

ISSN 0386-5878
Technical Report
of PWRI No.4218

PROCEEDINGS OF THE 27th U.S. – JAPAN BRIDGE ENGINEERING WORKSHOP

Tsukuba, Japan
November 7, 8 and 9, 2011

CENTER FOR ADVANCED ENGINEERING STRUCTURAL ASSESSMENT AND RESEARCH
PUBLIC WORKS RESEARCH INSTITUTE
Incorporated Administrative Agency

1-6, Minamihara, Tsukuba-shi, Ibaraki-ken, 305-8516 Japan

Opinions, findings, conclusions and recommendations expressed in the papers contained in this publication are those of the author(s).

Copyright © (2012) by P.W.R.I.

All rights reserved. No part of this book may be reproduced by any means, nor transmitted, nor translated into a machine language without the written permission of the Chief Executive of P.W.R.I.

この報告書は、独立行政法人土木研究所理事長の承認を得て刊行したものである。したがって、本報告書の全部又は一部の転載、複製は、独立行政法人土木研究所理事長の文書による承認を得ずしてこれを行ってはならない。

Technical Report
of PWRI No.4218

PROCEEDINGS OF THE 27th U.S. – JAPAN BRIDGE ENGINEERING WORKSHOP

By

Editor: Hideaki Nishida

Synopsis:

The proceeding documents the results of the 27th U.S. – Japan Bridge Engineering Workshop which was held at Tsukuba, Japan, on November 7, 8, and 9, 2011, as a part of the activities of the Panel on Wind and Seismic Effects, UJNR. The Workshop was organized by Task Committee G “Transportation System” (U.S. side chair: Dr. W. Philip Yen, FHWA, Japan side chair: Mr. Tetsuro Kuwabara, CAESAR, PWRI) of the Panel.

Key Words: Bridge, Design, Construction, Maintenance, Seismic, UJNR

Page Left Blank

PREFACE

The 27th US-Japan Bridge Engineering Workshop is a continuation of a series of technical interchanges between the United States and Japan on all topics related to bridge engineering. This series of workshops has been conducted under the auspices of Task Committee "G" of the US-Japan Panel on Wind and Seismic Effects, which is one of the 18 panels making up the United States-Japan Cooperative Program in Natural Resources (UJNR). The previous workshops are indicated below.

1 st	February 20-23, 1984	Tsukuba Science City, <i>Japan</i>
2 nd	August 19-20, 1985	San Francisco, California, <i>United States</i>
3 rd	May 8-9, 1987	Tsukuba Science City, <i>Japan</i>
4 th	May 11-12, 1988	San Diego, California, <i>United States</i>
5 th	May 9-10, 1989	Tsukuba Science City, <i>Japan</i>
6 th	May 7-8, 1990	Lake Tahoe, Nevada, <i>United States</i>
7 th	May 8-9, 1991	Tsukuba Science City, <i>Japan</i>
8 th	May 11-12, 1992	Chicago, Illinois, <i>United States</i>
9 th	May 10-11, 1993	Tsukuba Science City, <i>Japan</i>
10 th	May 10-11, 1994	Lake Tahoe, Nevada, <i>United States</i>
11 th	May 30-31, 1995	Tsukuba Science City, <i>Japan</i>
12 th	October 29-30, 1996	Buffalo, New York, <i>United States</i>
13 th	October 2-3, 1997	Tsukuba Science City, <i>Japan</i>
14 th	November 3-4, 1998	Pittsburgh, Pennsylvania, <i>United States</i>
15 th	November 9-10, 1999	Tsukuba Science City, <i>Japan</i>
16 th	October 2-4, 2000	South Lake Tahoe, Nevada, <i>United States</i>
17 th	November 12-14, 2001	Tsukuba Science City, <i>Japan</i>
18 th	October 22-24, 2002	St. Louis, Missouri, <i>United States</i>
19 th	October 27-29, 2003	Tsukuba Science City, <i>Japan</i>
20 th	October 4-6, 2004	Washington, DC, <i>United States</i>
21 st	October 3-5, 2005	Tsukuba Science City, <i>Japan</i>
22 nd	October 23-25, 2006	Seattle, Washington, <i>United States</i>
23 rd	November 5-7, 2007	Tsukuba Science City, <i>Japan</i>
24 th	September 22-27, 2008	Minneapolis, Minnesota, <i>United States</i>
25 th	October 19-21, 2009	Tsukuba Science City, <i>Japan</i>
26 th	September 20-22, 2010	New Orleans, Louisiana, <i>United States</i>
27 th	November 7-9, 2011	Tsukuba Science City, <i>Japan</i>

The steering committee for the 27th US-Japan Bridge Engineering Workshop consisted of Tetsurou Kuwabara, Phillip Yen, David Sanders, and Hideaki Nishida. The workshop was held at the NILIM and the CAESAR, PWRI, in Tsukuba, Japan. The 2-1/2 day workshop focused on: 1) Great East Japan Earthquake, 2) Tsunami 3) Load and Strength Evaluation, 4) Maintenance, 5) Inspection, 6) Design and Analysis, and 7) Acceleration Bridge Construction. Thirteen participants from the US and thirty-seven participants from Japan attended the workshop who were arranged by both T/C chairs in terms of the focused themes. The papers contained within this proceeding are the papers that were presented at the workshop (17 papers from the Japan side and 13 papers from the US side).

In addition to the workshop, there was a bridge study held after the workshop, November 10-12, 2011, visiting bridge sites:

- Long-term Bridge Management Plan for Old Bridges, Kiyosu Bridge and Eitai Bridge (Tokyo Metropolitan Government)
- Improvement of Seismic Performance, Katsushima area (Metropolitan Expressway)
- Damaged Bridges due to Great East Japan Earthquake
 - (a) Arakawa Wangan Bridge (Metropritan Expressway)
 - (b) Koizumi Oh-hashi Bridge, Kesen Oh-hashi Bridge, Osaragi Bridge and Kameda Oh-hashi Bridge (Tohoku Regional Development Bureau ,MLIT)
 - (c) Kamata Oh-hashi Bridge (Fukushima city)

in the Kanto and Tohoku regions.

ACKNOWLEDGEMENTS

There are many people that made the 27th US-Japan Bridge Engineering Workshop a success. I really appreciate cooperation of Tokyo Metropolitan Government, Metropolitan Expressway, Tohoku Regional Development Bureau and Ibaraki Prefecture.

Editor: Hideaki Nishida, Senior Researcher, Bridges and Structures Research Group, Center for Advanced Engineering Structural Assessment and Research (CAESAR), Public Works Research Institute (PWRI)

TABLE OF CONTENTS
27th US-Japan Bridge Engineering Workshop
Tsukuba, Ibaraki November 7 to 9, 2011

PREFACE

TABLE OF CONTENTS

WORKSHOP PROGRAM	1
SESSION 1: Great East Japan Earthquake	9
1-1 Damage of Highway Bridges due to the Great East Japan Earthquake By <u>Junichi Hoshikuma</u>	11
1-2 Ground Motion and Tsunami Induced Damage of Bridges during 2011 Great East Japan Earthquake By <u>Kazuhiko Kawashima</u> , Kenji Kosa, Yoshikazu Takahashi, Mitsuyoshi Akiyama, and Hiroshi Matsuzaki	23
1-3 Bridge Performance during the Great East Japan Earthquake of March 11, 2011 By <u>M. Lee Marsh</u> , Ian G. Buckle, W. Phillip Yen, Shideh Dasti, David Frost, and Eric Monzon.....	39
SESSION 2: Tsunami and Seismic1	53
2-1 Damage Analysis of Bridges Affected by Tsunami due to Great East Japan Earthquake By <u>Kenji Kosa</u>	55
2-2 Development of Tsunami Design Criteria for Oregon Coastal Bridges By <u>Bruce Johnson</u> and Solomon Yim.....	67
2-3 FHWA Seismic Hazard Mitigation Research Program By <u>W. Phillip Yen</u>	83

SESSION 3: Seismic2 91

3-1	Failure Investigation and Retrofit Strategies of a 22-Span Steel Girder Bridge during the 2010 Chile Earthquake By <u>Genda Chen</u> , Zuocai Wang, Phillip W. Yen, and Ian Buckle	93
3-2	Earthquake Response of Highway Bridges Subjected to Long Duration Seismic Motions By <u>Shojiro Kataoka</u>	107
3-3	Experimental Investigation of Influence of Live Load on Seismic Response of a Horizontally Curved Bridge By <u>Ian G. Buckle</u> , Hartanto Wibowo, Danielle M. Smith, and David H. Sanders	119
3-4	Discussion Method by Using Dynamic Analysis for Quakeproofing Long-Span Bridges By <u>Shunji Nagahashi</u> , Takumi Nishikawa, Mutsuji Kawakami, and Tatsumi Ujie	133

SESSION 4: Management and Maintenance1 143

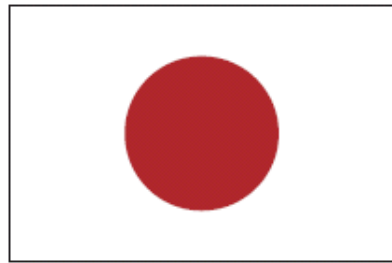
4-1	Analysis Examples of Periodic Inspection Results of National Highway Bridges in Japan -Application of Degree of Damage for Element Level- By <u>Fumihiko Nomura</u> , Masanori Okubo, and Takashi Tamakoshi	145
4-2	The Importance of Partnerships in the Implementation of Bridge Preservation Practices By <u>Peter J. Weykamp</u>	157
4-3	Maintenance of ASR-Affected Structures in Hokuriku Expressway, Japan By <u>Yoshifumi Adachi</u> , Mamoru Moriyama, and Masahiro Nomura	167

SESSION 5: Load and Strength Evaluation 175

5-1	Load-Carrying Capacity of Reinforced Concrete Beams with Adhesively Bonded Steel Plates By <u>Yoshiki Tanaka</u> , Jun Murakoshi, and Eiji Yoshida.....	177
------------	--	-----

5-2	Summary of NCHRP Research on Recalibration of the LRFR Load Factors in the AASHTO Manual for Bridge Evaluation By <u>Waseem Dekelbab</u>	191
5-3	Compressive Loading Test of Corroded Gusset Plate Connection in Steel Truss Bridge By <u>Jun Murakoshi</u> , Naoki Toyama, Mamoru Sawada, Kentaro Arimura, Lu Guo, Kuniei Nogami, Teruhiko Yoda, and Hideyuki Kasano.....	201
SESSION 6: Maintenance2		219
6-1	Introduction of Non-Destructive Highway Inspection Methods Using High Definition Video and Infrared Technology By <u>Koji Mitani</u> and Masato Matsumoto.....	221
6-2	Charpy Impact Tests with Test Specimens Made with Stop-Hole-Size Cores By <u>Kiyoshi Ono</u> , Kengo Anami, and Mitsuharu Oikawa.....	233
6-3	The Next Generation of Experimental Research in Structural Fires By <u>John L. Gross</u> and Stephen A. Cauffman	243
6-4	New Attempt to Maintenance of Steel Bridge Coating in Expressway By <u>Shuhei Sakai</u> and Dai Wakabayashi	255
6-5	FHWA's New Infrastructure Research and Technology Strategic Plan By <u>Ian M. Friedland</u>	267
SESSION 7: Design and Analysis		279
7-1	Unbonded Prestressed Columns for Earthquake Resistance By <u>David H. Sanders</u> , Alex S. Larkin, and M. Saiid Saidi	281
7-2	Study on Corrosion Analysis with Fiber Model of Long-Span Truss Bridge By <u>Kunihiro Hayashi</u> , Hideo Ohishi, Yukio Adachi, Misa Fujibayashi, and Koichi Sugioka.....	291

7-3	Seismic Performance Assessment of Concrete Bridges Designed by Displacement-Based Methods By <u>Kevin Mackie</u> , Vinicio Suarez, and Oh-Sung Kwon	301
7-4	Local Buckling Analysis of Steel Truss Bridge under Seismic Loading By <u>Eiki Yamaguchi</u> and Keita Yamada	315
SESSION 8: Construction and Maintenance3		323
8-1	Use of Precast I-Girders for Accelerated Bridge Construction in High Seismic Regions By <u>Sri Sritharan</u> , Justin Vander Werff, and Rick Snyder.....	325
8-2	How to Build a Bridge – Fast By <u>John Stanton</u>	337
8-3	Research and Repair of Reinforcement by Overlaying Floor Slab Method in Expressway By <u>Hidekazu Hayashi</u>	349
8-4	Repairing Fatigue Cracks in a Steel Deck Plate Girder Bridge of Unusual Structure By <u>Haruhiko Nakata</u> , Yoshiyuki Takamura, and Ken Tokumasu	359
8-5	Development of Eddy Current Test to Detect Fatigue Damages on Orthotropic Steel Deck By <u>Hiroki Sugiyama</u> , Akiko Tabata, Hiroyuki Nakajima, Tetsuji Yamagami, Sigeaki Tsukamoto, Akira Shiraishi, and Takaaki Yamada	373
APPENDIX 1 : JAPAN PARTICIPANTS		383
Resume of Japan Participants		
APPENDIX 2 : US PARTICIPANTS		393
Resume of U.S. Participants		



**27th US-Japan
Bridge Engineering Workshop
Workshop Program**

Page Left Blank

27th U.S.-JAPAN BRIDGE ENGINEERING WORKSHOP

PROGRAM SCHEDULE

November 7, 8 and 9, 2011
Tsukuba, Japan

November 7th (Monday) ... Day 1

9:00- 9:30 Opening Session (Conference Hall)

Moderators: Hideaki Nishida & David Sanders

Welcome Remarks: Taketo Uomoto (Chief Executive, PWRI)

Remarks: W. Phillip Yen (Chairman for the U.S.A Side)

Remarks: Tetsuro Kuwabara (Chairman for the Japan Side)

9:30-10:40 Session 1: Great East Japan Earthquake

(70 min.) Moderators: Shigeki Unjoh & Ian Buckle

1. Junichi Hoshikuma Damage of Highway Bridges due to the Great East Japan Earthquake

2. Kazuhiko Kawashima Ground Motion and Tsunami Induced Damage of Bridges during 2011 Great East Japan Earthquake

3 Lee Marsh Bridge Performance during the Great East Japan Earthquake of March 11, 2011

11:00-12:10 Session 2: Tsunami and Seismic1 (Conference Hall)

(70 min.) Moderators: Kazuhiko Kawashima & Lee Marsh

1. Kenji Kosa Damage Analysis of Bridges Affected by Tsunami due to Great East Japan Earthquake

2. Bruce Johnson Development of Tsunami Design Criteria for Oregon Coastal Bridges

3 W. Phillip Yen FHWA Seismic Hazard Mitigation Research Program

12:10-12:30 Photograph (Entrance of NILIM Main Building)

12:30-13:30 Lunch

- 13:30- 15:00 **Session 3: Seismic2 (Conference Hall)**
(90 min.) Moderators: Kenji Kosa & John Stanton
1. Genda Chen Failure Investigation and Retrofit Strategies of a 22-Span Steel Girder Bridge during the 2010 Chile Earthquake
 2. Shojiro Kataoka Earthquake Response of Highway Bridges Subjected to Long Duration Seismic Motions
 3. Ian Buckle Experimental Investigation of Influence of Live Load on Seismic Response of a Horizontally Curved Bridge
 4. Shunji Nagahashi Discussion Method by Using Dynamic Analysis for Quakeproofing Long-Span Bridges
- 15:20-16:30 **Session 4: Management and Maintenance1 (Conference Hall)**
(70 min.) Moderators: Takashi Tamakoshi & Bruce Johnson
1. Fumihiko Nomura Analysis Examples of Periodic Inspection Results of National Highway Bridges in Japan
--Application of Degree of Damage for Element
 2. Peter Weykamp The Importance of Partnerships in the Implementation of Bridge Preservation Practices
 3. Yoshifumi Adachi Maintenance of ASR-Affected Structures in Hokuriku Expressway, Japan

November 8th (Tuesday) ... Day 2

9:00-10:10 Session 5: Load and Strength Evaluation (Conference Hall)

(70 min.) Moderators: Yoshitomi Kimura & Peter Weykamp

- | | | |
|----|------------------|---|
| 1. | Yoshiki Tanaka | Load-Carrying Capacity of Reinforced Concrete Beams
with Adhesively Bonded Steel Plates |
| 2. | Waseem Dekelbab | Summary of NCHRP Research on Recalibration of the LRFR
Load Factors in the AASHTO Manual for Bridge Evaluation |
| 3 | Jun
Murakoshi | Compressive Loading Test of Corroded Gusset Plate
Connection in Steel Truss Bridge |

10:30-12:20 Session 6: Maintenance2 (Conference Hall)

(110 min.) Moderators: Eiki Yamaguchi & Waseem Dekelbab

- | | | |
|----|---------------|---|
| 1. | Koji Mitani | Introduction of Non-Destructive Highway Inspection Methods
Using High Definition Video and Infrared Technology |
| 2. | Kiyoshi Ono | Charpy Impact Tests with Test Specimens Made with
Stop-Hole-Size Cores |
| 3. | John Gross | The Next Generation of Experimental Research in
Structural Fires |
| 4 | Shuhei Sakai | New Attempt to Maintenance of Steel Bridge Coating in
Expressway |
| 5. | Ian Friedland | FHWA's New Infrastructure Research and Technology
Strategic Plan |

12:20-13:20 Lunch

- 13:20- 14:30 **Session 7: Design and Analysis (Conference Hall)**
(70 min.) Moderators: Masahiro Ishida & Sri Sritharan
1. David Sanders Unbonded Prestressed Columns for Earthquake Resistance
 2. Kunihiro Hayashi Study on Corrosion Analysis with Fiber Model of Long-Span Truss Bridge
 3. Kevin Mackie Seismic Performance Assessment of Concrete Bridges Designed by Displacement-Based Methods
 4. Eiki Yamaguchi Local Buckling Analysis of Steel Truss Bridge under Seismic Loading
- 14:50–16:30 **Breakout Session**
(100 min.) **Group A Seismic Engineering (Conference Hall)**
Moderators: Jun-ichi Hoshikuma & Phil Yen
Group B Maintenance (ICHARM Auditorium)
Moderators: Tetsuro Kuwabara & Ian Friedland

November 9th (Wednesday) ... Day 3

9:00-10:50 **Session 8: Construction and Maintenance3 (Conference Hall)**

(110 min.) Moderators: Jun Murakoshi& Genda Chen

1 Sri Sritharan Use of Precast I-Girders for Accelerated Bridge
Construction in High Seismic Regions

2 John Stanton How to Build a Bridge - Fast

3 Hidekazu Hayashi Research and Repair of Reinforcement by Overlaying
Floor Slab Method in Expressway

4. Haruhiko Nakata Repairing Fatigue Cracks in a Steel Deck Plate Girder
Bridge of Unusual Structure

5. Hiroki Sugiyama Development of Eddy Current Test to Detect Fatigue
Damages on Orthotropic Steel Deck

10:50-11:30 **Closing Session (Conference Hall)**

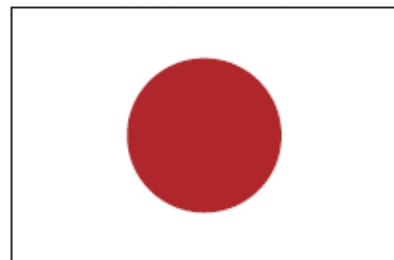
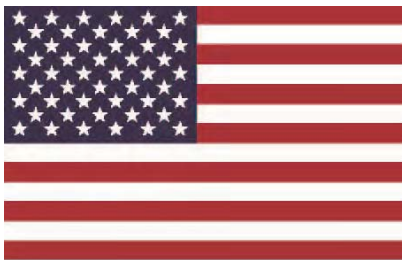
(40 min.) Moderators: Hideaki Nishida& David Sanders

Settlement of Resolution

Remarks: W. Phillip Yen (Chairman for the U.S.A Side)

Closing Remarks: Tetsuro Kuwabara (Chairman for the Japan Side)

Page Left Blank



27th US-Japan Bridge Engineering Workshop

Session 1

Great East Japan Earthquake

Damage of Highway Bridges Due to the Great East Japan Earthquake

By Junichi Hoshikuma

Ground Motion and Tsunami Induced Damage of Bridges during 2011 Great East Japan Earthquake

By Kazuhiko Kawashima, Kenji Kosa, Yoshikazu Takahashi, Mitsuyoshi Akiyama, and Hiroshi Matsuzaki

Bridge Performance during the Great East Japan Earthquake of March 11, 2011

By M. Lee Marsh, Ian G. Buckle, W. Phillip Yen, Shideh Dasti, David Frost, and Eric Monzon

Page Left Blank

DAMAGE OF HIGHWAY BRIDGES DUE TO THE GREAT EAST JAPAN EARTHQUAKE

Jun-ichi Hoshikuma¹

Abstract

The 2011 Great East Japan Earthquake struck the Tohoku and Kanto area on March 11, 2011. Immediately after the earthquake, research engineers in NILIM/PWRI were dispatched to Tohoku area to investigate the damage to bridges and suggest the technical advice to bridge administrators. On behalf of NILIM/PWRI joint reconnaissance team for bridge damage, author summarizes damage characteristic of bridges due to the earthquake in this paper. Technical issues learned from the damage of bridges were also described based on the investigation of bridge damage.

Introduction

The 2011 Great East Japan Earthquake occurred at 2:46 pm on March 11, 2011. The catastrophic damage resulting from strong ground motion and huge tsunami was caused in Tohoku and Kanto regions. More than 20,000 people were killed or missing and various infrastructures were damaged, especially in the coastal area of Iwate, Miyagi, Fukushima and Ibaraki Prefectures.

Many highway bridges were also damaged in these areas due to both large ground motion and tsunami inundation. Soon after the earthquake occurred, NILIM and CAESAR in PWRI jointly investigated bridge damage and provided the technical supports and suggestions to bridge administrators, including Regional Bureaus of MLIT and some Local Governments. Furthermore, Task Committee G of UJNR Panel conducted the U.S.-Japan joint reconnaissance to bridge damage in early June, 2011.

This paper presents damage characteristic of bridges. Following topics were focused; bridge damage due to tsunami inundation or strong ground motion effect, verification of seismic performance of bridges retrofitted after the 1995 Hyogo-ken Nambu earthquake, validations of effectiveness of the current seismic design specification.

The 2011 Great East Japan Earthquake and Ground Motion

The main shock of this earthquake ($M_w=9.0$, focal depth=24km) occurred at 2:46 pm (JST) on March 11, 2011. Maximum seismic intensity was observed at Tsukidate, Kurihara city in Miyagi prefecture (Seismic intensity of JMA was 7) and large seismic intensities were observed in Tohoku and Kanto areas. Fig. 1 shows acceleration ground motion waveforms and spectral response accelerations at representative strong ground motion observation sites.

¹ Chief Researcher, Center for Advanced Engineering Structural Assessment and Research, PWRI

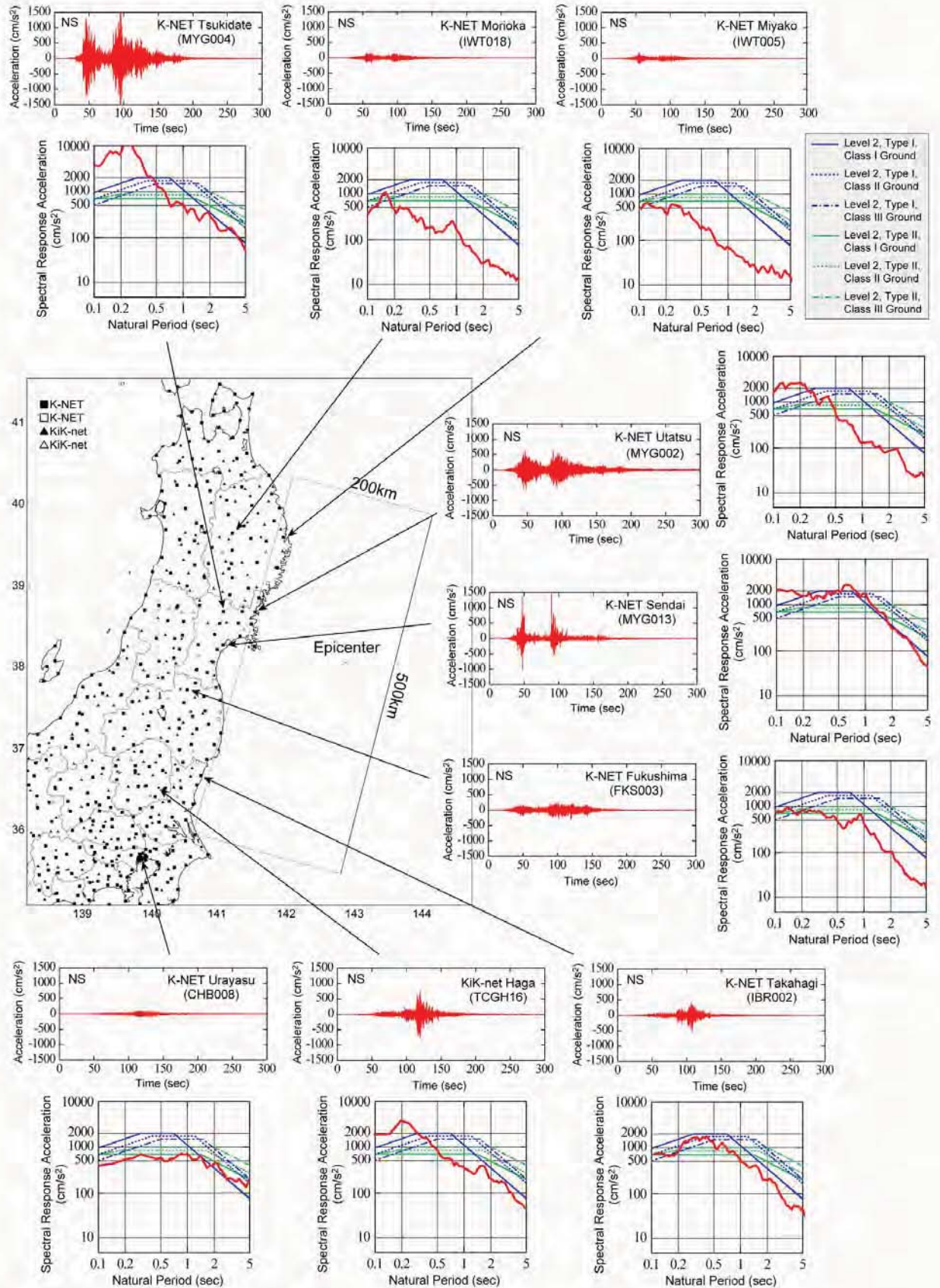


Fig. 1 Acceleration Waveforms and Spectral Response Acceleration at Main Shock (NS comp.)

It should be noted that 1) strong ground motion records with long duration were observed and 2) there were multiple pulses in some ground motion records observed near epicenter. This is because large fault areas collapsed continuously. It was observed at very large maximum response acceleration at the range of short predominant period such as Tsukidate record. The maximum response accelerations at the range of natural periods from 1.0 to 2.0 seconds, which relatively correlate with damage of ordinary road bridges, were equal or slightly less than those of the 1995 Hyogo-ken Nambu earthquake. Ground motions and maximum response accelerations at the coastal area of Tohoku region were not so large. However, strong ground motions and large response accelerations were observed at the sites where located slightly far from epicenter such as Fukushima, Tochigi and Ibaraki prefectures.

Huge tsunami induced by main shock struck at Tohoku and Kanto coastal areas and exceeding 10m in height of wave were observed.

Moreover, aftershocks with the JMA magnitude of 7.0 or over were occurred three times within a day and total of 89 aftershocks with the magnitude of 6.0 or over were occurred until August 3.

Overview of Damage in Bridges

Damage of the highway bridges due to this earthquake can be categorized as effect of strong ground motion, effect of tsunami inundation, and effect of soil liquefaction. It should be noted in this earthquake that the intensive damage in highway bridges was mainly caused by tsunami inundation. Superstructures in twelve bridges including service road for pedestrian on national highway route 45 (main route along the Pacific coast of Tohoku Area) were washed away, which resulted in the traffic close after the earthquake. About 91 highway bridges in total were washed away due to tsunami inundation in Iwate, Miyagi, Fukushima, Ibaraki and Chiba prefectures. On the other hand, as long as we have investigated, 105 bridges survived even though the superstructures of these bridges were inundated with the tsunami. The backfill of abutment in some bridges were also washed out even though super- and substructures survived.

The ground motion effect to damage of bridges was less significant than the tsunami effect. One bridge (Rokko Ohashi Bridge, an old steel girder bridge supported by steel pile-bent columns located in Ibaraki prefecture) was collapsed due to the ground motion of the earthquake. Although the collapsed bridge was observed at the only Rokko Ohashi in the highway bridges, it was found in the bridge designed in accordance with pre-1980 design specifications that damage to RC columns at section of cut-off of longitudinal rebars, damage to RC pier-wall with small amount of reinforcement, damage to steel bearings and attachment of bearings, damage to bracing and steel members, and subsidence of backfill soil of abutment. These damage modes have already observed in the past earthquakes. However, rupture of elastometric rubber bearings were observed at the Sendai-Tohbu viaduct designed based on Post-1995 design specifications.

After the Kobe Earthquake, the seismic retrofit project has been performed for existing bridges columns designed in accordance with pre-1980 specifications with high priority, to prevent the collapse of the bridge structure and unseating of the deck.

Almost of retrofitted bridge columns were not damaged due to the ground motion of the earthquake, which would exhibit the effectiveness of the seismic retrofit.

Soil liquefaction was widely observed in particularly Tokyo Bay area. Although the effect of the soil liquefaction on the bridge damage was minor, subsidence of backfill soil of abutment due to the soil liquefaction effect was developed in some bridges. Deck-end gap was shortened resulting from movement of substructure, which caused steel bearings damage and cracks in parapet wall.

Bridge Damage Due to Ground Motion

Damage of Unretrofitted Bridges Designed in Accordance with Pre-1980 Design Specifications

Intensive damage due to the ground motion was developed in many unretrofitted bridges designed in accordance with pre-1980 design specifications. Almost of damage modes of those bridges have ever been observed in the past earthquakes. Photos 1 to 3 show the damage to reinforced concrete piers, steel bearing supports and the attachment of the bearing support to pier top or the superstructure, respectively. Although some bridge columns collapsed during the 1995 Kobe earthquake, the only one bridge collapsed during the 2011 Great East Japan earthquake. As shown in Photo 4, an old steel girder bridge supported by steel pile-bent columns (Rokko Ohashi Bridge) in the local roadway was collapsed due to the ground motion of the earthquake. Rokko Ohashi is to be replaced a new bridge and the new one was being constructed at the time of the earthquake.

Damage of Bridges Designed in Accordance with Post-1995 Design Specifications

There were few intensively-damaged bridges designed in accordance with post-1995 design specifications, where the seismic design acceleration increased based on the ground motion records of the 1995 Kobe earthquake and the details of the transverse steel was specified for improving the confinement effect and shear capacity of the RC columns.



Photo 1 Damage of Reinforced Concrete Columns at Cut-off Section of Longitudinal Reinforcement



Photo 2 Damage of Steel Bearing Support



Photo 3a Damage of Pier Top



Photo 3b Damage of Attachment of Bearings to Superstructure



Photo 4 Collapse of Steel Pile-bent Columns

However, as shown in Photo 5, it should be noted that elastometric rubber bearings ruptured at the Sendai-Tohbu viaduct designed based on Post-1995 design specifications. Fig. 2 illustrates the structure of the Sendai-Tohbu viaduct and the positions of the elastometric rubber bearing with the rupture. As seen in Fig. 2, bridge structure in this junction is very complicate. Bridge width changes significantly in the 4-span continuous box girder with the change of the section. Span length of the section from P52 to 56 is around 70m, while that from P56 to P58 is 39m. P52 and P53 are single-column hammerhead steel piers, while P54, P55 and P56 are two-column steel frames. Rupture of the elastometric rubber bearings in the transverse direction was observed at the deck-end of P52 side in 4-span continuous box girder, though there are few damaged elastometric rubber bearings at the other deck-end side of the box girder on Pier 56. Photo 6 shows failure mode of the elastometric rubber bearing with the rupture. Comparison of the failure mode with the result of the shear loading test should be made, to estimate the capacity of the elastometric rubber bearing and the applied seismic force combination.

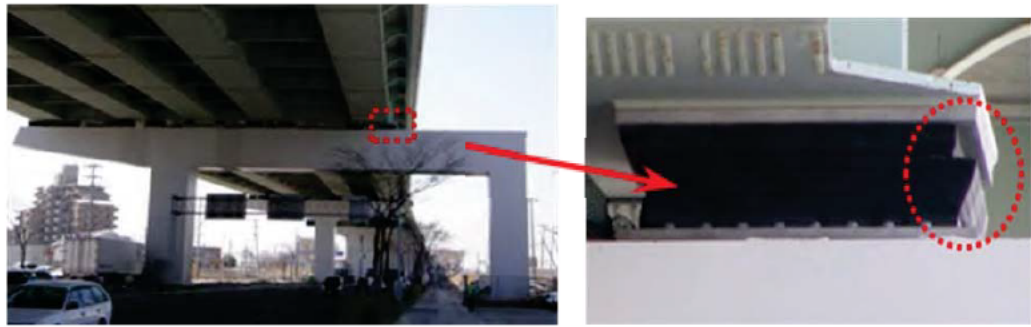


Photo 5 Rupture of Elastometric Rubber Bearings in Sendai Tobu Viaduct
(P54, Two-column Steel Frame)

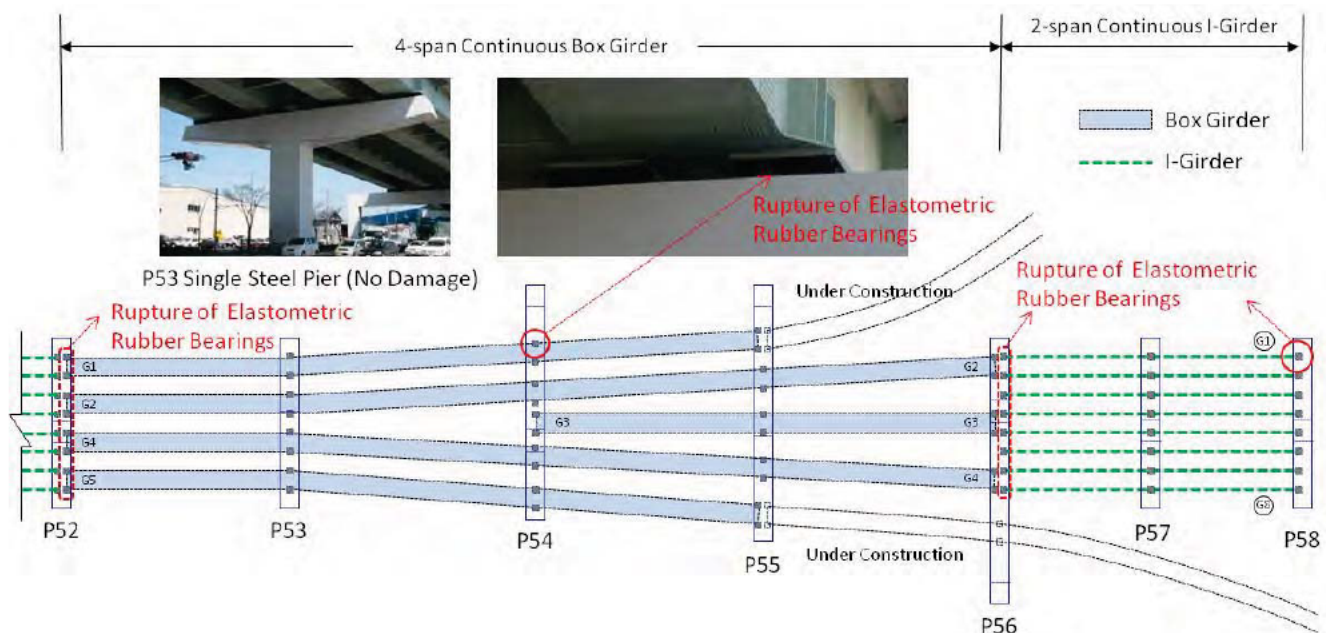


Fig. 2 Bridge Structure of Sendai-Tobu Viaduct and Position of Elastometric Rubber Bearing with Rupture



Photo 6 Details of Rupture of Elastometric Rubber Bearings

Damage of Retrofitted Bridges

Based on the lessons learned from the 1995 Kobe Earthquake, the seismic retrofit project has been performed for existing bridges columns designed in accordance with pre-1980 specifications with high priority, to prevent the collapse of the bridge structure and unseating of the deck. During the 2011 Great East Japan Earthquake, many retrofitted bridges were given a shake due to the ground motion.

Photo 7 exemplifies the effectiveness of the seismic retrofit for bridge columns. As seen in Photo 7, there are two adjacent river-crossing bridges. Since one bridge (Nakagawa Bridge) is on the designate emergency route, bridge columns designed with the pre-1980 specifications have already been retrofitted by reinforced concrete jacketing. The other bridge (Kunita Ohashi Bridge) is on the local roadway and the bridge columns have not yet been retrofitted at the earthquake. Although Kunita Ohashi Bridge suffered from the vulnerable damage and thus lost the serviceability for the bridge, Nakagawa Bridge did not suffer from the damage and kept the serviceability soon after the earthquake. Seismic performance shown in these two bridges clearly exhibits the effectiveness of the seismic retrofit.

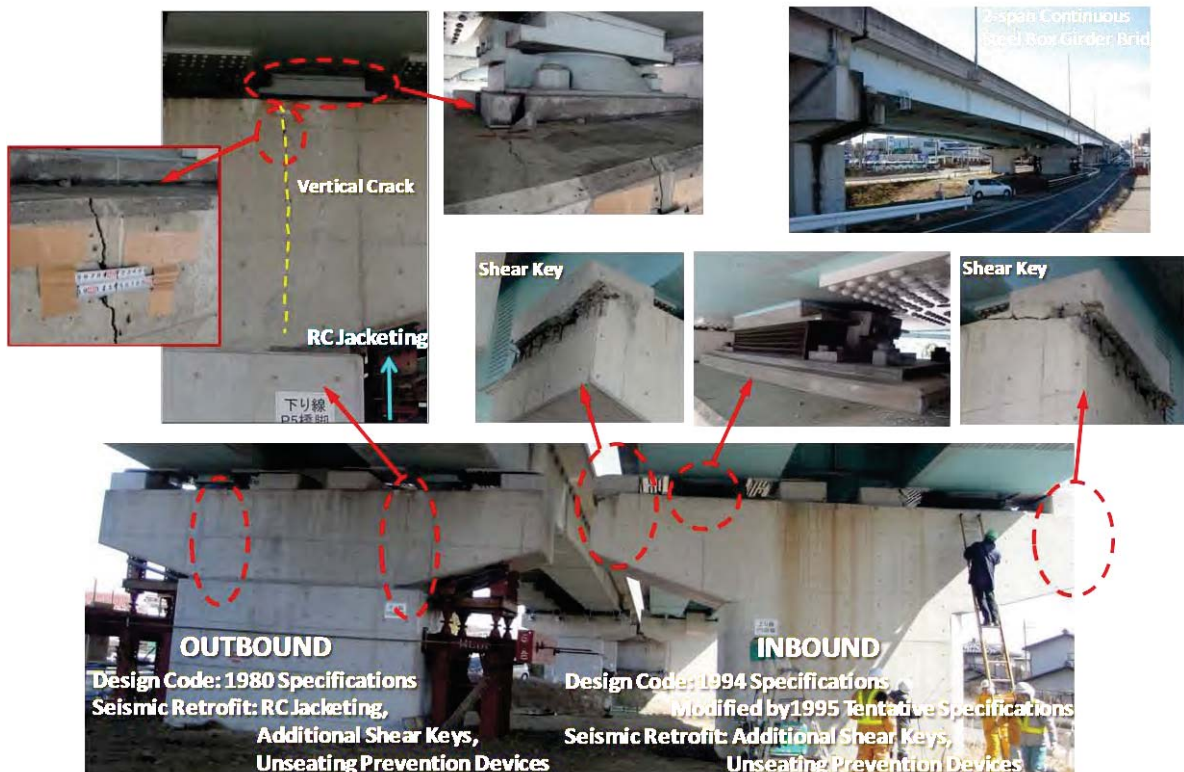


Photo 7 Comparison of Seismic Performance between Adjacent Two Bridges
(Nakagawa Bridge and Kunita Ohashi Bridge)

On the other hand, there are a few remarkable damage examples in the retrofitted bridges. Photo 8 shows adjacent two reinforced concrete columns in Kameda Ohashi Bridge. Each column supports 2-span continuous steel box girder at the middle. The outbound column was designed with 1980 specifications and retrofitted by reinforced concrete jacketing for strengthening the cut-off section without increasing the flexural strength of the column base. Furthermore, additional shear keys were anchored to column top to supplement the strength of the existing bearings. Although no damage was found to the steel bearings and shear keys, vertical cracks of nearly

10mm width were observed at the beam section as shown in Photo 8. The inbound column was designed with 1994 specifications basically and some modifications were made based on the 1995 tentative specifications (published soon after 1995 Kobe Earthquake). In the inbound column, elastometric rubber bearings were deformed in the transverse direction and the side stoppers were failed. Concrete of the beam edge portion attaching the supplemental shear keys also spalled off (see Photo 8) due to the transverse seismic force induced by the inertia of the superstructure, while vertical crack observed in the beam of the outbound column was not developed in the inbound beam.

Photo 8 Comparison of Damage Mode between Adjacent Two Bridge Columns



(Kameda Ohashi Bridge)

Photo 9 shows the failure of pier top. This type of damage has ever observed in the old bridge columns since the past earthquakes. Bearing capacity of the pier top was insufficient to transmit the seismic force to column. It should be noted in this bridge that the crack reaches the portion of the anchor bars of the steel bracket for attaching the unseating prevention devices. Since the unseating prevention devices should work at the unexpected situation of failure of bearing supports.



Photo 9 Crack to Pier Top Affects Attachment

Bridge Damage Due to Tsunami Inundation

Many bridges built along the coast line of the Pacific Ocean in Tohoku and Kanto areas were affected by the huge tsunami. Photos 10 and 11 show the typical damage modes of bridge due to the tsunami inundation.

The bridge shown in Photo 10a is a 6-span steel girder bridge (twin three-span continuous girders), namely Koizumi Bridge. The steel girder was supported by RC pier walls with steel pipe piles. The pier walls with the fix bearings (P2 and P4) were retrofitted by FRP sheets, furthermore viscous dampers were installed to the deck-ends. The height of tsunami has been estimated exceeding 10 meter high in this area, which means the steel girder was completely inundated with tsunami. Tsunami effect was so significant to Koizumi Bridge that the whole girder were washed away upstream and one RC pier-wall (P3) was also washed away. The pier-wall of P3 supported two girders with movable bearing supports was found about 50m away from original position, while the pile foundation and the footing for P3 remained at the original position. The pier-wall failed at the bottom section as shown in Photo 10b. The probable reason for only P3 being washed away was due to smaller ultimate strength than the other pier-walls. It is also noted that backfill soil of abutment was also washed away at both sides.

Photo 11 shows a 12-span PC single girder bridge, namely Utatsu Ohashi Bridge. Piers consisted of circular RC column (P1 and P2) and rectangular RC column with PC piles. Bridge columns were retrofitted by RC jacketing and the seat length was extended at the top of pier. Total of 8 spans (from P2 to P10) were washed away to the inland direction. It was found that additional concrete/steel shear keys, installed at the pier top for the seismic retrofit of existing bearings, were damaged and some hammerhead beams of piers in the inland side were cracked. A lot of diagonal cracks were also observed at both unseated and survived PC girders.

On the other hand, it is interesting to note that there are many survived bridges even though the superstructures of these bridges must be inundated with tsunami. Photo 12 exemplifies Yanoura Bridge survived washed away of superstructure due to the tsunami, while two spans of the water pipe bridge located adjacent to Yanoura Bridge were washed away. These survived bridges will hint the mechanism of resistance to the tsunami effect.

Impact of 2011 Great East Japan Earthquake on Seismic Design of Highway Bridges

The seismic performance of highway bridges, designed in accordance with the post-Kobe Japanese specifications, was very well and these bridges were functional without any long-term traffic stops after the earthquake. However, there are several important issues and lessons we should study and review for the latest seismic design specifications for highway bridges. Followings are the selected issues.



Photo 10a Washed Away of Steel Superstructure and Pier-wall (Koizumi Bridge)



Photo 10b Failure Section of Pier-wall (P3)



Photo 11 Washed Away of PC Superstructure (Utatsu Ohashi Bridge)



Photo 12 Bridge Survived Washed Away Due to Tsunami (Yanoura Bridge)

Ground Motion

In the 2011 Great East Japan Earthquake, many strong ground motion records were recorded and these records clearly showed that this earthquake generated ground motions with multiple pulses and thus the longer duration (more than 2 minutes) than other records observed in the past earthquakes. Similar ground motions were reported in the 2010 Chile Earthquake with the moment magnitude Mw 8.8. Therefore, the subduction-type earthquake with Mw of nearly 9 may induce the ground motion with long duration.

In general, the long duration would affect the number of cyclic inelastic response of the bridge system. Past experimental researches indicated that the loading pattern in the quasi-static cyclic loading test, particularly the number of cyclic loading affects the ductility capacity of flexural reinforced concrete column. In order to accommodate such effect into the seismic design, Japanese design specifications have determined two ductility/shear capacity factors based on the types of the ground motion, i.e. the subduction-type and the near-fault-type. Re-studies on the effect of the long duration will be required based on the ground motion observed in the 2011 Great East Japan Earthquake.

The long duration would also affect the soil liquefaction. Effect of the soil liquefaction on the seismic design of bridge foundation was introduced in the 1971 specifications in Japan based on the lessons learned from the 1964 Niigata Earthquake. Although there were no major liquefaction-induced damages in bridges during the 2011 Great East Japan Earthquake, the long duration effect on the bridge performance built on the liquefiable sandy soil condition should be verified through both geological and structural perspectives.

Since the ground motion effect propagated wide, bridge damage developed in wide area. Many ground motion records were also observed in wide area. It should be also important to study the relation between the properties of the ground motion and damage of bridges.

Tsunami Effect on Bridges

Superstructures in several bridges were washed away due to the tsunami effect. Backfill soil for the abutment was also washed out. Similar damage modes in bridge were also observed during the 2004 Indian Ocean Earthquake. Failure mechanism of bridge system due to the tsunami effect need to be studied, in which the resistance capacity of the existing bearing supports be analyzed based on both the washed-away and survived bridges. Also, more experimental researches on the bridge behavior due to the tsunami effect are required, to find the appropriate structural system for mitigating the tsunami effect.

On the other hand, the design concept of bridge for unexpected extraordinary event would be controversial, because structural resistance capacity has a limit. Basically, it would be one of the options for the extraordinary tsunami effect to avoid routing important highway network and locating important highway routes in the tsunami-inundation area. In terms of structural engineering, easy-to-recover bridge

system employing the temporary structure with the accelerated construction technique is also another option.

Validations of Effectiveness of Seismic Retrofit

Seismic retrofit have been performed step-by-step since 1995 Kobe earthquake. Based on the lessons learned from the past earthquakes, bridge columns in the important highway network designed by pre-1980 specifications have been retrofitted with high prioritization. Many seismic vulnerable bridges in the important route such as National Highway Route 4, 6, 45 etc were retrofitted up to the date of the earthquake, which resulted in quick recovery of the functional highway network after the earthquake. It should be, however, important review to investigate details of the new type of damage in the retrofitted bridges and evaluate the seismic behavior of the bridge during the earthquake.

Conclusion Remarks

This report preliminarily summarized damage to highway bridge due to the 2011 Great East Japan Earthquake with focus of the seismic performance of the retrofitted bridges and tsunami effect. Based on the damage caused by the earthquake and tsunami, more analytical and experimental researches should be required to clarify the mechanism of the damage. Investigation results also indicate that subsidence of the backfill soil in the abutment has been remarkable with the improvement of seismic performance for bridge structures, though details are not reported in this paper. It would be important to ensure the seismic performance of both bridge structures and embankment for highway.

Acknowledgments

Damage investigation was supported by a number of organizations. Special appreciation is extended to Iwate Pref., Ibaraki Pref., Chiba City, Kitakami City, Tohoku Regional Development Bureau, Kanto Regional Development Bureau and Headquarter of MLIT.

References

1. Genda Chen, Phillip W. Yen, Ian Buckle, Tony Allen, Daniel Alzamora, Jeffrey Ger and Juan G. Arias: 2010 Chile Earthquake Implication to the Seismic Design of Bridges, Proc. 26th US- Japan Bridge Engineering Workshop, 2010.
2. K. Kawashima, S. Unjoh, J. Hoshikuma and K. Kosa: Damage Characteristic of Bridges due to 2010 Chile Earthquake, Proc. 26th US- Japan Bridge Engineering Workshop, 2010.

GROUND MOTION AND TSUNAMI INDUCED DAMAGE OF BRIDGES DURING 2011 GREAT EAST JAPAN EARTHQUAKE

Kazuhiko Kawashima¹, Kenji Kosa², Yoshikazu Takahashi³, Mitsuyoshi Akiyama⁴,
and Hiroshi Matsuzaki⁵

ABSTRACT

This paper presents damage of road and railway bridges during the Great East Japan earthquake and tsunami on March 11, 2011 based on a JSCE damage investigation. Ground motion induced damage and tsunami induced damage of both road and railways bridges are presented.

INTRODUCTION

The Great East Japan earthquake (Off Pacific Coast of Tohoku Region, Japan earthquake) with moment magnitude of 9.0 occurred at 14:46 (local time) on March 11, 2011 along the Japan Trough in the Pacific. It was the sixth largest earthquake ever recorded in the world. The fault zone extended 450 km and 200 km in the north-south and west-east directions, respectively. Extensive damage occurred in the wide region in the east part of Japan.

The authors were dispatched by Japan Society of Civil Engineers for field damage investigation to bridges in Miyagi-ken and Iwate-ken between March 29-April 3, 2011. In addition to the first investigation, damage investigations were conducted several times. Since 1978 Miyagi-ken-oki earthquake and 2003 Sanriku-Minami earthquake affected this region, an emphasis was placed in the damage investigation to compare damage among 2011 Great East Japan earthquake and two previous earthquakes. This paper presents ground motion induced damage and tsunami induced damage of bridges during 2011 Great East Japan earthquake.

GROUND MOTIONS AND TSUNAMI

A number of strong motion accelerations were recorded by the National Institute of Earth Science and Disaster Prevention and Japan Meteorological Agency. Fig. 1 shows measured accelerations along the Pacific coast. Ground accelerations continued over 300s, and had at least two groups reflecting the fault rupture process. The highest peak ground acceleration of 27.0 m/s^2 was recorded at Tsukidate. However the high acceleration was resulted from a single pulse with high frequency components, and the response acceleration at 1.0 s was only 5.1 m/s^2 . Damage of buildings and other

¹ Professor, Tokyo Institute of Technology, Tokyo, Japan

² Professor, Kyusyu Institute of Technology, Kita-Kyusyu, Japan

³ Associate Professor, Disaster Prevention Research Institute, Kyoto University, Uji, Japan

⁴ Professor, Waseda University, Tokyo, Japan

⁵ Assistant Professor, Tokyo Institute of Technology, Tokyo, Japan

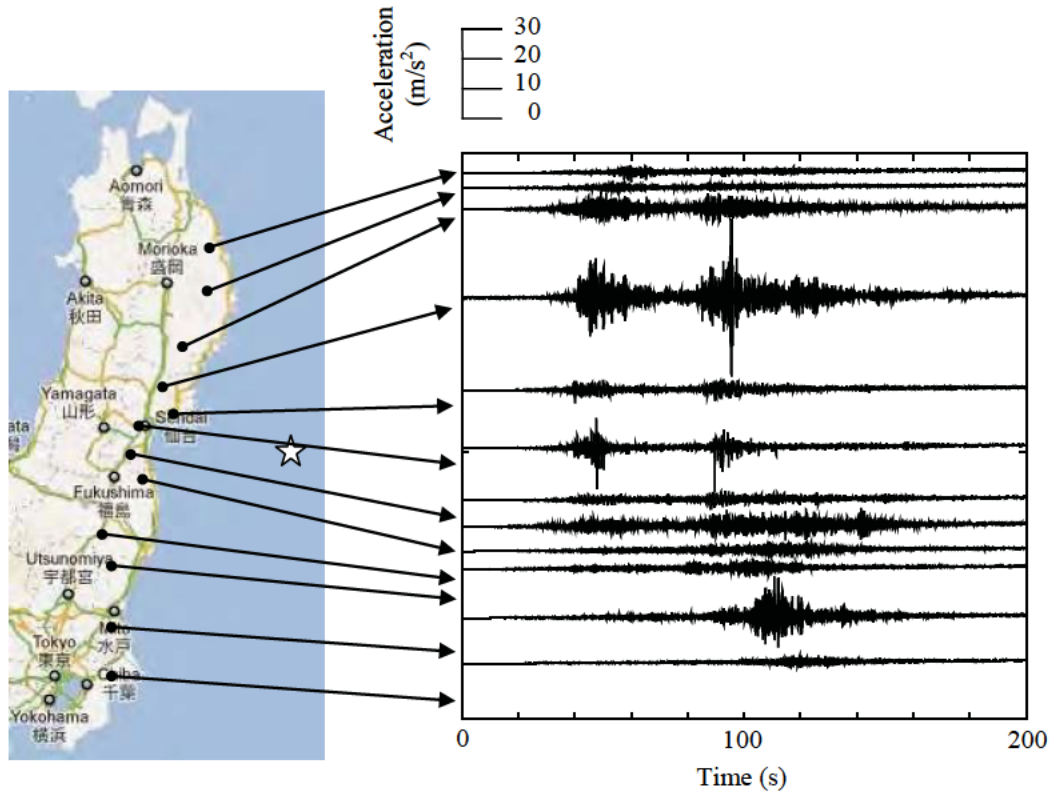


Fig. 1 Accelerations recorded by NIED

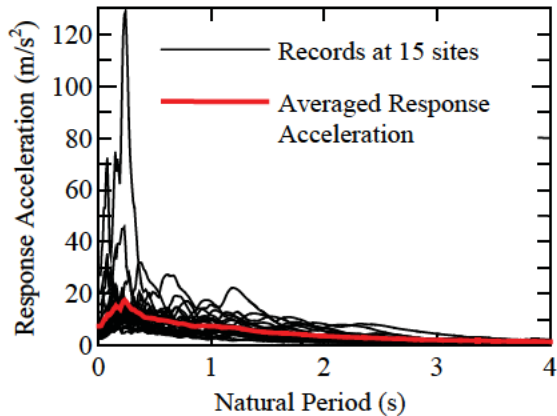


Fig. 2 Response accelerations ($\xi=0.05$) at 15 sites at the flat land north of Sendai City

infrastructures was minor in Tsukidate.

Fig. 2 shows acceleration response spectra at 15 sites in the flat region north of Sendai. It is general trend that high frequency components were predominant in the measured accelerations. However Fig. 3 shows ground accelerations and response accelerations of the records at Furukawa where soil condition is very weak such that the shear wave velocity is 80m/s at 2m thick top soil and 120 m/s between 2 m and 17 m below the ground surface. The response accelerations in the lateral components were nearly 15 m/s^2 at period between 0.2 s and 0.8 s, and $3-5 \text{ m/s}^2$ at 2 s period.

Ground accelerations with similar trend were recorded at other soft soil sites

such as K-NET Ichinoseki and Sendai and JMA Tome and Wakuya.

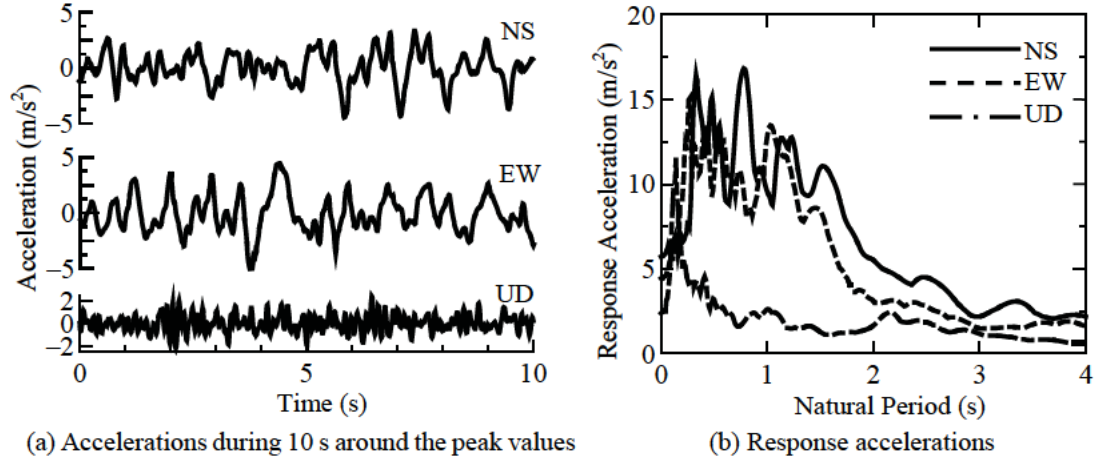


Fig. 3 Acceleration record at Furukawa, Osaki City (K-NET)

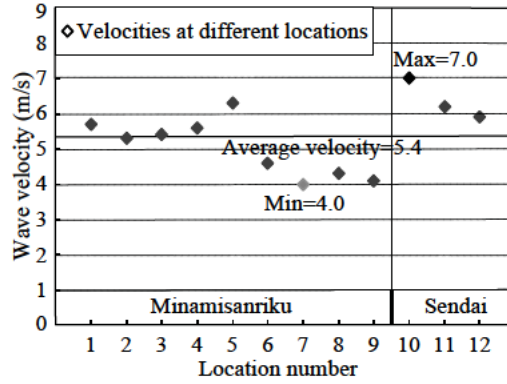


Fig. 4 Estimated tsunami particle velocity

Tsunami

Tsunami attacked coastal region as soon as 30 minutes after the earthquake. Tsunami inundation area reached as far as 10 km inland, engulfing virtually everything including peoples and structures. Japan Meteorological Agency (JMA) tidal stations recorded high tsunami at many locations. The highest tsunami was recorded 8.5m at Miyako. However due to saturation of the instrument, it must be higher than 8.5m. Other recorded heights at JMA stations include over 8.0 m in Ofunato and over 7.3 m in Soma. It is estimated that real tsunami height was as high as 15m at Onagawa fishery port.

For evaluating tsunami actions to bridges, it is important to know tsunami flow velocity. For this purpose, 12 videos which recorded tsunami flow in Minami-Sanriku Town and Sendai City were analyzed. Particle velocity was estimated based on the time required for a piece of debris to flow between two distinguished points. The distance between the two points and the time were measured using Google Earth's distance measurer and the video's timer, respectively.

Fig. 4 shows tsunami particle velocities evaluated at 12 locations. The maximum, average and the minimum tsunami particle velocities were 7.0m/s, 5.4m/s and 4.0m/s, respectively.



Photo 1 Shear failure of a column due to termination of longitudinal bars with insufficient development (Fuji Bridge) (courtesy of Dr. Hoshikuma, J., PWRI)



Photo 2 Yuriage Bridge



Photo 3 Damage of pin and roller bearings



Photo 4 Damage of PC girders near the support

GROUND MOTION INDUCED DAMAGE OF ROAD BRIDGES

Damage of bridges which were not yet retrofitted

Ground motion induced damage of road bridges was generally less significant. However extensive damage occurred at the bridges which were designed according to the pre-1990 design codes (JRA 1990) and were not yet retrofitted in accordance with the post-1990 design codes. For example, Photo 1 shows shear failure of a reinforced concrete column resulted from insufficient development at cut-off of longitudinal bars. This mode of damage occurred extensively in the 1995 Kobe, Japan earthquake [Kawashima and Unjoh 1997]. Extensive investigation was directed to clarify the failure mechanism of such columns [for example, Kawashima, Unjoh and Hoshikuma 2005], including a project consisting of series of large scale shake table experiments using E-Defense [Kawashima et al 2009]. Over 30,000 columns were so far retrofitted since 1995 Kobe earthquake. Consequently, during this earthquake, damage due to this mechanism was not predominant in the bridges which were retrofitted, but damage occurred at the bridges which were not yet appropriately retrofitted.

Yuriage Bridge as shown in Photo 2 suffered extensive damage at reinforced concrete hollow and solid columns, supports of prestressed concrete girders, and steel pin and roller bearings during 1978 Miyagi-ken-oki earthquake. Since the damaged

columns were repaired and strengthened by reinforced concrete jacketing, they did not



Photo 5 Buckled truss braces



Photo 6 Damage of a pier during 1978 Miyagi-ken-oki earthquake (Sendai Bridge)



Photo 7 Retrofitted pier of Sendai Bridge which did not suffer damage during 2011 Great East Japan earthquake

suffer damage this time. However pin and roller bearings suffered damage again in the similar way as shown in Photo 3. It is obvious that pin and roller bearings are vulnerable to seismic action, because the stress builds up until failure by allowing virtually no relative displacement at pin bearings and relative displacement accommodated in roller bearings is insufficient to realistic relative displacement developed under a strong excitation.

Furthermore, the same supports of prestressed concrete girder which suffered damage in 1978 Miyagi-ken-oki earthquake suffered again as shown in Photo 4. Taking account of likely concentration of seismic force at this region and the importance of anchorage of PC cables, more rigorous repair had have to be conducted after 1978 Miyagi-ken-oki earthquake.

Tennoh Bridge built in 1959 suffered extensive damage during 1978 Miyagi-ken-oki earthquake. This bridge suffered extensive damage again during this earthquake at the same members; truss braces and pin and roller bearings as shown in Photo 5.

On the other hand, damage of bridges which were already retrofitted suffered virtually no damage. For example, Sendai Bridge which is a symbolic bridge in Sendai suffered extensive damage at columns and bearings as shown in Photo 6 during 1978 Miyagi-ken-oki earthquake. However this bridge suffered no damage during this earthquake, because columns were retrofitted as shown in Photo 7 and steel bearings were replaced with elastomeric bearings.



Photo 8 Shin-Tenno Bridge



Photo 9 An end of deck supported by elastomeric bearings and unseating prevention devices



Photo 10 Piers where elastomeric bearings ruptured (Sendai-Tobu viaduct)



Photo 11 Transverse offset of a girder due to rupture of elastomeric bearings



Photo 12 One of elastomeric bearings ruptured

New bridges constructed by post-1990 codes

Since 1990, the seismic design code was extensively upgraded [JRA 1990]. Before 1990, only elastic static and dynamic analysis was used assuming unrealistically small seismic design force. However after 1990, inelastic static and dynamic analyses based on Type I/Level 2 design ground motions (middle-field ground motions by M8 events) and an evaluation method of inertia forces considering multi-span continuous effect were introduced, and introduction of those provisions much enhanced the ductility capacity of columns and the seismic performance of bridges. Furthermore in the 1996 code [JRA 1996, Kawashima 2000] which was revised taking account of

damage experience of 1995 Kobe earthquake, the Type II/ Level 2 design ground motions (near-field ground motions by M7 events), seismic isolation and use of elastomeric bearings were incorporated. Furthermore, strength of unseating prevention devices was enhanced.

As a consequence of the upgrading of seismic measures, damage of bridges which were built or were retrofitted in accordance with the post-1990 design codes suffered essentially no damage during this earthquake.

For example, Photo 8 shows Shin-Tenno Bridge which was constructed in 2002 suffered no damage. This bridge was located 150 m upstream of Tenno Bridge which suffered damage during 1978 Miyagi-ken-oki earthquake and suffered damage again at almost the same components. Photo 9 shows an end of girder at the left bank where it was supported by elastomeric bearings. New cable restrainers which satisfy the requirements by the post-1990 design code are set. No damage occurred in this bridge.

Elastomeric bearings including lead rubber bearings and high damping rubber bearings performed much better than vulnerable steel bearings. However it should be noticed that elastomeric bearings ruptured in several bridges. For example, at Sendai-Tobu viaduct as shown in Photo 10, several elastomeric bearings ruptured such that the deck offset in the transverse direction and settled aside the ruptured bearings as shown in Photo 11. Rubber layers detached from steel plates as well as rupture inside rubber layers as shown in Photo 12. Since extensive number of elastomeric bearings including high damping rubber bearings and lead rubber bearings are used, the damage should be critically investigated. It is pointed out that one of the possible reasons for the damage is that the interaction between adjacent bridges with different natural periods was not properly considered in design of elastomeric bearings. Since an expansion joint constrained relative displacement between adjacent decks in the transverse direction, it is likely that larger displacement demand of an adjacent deck is imposed to the elastomeric bearings which were designed based on smaller displacement demand [Quan and Kawashima 2009].

GROUND MOTION INDUCED DAMAGE OF SHINKANSEN VIADUCTS

Seismic retrofit program of Shinkansen

Tohoku Shinkansen started the service in 1982 between Omiya and Morioka Stations. Since Shinkansen viaducts were designed prior to the occurrence of 1978 Miyagi-ken-oki earthquake, they have smaller amount of shear reinforcements than required by the current code. Some viaducts of Tohoku Shinkansen between Morioka and Mizusawa-Esashi stations in Iwate-ken were extensively damaged during 2003 Sanriku-Minami earthquake [JSCE 2004].

It should be noted that all viaducts which suffered damage during 2011 Great East Japan earthquake had not yet been retrofitted. Most viaducts in Iwate-ken were single story RC moment resisting frame with a Gerber girder at both sides. Damage concentrated at the side columns during 2003 Sanriku-Minami earthquake as shown in Photo 13. Since the side columns were shorter than the center column, a parameter defined as a ratio of the shear capacity to the flexural capacity was smaller in the side columns than the center columns, which led shear failure in the side columns.

After 2004 Niigata-ken Chuetsu earthquake [Huyck et al 2006], the first seismic retrofit program was initiated for Shinkan-sen viaducts including Tohoku Shinkansen.

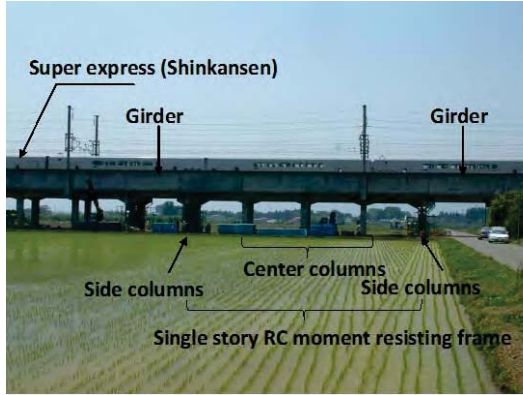


Photo 13 Single story RC moment resisting frame pier with a Gerber girder at both sides



Photo 14 Shear failure of RC columns at Odaki viaducts after 2003 Sanriku-Minami earthquake



Photo 15 No. 3 Odaki viaducts which were retrofitted after 2003 Sanriku-Minami earthquake performed well during 2011 Great East Japan earthquake

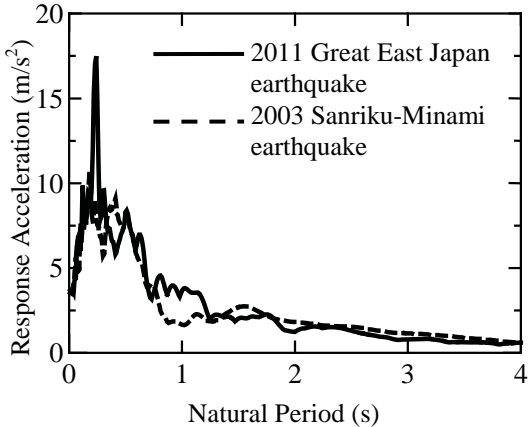


Fig. 5 Response accelerations in 2003 Sanriku-Minami earthquake and 2011 Great East Japan earthquake

Objectives of the program were to enhance the seismic performance of the columns with insufficient shear capacity. After retrofitting 12,500 columns, the program was completed by 2007. In 2009, the second retrofit program for enhancing columns flexural capacity was initiated.

No. 3 Odaki viaducts

No. 3 Odaki viaducts in Iwate-ken failed in shear as shown in Photo 14 during 2003 Sanriku-Minami earthquake. The viaducts were retrofitted so that they had sufficient shear capacity under the first retrofit program after 2004 Niigata-ken Chuetsu earthquake. The retrofitted columns of the viaducts performed well with almost no damage during 2011 Great East Japan earthquake as shown in Photo 15.

Fig. 5 compares the 5% damping response accelerations between 2003 Sanriku-Minami earthquake and 2011 Great East Japan earthquake. The records were measured at approximately 3km from No. 3 Odaki viaducts. Since the fundamental natural period of a single story RC rigid frame ranges between 0.4s to 0.6s, it is reasonable to consider that the response acceleration of No. 3 Odaki viaducts was

nearly the same between 2003 Sanriku-Minami earthquake and 2011 Great East Japan earthquake. It is considered that the seismic retrofit for No. 3 Odaki viaducts was



Photo 16 Damage of R7 column, No. 1 Nakasone viaduct during 2011 Great East Japan earthquake



Photo 17 Close view of damage of R7-1 and R7-2 columns

effective for preventing significant damage during this earthquake.

No. 1 Nakasone viaducts

No. 1 Nakasone Viaducts, constructed in 1978, is located between Kitakami and Shin-Hanamaki Stations. They had the similar structural shape with the No. 3 Odaki viaducts. No columns were retrofitted during the first seismic retrofit program since it was evaluated that the parameter was not small enough.

During 2011 Great East Japan earthquake, side columns suffered extensive damage as shown in Photo 16. All columns lost even the bearing capacity for vertical load. It was fortunate enough not to totally collapse because the viaduct was supported by eight columns. Side columns in other viaducts also suffered extensive damage. Shear failure occurred at the upper part of columns as shown in Photo 17. The damage was so extensive that original shear cracks could not be identified because of crash and spill out of the core concrete.

In the JR seismic evaluation, it was evaluated that shear failure occurred if the parameter α was smaller than 0.9. From the fact that the columns in No. 1 Nakasone viaducts failed in shear although α was not as small as 0.9, it is recommended to revise the criteria of failure mode in the future seismic retrofit program.

Table 1 Numbers of bridges which were washed away by tsunami

Types of bridges	Number of bridges washed away
Railways	101
National roads	9
Prefectural roads	14
City or town roads	More than 200
Total	324



Photo 18 Damage of Utatsu Bridge

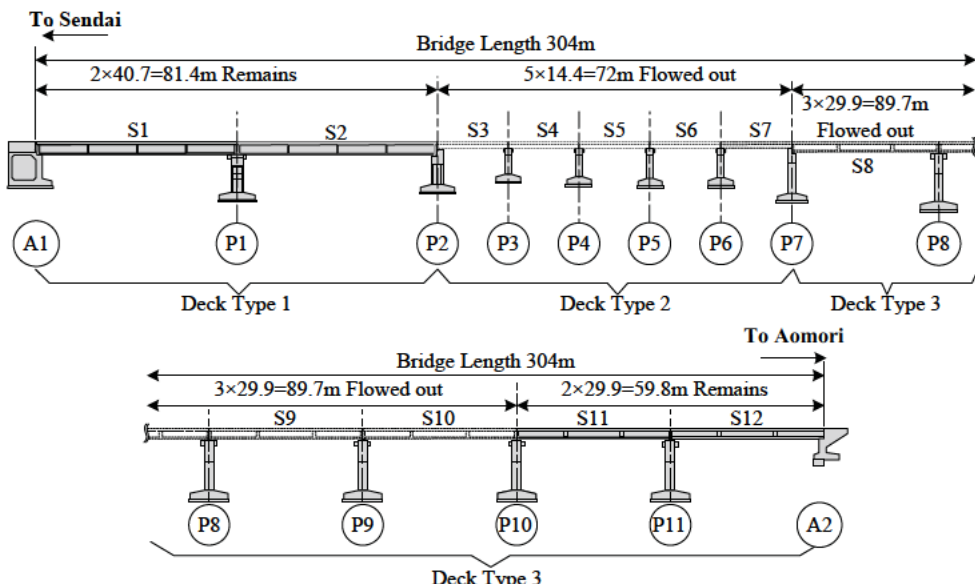


Fig. 6 Utatsu bridge

TSUNAMI INDUCED DAMAGE OF BRIDGES

More than 300 bridges were washed away by the tsunami. Jurisdiction of the bridges which were washed away by tsunami can be classified as shown in Table 1. A large number of bridges which suffered damage were either on railways or regional roads. Smaller and shorter span bridges which were built in the early days were vulnerable to tsunami effect. It was generally seen that either tall bridges or short bridges did not suffer damage by tsunami because tsunami front did not reach the bridges or over passed. The bridges with mid-range height suffered extensive damage because debris or ships directly attacked decks [JSCE 2011].

Utatsu Bridge at Minami-sanriku Town over Irimae Bay suffered extensive damage by tsunami as shown in Photo 18. It consisted of 3 types of superstructures with spans ranging from 14.4m to 40.7m, as shown in Fig. 6. The superstructures from S3 to S10 were completely washed away from their supports in the transverse direction due to tsunami while the superstructures S1, S2, S11 and S12 were not washed away. The

outflow displacements of S3~S10 are shown in Fig. 7. It should be noted that the spans located at the center such as S5-S7 and S8 were flowed 28 m and 41 m away from the original position, while the spans located at the sides such as S1, S2, S11 and S12 were

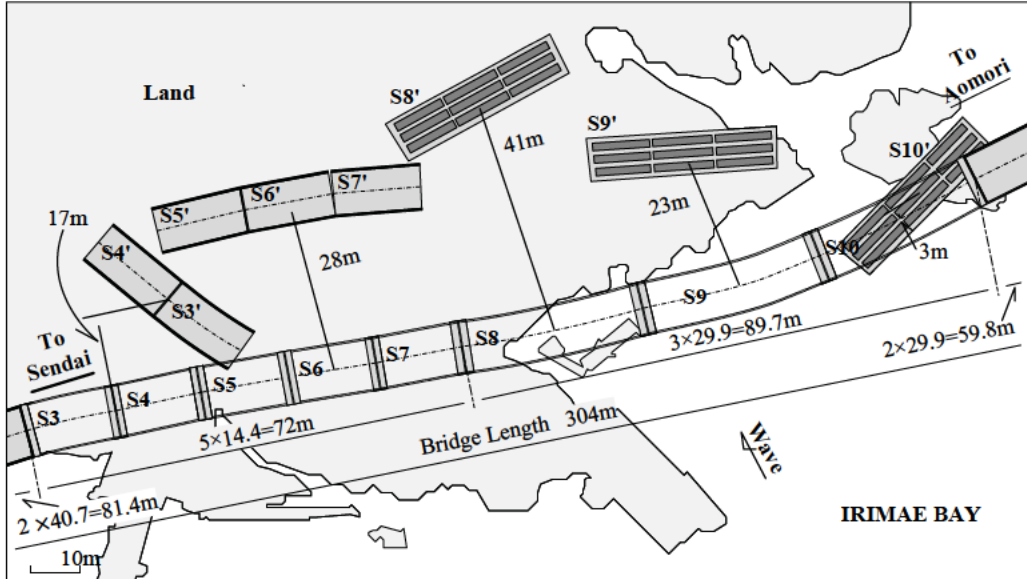


Fig. 7 Outflow of superstructure



Photo 19 Effective restrainers to tie together adjacent decks



Photo 20 An overturned superstructure

not washed away. It is noted that S3, S4 and S4', and S5, S6 and S7 which flowed out together because they were tied by cable restrainers for preventing excessive superstructure response under a large seismic excitation as shown in Photo 19. S8, S9 and S10 overturned during being floated as shown in Photo 20.

Photo 21 shows the top of a pier after superstructures were washed away. Two types of steel devices were set as an unseating prevention device in this column; one is the devices aiming of increasing seat length required by the recent code, and the other is the devices which were set for preventing excessive deck displacement in the longitudinal direction. It is important to know that none of those devices tilted or were

detached from the pier which must have happened if the decks were simply washed away laterally. It is likely that the decks were uplifted by tsunami buoyancy force and then they were washed away. Steel plate bearings used in this bridge was very simple as shown in Photo 22 such that both uplift and lateral force capacities were limited.



Photo 21 Steel devices for extending seat length (short device) and steel stoppers for preventing excessive longitudinal deck response due to ground motions (tall device)



Photo 22 Failure of a RC side stopper, and four steel stoppers for preventing excessive longitudinal deck response which were not damaged



Photo 23 An upper steel bearing after damaged

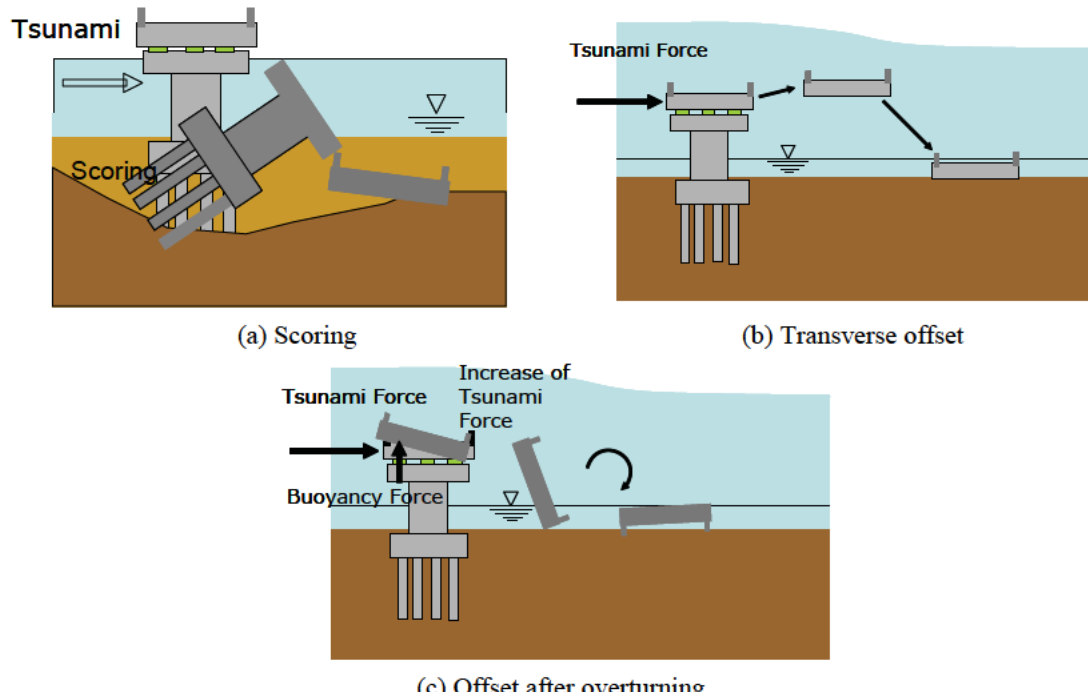


Fig. 8 Possible mechanism of bridge damage by tsunami

This is also the case at a column shown in Photo 23 in which four stoppers did not tilt. But a RC side stopper at the land side collapsed probably due to a transverse

force which applied from the deck. It is likely that due to tsunami force the deck uplifted at the sea side first being supported only at the land side, which resulted in larger tsunami force. Thus the side stopper at the land side collapsed due to excessive concentration of tsunami force.

Fig. 8 shows possible mechanism of damage of bridges due to tsunami. As mentioned earlier, overturning of foundation due to scouring did not occur in road bridges. It is likely that damage of decks in Photos 20 and 21 occurred due to mechanism shown in Fig. 8 (b) and (c), respectively.

In spite of the extensive damage of superstructures, none of piers suffered damage due to tsunami at Utatsu bridge.

CONCLUSIONS

Damage of road and railway bridges during 2011 Great East Japan earthquake was presented. Although more thorough collection of damage information as well as careful analyses is required, the following conclusions may be tentatively deduced based on the findings presented herein:

- 1) Ground motion induced damage of bridges which were built in accordance with the post-1990 design code was minor. Thus the effect of enhancing the shear and flexural capacity as well as ductility capacity, extensive implementation of elastomeric bearings and strengthening of unseating prevention devices were effective for mitigating damage during this earthquake. However, effectiveness of those measures against much stronger near-field ground motions has to be carefully investigated since the ground motion induced by 2011 Great East Japan earthquake was smaller than anticipated target ground motions.
- 2) On the other hand, ground motion induced damage of bridges which were built in accordance with old code (approximately pre-1990) or which were not yet retrofitted was still extensive. This was in particular true for railway bridges. Appropriate seismic retrofit is required in the near future.
- 3) Tsunami induced damage was extensive to bridges along the Pacific coast. It seems that decks were uplifted and washed away upstream. Tsunami force effect has to be studied more so that it can be considered in design for bridges along the coast.

ACKNOWLEDGEMENTS

The authors express their sincere appreciation for a number of organizations and persons for their kind support and cooperation for the field damage investigation. A joint investigation was conducted as a part of UJNR Panel on Wind and Seismic Effect activity. Special appreciation is extended to Dr. Yen, F., FHWA and Professor Buckle, I., University of Nevada, Reno, and members of National Institute of Land and Infrastructure and Public Works Research Institute including Drs. Tamura, K., Unjoh, S., and Hoshikuma, J.

REFERENCES

- 1) Huyck, C. K., Matsuoka, M., Takahashi, Y., and Vu, T. T.: Reconnaissance technologies used after the 2004 Niigata-ken Chuetsu, Japan, Earthquake, Earthquake Spectra, Vol.22, No. S1, pp. S133-S146, 2006.
- 2) Iemura, H., Takahashi, Y., Pradono, M. H., Sukamdo, P., and Kurniawan, R.: Earthquake and tsunami questionnaires in Banda Aceh and surrounding areas, Disaster Prevention and Management, Vol.15, No.1, pp.21-30, 2006.
- 3) Ishibashi, T, Ikeda, Y., Kanno, T. and Okamura, H.: The study on earthquake resistance on design and damage of reinforced concrete viaduct, Journal of JSCE, No.563/I-39, pp.95-103, 1997.
- 4) Japan Road Association: Design specifications of highway bridges, Part V Seismic design, 1990.
- 5) Japan Society of Civil Engineers: Report on reconnaissance damage investigation to civil engineering facilities resulted from 2011 Great East Japan earthquake, 2011.
- 6) Japan Society of civil engineers: Damage analysis of concrete structures due to the earthquakes in 2003, Concrete Library, 114, 2004.
- 7) Kawashima, K., Unjoh, S. and Hoshikuma, J.: A seismic evaluation method of RC bridge piers with inadequate anchoring length at termination of main reinforcements, Journal of JSCE, No. 525/I-33, pp. 83-95, 1995.
- 8) Kawashima, K., and Unjoh, S.: The damage of highway bridges in the 1995 Hyogo-ken-nanbu earthquake and its impact of Japanese seismic design, Journal of Earthquake Engineering, Vol. 1, No. 3, pp. 505-541, 1997.
- 9) Kawashima, K.: Seismic design and retrofit of bridges, Key note presentation, 12th World Conference on Earthquake Engineering, pp. 1-20, Paper No. 1818, Auckland, New Zealand, 2000.
- 10) Kawashima, K, Sasaki, T., Kajiwara, K., Ukon, H., Unjoh, S., Sakai, J., Kosa, K., Takahashi, Y., Yabe, M. and Matsuzaki, H.: Shake table experiment on RC bridge columns using E-Defense, Proc. 41st Panel on Wind and Seismic Effects, UJNR, Public Works Research Institute, Tsukuba Science City, Japan, 2009.
- 11) Quan, G. and Kawashima, K.: Effect of finger expansion joints on the seismic response of bridges, Journal of JSCE, A, Vol. 65, No. 1, pp. 243-254, 2009.

Page Left Blank

BRIDGE PERFORMANCE DURING THE GREAT EAST JAPAN EARTHQUAKE OF MARCH 11, 2011

M. Lee Marsh, Ian G. Buckle, W. Phillip Yen, Shideh Dasti, David Frost, Eric Monzon (See Acknowledgements for author affiliations)

Abstract

On March 11, 2011 the Great East Japan Earthquake struck the northeast coastal areas of Japan. Numerous bridges were damaged by either ground shaking or tsunami. A reconnaissance team from the US visited 11 bridge sites in June, and this report summarizes the observations and preliminary conclusions of several of those bridges. Staff from the PWRI hosted the reconnaissance effort and provided valuable technical data, excellent logistics, and useful insight into behavior and bridge practice throughout the reconnaissance effort.

Introduction

About 200 highway bridges and numerous rail bridges were damaged during the Great East Japan Earthquake of March 11, 2011, including span unseating, foundation scour, ruptured bearings, column shear failures and approach fill settlements. The causes of this damage can be broadly classified in two categories: ground shaking including ground failure (liquefaction), and tsunami inundation. Of these, the tsunami was responsible for about one-half of the number of damaged bridges.

A joint EERI/FHWA/GEER reconnaissance team visited the affected area from June 2 to June 6, 2011 and investigated 11 bridges: 2 had extensive bearing failures, 2 had column failures, 2 had combined bearing and column failures and 4 suffered tsunami-related damage (unseated spans, scour, loss of approach fill).

The location and names of ten of the eleven bridges visited by the reconnaissance team are shown in Figure 1. The eleventh bridge was the Arakawa Wangan Bridge across the Arakawa River in Tokyo. The performance of five of the eleven bridges is summarized in this report. A detailed description of all eleven bridges is given in FHWA, 2010.

Bridge Damage Due to Ground Shaking

In general the amount of damage due to ground shaking was remarkably light considering peak ground accelerations in some locations exceeded 1.0 g, with



FIGURE 1 – BRIDGES INVESTIGATED BY EERI(FHWA)/GEER RECONNAISSANCE TEAM (Graphic: L. Marsh)

short-period spectral accelerations in excess of 5g. The most likely explanation is that, most, if not all of the bridges on the national highway system had been seismically retrofitted over the last 10-15 years (in response to the widespread damage to bridges in the 1995 Hyogoken-Nanbu (Kobe) Earthquake). Bridges damaged in this earthquake by ground shaking were generally older structures owned by city and local governments, where retrofit programs have not been as active due to a lack of funding. With one exception, new bridges performed very well regardless of ownership most probably due to the adoption of conservative capacity design principles in the JRA Design Specifications in the 1990s. The one exception was the failure of elastomeric bearings in a section of the Sendai-Tobu Viaduct as described below. Three bridges are described in this section.

Sendai-Tobu Viaduct

The damage to this 4.4 km long, multi-span viaduct in north Sendai was largely confined to a 10-span section between Piers 52 and 62. Built in 2000, this section of the viaduct was being widened at the time of the earthquake. New on- and off-ramps were under construction between Piers 54 and 56 to connect Route 10 carried by the viaduct to Route 141 below. Span lengths and type between Piers 51 and 58 are shown in Table 1.

TABLE 1. SPAN DETAILS AND DISTRIBUTION OF FAILED STEEL STOPPERS AND ELASTOMERIC BEARINGS IN SENDAI-TOBU VIADUCT.

Span No.	Span (m)	Span Type	Pier No.	Pier Type	No. failed (damaged) ² stoppers in main event 3/11/2011	No. ruptured (damaged) ² bearings in main event 3/11/2011	No. failed (damaged) ² stoppers in aftershock 3/11/2011	No. ruptured (damaged) ² bearings in aftershock 4/7/2011
			51	1-col.	0	0	0	0
52	39.0	8 I-girders						
			52 ¹	1-col.	0/6	0/8	0	0
53	71.0	4 box girders						
			53	1-col..	5	0	0	0
54	72.0	4 box girders						
			54	2-col.	4(2)	1	0	0
55	72.0	5 box girders						
			55	2-col.	(6)	0	0	0
56	71.0	3 box girders						
			56 ¹	2-col.	6/6	(1)/8	0	0
57	39.0	8 I-girders						
			57	1-col.	1(1)	0	3	0
58	39.0	8 I-girders						
			58 ¹	2-col.	4(2)/5	1/0	0	(2)/0
59	39.0	8 I-girders						
			59	2-col.	(3)	0	0	0
TOTALS					37(14)	18(1)	3	(2)

Note 1. There are two lines of stoppers and bearings on Piers 52, 56, and 58.

2. Numbers in parentheses are numbers of stoppers and bearings damaged but not ruptured.

The superstructure comprises eight steel plate girders (I-girders) between Piers 50 and 52, three, four, or five steel box girders between Piers 52 and 56, and eight steel plate girders between Piers 56 and 63.

Elastomeric bearings are used exclusively with external stoppers to restrain transverse movement at almost every pier. Piers 54, 55, 56, 58, 59 and 60 had recently been converted from single steel box columns to two-column steel box frames to accommodate the new on- and off-ramps (Figure 2). The remaining piers (51, 52, 53 and 57) are single-column steel boxes (Figure 3).

The bridge suffered moderate-to-major damage during the earthquake but no span collapsed. This damage included the failure of 40 steel stoppers and 18 elastomeric bearings. Another 14 stoppers and 3 bearings were heavily damaged. In addition, girder stiffeners, gusset plates, and cross-frames were buckled or severely distorted. Locations of the failed and damaged stoppers and bearings, due to both the March 11 main shock and the April 7 aftershock, are given in Table 1.

The pattern of the bearing damage in Table 1 is particularly interesting. It is concentrated in regions of the viaduct where there is a significant change in lateral stiffness – from single-column hammerhead piers at Pier 57 to two-column frames at Piers 54, 55 and 56, for example. There is also a significant change in the in-plane stiffness of the superstructure in this section, from eight I-girders in Spans 52 and 57 to multiple single-cell box girders in Spans 53 to 56. This section of the viaduct is therefore very stiff (and particularly Spans 55 and 56) while sections to the north and south are comparatively flexible. When earthquake loads are applied, the difference in displacements at the two interfaces (Piers 52 and 56) generate high lateral forces in the stoppers at these two piers leading to their failure and the transfer of load to the bearings.

Inspection of the damage to the bearings showed that many had ruptured completely through the elastomer, as if in direct tension. Others showed damage to the internal shims which had been severely distorted (Figure 4). Typical dimensions of the bearings at Pier 56



FIGURE 2 – TWO-COLUMN FRAME, PIER 56
SENDAI-TOBU VIADUCT (Photo: E. Monzon)



FIGURE 3 – SINGLE COLUMN, PIER 57
SENDAI-TOBU VIADUCT (Photo: E. Monzon)

are 820 x 870 x 508 mm, with 8 x 33 mm layers of elastomer, 7 x 4.5 mm shims and 2 x 45 mm end plates. The masonry and sole plate connections were detailed to transfer both shear and axial forces (tension and compression) into the bearings.

It seems possible that the bearings failed due to the combination of two effects. First the high lateral forces in the steel stoppers at Piers 52 and 56 were probably not evenly distributed amongst the three effective stoppers. (Although there are six stoppers at each pier, only three are effective in any one direction at any point in time.) This uneven distribution arises because the gaps between the stoppers and the sole plates of the

bearings are not exactly the same at each location and one stopper will generally engage before the others. Overloading of this stopper is very likely, leading to its failure, followed by the transfer of load to the other stoppers which then fail in turn. Once all the stoppers have failed the transfer of load to the bearings places them under very high shear strain.

The second effect is the generation of high tensile forces in the bearings at these same locations due to the difference in pier type. For example Pier 56 is a 2-column frame and Pier 57 is a single column hammerhead pier. Under lateral load the hammerhead rotates about a longitudinal axis twisting the superstructure about the same axis. But the pier cap in the 2-column frame at Pier 56 does not rotate in this manner and this frame resists the twisting of the superstructure. High tensile forces are developed in the bearings as a result.

The simultaneous occurrence of high tension and high shear in the bearings could have led their failure.

The shim damage seen in Figure 4 most likely occurred when a ruptured bearing impacted a toppled stopper puncturing the cover rubber layers and distorting the edge of the shim plate. On the other hand, the expected failure mode of an elastomeric bearing is rupture within a rubber layer and not delamination at the shim plate. The clean surface of this plate in Figure 4 implies inadequate bond between the elastomer and shim during manufacture thus reducing the bearing's capacity for combined tension and shear.

Other damage to the superstructure included buckled cross-frame members, gusset plates and stiffeners, possibly due to the abrupt change in load path where the transverse member changes from a partial height diaphragm to a full depth cross-frame. But a more likely scenario is that this damage is due to the failure of the bearings below the girders leading to differential 'settlement' of the cross-frames and corresponding distortion and distress.

Yuriage Bridge

The Yuriage Bridge carries Route 10 over the Natori River near the Sendai airport. The area experienced tsunami run-up, but the wave passed under the bridge and the



FIGURE 4 – DAMAGED ELASTOMERIC BEARING FROM PIER 52, SENDAI-TOBU VIADUCT (Photo: E. Monzon)

superstructure was not impacted. The bridge was built in 1974 and is comprised of ten spans with an overall length 542 m. The three main spans, located between Piers 2 and 5, are cast-in-place concrete box-girders and the center of these three spans comprises two balanced cantilevers meeting at mid span (Figure 5). The approach spans are prestressed concrete I-girders, simply supported on steel bearings at the pier caps, founded on wall piers with caisson-type foundations.

Pier 1 was damaged during the 1978 Miyagi-Oki Earthquake and was repaired with a concrete jacket. No widening or other seismic retrofits have been made since that time.

Complete bearing failures occurred at Piers 2 and 5, at the transition between the approach spans and main spans. These failures are attributed to permanent pier movement possibly caused by liquefaction. Evidence of extensive liquefaction was found under the approach spans and in some cases 30 cm of ground settlement was observed adjacent to one of the piers under the south approach. Since Piers 2 and 5 are close to the river, lateral spreading may have caused these

piers to move towards the center of the river channel. Figure 6 shows this movement for Pier 2 to be of the order of 6 cm, which clearly exceeded the capacity of the roller bearing at this location. In addition damage to the transverse stopper is evident, indicating the simultaneous occurrence of significant shaking transverse to the bridge.

Shida Bridge and Levee

The Shida Bridge is a nine-span steel plate-girder bridge carrying Route 32 over the Naruse River east of Osaki. The bridge was built in 1957 and is comprised of a two-girder steel superstructure supported on concrete two-column piers. The foundation type is unknown. The bridge is straight, has no skew and only a slight vertical curvature. Typical piers are shown in Figure 7. The superstructure is articulated in every other span with drop-in spans, whose in-span seats form inflection points rendering the structure determinate (Figure 8). Such a drop-in span is visible in the center span of Figure 7 where rust stains from the



FIGURE 5 – MAIN SPANS OF THE YURAGE BRIDGE (Photo: E. Monzon)



FIGURE 6 - EJECTED ROLLER BEARING AND PERMANENT LONGITUDINAL MOVEMENT AT PIER 2, YURAGE BRIDGE (Photo: E. Monzon)

deck joint have discolored the two in-span hinge areas. Also visible are seat extensions installed on the piers throughout the bridge. No other seismic retrofitting was seen.

The drop-in spans have transverse guides that serve to restrain the movements of the spans and may help prevent dislodgment of the spans under seismic loading. These guides are positioned at the side of the drop-in bearings, the soffit of the plate girders, and the center of the transverse bracing near the bottom of the girders.



FIGURE 7 – PIERS 7 AND 8 OF PLATE-GIRDER SHIDA BRIDGE (Photo: L. Marsh)

The superstructure rests on steel bearings at each pier and each continuous span (i.e. alternate spans to the drop-in spans) has one fixed and one movable (sliding) bearing in the longitudinal direction arranged as shown in Figure 8.

Damage to the Shida Bridge included a dropped fixed bearing, a fixed bearing with sheared anchor bolts, abutment backwall failure due to soil pressure, yielded fixed bearing anchor bolts and cracked pier walls. None of the dropped-in spans became unseated and there was no apparent damage to the steel cross frames.

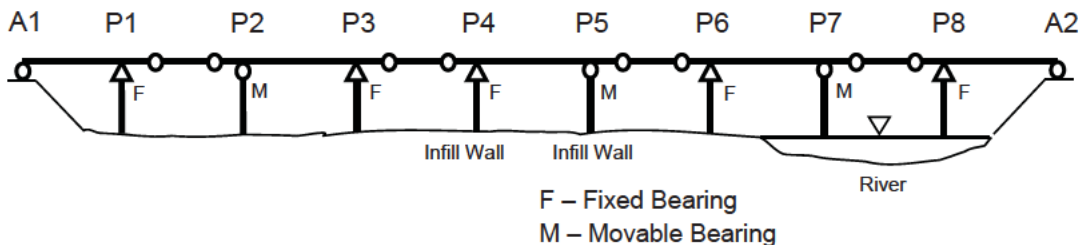


FIGURE 8 – LOCATIONS OF IN-SPAN HINGES AND F-M BEARINGS IN THE SHIDA BRIDGE (Graphic: L. Marsh)

Approximately 15 cm of settlement occurred in the backfill behind the abutment and pressure behind the abutment backwall was sufficiently large to crack and yield this wall. This likely occurred as the abutment fill settled and moved towards the river channel during the earthquake. The abutment is founded on a levee that parallels the river channel and movements in this levee, just upstream from the bridge, are described later in this section.

One of the fixed bearings at Pier 3 failed by dropping off its lower seat as seen in Figure 9. Also seen in this figure is a gap between the top of the bearing and the bottom of the girder. This indicates that the bolts of the other fixed bearing at Pier 3 have been sheared off and the girder at this location has lifted clear of the bearing. This means that the bearing that dropped on the other end of the pier must be supporting the gravity load at the pier, because no redundant load path exists. The bearing and girder have dropped far enough that the upper bearing has become wedged against the lower portion of the bearing, thus providing

vertical support. It is likely that the upper bolts of the left-hand bearing sheared before the right-hand bearing dropped from its pedestal. There is no vertical load path through the bearing pin to sustain tensile forces on the bolts and thus shear is the probable mode of failure. Following loss of shear capacity on the left side, all shear for this frame would have to be resisted by the right-hand bearing. This increase in shear demand likely caused the right-hand bearing to unseat. Failure of this bearing is probably the reason for the noticeable dip in the elevation of the bridge roadway and handrail (estimated at 10 cm) seen in Figure 10. It also possible that some of this deformation is due to foundation settlement due to widespread liquefaction in the area.

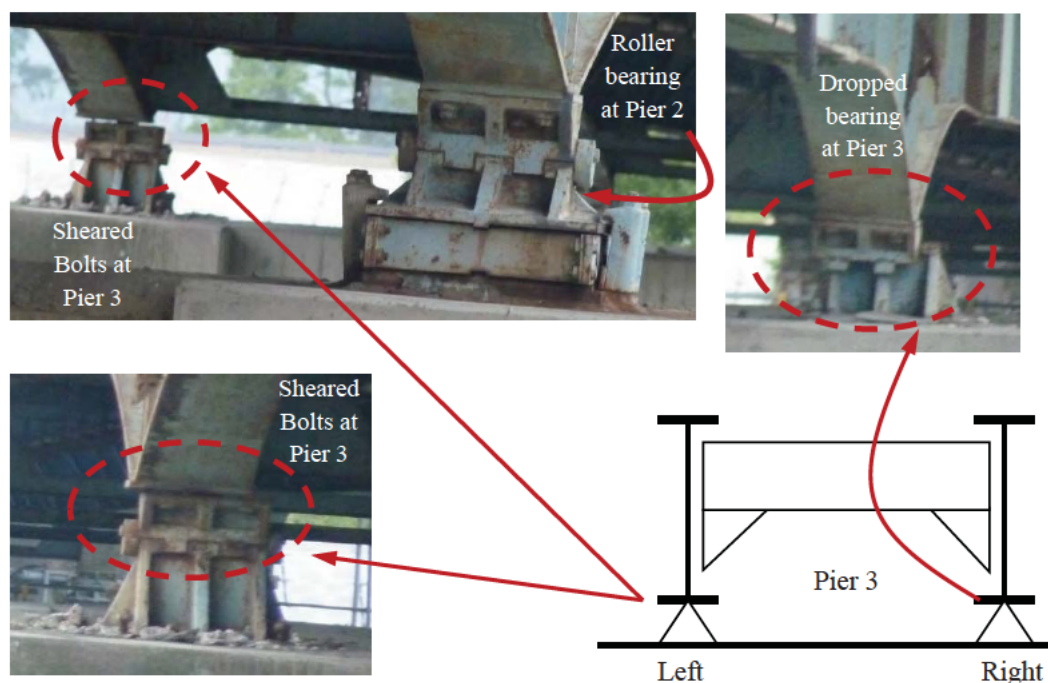


FIGURE 9 – UNSEATING AND FAILURE OF BEARINGS AT PIER 3, SHIDA BRIDGE
(Photos and Graphic: E. Monzon)

Pier 3 is one of the infill-wall piers. The infill probably increased the stiffness at Pier 3 in the longitudinal direction which the forces in the fixed bearing resulting in this dropped bearing. Close inspection of the anchor bolts at the top of the left side of Pier 3 indicates that those bolts were elongated or hammered outward more than any of the bolts on the other fixed piers of the bridge. This leads to the conclusion that the forces were higher at Pier 3 due to the infill wall.

Following the unseating of the right-hand bearing at Pier 3, the superstructure moved towards Abutment 1 as indicated by the final location of the right hand bearing at Pier 3. This is confirmed by the observed movement in the expansion bearing at Abutment 1 as indicated in Figure 11. The cracks in the masonry pedestal beneath the girder indicate that the shear keys were engaged as the superstructure moved in this direction.

At two other fixed piers, Pier 1 and Pier 6, the anchor bolts between the bearing and the top of the pier were either elongated or pulled out of their embedment by the longitudinal inertial action of the superstructure. The longitudinal response of the bridge was probably limited by the yielding or slippage of these bolts, and this action provided partial force limitation. However, it was not enough to prevent damage to the piers below the bearings. At both Piers 1 and 6, moderate cracking and potential yielding occurred. Figure 12 shows examples of such damage, and in fact both piers were undergoing repair at the time of the reconnaissance visit. This is evident by the scaffolding and enclosures present at these piers.

It is likely, due to the rust present in the exposed reinforcement of Pier 6, that delamination of the reinforcement had been present for some time before the March 2011 earthquake. Due to the age of the bridge – built in 1957 – it is likely to have experienced other significant earthquakes. Repairs to other piers, in particular the infill wall piers was evident, and it is not known if the infills were repairs to earthquake damage or were added at the time of construction.

While investigating the performance of the Shida bridge, it was observed that the crest of an 8-m high levee along the Naruse River just upstream of the bridge had settled 1.0 to 1.5 m. This settlement was accompanied by a lateral toe movement of up to 4 to 5 m downstream and significant slumping on the downstream face.

Due to concern that the levee might completely fail during the upcoming rainy season, a temporary repair was constructed consisting of a 240-m long, 3.8-m high, 4.5-m wide, double sided sheet pile cofferdam on top of a 3.8-m high berm.



FIGURE 10 – SETTLEMENT IN BARRIER AND DECK AT PIER 3, SHIDA BRIDGE (Photo: D. Frost)



FIGURE 11 – DAMAGE TO PEDESTAL AND ABUTMENT BACKWALL, SHIDA BRIDGE (Photo: E. Monzon)

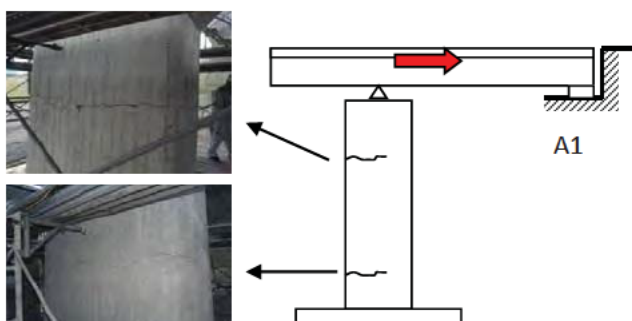


FIGURE 12 – FLEXURAL DAMAGE IN PIER 1 DUE TO LONGITUDINAL MOVEMENT, SHIDA BRIDGE (Photos and Graphic: E. Monzon)

Bridge Damage due to Tsunami Inundation

Twelve bridges on Route 45 were seriously damaged by the tsunami, which had wave heights from Sendai to Hachinohe ranging from 6.2 to 11.8 m. Damage to two of these bridges and nearby rail bridges are described in this section.

Koizumi Highway and Rail Bridges

The Koizumi bridge spans the Tsuya River on Route 45 just south of the city of Kesennuma. The bridge was constructed in 1975, has six 30.1-m spans (total length 182 m), and is 11.3-m wide. The superstructure comprised four steel plate girders supported by concrete piers on deep foundations. The bridge is without skew and only a slight vertical curve. The superstructure segments were continuous over three spans with expansion joints at the abutments and at the center pier (Pier 3). Piers 2 and 4 had fixed bearings, while Piers 1 and 5 had sliding bearings in the longitudinal direction.

The bridge had been seismically retrofitted using hydraulic dampers at the abutments. It is not known if similar restrainers or dampers had been installed at the expansion joint over the center pier. No other retrofitting, such as support length extensions or substructure strengthening was evident.

All six spans were swept away during the tsunami (Figure 13). Wave heights of the order of 11.8 m were registered at Ofunato City just north of this site and the tsunami clearly overtopped this bridge taking all six spans upstream. Based on damage to the levee on the north bank of the river, some of these spans were lifted off their piers and swept along the top of the levee on the north bank, then over the levee altogether on the north side, and later back over the levee into the main channel where they came to rest about 400 m upstream from the bridge (Figure 14). Other spans took a different path and came to rest about 300 m upstream but on the south side of the levee on the south bank of the river. Four of the five piers are still standing, but the center pier (Pier 3) was overturned and believed to be under water in the river channel just upstream of the bridge (Figure 13).



FIGURE 13 – REMAINING PIERS OF KOIZUMI BRIDGE. TEMPORARY BRIDGE IS UNDER CONSTRUCTION ON SEAWARD-SIDE OF ORIGINAL BRIDGE (Photo: E. Monzon)

It is clear that the longitudinal dampers installed at the abutments and the transverse keys (stoppers) over the piers, offered little restraint to the lateral loads imposed by tsunami. Once these devices failed, the relatively light weight of the steel I-girders, together with the buoyancy effects of air trapped between the girders, enabled the superstructure to be easily lifted and carried significant distances upstream. The loss of Pier 3 was probably due to scour but this could not be confirmed. Despite the low tide at the time of the visit, the foundation was still underwater.

About 900 m upstream of the Koizumi Bridge, the JR East rail line to Kesenuma crosses the Tsuya River on a multispan, prestressed concrete girder viaduct. Five of these spans were washed out, but the piers survived (Figure 15). The in-coming tsunami apparently breached the levee behind the piers allowing flow oblique to the channel. The piers are tilted toward the breach, and the simple span, three-girder superstructures came to rest on the opposite side of the levee.



FIGURE 14 – GIRDERS FROM KOIZUMI BRIDGE 400m UPSTREAM IN TSUYA RIVER CHANNEL (Photo: E. Monzon)



FIGURE 15 – DAMAGED PIERS OF THE JR RAIL VIADUCT AT THE TSUYA RIVER (Photo: S. Dashti)

Of interest is the damage to the lower portions of the piers. The exposed reinforcement seen on the left side of the each pier appears to have been pulled outward from the center of the column and rupturing the relatively light transverse steel. This type of behavior is seen in the failure of beams that are unreinforced for shear, where a shear crack precipitates failure and tearing of the tensile reinforcement from the beam. In the case of the JR East piers, potential buoyancy of the superstructure due to trapped air and the hydrodynamic forces produced lateral loads on the piers along with eccentric vertical loading. The piers may have failed in shear above the foundation after plastically deforming under the combined lateral and vertical effects. Following the loss of shear capacity at the base, the tension reinforcement was torn from the piers.

In this postulated mode of failure the tilting of the pier is due to structural failure and not to scour and subsequent rotation of the foundation. Inspection of the columns and footings below the water line is required to confirm this behavior.

Nijyu-ichihama Highway and Rail Bridges

The Nijyu-ichihama highway bridge spans a small stream on Route 45 south of Kesennuma and the Koizumi and Sodeo-gawa bridges. This bridge was built in 1971 and is a single-span prestressed concrete I-girder bridge supported on tall, cantilever abutments, which are in turn supported on steel pipe piles. The bridge has no skew, no curve and essentially no grade. The span is 16.64 m and the total width of the original structure is 8.7 m. End diaphragms engage each of the eleven I-girders comprising the deck and in turn, and were anchored to the abutment seats with tie-down rods in each bay. These same diaphragms acted as transverse shear keys restraining the lower flange of each girder from lateral movement.

The bridge has been widened on both sides at some time in the past using precast double-tee beams spanning between new abutments each founded on steel piles with heads at a much higher elevation than those of the original structure. The tsunami washed out the backfill behind both abutments and temporary approach spans, using steel I-girders, were placed to open the road to traffic. These spans are seen in Figure 16. Temporary steel towers to support these spans may also be seen in this figure.

Apart from the loss of the seaward extension, this bridge has performed remarkably well from a structural point of view. It is essentially intact and the principal reason for closure was the loss of back fill due to erosion. Despite the buoyancy of trapped air, the superstructure was well anchored both vertically and laterally to the abutment seats and was not dislodged by the tsunami despite being overtapped. It is of course possible that the erosion of the abutment backfills and the opening up of two alternative hydraulic channels took load off the bridge, but nevertheless the performance of this bridge under these circumstances is noteworthy.

About 100 meters upstream from the Nijyu-ichihama bridge is the JR East line to Kennesuma, which runs a distance of several hundred meters across the valley between tunnels at either end. This section of rail line was supported on a long fill embankment, two box culvert roadway underpasses, and a prestressed concrete, single span



FIGURE 16 – LOSS OF BACKFILL ON BOTH APPROACHES TO SINGLE-SPAN NIJYU-ICHIHAMA BRIDGE (Photo: L. Marsh)



FIGURE 17 – EXPOSED WINGWALLS OF JR RAIL BRIDGE 100m UPSTREAM OF NIJYU-ICHIHAMA BRIDGE DUE TO LOSS OF APPROACH EMBANKMENT (Photo: D. Frost)

bridge over the river (Figure 17). The unprotected embankment fill appeared to be a granular material. As the wave overtopped the embankment, it displaced the tracks and significantly scoured and removed the upper 4 to 5 m of the fill. Apart from the loss of the approach fills, all the bridges in the valley appeared to be intact.

Preliminary Conclusions

The following conclusions are based on observations made, and data recovered, during this reconnaissance exercise. They are, however, of a speculative nature due to the small number of bridges investigated and the absence of detailed field data such as foundation and soil details, bearing and tie-down details, superstructure weights, wave heights, and velocity profiles at each site. These conclusions are therefore likely to change as additional data becomes available and further studies are completed.

1. Despite the magnitude of this earthquake, bridge damage outside of the coastal zone was not heavy. This is believed to be partly due to the distance from the epicentral region, and partly to the fact that a conservative form of capacity design was implemented in Japan for new bridges in the 1990s. Furthermore an active retrofit program was undertaken for older bridges following the Kobe earthquake in 1995, especially on the national highway system.
2. Aftershocks that follow large magnitude main events can, themselves, be large and damaging. The damage sustained by some bridges was aggravated in subsequent aftershocks.
3. Retrofitting is an effective means for minimizing earthquake damage in older bridges. Most of the observed structural damage occurred in older bridges that had not yet been retrofitted, or only partly so. It is recommended that strong encouragement be given to owner agencies to accelerate their retrofit programs.
4. With the exception of several spans in the Sendai area, elastomeric bearings performed well and considerably better than older-style, steel bearings. The reason for the poor performance of the Sendai-Tobu bearings needs to be determined quickly for it has widespread implications on their growing worldwide use as movement and isolation bearings.
5. Damage to several older, un-retrofitted, bridge piers was concentrated in the reinforcement termination zone, and this vulnerability should be considered when prioritizing bridges for retrofitting. Bridges damaged in this manner are susceptible to additional damage during aftershocks that will lead to longer repair times and more restrictive load limits or even closure during repair.
6. Design methods to mitigate tsunami damage from inundation should be developed. Strategies to keep superstructures in place (such as using integral connections and venting trapped air to reduce buoyancy and equalize hydrostatic pressures on deck slabs) should be explored, along with armoring techniques to prevent undue scour of foundations and approach fills. In addition, the cost of deeper foundations should be weighed against the potential loss of a pier and the need for replacement of one or more spans.

7. Until analytical studies are complete it is not known to what extent the duration of this earthquake affected the observed damage, but it is expected to have been significant. The effect of duration on structural response should be investigated.

Acknowledgements

The team was hosted in Japan by Task Committee G of the UJNR Panel on Wind and Seismic Effects. Membership was as follows:

U.S. Members:

Ian Buckle, Professor, University of Nevada Reno, Reno
Shideh Dashti, Professor, University of Colorado at Boulder, Boulder
David Frost, Professor, Georgia Institute of Technology, Atlanta
Lee Marsh, Senior Project Manager, Berger/ABAM Engineers, Seattle
Eric Monzon, Graduate Research Assistant, University of Nevada Reno, Reno
W. Phillip Yen, Federal Highway Administration, Washington DC (Co-chair)

Japan Members:

Taku Hanai, Public Works Research Institute, Tsukuba
Jun-ichi Hoshikuma, Public Works Research Institute, Tsukuba
Kazuhiko Kawashima, Tokyo Institute of Technology, Tokyo
Tetuoru Kuwabara, Public Works Research Institute, Tsukuba (Co-chair)
Hideaki Nishida, Public Works Research Institute, Tsukuba
Keiichi Tamura, Public Works Research Institute, Tsukuba
Shigeki Unjoh, National Institute for Land and Infrastructure Management

The collegiality of members of the Japan team, the free exchange of technical data, the excellent field logistics, and many useful discussions about bridge performance are gratefully acknowledged.

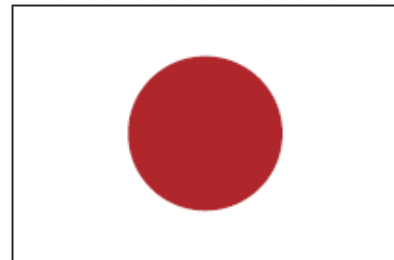
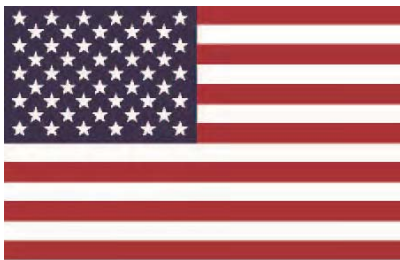
Acknowledgement is also made of generous funding provided by EERI, by FHWA under Contract DTFH61-07-C-00031 to the University of Nevada Reno, and by GEER under NSF Award #CMMI-1138203 to University of California, Davis.

References

EERI, 2011. *RAPID Proposal- Performance and Resilience Data Recovery from the Great East (Tohoku-Oki) Japan Earthquake Considering Bridges Buildings and Government and Community Response*, Proposal to National Science Foundation, Earthquake Engineering Research Institute, Oakland CA.

EERI, 2011. *Bridge Performance During the Great East Japan Earthquake of March 11, 2011*, Reconnaissance Report, to be published, Earthquake Engineering Research Institute, Oakland CA.

FHWA, 2011. *Bridge Performance During the Great East Japan Earthquake of March 11, 2011*, Reconnaissance Report, to be published, Federal Highway Administration, Washington DC.



27th US-Japan Bridge Engineering Workshop

Session 2

Tsunami and Seismic1

Damage Analysis of Bridges Affected by Tsunami due to Great East Japan Earthquake

By Kenji Kosa

Development of Tsunami Design Criteria for Oregon Coastal Bridges

By Bruce Johnson and Solomon Yim

FHWA Seismic Hazard Mitigation Research Program

By W. Phillip Yen

Page Left Blank

DAMAGE ANALYSIS OF BRIDGES AFFECTED BY TSUNAMI DUE TO GREAT EAST JAPAN EARTHQUAKE

Kenji Kosa¹

Abstract

Many bridges were washed away by Tsunami caused by the 2011 Great East Earthquake. We carried out the field survey and investigate the detailed damage to a lot of bridges in Tohoku Region. Utatsu Bridge, a prestressed concrete bridge, suffered enormous damage from the destructive tsunami. The detailed damage and the possible mechanisms of Utatsu Bridge have been conducted. Furthermore, from the study of the relation between β values (ratio between girder resistance and wave lateral load) and bridge damage extents of bridges in Tohoku Region and Sumatra Island, it is noted that ratio β is a significant indicator to judge the damage extent of bridge girders.

Introduction

During the Great East Earthquake, the outflow and excessive scour occurred to more than 300 bridges. **Fig. 1** illustrate the bridges which suffered damage Rank A (bridge is incapable). More than 300 bridges, including 9 national roads, 14 prefectoral roads and 101 railroads, suffered serious losses. Despite a lack of official data about the damage to city and village roads, by the use of Google Earth, it is noted that at least 200 bridges suffered serious losses.

Furthermore, the damage extent of the injured parts (girder, substructure, foundation) of bridges in Tohoku region is compared with the damage of bridges in Sumatra Earthquake by authors. **Fig. 2** shows the damage extent to the 26 bridges in the western coast of Sumatra and **Fig. 3** plots the damage extent to the 12 bridges in this tsunami attack. Based on **Fig. 2** and **Fig. 3**, many girders suffered damage Rank A, namely they were washed away entirely due to tsunami action. For substructures, although partial piers flowed out, comparing with girders, the occurrence rate is smaller.

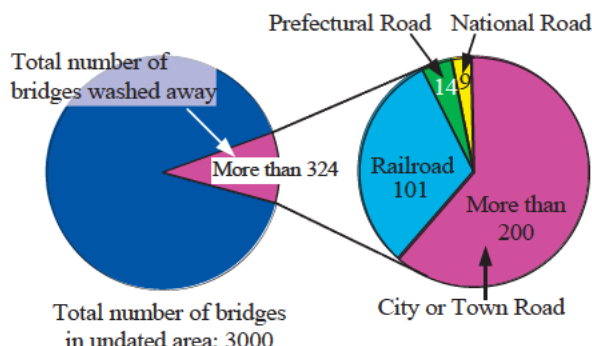


Fig. 1 Amount of bridges washed away

¹ Ph.D, Prof, Dept. of Civil Eng, Kyushu Institute of Technology

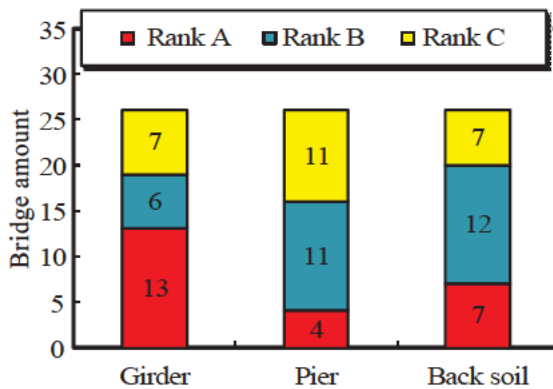


Fig. 2 Damage to bridge due to Sumatra Earthquake

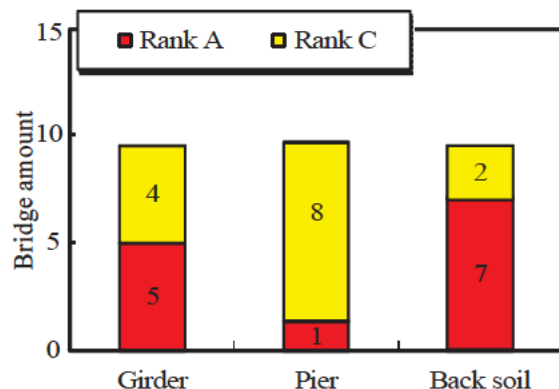


Fig. 3 Damage to bridge due to Great Japan Earthquake

Table 1 Video shot locations

Location		Distance to Shoreline [m]	Amount of Debris
A	Farm Field in Minamisanriku Town	1200	3
B	Wakabayashiku in Sendai City	1100	3
C	Hachiman River in Minamisanriku Town	1200	6
D	Kamaishi Port in Kamaishi City	0	2
E	Kitakami River in Ishinomaki City	4100	2

Besides that, it is frequent that foundations inflicted damage Rank A. The soils behind abutments were scoured. According to above data, the bridges in the 2 locations, where the wave heights were in excess of 10m, have many common points. The outflow of girders and the scour of foundations are the main damage to bridges.

Wave Height and Velocity

The tsunami arrived 30 minutes after the great earthquake and reached to approximately 5km inland. Further, it is reported the tsunami went upstream about 40km from the mouth of Kitakami River. The wave heights at the extensive region were measured by tidal observation station of Japan Meteorological Agency. For example, the wave height at Miyako was 8.5m, which is the highest one; in addition, the wave height at Oofunato and Souma are higher than 8.0m and 7.3m respectively (Japan Meteorological Agency, 2011). In order to evaluate the wave action on bridges, besides wave height, it is necessary to acquire wave velocities as well. Here, the authors apply the videos shot at the 5 locations in **Table 1**, which are close to shoreline, to estimate the wave velocity (Li, 2011) and these 5 locations are marked by A~E.

The rough measuring process of wave velocity is as follows. In one video, it is able to search for 2 distinguished place points where a pile of floating debris passed through. By using the Google Earth's distance measurer and the timer in video, it is available to obtain the distance between 2 points and the time span for the floating debris flowed from one point to the other. In the end by the Eq. (1), the velocity of

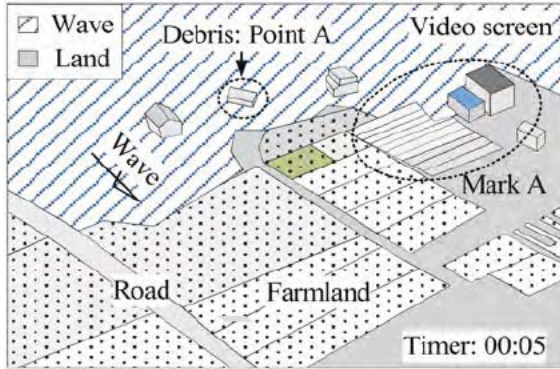


Fig. 4 Starting point for timing

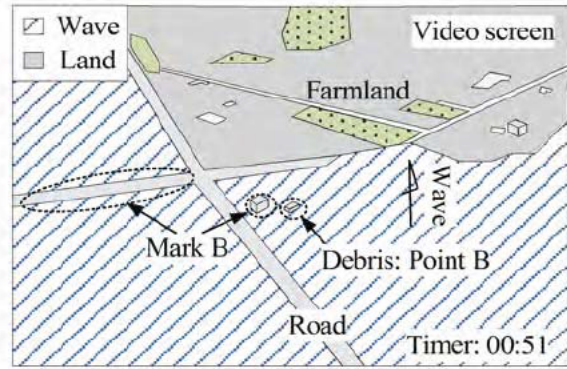


Fig. 5 Terminal point for timing

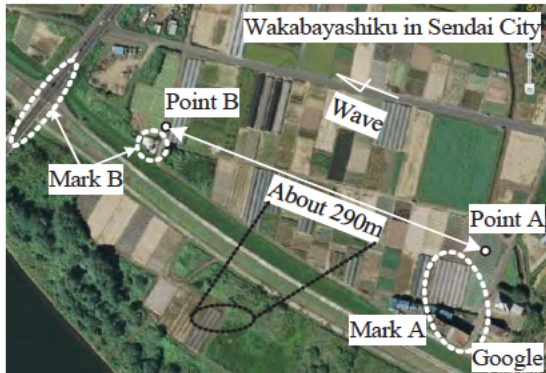


Fig. 6 Distance between 2 points

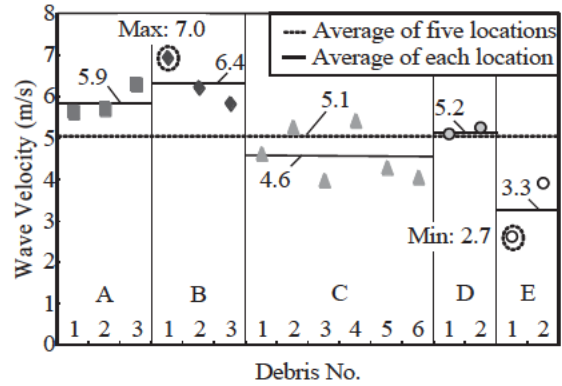


Fig. 7 Velocity result

debris was able to be computed roughly and this velocity can be regarded as the wave velocity at the video shot location.

$$v = \frac{l}{t} \quad (1)$$

Where v is the wave velocity (m/s); l is the distance between 2 place points (m); t is the time span for debris flowed from one point to the other (s).

In order to improve the precision, at each location, several different distinguished debris were selected to estimate the wave velocity repeatedly. The amount of debris used in each location is plotted in **Table 1**.

A velocity measurement of the debris at location B is described as an example. The time span for the debris flowed from one point to the other was obtained from the video. **Fig. 4** is drawn based on the video screen which shows the starting point for timing. When the debris passed Point A, from the timer of video, the time point was observed as 5sec. **Fig. 5** is drawn based on the video screen which shows the terminal point for timing. When the debris passed Point B, the time point was observed as 51sec. After that, the time span for the debris flowed from Point A to Point B was computed as $51 - 5 = 46$ sec.

Moreover the authors searched for the rough positions of Point A and B in the

Google Earth, with the use of Mark A and B, refer to **Fig. 6**. By the use of the distance measuring function of Google Earth, the distance between Point A and B was estimated around 290m. In the end, the Eq. (1) was applied to compute the velocity of the debris as 6.3m/s, refer to the velocity of B-2 in **Fig. 7**. By the same method, the wave velocity at location B was measured by 3 times with different debris. And the average velocity of the debris at location B was 6.4m/s. In the same way, the average wave velocities at the other 4 locations were computed as well. At last the average wave velocity of the 5 locations was computed as 5.1m/s, as shown in **Fig. 7**, and this velocity can be regarded as the average wave velocity in Tohoku Region.

Among the 16 velocity data, only the velocity of debris B-1 reached 7.0m/s, so it should be considered as an isolated phenomenon and the wave velocity at Utatsu Bridge should not exceed 7.0m/s. Besides that, since the Utatsu Bridge is located at location A (average: 5.9m/s) and the wave velocity is slightly larger than the velocity

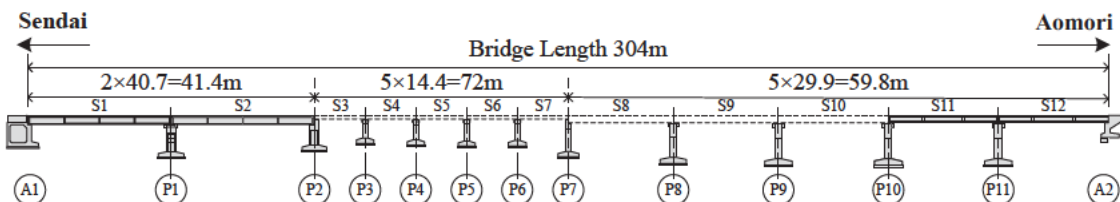


Fig. 8 Side view of Utatsu Bridge (before damaged, view from seaside)

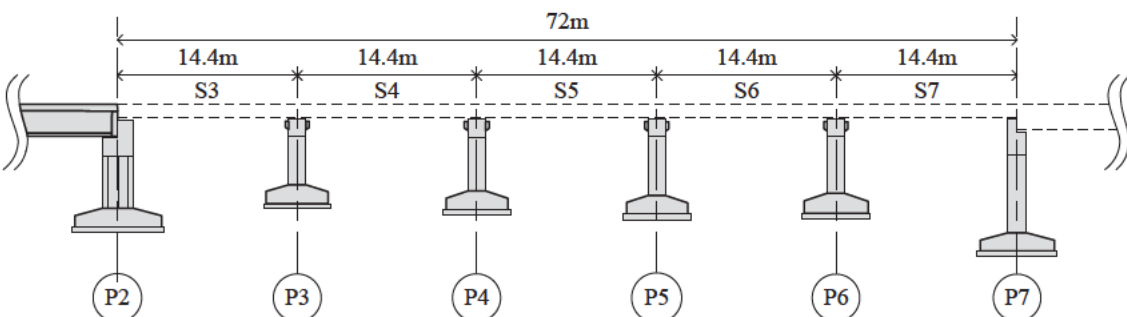


Fig. 9 Side view of damaged superstructures (S5~S7)

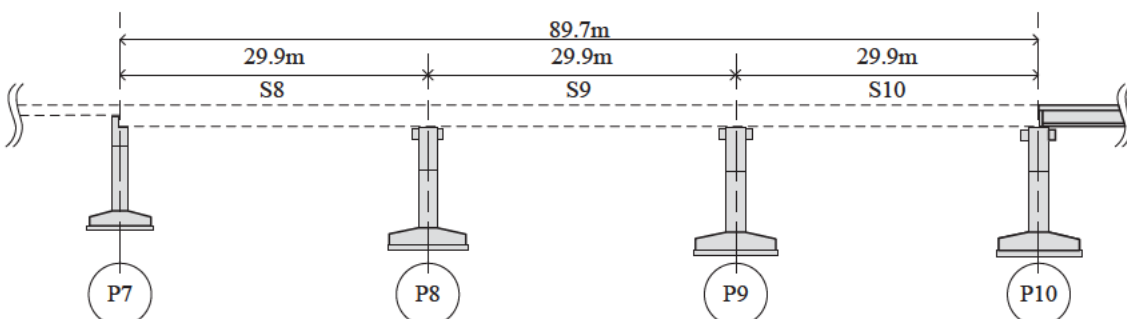


Fig. 10 Side view of superstructures (S8~S9)

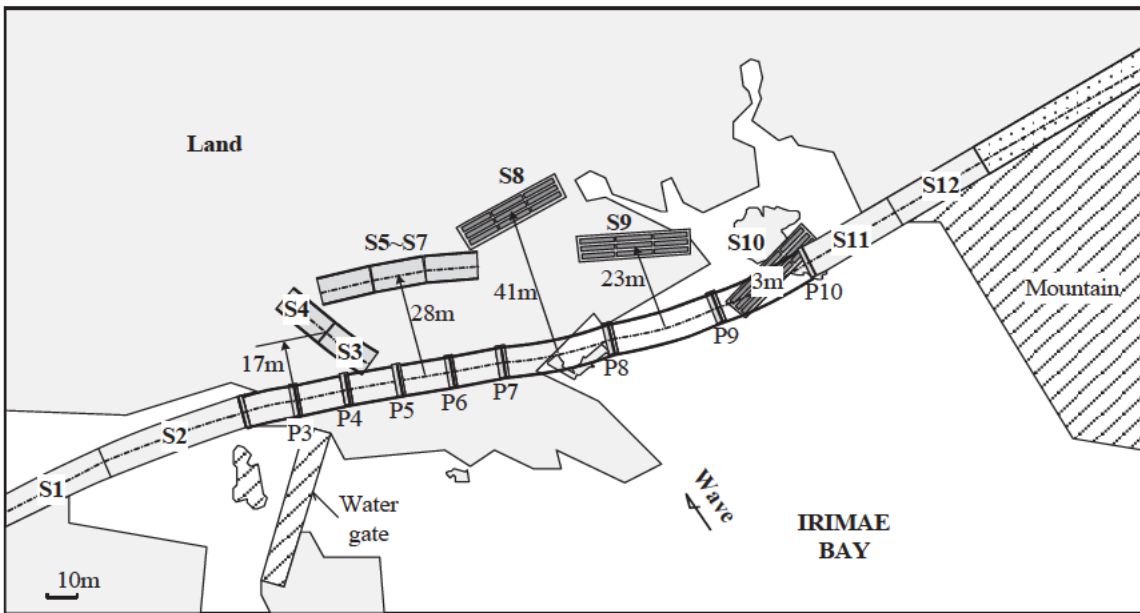


Fig. 11 Outflow condition of Utatsu Bridge

of debris due to the effect of obstacles, it is reasonable to define the wave velocity at Utatsu Bridge as 6.0m/s.

Damage to Utatsu Bridge

In the following content, the Utatsu Bridge which belongs to Line 45 of national road is analyzed as an example. The Utatsu Bridge, located at Minamisanriku Town over Irimae Bay, is composed of 3 types of superstructures varying in length from 14.4m to 40.7m, as shown in **Fig. 8**. For simplicity, the authors assigned numbers for the superstructures and piers from Sendai side to Aomori side. The 12 superstructures were numbered from S1 to S12 while the 11 piers were numbered from P1 to P11.

Based on the detailed survey, superstructures S3~S10 moved off their supports under the wave-induced lateral load while the superstructures of S1, S2, S11 and S12 did not flow out. In the flowed spans, S3~S7 and S8~S10 have different types and the details of them are shown in **Fig. 9** and **Fig. 10**. The displacements of S3~S10 have been illustrated in **Fig. 11**. The directions of displacements are transverse to the bridge axis. The characteristic of outflow condition is that the central spans such S5~S7 and S8 experienced long displacements (28m and 41m).

It was also observed that S3~S4 and S5~S7 flowed out with no separation. And due to a great wave-induced uplift force, S8~S10 were inverted when they flowed out.

However, contrary to the damage of superstructures, all piers of Utatsu Bridge withstand the wave action and did not collapse (**Fig. 12**, **Fig. 13**). The main damage to the piers is that the concrete surfaces of beams dropped due to a collision with girders and most of bridge collapse preventions were crushed or flowed out.

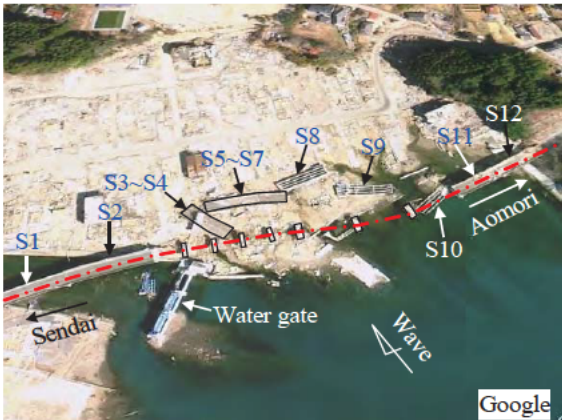
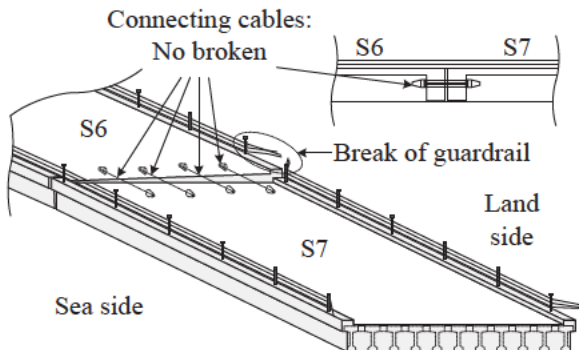


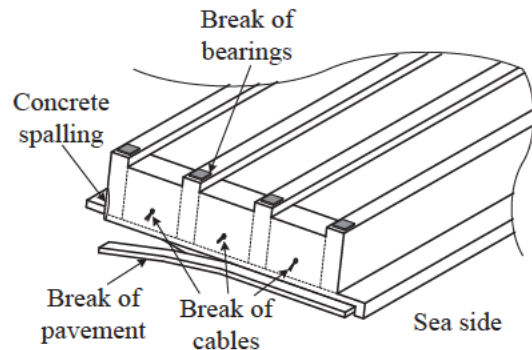
Fig. 12 Outflow condition



Fig. 13 General damage to piers



a. Damage to S6~S7



b. Damage to S9

Fig. 14 Detailed damage to superstructures

The damage to S3~S7 is one of the typical ones, which flowed out connecting with each other, and the damage of S6~S7 was selected as an example to state in the following content. Under the wave action, S6 and S7 experienced a displacement of 28m together thus it is proper to regard them as a whole. When the bridge was retrofitted, 4 cables, which were used to prevent the relative movement in axis direction of superstructures, were installed between S6 and S7. The details of cables are plotted in Fig. 14-a. These cables played an important role to keep S6 and S7 flowing out together. Besides, the damage to guardrails between S6 and S7 was observed as well.

S9 is one of the inverted superstructures, the damage to which is shown in Fig. 14-b. S9 experienced a displacement of 23m and was inverted by the wave-induced uplift. At the end surface of S8 side, different from the damage to S6 and S7, all of the cables which connected S8 and S9 were broken by the force between superstructures and the fracture traces could be found. Moreover, at the supporting area of girders, the remains of bearing plates were noted. In light of this, it is obvious that during the tsunami attack the bearings fractured. Besides that, at the connection of the 2 decks, the debris of pavement connection was observed.

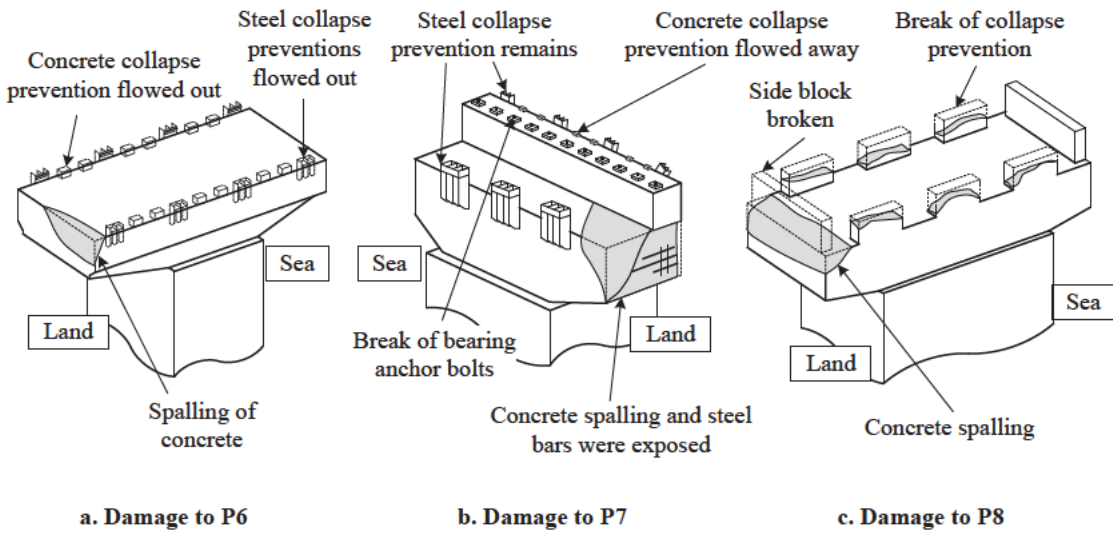


Fig. 15 Detailed damage to piers

It was found that the 11 piers supported 3 types of superstructures. In this section, 3 piers were selected basing on their different supporting superstructures. Pier 6 and Pier 8 respectively supported the type 2 and type 3 and in contrast, P7 supported both of these 2 types of superstructures (Fig. 9, Fig. 10). Therefore P6~P8 were selected to analyze. For P6 and P7, except for the concrete collapse preventions, they also had been installed steel preventions. Different from P6 and P7, only concrete collapse preventions were set up at the top of P8. These collapse preventions not only limit the superstructure's movement along the axis direction but also the transverse direction of bridge.

The detailed damage of P6 is shown in Fig. 15-a. When S6 and S7 were separated from P6, they imposed a horizontal collision on the concrete collapse preventions. Therefore, on the supporting plate of P6, 12 concrete collapse preventions were crushed. And for the same reason, the 8 steel collapse preventions, anchored on the sides of the beam, flowed out as well. Apart from the damage to the collapse preventions, the concrete surface of the beam which was located at the land side was crushed as well.

Fig. 15-b illustrates the detailed damage of P7 which supported 2 types of superstructures: S7 and S8. At S7 side, the installing details of superstructure collapse preventions were same as P6. Although the 6 concrete collapse preventions were crushed, the 4 steel ones were left. However, due to the girder-induced impact, the steel ones tilted. At S8 side, different from P6, only 3 larger steel collapse preventions were anchored and they did not flow out. The damage condition of steel collapse preventions demonstrates that when the superstructures, located on P7, displaced they were elevated by a wave-induced uplift. Because of this, the superstructures flowed from the top of the steel collapse preventions and did not impose a sufficient impact to make them separate from supports. Besides that, at the land side, the concrete surface of the beam was crushed and some steel bars could be observed.

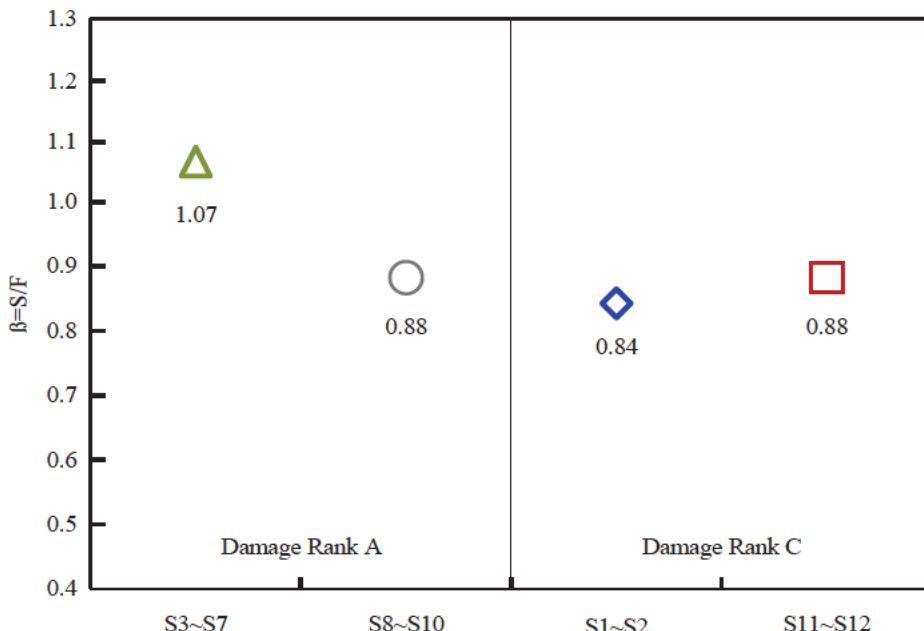


Fig. 16 β result of Utatsu Bridge

The damage of P8 is plotted in **Fig. 15-c**. On the top of beam, 6 concrete collapse preventions and 2 side concrete blocks were set up. By the same force situation as the preventions of P6, the 6 concrete collapse preventions and one side block, which was at the land side, were crushed. Besides, it was found while the side block flowed out, a damage of the concrete surface, which under the side block, occurred.

Simple Analysis of Utatsu Bridge

In this chapter, in order to confirm the outflow condition of Utatsu Bridge, the concept of ratio β to superstructure resistance and wave lateral load on is proposed. The relationship between the ratio and the outflow of girders has been analyzed. The expressions to compute the ratio β are listed as follows (Kosa, 2010):

$$\beta = \frac{S}{F} \quad (2)$$

$$S = \mu W \quad (3)$$

$$F = \frac{1}{2} \rho_w C_d v^2 A \quad (4)$$

Where, β is the ratio to resistance and lateral load; F is wave lateral load (kN); S is superstructure resistance (kN).

When computing β values, based on the result of last chapter, it is reasonable to apply $v=6.0\text{m/s}$. Further, based on the former experimental result the friction coefficient will be assumed as 0.6. For comparison, the damage extents of bridge

Table 2 Details of damaged bridges in Tohoku Region

Object Bridge	Object of Span(s)	Girder Type	Damage Rank	Span Length	Bridge Width	Bridge Height	Ratio β
				L[m]	B[m]	D[m]	
Utatsu Bridge	9th Span	Simple Post-Tension "T" Girder	A	29.9	8.3	2.5	0.89
Koizumi Bride	1st-6th Span	Continuorous Steel Plate Girder	A	181.8	11.3	2.6	0.90
Kesen Bridge	1st-5th Span	Continuorous Steel Plate Girder	A	181.1	13.3	2.7	0.99
Kawaharagawa Bridge	1st Span	Simple PC Hollow Girder	C	28.8	14.8	1.8	4.30
Nijyuichihama Bridge	1st Span	Simple Pre-Tension "T" Girder	C	16.6	8.3	1.5	1.23
Hamadagawa Bridge	1st Span	Simple Post-Tension "T" Girder	C	22.5	14.8	1.7	2.64
Numata-Kosen Bridge	2nd Span	Simple Post-Tension "T" Girder	A	20.0	13.5	2.6	1.34
Namiita Bridge	1st Span	Simple Pre-Tension "T" Girder	C	12.5	9.2	1.3	0.88
Sodeogawa Bridge	1st-4th Span	Continuorous RC hollow Girder	C	59.9	8.8	1.5	1.83
Mizujiri Bridge	3rd Span	Simple Steel "H" Girder	A	10.5	5.9	1.4	0.61
Shinkitagami Bridge	1st, 2nd Span	Continuorous Steel Truss Girder	A	155.0	8.6	3.6	0.45
Shiomi Bridge	1st Span	Simple PC "I" Girder	C	13.5	11.3	1.365	4.31
Shin-Aikawa Bridge	1st Span	Simple Steel Box Girder	A	67.2	11	3.835	0.57
Hachiman Railway Bridge	1st Span	Simple Post-Tension "I" Girder	A	22.9	5.5	2.05	0.62
Hachiman Highway Bridge	1st-3rd Span	Simple Post-Tension "I" Girder	C	12	8.2	1.07	5.97

girders is described by Rank A, B and C. Rank A means girders separated with substructures completely. Rank B means girders suffered displacements but still can be used. Rank C means girders only suffered partial damage such as damage to guardrails.

The β result is illustrated in **Fig. 16**. Based on **Fig. 16**, it is known that S3~S10 suffered damage Rank A and the remaining girders suffered damage Rank C. Most β values are smaller than 1.0 except for the β values of S3~S7 which is 1.07, slightly larger than 1.0. This trend of β values illustrates, comparing with wave lateral load, superstructure resistance is not sufficient to make S3~S10 survive, which is attributed to the relatively small girder width causing the comparatively small girder weight.

Simple Analysis of Bridges Damaged Due to Tsunami

Except for the Utatsu Bridge, 12 other damaged bridges in Tohoku region, the details of which are shown in **Table 2**, and the damaged bridges due to the Sumatra Earthquake have been analyzed as well. By the same method in last chapter, the β values of them are obtained and illustrated in **Fig. 17**.

Fig. 17-a and **Fig. 17-b** illustrate the β values of damaged bridges in Tohoku

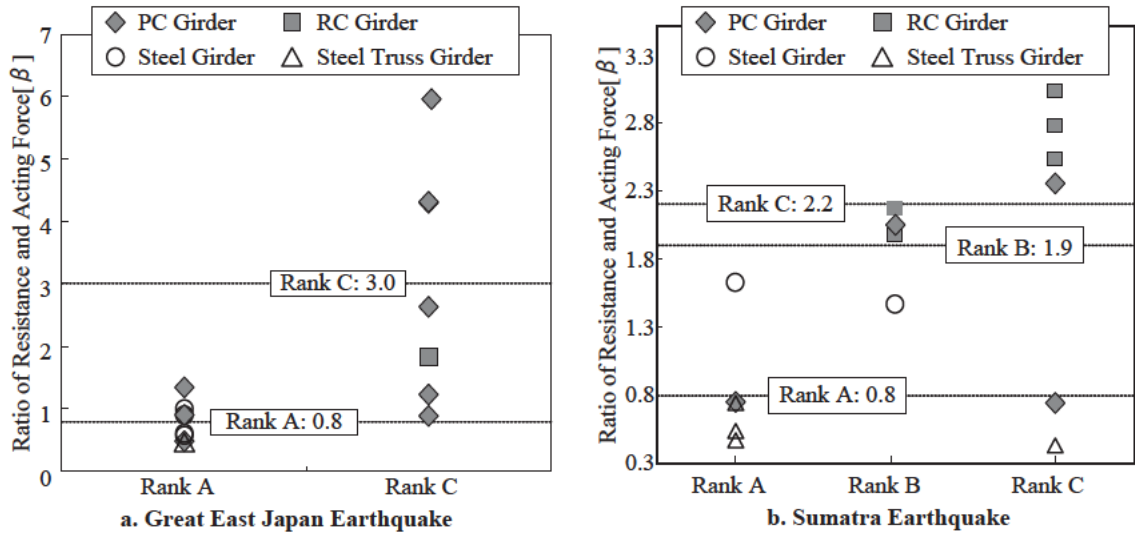


Fig. 17 β result of Sumatra and Great East Japan Earthquake

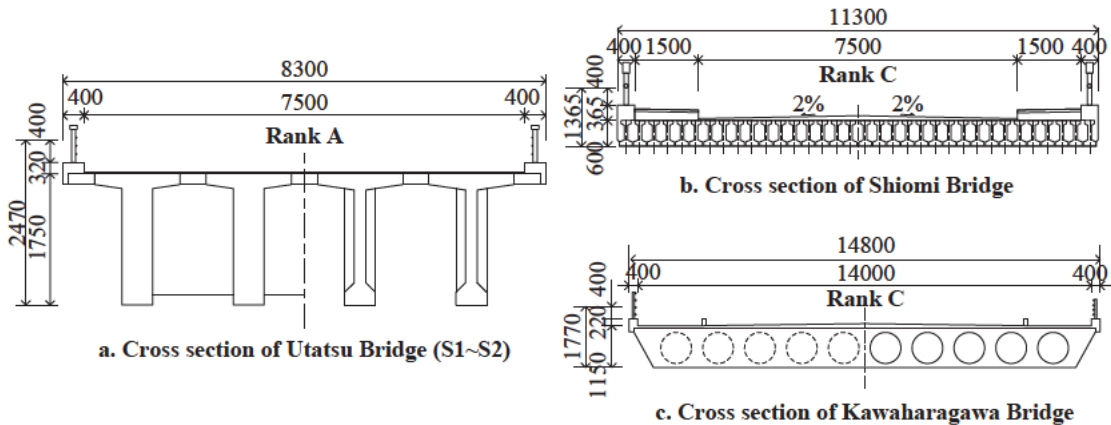


Fig. 18 Comparison of cross sections

region and the bridges damaged in Sumatra Earthquake respectively. In terms of the relationship between damage extents and β values, according to the former research as shown in **Fig. 17-a**, during the Sumatra Earthquake, the average β values of Rank A, Rank B and Rank C are respectively 0.8, 1.9 and 2.2 and the average β value of Rank A is around 2.5 times larger than Rank C. By the same method, for the situation of bridges in Tohoku region, refer to **Fig. 17-b**, the average β values of Rank A and Rank C are 0.8 and 3.0 respectively. And the average β value of Rank A is around 3.75 times larger than Rank C. Therefore, from the above result, it is noted that the β value is a significant indicator to judge the damage extent of bridges.

Fig. 18 is applied to describe the difference of typical girders of Rank A and Rank C. It is obvious that the ratio to girder width and height of Rank A (3.36) is smaller comparing with the girder of Rank C (b: 8.28, c: 8.36), which led to insufficient resistance and greater wave pressure area. Therefore, in future design, it should be

considered to increase the ratio to girder width and height for tsunami resistance.

Conclusions

- (1) Among the undated 3000 bridges subjected to the earthquake, around 10% suffered serious damage and could not be used.
- (2) Based on the flow velocities of debris in 5 inshore locations during the tsunami attack, the wave velocity at Utatsu Bridge can be estimated as 6.0m/s.
- (3) Based on the field survey, for the damage to the superstructures of Utatsu Bridge, S3~S10 experienced movement and for the damage to piers, although they did not collapse, the devices, which were used to prevent the collapse of superstructures, such as RC blocks, steel brackets and anchor bolts suffered serious loss.
- (4) With the comparison of damage appearances of bridges in Sumatra Earthquake and the bridges in Tohoku Region. As a result, when the tsunami heights were excess of 10m, the damage to bridges in 2 sites have many common points: outflow of girders and scour of foundations.
- (5) With the comparison of the β ratios of the damaged bridges in Sumatra Earthquake and the bridges in Tohoku Region. As a consequence, the β ratios of the bridges with same damage rank have the similar degrees, especially for the bridges of Rank A. Therefore, in the future work, it is reasonable to apply β ratio as the indicator to justify the function against tsunami of bridges.

References

1. Japan Meteorological Agency (JMA): The 2011 Off the Pacific Coast of Tohoku Earthquake (Quick Report #25), Strong 105 Reference Material 4 by the Subcommittee for Evaluation of Strong Ground Motion, the Earthquake Research Committee, 2011.
2. Li, Damage Analysis of Utatsu Bridge Affected by Tsunami due to Great East Japan Earthquake, The 14th Symposium on seismic design of bridges, The Earthquake Engineering Committee, Journal of Structural Engineering, pp .111-118, 2011. 7.
3. Kosa, Analysis of Damaged Bridge by Tsunami due to Sumatra Earthquake, Journal of Structural Engineering, Vol.55A, pp .483-494, 2010. 3.

DEVELOPMENT OF TSUNAMI DESIGN CRITERIA FOR OREGON COASTAL BRIDGES

Bruce Johnson¹

Based on research and documents by Solomon Yim² et al

Abstract

This paper describes Oregon Department of Transportation (ODOT) efforts to develop guidelines for estimating tsunami forces on bridges. ODOT contracted with Oregon State University (OSU) to conduct two studies. First we needed a model of the potential tsunami wave characterized by a height, direction and speed. Second, we needed a model to develop uplift and horizontal forces on a bridges generated from a wave with the three tsunami wave characteristics. OSU developed a numerical code to perform modeling of tsunami impact on bridge superstructures on four bridges located on US Highway 101 in the Siletz Bay area on the Oregon Coast. The numerical results were incorporated into a mathematical formula to provide a simplified, approximate method for estimating tsunami forces on bridge superstructures.

Introduction

The Oregon coast is vulnerable to large seismic events from the Cascadia Subduction Zone (CSZ) which shares common seismic characteristics with those at Sumatra that generated large tsunamis in the Indian Ocean in December 2004. Studies of tsunami deposits and evidences of coastal subsidence indicate that an average of large seismic events in CSZ occurs once every 300-500 years (Goldfinger et al. 2003). The most recent large seismic event in the CSZ occurred in 1700; therefore, there is a relatively high probability that a large seismic event will occur in the near future that could damage structures along the coastal area in the Pacific Northwest.

The bridges along the Oregon Coast are an important part of the transportation system. Any major damage to these bridges would result in traffic disruption and impede post-event emergency response. Since these bridges, mostly built in the 1950-70's, were not designed to resist large seismic or tsunami loads, they are at the risk of being severely damaged during large seismic events. However, unlike seismic loads, currently there is no specific design standard for estimating tsunami forces on bridge superstructures in the US in general and in Oregon in particular. Therefore, an understanding of tsunami impact on bridge superstructures is of major interest to the practicing engineering community. Consequently, the Oregon Department of Transportation (ODOT) initiated a research program to develop guidelines for estimating tsunami forces on bridge superstructures in the tsunami run-up zone along the Oregon Coast.

The study first developed numerical models to simulate tsunami impact on bridge superstructures, and calculate reaction forces due to tsunami loads on four selected bridges on

¹ State Bridge Engineer, Oregon Department of Transportation

² Professor, School of Civil and Construction Engineering, Oregon State University

the Oregon Coast. The four bridges – Schooner Creek Bridge, Drift Creek Bridge, Millport Slough Bridge, and Siletz River Bridge – are located on Highway 101 in the Siletz bay area. The study also developed a guideline for estimating tsunami forces on bridge superstructures to be used as preliminary guidance for design of bridges in the tsunami run-up zone. The developed guidance is based on existing literature and the time-history results obtained from the numerical models calculated in the first part.

OSU had conducted a previous case study of tsunami design criteria on the Spencer Creek Bridge, on US 101 in Oregon, conducted by Nimmala et al. (2006). The Spencer Creek project was conducted by developing numerical models of tsunami impact on bridge deck to determine the time-history forces on the bridge by using LS-DYNA software. The analysis is revisited in this paper to examine the applicability of the guideline developed in the present work.

Tsunami Flow Simulation

The input tsunami flow fields, water surface elevation and water velocity time-histories, for the simulation models were obtained from tsunami numerical models developed by Cheung and associates from the University of Hawaii (Cheung et al. 2010). The nonlinear shallow-water model by Yamazaki et al (2009) was utilized to capture hydraulic processes – wave overtopping, hydraulic jump formation, and bore propagation – describing flow conditions at the interested bridge sites.

The development of a rupture model based on 500-year return period CSZ earthquake scenarios from the National Seismic Hazard Maps. These rupture boundaries extend approximately 1,100 km from Cape Mendocino in northern California to Vancouver Island in British Columbia. The western boundary of the rupture is specified along the trench at the base of the continental slope. Additional conditions are provided by Wang et al (2003) to define the eastern rupture boundaries at the midpoint of the transition zone (MT) and the base of the transition zone (BT). Moreover, a global analog (GA) of shallow-dipping subduction zones, from Tichelaar and Ruff (1993), is used to define the eastern rupture boundary at 123.8°W at 30 km depth.

The tsunami flow model developed by Cheung included four hours of data simulating a 500-year Cascadia tsunami event at the Siletz Bay for six different scenarios. The six tsunami scenarios are based on four rupture configurations at moment magnitude (Mw) 9.0 and two additional moment magnitude 8.8 and 9.2 events at the rupture based on global analog zone. The first configuration assumes the rupture occurs within the locked zone (LZ) only. The eastern rupture occurs at the midpoint of the transition zone (MT) and at the base of the transition zone (TZ). The fourth rupture configuration is assumed to occur at 30 km depth based on global analog (GA).

A relative weight distribution probability of occurrence for the rupture configurations (0.1, 0.2, 0.2 and 0.5 for LZ, MT, BT and GA, respectively) and moment magnitudes (0.6, 0.2 and 0.2 for Mw 9.0, 8.8 and 9.2) are assigned based on the logic tree in the Pacific Northwest seismic source model in Cheung et al. (2010).

Currently, there is no specific code of practice to estimate forces on bridge superstructures due to tsunami loads. However, there is some relevant literature of wave forces on highway bridge decks and offshore platforms, and some literature on tsunami forces for other types of structures such as vertical walls, elevated slabs, and columns of different shapes.

Development of Equations to Estimate Forces from Tsunami Waves

Bea et al. (1999) presented a modification of the American Petroleum Institute (API) guidelines for estimating wind-induced wave forces on a platform deck of offshore structures by separating the total wave force into two components, horizontal force and vertical force. The horizontal force consisted of slamming force, drag force, and inertia force. The slamming force and drag force depended on the horizontal velocity of the waves while the inertia force depended on the acceleration. The vertical force consisted of a buoyant force and a lifting force, which depends on the vertical velocity of the waves.

Wave Forces on Bridge Decks

Douglass et al. (2006) presented a method for estimating wave forces on typical U.S. coastal bridge spans due to wind waves and storm surge to offer a preliminary guidance for design engineers. The estimated horizontal and vertical forces in that method mainly depend on the elevation of the wave crest. Other than water elevation, the horizontal force is also dependant on the number of girders supporting the bridge deck. This recommended approach was verified with post-storm damage on U.S. 90 Bridge across Biloxi bay, Mississippi by Hurricane Katrina.

$$F_H = [1 + C_r(N - 1)](C_{h-va} + C_{h-im})\gamma(\Delta h)A_h$$

$$F_V = (C_{v-va} + C_{v-im})\gamma(\Delta h)A_v$$

where C_r is a reduction factor for forces distribution on the internal girders; N is number of girders supporting bridge deck; C_{h-va} and C_{v-va} are empirical coefficients for slow varying horizontal and vertical force respectively; C_{h-im} and C_{v-im} are empirical coefficients for horizontal and vertical impact force respectively. The other parameters are generally defined in notation.

Previous Research on Wave Forces

FEMA P646 (2008), guidelines for design of structures for vertical evacuation from tsunamis, summarized the relevant design code, and presented equations for estimating tsunami forces on vertical evacuation structures. It also provided some suggestions on how to combine tsunami force with other loads such as dead load and live load. Load effects that had to be considered for tsunami forces consisted of hydrostatic, hydrodynamic, impulsive, buoyant and uplift forces. The hydrostatic force depended on water elevation and would be considered to be zero when water fills up on two opposite sides. Unlike the wave forces due to storm surge, the hydrodynamic force due to tsunamis depended on flux momentum (hu^2) where h is elevation of water crest and u is horizontal velocity. The impulsive force due to tsunami could be estimated by taking 1.5 times the corresponding hydrodynamic force for conservatism.

Douglass et al. (2006) developed a method for the Federal Highway Administration (FHWA) to estimate wave forces on highway bridge decks due to storm surge. Their approach was developed based on laboratory experiments of a scaled bridge deck model in a 3D wave basin. The resulting predictions were shown to be adequate for estimating the wave force induced by storm as verified by measured field damages from Hurricane Ivan and Katrina. However, the equations presented in that method depended only on wave crest elevation without considering the importance of water velocity, which is an important factor in tsunamis.

Numerical Models for Tsunami Impact Loads on Bridges

The models are developed to perform numerical testing of tsunami impact on realistic bridge superstructures to predict the magnitude of tsunami forces that could occur on specific types of bridge superstructure. This section presents details development of the numerical models, bridge descriptions as well as time-history of fluid loads on bridge superstructures under various tsunami flow fields. Effects of different cross-sectional bridge types and the effect of bridge rails to fluid loads are discussed followed by cumulative probabilities of tsunami forces and overturning moments. Furthermore, computational efforts are also summarized and presented in this section.

Two-dimensional (2-D) numerical models are developed using a finite-element based code. The provided tsunami flow velocities are assumed to be uniform over depth and resolved in the direction perpendicular to the longitudinal span of the bridge. The cross-section of the bridge superstructure normal to the longitudinal span is modeled by assuming simply supported under external girders.

In general, a simulation model consists of two major material parts: a fluid part and a rigid structure part. The fluid part is a composition of water and air materials which are demonstrated by appropriate material type combining with equation of states. For computational efficiency, an approximating rigid body material was used to represent the bridge part and reaction forces are determined by replacing four rigid elements at supports by elastic material. The OSU study focused on quantifying the maximum value of the horizontal force, vertical force, and overturning moment due to tsunami loads on the selected bridges; thus, the simulation began at a time immediately prior to first water impact the superstructure and terminated after obtaining the peak values of the time-history of the loads.

The Lagrangian-Eulerian coupling algorithm combined with an Arbitrary Lagrangian-Eulerian (ALE) solver was used in the numerical models as it is the most mature formulation to simulate the problem involving interaction between fluid with high velocity and rigid structure. The basic concept of the Lagrangian-Eulerian coupling algorithm is to track the relative displacements of the corresponding coupling points defined at the interfaced between the Lagrangian surface (bridge superstructure part) and inside the Eulerian elements (fluid part).

FIGURE 1 shows an example of the numerical model of the Millport Slough Bridge developed in this research. The model consists of three material parts: water, air, and bridge parts. Material

properties for each part – such as material mass density, pressure cut-off, fluid viscosity, modulus of elasticity, and Poisson's ratio – are specified appropriately as they are used in the ALE differential equation and in calculating of interface stiffness. Even though the numerical model is two dimensioned, it could be thought of as a three dimensional rectangular cross-section with unit thickness in z-direction. The cross-section is composed of water and air material parts with a bridge part inside.

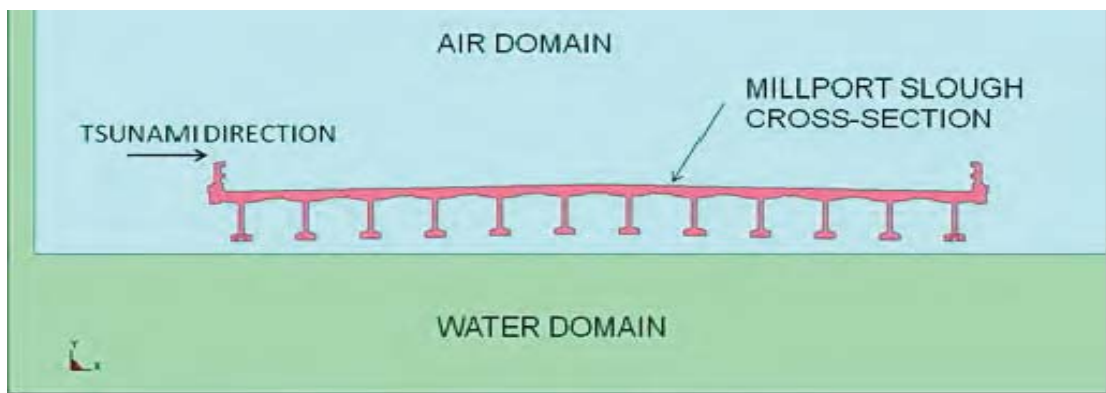


FIGURE 1, MILLPORT SLOUGH EXAMPLE SIMULATION MODEL

Example Bridges and Waves

Numerical models of four selected bridges in the Siletz bay are developed for this tsunami load estimation study. The first is the Schooner Creek Bridge located close to the open channel of the bay facing directly toward the incoming tsunamis. The reference bridge elevation measured at the support of the lowest (west-most) bridge girder is approximately 18 feet above mean sea level (MSL).

The second bridge is the Drift Creek Bridge located southeast of the Schooner Creek in a more open area. The bridge geometry is similar to that of the Schooner Creek Bridge (deck-girder section) with a smaller cross-sectional width and less number of girders supporting the bridge deck. The bridge is designed for a 2% slope with a reference elevation of approximately 14 feet above MSL. The third bridge is the Millport Slough Bridge located at the south end of the Siletz Bay on Highway 101. The bridge has a 2% slope crown with a reference elevation of 15 feet above MSL. Finally, the fourth bridge is the Siletz River Bridge. This bridge, which is a box section, with a reference elevation of approximately 33 feet above MSL, is at a higher elevation compared to the other three bridges.

Six different tsunami flow fields are provided for each bridge site (GA Mw 8.8, GA Mw 9.0, GA Mw 9.2, LZ Mw 9.0, MT Mw 9.0 and TZ Mw 9.0). However, the maximum water surface elevations generated in some scenarios are lower than the reference bridge elevation, and can be neglected because tsunamis in these scenarios would not induce forces on the superstructures. In particular, five tsunami scenarios – GA Mw 9.0, GA Mw 9.2, LZ Mw 9.0, MT Mw 9.0 and TZ Mw 9.0 – are applicable to the Schooner Creek Bridge, and the three of these scenarios – GA

Mw 9.2, LZ Mw 9.0 and MT Mw 9.0 – are also applicable to the Drift Creek Bridge and the Millport Slough Bridge. On the other hand, the tsunami flow of all six tsunami scenarios were below the beam elevation of the Siletz River Bridge, so no tsunami loads were modeled for that bridge.

Example Tsunami Force Time-History

Time-histories of the predicted horizontal and vertical reaction forces due to tsunami loads on the three affected bridges were calculated from the numerical models. The Schooner Creek horizontal tsunami forces are shown in FIGURE 2. The forces on the box section (black line) show a pattern of a short duration high intensity force at the time immediately after water impacting the bridge followed by fluctuating drag forces similar to those reported by Yeh et al. (2005). The impact forces on the box section are approximately 1 to 2.5 times the corresponding drag forces; whereas the maximum impact horizontal forces on the deck-girder section are sometimes smaller than the corresponding maximum drag force. A comparison of the vertical tsunami force time-histories on both box section and deck-girder for Schooner Creek is shown in FIGURE 3. The vertical tsunami forces on both sections show similar pattern as they are rapidly increased at the time water impacts the structure followed by steady forces for a while until the water subsides. Similar results were obtained for Drift Creek and Millport Slough.

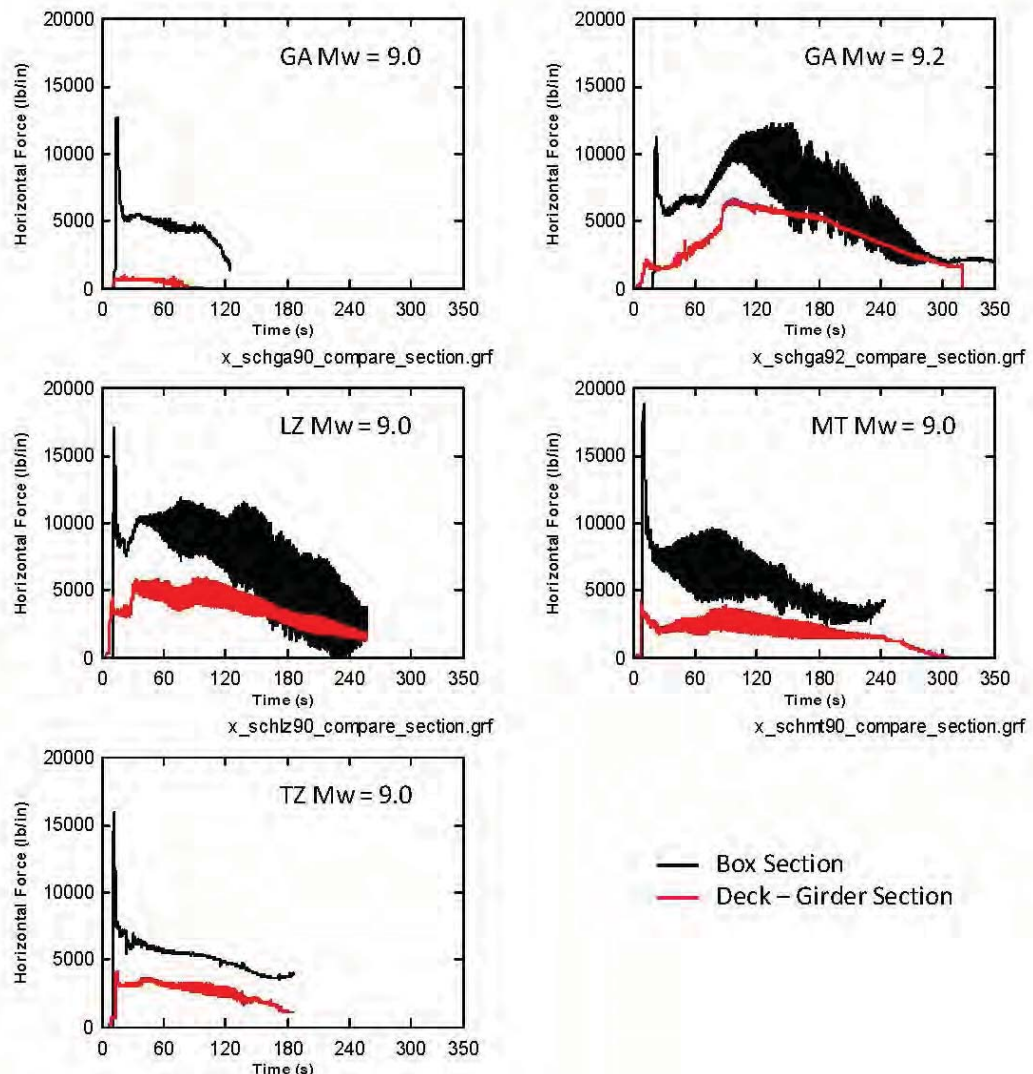


FIGURE 2, SCHOONER CK HORIZONTAL TSUNAMI FORCE TIME-HISTORIES

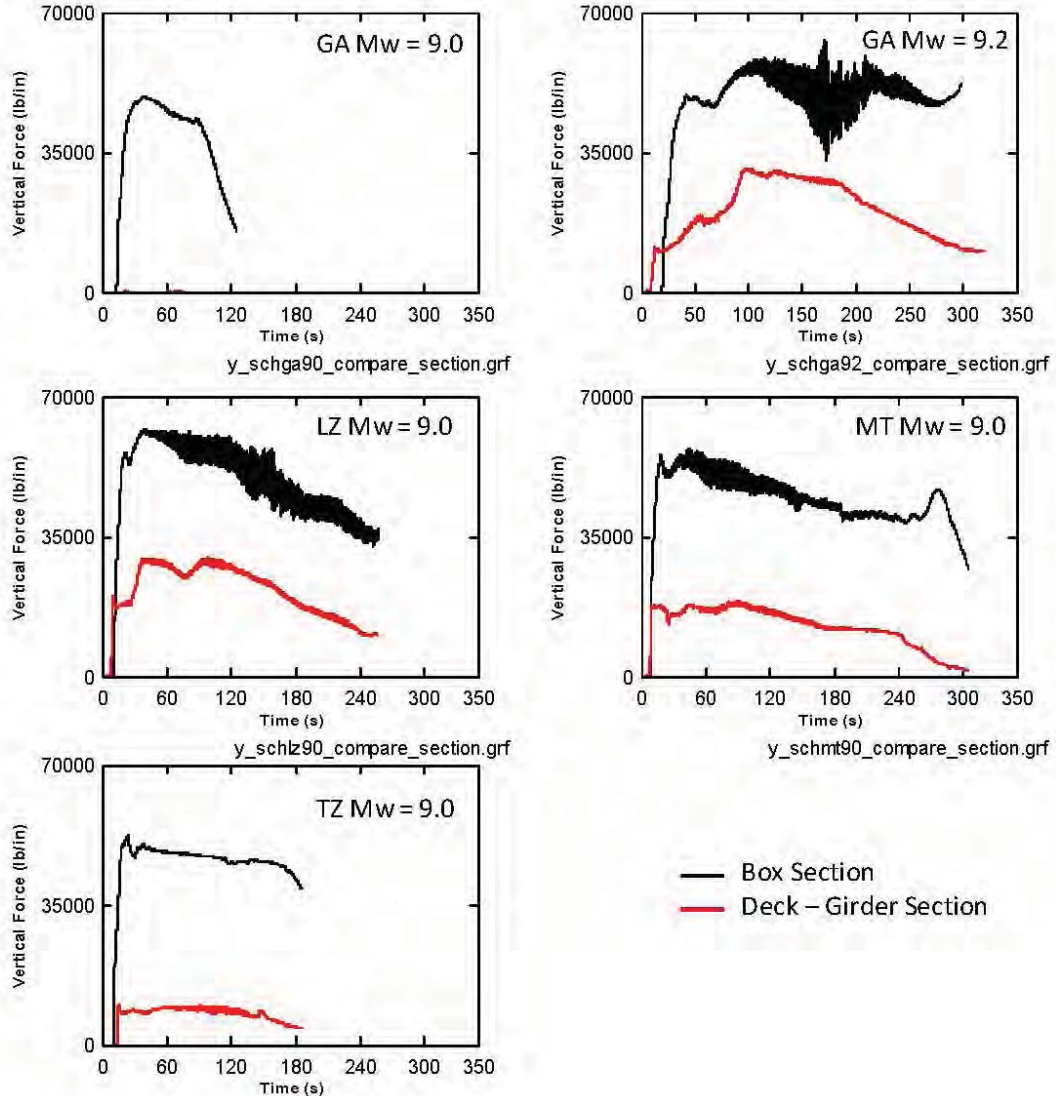


FIGURE 3, SCHOONER CK VERTICAL TSUNAMI FORCE TIME-HISTORIES

To summarize, tsunami forces on the superstructure of the selected bridges are quite difference given the same tsunami scenario. According to the results discussed above, the Siletz River Bridge could survive a 500-years Cascadia tsunami event because the designed reference elevation of the bridge superstructure is sufficiently high to avoid tsunami loads while the other three bridges are inundated in some scenarios. The Schooner Creek Bridge and the Drift Creek Bridges were subjected to large tsunami forces, compared to the forces on the Millport Slough Bridge, because they are located in an open area close to the inlet channel of the bay facing directly to the incoming tsunamis while the Millport Slough is located far from the inlet channel. A regression line relating the maximum horizontal forces and the corresponding maximum flux momentums is plotted in FIGURE 4. It is reasonable to assume that the maximum horizontal

force is approximately linearly proportional to the maximum flux momentum as suggested in FEMA (2008) and PBTE (2010).

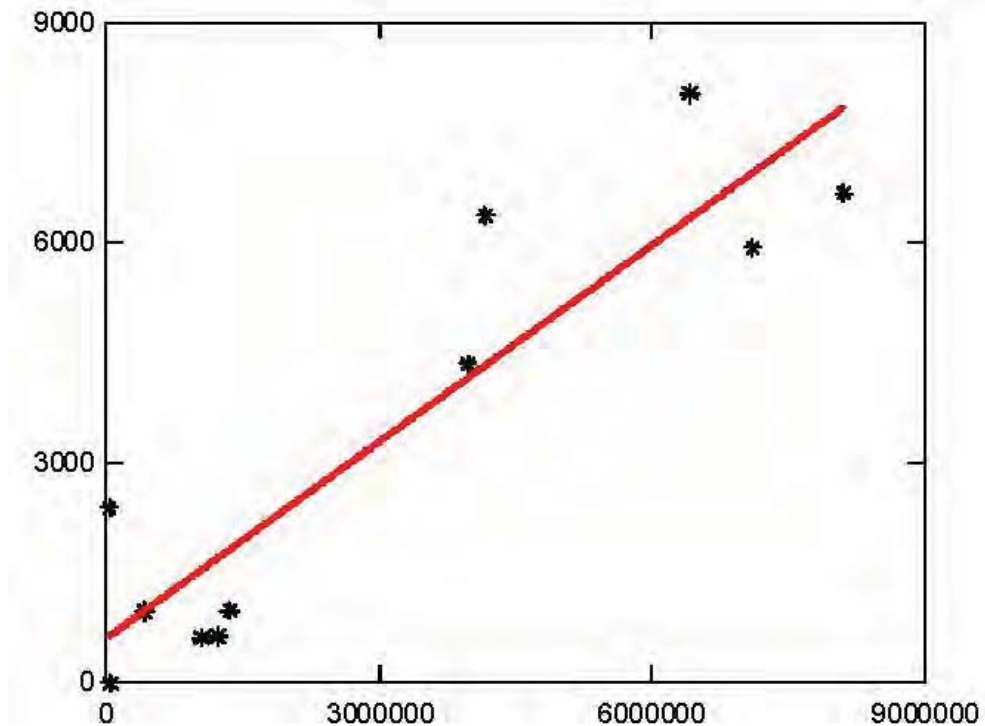


FIGURE 4, MAXIMUM FLUX (Horizontal axis, in^3/sec^2) VERSUS MAXIMUM HORIZONTAL TSUNAMI FORCE (Vertical axis, pounds/in)

According to the numerical results, the magnitude of the tsunami forces on a bridge superstructure generated from different rupture configurations and moment magnitudes can be significantly different.

Estimation of Tsunami Forces on Bridge Superstructures

This section presents a development of a guideline for estimating tsunami forces on superstructures for preliminary design of bridges in a tsunami run-up zone along the Oregon Coast. This approach is developed by incorporating the relevant existing literature and the tsunami forces obtained from the numerical models developed in the OSU Study for Oregon DOT.

The total tsunami force on a bridge superstructure can be considered separately as horizontal and vertical components. The horizontal component acts perpendicularly at the center of gravity of the longitudinal span of the bridge superstructure while the vertical component acts in upward and downward directions at the center of gravity of the superstructure normal to the wave direction.

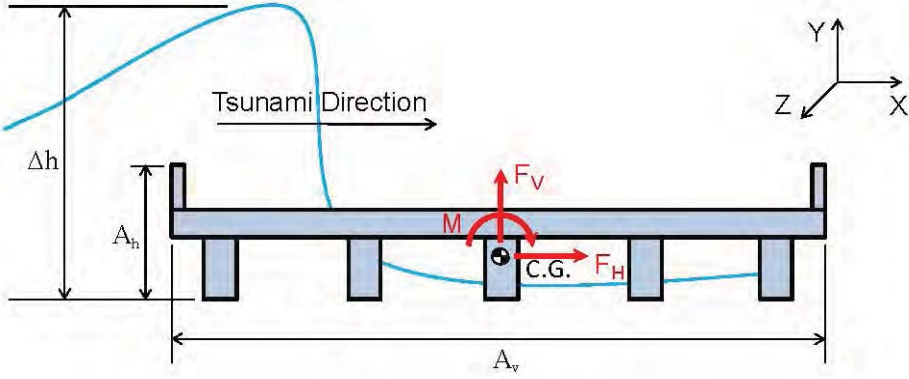


FIGURE 5, SIMULATED HORIZONTAL AND VERTICAL TSUNAMI FORCES

Horizontal Forces

The total horizontal forces on the bridge superstructures due to tsunami loads are a combination of hydrostatic and hydrodynamic pressures. The hydrostatic pressure is induced by gravity, and increases with water depth. The total force due to hydrostatic pressure is a result of imbalanced pressure, which could be considered zero when water filled up both side of the structure. The hydrodynamic pressure is induced by horizontal water velocity which is a significant factor in the tsunami events. The hydrostatic and hydrodynamic forces are considered linearly proportional to the water elevation and the flux momentum (hu^2), respectively.

The total horizontal wave-induced force on bridge superstructures presented by Douglass et al. (2006) is estimated by combining the hydrostatic pressure on the seaward external girder and the total pressure on the internal girders. The total force on the internal girders can be estimated by multiplying reduction factor with the corresponding force on the seaward external girder. The horizontal force due to hydrostatic (Douglass et al. 2006) and hydrodynamic (Yeh 2007) pressures, therefore, can be formulated as shown below.

$$F_h = (1 + C_r(N - 1))C_h F_h^* \\ F_d = 0.5 C_d \rho b (\Delta h u^2)_{\max}$$

Where $C_r = 0.4$ reduction coefficient for pressure on internal girders; $N = \text{number of girder supporting bridge deck}$; $F_h^* = \gamma(\Delta h_{\max})A_h$; $C_d = \text{empirical drag coefficient}$; $\rho = \text{seawater mass density}$; and $(hu^2)_{\max} = \text{maximum flux momentum}$.

The total horizontal force due to tsunami loads consists of hydrostatic force (water elevation-dependent term) and hydrodynamic force (flux momentum-dependent term). Even though the maximum of these forces might not occur exactly at the same time, combining these maximum forces together is considered reasonable (and conservative) for design purpose. Therefore, the

maximum horizontal force on bridge superstructure due to tsunamis can be estimated by combining the equations above as follows:

$$F_H = F_h + F_d \\ = (1 + C_r(N - 1))F_h^* + 0.5C_d \rho b(\Delta h u^2)_{\max}$$

An empirical drag coefficient, C_d , for bridge superstructures were evaluated in this research based on the time-history results obtained from the numerical models. A plot between the total horizontal force and flux momentum can be considered separately into two parts. The first part is where the horizontal force increases rapidly with a small change in the flux momentum (flux momentum-independent part). The second part is where the horizontal force increases proportionally to the corresponding flux momentum (flux momentum-dependent part) as shown in FIGURE 6. The empirical coefficient was estimated from the slope of the graph between flux momentum and the total horizontal force as $0.5C_d \rho b$ ($= \text{slope}$). Therefore, the drag coefficient is approximately 1.0 for the deck-girder bridge type.

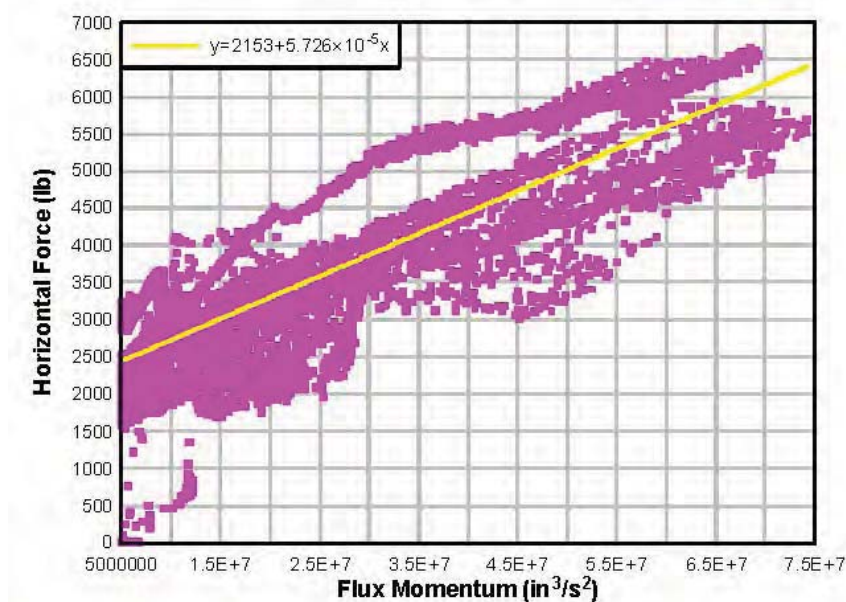


FIGURE 6, TOTAL HORIZONTAL FLUX VERSUS FLUX MOMENTUM

In determination of wave forces due to wind wave and storm surge, it is recommended that the total horizontal pressure on internal girders could be estimated as 40% of the pressure on the external seaward girder. However, horizontal pressure time-history results at the bottom of bridge girders are determined to evaluate an appropriate reduction coefficient for the distributed pressure on the internal girders under tsunami loads. The results (refer to the figures that show these results) show that the maximum pressure on the internal girders is approximately 20% to

50% of the corresponding pressure on the external seaward girder. Therefore, the reduction coefficient, C_r , for this study was taken as 0.4 until further information is obtained.

A comparison between the estimated maximum horizontal forces and the predicted forces calculated from the numerical models are shown in FIGURE 7. The straight line in that graphError! Reference source not found. represents a perfect fit between estimated force and the predicted force. It can be observed that the estimated forces could be overestimated or underestimated in some cases because the recommended empirical coefficients are based on an average value of the scattering data as shown above.

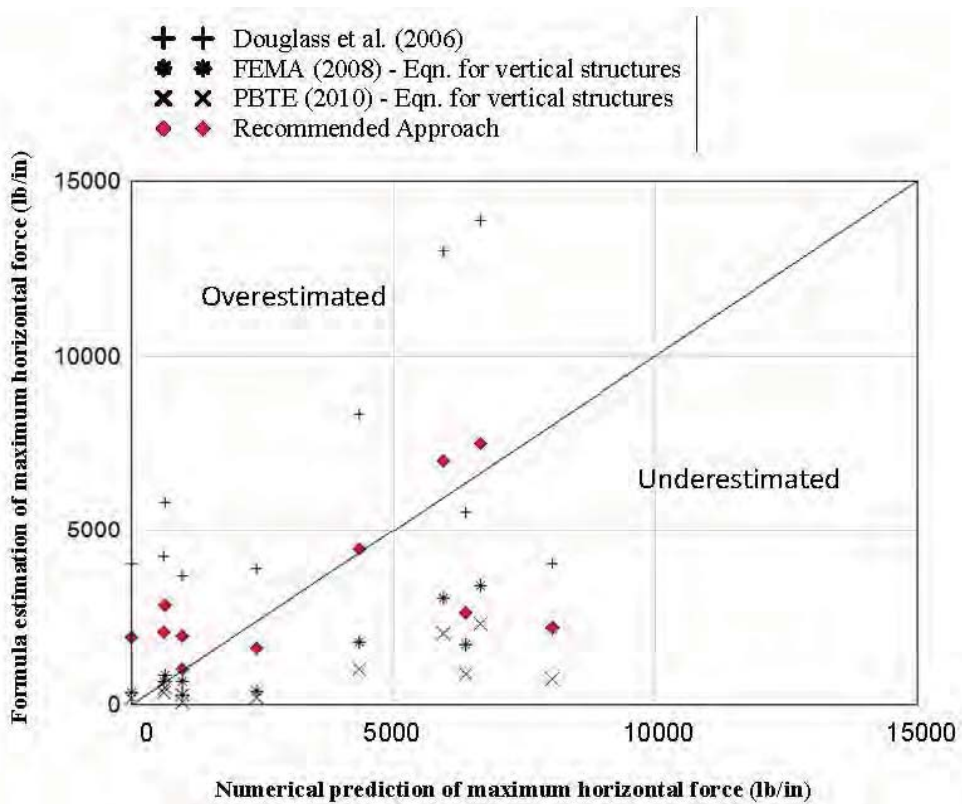


FIGURE 7, CCOMPARISON OF NUMERICAL PREDICTION OF HORIZONTAL FORCE VERSUS RECOMMENDED FORMULA ESTIMATE

Vertical Forces

Load effects due to tsunamis that must be considered for estimating vertical force under bridge girders consist of hydrostatic and hydrodynamic pressure. The hydrostatic pressure is induced by water elevation as mentioned earlier while the hydrodynamic pressure is induced by horizontal

and vertical water velocity. The summation of estimated pressures under the bridge superstructure can be estimated by following equation.

$$P = \gamma(\Delta h) + \frac{1}{2} \rho u_x^2 + \frac{1}{2} \rho u_y^2$$

However, the hydrodynamic force induced by the vertical component of water velocity is relatively small compared to the corresponding hydrostatic and hydrodynamic forces due to horizontal velocity; thus, it can be neglected. Consequently, the maximum vertical force due to tsunami loads can be estimated by the simplified equation below.

$$F_V = \{\gamma(\Delta h_{\max}) + \frac{1}{2} \rho u_{x,\max}^2\} A_v$$

It is important to remember that these maximum forces might not occur at exactly the same time. It is considered appropriately conservative to combine these maximum forces together for design purpose until model testing is conducted to verify the recommendations developed by the research.

In general, the provided tsunami flow field data – water velocity and water elevation – is based on tsunami flow without obstruction (which is a bridge superstructure in this study). The results from the numerical models suggest that the output water elevation and water velocity of tsunami waves near the bridge are higher than the input values. FIGURE 8 shows a plot between input value of water velocity and the output value of water velocity obtained from the numerical models. The output water velocities are measured near the bottom of the seaward external girder as pressures at this location represent up to 80% of total pressure under the bridge cross-section. It can be interpreted that the output water velocity near the bridge superstructure is approximately 3.5 times the input water velocity, based on scattering data shown in FIGURE 8. The relationship between these input and output water velocity can be formulated as shown in the following equation.

$$u_{x,\max} \cong 3.5 u_{x,\max}^*$$

where $u_{x,\max}$ = adjusted horizontal water velocity (output water velocity); and $u_{x,\max}^*$ = input horizontal water velocity.

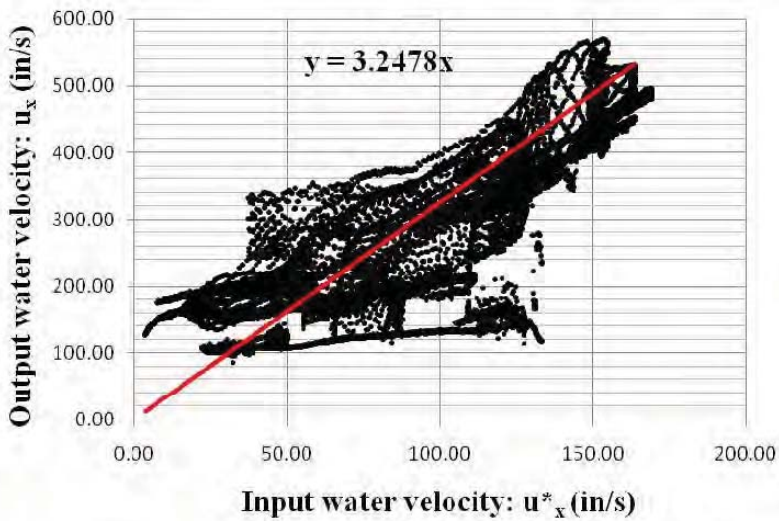


FIGURE 8, COMPARISON OF HORIZONTAL WATER VELOCITY WITH AND WITHOUT OBSTRUCTIONS (BRIDGE SUPERSTRUCTURE)

A comparison of the estimated maximum vertical force and the predicted maximum vertical force obtained from the simulations is shown in FIGURE 9. The estimated vertical forces are observed to be overly conservative for small values and slightly under-estimated for large values. However, the recommended equation is considered appropriate for estimating vertical force due to tsunamis until further study.

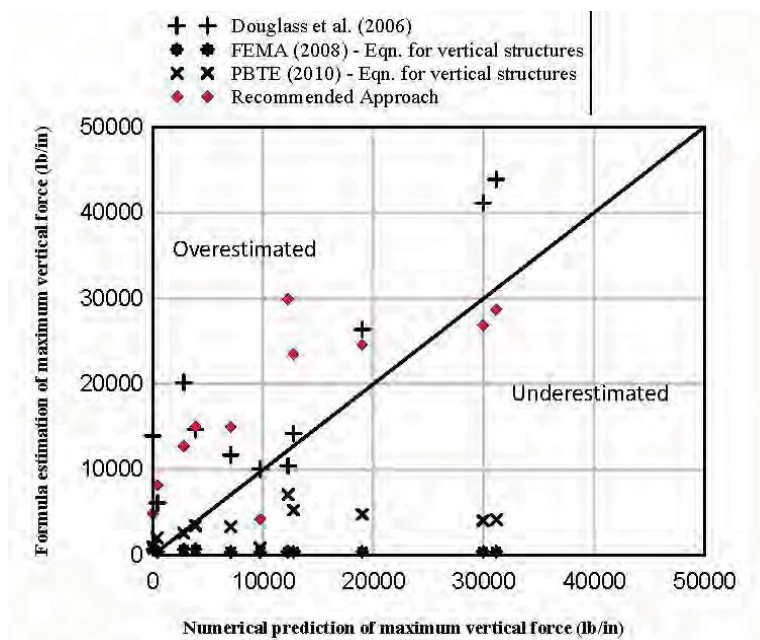


FIGURE 9, COMPARISON OF NUMERICAL PREDICTION OF VERTICAL FORCE VERSUS RECOMMENDED FORMULA ESTIMATE

The maximum percentage values of pressure distribution time-histories under each girder along the cross-section of the deck-girder bridges are not evenly distributed along the cross-section. The model found that a maximum 70 to 100% of total pressure is applied to the external seaward girder and it rapidly decreases for the internal girders. However, the total vertical force is assumed to interact with the bridge at the centroid of the cross-section for simplification at this time.

Conclusions

The recommended approach is intended to be used for estimating tsunami forces on bridge superstructures as preliminary guidance for design. This approach is developed by incorporating those proposed in literature and the time-history of the tsunami forces on bridge superstructures calculated from the numerical models developed in the OSU research. Given the uncertainties in tsunami flow field and lack of laboratory results on realistic bridge model, an appropriate factor of safety should be added into these equations.

The input parameters required for estimating tsunami forces by the recommended approach consist of maximum water elevation, horizontal water velocity, maximum flux momentum, and elevation of bridge superstructure. Moreover, tsunami waves usually loosen sediment saturated with seawater while surging inland increasing the effective fluid density above that of typical seawater. Thus, FEMA (2008) recommended the fluid density be set equal to 1.2 times typical freshwater density for tsunami forces calculation.

The recommended empirical coefficients are given here. The reduction factor for forces on internal girders, C_r , is given as 0.4 which corresponds to that presented in Douglass et al. (2006) as the maximum fluid pressure on the internal girders is approximately 20% to 50% of the pressure on the seaward external girder. The drag coefficient $C_d - 1$ was obtained for bridge superstructures under tsunami loads in this study.

The recommended approach is developed based on the deck-girder bridge section only. It might not be appropriate to apply these recommended equations directly to calculate tsunami forces on other types of bridge superstructures.

ODOT considers the research to be a good start in developing design criteria. However the proposed formulas for estimating forces need to be verified and the coefficient needs to be calibrated to actual experience. Wave tank model testing is one way we are considering to refine the results of the OSU research.

Acknowledgements

This paper is based on research conducted at Oregon State University under contract with Oregon DOT. The work was led by principle investigator, Solomon Yim, with contributors, Sutaporn Boon-Intra, Seshu B. Nimmala, Holly Winston, Mohsen Azadbakht. The tsunami wave simulation was developed by Kwok Fai Cheung, Department of Ocean and Resources

Engineering, University of Hawaii. This paper is a summary of research report to be published in late 2011 by Oregon DOT.

References

- Bea, R.G., Xu T., Stear J., and and Ramos R. "Wave Forces on Decks of Offshore Platforms." *Journal of Waterway, Port, Coastal and Ocean Engineering*, 1999: 136-144.
- Cheung, K.F., Wei Y., Yamazaki Y., adn Yim, S.C. Modeling of 500-year Tsunamis for Probabilistic Design of Coastal Infrastructure in the Pacific Northwest. *Coastal Engineering*, 2011: In Press.
- Douglass, S. L., Q. Chen, and J. M. Olsen. *Wave Forces on Bridge Decks*. Washington: Federal Highway Administration, 2006.
- FEMA P646. Guidelines for Design of Structures for Vertical Evacuation from Tsunamis. Federal Emergency Management Agency, Washington DC, 2008
- Goldfinger. "Deep-water turbidites as Holocene earthquake proxies: the Cascadia subduction zone and Northern San Andreas Fault systems." *Annals of Geophysics*, 2003: 1169-1194.
- Nimmala, S. B., Solomon C. Y., K. F. Cheung, and Yong W. *Tsunami Design Criteria for Coastal Infrastructure: A case study for Spencer Creek Bridge, Oregon*. Technical Report, Salem: Oregon Department of Transportation (ODOT), 2006.
- PBET, Riggs, R., Chock, G., Robertson, I., and Yim, S.C. Development of Performance-Based Tsunami Engineering, NEES Presentation, 2010.
- Tichelaar, B. W., and L. J. Ruff. "Depth of seismic coupling along subduction zone." *Journal of Geophysical Research*, 1993: 15829-15831.
- Wang, K., Wells, R., Mazzotti, S., Hyndman, R.D., and Sagiya, T. A revised dislocation model of interseismic deformation of the Cascadia subduction zone. *Journal of Geophysical Research*, 2003: 108(B1), 2026, doi: 10.1029/2001JB001227.
- Yamazaki, Y., and Cheung K.F. Shelf resonance and impact of near-field tsunami generated by the 2010 Chile earthquake. *Geophysical Research Letters*, 38, doi:10.1029/2011GL047508, in press. 2011
- Yeh, H. "Design Tsunami Forces for Onshore Structure." *Journal of Disaster Research Vol.2 No.6*, 2007: 531-536.
- Yeh, H., I. Robertson, and J. Preuss. *Development of Design Guidelines for Structures that Serve as Tsunami Vertical Evacuation Sites*. Olympia: Washington State Department of Natural Resources, 2005.

FHWA SEISMIC HAZARD MITIGATION RESEARCH PROGRAM

W. Phillip Yen, PhD, PE¹

Abstract

This paper describes the Federal Highway Administration's (FHWA) seismic research program to mitigate earthquake loss of highway infrastructures. Since 1992, FHWA has initiated three major research projects in the seismic hazard mitigation; they are Seismic Vulnerability Study for Existing and New Highway Constructions, Seismic Vulnerability of Highway System, and the SAFETEA-LU Seismic Research Program. Major products of these three research programs were introduced and future developments under the current studies and recommended future studies due to the effects of recent large devastated earthquakes were also discussed.

Introduction

The public relies on highways for the safe transport of goods and people across the country. Because roads serve as critical lifelines in the delivery of basic daily needs, they need to function even in the face of adverse weather and natural hazards. From 1993–1996, the United States spent approximately \$250 million per week responding to the impacts of natural disasters, with earthquakes, hurricanes, and floods being the major causes of monetary losses. At times, earthquakes can top the list. One of the most costly natural disasters in the United States between the late 1980s and late 1990s was California's Northridge Earthquake of 1994, which resulted in \$20 billion in damages.

The loss of life and extensive property damage inflicted by the 1989 Loma Prieta and 1994 Northridge earthquakes emphasized the need to minimize seismic risks to the U.S. highway system. Seismic research projects conducted by the Federal Highway Administration (FHWA) are developing mitigation approaches to reduce those risks, including a method for assessing seismic risks and various structural designs and retrofitting measures.

Since 1992, FHWA has initiated a series of comprehensive seismic research studies targeting retrofitting, design, and risk analysis issues and the seismic research has produced a number of nationally applicable seismic retrofitting manuals and design and risk analysis tools.

¹Principal Bridge Engineer, Office of Bridge Technology, Federal Highway Administration, 1200 New Jersey Ave. S.E., Washington, DC 20590 USA, Email address: Wen-huei.Yen@dot.gov

Early Earthquake Mitigation Research

FHWA initiated its earthquake investigations after the 1964 Prince William Sound Earthquake in Alaska. FHWA's followup focused on how bridge engineers could learn from the Alaska earthquake in terms of geotechnical issues such as soil properties.

Following the defective performance of bridges during the San Fernando Earthquake in 1971, FHWA and the California Department of Transportation (Caltrans) began exhaustive studies of the seismic performance of bridges. FHWA and Caltrans invested \$3 million in basic research to develop national guidelines for bridge seismic design. The study evaluated the criteria used at the time for seismic design, reviewed findings from seismic research for potential use in a new specification, updated guidelines for seismic design, and evaluated the impact of those guidelines on construction and costs.

In 1979, FHWA and Caltrans completed the guidelines, which the American Association of State Highway and Transportation Officials (AASHTO) adopted in 1983 as its *Guide Specification for Seismic Design of Highway Bridges*. This specification became the national standard in 1992, following the Loma Prieta Earthquake. The design philosophy underlying this specification was to prevent collapse of any span or part of a span during large earthquakes. In small to moderate seismic events, the code's intent was for bridges to resist seismic loads without significant damage to structural components. Under this code, the design earthquake has a 475-year return period.

ISTEA and the Seismic Research Program

FHWA's earthquake research did not end with the adoption of this 1992 standard. The agency renewed its commitment to mitigating effects on highway structures by establishing a seismic research program, as called for in the Intermodal Surface Transportation Efficiency Act (ISTEA) of 1991. The National Center for Earthquake Engineering Research, later renamed the Multidisciplinary Center for Earthquake Engineering Research (MCEER), conducted this program for FHWA. Under ISTEА, Congress funded the research with more than \$14.5 million between 1991 and 1997, and the program covered all major highway system components (bridges, tunnels, embankments, retaining structures, and pavements). Approximately 65 percent of the Nation's 600,000 highway bridges were constructed prior to 1971, with little or no consideration given to seismic resistance. In recognition of that situation, the FHWA seismic research program initiated two comprehensive studies. In the fall of 1992, the program began studying the seismic retrofitting of existing highways, and in spring 1993 began studying the seismic design of new highways.

The first product of this research, *Seismic Retrofitting Manual for Highway Bridges* (FHWA-RD-94-052), appeared in 1995 and summarized lessons learned from more than 20 years of earthquake engineering research and implementation, and provided procedures for evaluating and upgrading the seismic resistance of existing bridges. In 1999 the program published *Impact Assessment of Seismic Design of*

Highway Structures, which became the major documentation used to develop recommendations for the seismic design of new bridges. In 2006, FHWA issued the final products of this research, *Seismic Retrofitting Manual of Highway Structures—Part I (Bridges)* (FHWA-HRT-06-032) and *Part II (Retaining Structures, Slopes, Tunnels, Culverts, and Roadways)* (FHWA-HRT-05-067). These new seismic design specifications were performance-based, and the major difference between them and the 1992 design code was that they had a two-level design criterion. The higher level was based on a 1,000-year return period, and the lower on a 100-year period.

Seismic Research Under TEA-21

In 1998 FHWA launched a congressionally mandated seismic research program under the Transportation Equity Act for the 21st Century (TEA-21), funded by another \$12 million, to study seismic vulnerability. In cooperation with MCEER, the program conducted a series of studies to develop tools for evaluating and assessing the social costs and impacts of earthquakes on the U.S. highway system. The goal was to reduce the likelihood of damage to existing and future highway structures caused by moderate to significant seismic events.

The main tasks undertaken within this program were the following:

- Development of loss estimation methods for highway systems
- Preparation of a manual for the seismic design and retrofitting of long-span bridges
- Development of protective systems and a systems design manual for bridges
- Specialized ground motion, foundation, and geotechnical studies

Under TEA-21, FHWA worked with the National Cooperative Highway Research Program (NCHRP) in 2001 to develop new seismic design specifications. The project number and name was NCHRP 12-49, Comprehensive Specification for the Seismic Design of Highway Bridges. AASHTO then reviewed and revised the new design specifications and adopted them in 2007. The NCHRP 12-49 specification was developed from the 1999 recommendations and is about the same. The 2007 specification is a one-level design criterion for a 1,000-year return period.

With the TEA-21 seismic research program, FHWA developed a software package called REDARS: Risks from Earthquake DAmage to Roadway Systems to estimate the loss of highway system capacity due to earthquakes. The tool helps bridge owners estimate how earthquake damages affect post-earthquake traffic flows and enables them to consider those effects during pre-earthquake planning and prioritizations, and in post-earthquake responses, such as rescue and management of damage investigations. The seismic research program released REDARS in 2006.

REDARS is a multidisciplinary tool for seismic risk analysis of highway systems nationwide. For any given level of earthquake, REDARS uses state-of-knowledge models to estimate seismic hazards (ground motions, liquefaction, and surface fault rupture); the resulting damage (extent, type, and location) for each component in the highway system; and repairs of each component's damage, including costs, downtimes, and time-dependent traffic (that is, the component's

ability to carry traffic as the repairs proceed over time after the earthquake).

REDARS incorporates these traffic states into a highway network link-node model to form a set of system-states that reflect the extent and spatial distribution of roadway closures at various times after the earthquake. REDARS then applies network analysis procedures to each system-state in order to estimate how these closures affect systemwide travel times and traffic flows. Finally, REDARS estimates corresponding economic losses and increases in travel times to and from key locations or along key lifeline routes. Users can apply these steps for single earthquakes with no uncertainties (deterministic analysis) or for multiple earthquakes and in estimates of seismic hazards and component damage (probabilistic analysis).

Although REDARS adequately replicated the performance of the highway system in the San Fernando Valley during the Northridge Earthquake, much work still needs to be done to enable engineers to use the methodology with confidence. Indeed, the researchers developed REDARS with the expectation that new and more sophisticated modules will be developed over time to improve its accuracy and expand its range of application.

Also in 2006, the program published the *Seismic Retrofitting Manual for Truss Bridges*, particularly addressing truss bridges that are more than 500 feet (152 meters) long. The program also released a third report, *Isolation Bearing Design/Retrofit Manual*, in 2006.

SAFETEA-LU Seismic Research

In 2005, Congress passed the Safe, Accountable, Flexible, Efficient Transportation Equity Act: A Legacy for Users (SAFETEA-LU). Under the new legislation, FHWA oversaw \$12.5 million in seismic research to work with the bridge engineering community and enhance the earthquake resistance of U.S. highway bridges.

Also, SAFETEA-LU mandated a technology exchange and transfer task, which FHWA conducted through a series of bridge engineering workshops and conferences held nationally and internationally. The meetings involved exchange of technical information and performance of cooperative studies.

The outcomes of the succession of programs held over the past four decades include greater understanding in three areas: seismic vulnerability of specific locations, geotechnical hazards, and infrastructure vulnerability. Building on this increased body of knowledge, FHWA currently is developing improved seismic designs for new and retrofitted bridges, plus instrumentation to monitor performance.

(1) Assessing Seismic Vulnerability: Hazard Maps

To design a bridge to resist earthquakes, understanding the seismic vulnerability or earthquake intensity of the bridge's location is essential. This vulnerability usually is described as seismic hazard. The U.S. Geological Survey (USGS) publishes National Seismic Hazard Maps that display various probability levels of earthquake

ground motions across the United States. The seismic provisions of building codes, insurance rate structures, risk assessments, and other public policy provisions commonly apply probability levels based on the hazard maps.

A 2003 update of the maps incorporates new findings on earthquake ground shaking, faults, and seismicity (that is, how prone a region is to earthquakes). USGS derived the new maps for a grid of sites across the United States by calculating seismic hazard curves that describe the frequency of exceeding a set of ground motions. Currently, the new seismic design and retrofitting criteria for bridges use a 1,000-year return period for a given level of earthquake, which represents not greater than a 7 percent probability of that earthquake occurring during a bridge design life of 75 years. AASHTO and USGS issued the new maps and computer software for obtaining seismic hazards by entering ZIP Codes or longitudes and latitudes.

(2) Assessing Geotechnical Hazards

Another factor in designing and retrofitting highway bridges is the geotechnical hazards that earthquakes can trigger, such as soil liquefaction and settlement, slope failure (landslides and rockfalls), surface fault ruptures, and flooding. Assessing geotechnical hazards is a two-part procedure. First, engineers conduct a quick screening evaluation, generally using information available from field reconnaissance.

If various criteria are satisfied, they consider the risk to be low and require no further evaluations. If a hazard cannot be screened out, they conduct more detailed and rigorous evaluations, which usually require obtaining additional data to assess the hazard and its consequences.

(3) Assessing Infrastructure Vulnerability

To assess the seismic vulnerability of the U.S. bridge inventory, researchers often use an indices method to determine a seismic rating. The method involves assessing a bridge's structural vulnerability, the site's seismic and geotechnical hazards, the socioeconomic factors affecting the structure's importance, and other issues such as bridge redundancy and nonseismic structural issues. Through this method, researchers arrive at a final, ordered determination of the retrofitting priority of individual bridges and, ultimately, for the Nation's entire infrastructure inventory.

The rating system has two parts. The quantitative part produces a seismic rating based on structural vulnerability and site hazard. The qualitative part modifies the rank in a subjective way that accounts for importance, network redundancy, nonseismic deficiencies, remaining useful life, and similar issues to arrive at an overall priority index.

(4) Mitigation Design of New Bridges

Based on advanced seismic research and experience with destructive earthquakes, AASHTO, NCHRP, and FHWA have improved seismic designs for new bridges. The results include design details that directly affect bridge performance under increased loadings due to earthquakes and other natural hazards.

The performance of U.S. highway bridges in recent large earthquakes has shown

that the current state of the art has saved many bridges from collapse caused by unseating of the superstructure or shear failure of the columns,”

The fundamental design objective of current seismic specifications in small to moderate events is to resist seismic loads within an elastic range without significant damage to structural components. The objective in large earthquakes is that no span, or part of a span, should collapse. The specifications consider limited damage to be acceptable in these circumstances, provided it is confined to flexural hinging (that is, a hinge that allows an angle to be adjusted while it remains in place) in pier columns. Further, damage above ground is preferable so that it is visible in sections of the bridge that are accessible for inspection and repair.

Under current specifications, the seismic performance objective is no collapse based on a one-level rather than a two-level design approach. The current single-level design criterion is based on a 1,000-year return period event with not greater than a 5 percent probability of occurring during a bridge’s 50-year design life. As an operational objective, a bridge’s designers may use a higher, two-level performance level, but only with authorization from the bridge’s owners. Current specifications, however, do not provide guidance beyond the one-level approach.

(5) Seismic Retrofitting of Existing Bridges

Retrofitting is the most common method of mitigating risks; in some cases, however, the cost might be so prohibitive that abandoning the bridge (total or partial closure with restricted access) or replacing it altogether with a new structure may be favored. Alternatively, doing nothing and accepting the consequences of damage is a possible option. The decision to retrofit, abandon, replace, or do nothing requires careful evaluation of the structure’s importance and degree of vulnerability. Limited resources generally require that deficient bridges be prioritized, with important bridges in high-risk areas being retrofitted first.

Bridges constructed prior to 1971 in particular need to be retrofitted, based on seismicity and structural types. Toward this end, FHWA issued several publications, including *Seismic Retrofitting Guidelines for Highway Bridges* (FHWA-IRD-83-007) in 1983 and *Seismic Design and Retrofitting for Highway Bridges* (FHWA-IP-87-06) in 1987. In 1995, FHWA updated these manuals with more current knowledge and practical technology; *FHWA Seismic Retrofitting Manual of Highway Bridges* (FHWA-RD-94-052).

Then, as mentioned earlier, FHWA published *Seismic Retrofitting Manual of Highway Structures—Part I and Part II*. This two-volume manual contains the following procedures for evaluating and upgrading the seismic resistance of existing highway bridges:

- A screening process to identify and prioritize bridges that need to be evaluated for seismic retrofitting
- A methodology for quantitatively evaluating the seismic capacity of a bridge
- Retrofitting approaches and techniques for increasing the seismic resistance of existing bridges
- A methodology for determining the overall effectiveness of alternative retrofitting

measures, including cost and ease of installation

The manual does not prescribe rigid requirements as to when and how bridges are to be retrofitted. The decision to retrofit depends on a number of factors, several of which are outside the engineering realm. These other factors include, but are not limited to, the availability of funding and a number of political, social, and economic issues. A bridge may be exempt from retrofitting if it is located in a seismic zone with very little ground motion or has limited remaining useful life. Temporary bridges and those closed to traffic also may be exempt.

Future Developments

The recent huge earthquakes in Japan, Chile, and China have challenged earthquake engineering communities around the world. The intensity of peak ground accelerations and long duration of shaking in large earthquakes create greater difficulties for designing and retrofitting highway bridges. FHWA's seismic research program is exchanging technical information and collaborating on research with seismically active States in the United States and with other countries, including Chile, China, Italy, Japan, Taiwan, and Turkey.

Over the past 15 years, the program has held a series of conferences around the United States and bilateral workshops with other countries to promote new technology and exchange technical information. In 2009, the 25th U.S.–Japan Bridge Engineering Workshop, held in Tsukuba, Japan, marked the silver anniversary of this technology exchange and cooperation.

Under SAFETEA-LU, FHWA is working with MCEER, located at The State University of New York at Buffalo, and the University of Nevada, Reno, to initiate two major seismic research studies to help highway infrastructure face the challenges of big earthquakes yet to come. These studies focus on innovative protection techniques and seismic resilience.

(1) Developing Innovative Technologies

The first study's objective is to improve the seismic resistance of the U.S. highway system by developing innovative technologies, expanding their applicability, and developing cost-effective methods for implementing design and retrofitting technologies. As FHWA applies accelerated techniques to construction of new bridges and maintenance of existing bridges in high seismicity areas, this study is attempting to develop more advanced design details to accommodate large ground motions and increase the mobility and safety of the surface transportation system.

(2) Improving Seismic Resilience

Life-safety (no collapse and no loss of human life) is no longer the sole requirement for success in designing a highway system capable of resisting the impacts of a major earthquake. The traveling public now expects resilience as well—

that is, rapid recovery and minimal impact on the socioeconomic fabric of modern society.

The need for resilience has led to development of the concept of performance-based seismic design. Performance measures calculated by REDARS include congestion and delay times. These measures allow system-level performance criteria to be specified for earthquakes of various sizes, such as maximum permissible traffic delay times and minimum restoration times. Thus, these measures allow resilience of a highway system to be defined and measured in quantitative terms, such as the time it takes to restore the system's pre-earthquake capacity. Accordingly, local transportation authorities can develop financial and societal incentives that will improve resilience and at the same time reduce risk to life and property.

FHWA and others have made substantial progress in this area, particularly with respect to the performance of individual components of the built environment, such as buildings and bridges. But the real potential for performance-based design comes when these concepts are applied to systems and subsystems of the infrastructure, such as transportation networks, subject to both service load conditions and extreme events.

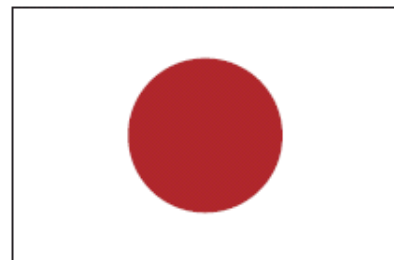
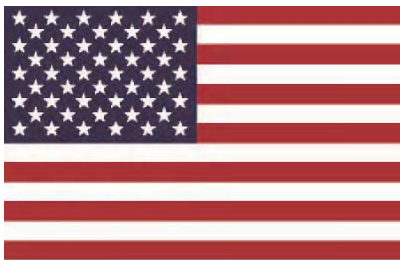
This project's objective is to study the resilience of highway systems with a view to improving performance during major earthquakes. By improving current loss estimation technologies such as REDARS, the FHWA researchers will develop a comprehensive assessment tool to measure highway resilience. They will identify factors affecting system resilience, such as damage-tolerant bridge structures and network redundancy, and develop design aids for curved bridges and structures in near-fault regions. To the extent practical, they will implement the new methodologies and technologies in REDARS and conduct outreach to improve seismic safety.

Concluding Remarks

The greatest difficulty in mitigating earthquake hazards is that seismic events occur without any notice and without any way of accurately predicting when they will occur, nor what their magnitude will be. Earthquakes are devastating, often resulting in a large number of deaths, injuries, and extensive infrastructure damage. These losses occur within minutes. Systematic approaches to evaluating earthquake risks, including indirect losses such as economic impacts, have become an important issue to the engineering community. Hazard mitigation methods to reduce earthquake losses require an enormous effort for development and implementation. FHWA is working closely with AASHTO and NCHRP to mitigate earthquake hazards and reduce losses, and the efforts to implement all practical measures to enhance the safety and mobility of the highway infrastructure are in a race against time with earthquakes.

Reference:

FHWA Congressional Seismic Research Studies under the ISTEA, TEA-21, and SAFETEA-LU Program.



27th US-Japan Bridge Engineering Workshop

Session 3

Seismic2

Failure Investigation and Retrofit Strategies of a 22-Span Steel Girder Bridge during the 2010 Chile Earthquake

By Genda Chen, Zuocai Wang, Phillip W. Yen, and Ian Buckle
Earthquake Response of Highway Bridges Subjected to Long Duration Seismic Motions

By Shojoiro Kataoka
Experimental Investigation of Influence of Live Load on Seismic Response of a Horizontally Curved Bridge

By Ian G. Buckle, Hartanto Wibowo, Danielle M. Smith,
and David H. Sanders

Discussion Method by Using Dynamic Analysis for Quakeproofing Long-Span Bridges
By Shunji Nagahashi, Takumi Nishikawa, Mutsuji Kawakami, and Tatsumi Ujie

Page Left Blank

FAILURE INVESTIGATION AND RETROFIT STRATEGIES OF A 22-SPAN STEEL GIRDER BRIDGE DURING THE 2010 CHILE EARTHQUAKE

Zuocai Wang¹, Genda Chen², Phillip W. Yen³, and Ian Buckle⁴

Abstract

This paper presents a case study on the Cardinal Raúl Silva Henríquez Bridge that was significantly damaged during the Chile Earthquake on February 27, 2010. Field observations and finite element simulations indicated that the bridge failed mainly because the excessive longitudinal load of 22 continuous steel-girder spans was transferred from the girders to their bearing masonry plates at two abutments with a weld connection detail, locally bending the girders due to axial load eccentricity. Parametric studies demonstrated that an effective retrofit strategy can be developed by reducing the number of continuous spans, modifying the connection detail, and increasing the capacity of girders with enlarged bearing seats, additional stiffeners for girders, and thicker flanges and webs.

Introduction

On February 27, 2010, the M8.8 offshore Maule earthquake occurred on a thrust fault along the boundary between the Nazca and South American tectonic plates [USGS, 2010]. The Chile earthquake damaged about 200 bridges and led to 20 collapses. One of the significantly damaged bridges is the Cardinal Raúl Silva Henríquez Bridge. Based on the field inspections by Chen et al. [2010], bottom flanges and webs of the steel girders at abutment supports and the girder-to-abutment weld connections were severely fractured during the earthquake. This type of damage is indicative of the presence of excessive longitudinal loads in the bridge superstructure since only one center expansion joint exists in the entire bridge structure. In addition, the bottom flanges of the girders were welded on masonry steel plates at abutments. This detail is not representative to the common practice in continuous steel girder bridge constructions where a continuous bridge section is simply supported on one fixed bearing and multiple expansion bearings [Saadeghvaziri et al., 2000]. The specific girder-to-abutment connection detail in the Cardinal Raúl Silva Henríquez Bridge attracted not only axial and shear forces but also a bending moment in the longitudinal plane of the bridge under earthquake loads.

¹ Ph.D. Candidate, Dept. of Civil, Architectural, and Environmental Engineering, Missouri University of Science and Technology, Rolla, MO, USA

² Professor, Dept. of Civil, Architectural, and Environmental Engineering, Missouri University of Science and Technology, Rolla, MO, USA

³ Research Structural Engineer, Turner Fairbank Highway Research Center, Federal Highway Administration, McLean, VA, USA

⁴ Dept. of Civil and Environmental Engineering, University of Nevada, Reno, NV, USA

Previous research concluded that steel bridge superstructures are susceptible to damage under low or moderated earthquakes and even more fragile than concrete superstructures if designed improperly [Itani et al., 2004]. For example, bearing failure in the steel girder bridges that were designed without seismic considerations has been commonly seen during previous earthquake events due to insufficient seat length. The load path and the capacity of a bridge system and its individual components at end supports must be evaluated case by case.

The objectives of this study are to investigate the failure mechanism of girders and end bearings at two abutments of the Cardinal Raúl Silva Henríquez Bridge during the 2010 Chile Earthquake and develop various effective retrofit strategies for them through sensitive studies with a finite element model of the bridge.

Bridge Description and Field Observed Damage

(1) Configuration of the Bridge

Built in 2002, Cardenal Raúl Silva Henríquez Bridge is a 22-span, steel-girder structure crossing the Maule River near Constitución in the NE-SW direction. Each span length is 41.5 m. The bridge is supported by two seat-type abutments and twenty-one intermediate bents. As partially shown in Fig. 1, the first five bents from the NE abutment are supported on two reinforced concrete (RC) columns and drilled shafts. The next six bents are supported on three RC columns and drilled shafts. The following eight bents are steel pile bents with three legs (one vertical and two inclined) with horizontal struts and diagonal braces interconnecting the legs in each bent. The last two bents are supported on three RC columns that rest on footings. The bridge superstructure is comprised of two continuous 11-span-long segments with three expansion joints at the two ends and in the middle of the bridge. It is connected to the bridge substructure by elastomeric pads at all piers to allow for longitudinal movement except for two abutments. At each abutment, three girders were welded to their bearing masonry plates that are anchored into the abutment.



Fig. 1 Cardenal Raúl Silva Henríquez Bridge

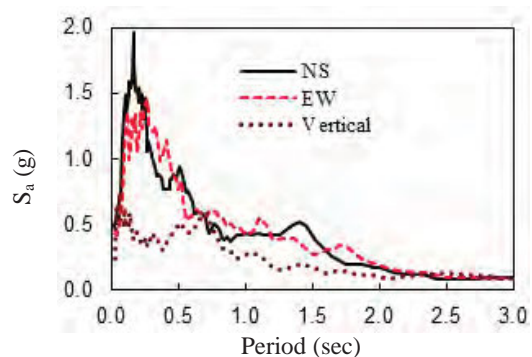


Fig. 2 Acceleration Response Spectra

(2) Acceleration Response Spectra

The 2010 Chile earthquake generated ground motions with long duration and multiple pulses [Boroschek et al., 2010]. The three-component earthquake ground motions at the Hospital Station in Curicó near the bridge site were successfully recorded but not released to the public as of today. However, their acceleration response spectra were made available as shown in Fig. 2. It can be seen from Fig. 2 that the NS and EW acceleration spectra are much larger than the vertical acceleration spectrum in a period range from 0.2 sec to 0.6 sec and from 0.8 sec to 1.5 sec. On the other hand, the natural periods of the particular steel-girder bridge almost fall in this range. In other words, the bridge is more sensitive to the longitudinal and transverse motions.

(3) Field Observed Damage

During the earthquake, the NE portion of the bridge moved transversely from west to east as shown in Fig. 3(a). All steel stoppers were deformed and girders were displaced from their elastomeric pads, resulting in the web and flange bending of the exterior girder about its weak axis. At the NE abutment, the webs and bottom flanges were fractured in all three girders, and both bearing stiffener and web buckled as illustrated in Fig. 3(b). The cause of this type of damage is indicative of excessive longitudinal loads in the superstructure that was resisted by the weld bearing connection at the abutment. At the SW abutment, the welds from the girder bottom flanges to the masonry plates were fractured [Chen et al., 2010].



(a) Girder offset and cross frame buckling (b) Girder fracture at the north abutment

Fig. 3 Superstructure Damage at the NE Portion

Response Spectrum Analysis of the Bridge System

(1) The Grillage Finite Element Model

A typical cross section of the bridge is schematically shown in Fig. 4. The

bridge has a total of 12 types of cross sections with various flange widths and thicknesses. The flange width of steel girders varies from 0.25 m to 0.62 m, and the thickness changes from 12 mm to 40 mm. The height and thickness of girder webs are 2.06 m and 12 mm, respectively. The bridge has two types of steel diaphragms spaced every 2 m. It also has two types of piers: concrete and steel pile bents. The diameter of circular concrete columns is 1.5 m while the outer diameter of the 12-mm thick thin walled circular steel pile is 1.0 m. The concrete bridge deck is 10 m wide and its thickness is 0.25 m.

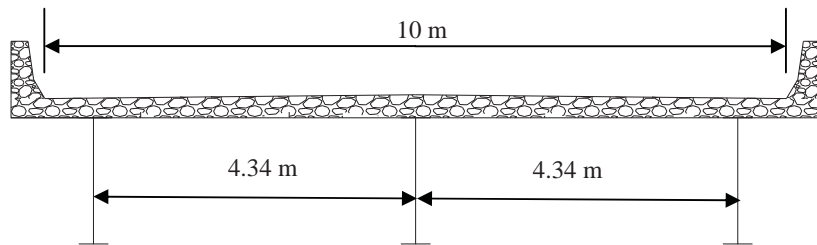


Fig. 4 Bridge Cross Section

To understand its complicated seismic behavior, a grillage mesh finite element model was established to represent the global responses of the entire bridge, and a detailed three-dimensional (3-D) model was created for the local failure analysis of the fractured girder portion. In the global grillage model as shown in Fig. 5, the beam elements were used to represent the bridge decks and other components (girders, bent caps, and columns). The longitudinal beam elements represent the centerline of bridge members passing through the neutral axis of all cross sections. The moment of inertia, cross sectional area and unit mass of the longitudinal grillage members were determined from the properties of as-built girders and a portion of bridge decks based on the effective width of composite beams [Eugene and Damien, 2005].

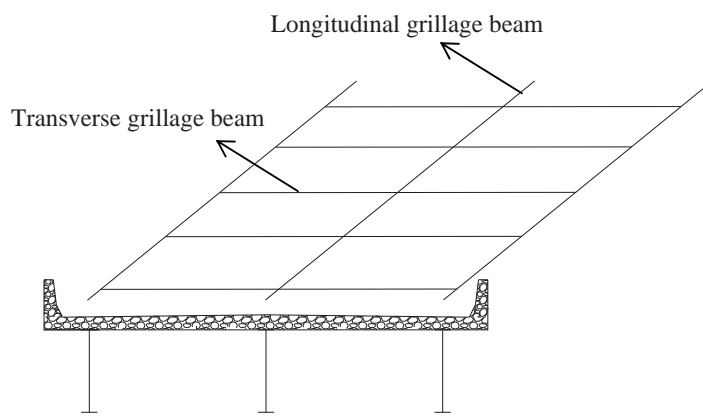


Fig. 5 Grillage Modeling of the Bridge

All transverse grillage members were placed at the location of diaphragms. Their properties were directly calculated from the as-built diaphragm frames. The

equivalent cross area and moment of inertia of each diaphragm frame were calculated based on the equivalent displacement criterion. The properties of bent caps and columns (reinforced concrete or steel tube) were estimated based on their as-built cross sections. The cross sectional areas and moments of inertia of various grillage members are presented in Table 1. Here, I_x and I_y represent the moments of inertial about the strong (horizontal) and weak (vertical) axes of a cross section, respectively. The Young's Modulus of Elasticity for the longitudinal and transverse grillage beams and steel tubes is 2×10^{11} N/m², while that for the concrete bent caps and columns is 2.5×10^{10} N/m².

Table 1 Section Properties of Grillage Beam Elements

Grillage beams		Area (m ²)	$I_x (10^{-3} \text{ m}^4)$	$I_y (10^{-3} \text{ m}^4)$
Longitudinal	1	0.17	51.4	3.3
	2	0.18	92	3.5
	3	0.19	107	3.7
	4	0.19	119	3.9
	5	0.19	123	4
	6	0.18	99	3.5
	7	0.17	84	3.4
	8	0.19	116	3.8
	9	0.21	159	4.4
	10	0.17	78	3.4
	11	0.19	130	4.2
	12	0.18	98	3.5
Transverse	1	0.003	0.002	0.0002
	2	0.007	4.67	0.001
Concrete column		1.78	249	249
Steel pipe		0.04	4.55	4.55

To take into account soil-foundation-structure interaction, all columns in each bent were simply considered to be fixed at certain depth that can be estimated by [Davisson and Robinson, 1965]:

$$L_f = 1.8 \left[\frac{EI}{n_h} \right]^{0.2} \quad (1)$$

in which E and I are the modulus of elasticity and the moment of inertia of columns, respectively, and n_h is the coefficient of the horizontal subgrade modulus of soil materials. The grillage finite element model of the entire bridge was set up with SAP2000 as shown in Fig. 6.

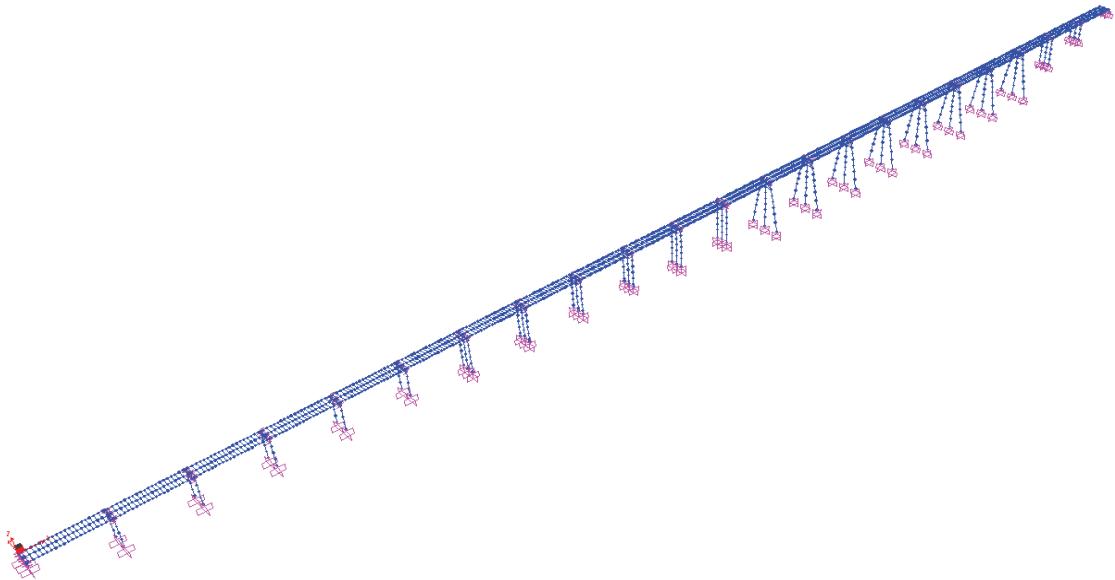


Fig. 6 Finite Element Model of the Bridge based on Grillage Method

(2) Response Spectrum Analysis

The complete quadratic combination (CQC) rule was applied to combine the effects of modal responses [Chopra, 2007]. Therefore, the peak value of a structural response can be written as:

$$r_0 = \left(\sum_{i=1}^N \sum_{n=1}^N \rho_{in} r_{io} r_{no} \right)^{1/2} \quad (2)$$

where N represents the total number of vibration mode of engineering interest; r_0 is a peak response of the bridge system; r_{io} and r_{no} are the peak responses of the i th and n th modes of vibration, respectively; and ρ_{in} is the correlation coefficient between the two modes.

The natural frequencies of the first transverse, first vertical, and first torsional modes of vibration are listed in Table 2. The maximum axial force, bending moment, and shear of the NE end girders where significant damage was observed are presented in Table 3. It can be seen from Table 3 that the maximum axial force is 8750 kN mainly due to the longitudinal earthquake ground motion. Due to load transfer eccentricity (2 m) at each end of the bridge, the axial force causes a significant bending moment at the end of each girder, which is most likely underestimated in design. This moment is almost 6 times as large as that of the bending moment directly caused by the earthquake load.

Table 2 Natural Frequencies of the First Transverse, Longitudinal, Vertical and Torsional Modes

1st Mode	Transverse	Longitudinal	Vertical	Torsional
Natural frequency (Hz)	0.45	1.21	1.85	2.05

Table 3 Maximum Axial Force, Bending Moment, and Shear at the NE End Girders

Axial force (kN)	Moment (kN-m)	Shear (kN)
8750	2970	240

3D Finite Element Model for the Fracture Analysis of Girders

To better understand the stress concentration around the fracture location of girders, the area of crack initiation, and the process of failure, a 3D finite element model of a small portion of girder (including bearing stiffeners) was established with ABAQUS. Considering 0.7 m fillet weld on the bottom flange of each girder at the abutments or 0.7 m bearing seat length, the detailed 3D model is selected to be 1.7 m long as schematically illustrated in Fig. 7(a). The steel girder and reinforced concrete deck were modeled by plate and solid elements, respectively, as shown in Fig. 7(b). The portion of the bottom flange of the girder, welded on the masonry plate at abutments, was fixed in the fracture analysis of girders. The flange width and thickness of the girder are 0.28 m and 12 mm, respectively. The web and stiffener thicknesses are 12 mm and 20 mm, respectively. The maximum axial force obtained at the end of girders from the global grillage model of the bridge system was divided into two components based on the weight ratio between the bridge deck and steel girders. Each component was uniformly distributed and applied on its respective deck or girder cross section.

To understand the crack initiation and failure process, four (4) load cases were considered for elastic-plastic analysis: 130, 300, 440, and 700 kN. The stress distribution for each case is presented in Fig. 8. It can be observed from Fig. 8 that damage likely initiated at the bottom flange of the girder under an axial load of 130 kN. Cases 2 and 3 in Fig. 8 indicate that the maximum stress will extend into the girder web in the area of observed damage after the Chili Earthquake. Eventually, the girder failed at an axial force of 700 kN, which is 8% of the maximum axial load obtained from the response spectrum analysis. Based on the stress distributions under various load cases and field observations, it was verified that the web fracture was indeed caused by the excessive longitudinal load, which can be estimated to be approximately 12 times of the actual capacity of the steel girder bearing system.

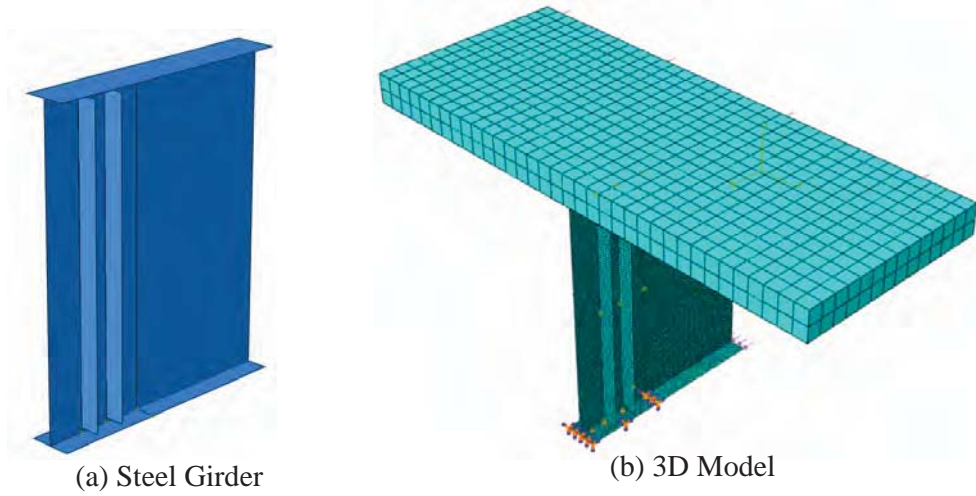


Fig. 7 Modeled Portion of Steel Girder and ABAQUS 3D Finite Element Model

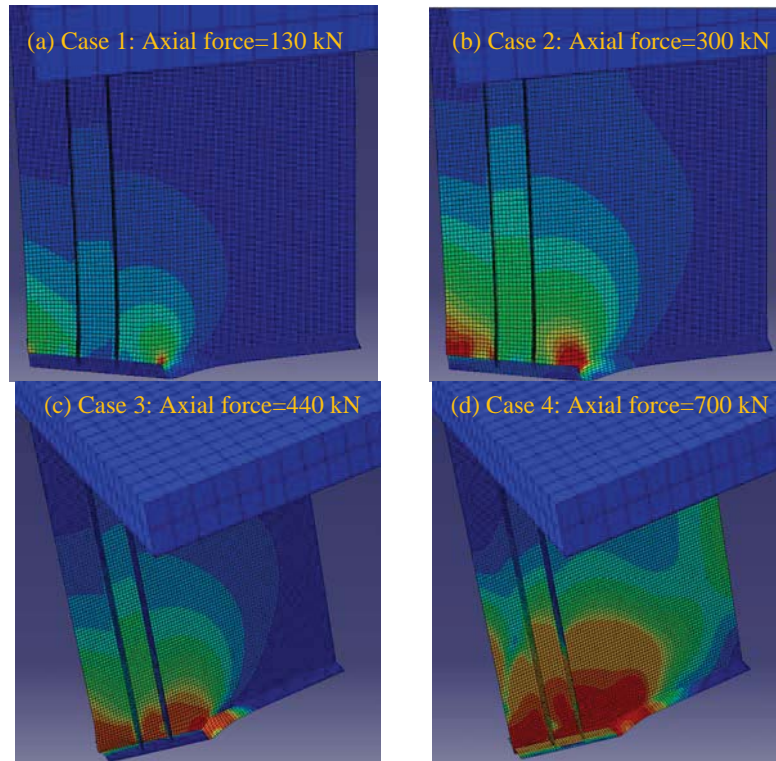


Fig. 8 Stress Distribution under Each of Four Axial Forces

Parametric Study

In this section, several potential retrofit strategies are investigated either by reducing the longitudinal earthquake load or increasing the seismic capacity to ensure a smooth transfer of the seismic load from the girder to abutment. To limit the scope of

work, it is assumed that both abutments are adequate to transfer the seismic loads from the bridge superstructure to ground. Example retrofit strategies for the bearing connections include:

1. Reducing the longitudinal seismic load by increasing the number of joints in bridge superstructure (both deck and girder) so that bearing elements between the super- and sub-structure can transfer the seismic load satisfactorily,
2. Changing the bearing connection detail between the bottom flange of girders and the masonry plate of abutments, and
3. Increasing the seismic capacity of the girder-to-abutment system by increasing the thicknesses of web and bottom flange, the number of stiffeners, and the bearing area at abutments.

More advanced retrofit strategies include the use of base isolators at each bent and abutment so that the longitudinal load on each bent can be regulated based on its available capacity for load transfer, and the use of passive energy dissipation systems so that earthquake energy can be dissipated. In what follows, only the three strategies that are detailed above are discussed.

(1) Number of Joints

One effective way to reduce the longitudinal seismic force is to increase the number of joints at intermediate bents. Towards this endeavor, the number of continuous spans was considered to be 1, 2, 3, 4, 5, and 6. In each case, the longitudinal force calculated from the response spectrum analysis based on the grillage beam model is shown in Fig. 9. It can be clearly seen from Fig. 9 that the axial force is significantly reduced as the number of continuous spans is reduced.

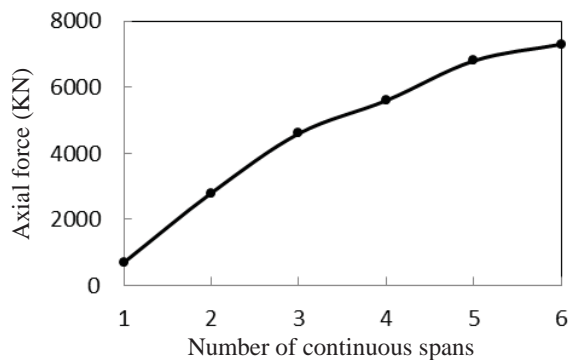


Fig. 9 Axial Force at the End Girder of Bridge with Various Continuous Span Numbers

On the other hand, more expansion joints in bridge deck mean more maintenance since these are often the areas for water leakage and corrosion developed over the years. Furthermore, as the number of expansion joints increases, the redundant effects for extreme loads diminish. Therefore, there must be a tradeoff between seismic performance and maintenance cost in practical applications or advanced retrofitting strategies with dampers and isolators can be developed.

(2) Bearing Connection Detail

Bearing capacity can be increased by using thicker web and bottom flange of girders, additional stiffeners, and extended bearing seat. For parametric studies, a total of 18 elastic-plastic analyses of the 3D finite element model of girders were conducted with complete combinations of the following parameters:

1. Thickness of web and bottom flange = 12, 25, and 50 mm,
2. Bearing seat length = 0.7, 1.0, and 1.2 m, and
3. Additional web stiffener of 30 mm thick = 0 and 3 as illustrated in Fig. 10.

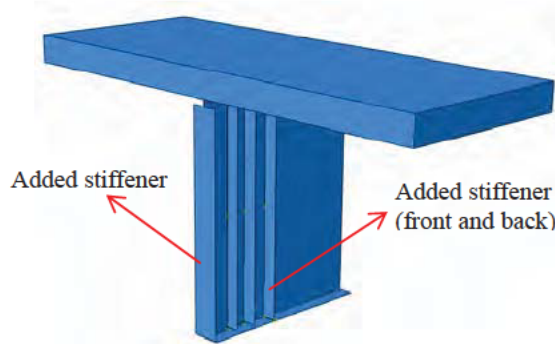


Fig. 10 Three Added Stiffeners at the End of the Girder

The additional stiffeners were considered to be welded on the web and the bottom flange of the girder. They function as tension and compression members under the end bending moment caused by the longitudinal earthquake load and help transfer them from the girder to the masonry plate and then abutment.

The axial force capacities of the retrofitted bearing connection at the end of the girder are listed in Table 4 with no added stiffeners and in Table 5 with three added stiffeners. The axial force is considered to be applied at the same location as the seismic axial load determined from the global bridge analysis.

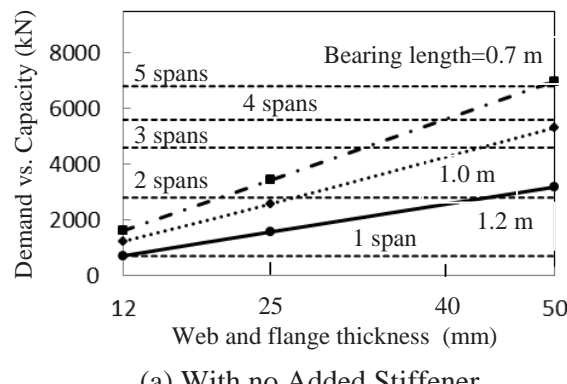
Table 4 Axial Load Capacities of Retrofitted Bearing Connections with no Added Stiffeners (kN)

Plate thickness (mm)	Bearing seat length (m)		
	0.7	1	1.2
12	710	1226	1612
25	1568	2575	3425
50	3180	5309	6982

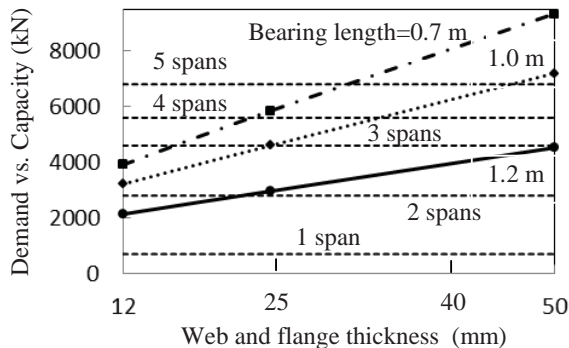
Table 5 Axial Force Capacities of Retrofitted Bearing Connections with Three Added Stiffeners (kN)

Plate thickness (mm)	Bearing seat length (m)		
	0.7	1	1.2
12	2137	3215	3907
25	2961	4599	5843
50	4520	7192	9329

In retrofitted design, the seismic capacity of the structure must be larger than the seismic demand by a certain safety margin. As indicated in Tables 4 and 5 for the Cardenal Raúl Silva Henríquez Bridge, only when the thickness of the web and flange is increased to 50 mm, three 30 mm thick stiffeners are added at the girder end, and the bearing seat is lengthened to 1.2 m can the retrofitted bearing connection transfer the excessive longitudinal earthquake load from the girder to abutment without requiring additional expansion joints over intermediate bents. If the number of continuous spans is reduced, the longitudinal earthquake load can be significantly reduced and thus more bearing connection retrofitting options in Tables 4 and 5 are viable in design. For instance, Fig. 11 shows the seismic demand versus seismic capacity for various combinations of reducing span numbers and increasing web/flange thickness and bearing seat length; when the bridge girders are simply supported, the current bridge design can transfer the earthquake-induced load. For a specified continuous span number, the seismic demand (axial load) can be determined from a global bridge analysis as shown in dash line in Fig. 11. Various retrofitting options as shown in solid, dotted, and long dash dotted lines in Fig. 11, which can increase the seismic capacity (axial force) above the seismic demand, can be considered as viable designs with adequate performance.



(a) With no Added Stiffener



(b) With Three Added Stiffeners

Fig. 11 Seismic Demand (Load) versus Seismic Capacity (Force) for Various Continuous Span Numbers and Bearing Connection Retrofit Designs

Fig. 11 also indicates that if the bearing weld connection were changed to a pin connection, the bending moment due to the welded bottom flanges of girders at abutments would disappear and the bending moment due to load eccentricity would be approximately $8750 - 2970 = 5780$ kN. Indeed, re-running the grillage beam model with pin supports at two abutments gave a moment of 6800 kN. Even with pin supports, the bridge must be retrofitted further by increasing seismic capability such as adding three stiffeners and/or increasing web/flange thicknesses. The main difference between the pin and fixed supports, however, lies in the design of masonry plates and abutments. With pin supports, the masonry plates are subjected to both axial and shear forces only, which can be significantly less demanding in comparison with the fixed supports as seen in the current bridge design.

Conclusions

To understand the main causes of the steel girder fracture and weld fracture of a 22-span Cardenal Raúl Silva Henríquez Bridge during the 2010 Chile Earthquake, a grillage beam model of the entire bridge system and a 3D finite element model of the bearing connection at bridge abutments have been developed. The representative acceleration response spectra at the Hospital Station in Curicó near the bridge site were used for the global bridge analysis. Parametric studies were conducted to investigate the effects of various retrofit designs at bearing connections. Following is a summary of the preliminary findings from this study:

1. The current bridge design has 11 continuous spans that are all rested on elastomeric bearings except for end bearing connections at abutments. The elastomeric bearings allow for some longitudinal displacement under the longitudinal component of ground motions. Therefore, the fixed girder-to-abutment bearing connection attracted the longitudinal load of all continuous spans, causing fracture damage at abutments.
2. Reducing the number of continuous spans can significantly reduce the longitudinal load applied at the bearing connection system. However, the

current bearing connection design is still inadequate to transfer the longitudinal load unless all girders are simply supported. Their combinations may be necessary to transfer the loads induced by a mega earthquake such as the 2010 M8.8 Chile Earthquake.

3. Increasing the web and flange thickness of girders, number of stiffeners, and length of bearing seats at the bearing connection are all effective measures for seismic retrofitting of the bridge.
4. For the multi-span bridge structure, the longitudinal component of the 2010 Chile Earthquake induced ground motions caused more significant damage than the vertical earthquake motion. Therefore, due considerations must be taken of the longitudinal ground motion effect in bridge design and a decision may have to be made to trade off the seismic design load and the seismic redundancy in lieu of the number of continuous spans.

References

- USGS, Magnitude 8.8 – Offshore Maule, Chile, February 27, 2010, <http://earthquake.usgs.gov/earthquakes/equinthenews/2010/us2010tfan/>, Earthquake Hazards Program, 2010.
- Chen, G.D., Yen, P. W., Buckle, I., Allen, T., Alzamora, D., Ger, J., and Arias, J. G.: 2010 Chile Earthquake Implications to the Seismic Design of Bridges, Proceedings of the 26th US-Japan Bridge Engineering Workshop, pp. 203-216, 2010.
- Saadeghvaziri, M. A., Yazdani-Motlagh, A. R., and Rashidi, S.: Effects of Soil-Structure Interaction on Longitudinal Seismic Response of MSSS Bridges, Soil Dynamics and Earthquake Engineering, vol. 20, No. 1-4, pp. 231-242, 2000.
- Itani, A. M., Bruneau, M., Carden, L., and Buckle, I. G.: Seismic Behavior of Steel Girder Bridge Superstructures, Journal of Bridge Engineering, Vol. 9, No. 3, pp. 243-249, 2004.
- Boroschek, r., Soto, P., Leon, R., and Comte, D.: Terremoto Centro Sur Chile-27 de Febrero de 2010, Informe Preliminar N° 4, Universidad de Chile-Depto. Ingenierial Civil, and Depto. De Geofisica, 2010, 29pp.
- Eugene J. and Damien L. K.: Bridge Deck Analysis, Taylor & Francis e-Library, 2005, 278pp.
- Davisson, M. T., and Robinson, K. E.: Bending and Buckling of Partially Embedded Piles, Proceedings of 6th International Conference on Soil Mechanics and Foundation Engineering, Canada, Vol. III, pp. 243-246, 1965.
- Chopra, A. K.: Dynamics of Structures-Theory and Application to Earthquake Engineering, Prentice-Hall, Inc., New Jersey, U.S.A., 2007, 876pp.

EARTHQUAKE RESPONSE OF HIGHWAY BRIDGES SUBJECTED TO LONG DURATION SEISMIC MOTIONS

Kataoka Shojiro¹

Abstract

Strong motion records obtained during the 2003 off Tokachi, Japan, earthquake (Mw8.0) and the 2010 Maule, Chile, earthquake (Mw8.8) are used to investigate effects of duration of seismic motion on earthquake response of highway bridges. Not much difference was found between the responses excited by the seismic motions from the two earthquakes despite difference of the duration.

Introduction

Current Japanese design specifications (Japan Road Association, 2002) require highway bridges to be checked if the bridges satisfy target seismic performances against Level 1 and Level 2 earthquake motions. Level 1 earthquake motion covers ground motion highly probable to occur during service period of bridges and its target seismic performance is set to have no damage. Level 2 earthquake motion is defined as ground motion with high intensity with less probability to occur during the service period of bridges. The target seismic performance against Level 2 earthquake motion is set to prevent fatal damage for bridges with standard importance and to limit damage for bridges with high importance.

There are two types of Level 2 earthquake motion, i.e. Type I and Type II earthquake motions. Type I represents ground motions from large-scale plate boundary earthquakes, while Type II from inland earthquakes and directly strike the bridges. These design earthquake motions are defined as design acceleration response spectra with damping ratio of 0.05. Time history waveforms are also shown in the design specifications as examples for seismic design using dynamic response analyses. The time history waveforms were produced by spectral fitting using strong motion records as original waveforms; their acceleration response spectra were adjusted to fit to the design spectra by means of a spectral fitting technique.

As for Type I earthquake motion, strong motion records obtained during plate boundary earthquakes of which magnitudes ranging from 7.4 to 8.2 were used as original waveforms. Duration of the example waveforms are up to only 55[s] (duration in this paper will be defined in the next section). Ground motion records with long duration, however, were obtained during the 2003 off Tokachi, Japan, earthquake (Mw8.0) and the 2010 Maule, Chile, earthquake (Mw8.8). Besides, it has been pointed out that super-giant earthquakes, of which magnitudes are as large as 9, may occur in Suruga-Nankai trough, south-western Japan, in the near future – though the 2011 off the Pacific coast of Tohoku earthquake (Mw9.0) had never been imagined.

¹ Senior Researcher, Earthquake Disaster Prevention Division, National Institute for Land and Infrastructure Management (NILIM)

In this paper, effects of long duration seismic motions on earthquake response of highway bridges are investigated using the strong motion records from the 2003 off Tokachi and the 2010 Maule earthquakes.

Strong Motion Records and Adjusted Waveforms

Table 1 lists 10 observation stations where strong motion records were obtained by the Department of Geophysics, the University of Chile, during the 2010 Maule earthquake. The digital data were downloaded from its website (<http://ssn.dgf.uchile.cl>). Locations of these observation stations are shown in Figure 1 with the epicenter and surface projection of the source fault. The strong motion recorded at CCSP (Figure 2) has the largest PGA and the longest duration. In this paper, the duration is defined as the time between first and last moments when amplitudes exceed 50 [cm/s²]. The durations of NS, EW, and UD components of the strong motion at CCSP are 151[s], 152[s], and 122 [s], respectively.

The acceleration response spectrum of EW component of the strong motion at CCSP was adjusted to target response spectra by spectral fitting. The target response spectra are set as shown in Figure 3. Type I, II, and III grounds are stiff, medium, and soft soil conditions, respectively. Since there was no available information about the soil condition at CCSP, three acceleration waveforms that represent Type I, II, and III grounds were produced as shown in Figure 4; the acceleration response spectra of these waveforms were adjusted to the target response spectra (Figure 3) by spectral fitting. The durations of the waveforms produced here are very close to the duration of the original waveform (152 [s]).

Acceleration response spectra of strong motion recorded during the 2003 off Tokachi earthquake were also adjusted to the same target response spectra by spectral fitting. The strong motion records obtained at UKE (Urakawa-Efue), CKB (Chokubetsu), and TCS (Taikicho-Seika) stations were chosen to represent Type I, II, and III grounds, respectively. The original and adjusted waveforms are shown in Figures 5, 6, and 7. The durations of the adjusted waveforms are 75[s], 78[s], and 96[s], which are more than 50[s] shorter than those produced from the strong motion during the 2010 Maule earthquake.

Analytical Models of Highway Bridges

Analytical model of highway bridges and nonlinear models for plastic hinge section of RC piers and seismic isolation bearings are shown in Figures 8 and 9. Rubber bearings, seismic isolation bearings, and fixed bearings were chosen for Type I, II, and III grounds, respectively. Spread foundation was chosen for Type I ground, while pile foundation was chosen for Type II and III grounds. All three analytical models were designed under the current seismic design specifications and their fundamental natural periods are 1.25[s], 1.15[s], and 0.71[s] for Type I, II, and III grounds, respectively.

Earthquake Response of Highway Bridges

Figure 10 shows hysteretic force-displacement response of the analytical model subjected to the long duration seismic motions produced from the strong motion records obtained during the 2003 off Tokachi and the 2010 Maule earthquakes. The amplitudes of the adjusted waveforms were magnified to 1.2 times for seismic input to check nonlinear response of the model more clearly. We can see that peak response displacements of the bridge models due to the adjusted waveforms from the 2003 off Tokachi earthquake are as large as or larger than those from the 2010 Maule earthquake.

Hysteretic force-displacement response of the seismic isolation bearings, adopted for Type II ground, subjected to the long duration seismic motions from the two earthquakes are compared in Figure 11. The amplitudes of the adjusted waveforms were magnified to 1.2 times for seismic input as well. The peak response displacements of the bearings are not much different and do not exceed 250% shear strain.

Table 2 summarizes residual displacements of the analytical models subjected to the long duration seismic motions. The amplitudes of the adjusted waveforms were magnified to 1.2 times and 1.4 times for seismic input. It was found that the residual displacements vary case by case and that seismic motions with longer duration are not always more severe in terms of the residual displacement.

Conclusions

In this paper, strong motion records obtained during the 2003 off Tokachi earthquake (Mw8.0) and the 2010 Maule earthquake (Mw8.8) are used to investigate effects of duration of seismic motion on earthquake response of highway bridges. We could not find notable difference between the responses, i.e. the peak response displacements of RC piers and seismic isolation bearings and the residual displacement, excited by the seismic motions from the two earthquakes though there are differences of more than 50 [s] between their durations. Further investigations will be carried out using the abundant strong motion records obtained during the 2011 off the Pacific coast of Tohoku earthquake.

References

Japan Road Association (2002): Specifications for highway bridges, Part V: Seismic design.

Table 1 Strong motion records obtained from website of the Department of Geophysics, the University of Chile. Directions of horizontal component of olmu are unknown.

Station code	Place	Location			Sampling [Hz]	Number of data	PGA [cm/s^2]		
		Lat. (S)	Lon. (W)	Elev. [m]			NS	EW	UD
ANTU	Campus Antumapu, Santiago	33.569	70.634	640	50	22,779	230.0	265.0	162.3
CCSP	San Pedro, Cancepcion	36.844	73.109	38	100	20,200	633.7	602.3	566.8
CLCH	Cerro Calan, Santiago	33.396	70.537	865	50	22,533	195.3	216.6	103.3
csch	Casablanca	33.321	71.411	260	100	9,000	285.0	322.0	221.0
lach	Colegio Las Americas, Santiago	33.452	70.531	729	100	19,100	304.7	228.7	158.2
melp	Melipilla	33.687	71.214	180	100	9,000	556.1	761.2	377.9
olmu	Olmue	32.994	71.173	173	100	9,000	(244.3)	(346.8)	150.4
ROC1	Cerro El Roble, TilTil	32.976	71.016	2,191	100	60,261	168.4	135.8	113.0
sjch	San Jose de Maipo	33.452	70.531	728	100	18,800	457.4	470.9	234.0
stl	Santa Lucia, santiago	33.440	70.643	614	100	17,900	233.1	330.0	235.7

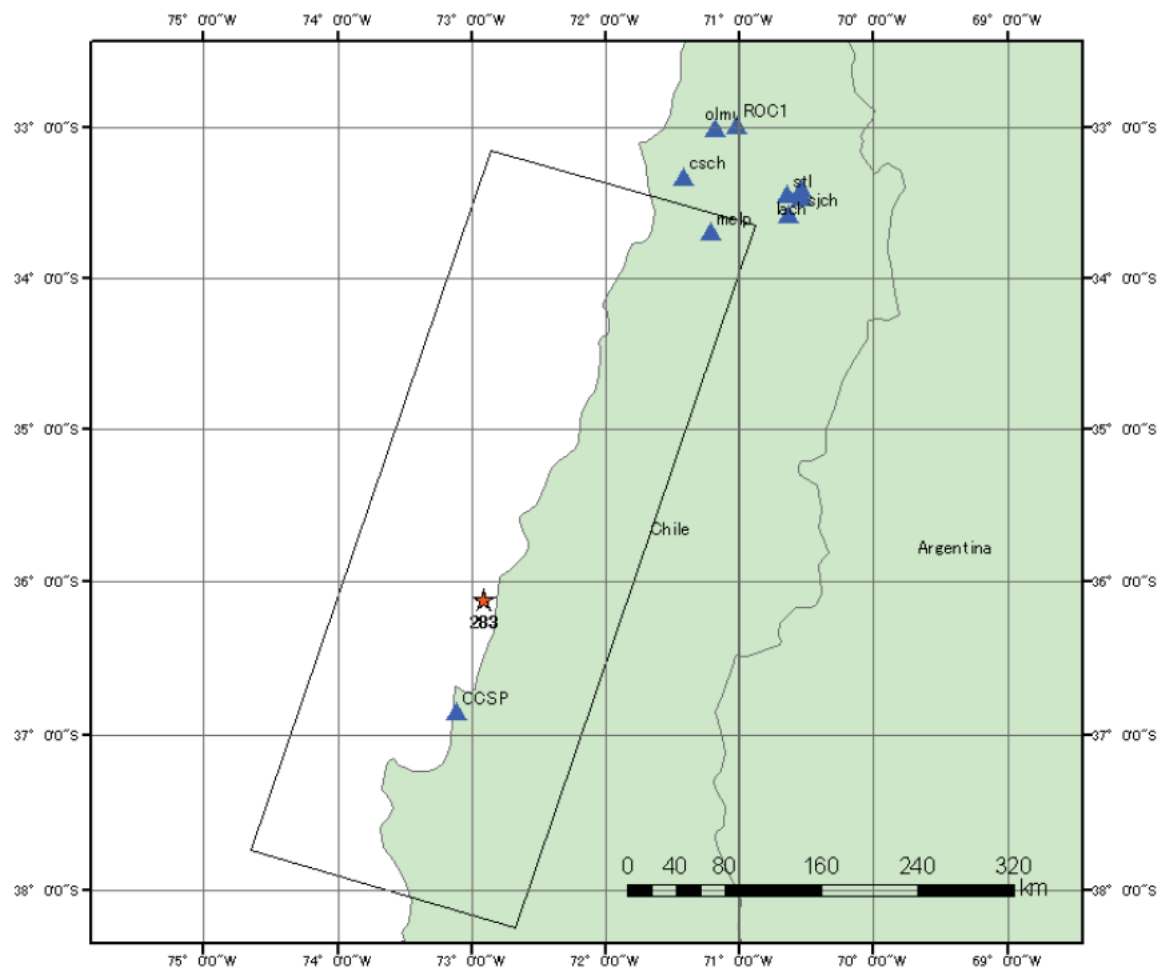


Figure 1 Locations of observation stations of which strong motion records obtained during the 2010 Maule earthquake are available from website of the Department of Geophysics, the University of Chile.

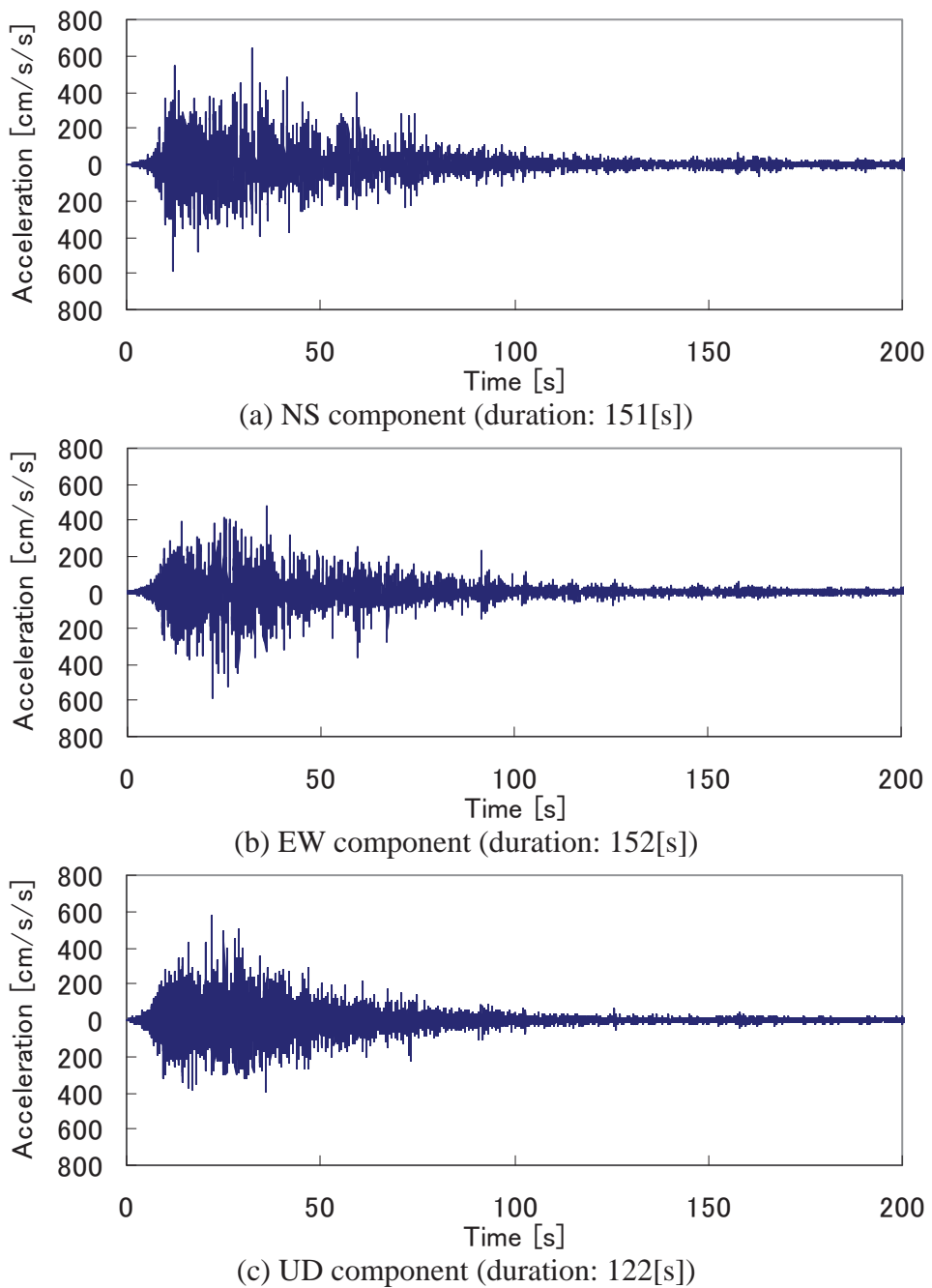


Figure 2 Strong motion recorded at CCSP during the 2010 Maule earthquake.

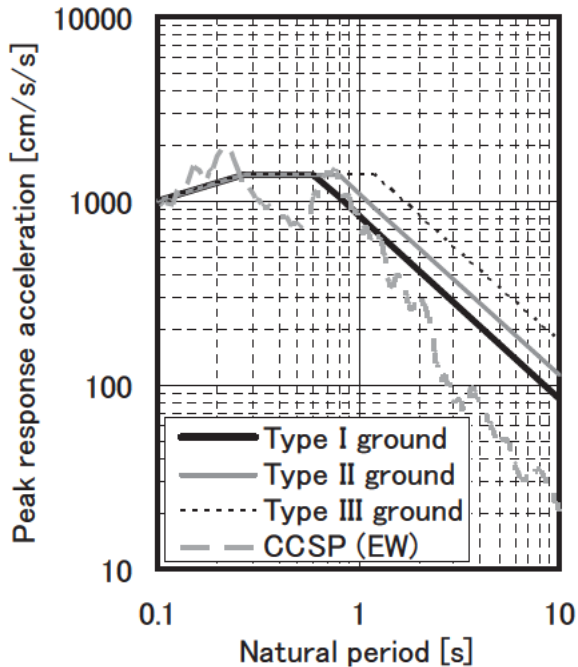
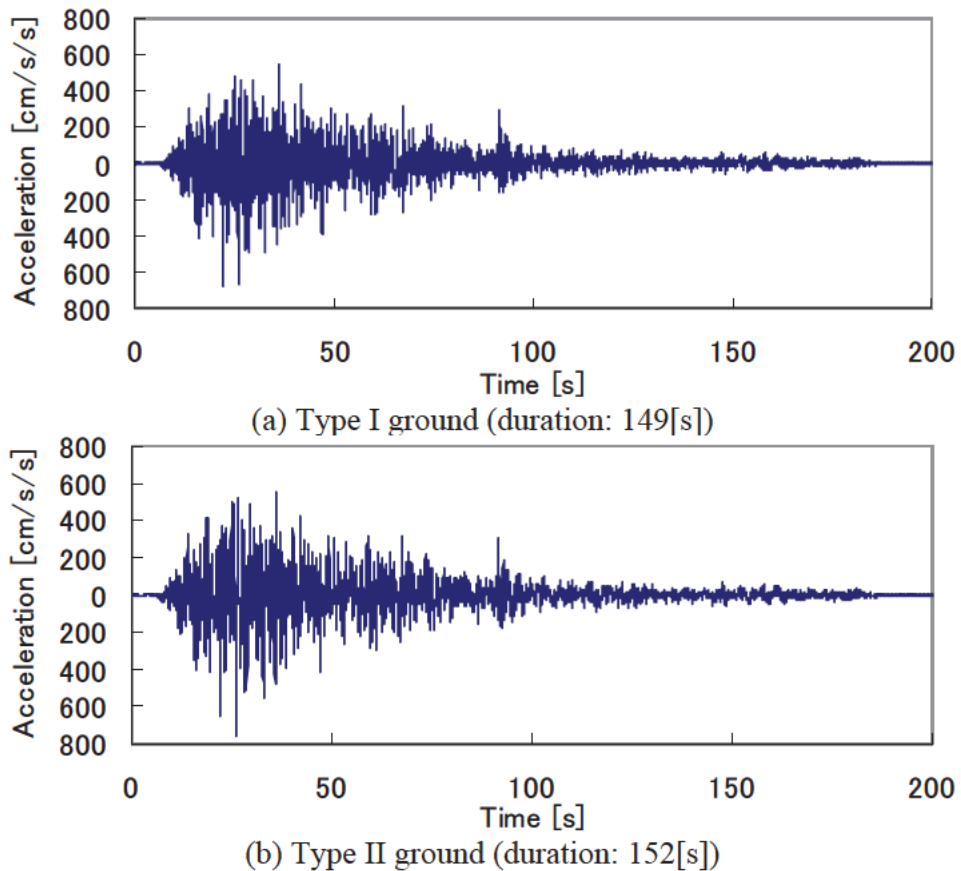
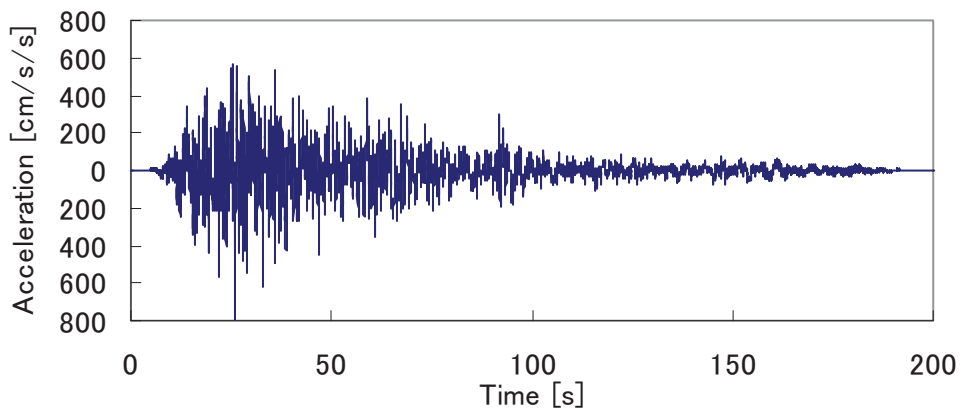


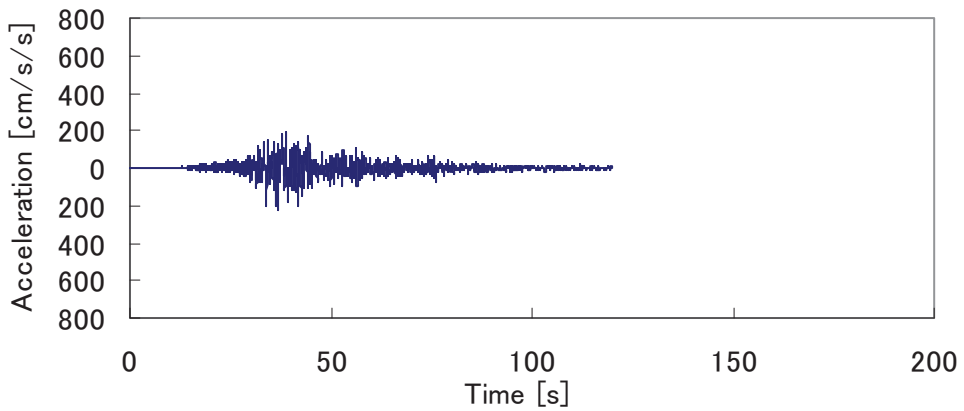
Figure 3 Target acceleration response spectra for spectral fitting of the strong motion records. Type I, II, and III grounds correspond to stiff, medium, and soft soil conditions, respectively. The peak levels of the target response spectra are 1,400 [cm/s²]. The acceleration response spectrum of EW component of the strong motion at CCSP is also shown.



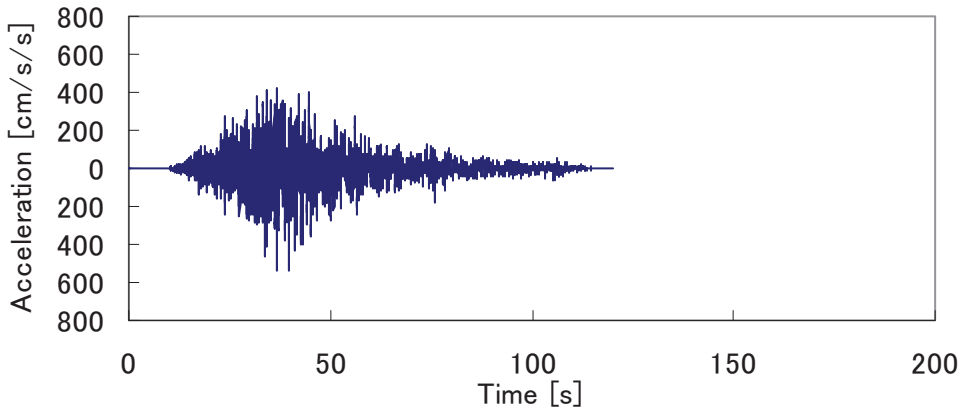


(c) Type III ground (duration: 152[s])

Figure 4 Acceleration waveforms produced by spectral fitting from EW component of the strong motion at CCSP. The acceleration response spectra of these waveforms were adjusted to the target spectra shown in Figure 3.

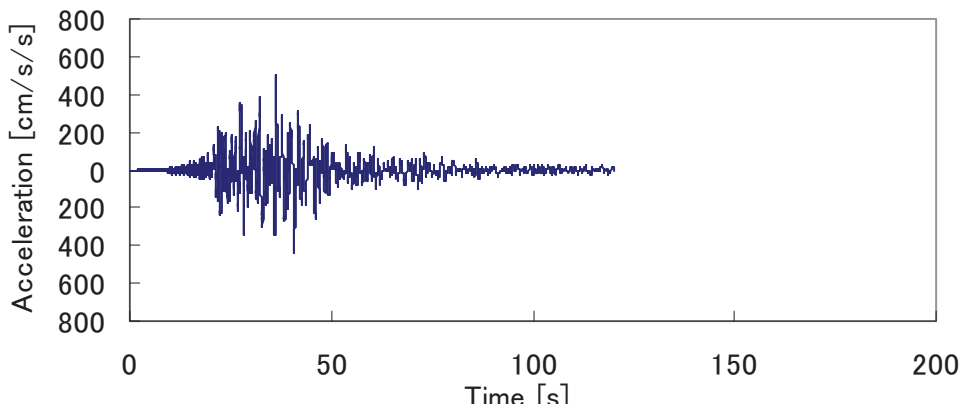


(a) Original waveform (duration: 46[s])

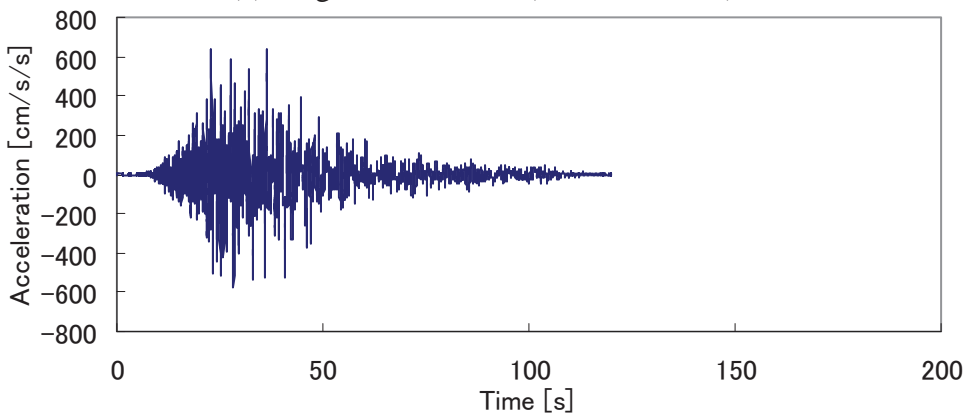


(b) Adjusted waveform (duration: 75[s])

Figure 5 Original (a) and adjusted (b) waveforms for Type I ground. The original strong motion is observed during the 2003 off Tokachi earthquake at UKE (Urakawa-Efue) station. Adjusted waveform was produced by spectral fitting



(a) Original waveform (duration: 68[s])



(b) Adjusted waveform (duration: 78[s])

Figure 6 Original (a) and adjusted (b) waveforms for Type II ground. The original strong motion is observed during the 2003 off Tokachi earthquake at CKB (Chokubetsu) station. Adjusted waveform was produced by spectral fitting

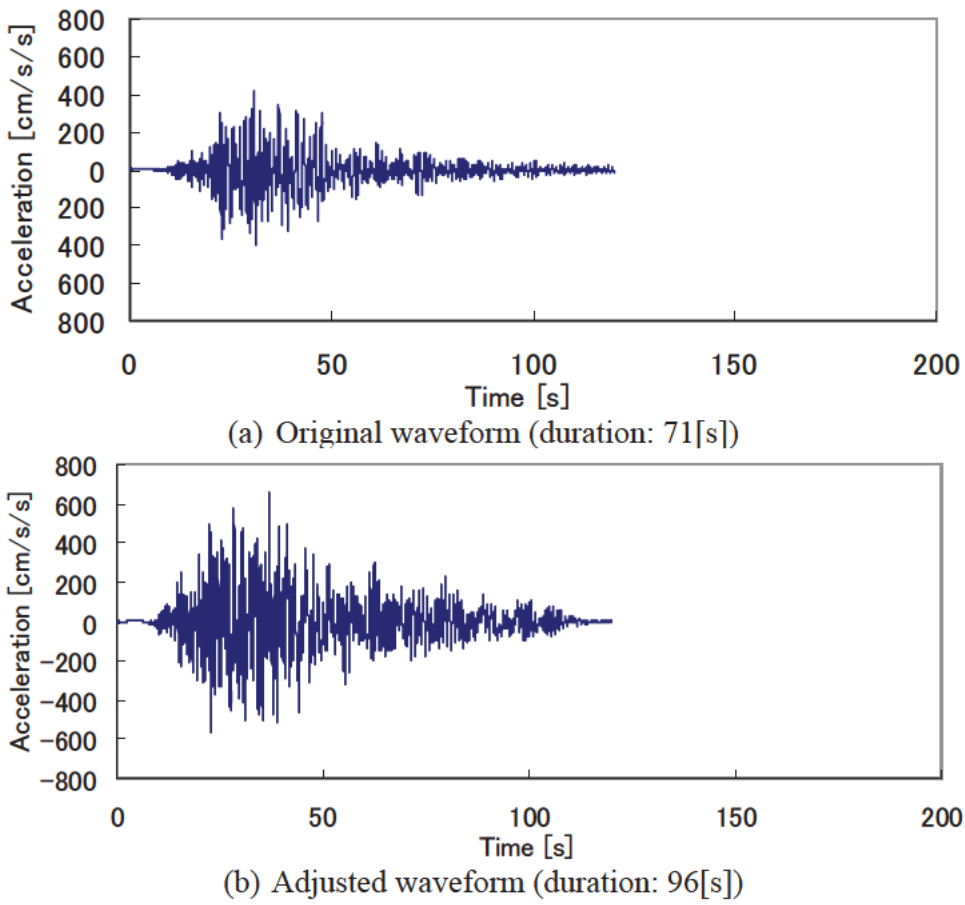


Figure 7 Original (a) and adjusted (b) waveforms for Type III ground. The original strong motion is observed during the 2003 off Tokachi earthquake at Taikicho-Seika (TCS) station. Adjusted waveform was produced by spectral fitting

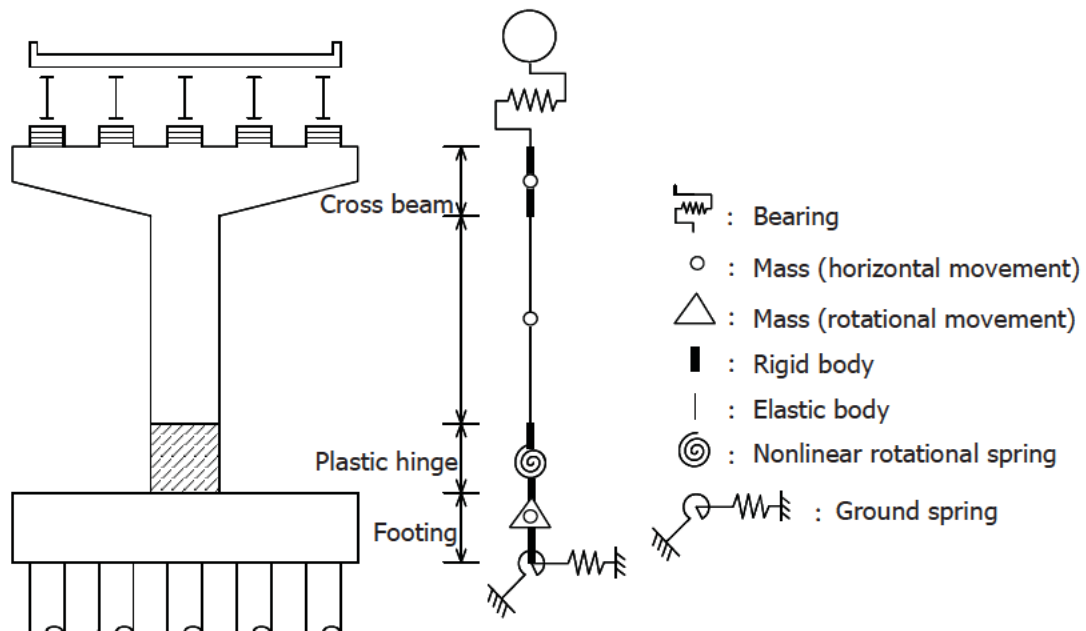
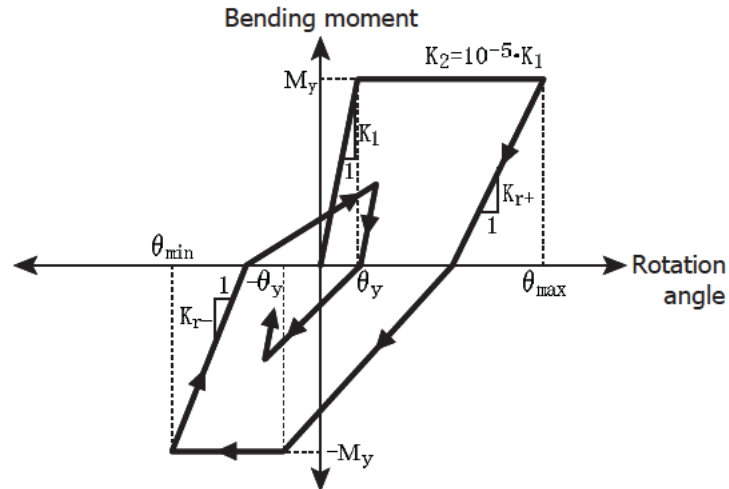
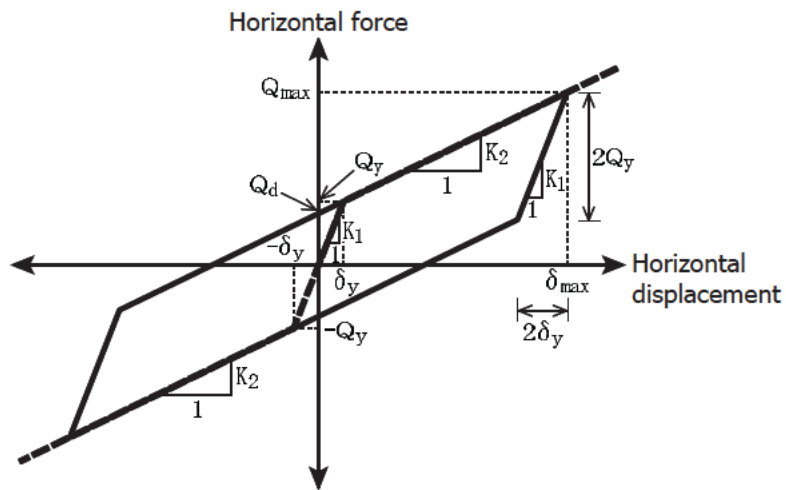


Figure 8 Analytical model of highway bridges. Rubber bearings, seismic isolation bearings, and fixed bearings were chosen for Type I, II, and III grounds, respectively.



(a) Plastic hinge section of RC piers



(b) Seismic isolation bearings

Figure 9 Nonlinear models for: (a) Plastic hinge section of RC piers; (b) Seismic isolation bearings. Seismic isolation bearings are adopted for the highway bridge on Type II ground.

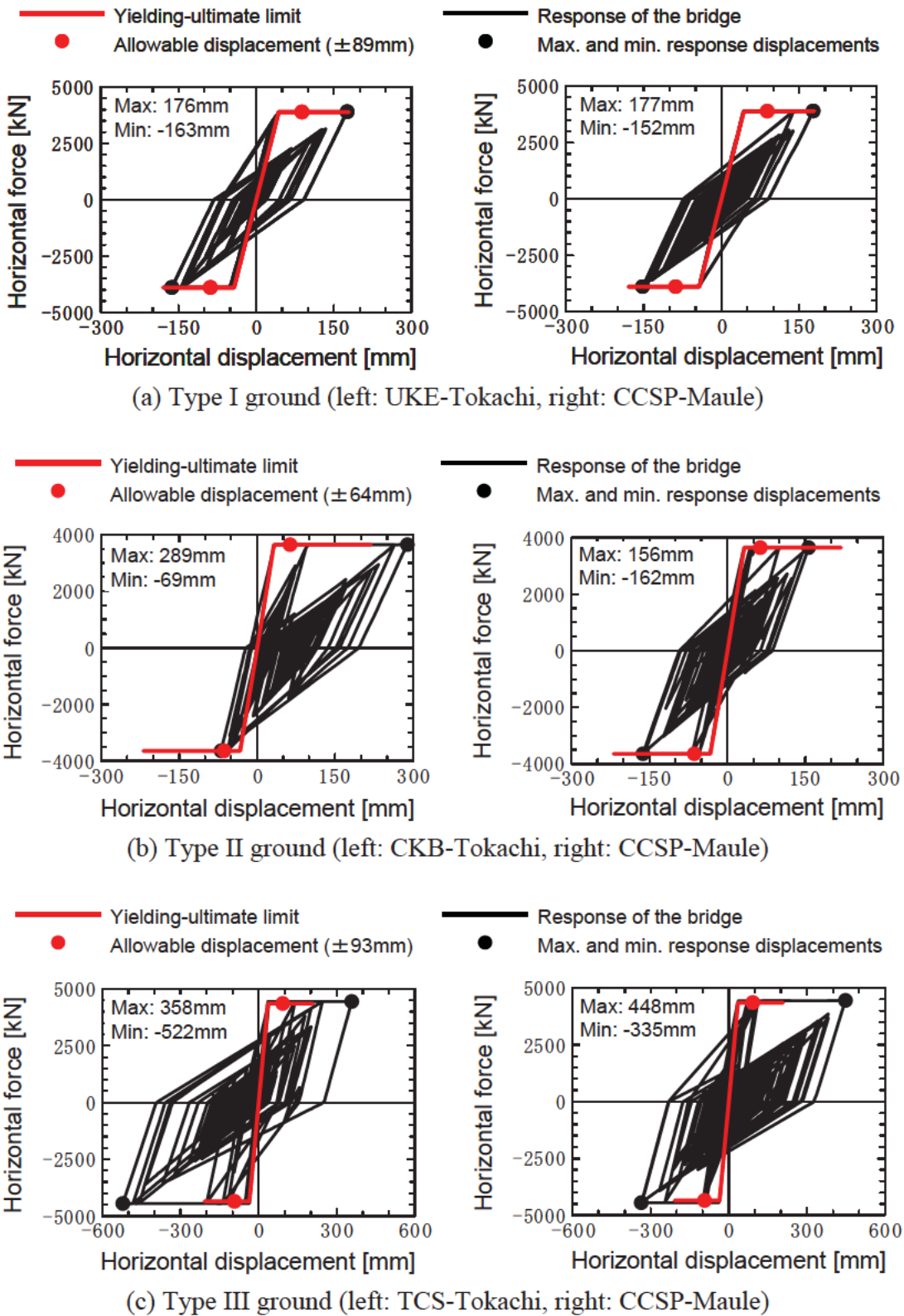


Figure 10 Hysteretic force-displacement response of the analytical model subjected to the long duration seismic waves produced from the strong motion records obtained during the 2003 off Tokachi and the 2010 Maule earthquakes. The amplitudes of the adjusted waveforms were magnified to 1.2 times for seismic input.

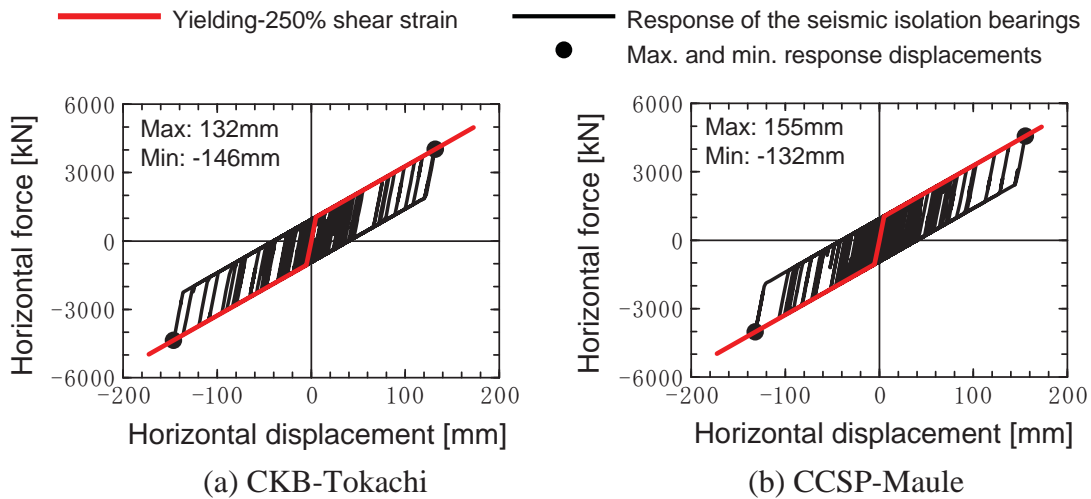


Figure 11 Hysteretic force-displacement response of the seismic isolation bearings, adopted for Type II ground, subjected to the long duration seismic waves. The amplitudes of the adjusted waveforms were magnified to 1.2 times for seismic input.

Table 2 Residual displacements of the analytical models subjected to the long duration seismic motions. The amplitudes of the adjusted waveforms were magnified to 1.2 times and 1.4 times for seismic input.

Ground	Fundamental natural period	Strong motion record	Residual displacement [mm]	
			1.2 times	1.4 times
Type I	1.25 [s]	UKE-Tokachi	11	34
		CCSP-Maule	17	39
Type II	1.15 [s]	CKB-Tokachi	73	82
		CCSP-Maule	1	2
Type III	0.71 [s]	TCS-Tokachi	57	156
		CCSP-Maule	100	57

EXPERIMENTAL INVESTIGATION OF INFLUENCE OF LIVE LOAD ON SEISMIC RESPONSE OF A HORIZONTALLY CURVED BRIDGE

Hartanto Wibowo¹, Danielle M. Smith¹, Ian G. Buckle², and David H. Sanders³

Abstract

Little is understood about the dynamic interaction between heavy vehicles and bridge systems during strong earthquakes. An experimental study was therefore undertaken to investigate this phenomenon. Six, full-scale, pickup trucks were placed on a 3-span, large-scale bridge model, which was supported on the 4 shake tables at the NEES Equipment Site at the University of Nevada Reno. Comparison of behavior when the same model was tested without trucks showed their presence to have a beneficial effect up to a level of shaking defined by the Design Earthquake, and an adverse effect for shaking greater than the Design Earthquake. This bimodal result has been reported by other researchers and confirms the difficulty of isolating and quantifying the critical parameters that govern response.

Introduction

Design procedures for earthquake-resistant bridges in most countries do not require the simultaneous presence of live load and earthquake load to be considered. This decision is based on two major assumptions. First, it is assumed the full design live load will not be on the bridge at the time of the design earthquake, and second, the seismic response of a bridge is dominated by its dead load and live load inertial effects are negligible by comparison. However for bridges in urban areas where congestion is a frequent occurrence, some fraction of the design live load (usually 50%) is now recommended to be included with the dead load when computing gravity load effects (AASHTO, 2010). But this recommendation applies only to gravity load effects and not to inertial effects.

The omission of inertial effects in design is the result of a prevailing attitude that the suspension system of a heavy vehicle acts as a tuned mass damper and reduces the motion in the bridge. It is therefore believed to be conservative to ignore these effects. But in fact little is understood about the dynamic interaction between heavy vehicles and bridge systems during strong shaking and there is no hard evidence that the tuned mass damper model is universally applicable. It is equally possible that the added weight increases the inertial loads in the bridge and the corresponding displacements and forces.

Currently, very little research has been conducted to resolve this issue, and the first step is to understand and model vehicle suspension systems and their interaction

¹ Graduate Research Assistant, Department of Civil and Environmental Engineering

² Foundation Professor and Director of Center for Civil Engineering Earthquake Research

³ Professor, Department of Civil and Environmental Engineering, University of Nevada, Reno, MS 0258, Reno, NV, 89557

with the bridge structural systems. Then these numerical models need to be calibrated against experimental work, and finally the validated models should be used to study bridge-vehicle interaction during earthquake ground shaking.

This paper describes an experimental study to calibrate a previously developed numerical model and give some insight into the circumstances leading to beneficial and adverse behavior of live load during an earthquake. This study is part of a larger project involving the development of a set of findings and recommendations concerning the effect of live load on seismic response and how these effects may be included in the seismic analysis and design of bridges in the future.

Literature Review

Most of the research reported in the literature to date on the effect of live load is related to the calculation of impact factors (vehicle dynamic load allowance) for gravity load design. It appears that very little work has been done on the influence of live load on seismic response of bridges. Also, experimental tests on large-scale bridges to study the effects of vehicle-bridge interaction under seismic load do not appear to have been previously carried out.

A study by Sugiyama *et al.* (1990) used a single degree-of-freedom vehicle system that can model rolling in the transverse direction and pitching in the longitudinal direction, but the properties are not given. The bridge was idealized as a nine-mass system with transverse and rotation inertia connected by linear springs and damper elements. A vibration test is reported on an existing steel girder bridge with and without trucks in the longitudinal and transverse directions to verify the results. In the test, two large trucks were parked facing the same direction on a portion of an existing off ramp whose girders were vibrated with an electro-hydraulic exciter. The bridge was tested with the vehicles empty and loaded to various capacities. The results show that the dynamic effect of the vehicle is more dominant in the transverse direction and the vehicle tends to reduce the response of the bridge. The authors also note that as the exciting force level increases, the effects of nonlinearity become more apparent since the dynamic characteristics of the vehicle itself are nonlinear. These results are corroborated by Kameda *et al.* (1992) who used a 5 degree-of-freedom model in their study. These authors state that the vehicle tends to increase the bridge response when the vehicle is in the in-phase mode with the bridge and decrease the bridge response when it is in the out-of-phase mode. Moreover, they also concluded that the ratio of the fundamental frequency of the bridge to the vehicle plays an important role for the response of the bridge.

Another study of the seismic response of a bridge with live load was done by Kawatani *et al.* (2007). These authors analyzed the seismic response of a steel plate girder bridge under vehicle loadings during earthquakes. The vehicles were modeled with 12 degrees-of-freedom that took sway, yaw, bounce, pitch, and roll into account. The observations from the numerical analysis showed that heavy vehicles, acting as a dynamic system, can reduce the seismic response of bridges under a ground motion

with low frequency characteristics, but the vehicles have the opposite effect and slightly amplify the seismic response of the bridge under high frequency ground motions.

Kawashima *et al.* (1994) and Otsuka *et al.* (1999) performed a series of studies to determine the effect of live load on a bridge when combined with seismic load. The study modeled a two-span simply supported girder bridge with a mix of ordinary cars, modeled as additional dead load, and large trucks, each modeled with 5 degrees-of-freedom. The bridge was only analyzed in the transverse direction because it was estimated that the deck response would be significantly affected by the rolling of the large trucks. The studies found that the displacement response of the girders increased by 10% when the live load was included; ductility demand at the bottom of the column also increased by 10% with live load on the bridge. This study concluded that these increases were not enough to be significant and that existing safety factors should be adequate to cover these effects. It was also concluded that the increase in response was due to the increase in weight. However, the effect of the large trucks was not just to increase the dead weight, they also behaved as a mass damper.

Scott (2010) developed a simplified modeling approach for dynamic analyses to account for combined live load and seismic load. It is shown that for short-span bridges, the displacement responses are mainly due to the fundamental bridge mode. In addition, for long-span bridges, vehicle speed had small influence on the displacement and acceleration responses of the bridge.

A recent study on the effects of live load a highway bridge under a moderate earthquake in the horizontal and vertical directions is reported by Kim *et al.* (2011). The study concluded that the seismic response of the bridge is amplified when the vehicle is considered as merely additional gravity load or mass and the amplification is dependent on the relationship between the fundamental frequency of the bridge and the response spectrum of the ground motion. However, when the vehicle is considered as dynamic or mass-spring-damper system, which is more realistic, the dynamic effect of the vehicle is greater than its gravity load effect and thus it reduces the seismic response. In addition, the study also showed that the effect of a moving vehicle as compared to a stationary vehicle is negligible, and it is sufficient to model the vehicle as stationary for these studies.

Bridge Model

A three-span, curved bridge model was tested in the Large-Scale Structures Laboratory at University of Nevada, Reno. This 2/5-scale model has a steel plate girder superstructure, single-column reinforced concrete substructures, and seat-type abutments. Overall dimensions are shown in Table 1.

The bridge model has a total length of 145 ft, a total width of 12 ft, and subtended angle of 104° as shown in Figures 1 and 2. Each bent has a single circular column. The column height is 7 ft - 8 in with a diameter of 24 in. The superstructure is

a three-span, three-girder steel bridge with concrete deck. The detail of the superstructure and the column can be seen in Figure 3. The superstructure is supported by fixed (rotation-only) pot bearings at the bent locations and slider bearings at the abutments. Moreover, shear keys are provided at the abutments to restrain movement in the radial direction during small amplitude earthquakes, but are designed to fail at higher events to protect the abutment foundations against damage.

The prototype bridge was designed for a site in Seismic Zone 3 (AASHTO 2010) with a 1,000-year spectral acceleration at 1.0 sec (S_1) of 0.4 g. Under this Design Earthquake (DE), the bridge is expected to be damaged but not collapse. The record selected as the input motion for the experimental studies was the Sylmar record from the 1994 Northridge Earthquake near Los Angeles, scaled to have the same spectral acceleration at 1.0 sec. A scale factor of 0.475 was therefore applied to both the NS and EW time histories of ground acceleration from this station.

Table 1. Bridge Geometry Summary.

Parameter	Prototype	Model
Total Length	362'-6"	145'-0"
Span Lengths	105'-0", 152'-6", 105'-0"	42'-0", 61'-0", 42'-0"
Radius at Centerline	200'-0"	80'-0"
Subtended angle	104° (1.8 rad)	104° (1.8 rad)
Total Width	30'-0"	12'-0"
Girder Spacing	11'-3"	4'-6"
Total Superstructure Depth	6'-6.125"	2'-7.25"
Column Height	19'-2"	7'-8"
Column Diameter	5'-0"	2'-0"

Test Vehicles

The vehicles used in these experiments were six Ford F-250 trucks, each weighing 10,000 lb (10 kip). Dynamic properties of a typical truck were found by shake table testing using the 6 degree-of-freedom shake table in the Structures Laboratory. The ratio of the total vehicle weight to the superstructure weight is around 22%. The rationale of selecting the vehicle is discussed below.

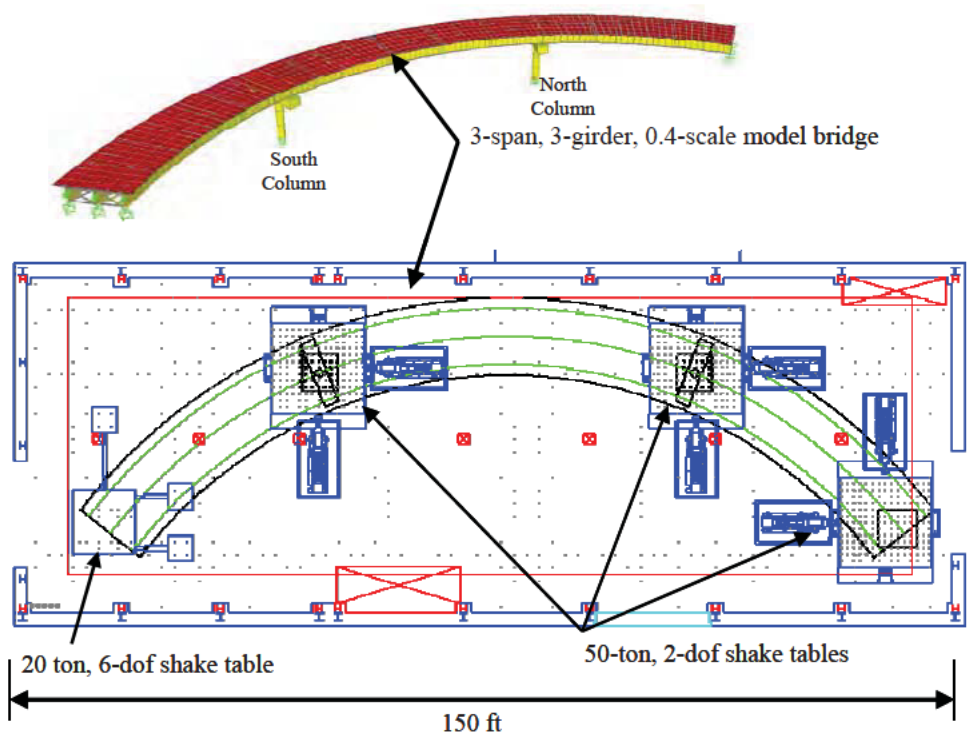


Figure 1. Bridge Model and Layout in Large-Scale Structures Laboratory.



Figure 2. Bridge Model Assembled in Large-Scale Structures Laboratory.

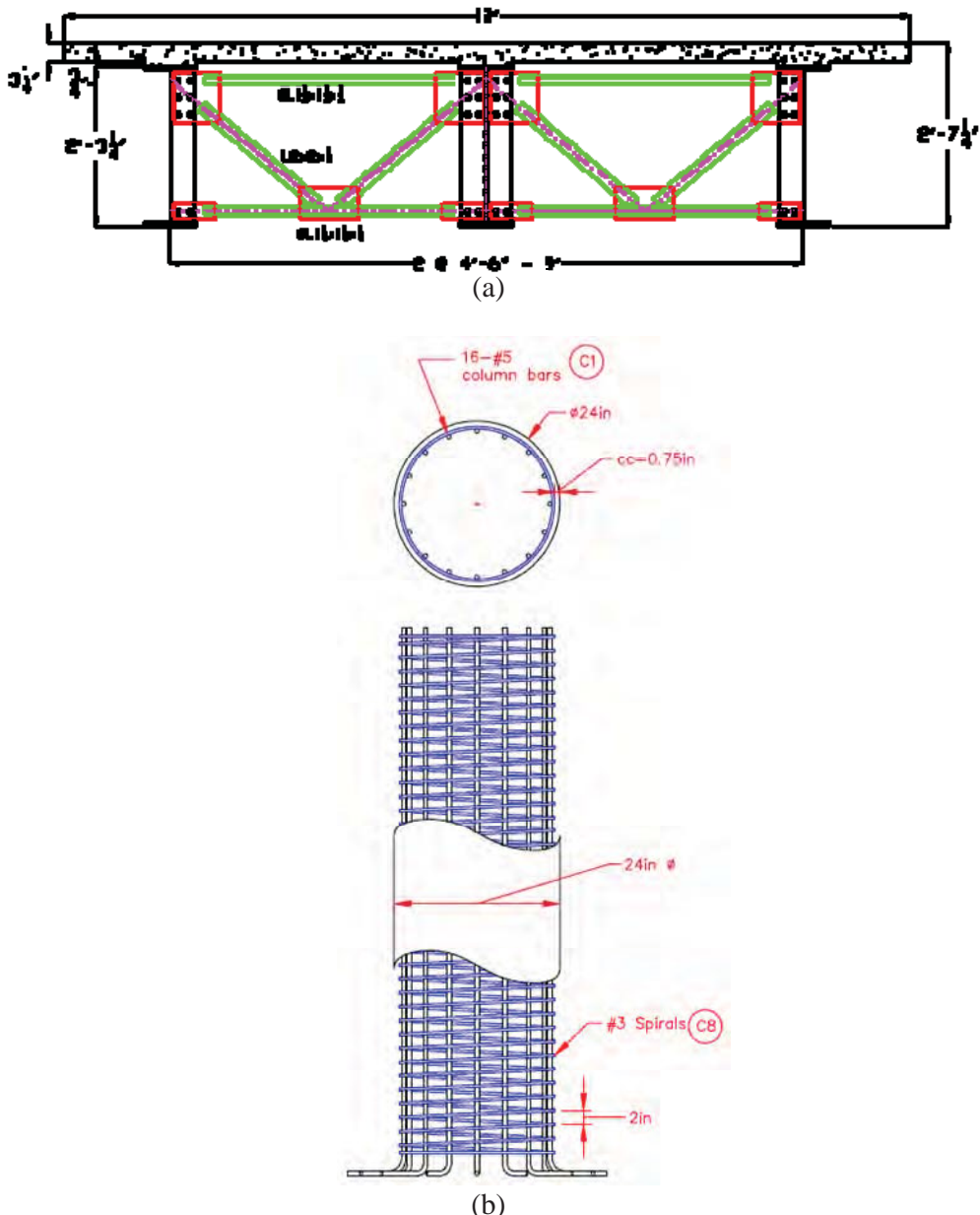


Figure 3. Typical Superstructure and Column Details.

The starting point for selection of the test vehicle was the H-20 truck from the Caltrans Bridge Design Specifications. This truck is a two-axle vehicle weighing 40 kips (8 kips on the front axle and 32 kips on the rear axle) with a 14 ft wheel base. For a 0.4-scale model, the model truck would have a wheel base of 5.6 ft, be 2.4 ft wide, and weigh 6.4 kip. Since such a vehicle would most likely have to be custom-built, the decision was made to select from commercially available vehicles. The closest possible vehicle to match the modeling requirements was found to be the Ford F-250. Although the similitude requirements are not fully satisfied, the dynamic properties of the chosen vehicle can produce similar effects to those of the target vehicle.

Table 2. Ford F-250 Dimensions and Weight Ratings

Parameter	Value
Overall Length	247 in
Overall Width	68 in
Overall Height	80 in
Wheel Base Length	156 in
Ground Clearance	7.9 in
Curb Weight	6.7 kip
Gross Vehicle Weight Rating	10 kip
Max Allowable Payload	2.3 kip

Experimental Setup

The bridge model was assembled on the four shake tables in the Large-Scale Structures Laboratory and the vehicles positioned on the deck as shown in Figure 4. Instrumentation has been installed on the columns, bridge girders, and trucks to gather response data during testing. The types of instruments range from strain gauges on the column rebar, string pots on the bridge girders and trucks (to measure displacements), and accelerometers on the bridge deck and trucks (to measure accelerations). During the experiment, 383 data acquisition channels were used.

The test protocol followed for this experiment started with 10% of the DE and then the motion was increased in successive increments to 20%, 50%, 75%, 100%, 150%, 200%, 250%, 300%, and 350% of the DE. Before each run, a series of white noise excitations were run to characterize the system's dynamic properties.

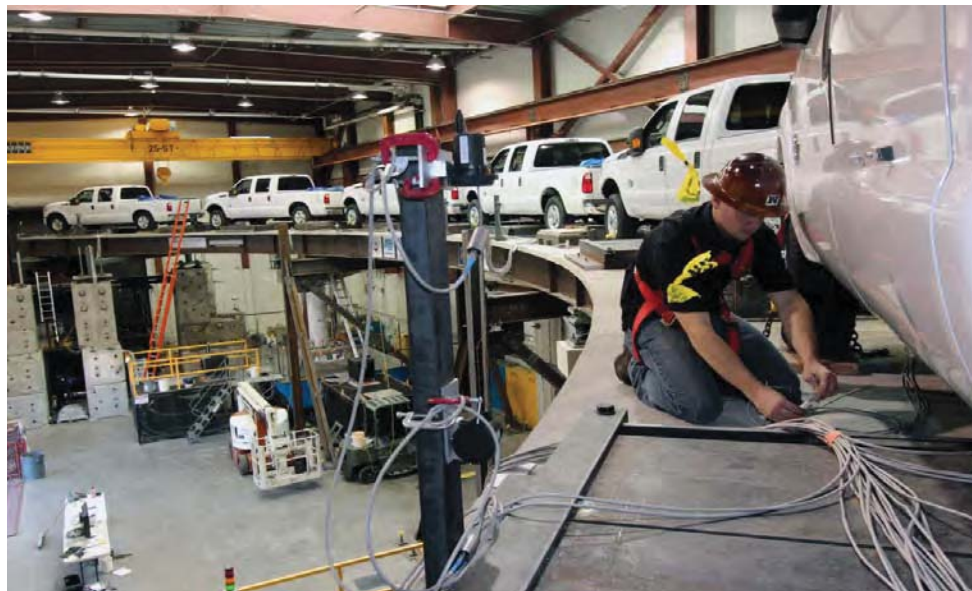


Figure 4. Bridge Model with Live Load (Courtesy of M. Wolterbeek, 2011)

Preliminary Results

One of the parameters that may be used to quantify the effect of live load is the column displacement. Figures 5 and 6 show the north and south column displacements with and without live load under 75% and 100% of DE, respectively. It is shown that for these two runs, the maximum displacement is less when live load is present. It is also important to note that during the no-live load case, the shear keys at the abutment failed during the 75% DE run, whereas it took a stronger ground motion (100% DE) to fail these keys when live load was present, i.e. the live load reduced the forces in the shear keys at the same level of excitation. This shows that at these levels of shaking, the existence of live load caused less demand in the column and reduced the radial shear forces at the abutments. The damage in the column was also found to be minor and not as severe as for the no-live load case.

On the other hand, observations from the higher amplitude runs, after the shear keys at the abutments had failed, show a different result. Figures 7 and 8 show the displacements in the north and south columns with and without live load after 250% and 300% of DE, respectively. It is seen at these levels of shaking (and after the keys had failed), the live load exercises the columns to a greater extent and the maximum displacements at the top of the columns became closer to the no-live load case. It is also seen that the residual displacements in the columns for the live load case are about double those without live load. These larger residual displacements indicate greater distress to the columns, and especially the south column, due to the presence of the live load.

Concluding Remarks

A recent experiment was conducted in the Large-Scale Structures Laboratory at University of Nevada, Reno, to study the effects of live load on a 0.4-scale horizontally curved bridge model. From the experimental results for the column displacements and radial shears forces at the abutments, with and without live load, some preliminary conclusions can be drawn. In lower amplitude motions, when the shear keys were still intact, live load gave a beneficial effect. In higher amplitude motions, after the abutments were free to move, live load gave an adverse effect. It is not known at this stage whether this reversal in effect is due to (1) the deteriorating nature of the bridge under increasing levels of shaking and thus a changing vehicle-to-bridge frequency ratio, or (2) the changed configuration of the bridge when the abutments were released in the radial direction after the shear keys failed, or 3) both of the above. Studies are continuing to better understand this phenomenon.

Acknowledgments

This project is funded by California Department of Transportation under contract number 59A0695 and Federal Highway Administration under contract number DTFH61-07-C-00031. The experimental study was conducted at the George E. Brown, Jr. Network for Earthquake Engineering Simulation (NEES) Equipment Site located at University Nevada, Reno. The use of NEES shake tables at University of Nevada, Reno was provided under a Shared-Use Agreement with NEEScomm.

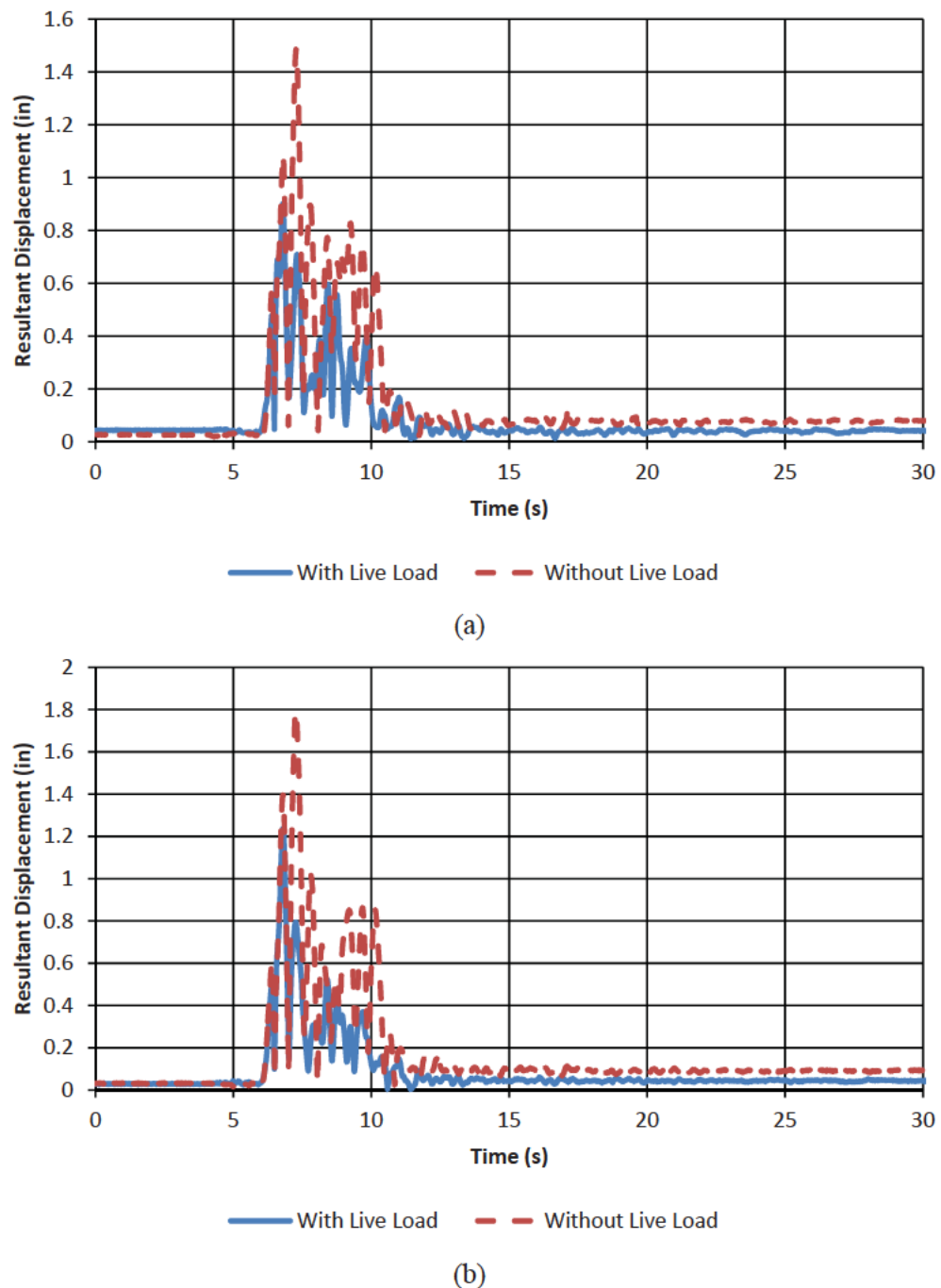
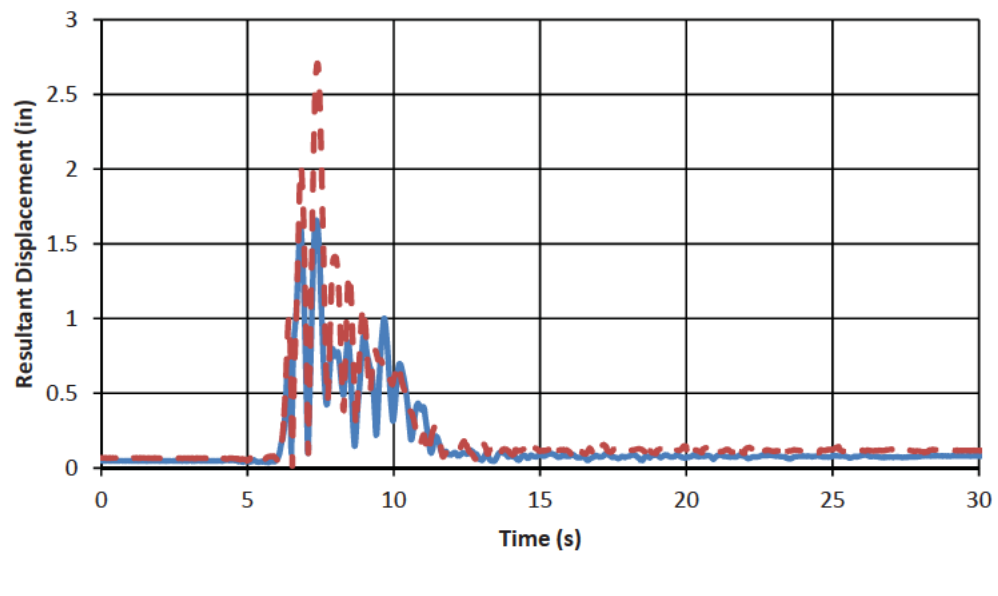
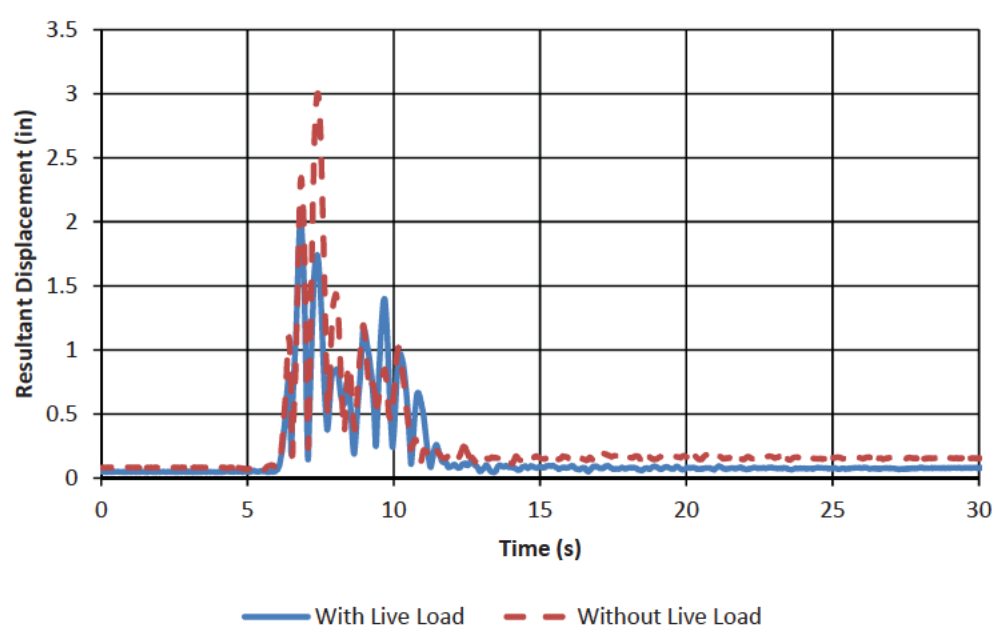


Figure 5. (a) North and (b) South Column Displacements during 75% DE Run.

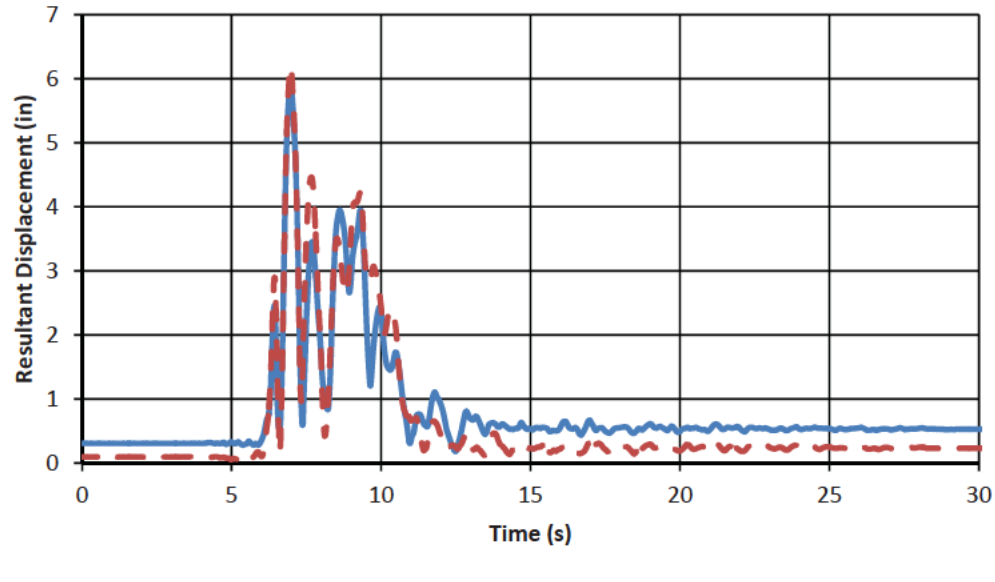


(a)

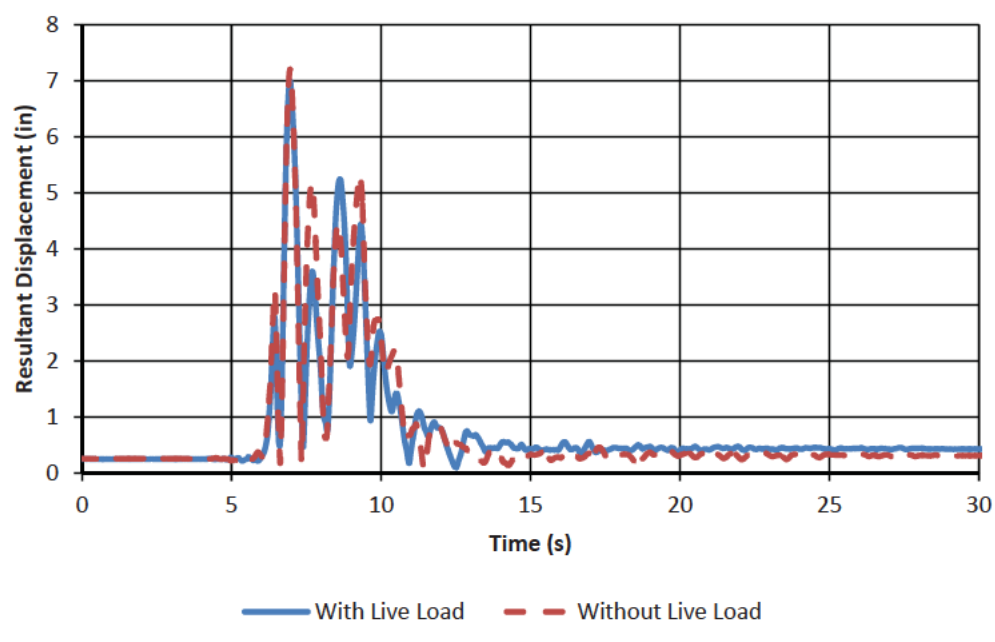


(b)

Figure 6. (a) North and (b) South Column Displacements during 100% DE Run.

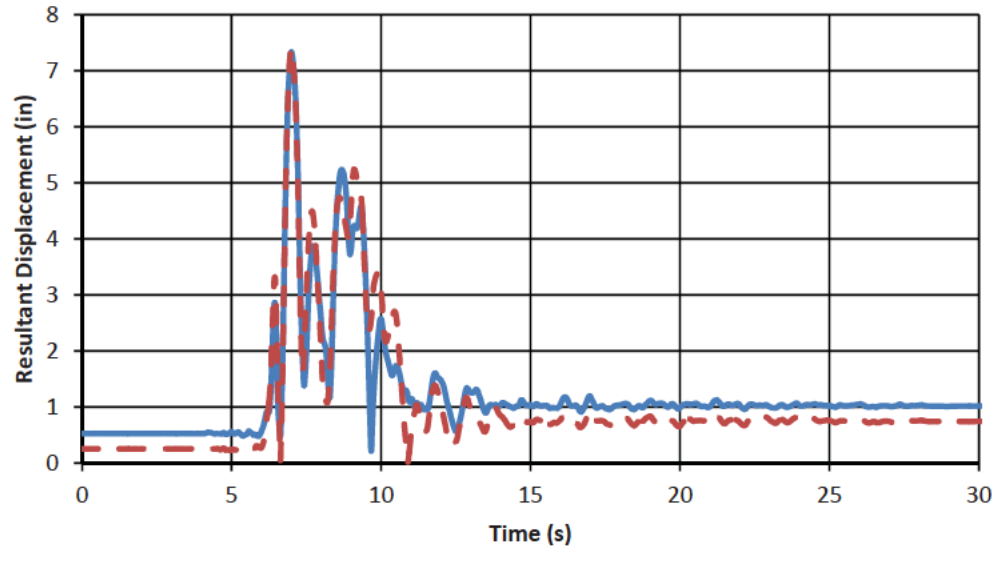


(a)

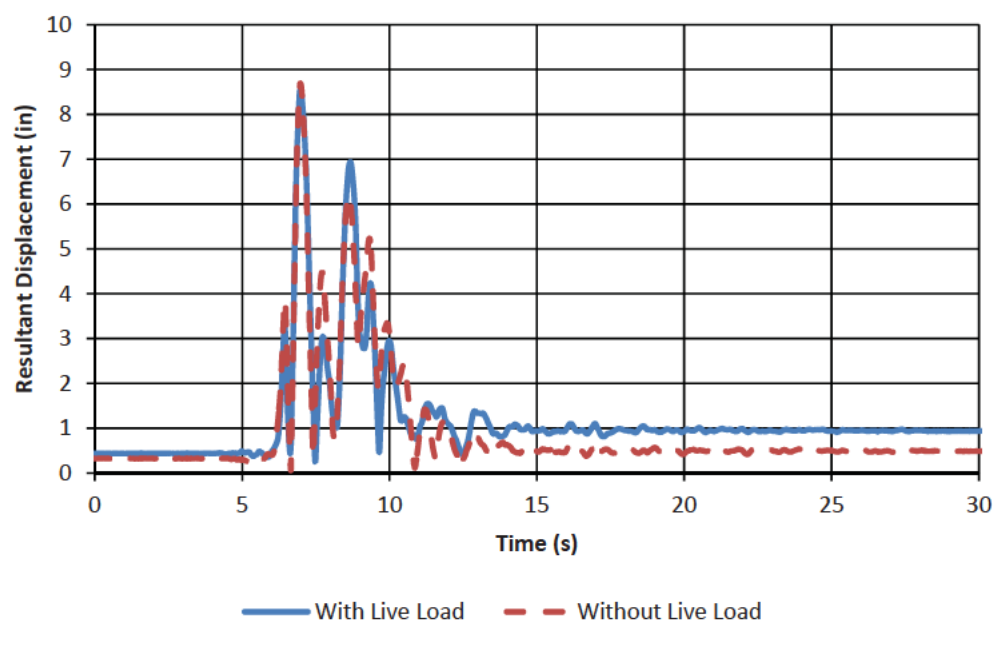


(b)

Figure 7. (a) North and (b) South Column Displacements during 250% DE Run.



(a)



(b)

Figure 8. (a) North and (b) South Column Displacements during 300% DE Run.

References

- AASHTO. (2010). *AASHTO LRFD Bridge Design Specifications, Customary U.S. Units, 5th Edition*. Washington, DC: AASHTO.
- Kameda, H., Murono, Y., Maekawa, Y., and Sasaki, N. (1992). Dynamic Structure-Vehicle Interaction for Seismic Load Evaluation of Highway Bridges. *Proceedings of the Tenth World Conference on Earthquake Engineering*, Madrid, Spain, July 19-24, pp. 4861-4866.
- Kawashima, K., Unjoh, S., and Mukai, H. (1994). Research on Live Load Effect to Earthquake Response of Bridges (Part 1). *PWRI Research Report No. 3316*, 59 pp. (*In Japanese*)
- Kawatani, M., Kim, C. W., and Yasui, K. (2007). Seismic Response of a Highway Bridge under Traffic Loadings. *Proceedings of Pacific Structural Steel Conference 2007: Steel Structures in Natural Hazards*, Wairakei, New Zealand, March 13-16, pp. 183-188.
- Kim, C. W., Kawatani, M., Konaka, S., and Kitaura, R. (2011). Seismic Responses of a Highway Viaduct Considering Vehicles of Design Live Load as Dynamic System during Moderate Earthquakes. *Structure and Infrastructure Engineering*, 7 (7-8), pp. 523-534.
- Otsuka, H., Unjoh, S., and Mukai, H. (1999). Research on Live Load Effect to Earthquake Response of Bridges (Part 2). *PWRI Research Report No. 3355*, 40 pp. (*In Japanese*)
- Scott, M. H. (2010). *Combined Seismic Plus Live Load Analysis of Highway Bridges, Report OTREC-RR-09-261*. Portland: Oregon Transportation Research and Education Consortium.
- Sugiyama, I., Kameda, H., Sasaki, N., and Kawakita, S. (1990). Dynamic Structure-Vehicle Interaction of Highway Bridges and Its Implication to Seismic Design. *Proceedings of the 6th U.S.-Japan Bridge Engineering Workshop*, Lake Tahoe, NV, May 7-8, pp. 379-392.

Conversion Table

From	To	Multiply by
in	mm	25.4
ft	mm	304.8
lb	kg	0.45

Discussion Method by using Dynamic Analysis for Quakeproofing Long-Span Bridges

Manager, Bridge Section, Road Department.

Takumi Nishikawa

Deputy Manager, Bridge Section, Road Department

Mutsuji Kawakami

Assistant Manager, Bridge Section, Road Department

Tatsumi Ujie

Bridge Section, Road Department

Shunji Nagahashi

1. Introduction

The capital in Western Japan, Osaka City, is the second largest city in Japan, with only Tokyo surpassing it, and is the center for finance and culture. Osaka City is known as the “City of water”, and its bridges have been loved by the Japanese, down through the ages. Currently, the Construction Section of Osaka City manages 764 bridges, which includes about 720,000 square meters of bridge. There are a great variety of bridges, including continuous viaducts where 100,000 or more cars a day pass through, long-span bridges across large rivers (Picture 1), and bridges (Picture 2) that have been loved by the locals throughout history and are closely connected to the lives of the average person.

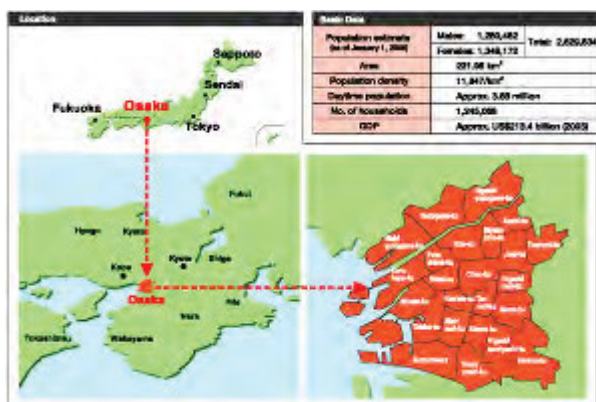


Figure 1 Location of Osaka City



Picture 1 Continuous viaduct
(New Midosuji line)



Picture 2 Historical bridge
(Namba Bridge)

The Southern Hyogo Prefecture Earthquake in 1995 caused much damage to many of the bridges. Even Osaka City (Figure 1), which is about 30 km east of Kobe City, suffered major damages, such as cracks in the reinforced concrete bridge supports of the viaduct, although no bridges actually collapsed. Thus, since 1996, Osaka City has advanced earthquake-resistant projects for 331 bridges (about 43%), which need earthquake-resistant measures, among the 764 bridges managed by the Construction Section. Earthquake-resistant projects have reinforced the bridge supports of viaducts, installed travel-limiting devices and devices for the prevention of collapse, and widened bridge seats. At present (March 2011), the project has been implemented to about 94% of the bridges that have been chosen for this project.

On the other hand, there have been many problems on quakeproofing long-span bridges that a river impedance ratio (Cabinet Order concerning Structural Standards for River Management Facilities, etc) is not satisfied as a building frame of bridge supports becomes thicker after a reinforcement, reinforcement constructions are prolonged because reinforcement construction periods are limited to non-flood seasons and it takes large money and time for temporary cofferdam. Therefore, we determined to improve better earthquake resistance of the long-span bridge by changing the support conditions of the bridge by replacing bearing supports and installing damper devices as well as adopting discussion methods with dynamic analyses. This paper will report on the earthquake-resistant project where support conditions of the long-span bridge, Nagara Bridge, were changed and dynamic analyses were used as a discussion method.

2. Outline of the Nagara Bridge

The Nagara Bridge, which will be reported in this paper, is located on the main road that connects the major cities of Osaka and Kyoto, and crosses the Yodo River, going to Osaka City. This river dates back a long way (Figure 2). A reliable book says that the bridge had already been constructed in the 9th century and many Japanese old poems, wakes, speak of the Bridge. The current Nagara Bridge was completed in 1983, with a Nielsen-Lohse beams located at the center of the Bridge, the 4 span continuous steel floor plate 2 main beam on the left bank of the Bridge (length 294 m) and the simple steel floor box-girder (length 76 m) and 2 span continuous steel floor plate 2 main beam (length 131 m) located on the right bank of the Bridge.

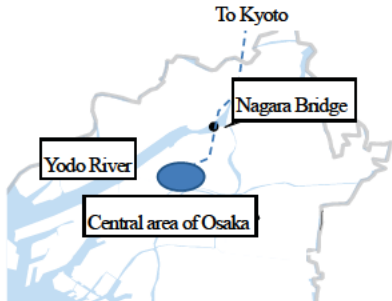


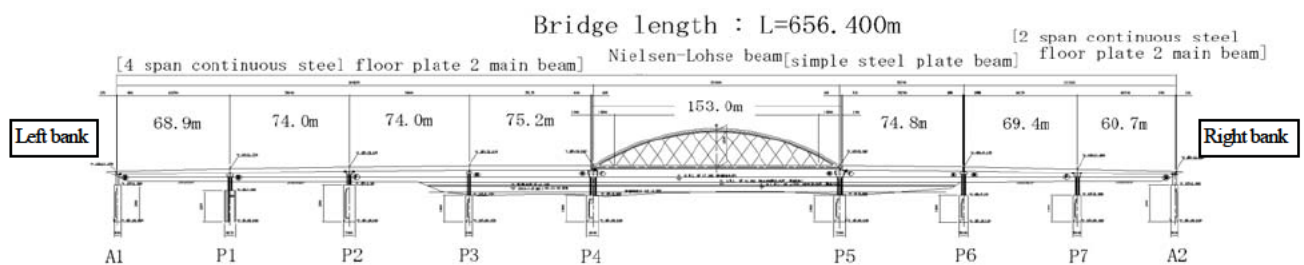
Figure 2 Location of Nagara Bridge



Picture 3 Nagara Bridge
(Nielsen-Lohse bridge)



Picture 4 Nagara Bridge
(Steel plate floor beam bridge)



3. Earthquake-resistant design concept, analysis model and designed ground motion

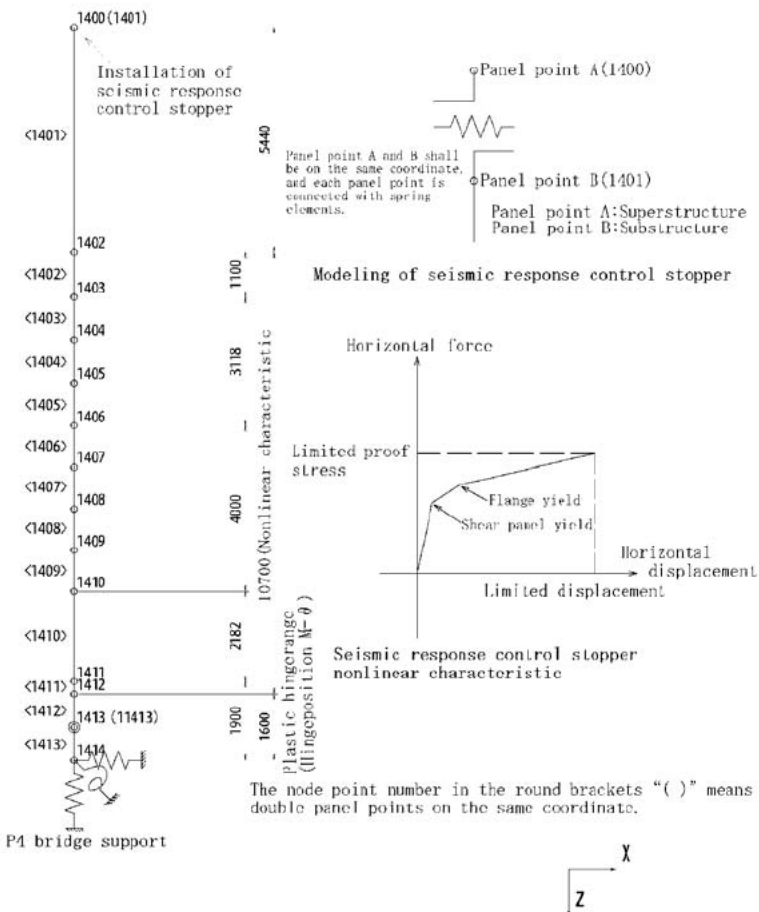
The concept for the earthquake-resistant reinforcement design complied with the national design standard 1) and is designed for ground motion at 2 levels. That is, the purpose of considering the levels is to prevent damage to the Bridge (to insure the same function of the Bridge before an earthquake occurs) during ground motion (level 1 ground motion) which is very likely to occur during the in-service period of the Bridge, and to prevent fatal damage, such as the collapse of the Bridge, during an earthquake which occurs rarely (level 2 ground motion). Two types of earthquakes are assumed: the inner-plate earthquake that infrequently occurs, but that has large scale ground motion, and the inland local earthquake). Because the Nagara Bridge is designated as an emergency traffic route in the regional disaster prevention plan of Osaka City, it is especially necessary to prevent the bridge from sustaining extensive damages which may lead to collapse of the Bridge, and to insure its earthquake resistance so that it can function after an earthquake; therefore, we designed the reinforcement so that deformation of the bridge support foundation would not exceed the plastic deformation capacity in order to enable it to be easily repaired even if the Bridge suffers some damage.

Next, the analysis models used for discussion are described. The Nagara Bridge is composed of four bridges (4 span continuous steel floor plate 2 main beam , Nielsen-Lohse beam, simple steel floor box-girder, and 2 span continuous steel floor plate 2 main beam) and designed vibration units of the bridges are assumed to operate separately, without transferring the earthquake load to each other. For dynamic analysis modeling of the bridge

axis direction, each bridge unit was used. At the transverse direction to the bridge axis, as the earthquake loads are influenced each other through the staggered bridge supports, the whole Nagara Bridge, with all four beams combined, could be seen as one analysis model. The superstructure is an elastic frame model, reinforced concrete bridge supports are a trilinear model (Takeda model 2)) and the foundation is a nonlinear spring element as to analysis conditions (Figure 4).

The most distinctive feature of improvement for earthquake resistance of the Bridge is the distribution of the load to make it resistant to earthquakes, and to make the structure of the bridge to be the structure with the primary natural period by changing the bearing support conditions of the existing bridges, which is a one-point fixation that bears inertia force from the bridge axis direction, to elastic bearing supports. Another feature is a change in the structure so that the bearing supports can be expected to have an attenuation effect by using shear and friction hysteretic dampers. The hysteresis of these dampers is shown below.

Superstructure	Elastic girder model
Abutment	Elastic girder (total cross-section rigidity)
Bridge support	Girder Elastic girder model(rigid zone) Column General material M- ϕ trilinear model(takeda model) Plastic hinge M- θ trilinear model(takeda model)
Foundation	Intensive ground spring



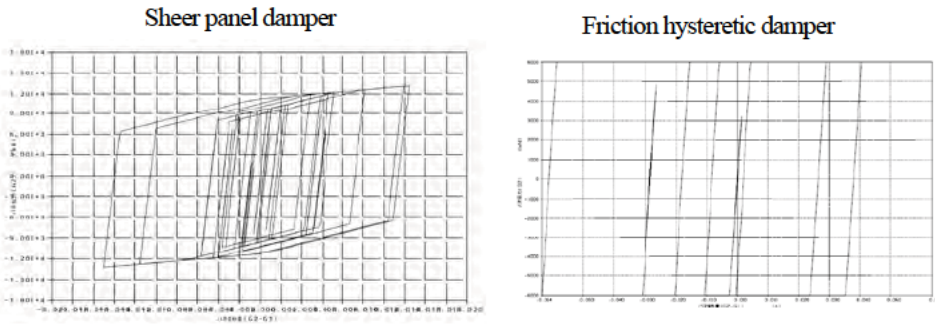


Figure 5 Example of response hysteresis

The seismic wave used as the national standard and input seismic wave 3) set by Osaka City were used as the input ground motion used for the dynamic analyses of earthquake-resistant design for the Nagara Bridge in this paper. These are seismic waves due to Uemachi faulting directly under Osaka City, and specify the standard input ground motion used for earthquake-resistant design for civil engineering structures, in response to the earthquake in the Southern Hyogo Prefecture Earthquake in 1995. Figure 6 shows the acceleration response spectrum of the input seismic wave adopted in this paper.

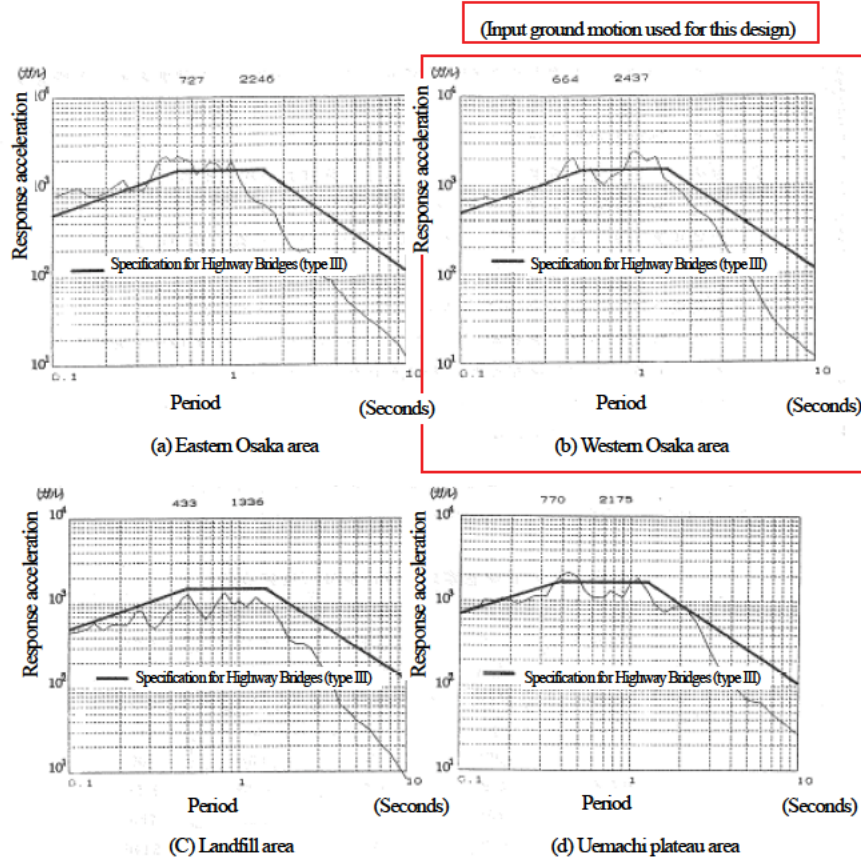


Figure 6 Seismic wave in Osaka City

4. Survey on earthquake resistance of the current reinforced concrete bridge support

The basis of earthquake-resistant reinforcement for a reinforced concrete bridge support is to change the failure mode to a flexure failure mode on the bridge support foundation where toughness is expected, while avoiding shear failures which show drastic failure on the bridge support.

The method described in “Existing bridge earthquake resistant reinforcement method cases” 4) published by the Japan Bridge Engineering Center was used to evaluate the damage on the cut-off area of longitudinal reinforcing steel. If the reinforcement of the bridge support foundation was implemented on a large scale, and it was difficult to change a failure mode to a flexure failure mode of the bridge support foundation, we surveyed that the plasticity rate of the cut-off area was to the extent that the proof strength will not lower (the maximum response yield curvature of the cut off area should be twice the initial yield curvature or less).

In order to confirm safety, the response rotation angles of the plastic hinges, the response shear force of the bridge supports, and the values of the residual displacement of the bridge supports, acquired from dynamic analyses were surveyed. Concretely, we surveyed that the maximum response rotation angle of the plastic hinges shall be the allowed rotation angle specified in Specification for Highway Bridges with Commentary, PART V:SEISMIC DESIGN Section 10.2, or smaller, the maxim response shear force of the bridge supports shall be shear force of the reinforced concrete bridge support or lower, and the residual displacements of the bridge supports calculated using the maximum response plastic rate shall be the allowed residual displacement (1/100 of bridge support height) or lower. As the bridge support is a wall type bridge support, the effects of the deep beams are considerate for calculation of the shear proof strength at the transversal direction to the bridge axis.

Earthquake resistance of a structure with the current bearing support condition (Table 2 CASE 1) being maintained was surveyed in the case of a ground motion at level 2. The bridge support foundation and cut-off area of P2, P4, P5 and P7 bridge supports lacked flexural and shear proof strength to the bridge axis direction (Table 3 CASE 1). P1 bridge support showed an adequate earthquake resistance. Although the cut-off area of P3 and P6 bridge supports reached to the plastic field, that range was only to the extent in which proof strength did not decrease.

All bridge supports showed the shear failure type to the transverse direction to the bridge axis. The shear proof strength calculated in consideration of the effects of the deep beams exceeded the maximum response shear force, and met the required earthquake-resistant strength. Therefore, if the bridge supports were mechanically reinforced against earthquake loads acting on each support, while the current bearing support conditions were maintained, the reinforcement of the cut-off area of P2, P4, P5 and P7 bridge supports, and the shear reinforcement and flexural reinforcement of the foundation would be necessary. Especially, the flexural reinforcement of the bridge support

foundation should be large scale reinforcements in which longitudinal reinforcing steel is established to the footing.

5. Discussion on earthquake-resistant reinforcement

5-1. Determination of the policy for reinforcement

For discussion of the whole structure of the Bridge, under the conditions of bearing supports indicated in Table 2, a bridge support reinforcement method where reinforcement against earthquake loads acting on the bridge support was implemented (CASE 1), a seismic isolation method which makes vibration periods of the structures longer and enhances attenuation (CASE 2) and a seismic response control method which enhances attenuation and distribution of earthquake loads (CASE 3) were weighed. Table 3 shows the results of the need of bridge support reinforcement.

In CASE 2, the natural period was lengthened by using seismic isolation bearing supports, such as a laminated rubber bearing, and the inertial force was expected to be reduced by improving the attenuation performance. Reinforcement of P1 and P6 bridge supports was necessary, as well as reinforcement of P2, P4 and P5 bridge supports, and the scales of flexural reinforcement, shear reinforcement and the cut-off reinforcement were larger, resulting in the construction costs being high. The traveling distances of the beam on A1 abutment, P6 bridge support and A2 abutment were greater than those of the expansion gap, resulting in a collision of the beams.

CASE 3 was a construction method which controls deformation of the entire bridge and attenuates the inertia force transmitted to the bridge support by installing dampers that deforms during an earthquake and absorbs the energy around the bearing supports. The seismic response control dampers were located at A1 and P2 supporting points of the 4 span continuous beam ranging from A1 to P4, P4 supporting point of the Nielsen-Lohse beam ranging from P4 to P5, P5 supporting point of the simple beam ranging from P5 to P6, P7 supporting point of the 2 span continuous beam ranging P6 to A2, and A2 supporting point. In this structure, the inertia force transmitted to the substructure dramatically decreased, shear and cut-off reinforcements were necessary only for P2, P4 and P5 bridge supports. As flexural reinforcement (establishment of longitudinal reinforcing steel to the foundation) was unnecessary, the earthquake loads to the foundation did not increase. A travelling distance of the beam at staggered areas was shorter than the expansion gap with the adjacent beam, and beams did not collide with each other.

As a result of a comparison of the construction costs of these three methods, we decided on the earthquake-resistant measure based on CASE 3, which controlled deformation of the entire bridge and attenuated the energy by installing seismic response control dampers. For this basic structure, construction methods for the reinforcement of the bridge supports were compared, types of seismic response control dampers were compared, and shear plate type dampers and friction hysteretic dampers were designed.

Table 2 Bearing support conditions

	A1	P1	P2	P3	P4		P5		P6		P7	A2
CASE 1	M	M	F	M	M	F	M	F	M	M	F	M
CASE 2	E	E	E	M	M	E	E	E	E	M	E	E
CASE 3	M Damper	M	F(M) Damper	M	M	F+ shear panel	M	F+ shear panel	M	M	F Damper	M Damper

Table 3 List of need of bridge support reinforcements

	A1	P1	P2	P3	P4	P5	P6	P7	A2	Remarks
CASE 1	-	-	•	□	•	•	-	•	-	⊕.. Plastic
CASE 2	-	•	•	-	•	•	•	-	-	Beams may collide.
CASE 3	-	-	•	-	•	•	-	-	-	

5-2. Bridge support reinforcement

A PC confined method was adopted for reinforcement of the bridge support at the low-water channel of a river. The PC confined method enables improvement of the horizontal proof strength and toughness during an earthquake by prestressing the PC steel wires inserted into the sheath in the PC precast panel after the panel is installed around the bridge supports, as well as improvement of work efficiency at the site, by using precast panels manufactured at a plant.

A reinforced concrete lining method, a carbon fiber material lining method, and a steel plate lining method were compared and studied for the reinforcement of the bridge support at the high-water channel of a river. As the carbon fiber material lining method has excellent work efficiency but is vulnerable to fires and shocks, this method still has operation and maintenance problems. The least expensive method of these methods, the reinforced concreted lining method was adopted.

5-3. Seismic response control dampers

Seismic response control dampers have shear panel and friction hysteretic dampers. The shear panel damper (Picture 5) absorbs earthquake energy and reduces the cross-sectional force which transmits to the substructure due to the shear deformation of the panels which are composed of low yield point steel. This damper normally works as a fixation device and when a level 1 earthquake occurs. The shear panel yields with ground motion due to an earthquake at level 2 and this damper absorbs earthquake energy with hysteresis attenuation of shear plastic deformation. As this damper normally works as a fixation device, it was installed at one supporting point of each beam, so that the beam could be elastic during temperature changes (P4 supporting point of the Nielsen-Lohse beam and P5 supporting point of the simple steel plate 2 main beam I beam).

The friction hysteretic damper (Picture 6) absorbs vibration with the flow resistance force that occurs during piston movement in the high viscosity material filled into the cylinders, and normally works as a movable point. This damper is an elastic fixation against the large shaking of an earthquake. This damper can be installed at several supporting points in the 1 structure system to ensure elasticity during normal temperature changes. In this paper, this damper was installed at A1 and P2 supporting points of the 4 span continuous steel plate 2 main beam I beam and P7 and A2 supporting points of the 2 span continuous steel plate 2 main beam I beam.



Picture 5 Shear panel damper
(Static loading test)



Picture 6 Friction hysteretic damper
(Nagara Bridge)

5-4. Stimulated fixation of P2 bearing support

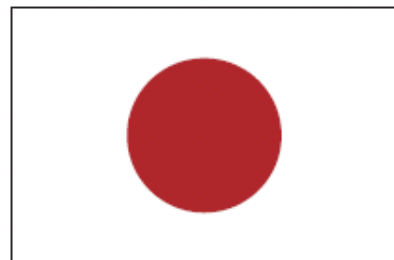
In the 4 span continuous steel floor 2 main beam bridge ranging from A1 to P4, only P2 supporting point was a fixation bearing and the rest of the supporting points were movable bearings. In this earthquake-resistant measure, all of the supporting points were changed to movable supporting points and the friction hysteretic dampers were installed at A1 and P2 supporting points. When all supporting points are made to be movable, the fixed point against temperature change is unclear. As a measure against this issue, we stimulated fixation to P2 bearing support by installing blocks which limit travelling toward the bridge axis so that the beam could normally stretch around P2 supporting point. In this case, the number and radius of the bolts were adjusted so that the seismic response control dampers would work effectively at ground motion at level 2 and the fixation bolts of the block would fracture with the horizontal loading due to ground motion at level 1 or higher.

6 Conclusion

For earthquake-resistant reinforcement, structures of a general reinforcement method which reinforces each bridge support against cross-sectional force acting on the bridge support while the current bearing support conditions are maintained were discussed as well as the seismic isolation construction method, and the earthquake response control method. Accordingly, the optimal method was selected where a high attenuation device, such as a seismic response control damper, could absorb the earthquake energy, reduce the earthquake loads transmitted to the bridge supports, and control the deformation of the entire bridge. Then, the friction hysteretic damper and shear panel damper that use a low yield point steel were designed, in consideration of the structure characteristics of the Bridge. Currently, the reinforcement construction of the Nagara Bridge has been conducted for early completion. We received guidance from Hirokazu Iemura (professor emeritus at Kyoto University) for this paper. We will express our sincere gratitude to him.

Reference

- 1) Japan Road Association: Specification for Highway Bridges with Commentary, PART V: SEISMIC DESIGN, Published by Maruzen, 2002-3
- 2) Takeda, T., Sozen, M.A. and Nielsen, N. M: Reinforced Concrete Response to Simulated Earthquakes, Journal Division, ASCE, Vol. 96, No. ST12, PP. 2557-2573, December, 1970
- 3) Osaka City Planning Section: Osaka City Civil Engineering and Architectural Buildings Earthquake Measure Technology Conference Report, 1997-3
- 4) Japan Bridge Engineering Center: Existing bridge earthquake resistant reinforcement method cases, 2005-4
- 5) Maruyama. T. Seismic Retrofitting for Bridges in Osaka City, Osaka and Its Technology, Osaka Municipal Government, No.32, PP7-18, 1998.1



27th US-Japan Bridge Engineering Workshop

Session 4

Management and Maintenance

Analysis Examples of Periodic Inspection Results of National Highway Bridges in Japan

-Application of Degree of Damage for Element Level-

By Fumihiko Nomura, Masanori Okubo, and Takashi Tamakoshi

The Importance of Partnerships in the Implementation of Bridge Preservation Practices

By Peter J. Weykamp

Maintenance of ASR-affected Structures in Hokuriku Expressway, Japan

By Yoshifumi Adachi, Mamoru Moriyama, and Masahiro Nomura

Page Left Blank

Analysis Examples of Periodic Inspection Results of National Highway Bridges in Japan -Application of degree of damage for element level-

Fumihiko Nomura¹, Masanori Okubo², Takashi Tamakoshi³

Abstract

In order to have enormous highway bridge stocks in Japan already, it is important to save safe and smooth traffic networks and to have them maintained both economically and rationally. Thus, it is a matter of urgent business to grasp and evaluate their states appropriately, and to develop well-planned maintenance methods.

National Institute for Land and Infrastructure Management (NILIM) conducts feature arrangements and analyses of damage by statistical processing of national highway bridges periodic inspection data, and provides the insights into the further rationalization and standardization of their periodic inspection.

In this paper, the features of generation and progress of damage on bridges are reported based on analysis examples of element periodic inspection results, and the direction of the goal of bridge maintenance in Japan is explained.

Introduction

Periodic inspection of national highway bridges in Japan based on ‘Bridge Inspection Manual’ (Public Works Research Institute Document No.2651, July 1988) had been conducted every 10 years, and that based on ‘Bridge Periodic Inspection Manual’ (National Highway and Risk Management Division, March 2004) (hereinafter referred to as ‘Periodic Inspection Manual’) has been being conducted within two years for initial inspection, and every five years after that since 2004.

Data as objective facts for damage and deterioration obtained from inspections is made use of future projections and trend analyses by grasping continuously as well as be indispensable for cause estimation and evaluation of current performances. In order to be used for statistical processing and quantitative projection, it is important that the data is the objective one based on a uniform standard possible to be used for relative comparison over time.

On the other hand, for road administrators who do not always have the knowledge enough to judge effects on bridge performance, primary diagnosis as evaluation of functional states of bridges is essential to take action to make appropriate decisions for taking measures to traffic regulations, and repairs and retrofits. In other words, except the facts as individual kinds of damage and damage progression, it is possible for road administrators to make responses to conduct the further surveys right after obtaining measures for effects of damage on functional states of bridges. So, in case primary diagnosis has no troubles, it is so difficult for them to have suspicions about the results.

¹ Researcher, Bridge and Structural Division, Road Department, NILIM

² Senior Researcher, Bridge and Structural Division, Road Department, NILIM

³ Head, Bridge and Structural Division, Road Department, NILIM

Thus, the revision of 2004 regulates that objective facts as size of the damage are recorded as ‘evaluation of degree of damage’, at the same time, primary diagnosis for functional states of bridges by appropriate engineers is evaluated as ‘judgment of measure classification’. Moreover, the evaluation system is set to taking saving the continuity with the existing inspection data into consideration. In this way, for national highway bridges, data for the new manual converting into inspection data based on manual of 1988, and data based on the new inspection manual operating from 2004 are gradually saved.

As for periodic inspection, damage states for element levels and every kinds of damage are surveyed. Figure 1¹⁾ shows examples of element numbers of a main steel girder and a concrete slab. For the main girder and concrete slab, one element is defined as the element enclosed by the main girder and a cross frame, indicating the main girder divided by 16 elements and the concrete slab by 14 elements per a span. ‘Evaluation of Damage States’ is judged and recorded based on ‘Evaluative Standard of Damage States’. The evaluative standard of damage states is set to be 5 stages (from ‘a’ to ‘e’) by every sorts of damage. ‘a’ means to be sound, while ‘e’ to be the most severe damage of all five stages. As shown in Table 1-1, sorts of damage are set for every regions and members. On the other hand, judgment of measure classification is conducted by appropriate engineers as primary checks for functional states of bridges.

Thus, periodic inspection of national highway bridges in Japan is the most fundamental action to grasp the bridge states comprehensively, and at the same time, it plays an important role in obtaining the fundamental information for well-planned and effective maintenance.

Main girder (Mg), Stringer (St)

	0101	0102	0103	0104
1行目				
2行目	0201	0202	0203	0204
3行目	0301	0302	0303	0304
4行目	0401	0402	0403	0404
	1列目	2列目	3列目	4列目

Slab (Ds)

	0101			
	0201	0202	0203	0204
	0301	0302	0303	0304
	0401	0402	0403	0404
	0501			

direction perpendicular to bridge axis

bridge axis direction

(a) Steel main girder

(b) concrete slab

Figure 1 Examples of element number

Features of damage occurrence for each member & region

Since element level inspection results are gradually saved, and it is possible to grasp damage occurrences for each member and region, the damage occurrences for each were analyzed. The number of the parameters was 21,636 bridges, and objective bridges of them were extracted.

In this case, corrosion of steel members, cracks, cracks at concrete girders, and cracks at reinforced-concrete (RC) slabs of steel bridges with the significant features of damage for each member and region are shown as the analysis examples.

(1) Corrosion of steel girder bridges

For corrosion of main girder in the steel plate girder bridge, Figure 2 shows the degree of corrosion at the end and middle of the same girder. The degree of the corrosion at the end of the main girder has a tendency to be worse than that at the middle.

For corrosion of main girder at the middle in the steel plate girder bridge, Figure 3 shows the degree of corrosion at the outside and inside of the same span. The degree of the corrosion at the outside of the main girder has a tendency to be a bit worse than that at the inside.

In this way, it was indicated that there was a difference of the degree of corrosion between the end and the middle of the girder, and the outside and the inside girder. That means there is a possibility of taking measures of bridge maintenance economically and rationally for corrosion at the end girders by partial coating. Moreover, there is a possibility of making inspections effectively by restricting the inspection region.

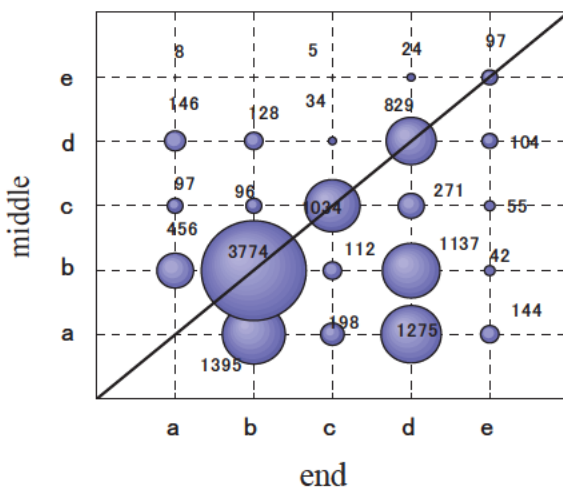


Figure 2 Corrosion, Steel plate girder bridge, main girder, Degree of damage for each region

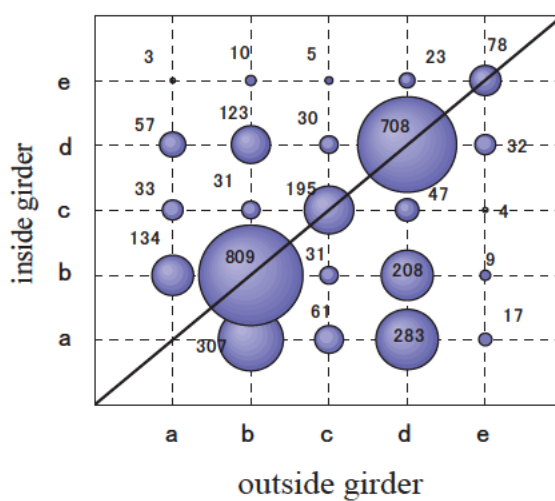


Figure 3 Corrosion, Steel plate girder bridge, main girder at the middle, Degree of damage for each region

(2) Cracks of steel plate girder bridge

For cracks of steel plate girder bridge, Figure 4 shows the degree of cracks at the end and middle of the same girder. The degree of the cracks at the end of the main girder has a tendency to be worse than that at the middle.

For cracks of main girder in the steel plate girder bridge, Figure 5 shows the degree of cracks at the outside and inside of the same span. Since there are some cracks at any objective region such as outside, inside, and all span of the girder.

In this way, it is considered that there is a possibility of reducing a risk of missing at the inspection time due to incorporating into specific inspection of fatigue, which the government is planning.

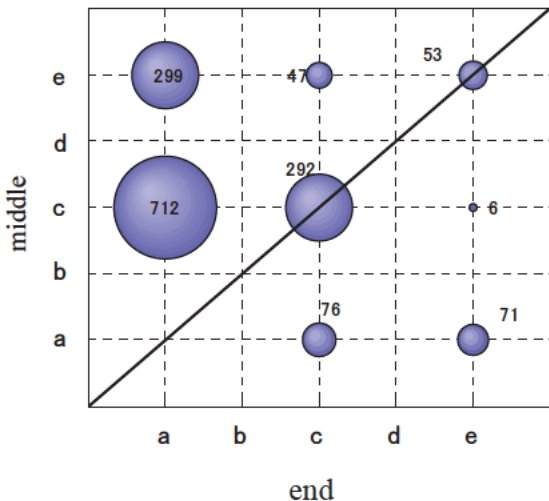


Figure 4 Crack, Steel plate girder bridge, main girder, Degree of damage for each region

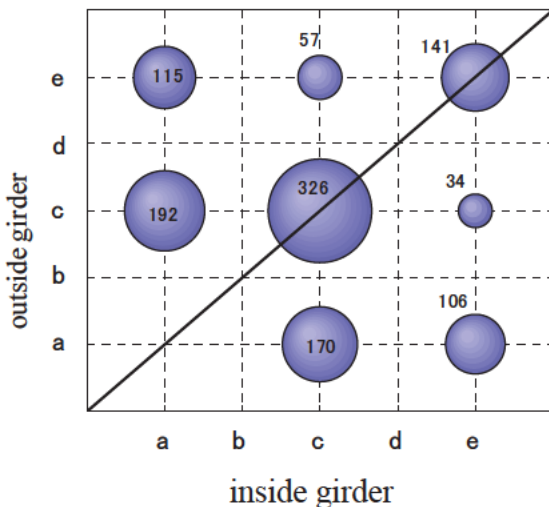


Figure 5 Cracks, Steel plate girder bridge, main girder, Degree of damage for each region

(3) Cracks of concrete bridges

For cracks of concrete bridges, Figure 6 shows the degree of cracks at the end and middle of the T-girder bridges with pre-tensioning system, Figure 7 shows those with post tensioning system, and Figure 8 shows those of RC-T-girder bridges. Most of the T-girder bridges with pre-tensioning and post tensioning system have cracks only at the end or the middle of the main girders. The degree of the cracks at the end of the main girder has a tendency to be worse than that at the middle. On the other hand, RC-T-girder bridges have a tendency to have cracks at all of the main girders.

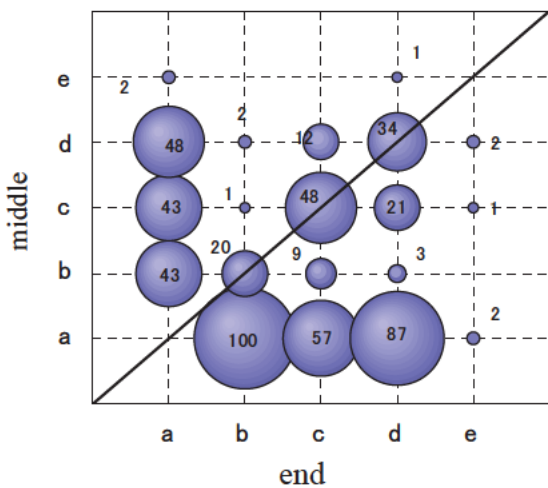


Figure 6 Cracks, T-girder bridges with pre-tensioning system, main girder, Degree of damage for each region

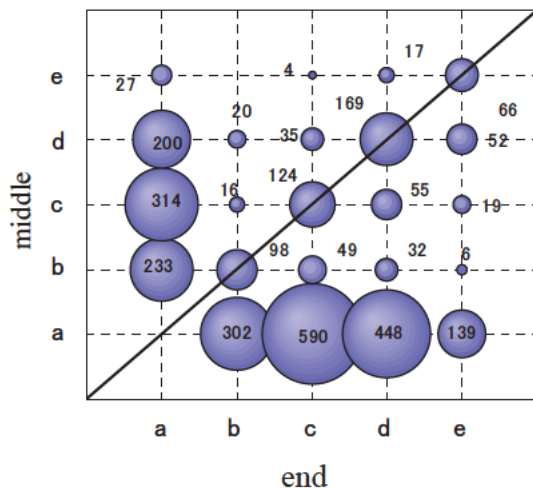


Figure 7 Cracks, T-girder bridges with post tensioning system, main girder, Degree of damage for each region

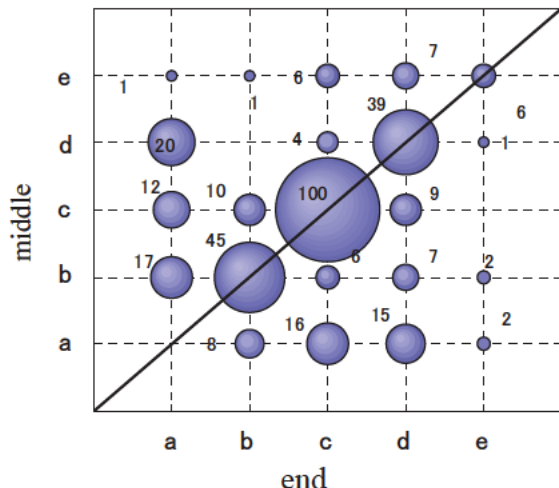


Figure 8 Cracks, RC-T-girder bridges, main girder, Degree of damage for each region

For cracks of concrete bridges, Figure 9 shows the degree of cracks at the outside and inside of the T-girder bridges with pre-tensioning system, Figure 10 shows those with post tensioning system, and Figure 11 shows those of RC-T-girder bridges. Most of the T-girder bridges with pre-tensioning and post tensioning system have cracks only at the outside or inside of the main girders. The degree of the cracks at the end of the main girder has a tendency to be worse than that at the middle. On the other hand, RC-T-girder bridges have a tendency to have cracks at all of the main girders

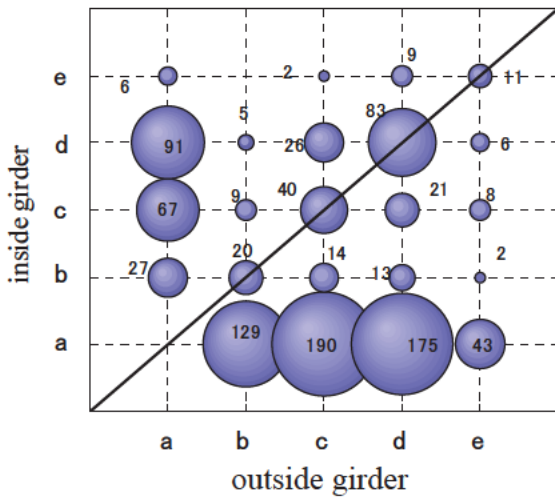


Figure 9 Cracks, T-girder bridges with pre-tensioning system, main girder, Degree of damage for each region

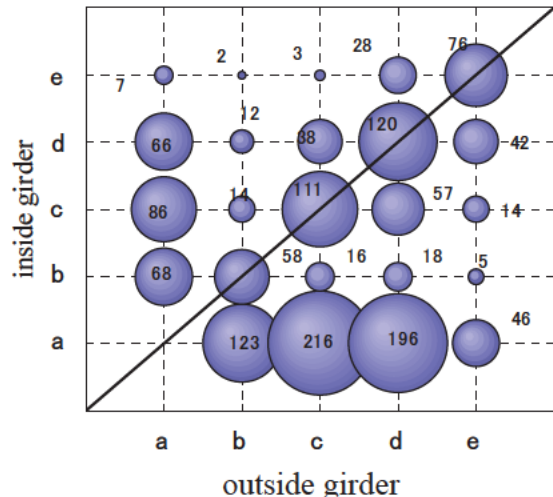


Figure 10 Cracks, T-girder bridges with post tensioning system, main girder, Degree of damage for each region

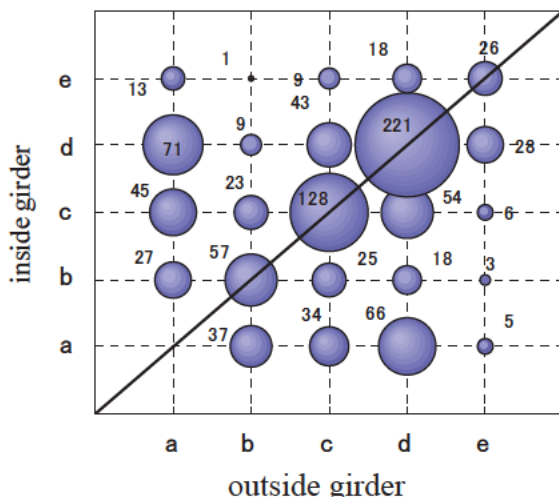


Figure 11 Cracks, RC-T-girder bridges, main girder, Degree of damage for each region

For cracks, adding to recording the degree of damage at the element level, typical crack types are divided into 20 patterns and the pattern number is recorded.

For concrete T-girder bridges, Figure 12 shows the number of members with crack for each pattern for T-girder bridges with pre-tensioning system, Figure 13 shows that with post tensioning system, and Figure 14 shows that for RC-T-girder bridges. The number of members with 'pattern' (vertical cracks at the girders on the bearings) for pre-tensioning system, 'pattern' (vertical cracks at the bottom/side of the girders of the center of the span) for post-tensioning system, and 'pattern' (longitudinal cracks at the bottom of the girders of the center of the span) for RC-T-girder bridges were the largest.

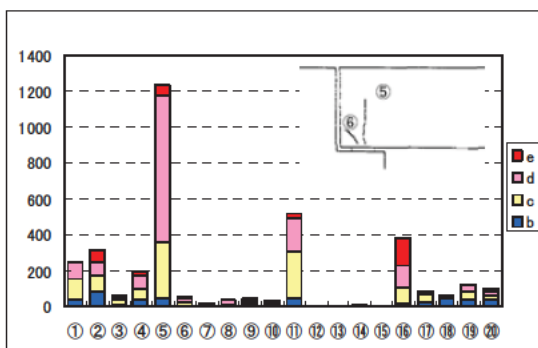


Figure 12 Cracks, T-girder bridges with pre-tensioning system, The number of members with crack for each pattern

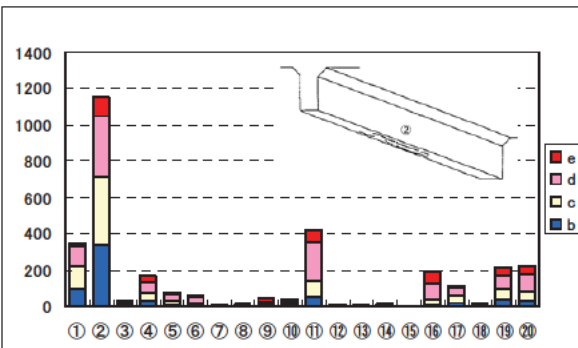


Figure 13 Cracks, T-girder bridges with post tensioning system, The number of members with crack for each pattern

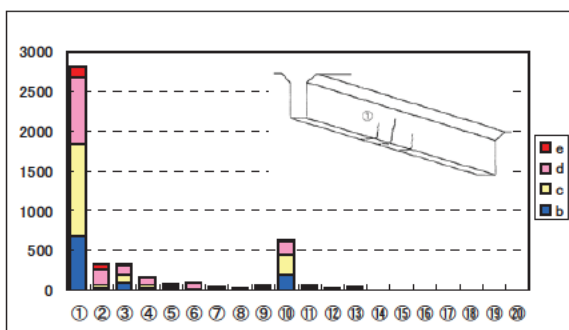


Figure 14 Cracks, RC-T-girder bridges, The number of members with crack for each pattern

For concrete cracks, it was indicated that there was a difference of the degree of cracks depending on types (pre-tensioning system, post-tensioning system, and RC-T-girder) and girder regions (end and middle, and outer and inside girder). In this way, since the features of cracks by bridge types can be grasped, it is possible to implement crack control measures at the design-time, and to improve the initial material qualities. Moreover, there is a possibility of making inspections effectively by restricting the inspection region.

(4) Cracks of RC slabs of steel bridges

For cracks of slabs of steel plate girder bridges, Figure 15 shows the relationship between passed years and degree of damage for cracks of slabs at each general and cantilever parts. Degree of damage for cracks of slabs at the general parts has a tendency to be worse over years, while that at the cantilever parts does not.

In this way, for the cracks at the RC slab, there was a difference of the degree of cracks depending on slab types (general and cantilever parts). In this way, it was indicated that there is a possibility of improving the initial material qualities economically and rationally especially for the cantilever parts by taking measures at the initial design-time.

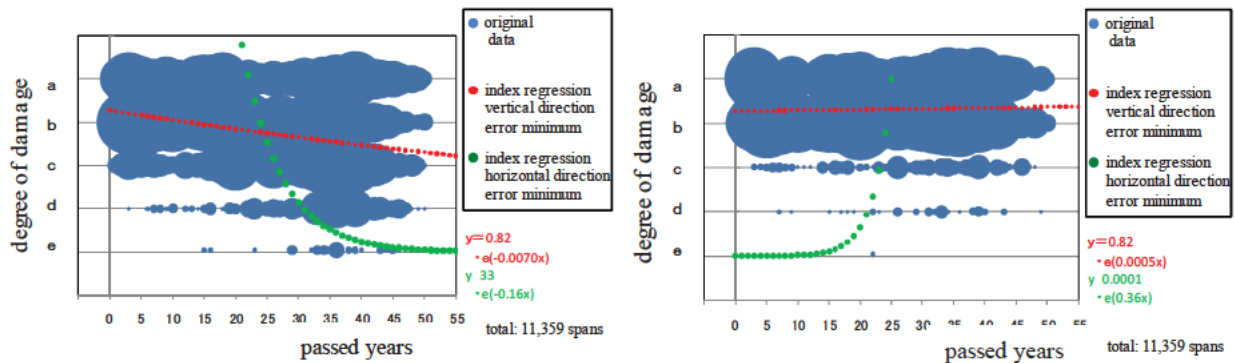


Figure 15 Relationship between passed years and degree of damage at general and cantilever parts

(Cracks of slabs, Steel plate girder bridges, RC slabs)

DAMAGE PROGRESSION

A tendency of damage progression was analyzed by calculating transition probability of degree of damage (from ‘a’ to ‘e’) for each member and region in order to grasp how the degree of damage will progress within 5 years by using two periodic inspection results (hereinafter called ‘the new inspection’ for the most recent inspection, and ‘the old inspection’ below) conducted to the same bridge in the different time.

A group of data consisting of the most recent periodic inspection results based on the manual and the results based on the manual of 1988, and a group of two data of bridges conducting two periodic inspection based on the manual are used for the analyses.

For the verification of the old and new inspection results, the results which satisfy the following extracted conditions were regarded as the effective data.

- i) Inspection interval is within five years.
- ii) The old and new inspection data for the same elements exist.
- iii) No repairs were done between the old inspection and the new inspection.
- iv) Degree of damage for the new inspection is the same or the worse as compared to that for the old.

The total is 5,109 bridges, and the objective bridges were extracted for each analysis.

In this chapter, analysis examples of steel corrosion and crack of slab remarkable for features of damage for each member and region in the previous chapter were indicated. The analysis contents are a transition probability made up the degree of damage for the new inspection to the old one, Markov chain based on that, an expected value for Markov chains every five years weighting each degree of damage (‘a=1.00’, ‘b=0.75’, ‘c=0.50’, ‘d=0.25’, and ‘e=0.00’), and standard deviation in some of these graph.

(1) Corrosion of steel plate girder bridges

For corrosion of main girder of steel plate girder bridges in a A & B type of painting, Figure 16 shows transition probability, Markov chain, and expected values for whole members (from the left to the right), Figure 17 for the end of the girders, Figure 18 for the middle, Figure 19 for the outside girders, and Figure 20 for the inside girder.

For the transition probability of the left figure, for example, 80% of the degree of damage ‘a’ (no corrosion) for the old inspection keeps the same state, while most of the rest of 20% progress the degree of damage ‘b’, others progress ‘c’, ‘d’, and/or ‘e’. Thus, the damage progression depends on the bridges, and so it has a tendency to vary to some extent.

In this way, features shown in the damage progression states were also shown in the damage occurrence states.

Moreover, the deterioration prediction distribution varies, however, the accuracy improvement of the deterioration curve by each region in Figure 17 & 18

more than that by the whole members in Figure 16 is expected.

For Markov chain (the middle figure) and the expected values (the right figure) obtained from the transition probability (the left figure), the degree of damage at the end of the girders has a tendency to be worse than the middle of the girders, as seen in Figure 2. Also, the degree of damage at the outside girders has a tendency to be a bit worse than the inside girders, as seen in Figure 3.

Also, Markov chain shows the probability of occurrence of the degree of damage after some years. However, it is common to use the expected values for the application of future prospects of the individual bridges instead of Markov chain. In this case, since the expected values are the uniform ones, the values have a possibility to be confused with the fixed ones. In order to prevent this confusion, standard deviation of the expected values were shown to the right figure. Future prospects should be used with the recognition that it just shows the probability with variation.

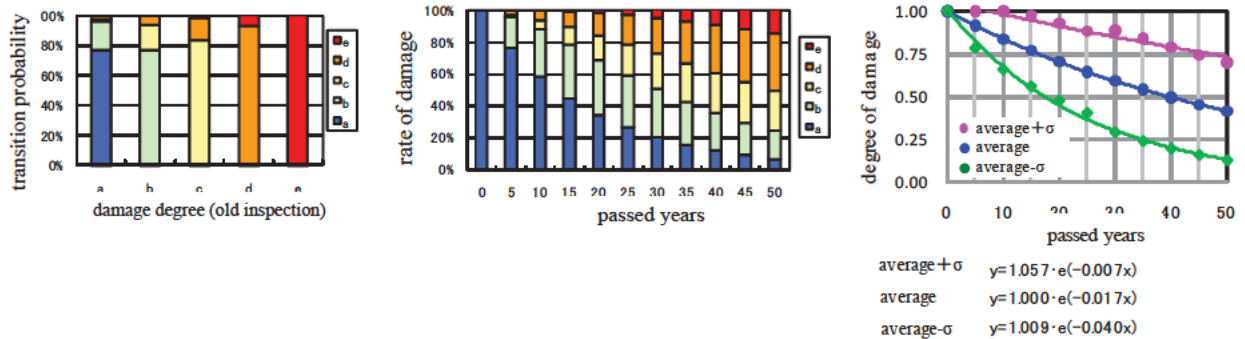


Fig. 16 steel plate, main girder, corrosion, A & B type of painting, whole member

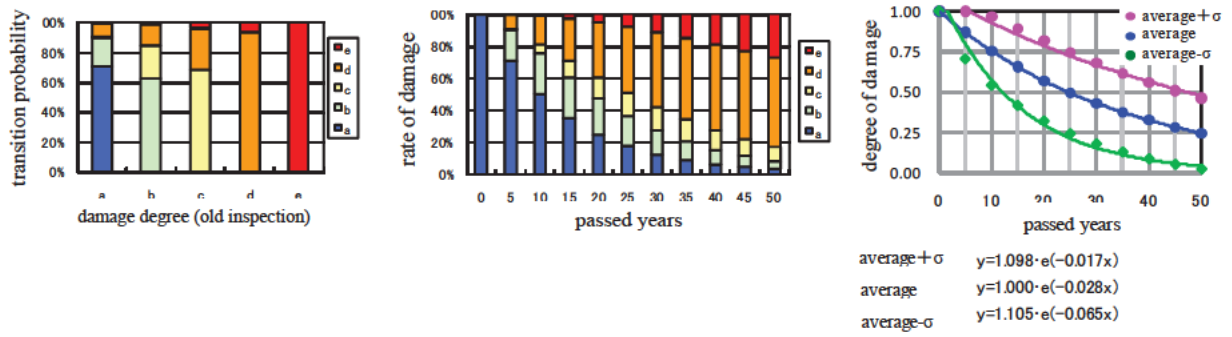


Fig. 17 steel plate, main girder, corrosion, A & B type of painting, end of girder

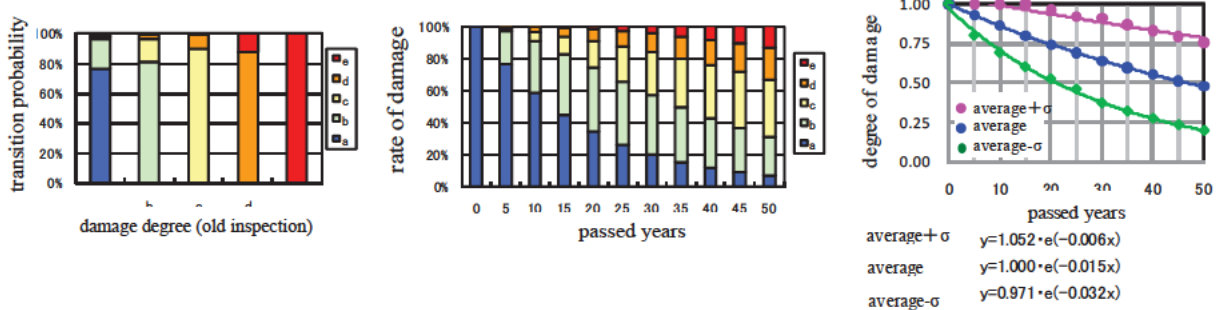


Fig. 18 steel plate, main girder, corrosion, A & B type of painting, middle of girder

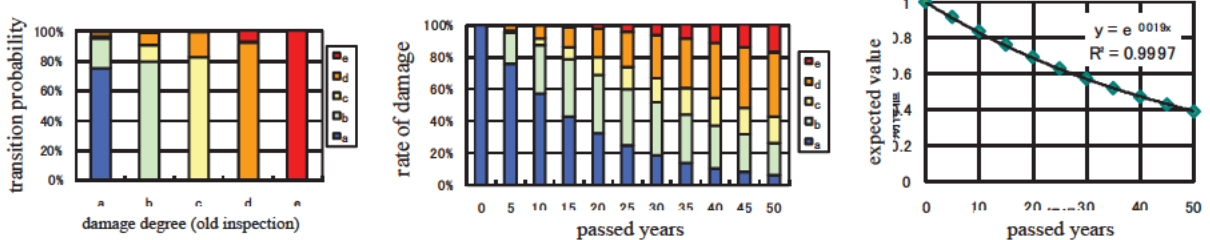


Fig. 19 steel plate, main girder, corrosion, A & B type of painting, outside girder

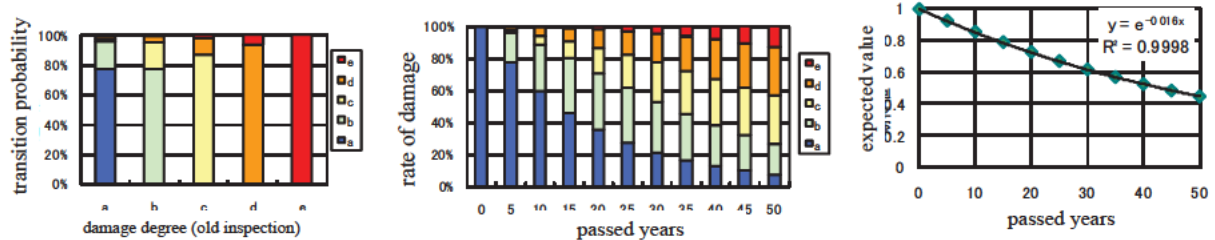


Fig. 20 steel plate, main girder, corrosion, A & B type of painting, inside girder

(2) RC slab of steel bridges

For crack of RC slab of steel plate girder bridges, Figure 21 shows transition probability, Markov chain, and the expected values (from the left to the right) for the cantilever parts, Figure 22 for the general parts. The degree of damage for crack of the slabs for the cantilever parts progresses up to 'b', as seen in Figure 15. In this way, features shown in the damage progression states were also shown in the damage occurrence states. Results obtained from the deterioration prediction were already shown in the above (1).

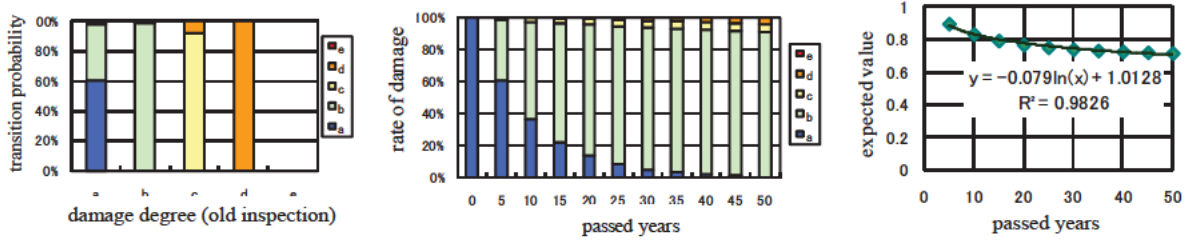


Fig. 21 steel plate, RC slab, crack of slab, cantilever part

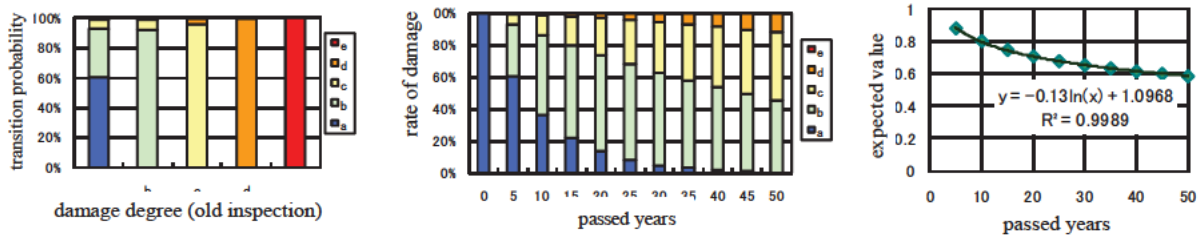


Fig. 22 steel plate, RC slab, crack of slab, general part

Summary

Since the periodic inspections in the element level are conducted, it is possible to analyze the degree of damage for each member and region. Thus, differences of the degree of damage and damage progression for each member and region in the same bridge were recognized. Also, transition probability, Markov chain, and the expected values and standard deviation using the probability could be calculated by analyzing the old and new inspection data in the element level.

Based on features of damage occurrence and its progression adding material, bridge types, and environments, improvements of the frequency and the method of the periodic inspection, accuracy improvements for the data analyses, and improvements of the initial design, lead to rationalization of bridge maintenance. Saving the data in the element level, the more detailed survey analyses for identification of damage progression, their correlation, and quantitative evaluation for variation of the degree of damage will be conducted. In the future, the further research plans to be conducted toward the achievement of the smart bridge maintenance system, which the life-cycle costs and the risk among the users can be minimized due to the use of the recent information technologies and the appropriate maintenance for individual bridges.

References

- [1] National Highway and Risk Management Division, MLIT: Bridge Periodic Inspection Manual (Draft), March, 2004

THE IMPORTANCE OF PARTNERSHIPS IN THE IMPLEMENTATION OF BRIDGE PRESERVATION PRACTICES

Peter J. Weykamp¹

Abstract

This paper discusses the advantages of multi-discipline partnerships for instituting bridge preservation programs from the perspective of the bridge maintenance engineer. FHWA, AASHTO, and other stakeholders, including the bridge maintenance community, are working collaboratively to increase communications in developing a more holistic approach to managing highway structures. This paper will briefly review a few of the communication initiatives implemented, describe several “best practices”, and identify topics for further development within three areas pertinent to bridge maintenance; 1) bridge management; 2) bridge design; and 3) “maintenance friendly” materials.

Introduction

FHWA and AASHTO have been instrumental in providing avenues for bridge maintenance practitioners to meet and discuss issues through peer exchanges and web-based formats. Though bridge maintenance was discussed in such circles as TRB Committees and the AASHTO Subcommittee on Bridges and Structures, most often bridge maintenance engineers were in the minority or not in attendance. The Bridge Technical Working Group (BTWG) to the AASHTO Subcommittee on Maintenance was one of the only conferences specifically focusing on bridge maintenance. A few regional groups, such as the Midwest Working Group and the Pacific Northwest Maintenance Conference, invited bridge maintenance practitioners to meet and discuss the issues specific to bridge maintenance. On the whole, however practicing maintenance engineers had limited opportunities to participate in peer to peer discussions.

In 2007 the BTWG to the AASHTO Sub Committee on Maintenance developed a Bridge Preservation and Maintenance (BPAM) Strategic Plan. The document was created to provide a comprehensive strategic plan for highway bridge preservation and maintenance. The plan listed objectives of identifying good practices and strategies, succession planning strategies, communication needs, identified suggested research topics, promoted management systems, materials innovations, and requested the creation of regional partnerships consisting of bridge preservation and maintenance stakeholders. The BPAM was included in a resolution entitled AASHTO Bridge Preservation Strategic Plan Recommended Strategy Focus Areas 2008 - 2013 adopted by the AASHTO Standing Committee on Highways in 2008. The document continues to serve as a roadmap for bridge preservation stakeholders.

¹ Bridge Maintenance Program Engineer, New York State Department of Transportation.

In 2009, AASHTO contracted with the National Center for Pavement Preservation (NCP) to include bridge preservation in their Transportation System Preservation Technical Services Program (TSP²), which was formed only a few years earlier to focus on pavement preservation. The TSP² now provides administrative services, a website, FAQs web board, and on-line library assisted in the creation and continues to support regional partnerships on bridge preservation. All stakeholders involved with bridge preservation were invited to become members. Owners, consultants, suppliers, academics, and contractors were invited to join one of four regional partnerships covering all AASHTO members.

During the same period, FHWA held a national meeting to develop a research roadmap for bridge preservation. Stakeholders representing a variety of disciplines gathered to develop and prioritize research needs statements. The process has been successful as topics related to bridge preservation continue to receive funding through the NCHRP.

The multi-disciplined approach was also used by FHWA in 2010 to define the term “Bridge Preservation”. Again, owners, product manufacturers, consultants, FHWA officials, and academics were brought together to work toward a definition. The definition is currently under consideration for adoption by AASHTO.

The draft definition states: “Bridge Preservation: Actions or strategies that prevent, delay or reduce deterioration of bridges or bridge elements, restore the function of existing bridges, keep bridges in good condition and extend their useful life. Preservation actions may be preventive or condition-driven.” (Ahmad, 2011)

Bridge preservation is more than bridge maintenance. AASHTO, FHWA, and others advocate for owners to adopt preservation strategies that “employ long term strategies”, include “sustained and adequate funding sources”, and ensure the “appropriate treatments are applied at the appropriate time”. The concept of preservation necessitates that treatments are available for various condition states, that management systems are based on element level condition assessment, and have the capability of identifying, prioritizing, and estimating bridge needs. Bridge maintenance engineers support the implementation of these concepts.

Bridge Management

Bridge management until recently was essentially a “worst-first” program. Federal funding was primarily focused on structurally deficient and functionally obsolete bridges. Much has changed. Perhaps the precursor to a review of all bridges began with the implementation of Pontis, offered by AASHTO as a national bridge management system.

Pontis provides for element level bridge condition ratings, perhaps the singularly most significant enhancement in managing a network of bridges. Bridge

conditions could now be described on an element level basis as opposed to the three components used in the National Bridge Inspection program (deck, superstructure and substructure). Element level conditions are critical in identifying and addressing early failures thereby avoiding more costly repairs. Recording the “condition state” goes even further as it provides the maintenance engineer with a comprehensive review of the condition of the element.

Pontis Task Force members are primarily state bridge management engineers with input from other groups, including bridge maintenance engineers. Pontis enhancements currently under development include condition rating information for steel coatings and wearing surfaces. These protective systems are currently rated in a review of the primary member and the structural deck, respectively. Maintenance engineers will thereby be informed when protection systems have been compromised. Pontis will also be able to group bridge needs. It currently lists response options for individual needs. Grouping bridge needs is expected to improve system derived options for treatment selection and improve repair estimates.

The requirements instituted to obtain high quality condition data are not matched for inventory data. Uncertainty in data quality, missing data, and incorrect inventory data hamper reviews on the performance of new materials, investment strategy outcomes, feedback on changes in design details, compliance with technical memorandum on assessments, or improvement in element level deterioration modeling. It is not unusual for a maintenance crew to remove an armored angle expansion joint and replace it with a polymer-based system without the inventory being updated. Most agencies do not currently have a link between their maintenance management system and their bridge management system.

Needs lists, derived from data from the bridge inspection program, do not capture all the needs of the network structures. U.S. Domestic Scan 07-05 entitled Best Practices in Bridge Management Decision-Making identified the need for management systems to be flexible and work to include the experiences of the regional or district personnel. Host states mentioned the needs list developed by the agency's bridge management system contained, at best, 50 to 55% of the needs identified by field reviews. Management systems using safety-based inspection criteria are not capturing the same information collected by regional staff. Regional or District bridge maintenance engineers and crews may have 20 plus years of experience with a set of bridges. Agencies recognize the value of this experience and allow regional management to edit the needs lists.

Durability is not captured in current inspection systems and as a result management systems are not able to differentiate between a good performing bridge with a low condition rating, health index, or sufficiency rating or a poor performing bridges with good ratings. Bridge maintenance engineers determine durability through experience, either by bridge design type or knowledge of the performance of an individual bridge. To illustrate: a jack arch structure with a low condition rating does not concern the maintenance engineer. Ratings for those structures do change

significantly and the structure still has ample service life even in poor condition. On the other hand, even a slight change in the condition rating of adjacent pre-stressed box beams causes alarms. These structures do not age well and can fail catastrophically.



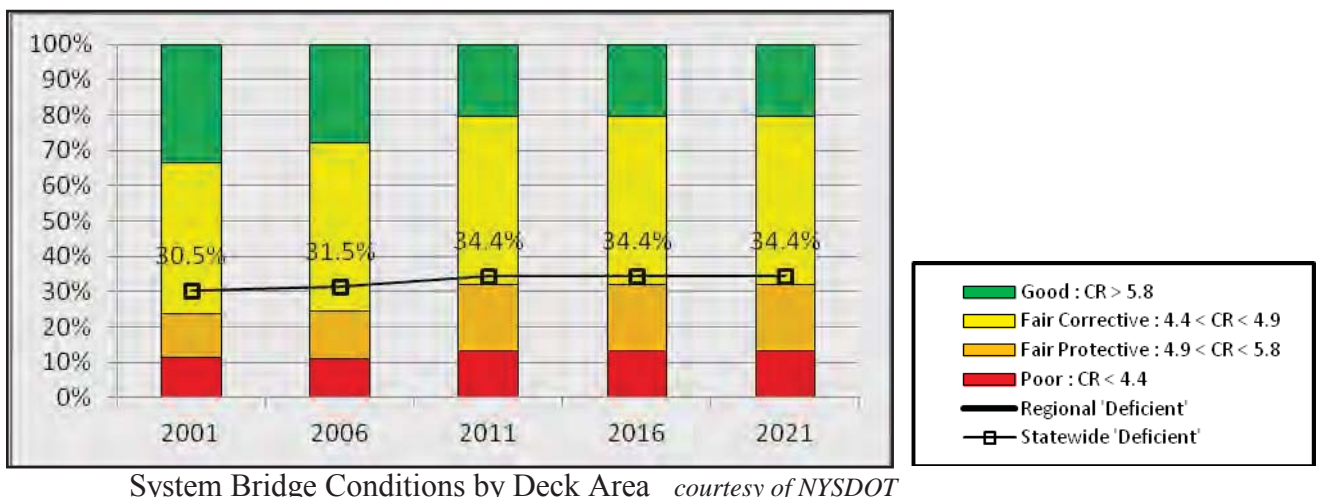
BIN 3346310 Built 1925



BIN 1011510 Built 1983

An international scan tour on Bridge Evaluation Quality Assurance in Europe outlined the German SIB-Bauwerke system of rating bridges. German inspectors rate structures for 1) structural stability, 2) traffic safety, and 3) durability. The study found that “in Europe, the emphasis is greater on determining the cause of a particular defect in the bridge.” This is in contrast to the U.S. approach of characterizing the element or component, which essentially characterizes the effect of the defect”. (Everett, 2008)

Many agencies are moving to include alternative indicators to measure network conditions. Bridge programming now looks to minimize the percentage of structurally deficient structures by including a review of the conditions of the entire network. Agencies have increased efforts to keep bridges from becoming deficient. The most common approach divides the network into categories of Good–Fair–Poor based on condition. Historic data and forecasting methods can be used to track the movement of bridges over time.



Municipalities, counties, cities, and towns own slightly more than 50% of the

bridges in the U.S. In most cases, they do not have the resources to adequately maintain their structures. Consultants are typically held on retainer to provide designs for emergency repairs and design services for bridge rehabilitation or replacement projects. Some consultants, however, have found a niche by providing municipalities network management services. The City of Rochester, New York has secured consultant services for the inspection, needs assessment, maintenance program development & design, and construction inspection services for the city's 70 bridges. The consultant essentially acts as the manager of the inventory, determines bridge needs, and develops the bridge preservation plan for the network.

Designing for Access

A vast amount of effort has gone into research of new materials and design parameters expected to improved bridge performance. Epoxy coated bars, joint-less bridges, and high performance concrete are some examples of common enhancements aimed at improving the service life of highway structures. Comparably, however, little attention has been paid to designing for the maintenance of the bridge. Bridge maintenance engineers generally adhere to the realization that “all concrete cracks, all joints leak, and rust never sleeps” (Welch 2005). Some of the following suggestions would facilitate maintenance and inspection efforts throughout the life of the structure.

Increasing the size of the pedestals and/or diaphragms would facilitate bridge jacking operations. Steel sliding bearings need to be lubricated approximately every six years. To properly lubricate the bearing, the bridge has to be raised. Bearing manufactures do not supply a parts list or maintenance requirements for their bearings. It would be helpful if the expansion bearings included a means to indicate if they were still capable of movement. If “frozen”, a maintenance action could be programmed to avoid deterioration of the anchor bolts and pedestals.

Access to the substructure is not easy. Traversing 1 on 2 slopes, even without tools and ladders, is difficult. When 10” (254 mm) sized loose stones (rip-rap) are used for slope protection footing becomes hazardous. Setting up ladders and scaffolding on narrow or non-existing berms is difficult. A level six foot (1 meter) wide concrete berm for tall abutments would facilitate inspection and maintenance operations.

Designers should consider the possibility that typical maintenance activities may not be possible to perform for standard bridges carrying high volumes or high speed traffic. It is difficult to obtain approval for multi-lane closures on interstate roadways for maintenance actions. Joint repair, deck sealing, and deck repairs may not be performed until serious conditions exist. Alternative means of access, stainless rebar, and durable waterproofing membranes could be included in the design for these service conditions.

Materials

Most materials adopted by an agency come through the maintenance

organization first. To be able to “apply the right treatment at the right time”, maintenance managers need a tool box of products for assorted conditions. Typical activities performed by maintenance crews focus on deck waterproofing systems, correcting leaking joints, protecting steel elements, and concrete repairs. Perhaps the primary factor, after safety considerations, in selecting repair materials is speed. Not only is it hazardous to be working next to high speed traffic, but traffic delays are unacceptable. Overnight lane closures or concrete barrier protection for bridge maintenance activities are seldom employed. Field crews need to “get in and get out”.

The most common deck waterproofing system, bituminous sheet membranes, were developed for the roofing industry. These peel and stick sheet membranes are labor intensive and time consuming. Spray applied applications with automated equipment increase productivity but are more costly. Manufacturers have responded to failures attributed to bond by introducing hot applied membrane systems. Some agencies now specify only hot or torch applied systems.

Polymer manufacturers attentive to deck maintenance needs have developed materials and application techniques. Thin Polymer Overlays (TPOs) are easily applied by maintenance crew using a “broom and seed” or a slurry method and have provided satisfactory performance for a number of years. These materials offer minimal dead load, require no adjustments to bridge rails or existing expansion joints, but are more costly than sheet membranes.

The use of second generation polymer modified binders, developed for pavement preservation applications, has promising potential for use as a deck waterproofing system. These materials require minimal surface preparation, are comparatively cost-effective and placement rate are similar to those of HMA applications. They have minimal dead load (typical thickness of 3/8" (9.5 mm), and may provide a long term waterproofing barrier. The material and



application technique, commonly called Nova-chip, can be formulated with a high percentage of rubber and a low modulus of elasticity. Representatives from the pavement preservation industry now attend bridge preservation conferences.

The New York Department of Transportation is working with a local inventor who has developed a moisture sensor using the concept of a “beneath the surface” wireless technology. These sensors measure moisture of the concrete through wires on the side of the units. Resistivity readings are taken through the membrane by a computer surface unit that excites the sensor. The low cost sensors are being placed in shallow cavities in existing bridge decks. Wiring or batteries are



not required. A variety of waterproofing systems are being reviewed to determine if they are effective as a waterproofing barrier.

Bridge maintenance engineers probably spend more time attempting to correct leaking expansion joints and avoid the subsequent deterioration of elements under the joint, than any other bridge activity. Manufacturers have responded. Innovations in design and materials, especially for small movements allow for rapid replacement using “maintenance friendly” materials and techniques. Polymers with low modulus of elasticity provide a resilient anchoring material, an important characteristic for protection against the impact of snow plows. These two part materials, most commonly epoxies, are easy to use, and are traffic ready in 3 hours depending on ambient temperature.

Various seals are available. Pourable silicones are useful for non-parallel, and irregular surfaces, but surface preparation is critical. Pre-formed closed cell foams are more tolerant of contaminated surfaces, are inexpensive, but must be sized accurately and can be difficult to install. Manufacturers have responded by developing W and V-shaped pre-formed seals of neoprene or silicone which provide for a wider range of movement. These seals are very easy to install but are considerably more expensive.

When these joints fail, it can most often be attributed to improperly sizing of the seal. All too common a measurement of the opening is taken on the day of installation without consideration of the movement range of the structure. A common misconception is to measure the opening on the day of installation and size the seal (typically foam) $\frac{1}{4}$ " (6.35 mm) wider than the opening. Despite manufacturers claims to the contrary, a good practice is to size the seal so it does not go into tension. Manufacturers are working to make the installation of the seal as foolproof as possible.

A notable innovation is the use of urethane-based repair materials. A small company in Washington has developed an application where the ultra-low viscosity resin is pumped from barrels, mixed in the nozzle and gravity-fed onto gap graded $\frac{3}{8}$ " (9.5 mm) angular aggregate. This application has been well received by maintenance crews. Modified urethanes are traffic ready in 30 minutes, can be placed in below freezing temperatures and significantly increase productivity. Mixing in 5 gallon (3.78 liter) containers and placing with hand trowels is eliminated. Several other manufacturers are developing similar applications.



Silane sealers provide an inexpensive barrier to the ingress of chlorides for reinforced concrete. They perform well in the laboratory testing. However, the effectiveness of silane sealers on in-place structures is not well documented. Effectiveness studies for in-place applications are difficult to conduct and require a lengthy assessment period. A comparative review of deck condition data of agencies known to have a generally consistent sealing program to that of those known that do not

seal bridge decks could prove informative. Sealers do not prevent contaminates from entering through cracks in the concrete. Manufactures are working to enhance sealers with corrosion protection properties. Studies on the effectiveness of a penetrating sealer on vertical surfaces, such as columns and abutments would also be helpful.

Coatings of paints are the primary means of protecting steel superstructures. Blasting the surface is necessary because the paint systems specified require a white metal or near-white metal surface profile. Most agencies have dropped their in-house painting programs because of prohibitions against open blasting. The efforts of the manufactures and the coatings industry have been on extending the service life of the paint system, whereas the bridge maintenance engineer is focusing on extending the life of the superstructure. Coatings that could be applied on surfaces requiring much less preparation and capable of providing some years of protection are being sought by maintenance engineers. Manufacturers of older technologies such as high content calcium sulfonate, long chain non-polar hydrocarbons, such as marine grease are working with bridge maintenance engineers to assist in providing some protection against section loss between painting projects.

Summary

The multi-disciplined approach of including all stakeholders in the discussion of needs to address bridge preservation concerns has yielded immeasurable benefits. The ability to respond to the needs of an aging infrastructure with limited funding will require input from many sources. Peer exchanges, such as the Regional Bridge Preservation Partnerships, now only in it's second year of existence, has already proven beneficial for bridge designers, maintenance managers, industry, and the consultant community.

Coordinating the energies and interests of the various stakeholders becomes a much more realistic endeavor when done through partnerships. Through the communication of needs, sharing good practices, and developing a unified statement of objectives, partnerships are assisting in developing a more holistic approach toward bridge management.

References

1. AASHTO Standing Committee on Highways (PPR-AM08 Attachment)
Subcommittee on Maintenance Title: AASHTO Bridge Preservation Strategic Plan Recommended Strategy Focus Areas 2008 - 2013 SCOH Business Agenda Resolutions Hartford, Connecticut – October, 2008
2. Ahmad, Anwar: Bridge Preservation Guide Maintaining a State of Good Repair Using Cost Effective Investment Strategies; FHWA-HIF-11-042, 2011
3. Everett, Thomas: Bridge Evaluation Quality Assurance in Europe: FHWA-PL-08-016, 2008
4. Hearn, George: Bridge Preservation and Maintenance in Europe and South Africa: FHWA-PL-04-007, 2005
5. Memmott, Jeffery: "Highway Bridges in the United States—an Overview"
Bureau of Transportation Statistics USDOT Research and Innovative Technology Administration, 2007
6. Welch, Ed et al: "The Bridge Maintenance Credo", 2005
7. Weykamp, Peter et al: Best Practices in Bridge Management Decision-Making: NCHRP 20-68A Scan 07-05, 2009

Maintenance of ASR-affected Structures in Hokuriku Expressway, Japan

Mamoru Moriyama¹, Masahiro Nomura²

Abstract

Increasing amounts of deicing salts have been used to ensure the safety of road surfaces in Hokuriku district, Japan. Sodium chloride, which accounts for the majority of deicers, has been causing damage to road concrete structures due to alkali-silica reaction. This report describes the current state of maintenance and repair techniques of these road structures affected by deicer-related alkali-silica reaction.

Introduction

Increasing amounts of deicing salts have been used to ensure safety of road surfaces in Hokuriku district, in Japan. The deicers used in this area have been mainly of sodium chloride (NaCl) type. In addition, the structures alongside the Japan sea coastline are subjected to monsoons, which increase its exposure to airborne chlorides from the sea. Therefore, these natural conditions set the road structures of the Hokuriku district in a permanent saline environment. As the effect of this chloride supply, the cases that alkali-silica reaction (ASR) deteriorates road structures have been increasing. On the other hand, river gravels and river sands have been used as concrete aggregates for a long time and these aggregates have been found in seriously ASR-affected structures. ASR has occurred mainly in structures primarily built from 1970 to 1985, a time when high alkali cement had been produced in Japan. Over the course of time, reactive river sands and gravels may not be properly assessed since these aggregates contain a wide variety of rock types, as well as different types and contents of reactive minerals.

Central Nippon Expressway Company has covered the sections from Kinomoto IC (Shiga Prefecture) to Asahi IC (Toyama Prefecture) in Hokuriku Expressway and Oyabe-tonami JCT (Toyama Prefecture) to Shirakawago IC (Gifu Prefecture) in Tokai-Hokuriku Expressway, a total of 300km (9-39 years in service). There are 545 bridges, 1200 C-Boxes and 45 tunnels in these sections. ASR occurs in some of these structures and the application of efficient maintenance techniques have been put in place.

This report presents the current state of inspection and survey of road structures under saline environment in the Hokuriku district, the methods of diagnosis, repair and repair prioritization of ASR damaged structures.

¹ Central Nippon Expressway Company Limited Kanazawa Branch

² Researcher, Central Nippon Highway Engineering Nagoya Company Limited Kanazawa Branch

The ASR Characteristics in Hokuriku district

The Hokuriku district is located approximately in the center part of the Japan Sea coastline and is characterized by severe weather conditions: hot and humid summers and cold and snowy winters (see Fig. 1~Fig. 3).

Figure 4 shows the map of deteriorated structures in the Hokuriku district. In the expressways ASR occurs in almost all areas of Toyama Prefecture and parts of Ishikawa and Fukui Prefectures. The reactive aggregates were confirmed as andesite, rhyolite and tuff, from volcanic rock deposits (see Fig. 5). Deterioration of road structures by ASR has been often assessed as a combined effect of rainwater, road drainage and deicer application (see Fig. 6).

Maintenance

The inspection of road structures is classified as regular inspection or detailed inspection. Regular inspections are conducted once a year, while detailed inspections are carried out in the span of 2 to 5 years. These inspections have been mainly visual. In addition, continuous survey of the expansion behavior of the structures (by contact gauge or by π gauge) is conducted every year and followed by a thorough investigation.

Fig. 7 shows the flow of assessment of ASR-deteriorated structures, which has been applied in reference to the case-studies shown in Fig. 6. In addition, the structure's database is comprised with the construction company, concrete plant, cement maker, aggregate quarry or supplier once construction is elaborated. In the deterioration cases where the assessment is inconclusive, ASR occurrence is determined by a comparative evaluation of the database of other structures supplied from the same concrete plant. If it cannot provide a proper judgment, then a detailed investigation has to be carried out.

Detailed ASR investigation includes the mineralogical composition of coarse aggregates, thin section observation with a polarizing microscope, alkali and chloride contents in concrete, and the residual expansion of concrete cores drilled from the structures. In particular, considering the feature of Hokuriku district, the residual expansion test of concrete cores, which is a technique that conforms with the alkali external supply, has been adopted. The test method is described in Table 1 and shown through Fig.7~Fig. 11.

Repair and monitoring

Figure 12 shows the flow of repair method selection of ASR-deteriorated structures. Since there are a considerable number of ASR deteriorated structures in the Hokuriku district and, therefore, a need for reducing maintenance costs, a ranking system based on the visual inspection has been created for choosing the ASR repair method. For

ranking “A” structures, crack injection and surface coating is applied, including the time reference results of residual expansivity tests of concrete cores. For ranking “B or C” structures, the road surface drainage countermeasures are applied, followed by close observation of the improvements. Repair rankings are priority for important intersections (such as national road and railway) and the areas affected by concrete spalling or peeling off, works include section repair and coating with fiber sheets. In addition, due to the severe environment conditions in the Hokuriku region, the rehabilitation period has been set to about one or two year long to ensure quality control.

After the repairing is concluded, monitoring is applied for inspection purposes. Focus point is the effect of road surface drainage. Also, a special attention is paid to bridge abutment front, where the water absorption from the back part often leads to swelling of the surface coating. The effective countermeasures for stopping water migration from the back part of bridge abutments are a matter of serious concern.

Concluding Remarks

The extent of ASR deterioration of concrete structures in the Hokuriku district is significant if compared to other areas of Japan. In some cases, fracture of reinforcing steel bars due to ASR expansion has been reported. The lack of appropriate repairing countermeasures to stop ASR progress is still a matter of fact. If the repair occurs ASR, there will be no drastic measures. At present, ASR in bridge superstructure has not reached deterioration levels which exert influence on the load bearing capacity. In the future we will plan to continue the conduction of detailed inspections and surveys on these ASR-affected structures.

Table 1 Outline of ASR test methods

Lithological composition of gravel	In regard to particles 5mm or more in diameter visible on the surfaces of concrete cores, the lithological composition is calculated by the point count method using a 5mm mesh.
Alkali-silica reactivity:	Alkali-silica reactivity is judged by the presence of rims and/or alkali-silica gel around aggregate particles. Thin sections are prepared from some specimens for polarization microscopy observation.
Alkali content of concrete:	A 10-g sample ground to particles less than 150 μm in diameter is added to 100ml of distilled water at 40°C and agitated for 30 min. The mixture is then filtered, and the alkali concentration of the filtrate is measured by atomic absorption photometry, to calculate the Na ₂ O equivalent (Na ₂ O + 0.658 K ₂ O).

Chloride ion content:	A 20-g sample ground to between 150 and 300 μ m particle size is dissolved in a 2N HNO ₃ solution and boiled for 5 min. The chloride ion (Cl ⁻) concentration of the filtrate is then measured by potentiometric titration.
Residual expansion (Canadian method, ASTM C 1260)	The time-related changes in the expansion of drilled concrete cores (ϕ 55mm) are measured while being immersed in a 1N NaOH solution at 80°C.
Residual expansion (Danish method):	The time-related changes in the expansion of drilled concrete cores (ϕ 55mm) are measured while being immersed in a saturated NaCl solution at 50°C.



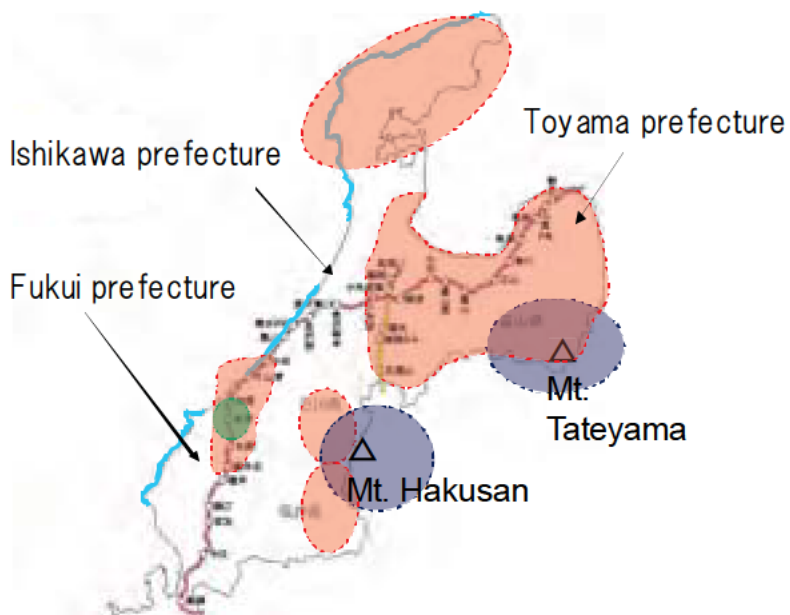
Fig. 1 Location of Hokuriku district



Fig. 2 Highway snow removal work in winter



Fig. 3 Scattering of deicing salts



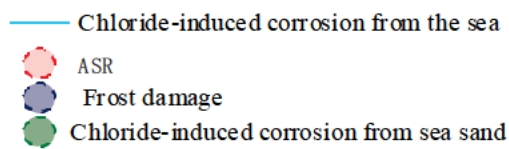


Fig.4 Map of deterioration in Hokuriku district



Fig.5 ASR gel (Core fracture surface)

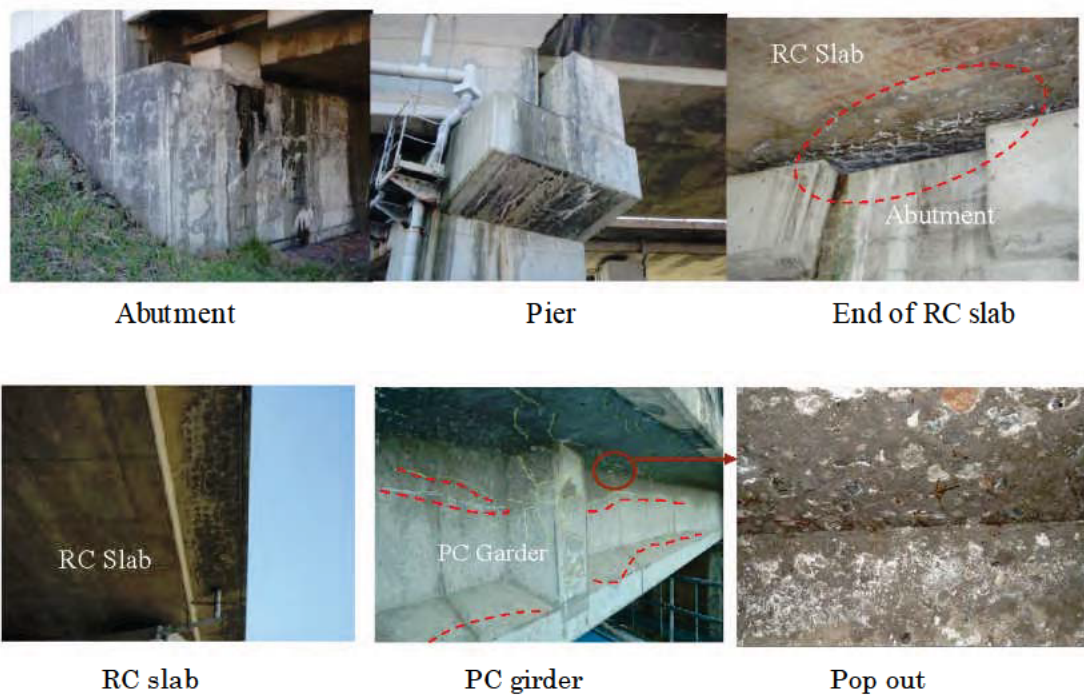


Fig.6 Cases of ASR deterioration

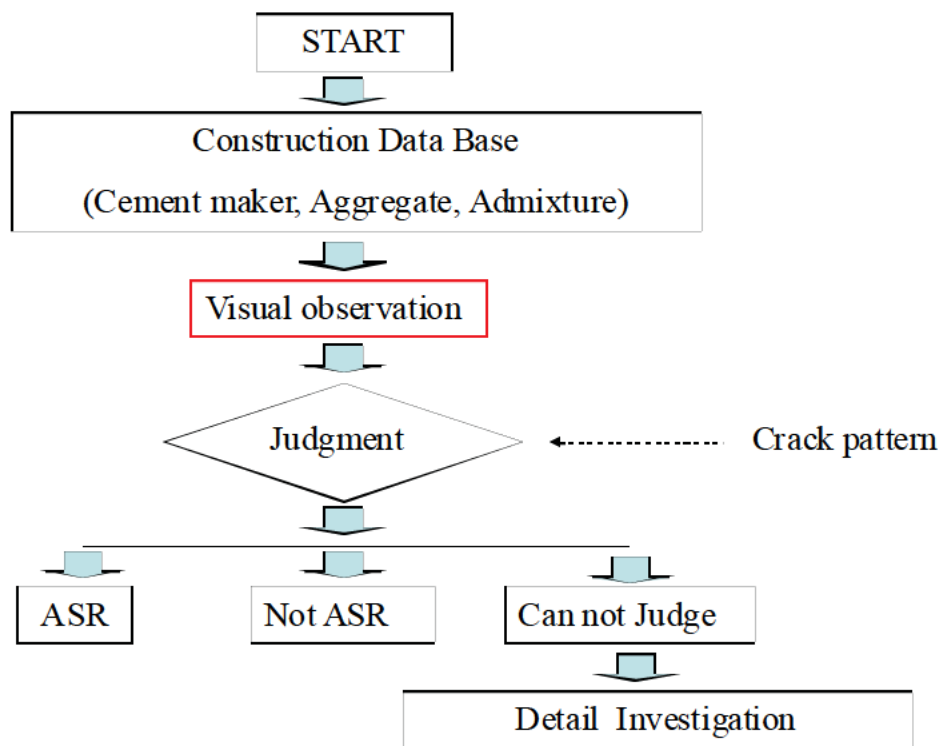


Fig.7 Flow of Assessment of ASR Structures



Fig.7 Lithological composition of gravel

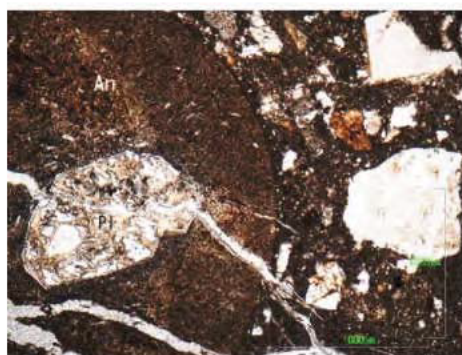


Fig.8 Observation of thin section by polarization microscopy



Fig.9 Alkali content of concrete by Atomic Absorption Spectroscopy Apparatus

Fig.10 Chloride ion content by Potentiometric Titration Apparatus



Fig.11 Residual expansion test of concrete cores

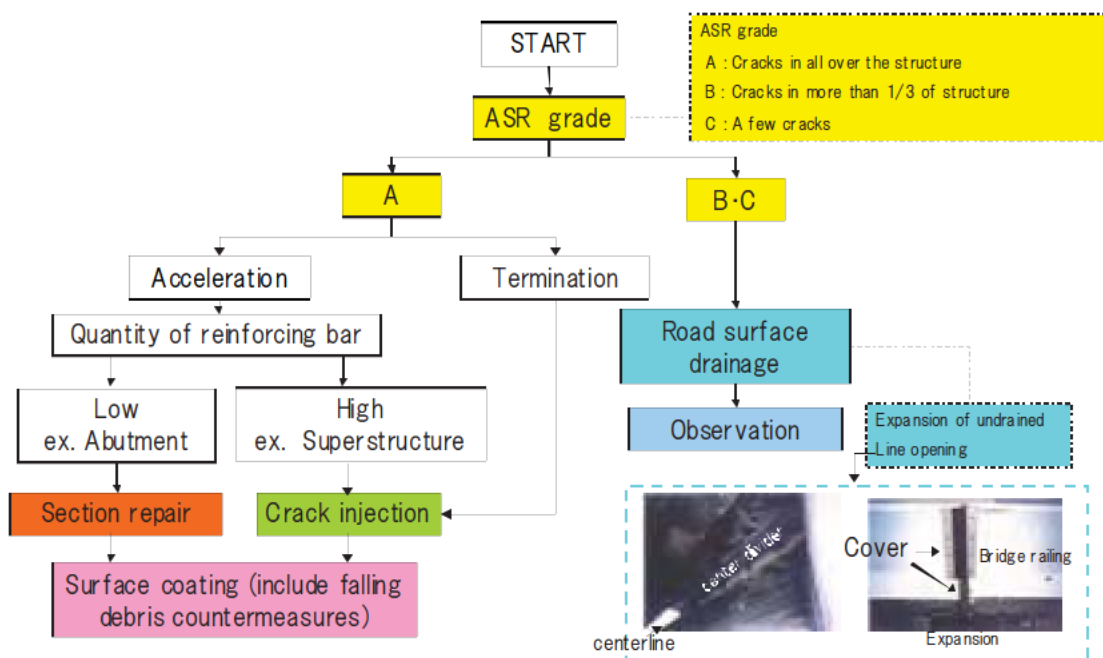


Fig.12 Selection of ASR Maintenance Method



Crack injection

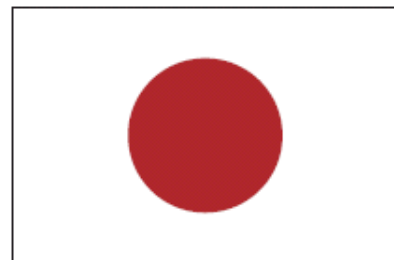
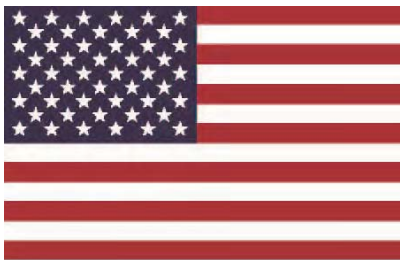
Surface coating

Water jet



Section repair with shotcrete Execution of fiber sheet coating Completion of repairing works

Fig.13 Maintenance of ASR-affected bridges



27th US-Japan Bridge Engineering Workshop

Session 5

Load and Strength Evaluation

Load-Carrying Capacity of Reinforced Concrete Beams with Adhesively Bonded Steel Plates

By Yoshiki Tanaka, Jun Murakoshi and Eiji Yoshida

Summary of NCHRP Research on Recalibration of the LRFR Load Factors in the AASHTO Manual for Bridge Evaluation

By Waseem Dekelbab

Compressive Loading Test of Corroded Gusset Plate Connection in Steel Truss Bridge

By Jun Murakoshi, Naoki Toyama, Mamoru Sawada, Kentaro Arimura,
Lu Guo, Kuniei Nogami, Teruhiko Yoda, and Hideyuki Kasano

Page Left Blank

LOAD-CARRYING CAPACITY OF REINFORCED CONCRETE BEAMS WITH ADHESIVELY BONDED STEEL PLATES

Yoshiki Tanaka¹
Jun Murakoshi¹
Eiji Yoshida¹

Abstract

To evaluate the load-carrying capacity of reinforced concrete beams with externally bonded steel plate, the influence of the bonded steel plates to the soffit on the shear strength of the beams, and the effect of shear strengthening using wing-type side steel plates for stocky concrete beams (broad and low web) have been examined. From the results, it was found that the shear strength is properly evaluated by shear capacity equations for non-plated reinforced concrete beams unless a crack develops at the edge of the steel plate, and that the side plate bonding is likely to have a potential to be effective in strengthening for the stocky beams without stirrup. Additionally, loading tests using two 75-year-old deteriorated reinforced concrete beams with adhesively bonded steel plates to the soffit were carried out. The bonded steel plates no longer contributed to the load carrying capacity after the joints between the steel plates failed due to debonding.

Introduction

In Japan, a number of the concrete girders and decks of existing highway bridges were strengthened with adhesively bonded steel plates or fiber reinforced polymer (FRP) sheets when design loads were changed or when the members deteriorated (Figs. 1 and 2). For the efficient management of existing bridges, the load-carrying capacity of not only conventional concrete beams but also concrete beams with the bonded steel plates should be properly evaluated.

The late 1960s, several researchers dealt with the strengthening method that steel plates were adhesively bonded with a two-part epoxy resin adhesive on the soffit of reinforced concrete beams. In those days, because the fatigue deterioration of concrete decks was frequently found on the Japanese highway bridges, experimental studies on the steel plate bonding technique applying to the bridge decks were carried out.¹⁻⁴ Then the FRP sheets were not major materials for construction. The steel plate bonding immediately became a major tool to improve the durability of bridge decks, having the advantage of applicability in service, and the efficient strengthening with the minimum change in

¹ Public Works Research Institute, Japan

appearance. The strengthening method using FRP sheets for reinforced concrete was developed in early 1990s. Currently, the materials became used commonly to improve the durability of bridge decks after a revision of the legal maximum weight for trucks from 20 tons to 25 tons in 1993, and the ductility of existing bridge piers after the great Hanshin earthquake in 1995. Extensive research works were carried out not only in Japan, but also in the world. Based on the results, several design guidelines for strengthening reinforced concrete members using FRP have been established.⁵⁻⁸ On the other hand, the effects of the steel plate bonding technique has not been so sufficiently identified as a guideline could be established. In a research program from FY2008 to 2010, the effect of shear strengthening using the steel plate bonding on reinforced concrete beams was examined. This summary report provides the outlines of three series of experimental studies focusing on; Series I: the influence of the steel plate bonded to the soffit on the shear capacity of reinforced concrete beams (further for the evaluation of plated concrete decks), Series II: the effect of side steel plate bonding on the shear capacity of stocky reinforced concrete beams,⁹ and Series III: the load-carrying capacity of two 75-year-old deteriorated concrete girders with the steel plate bonded to the soffit.¹⁰

Series I: Influence of Steel Plate Bonded to the Soffit on Shear Capacity of Reinforced Concrete Beams

Test Program: A test scheme and details of specimens are shown in Fig. 3 and Table 1. The height of the specimens, except Specimens A-7 and A-8, was set as 190 mm, referring to the thickness of the typical bridge decks built in 1960s. No stirrup was arranged except that on the support points for arranging main reinforcing bars. Specimens A-1 to A-8 had two longitudinal reinforcing bars. For Specimens A-4 to A-8, the steel plate with a thickness of 4.5 mm was adhesively bonded on the soffit of concrete beams. The steel plate and an adhesive layer for every beam were as wide as the beam with a width of 150 mm. The thickness of the adhesive layer was 5 mm. The distance from the center of each the support point to the end of the steel plate x_a was 80 mm, and that from the edge of a steel plate for the support was 30 mm.

The test parameter of Specimens A-4 to A-6 is the ratio of shear span a to effective depth d_s , which excludes the dimension of the steel plate. The effective depth and shear span of Specimens A-7 and A-8 were larger than those of Specimen A-5 with the same a/d_s ratio. Control specimens A-1 to A-3 with no steel plate had different reinforcement ratios, respectively.

Specimens B-4 to B-6, and B-8 had a main reinforcing bar and a doubly reinforcing bar, the steel plate being bonded to the soffit. The thickness of the steel plate of Specimens B-4, B-5, and B-6 was 4.5, 6, and 12 mm, respectively. Specimens B-4 to B-6 were simply supported on the bonded steel plate, as the shear span was 400 mm. Then the bonded steel plate had no curtailment near the supports. For Specimen B-8, the steel plate was bonded after the concrete beam had been precracked under cyclic loading with a shear span of 500

mm. Specimen B-8 was monotonically loaded with a shear span of 1000 mm, having the curtailment of the steel plate with a distance to the center of the support x_a of 80 mm.

Plate bonding was carried out at three weeks or more after casting. Anchor holes were drilled and mechanical steel anchors were installed on the soffit of concrete beams, which was roughened with a hand grinder. The steel plate was supported with the anchors as the gap to the surface of concrete was held with 5 mm spacers. Side openings were capped with epoxy resin putty. The epoxy resin adhesive was filled into the gap by grouting. In Specimens A-4 to A-8, inorganic zinc-rich primer for protecting the steel plate up to bonding remained similarly to practice. The steel plates for Specimens B-4 to B-6, and B-8 were not coated.

Loading tests were conducted at a week or later after the grouting. The putty on the sides was ground; that at the ends of the steel plates remained. The tensile-shear bond strengths of the epoxy resin adhesives were 12.3 MPa to 18.4 MPa.

Results: All test results are also shown in Table 1. Specimens A-4 to A-6 failed due to cracking at the end of steel plate (Fig. 4). The shear force at cracking at the end of the steel plate V_{p2} may be calculated based on a model provided by Tumialan et al.¹¹ In the model, the maximum (tensile) principal stress acting on the concrete near the end of the bonded steel plate is estimated based on the approximate solution by Roberts¹², being compared with the tensile strength of concrete. Although Tumialan et al.¹¹ applied the modulus of rupture f_r to the threshold tensile strength, the splitting tensile strength f_s is applied in this report, because it is more understandable for the model. Figure 5 shows the relationship between the calculated shear force at the cracking V_{p2} and the experimental results V_{ex} including the results of Specimens A-4 to A-6 and the other experimental results obtained from previous research¹³⁻²⁴ except the results of specimens with a ratio x_a/a of more than 0.25. The calculated values V_{p2} are somewhat larger than the experimental values when the value is larger. However, considering that the previous data contain the several unknown parameters, it appears that the shear force at the cracking can be properly estimated. Incidentally, the database based on the previous research shows that the results of specimens with a ratio x_a/a of more than 0.25 showing debonding failure do not depend on the value of V_{p2} , rather they mainly depend on the ultimate flexural strength of non-plated reinforced concrete beams.

In Fig. 6a, the results of specimens exhibiting flexure-shear failure in concrete are shown in relation to the calculated shear strength V_{sh} based on the conventional empirical equation²⁵ for estimating a shear force at flexure-shear failure. The influence of the bonded steel plates is estimated by substituting the dimensions containing the steel plate for the calculation of the reinforcement ratio and the effective depth in the equation. The other triangle symbols indicate the results of control specimens containing Specimens A-1 to A-3 and the previous research related. For the results of specimens with a ratio a/d of 1.7 to 1.75, the other empirical equation for deep beams²⁶ is applied. From the results, it was

found that the shear capacity of the plated beams can be estimated by the conventional equations. For reference, the calculated shear strength based on an equation in ACI318 (Eq. 11-5)²⁷ with a factor of 1.3 is also compared with the test results except the deep beam in Fig. 6b.

Series II: Effect of Side Steel Plate Bonding on Shear Capacity of Stocky Reinforced Concrete Beams⁹

Test Program: Configurations of specimens and a test setup are shown in Figs. 7 to 8. Of the same dimension of two reinforced concrete beams, Specimen S, of which wing-type steel plates was adhesively bonded on the sides of web at both shear spans. The other beam with no steel plate was named Specimen N. The concrete beams were designed as a simply supported T-shaped beam with a stocky cross section consisting of a web width of 600 mm and a height of beam of 850 mm, containing ten No.11 longitudinal reinforcing bars with a yield point of 534 MPa. For both specimens, four 9 mm dia. stirrups with a spacing of 250 mm were arranged at a shear span (right side in Fig. 8), no stirrup being at the other shear span. Similarly to the old reinforced concrete bridges, all the stirrups were round steel bars with a yield point of 292 MPa. The compressive cylinder strength of concrete was 33 MPa.

Four steel plates with a size of 2400 mm x 520 mm x 4.5 mm and a yield point of 360 MPa, coated by inorganic zinc-rich primer, were prepared. The procedure for bonding was the same as Series I. The tensile-shear bond strength of the epoxy resin adhesive was 16.1 MPa. Twelve steel anchors with a size of M10 and an embedded length of 70 mm for supporting each the steel plate at grouting were preinstalled before casting. The thickness of adhesive of 5 mm was kept.

Two point loading were monotonically applied to the beams with a shear span of 2 m. Cracking inside the web concrete covered by the steel plates were monitored using molded gauges and gauges on the stirrups. After shear failure occurred at the shear span with no stirrup, once unloaded. Then a vertical restrainer consisting of four tendon bars with 13 mm dia. were installed at 1/3 of the shear span with no stirrup from the near loading point. Reloading beyond the yielding of stirrups became available by using the restrainer, although finally the flange yielded at the shear span with no stirrup.

Results: Relationships between load and deflection at midspan for both specimens are shown in Fig. 9. Cracks observed on the web at the first peak due to shear failure at the shear span with no stirrup are shown in Fig. 10. The load at each event in the loading tests is summarized in Fig. 11. The load at diagonal cracking (detected with the molded gauges in Specimen S) was attributed to neither the stirrup nor the bonded steel plate. For the web without stirrup, the bonded steel plates showed an appreciable effect of improving the shear capacity, which was approximately 1.5 times as high as that of the non-plated specimen.

The side steel plates of both shear spans were debonded at similar loads regardless of stirrups, while the debonding of the steel plates on the web with stirrups did not immediately expand compared with that on the web without stirrup. At the shear span with stirrups, even after debonding, the steel plates were to some extent likely to contribute to the delay in failure. The stirrups, however, showed ductile behavior compared with an estimated level based on the modified truss theory despite the bonded steel plates.

Series III: Loading Tests of Old Concrete Beams with Steel Plate Bonding¹⁰

Outline of test beams: To examine the load-carrying capacity of old reinforced concrete beams with externally bonded steel plates to the soffit, six beams with a span length of 10 m were taken from the first and seventh spans of a concrete highway bridge built in 1935 (Fig. 1). In about 1981, steel plates were bonded to the soffit of most decks and beams in the bridge. Because the significant deterioration of the decks and beams was found when the administrator was considering the delivery of the bridge to the other small administrator, eight deteriorated spans of the bridge were replaced in 2010. According to the results of the investigation and observation before the removal, the degree of the deterioration of eight spans differed widely from each other. On the beams at the first span, corrosion of steel plates, water leakage and cracks in concrete were widely observed. The beams at the seventh span less deteriorated than that at the first span. Of six beams obtained, a beam from the seventh span and another beam from the first span, named Specimen S1 and S2, respectively, were tested.

Observations and survey of materials: Cracks observed on the test beams before the loading test and each cross section cut after the test are shown in Fig. 12. Coating partially covering web concrete was removed for the observations. The cracks were widely observed on the web of Beam S2. The crack depth, however, was found to be shallower than that concerned. Innumerable horizontal cracks were found in the flanges of both beams. Hammer soundings detected the debonding area of the steel plates as shown in Fig. 12. From a partial dissection survey conducted after the loading tests, two 8 mm dia. stirrups with a spacing of approximately 200 mm were found. The mechanical properties of concrete cores at uncracked parts, reinforcing bars and the steel plate taken from the tested beams are shown in Tables 2 to 3. It should be noted that the modulus of elasticity of the concrete cores taken from Beam S2 was considerably lower than that of Beam S1.

Test program: Two point loading were carried on the beams with a span length of 10 meters as the original span. Two strain gauges were mounted on the main reinforcing bars at a loading point section, after the web concrete was dug as small as possible. Asphalt surfacing remained at loading, because the removal would affect the cracked flange, and an additional preparation for the surface would be required. The tests were carried out in winter. For Beam 2, vertical restrainers were installed at the joints between the bonded steel plates in order to temporarily attempt to mitigate the debonding of the splice plate, although no effect was found from the result.

Results: Relationships between load and deflection at midspan of both the old beams are shown in Fig. 13. In Table 4, the maximum loads are compared with calculated ultimate loads, which were obtained using the measured dimensions and the properties of materials, except the asphalt surfacing. The sign of debonding of splice plates in Beam S1 was detected at 400 kN by using LVDTs (Fig. 14a), and in Beam S2 at 320 kN. After the sign of debonding in Beam S1, the load further increased up to the ultimate flexural capacity of the conventional reinforced concrete beam with no deterioration, while the rigidity significantly decreased. The flexural capacity of the deteriorated beam S2 was 8% lower than that of Beam S1, being 5% lower than the estimated value. After the peak, yielding of the main reinforcing bars was recognized by strain readings, and the flange was moderately crushed (Fig. 14b).

Conclusions

- 1 - From the test results and the previous research, it was found that the shear capacity of reinforced concrete beams with a steel plate bonded to the soffit is properly evaluated by substituting the dimension containing the steel plate for the calculation of the reinforcement ratio and the effective depth in the shear capacity equations for non-plated reinforced concrete beams, unless a crack develops at the edge of the steel plate.
- 2 - The side plate bonding is likely to have a potential to be effective in strengthening for the stocky reinforce concrete beams without stirrup. The effect of the side steel plates, however, may be limited depending on the web reinforcement ratio in existing beams.
- 3 - In the results of loading tests using old reinforced concrete beams, the bonded steel plates no longer contributed to the load carrying capacity after the steel splice plates failed due to debonding.

Acknowledgments

The authors thank Nagano prefecture and engineers who assisted with the survey of the old bridge.

References

1. Ohta, M., Aizawa, I., Momota, K., and Nakamura, T., *Experimental Study on Strengthening Using Steel Plate Bonding for Reinforced Concrete Decks*, Tech. Note of PWRI, No. 681, April 1971. (in Japanese)
2. Ishitani, T., Higai, T., and Hosoda, K., *Experimental Study on Strengthening Methods for Reinforced Concrete Decks, -Steel Plate Bonding Technique-*, Report of Japan Highway Corporation Laboratory, pp.150-157, Dec. 1975. (in Japanese)
3. Iioka, Y., and Higai, T., *Experimental Study on Strengthening Methods for Reinforced Concrete Decks, -Steel Plate Bonding Technique (Part 2)-*, Report of Japan Highway Corporation Laboratory, pp.142-154, Nov. 1976. (in Japanese)
4. Iioka, Y., Higai, T., and Hosoda, K., *Experimental Study on Strengthening Methods for Reinforced Concrete Decks, -Steel Plate Bonding Technique (Part 3)-*, Report of Japan Highway Corporation Laboratory, pp.143-151, Dec. 1977. (in Japanese)

5. *Recommendations for Upgrading of Concrete Structures with Use of Continuous Fiber Sheets*, Concrete Library 101, Japan Society of Civil Engineers, July, 2000. (in Japanese)
6. Mufti, A.A., et al., New Canadian Highway Bridge Design Code design provisions for fibre-reinforced structures, *Can. J. Civ. Eng.*, 34, pp.267-283, 2007.
7. ACI 440 Committee, *Guide for the design and construction of externally bonded FRP systems for strengthening concrete structures*, ACI, July 2008.
8. Zureick, A., Ellingwood, B. R., Nowak, A. S., Mertz, D. R., and Triantafillou, T. C., *Recommended Guide Specification for the Design of externally Bonded FRP Systems for Repair and Strengthening of Concrete Bridge Elements*, NCHRP Report 655, TRB, 2010.
9. Yoshida, E., Murakoshi, J. and Tanaka, Y, Effect of Adhesively Bonded Steel Plates on Web Reinforcement for Reinforced Concrete Beams, *Proceedings of JCI*, pp.703-708, 2010. (in Japanese)
10. Yoshida, E., Murakoshi, J. and Tanaka, Y, Structural Testing of Deteriorated Reinforced Concrete Girders Strengthened by Externally Bonded Steel Plates, *Proc. JSCE Annual meeting*, V, pp.377-378, 2010. (in Japanese)
11. Tumialan, J. G., Belarbi, A., and Nanni, A., *Reinforced Concrete Beams Strengthened with CFRP Composites: Failure due to Concrete Cover Delamination*, Center for Infrastructure Engineering Studies, 99-01, Department of Civil Engineering, Univ. of Missouri - Rolla, March 1999.
12. Roberts, T. M., Approximate analysis of shear and normal stress concentrations in the adhesive layer of plated RC beams, *Structural Engineer*, 67(12), pp.229-233, 1989.
13. Jones, R., Swamy, R. N., Bloxham, J., and Bouderbalah, A., Composite behaviour of concrete beams with epoxy bonded external reinforcement, *Int J Cem Compos*, 2(2), pp.91-107, 1980.
14. Macdonald, M. D., *The flexural performance of 3.5m concrete beams with various bonded external reinforcements*, TRRL Supplementary Report 728, 1982.
15. Jones, R., Swamy, R. N., and Ang, T. H., Under- and over-reinforced concrete beams with glued steel plates, *Int J Cem Compos Lightweight Concr*, 4(1), pp.19-32, 1982.
16. Swamy, R. N., Jones, R., and Bloxham, J. W., Structural behaviour of reinforced concrete beams strengthened by epoxy-bonded steel plates, *Structural Engineer*, 65A(2), pp.59-68, Feb. 1987.
17. Jones, R., Swamy, R. N., and Charif, A., Plate separation and anchorage of reinforced concrete beams strengthened by epoxy-bonded steel plates, *Structural Engineer*, 66(5), pp.85-94, 1988. Correspondence from Roberts, 67(12), pp.187-188, 1988.
18. Oehlers, D. J., and Moran, J. P., Premature failure of externally plated reinforced concrete beams, *J. of Structural Engineering*, ASCE, 116(4), pp.978-995, April 1990.
19. Basunbul, I. A., Gubati, A. A., Al-Sulaimani, G. J., and Baluch, M. H., Repaired reinforced concrete beams, *ACI Materials J.*, 87(4), pp.348-354, July-Aug. 1990.
20. Oehlers, D. J., Reinforced concrete beams with plates glued to their soffits, *J. Structural Engineering*, ASCE, 118(8), pp.2023-2038, 1992.
21. Hussain, M. et al., Flexural behavior of precracked reinforced concrete beams strengthened externally by steel plates, *ACI Structural J.*, 92(1), pp.14-22, Jan.-Feb. 1995.
22. Baluch, M. H., Ziraba, Y. N., Azad, A. K., Sharif, A. M., Al-Sulaimani, G. J. and Basunbul, I. A., Shear strength of plated RC beams, *Mag. of Concrete Res.*, 47, No. 173, pp.369-374, 1995.
23. Swamy, R. N., Jones, R., and Charif, A., Contribution of externally bonded steel plate reinforcement to the shear resistance of reinforced concrete beams, *Repair and Strengthening of Concrete Members with Adhesive Bonded Plates*, SP-165, ACI, pp.1-24, 1996. (The session was held in 1992)
24. Sano, M., and Miura, T., A study on a design method for strengthening concrete members by steel-plate-bonding, *Proc. of JSCE*, 550, pp.117-129, Nov. 1996. (in Japanese)
25. Okamura, H., and Higai, T., Proposed design equation for shear strength of reinforced concrete beams without web reinforcement, *Proc. of JSCE*, 300, pp.131-141, Aug. 1980.
26. Niwa, J., Equation for shear strength of reinforced concrete deep beams based on FEM analysis, *Proc. of JCI 2nd Colloquium on Shear Analysis of RC Structures*, pp.119-128, Oct. 1983. (in Japanese)
27. ACI 318 *Building Code Requirements for Structural Concrete and Commentary*, ACI, 2005.



Fig. 1 Steel plates bonded to the soffit of decks and girders in a concrete bridge



Fig. 2 Steel plates bonded on the webs of concrete girders

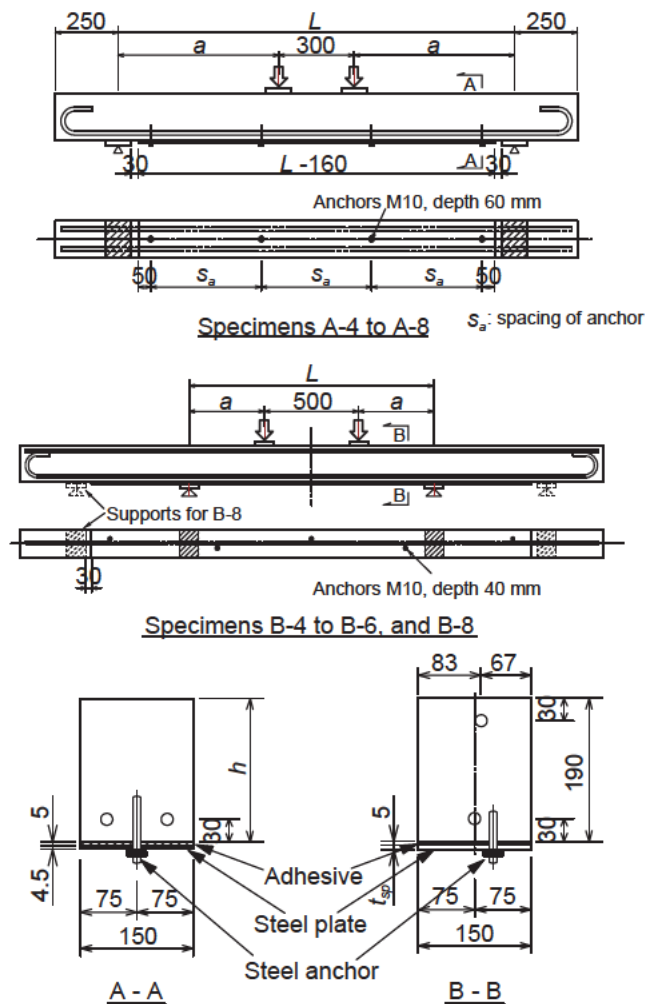


Fig. 3 Configurations of specimens in Series I

Table 1 Details and test results of specimens in Series I

Specimen	A-1	A-2	A-3	A-4	A-5	A-6	A-7	A-8	B-4	B-5	B-6	B-8
Steel plate strengthening	No	No	No	Yes								
Continuity of steel plate at support	—	—	—	No	No	No	No	No	Yes	Yes	Yes	No
Height of beam h , mm	190	190	190	190	190	190	250	330	190	190	190	190
Shear span a , mm	480	480	480	320	480	640	660	900	400	400	400	1000
Effective depth d , mm (after strengthening)	160	160	160	183	183	183	237	315	189	191	197	189
a/d	3.0	3.0	3.0	1.7	2.6	3.5	2.8	2.9	2.1	2.1	2.0	5.3
Longitudinal reinforcing bars	2-#7	2-#5	2-#6	2-#5	2-#5	2-#5	2-#7	2-#8	1-#5	1-#5	1-#5	1-#5
Ratio of reinforcement before strengthening, %	3.23	1.66	2.39	1.66	1.66	1.66	2.35	2.25	0.83	0.83	0.83	0.83
Ratio of reinforcement after strengthening, %	-	-	-	3.90	3.90	3.90	4.07	3.57	3.09	3.83	6.77	3.09
Doubly reinforcing bars	-	-	-	-	-	-	-	-	1-#5	1-#5	1-#5	1-#5
Thickness of steel plate t_{sp} , mm	-	-	-	4.5	4.5	4.5	4.5	4.5	4.5	6.0	12.0	4.5
Comp. cylinder strength of concrete, MPa	27.7	28.0	28.5	29.4	28.6	29.7	29.8	30.6	27.8	27.8	27.8	28.3
Splitting tensile strength of concrete, MPa	2.3	2.3	2.3	2.3	2.3	2.3	2.3	2.3	2.0	2.0	2.0	2.4
Yield point of reinforcing bars, MPa	369	390	374	390	390	390	369	362	348	348	348	348
Yield point of steel plate, MPa	-	-	-	300	300	300	300	300	306	318	330	306
Diagonal cracking load $P_{cr,ex}$, kN	88	77	79	78	75	73	121	158	90	112	131	86
Maximum load $P_{max,ex}$, kN	122	94	79	121	78	74	121	158	-	-	-	86
Type of failure	S	S	S	D	D	D	S	S	**	**	**	S†

Note: 1) Width of beams and plates : 150 mm, Thickness of adhesive layer : 5 mm

2) **: Loading was stopped at diagonal crack load.

3) A steel plate was installed on the soffit of Specimen B-8, after initial cracks developed due to cyclic loading when the shear span was set as 500 mm.

4) S : shear failure, D : failure due to cracking at the edge of steel plate,

† : Shear failure happened after the yielding of steel plate.



Fig. 4 Failure due to cracking at the edge of the bonded steel plate in Specimen A-6

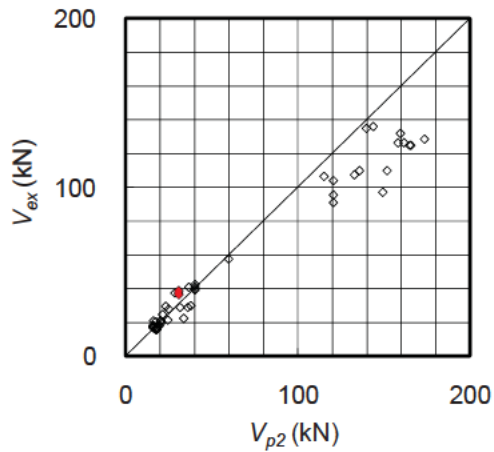


Fig. 5 Comparison between the measured shear forces at cracking at the edge of steel plate and the calculated shear force at debonding of steel plate

Note: Painted symbols indicate the results obtained from this study.

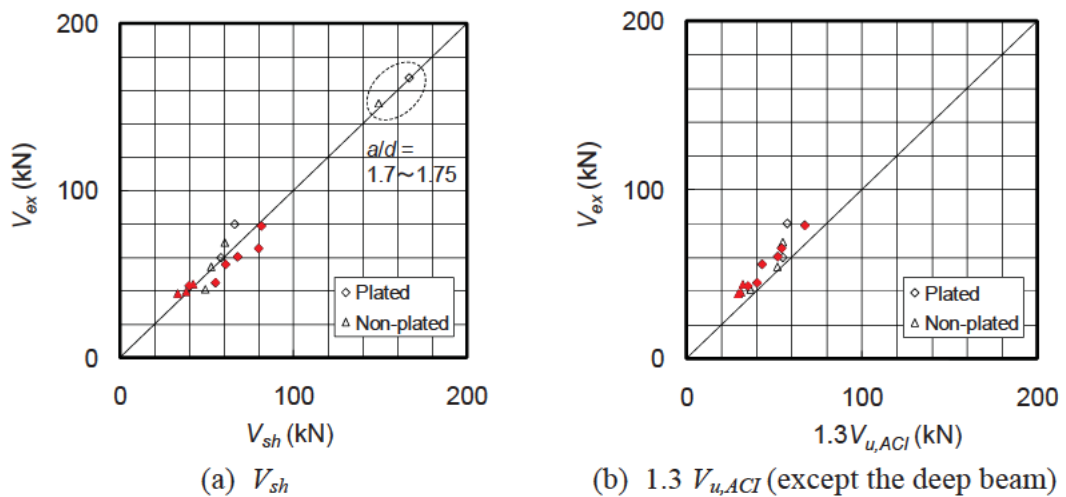


Fig. 6 Comparisons between the measured shear force of the plated beams at diagonal cracking and the calculated shear capacity for flexure-shear cracking.

Note: Painted symbols indicate the results obtained from this study.



Fig. 7 Wing-type steel plates bonded to the sides of web in Series II

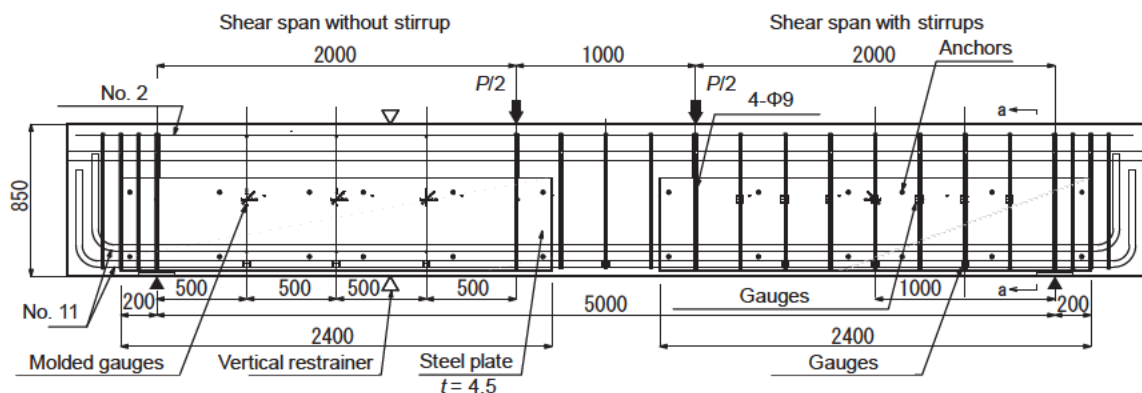
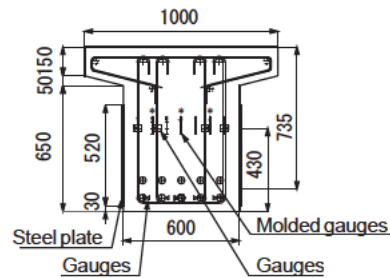
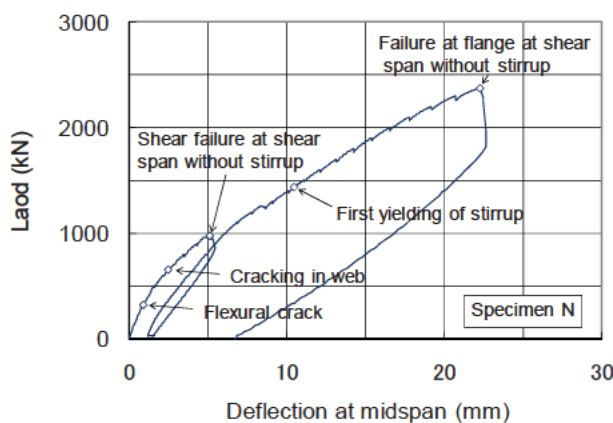
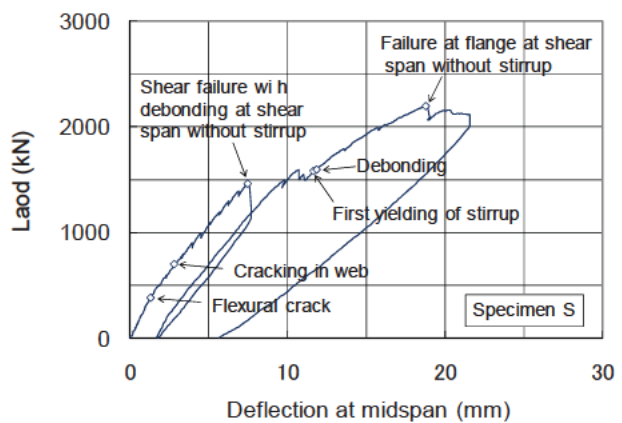


Fig. 8 Details and test setup of side-plated beams in Series II
Note: Steel plates were bonded on the web in Specimen S.

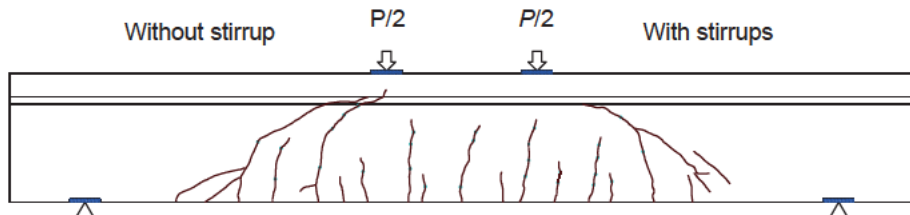


(a) Specimen N (no plate)

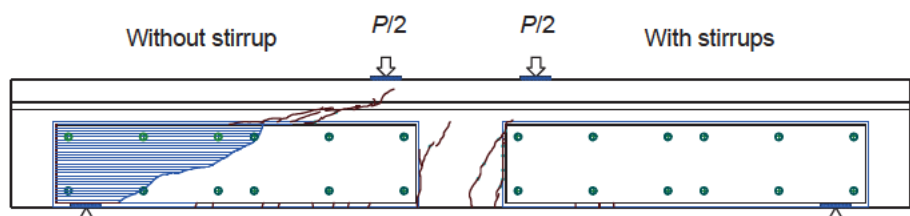


(b) Specimen S (plated)

Fig. 9 Relationship between load and deflection of side-plated reinforced concrete beams



(a) Specimen N (no plate)



(b) Specimen S (plated)

Fig. 10 Cracks observed at shear failure at the shear span without stirrup
Note: Hatching indicates the area of debonding of the steel plates.

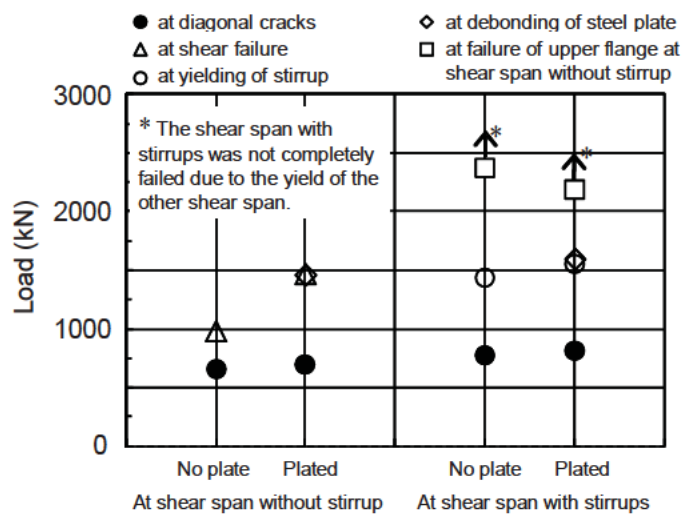


Fig. 11 Comparisons of the load at diagonal cracking, the load at debonding, and the maximum load in Series II

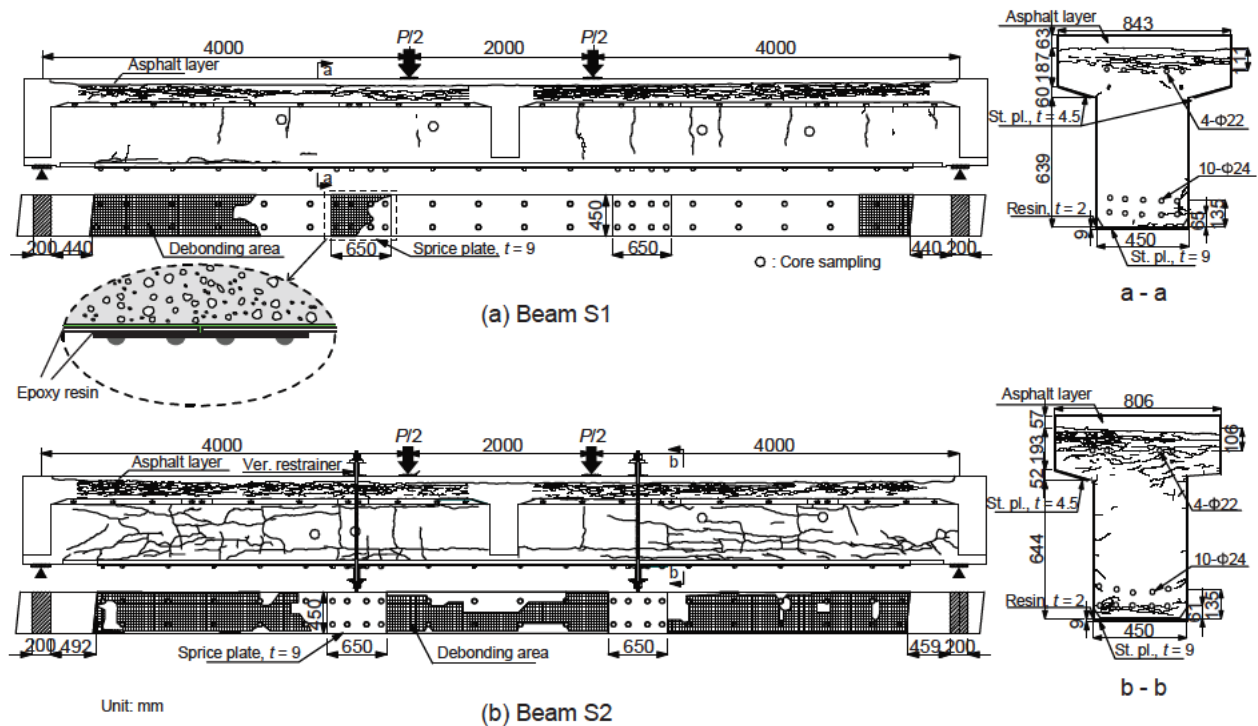


Fig. 12 Deterioration of old reinforced concrete beams with bonded steel plates

Note: Cracks in decks near cross beams are not drawn.
Cracks observed in cross sections were investigated after loading tests.

Table 2 Test results of concrete cores taken from the old beams

Beam	Core No.	Cylinder strength, MPa	Modulus of elasticity, GPa	Density, kg/m³
S1	1	23.0	26.1	2390
	2 *	35.2	30.9	2400
	3	30.2	18.6	2360
	4	28.7	30.6	2380
S2	1 *	32.3	10.9	2400
	2	24.4	4.6	2400
	3	31.0	9.7	2430
	4	17.4	-	2420

*) The values of the cores were used for the calculation of the ultimate loads shown in Table 4.

Table 3 The results of tensile tests of reinforcing bars and steel plates

Types and sizes		Yield point (MPa)	Tensile strength (MPa)	Modulus of elasticity (GPa)
Stirrups	8 mm dia.	299	418	209
Doubly reinforcing bars	22 mm dia.	301	460	209
Main reinforcing bars	24 mm dia.	287	400	212
Steel plates	9 mm thick.	393	530	205

Note: All data were obtained from tensile tests, being the averages of three test pieces.

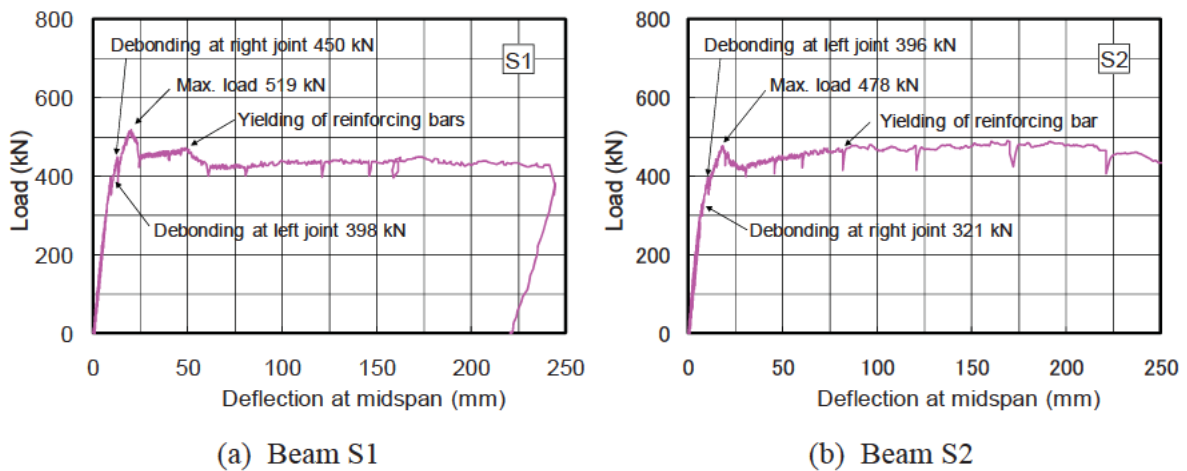


Fig. 13 Relationship between load and deflection at midspan of the old beams



(a) At sign of debonding of a splice plate

(b) Flexural failure

Fig. 14 Failure observed in Beam S1

Table 4 Comparisons of ultimate loads of the old beams

Beam	Measured ultimate load, $P_{u,ex}$ (kN)	Calculated ultimate load, $P_{u,cal}$ (kN)	$P_{u,ex} / P_{u,cal}$
S1	519	1130 (502)	0.46 (1.03)
S2	478	1110 (501)	0.43 (0.95)

Note: Parentheses indicate the calculated ultimate loads of reinforced concrete beams without steel plates.

Summary of NCHRP Research on Recalibration of the LRFR Load Factors in the AASHTO Manual for Bridge Evaluation

Waseem Dekelbab¹

Abstract

This paper summarizes the findings of research conducted under NCHRP Project 20-07, Task 285 “Recalibration of the LRFR Load Factors in the AASHTO Manual for Bridge Evaluation”. The objectives of the project were to (1) develop and recommend reliability indices better aligned with current permit operations for routine and special permit calibrations and (2) recalibrate LRFR live load factors for the recommended reliability indices for use with either the LRFD distribution formulas or refined methods of analysis such as finite element analysis.

Introduction

For single and multiple-trip special permits that are allowed to mix with traffic (without restrictions on other traffic), the Load and Resistance Factor Rating (LRFR) live load factors were derived to provide a higher level of reliability consistent with the AASHTO inventory ratings and Load and Resistance Factor Design (LRFD) design loading. The prescribed higher target reliability considers the increased risk of structural damage and benefit/cost associated with very heavy special permit vehicles compared to other truck classes. Though this higher level reliability index is justified based on structural safety, it has caused operational difficulties for bridge owners because the past permitting practices have allowed permits to operate at a lower reliability level.

The target reliability index for routine permit crossings is currently established at either a reliability index beta of 2.5 or 3.5. This reliability index needs to be compared with reliability indices used in current routine permit practices and adjusted as appropriate to meet operational needs.

The live load distribution for special permits is based on the tabulated LRFD one-lane distribution factors with the built-in multiple presence factor (i.e., 1.2) divided out. The live load distribution analysis for routine permits uses LRFD two-lane distribution factors assuming the simultaneous side-by-side presence of non-permit heavy trucks on the bridge. The load factors are higher for spans with higher average daily truck traffic (ADTT) and lower for heavier permits. The current LRFR permit load factor calibration for routine and special permits is tied to the LRFD distribution analysis method and does not provide guidance on the use of refined methods of analysis for heavy permits or for permits with non-standard gage widths. Therefore, live load factors and analysis guidance that are appropriate for analysis methods other than the LRFD distribution formulas need to be derived.

This paper summarizes the research conducted under this project to achieve the research objectives. This summary is based on the contractor's final report authored by Mr. Bala Sivakumar of HNTB Corp., New York and Dr. Michel Ghosn of the City College of New York, New York.

Analysis of Representative WIM Data

To verify that the AASHTO LRFR produces acceptable and uniform levels of reliability for typical U.S. bridges under current loading conditions, it is critical to use the most representative statistical information on truck weights, truck configurations, and multiple presence data. In this study, weigh-in-motion (WIM) data were analyzed to obtain projections for the maximum bridge load effects from six sites located on interstate highways in New York, Mississippi, Indiana, Florida, California, and Texas. The data were gathered in 2005 and 2006 for each traffic direction and included the number of axles, axle spacings, and axle weights for each truck. Multiple presence probabilities were assembled from a representative site in New York (Sivakumar et al 2008). Table 1 lists descriptive information for each site including the average daily truck traffic (ADTT) and the number of truck records after filtering the data to eliminate any questionable data.

Table 1 WIM Data for LRFR Recalibration

Site	State	Interstate Route (Direction)	#Trucks Recorded	ADTT	Mean GVW (kips)	Mean of top 10% GVW (kips)
0001	CA	I-5 (E/N)	1,537,613	5,058	56.0	80.6
		I-5 (W/S)	1,470,924	4,839	53.3	81.9
0526	TX	I-20 (E/N)	1,330,799	4,070	55.6	80.8
		I-20 (W/S)	1,174,954	3,593	56.7	81.5
2606	MS	I-55 (N)	564,393	1,622	66.5	108.7
		I-55 (S)	604,919	1,733	63.2	83.5
9121	NY	I-81 (N)	531,042	1,715	57.2	101.7
		I-81 (S)	525,733	1,614	57.8	98.3
9512	IN	I-74 (E)	931,971	2,596	60.7	82.5
		I-74 (W)	1,003,443	2,795	60.1	87.3
9926	FL	I-75 (N)	1,096,076	4,136	48.4	84.1
		I-75 (S)	1,032,680	3,897	53.5	84.6

Maximum Live Load Effects

The statistical analysis of the WIM data for each direction of the six WIM sites was performed to project the expected maximum live load (L_{max}) effects on simple span bridges for five-year projection periods. The load effects studied are the moment at midspan and the shear near the supports for a single truck and side-by-side trucks.

As an example, Figures 1 through 4 present the plots of the L_{max} values versus span length for each direction of the six WIM sites with ADTT of 5000. L_{max} values were normalized by the corresponding effect of the HL-93 load. These plots show large variability in L_{max} between the sites.

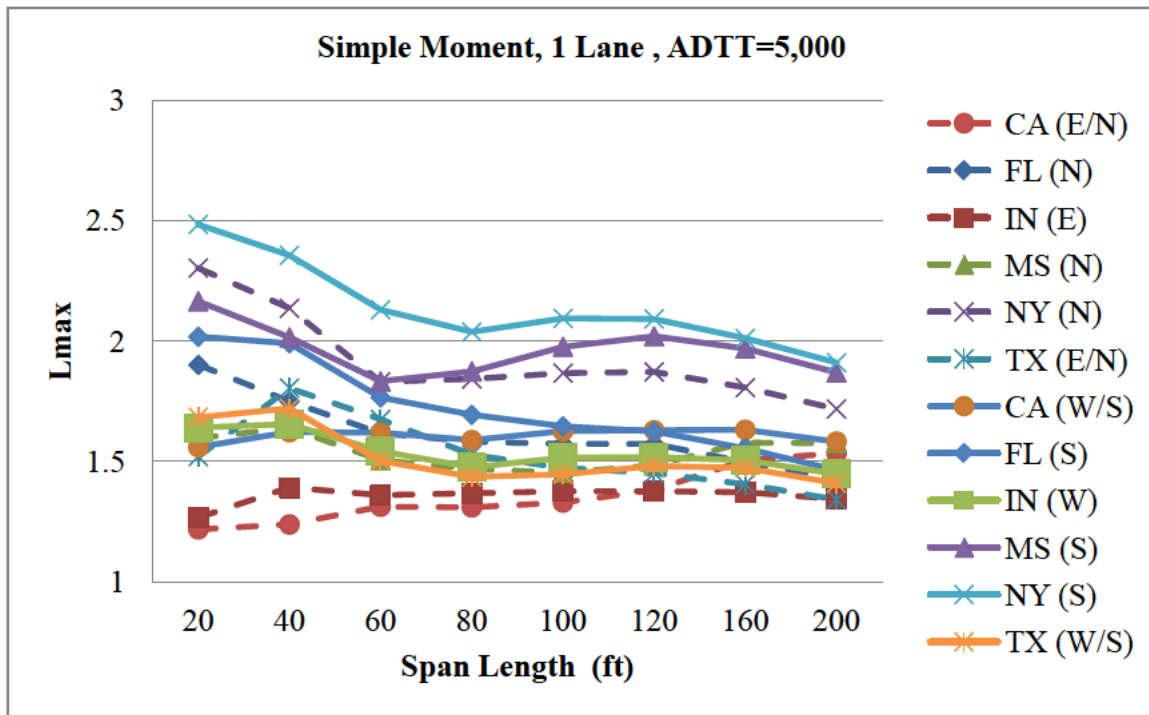


Figure 1 L_{max} Versus Span Length for Single Truck Moment

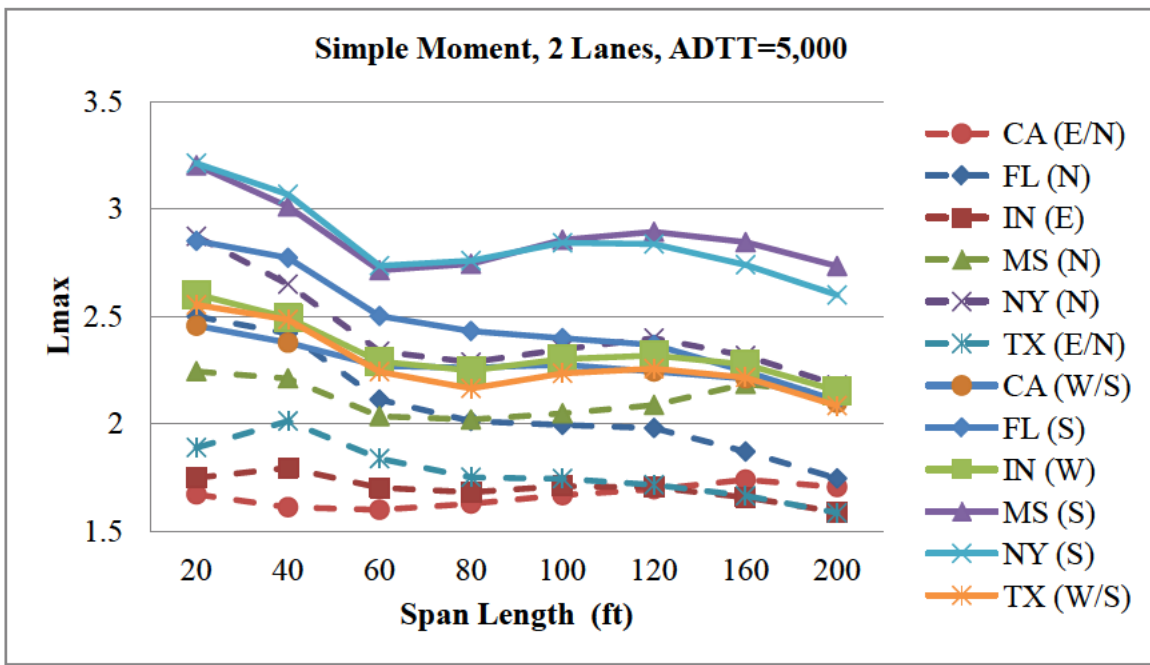


Figure 2 L_{max} Versus Span Length for Side-by-Side Truck Moment

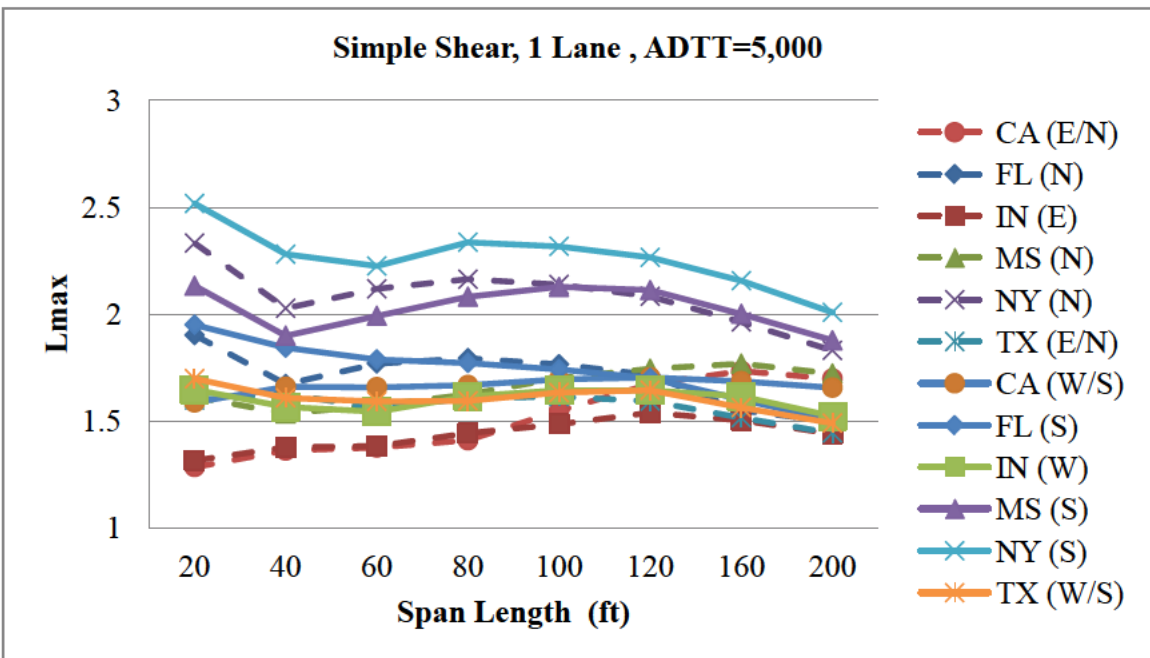


Figure 3 L_{max} Versus Span Length for Single Truck Shear

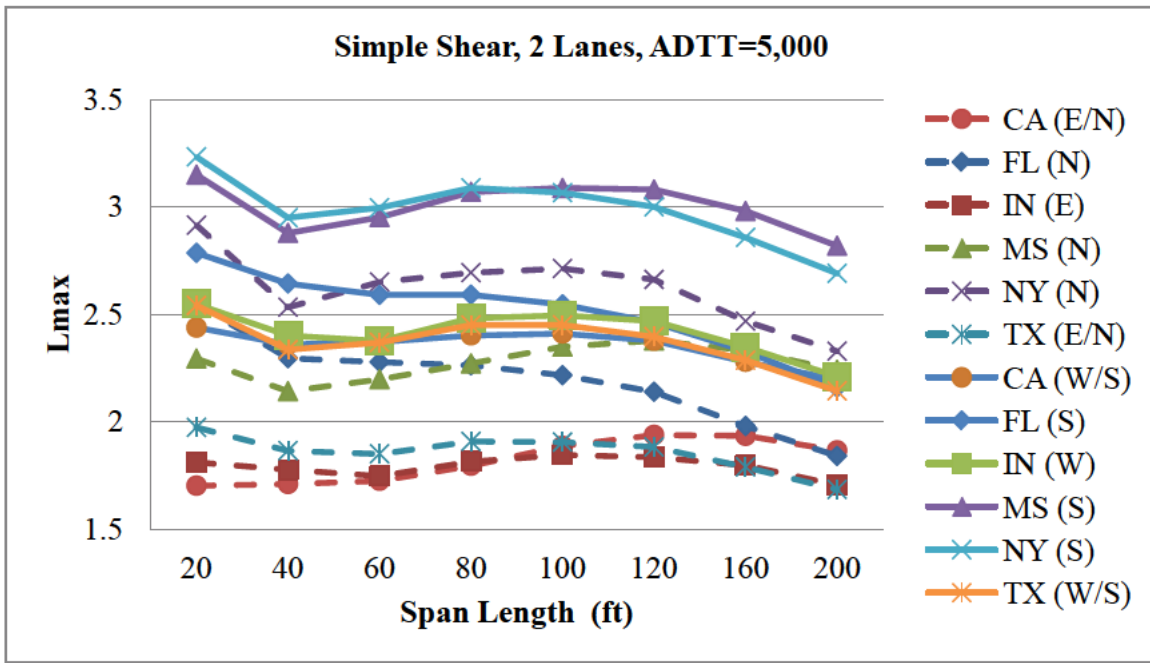


Figure 4 L_{max} Versus Span Length for Side-by-Side Truck Shear

Current Reliability Levels for LFR Ratings at the Operating Level

To find the reliability levels implied when a bridge is rated using the current AASHTO Load Factor Rating (LFR) criteria, the set of bridge configurations previously used for the AASHTO LRFD calibration is used with three different ADTT volumes: 5000, 1000, and 100. The analyzed bridge configurations are: T-beam, prestressed concrete, and noncomposite and composite steel bridges with spans varying between 20 ft and 200 ft with beams spaced from 4 ft to 12 ft center to center. The analysis was performed for the midspan moment and maximum shear. The current reliability levels for LFR rating at the operating level was calculated for the three different cases: Random trucks on two-lane bridges, permit trucks on two-lane bridges, and permit trucks on single lane bridges.

Random Trucks on Two-Lane Bridges

In this case, all the bridges are assumed to be two-lane bridges. The bridge member resistances were calculated assuming that LFR operating rating factor is 1.00, live loads are the AASHTO legal loads (Type3, Type 3S2, and Type 3-3), and live load factor is 1.30. Table 2 provides a summary of the average reliability index values for each bridge type and ADTT for both moment and shear; the overall average is 1.35. This relatively low value is due to the high loads observed on many of the WIM sites used to project the L_{max} values. This indicates that the AASHTO legal trucks do not provide an adequate envelope of the actual loads on highway bridges leading to lower reliability levels than might have been anticipated.

Table 2 Average Reliability Index Values for Random Trucks on 2-Lane Bridges

Bridge Type	ADTT=5000		ADTT=1000		ADTT=100	
	Moment	Shear	Moment	Shear	Moment	Shear
T-Beam	1.291	0.978	1.855	1.180	1.855	1.558
Prestressed Concrete	1.083	0.995	1.329	1.204	1.783	1.595
Noncomposite Steel	1.124	0.809	1.361	1.067	1.799	1.547
Composite Steel	1.113	0.793	1.351	1.052	1.790	1.533

Permit Trucks on Two-Lane Bridges

The reliability analysis was performed for the selected bridge configurations assuming that AASHTO LFR operating rating factor for each permit truck of the set of typical permit trucks is equal to 1.00. The member resistances that would be required to allow a permit truck to cross each bridge are calculated assuming that the bridges are being evaluated using the current AASHTO LFR operating rating criteria with a live load factor 1.3 applied on the routine permit and using the two-lane distribution factor.

Table 3 provides a summary of the average values for each bridge type and ADTT for both moment and shear. The overall average reliability index is 2.94. This average value is considerably higher than that observed for previous case (random trucks on span). This difference is because the rating process uses the actual permit load and assumes that the random truck alongside the permit is of equal weight. The difference is also due to the fact that the permit trucks weights are much better known and are associated with lower coefficient of variation values than the random trucks. Although the permit truck may still cross the bridge with a random truck, the chances of having a permit truck alongside a truck of equal or higher weight are relatively low. These factors lead to significantly higher reliability index values for the permit trucks than in the cases of random loading.

Table 3 Average Reliability Index Values for Permit Trucks on 2-Lane Bridges

Bridge Type	ADTT=5000		ADTT=1000		ADTT=100	
	Moment	Shear	Moment	Shear	Moment	Shear
T-Beam	2.71	2.58	2.75	2.61	2.83	2.68
Prestressed Concrete	2.99	2.66	3.05	2.69	3.25	2.76
Noncomposite Steel	3.01	3.10	2.99	3.14	3.10	3.23
Composite Steel	2.93	3.09	2.98	3.13	3.10	3.23

Permit Trucks on Single Lane Bridges

The reliability analysis approach used for permit trucks on two-lane bridges was applied using the one lane distribution factor; the results are presented in Table 4. The

average reliability index for all the cases considered is 3.62, which is higher than that obtained for the permits crossing over two-lane bridges. This difference is because the permit truck on a 1-lane bridges is alone on the bridge and thus the total applied load is better known than in the case where the truck may cross alongside a random truck which would govern the analysis of permit truck crossing two-lane bridges.

Table 4 Average Reliability Index Values for Permit Trucks on Single Lane Bridges

Bridge Type	All ADTTs	
	Moment	Shear
T-Beam	3.60	3.39
Prestressed Concrete	4.01	3.04
Noncomposite Steel	3.91	3.56
Composite Steel	3.91	3.55

Reliability Targets for Permit Load Recalibrations

Target reliability index for the calibration is set at 2.5 with the goal of achieving a minimum reliability index values for all conditions above 1.5.

Permit Load Classifications

The recalibration of the live load factors for permits considered the following four cases:

- I. Permit vehicle alone on a bridge which can occur whether the permit has been issued for a single trip or multiple trips.
- II. Unlimited crossings of multiple trip permits in which two permit trucks could cross a bridge simultaneously side-by-side.
- III. Unlimited crossings where a permit truck mixes with other random vehicles.
- IV. Limited number of trips (1 and less than 100) where the permit truck can mix with other random trucks.

Cases I, II, and III consider routine permits where the actual truck weight may sometimes exceed the weight limit. Cases I, II, and IV consider special permits where the weights are assumed to be fully controlled and are not expected to exceed the permit weight allowed. For routine permits, it is Case III that is expected to govern, while Case IV should govern for special permits. Case I is analyzed to check the safety of escorted permit trip. The analysis of Case II is performed to verify that it will be overshadowed by Cases III and IV.

Case I is not affected by the WIM data for the random trucks. Case II considers the probability of having two permit trucks side-by-side cross a bridge within the five year rating period. In the reliability analysis, it assumed up to 100 permits per day as an upper limit for the number of trips (Moses 2001). The probability of having two side-by-

side permits is 0.5% based on the WIM data collected on New York state sites on low truck traffic volume days (Sivakumar et al, 2008).

For cases III and IV, the reliability analysis should account for the number of random vehicles that may cross the bridge simultaneously with the permit truck. Following the AASHTO LRFR classifications sites with ADTT of 5000, 1000, and 100 are considered. The percentage of side-by-side vehicles (P_{sxs}) is 2%, 1.25%, and 0.5% for sites with ADTT of 5000, 1000, and 100, respectively. These P_{sxs} values are upper bounds obtained from the headway data collected at ten WIM sites in New York State (Sivakumar et al 2008).

Key Findings

The calculations performed demonstrate that using a live load factor of 1.10 for escorted special permit loads will provide average reliability index values greater than 2.5 when the single lane AASHTO LRFD load distribution factors are used to check whether the permit truck can be allowed to cross a bridge. When performing a refined analysis of the bridge, it is recommended to use the same live load factor (i.e., 1.10) for escorted special permits. Special permits travelling over bridges at crawl speed should still be checked with a dynamic allowance factor of 1.05 to satisfy the minimum reliability index of 1.5.

For the case when a refined analysis is performed for special permits that may mix with traffic, the target reliability is also exceeded when a live load factor of 1.00 is applied on the permit truck while a live load factor of 1.10 is applied on the governing AASHTO legal truck placed in the adjacent lane.

For the cases of routine permits, where data shows that permit loads may exceed the permit weight limits, having live load factors varying from 1.40 for sites with ADTT of 5000, 1.35 for sites with ADTT of 1000, to 1.30 for sites with ADTT of 100 will lead to average reliability index greater than 2.5 while the minimum reliability index values remain above 1.5. These checks should be performed with the two-lane AASHTO LRFD load distribution factors.

The above live load factors for routine permits can be reduced for the cases where the permit truck's gross vehicle weight is high in order to reflect the lower probability of having a random truck of equal or higher weight crossing alongside the permit truck. Specifically, for trucks with $GVW/AL < 2.0$ kip/ft (i.e., gross vehicle weight (GVW) over front axle to rear axle length (AL)), it recommended to use the above mentioned live load factors (1.40, 1.35, and 1.30 for sites with ADTT of 5000, 1000, and 100, respectively). For trucks with GVW/AL between 2.0 and 3.0 kip/ft, the recommended live load factors are 1.35, 1.25, and 1.20 for sites with ADTT of 5000, 1000, and 100, respectively. For trucks with GVW/AL above 3.0 kip/ft, the live load factors are 1.30, 1.20, and 1.15 for sites with ADTT of 5000, 1000, and 100, respectively.

The research also recommended revisions to LRFR permit rating specifications with commentary suitable for inclusion in the AASHTO Manual for Bridge Evaluation including a new table of LRFR permit load factors.

Acknowledgments

The work summarized herein was performed under NCHRP Project 20-07, Task 285 and was guided by NCHRP Project Panel 20-07, Task 285. Dr. Waseem Dekelbab served as the responsible NCHRP staff officer. The final report was prepared by Mr. Bala Sivakumar of HNTB Corp., New York and Dr. Michel Ghosn of The City College of New York, New York.

References

Moses, F. (2001). "Calibration of Load Factors for LRFR Bridge Evaluation," NCHRP Report 454, Transportation Research Board, National Research Council, Washington, DC.

Sivakumar, B., Ghosn, M., and Moses, F. (2008). "Protocols for Collecting and Using Traffic Data in Bridge Design," Unpublished draft final report for NCHRP Project 12-76, National Cooperative Highway Research Program, Transportation Research Board, Washington, DC.

Sivakumar, B. and Ghosn, M. (2011). "Recalibration of the LRFR Load Factors in the AASHTO Manual for Bridge Evaluation," Final report for NCHRP Project 20-07/Task 285, National Cooperative Highway Research Program, Transportation Research Board, Washington, DC.

COMPRESSIVE LOADING TEST OF CORRODED GUSSET PLATE CONNECTION IN STEEL TRUSS BRIDGE

Jun Murakoshi¹, Naoki Toyama¹, Mamoru Sawada¹, Kentaro Arimura¹, Lu Guo¹
Kuniei Nogami², Teruhiko Yoda³, Hideyuki Kasano³

Abstract

With the stock aging of the majority of highway bridges in Japan constructed during the 1950s–1970s, some serious corrosion deterioration cases of fracture critical members in steel truss bridges have been reported recently. In this paper, compressive loading test of severely-corroded gusset plate connections cut out from a demolished truss bridge were conducted in order to assess the remaining load capacity.

Introduction

The majority of highway bridges in Japan were constructed during the 1950s–1970s which coincides with Japan's high economic growth period, and the number of bridges over 50 years is increasing drastically. With increase of aged bridges, since these bridges are exposed to heavy traffic and severe natural environment, it is highly probable that the deterioration and damage will increase rapidly. Improvement of technologies related to inspection, diagnosis, repair, and rehabilitation needed. Concerning steel bridges, some serious deterioration cases of FCMs on steel truss bridges have been reported recently. A tension diagonal member of steel truss embedded inside the deck concrete fractured in the Kiso River Bridge and Honjo Bridge on the National Route because of corrosion that invisibly progressed inside the concrete in 2007. Fracture of diagonal members or gusset plate connections of truss bridge is likely to lead to fatal damage of whole bridge. On the other hands, there was no effective measure to evaluate remaining strength of such deteriorated components and the whole bridge system with the uncertain section loss from corrosion.

The authors initiated research project in order to identify the remaining load capacity and to investigate how to evaluate the remaining strength of deteriorated diagonal members and riveted gusset plate connections subjected to severe corrosion. In this research project, several corroded specimens are going to be tested within a few years. These specimens consist of diagonals and gusset plate connections which were cut out from demolished steel bridges which were in service about 50 years near coastal area.

This paper reports the preliminary results from of compressive loading test of the first one specimen conducted in September, 2011, and discusses compressive behavior and the ultimate strength for severely-corroded gusset plate connection.

¹ Center for Advanced Engineering Structural Assessment and Research(CAESAR),
Public Works Research Institute(PWRI)

² Department of Civil and Environmental Engineering, Tokyo Metropolitan University

³ Department of Civil and Environmental Engineering, Waseda University

Before the test, section loss was measured using laser measurement equipment, and the effect of the section loss on failure behavior and the ultimate strength were examined by Finite Element analyses to complement experimental results. Then the authors compare experimental results with analysis results and strength equations in gusset plate connections.

Bridge Description

Figure 1 shows a bridge utilized in this project, which is called Choshi Bridge. It was built in 1962 across Tone River, called Choshi Bridge. It was 5-span steel through truss bridge with total length of 407.4m. Figure 2 shows general and section view of the bridge. The average daily traffic is about 20,000 with 10% of heavy vehicles. It was located in river mouth and had suffered from salt damage by airborne salt and heavily corroded. Although repainting, strengthening and partial replacement of severely corroded members were conducted several times through its service life, it was finally replaced in 2009 at 47 years old, because the corrosion was unlikely to stop and it is considered to be impossible to assess remaining strength and remaining service life.

Figure 3 shows corrosion damage focusing on main members and gusset plate connection that influence safety of the whole bridge. Steel members of this bridge have been repainted by the thick fluorine coating material, so section loss was not able to be observed exactly by visual inspection. Corrosion of gusset plate connections are shown in Figure 3(a) (b). Several connections and diagonals were strengthened with steel plate bonding (see Figure 3(c)). Intense corrosion of diagonal joint is shown in Figure 3(d). Pitting of diagonal was observed in Figure 3(e). Concerning floor beams, Figure 3 (f) shows typical area of deterioration of floor beam with debris accumulation.

Compression Load Test

Specimen Description and Experimental Setup

After demolished, several connection parts and diagonal members were cut out as experimental specimens, and carried to our laboratory after the coating was removed. For the present, we are planning to conduct the loading test for 4 specimens which have different gusset configurations. Figure 4 shows the first one test specimen, which was cut out from upper chord connection P25d near intermediate support. The diagonal is square box type section with flange of 500mm width and 10 and 12 mm thickness at the connection, and thickness of gusset plate is 12mm. Design axial force/stress of the diagonal members are listed in Table 1. Steel grade is SM40 (400MPa nominal tensile strength), the yield strength is 284MPa by tensile material test of the diagonal member.

Section loss at the outer and inner surface of the specimen was measured using laser surface measurement equipment (see Figure 5). The measurement interval was set to 1mm to understand the mechanical behavior for uneven surface. As it was difficult to measure the inner surface directly, the surface shape was taken using plaster, and then it was measured. Figure 6 shows contours of corrosion areas. Red area means

large section loss, and yellow color means non-corrosion areas. Severe section loss was observed at connection parts of diagonal and gusset plate. As for the gusset plates, severe sections loss on the outer surface was not be seen except the rivets areas. Severe section was observed on the inner surface, where humidity seems high and airborne salt is likely to accumulate. As for the compression diagonal, large section loss on the outer surface was hardly found except the edge of flange, however, large section loss was shown on the inner surface around the gusset plate boundary. The maximum corrosion depth on the inner surface of the compression diagonal is 8.0mm (thickness of the diagonal flange: 12mm), the average corrosion depth is 3.4mm. The maximum and the average corrosion depths on the inner surface of the gusset plate are 9.0mm and 4.0mm respectively. The average corrosion depth at the plate area underneath the diagonal is 6.7mm. The average remaining thickness of the gusset plate is 8.0mm. The average reduction area ratio is 19% for the compression diagonal and 33% for the gusset plate. Comparing the measured section loss distribution with FE analysis results, it was found that severe corrosion part generally corresponded to the part where large stress appears. As a result, gusset plate connections may be structural weakpoint.

Figure 7 shows outline of specimen and loading frame. Figure 8 shows experimental setup. The compression and the tension axial loads were applied to the diagonal members at the same load increment step, because the absolute values of the design axial forces of both diagonals are almost equal. However, by the restriction of capacity of tension jack, tensile load was fixed to 2000kN. 30MN testing machine for compression and loading frame with jacks for tension were used for bi-axial loading.

Analysis Method

FE analyses were carried out to investigate the effect of section loss on compressive behavior by using a model shown in Figure 9. The analysis model simulated test condition. In modeling, 4 nodes shell elements were used for gusset plates and diagonals. Rivet fasteners were modeled by spring elements. The stress-strain relation of steel was assumed to be bi-linear, with a second modulus of $E/100$ ($E=2\times 10^5$ MPa). Upper chord was restrained with the loading frame at connection part. The displacement along the loading direction at the loading point is free, and the displacements of two other directions are fixed. In this analysis, the initial imperfection is not considered.

Analyses were conducted for two cases of non-corroded and corroded model simulating test specimen. Figure 10 shows assumed plate thickness of corroded model which reflects the measured data. Average thickness reductions were 2.0mm for the diagonal flange, 3.0mm for the diagonal web and 4.0mm for the gusset plate, respectively.

Experimental and Analysis Results

Figure 11 shows the curves of load versus vertical displacement at the loading head. The analytical ultimate strengths were 4953kN for the un-corroded model and 3346kN for the corroded model. The ratio of the strengths is about 2/3, which is similar

to average thickness loss of the gusset plate. The measured ultimate strength was 3598kN, that is about 1.1 times the analytical value for the corroded model. Linear behavior was observed until the out-of-plane deformation of gusset plate become large. After that, the load reached maximum load gradually and fell down moderately. The measured value and analytical value show generally the same curves and ultimate loads.

Figure 12 shows failed specimen after the test. The failure mode of the specimens was plate local buckling of the gusset. Figure 13 shows out-of-plane deformation and relations between load and the deformation of the both side of gusset plates at major points. With increase of vertical load, deformation of one side of the gusset plate preceded with the other side of the gusset. As a result, the buckling shape of unsupported edge shows unsymmetry. As for the analytical results of the corroded model, Von Mises stress contours and yielded area at the peak load are shown in Figure 14 and Figure 15, respectively. The local buckling occurred at the plate area underneath the diagonals and free edges of the gusset plate. Figure 16 compares the out-of-plane deformation at major points where large deformations were measured and shows good agreement. For reference, analytical out-of-plane deformation contours of the corroded model are also shown in this figure. The results in these figures provide verification of the corroded model using shell element to evaluate compressive behavior of the corroded gusset plate connection. About the modeling of the corrosion, the use of average reduction thickness of gusset plate seems reasonable to evaluate the behavior of the gusset plate in this specimen, however detailed investigation is required. Figure 17 shows the out-of-plane displacement along the line parallel to the centerline of the compression diagonal.

Strength Estimation Equations of Truss Gusset Plate Connections

Strength Equations

After the collapse of I-35W Bridge, “Load Rating Guidance and Examples for Bolted and Riveted Gusset Plates in Truss Bridges” [2] was issued by FHWA in 2009. By referencing the Guidance and previous experimental research results [3]- [7], limit state of gusset plate and diagonal members are assumed as follows as shown in Figure 18,

- a) Strength of fasteners in compression and tension
- b) Cross section yielding or net section fracture strength of gusset plate
- c) Block shear rupture strength in tension
- d) Cross section yielding or net section fracture strength of diagonal member
- e) Compressive strength
- f) Shear fracture strength

This paper only discusses compressive strengths of b), d) and e). The resistance factors are 1.0 in this study.

Cross section yielding strength of gusset plate in compression

The Whitmore effective width[3] is used for estimating yielding of the gusset plate. The effective width is bound on either side by the closer of the nearest adjacent plate edges or lines constructed starting from the external fasteners within the first row and extending from these fasteners at an angle of 30 degrees with respect to the line of action of the axial force (see Figure 19). The cross section yielding is taken as:

$$P_{gy} = f_y A_e \quad (1)$$

where:

A_e : gross cross-sectional area of Whitmore effective width of the plate, $A_e=L_e t(\text{mm}^2)$

f_y : yield strength of the plate (N/mm^2)

L_e : Whitmore effective width (see Figure 19)(mm)

t : thickness of the plate (mm)

Cross section yielding of diagonal member

The smallest sectional area of the diagonal members near the gusset plate boundary is assumed to be yielded. The cross section yielding strength is expressed by:

$$P_{dy} = f_y A_g \quad (2)$$

where:

f_y : yield strength of the diagonal (N/mm^2)

A_g : gross cross-sectional area of the diagonal (mm^2)

Local buckling at the plate area underneath the splice member of diagonals

The Whitmore effective width and an unbraced gusset plate length which is average of the three lengths was used for estimating buckling strength. Standard buckling equations specified in Japanese Design code (JSHB) was used. Ignoring any lateral constraint to the gusset plate, the effective length factor, β ($\beta=1.2$) was used for unbraced gusset plate assuming the buckled shape as shown in Figure 20. The local buckling equation is taken as:

$$P_{gcr} = f_y A_g \quad (\bar{\lambda} \leq 0.2) \quad (3a)$$

$$P_{gcr} = (1.109 - 0.545\bar{\lambda}) f_y A_g \quad (0.2 < \bar{\lambda} \leq 1.0) \quad (3b)$$

$$P_{gcr} = (1.0 / (0.773 + \bar{\lambda}^2)) f_y A_g \quad (1.0 < \bar{\lambda}) \quad (3c)$$

where:

f_y : yield strength of the plates (N/mm^2)

A_g : gross cross-sectional area (mm^2)

The column slenderness ratio $\bar{\lambda}$ is given by:

$$\bar{\lambda} = \frac{1}{\pi} \cdot \sqrt{\frac{f_y}{E}} \cdot \frac{\beta L_c}{r_s} \quad (4)$$

where:

E : Young's modulus of plate (N/mm²)

β : effective length factor (=1.2)

L_c : $L_c = (L_1+L_2+L_3)/3$

L_1, L_2, L_3 : distance from center or each end of the Whitmore width to the edge in the closest adjacent member, measured parallel to the line of action of the compressive axial force (see Figure 19).

r_s : radius of gyration about the plane of buckling, $r_s = \sqrt{I_g / A_g}$ (mm)

I_g : moment of inertia (mm⁴)

Comparison of Analysis Results and Calculation Results

Table 2 outlines the comparison of the experimental results, FE analysis results and the calculation results for the specimen. The ratio means the calculated or measured value to the analytical value. The calculated yield strength by the Whitmore effective width was to some extent close to the analytical ultimate strength with ratios of 0.97 (un-corroded model) and 0.95 (corroded model). On the other hand, the calculated yield strength of the diagonal was larger than the analytical value with ratios of 1.23 and 1.39. It is indicated that the gusset plate failure preceded with yielding of the diagonal. Strength equation for local buckling gives conservative estimates with strength ratio of 0.59 (un-corroded model) and 0.36 (corroded model), much below 1.0.

Regarding the compressive strength of the gusset plate connection, the results in this study were compared with experimental results[4]-[8]. Figure 21 shows comparison of the measured ultimate loads and the calculated values for local buckling and yielding respectively. Figure 22 shows relations of ultimate strength and slenderness ratio. Calculated values are also conservative for the experimental data, and the correlation is not good. Then, we are investigating more accurate estimation of ultimate strength of the gusset plate. According to the failure mode, the ultimate strength is likely to depend on the buckling strength of the compressive unbraced area parts and the strength of its surrounding plate area. As one of our ideas, we are trying to evaluate the compressive strength by the summation of following strength equations of gusset plate divided into 3 areas as shown in Figure 23.

$$P_{gcr} = P_{gcr1} + P_{gcr2} + P_{gsy} \quad (5)$$

P_{gcr1} is expressed by:

$$P_{gcr1} = f_y A_g \quad (\bar{\lambda} \leq 1.0) \quad (6a)$$

$$P_{gcr1} = \frac{1}{\bar{\lambda}^2} f_y A_g \quad (1.0 < \bar{\lambda}) \quad (6b)$$

The column slenderness ratio $\bar{\lambda}$ is given by:

$$\bar{\lambda} = \frac{1}{\pi} \cdot \sqrt{\frac{f_y}{E}} \cdot \frac{\beta L_c}{r_s} \quad (7)$$

where:

β : effective length factor ($=0.65$)

L_c : $L_c = (L_1 + L_2 + L_3) / 3$

L_1, L_2, L_3 : The distance from center or each end of the width of diagonal end to the edge in the closest adjacent member, measured parallel to the line of action of the compressive axial force (see Figure 23).

P_{gcr2} is expressed by:

$$P_{gcr2} = f_y A_g \sin \theta_i \quad (R \leq 1.0) \quad (8a)$$

$$P_{gcr2} = \frac{1}{R^2} f_y A_g \sin \theta_i \quad (1.0 < R) \quad (8b)$$

The plate slenderness ratio R is given by:

$$R = \frac{b}{t} \cdot \sqrt{\frac{f_y}{E} \cdot \frac{12(1-\nu^2)}{\pi^2 k}} \quad (9)$$

where:

ν : The Poisson's ratio ($=0.3$)

k : The buckling coefficient , $k = \frac{4}{\alpha^2} + \frac{40}{3\pi^2} + \frac{15\alpha^2}{\pi^4} - \frac{20\nu}{\pi^2}$

α : $\alpha = h_c / b_2$

h_c : $h_c = (h_1 + h_2) / 2$

P_{gsy} is expressed by:

$$P_{gsy} = \frac{f_y}{\sqrt{3}} A_g \cos \theta_2 \quad (10)$$

Figure 24 shows comparison of the measured ultimate loads and the calculated values. It is noticed that failure modes of all data are local buckling, not compressive and block shear failure which is described in [8]. Considering that previous experimental data contain various gusset configurations, it appears the ultimate strength can be approximately estimated. Still there is a difference, further study is required to estimate the ultimate strength for compressive load.

Conclusions

Compressive loading test of the corroded gusset plate connection specimen from decommissioned truss bridge was performed, and the FE analyses were conducted to complement experimental results. As for compressive strength estimation of gusset plate connection, from practical viewpoint, application of strength equations were discussed with use of previous experimental research results. The major findings are summarized as follows.

- 1) Based on thickness loss measurement of gusset plate connection, advanced corrosion of diagonals and gusset plate was observed around the connection parts. Severe corrosion part generally corresponded to the part where large stresses appear.
- 2) The effect of the section loss on the compressive strength of the gusset plate was evaluated by experimental and analytical results. Compressive behavior of the gusset plate was properly evaluated by shell element model in consideration of the average thickness reduction.
- 3) Local buckling strengths by the Whitmore effective width provided conservative estimates to the experimental ultimate strength. Taking the buckling strength of the compressive area and the strength of its surrounding plate area into consideration gave more proper prediction.

Acknowledgment

This research was undertaken as part of the collaborative research project between Public Works Research Institute; Tokyo Metropolitan University; and Waseda University, and funded by the Ministry of Land, Infrastructure, Transport and Tourism based on the Construction Technology Research and Development Subsidy Program. Finally, the authors express appreciation to Choshi Public Works Office, Chiba Prefecture for their cooperation.

References

- [1] Japan Road Association (JRA), “Specification for Highway Bridges, Part II Steel Bridge”, 2002.(in Japanese)
- [2] Federal Highway Administration, “Load Rating Guidance and Examples For Bolted and Riveted Gusset Plates In Truss Bridges”, Publication No.FHWA-IF-09-014, 2009.
- [3] Whitmore, R.E., “Experimental Investigation of Stresses in Gusset Plates, Bulletin No.16, Engineering Experiment Station”, University of Tennessee, 1952.
- [4] Yam, M. and Cheng, J., “Experimental Investigation of the Compressive Behavior of Gusset Plate Connections”, Structural Engineering Report No.194, Dept. of Civil Engineering, University of Alberta, 1993.

- [5] Ocel, J. M., Hartman, J.L., Zobel, R., White, D. and Leon, R., "Inspection and Rating of Gusset Plates - A Response to the I-35W Bridge Collapse", Proceedings of the 26th US-Japan Bridge Engineering Workshop, pp.11-23, 2010.
- [6] Matsuhsisa, S., Yamamoto, K. and Okumura, T., "Loading Experiment of Truss Gusset Plate Connections", Proceedings of the 31st Annual Conference of Japan Society of Civil Engineers, pp.297-298, 1976. (in Japanese)
- [7] Matsuhsisa, S., Yamamoto, K. and Okumura, T., "Loading Experiment of Truss Gusset Plate Connections", Proceedings of the 32nd Annual Conference of Japan Society of Civil Engineers, pp.631-632, 1978.(in Japanese)
- [8] Kasano, H., Yoda, T., Nogami, K., Murakoshi, J., Toyama, N., Sawada, M., Arimura, K. and Guo, L., "Study on Failure modes of Steel Truss Bridge Gusset Plates Related to Compression and Shear Block Failure", Proceedings of the 66th Annual Conference of Japan Society of Civil Engineers, pp.149-150, 2011. (in Japanese)

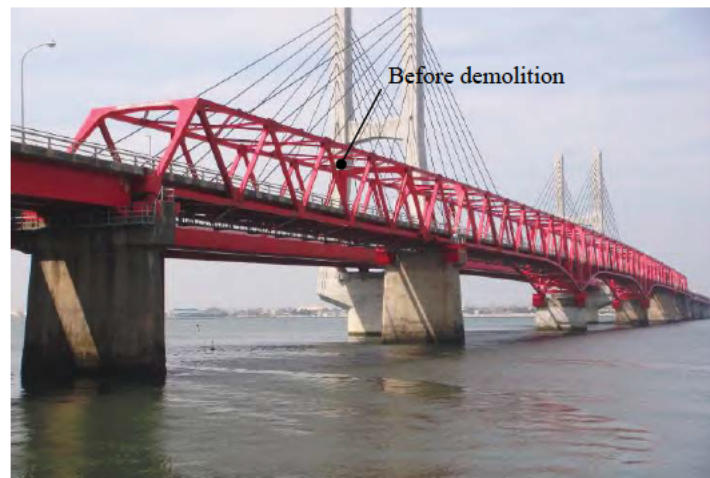


Figure 1 Old Bridge and New Bridge (cable-stayed bridge)

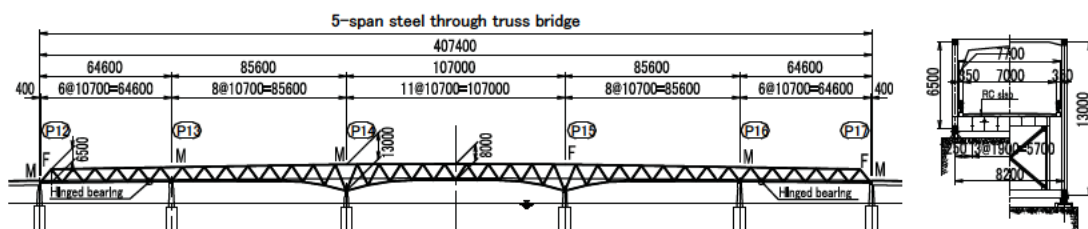


Figure 2 General View of Choshi Bridge

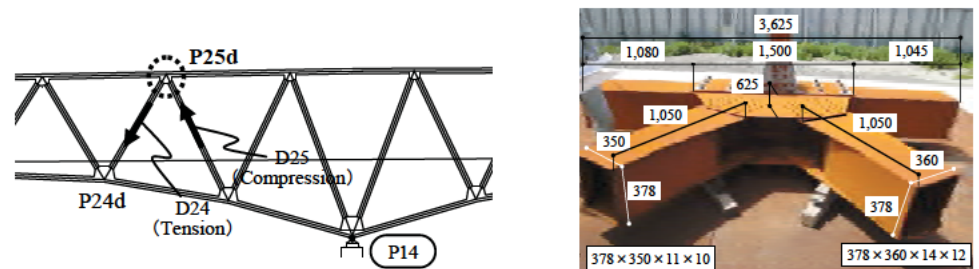


a) Lower chord connection b) Upper chord connection c) Plate bonding of lower chord connection



d) Diagonal joint e) Pitting of diagonal f) Section loss of end floor beam

Figure 3 Corrosion Damage of Main Members



a) The test Specimen



b) The edge of flange



c) Inside gusset plate connection

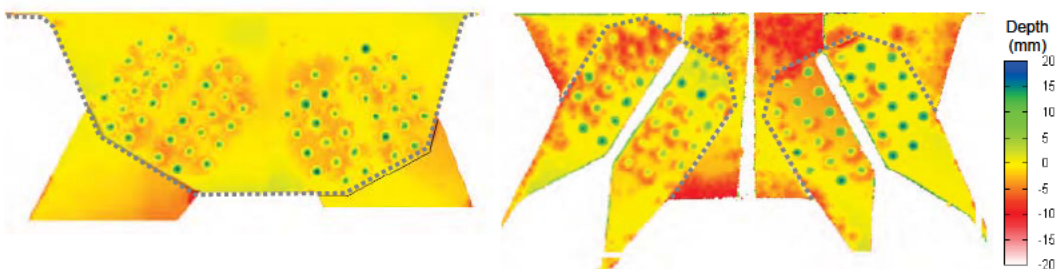
Figure 4 P25d Connection Cut Out as Specimen

Table 1 Design Axial Force and Design Stress

Design load	D24(Compression)		D25(Tension)		Notes
	Axial force(kN)	Stress(MPa)	Axial force (kN)	Stress(MPa)	
Dead load	1,027	69	-973	-52	
Live load	785	53	-742	-40	TL-20
Total (Ratio)	1,812(-1.06)	112	-1,715(1.0)	-92	
Allowable stress	—	128	—	-93	SM40



Figure 5 Thickness Loss Measurement by Laser Measurement Equipment



a) Outside gusset plate

b) Inside gusset plate

Figure 6 Thickness Reduction of Corroded Specimen

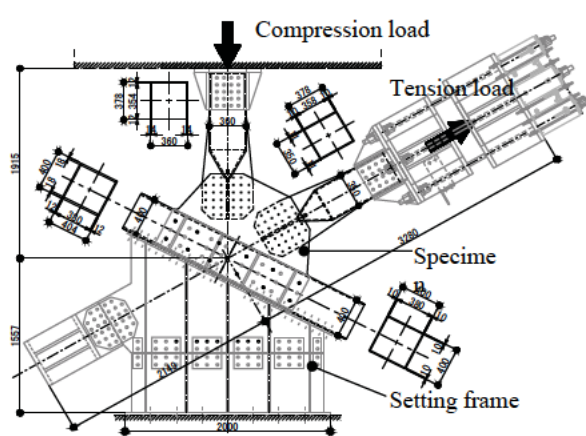


Figure 7 Outline of Specimen and Loading Frame

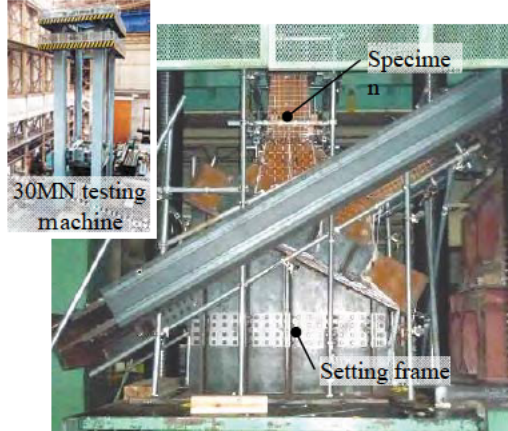


Figure 8 Test Setup of P25d Connection

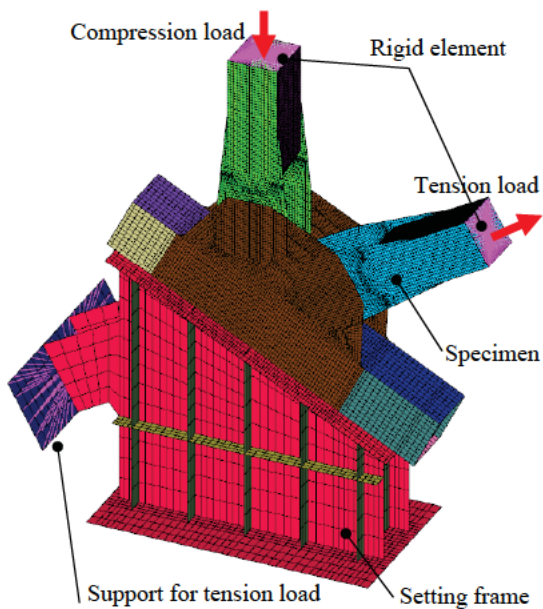


Figure 9 Analysis Model

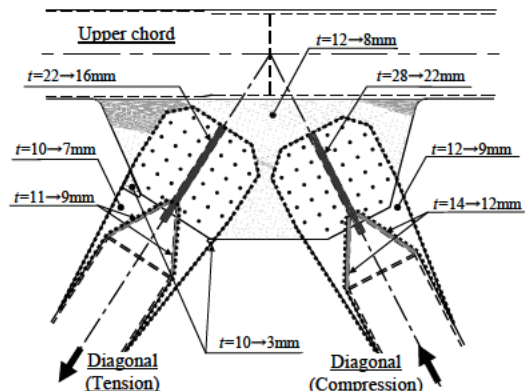


Figure 10 Plate Thickness Reduction of Corroded Model

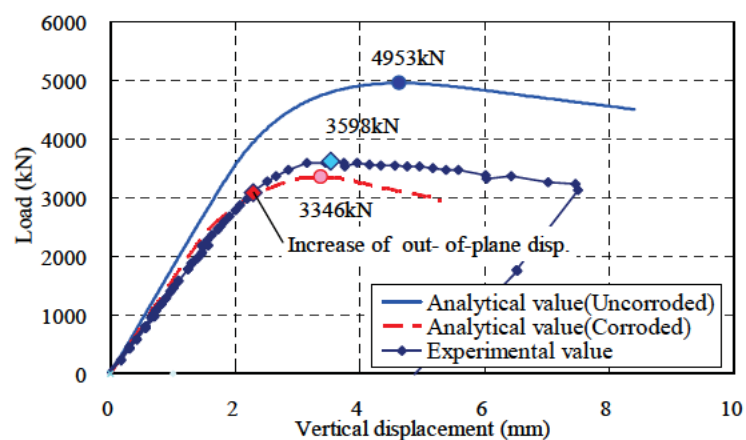


Figure 11 Compression Load vs. Vertical Displacement Curves



Figure 12 Failed Specimen after the Test

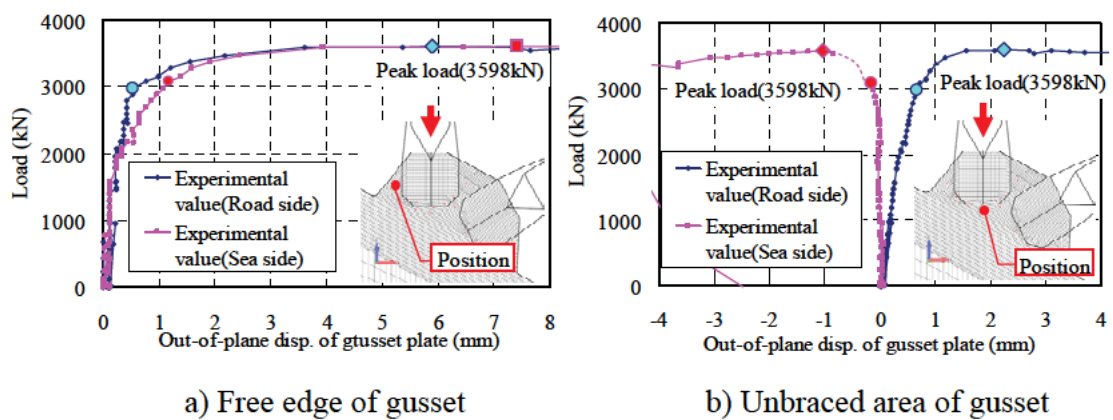


Figure 13 Compression Load vs. Out-of-displacement of gusset plate Curves

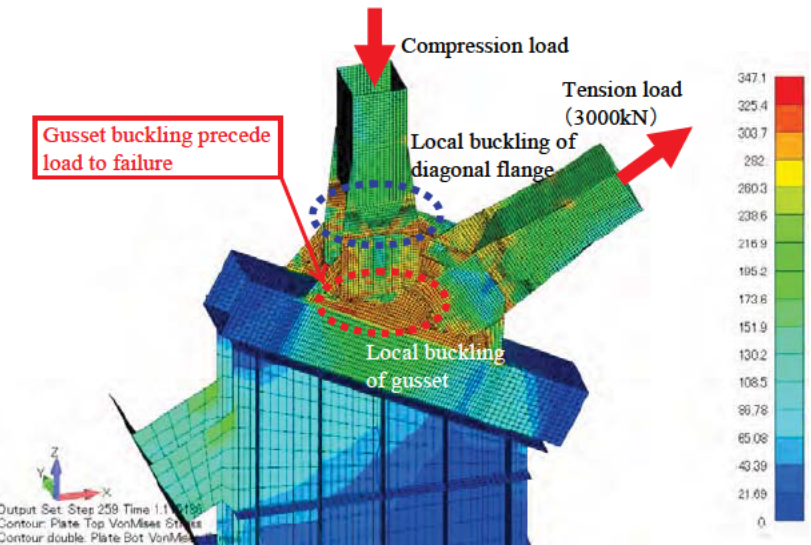


Figure 14 Von Mises Stress Contour of Corroded Model Gusset at Peak Load

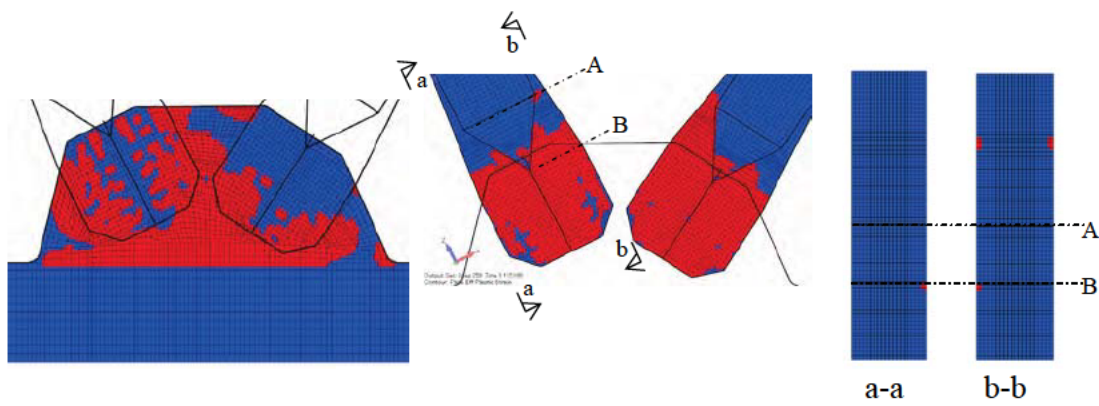


Figure 15 Yield Strain Distribution of Outside Web at Peak Load

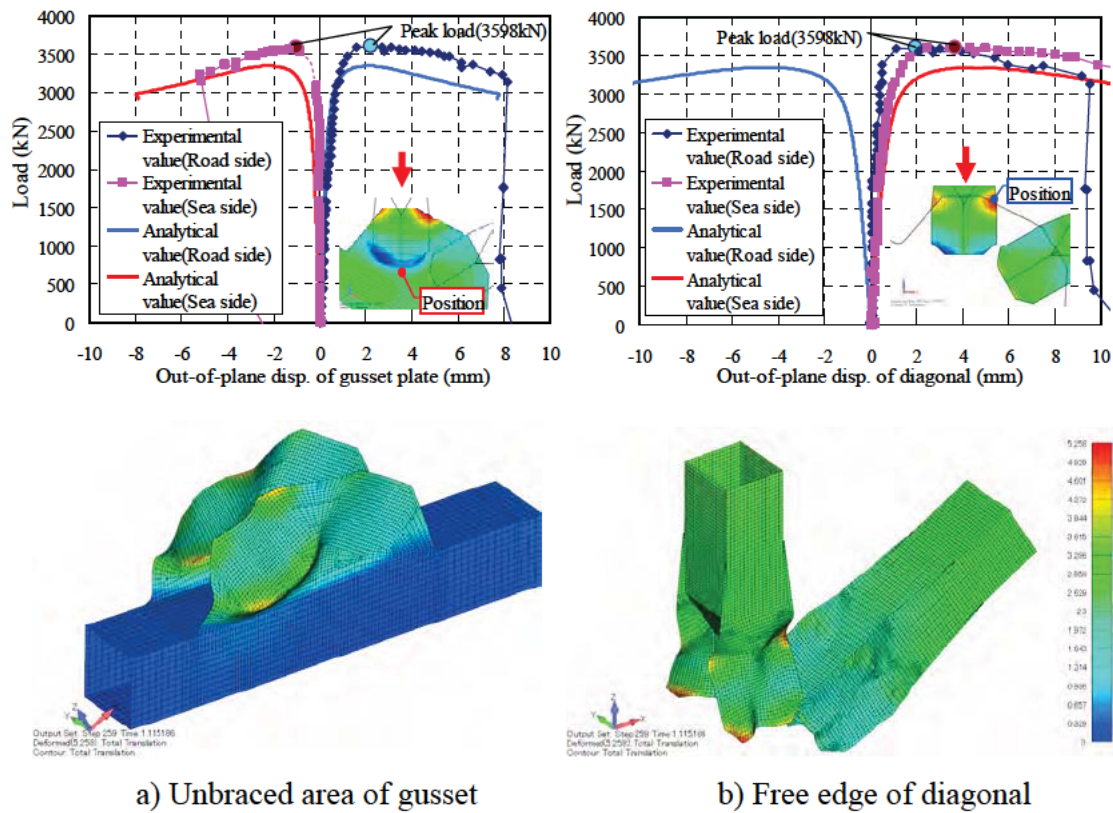


Figure 16 Load vs. Out-of-plane Displacement Curves

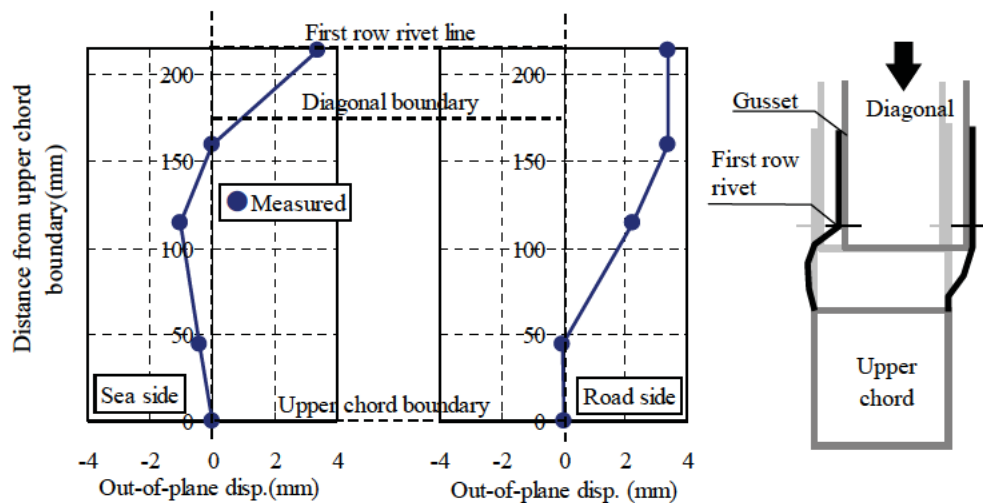


Figure 17 Deflected Mode of Unbraced Area

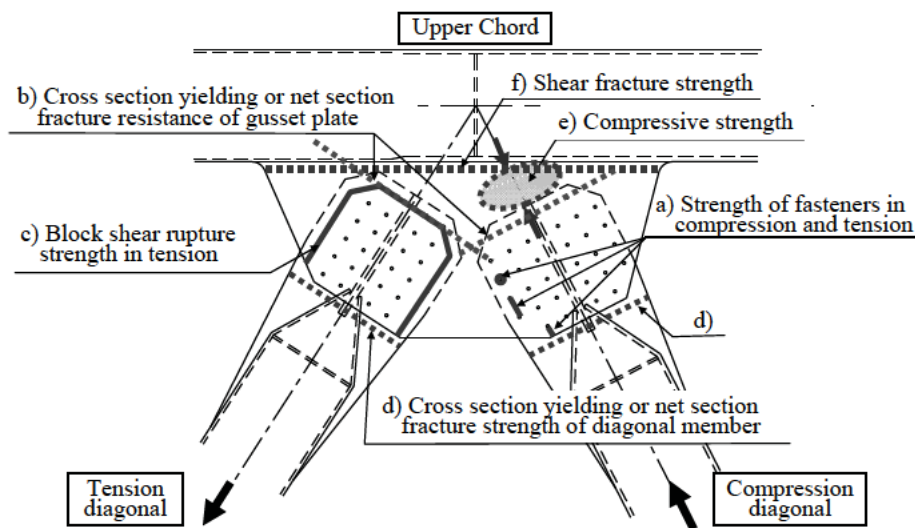
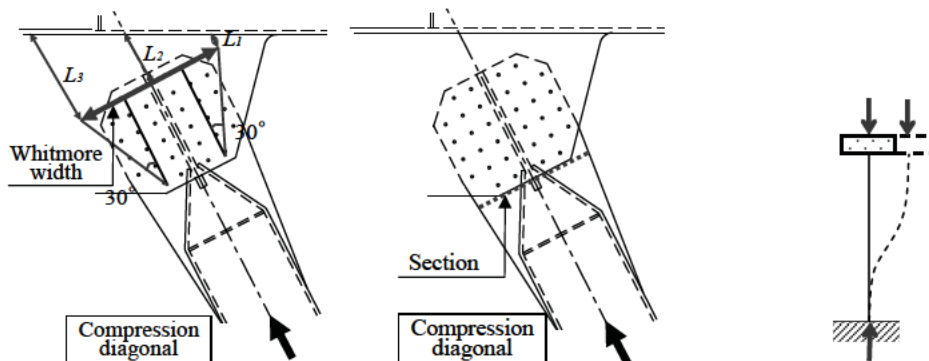


Figure 18 Limit State of Gusset Plate Connection



a)Yielding or local buckling of gusset plate b) Yielding of diagonal

Figure 19 Strength Equations for Compression

Figure 20
Effective length
Factor ($\beta=1.2$)

Table 2 The Comparison of the Ultimate Strength

	Compressive ultimate strength	Uncorroded model	Corroded model
	Analysis Value (Ultimate Load) kN (ratio)	4,953 (1.00)	3,346 (1.00)
Calculated Value	b) Cross section yielding of gusset plate kN (ratio)	4,792 (0.97)	3,194 (0.95)
	d) Cross section yielding of diagonal member kN (ratio)	6,087 (1.23)	4,666 (1.39)
	e) Compressive strength kN (ratio)	2,948 (0.59)	1,220 (0.36)
	Experimental Value (Ultimate Load) kN (ratio)	—	3,598 (1.08)

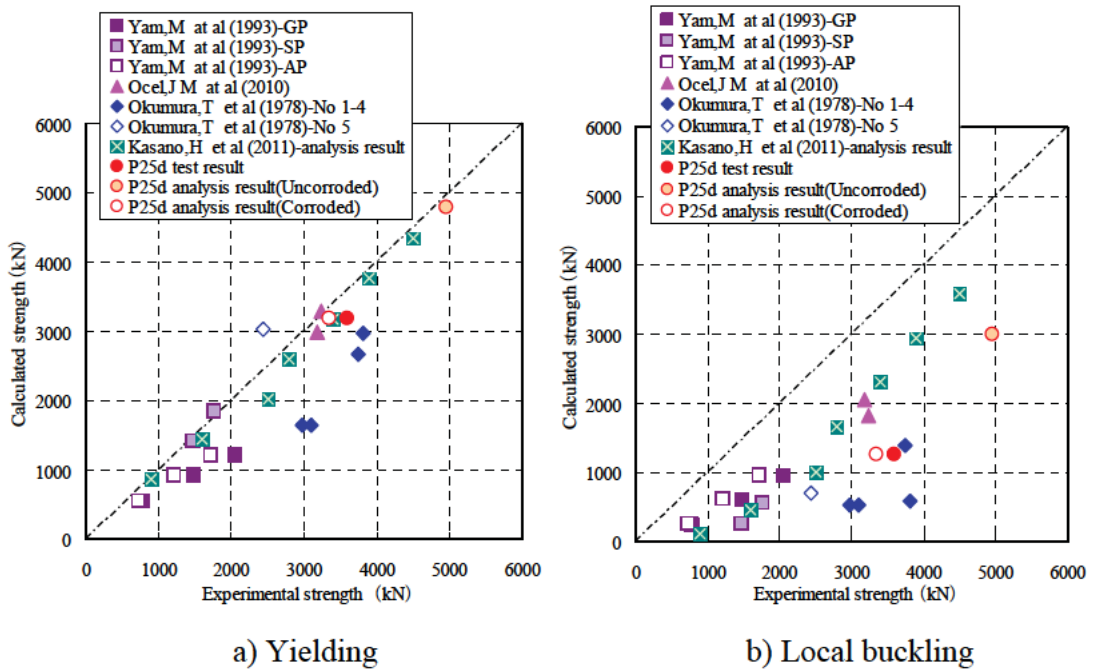


Figure 21 Comparison of the Experimental Ultimate Strength and the Calculated Strength

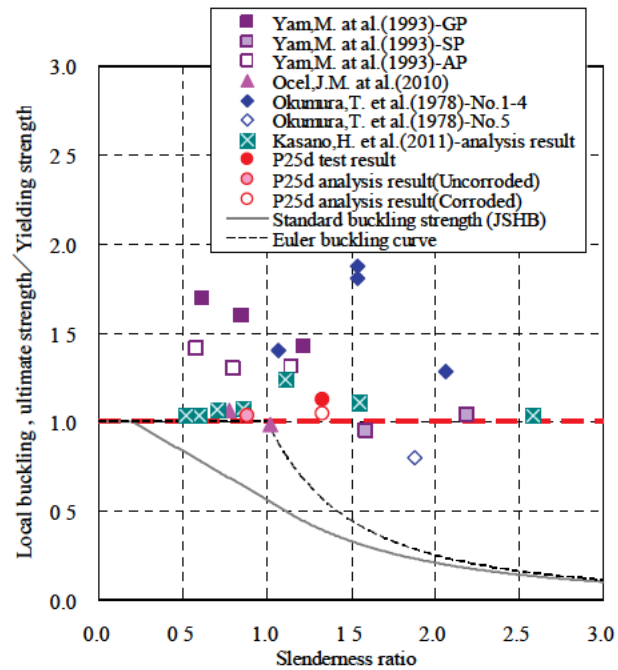


Figure 22 Relations of Strength and Slenderness Ratio

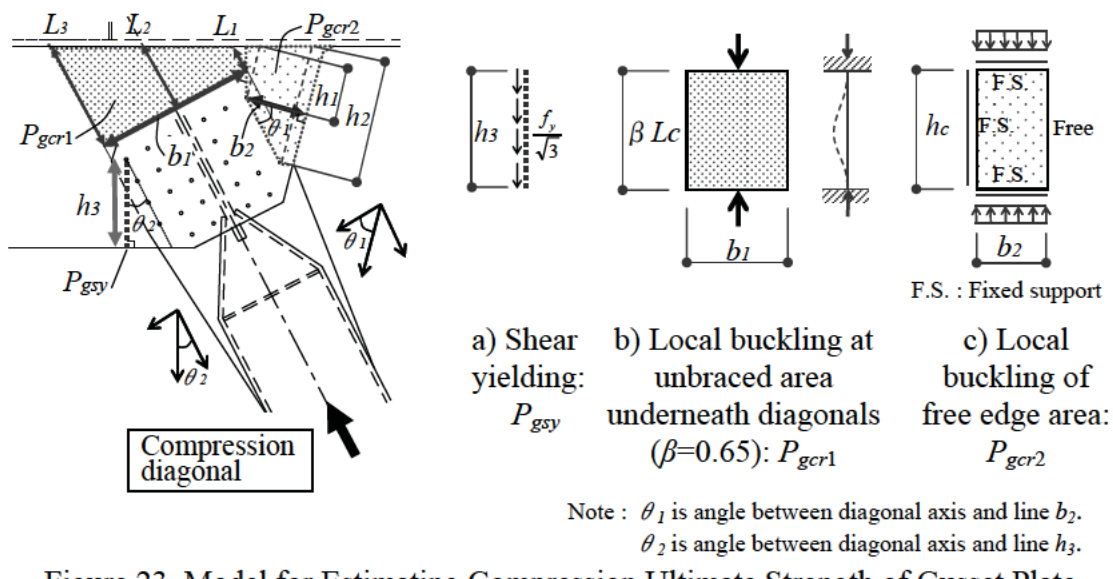


Figure 23 Model for Estimating Compression Ultimate Strength of Gusset Plate

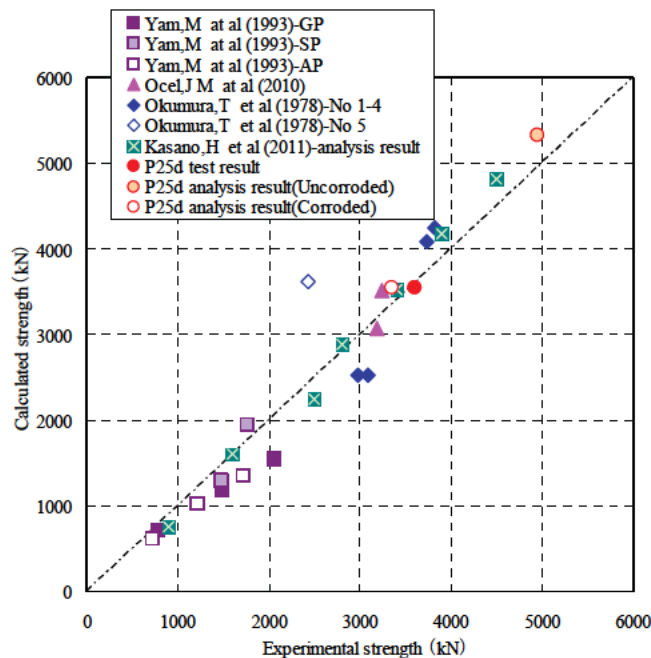
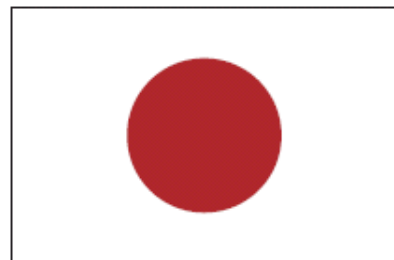
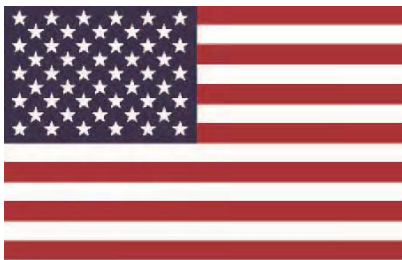


Figure 24 Comparison of the Experimental Strength and the Calculated Strength



27th US-Japan Bridge Engineering Workshop

Session 6

Maintenance2

Introduction of Non-Destructive Highway Inspection Methods Using High Definition Video and Infrared Technology

By Koji Mitani and Masato Matsumoto

Charpy Impact Tests with Test Specimens Made with Stop-Hole-Size Cores

By Kiyoshi Ono, Kengo Anami, and Mitsuharu Oikawa

The Next Generation of Experimental Research in Structural Fires

By John L. Gross and Stephen A. Cauffman

New Attempt to Maintenance of Steel Bridge Coating in Expressway

By Shuhei Sakai and Dai Wakabayashi

FHWA's New Infrastructure Research and Technology Strategic Plan

By Ian M. Friedland

Page Left Blank

INTRODUCTION OF NON-DESTRUCTIVE HIGHWAY INSPECTION METHODS USING HIGH DEFINITION VIDEO AND INFRARED TECHNOLOGY

Koji Mitani¹ and Masato Matsumoto²

Abstract

In order to make timely and appropriate maintenance and rehabilitation decisions for deteriorating highway structures, constant monitoring of structural conditions is necessary. While most agencies recognize the importance of timely bridge inspections, such programs tend to be time consuming and expensive. Under these circumstances, NEXCO-West has been able to reduce highway structure inspection costs by introducing an innovative highway inspection technical approach that uses a combination of high definition video (HDV) and infrared (IR) thermographic technology. This paper describes these inspection methods using HDV and infrared technologies and introduces some examples of practical on-site application to highway bridge superstructures.

1. Introduction

Today, proper maintenance and management of deteriorating infrastructure under severe budget constraints have become serious issues for bridge owners. Traditionally, highway bridge conditions have been monitored by visual inspection with structural deficiencies being manually identified and classified by qualified engineers and inspectors. However, the quality of inspection results obtained through the traditional approach depends on the individual inspector's subjective judgment based on his/her knowledge and experience. In addition, these traditional inspection procedures require significant investments in both time and labour cost. These factors support the necessity for research and development for more reliable, objective and efficient bridge inspection methods.

With traditional site inspections, qualified inspectors are performing close-up visual inspections and sounding tests, often from crane suspended lifting cages or built-in inspection staging; arguably putting inspectors at some safety risk. The need for safer inspection methods calls for new innovations in bridge inspection technologies. In addition, new technologies that improve inspection efficiencies will help address the upcoming shortage of qualified bridge inspectors.

Bridge inspector responsibilities include preparing summaries of bridge condition factors that, by their nature, reflect the individual inspector's engineering judgement. If we can improve data collection efficiencies and reduce the time required

¹ President and CEO, NEXCO-West USA, Inc.

² Executive Vice President, NEXCO-West USA, Inc.

by inspectors in the field to make general structure condition assessments, more time will be made available for these same inspectors to perform detailed hands-on inspection for those pre-screened bridge elements where structural defects require special attention.

The West Nippon Expressway Company Ltd. (NEXCO-West) has been working to develop efficient non-destructive highway bridge inspection methods using High Definition Video (HDV) and Infrared (IR) Imagery technologies. This paper describes the mechanisms of these inspection technologies and presents results from an on-site pilot project performed to evaluate the feasibility of these technologies in Florida, USA.

2. New Inspection Technologies

2.1 Inspection Methods Using High Definition Video (HDV)

Recently, research and development on crack detection methodologies for efficient highway bridge inspection using digital images of the structures have seen significant technological progress. In the past, conventional inspection techniques using digital image processing had not been widely applied for practical use due to its limited image quality. The equipment was typically expensive and their application was limited primarily to technical research applications and special forensic professional services. However, recent innovations and improvements in image quality and data processing technology have contributed greatly to the technical viability of this inspection technology.

FIGURE 1 shows the mechanism of pavement crack detection using HDV. The technology is the combination of GPS, GIS and HDV image pictures. The GPS navigation system, HDV and laptop computer are included inside the inspection vehicle. The HDV camera is attached on top of the inspection vehicle to record the surface condition (FIGURE 2). The recorded data is analyzed by image processing to determine an individual structure's current condition as related to crack size, location and distribution. The detected cracks are identified in a digital crack map. The crack size and length are determined by computer software, and these quantitative characteristics are also summarized in spreadsheet format. The obtained crack maps and related data are provided to engineers for their subsequent structural diagnosis and rehabilitation planning.

A special advantage of HDV technology, with respect to crack identification and measurement, is the ease of maintaining a historical record of bridge cracks for use in monitoring crack propagation over time. The image processing includes a two-gradation analysis and line featuring analysis. The first step of the two-gradation analysis converts the digital picture into binary (black-and-white) data by analyzing the degree of color transition from the nearby pixels, enabling our computer program to differentiate the spectrum and identify individual cracks. The second step then identifies the lines of black pixels in order to confirm the existence of cracks (see FIGURE 3).

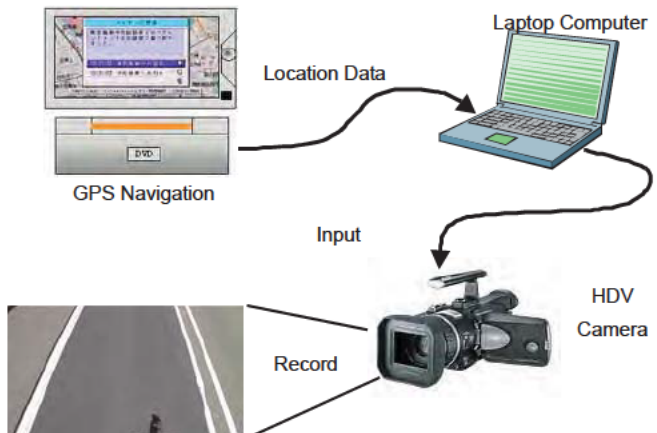


FIGURE 1 - HDV RECORDING FOR PAVEMENT CRACK DETECTION

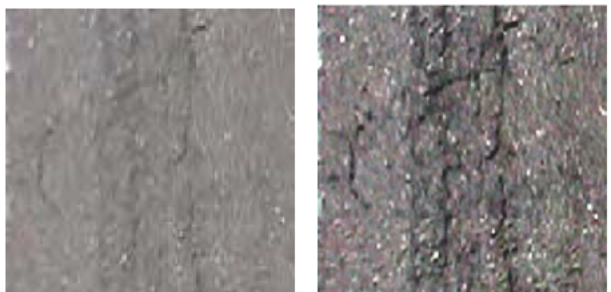


FIGURE 2 - HDV-EQUIPPED INSPECTION VEHICLE (LEFT)

FIGURE 3 - IMAGE PROCESSING (RIGHT)

2.2 Inspection Method Using Infrared (IR) Imagery Technology

Infrared imagery technology is a non-destructive testing method to locate possible delamination and spalling of concrete through the monitoring of temperature variations on a concrete surface using infrared thermography technology. IR technology offers inspectors the advantage of being able to identify likely delaminated, spalled and inner void areas from a distance of up to 5 meters with reasonable accuracy; thus avoiding the time and expense of gaining immediate access to the concrete surface to conduct traditional sounding tests. The results of IR images provide bridge owners a reliable screening of potential concrete defects on concrete structures that have been traditionally obtained by more time consuming (and probably more expensive) sounding tests. By applying IR technology to the concrete inspection process, inspectors can focus their hand-on sounding test activities on those areas shown through IR imaging as likely to be defective.

FIGURE 4 shows the mechanism of infrared thermography method. The red line shows daily temperature variation for delaminated concrete, while the blue line shows the daily temperature variation for concrete in good condition. The delaminated concrete surface shows different temperature variation (see FIGURE 5). Infrared imagery technology is applicable during the periods when temperature differentials are

detectable over time (IR imagery period A and B in FIGURE 4). It is not always possible to detect delamination of concrete only from the color variation of infrared imagery since the concrete structure itself tends to have a temperature gradient depending on location and orientation with respect to the sun. Akashi et al. (2009) performed the statistical and analytical study on the relationship between characteristics of temperature variation and inherent damage of the concrete, and developed an automatic damage classification system (J-System) that can classify the damage rate into three categories; the classification categories being “Critical” (crack exists on concrete surface and immediate attention is required), “Caution” (crack exists within 2cm from the concrete surface and close monitoring is recommended) and “Observation” (currently satisfactory) (see FIGURE 6). In Japan, spalling of concrete debris from expressway bridges has become a serious issue. In order to prevent hazards to the third parties, comprehensive sounding tests have been performed on all potentially hazardous concrete surfaces exposed to motorist and pedestrian traffic. Using IR thermography technology, engineers can check the delamination and/or spalling of concrete about three times faster than they can by conducting conventional sounding tests because IR technology applications require significantly less staging to secure adequate site access and correspondingly less traffic control to collect the required field data. Concurrently IR versus traditional sounding tests offer a 40% cost savings.

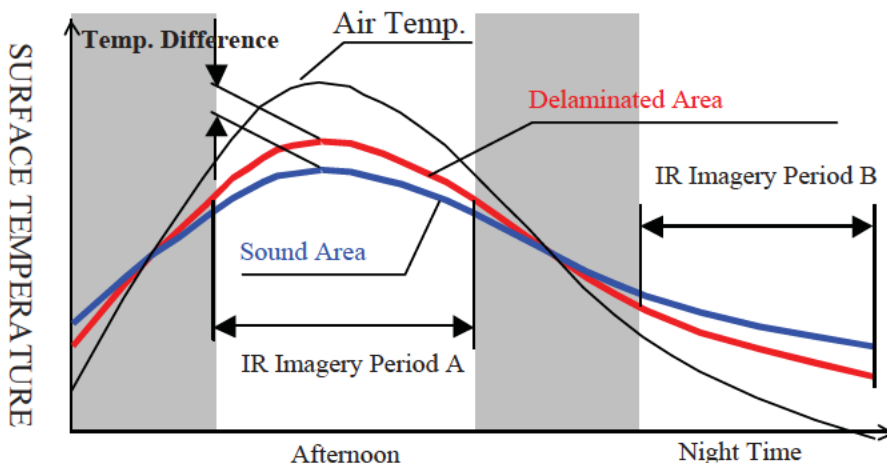


FIGURE 4 - TEMPERATURE VARIATION DURING THE DAY

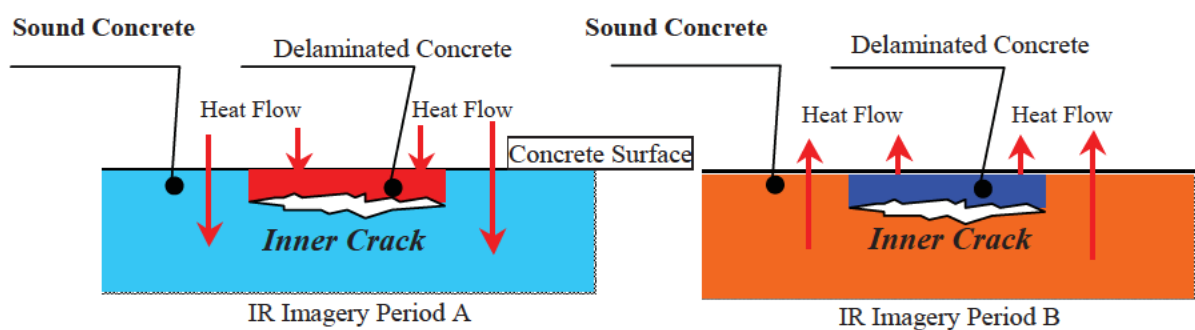


FIGURE 5 - MECHANISM OF INFRARED IMAGERY TECHNOLOGY

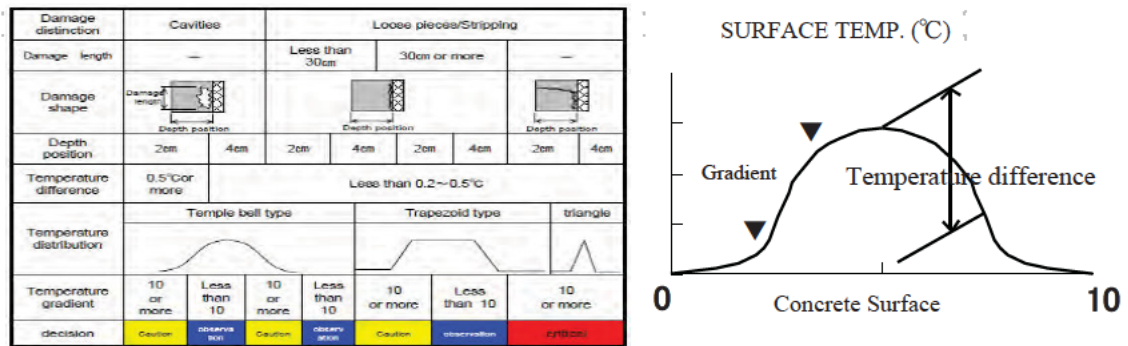


FIGURE 6 - DAMAGE RATING BY INFRARED IMAGERY TECHNOLOGY

2.3 Combination of HDV and IR Imagery Technology

HDV technology provides bridge inspectors visual digital information on concrete surface conditions that have traditionally been obtained from close-up visual inspections. Concurrently, the IR imagery technology corresponds to the sounding tests that traditionally have been used to detect voids, delaminations, and/or areas of spalled concrete (see TABLE 1). Most of the information from the visual inspection and the sounding tests can be obtained by a combined inspection using HDV and IR imagery technology. Effectively combining these technologies can contribute to reduced time for on-site inspection and inspection report preparation, allowing engineers to have more opportunities to devote themselves to the engineering issues such as structural diagnosis and strategic rehabilitation planning. The advantages of applying new inspection technology include;

- Minimizing the human error factors (improve objectivity)
- Providing digital record for historical inspection data comparisons
- Improve efficiencies in bridge inspection resource application

TABLE 1 - PURPOSE OF THE NEW INSPECTION TECHNOLOGIES

		Purpose of Inspection	Traditional Approach
HDV	IR Imagery	Surface Condition of the Structure (ex. Crack Map) Inner Void, Delamination and Spalling of Concrete	Visual Inspection Sounding Test

3. The On-site Pilot Project in the United States

3.1 Introduction to the Pilot Project

In order to validate effectiveness of the new inspection technologies, a pilot inspection project was conducted at the Seven Mile Bridge on US Route 1 in Florida

Keys (see FIGURE 7). Currently, condition of the bridge is regularly monitored through established visual inspection procedures performed by qualified inspectors.

3.2 The Pilot Project Results

(1) Deck Surface Inspection Using HDV

In order to record the deck surface cracks using an HDV camera, proper height (approximately 3 meters) and recording angle (no greater than 45° from vertical) are required. The HDV camera was attached to a custom-made camera mount and video data was gathered facing in the backward direction. HDV recordings of the concrete deck surface were conducted at a speed of 70km/h.

FIGURE 8 shows an example of a crack map for a concrete deck surface. Cracks of 3mm or greater were detected by a software supported automatic crack detection program, followed by supplemental manual crack checking by an experienced engineer. Manual crack checking successfully detected cracks of 0.8mm or greater. According to the Bridge Inspectors Field Guide (Florida Department of Transportation (2008)), cracks should be classified into three categories as shown in Table 2, and the NBI (National Bridge Inventory) specified “Distressed Area” is calculated for the rectangular area including “Significant,” “Moderate,” or “Severe” cracks. Inspectors are responsible for proposing priorities on rehabilitation to the bridge owners by comparing the “Distressed Area” for each span or bridge. The results of pilot area bridge deck surface inspections proved the accuracy of crack detection using HDV technology to be satisfactory for routine in-service deck inspections. The new inspection technology provides additional benefits by increasing the level of safety for both inspectors and motorists and storing position recorded historical inspection data for monitoring of crack propagation. The digital crack map database can be a powerful tool for supporting those engineers responsible for maintenance plan preparation and work task priority decision-making.



FIGURE 7 - LOCATION OF THE SEVEN MILE BRIDGE

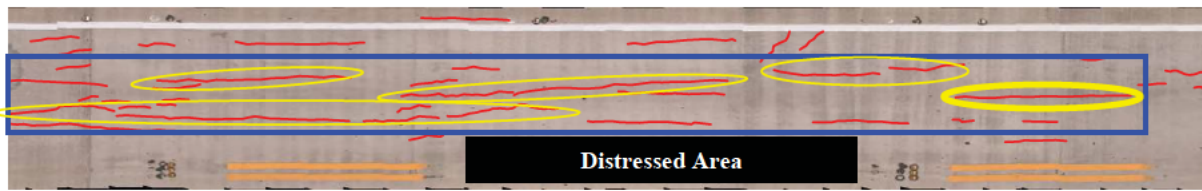


FIGURE 8 - AN EXAMPLE OF CRACK MAP FOR CONCRETE DECK TOP

TABLE 2 - CATEGORIZATION OF CRACK SIZE (Florida Department of Transportation (2008))

	Insignificant	Moderate	Severe
Crack Size	<1.6mm	1.6mm-6.3mm	>6.3mm

(2) Bridge Inspection using High Definition Video (HDV)

The underside of the bridge superstructure was photographed by HDV from a boat. Due to the boat's motion from wave action, the allowable recording range needs to be addressed by using three HDV cameras with a combined 1.56 million pixel image, a resolution that enables the user to include a 2-meter wide targeted object within a 3600 wide pixel image. This approach enabled identification of cracks in the 0.2mm to 0.5mm range through an analysis of the relative grey tone of the pixels denoting the cracks. The pilot project section consists of seven continuous spans of a post tensioned segmental box girder bridge. HDV photography involved seven separate passes of the boat beneath the bridge as shown in FIGURE 9 in order to capture all of the required HDV images. The time required to record HDV images for the lower surface of all seven spans was about 2.5 hours. The recorded data obtained by the three cameras were combined automatically using proprietary computer software. By magnifying the digital image on the computer, existing cracks were visually detected by an experienced engineer trained to interpret HDV images.

To validate the results of the computer generated HDV crack detection assessment and to perform more detailed crack detection, an 'electronic crack gauge' is superimposed onto the HDV image. Engineers can maneuver the gauge on the HDV image and manually validate computer based crack width measurements. The detected cracks are categorized into three ranks (Rank 1: $\leq 0.5\text{mm}$, Rank 2: $>0.5\text{mm}$ to 0.7mm , Rank 3: 0.7mm or greater). The crack width, length and location data developed by using HDV applications can provide powerful decision making support information for engineers with bridge maintenance planning responsibilities.

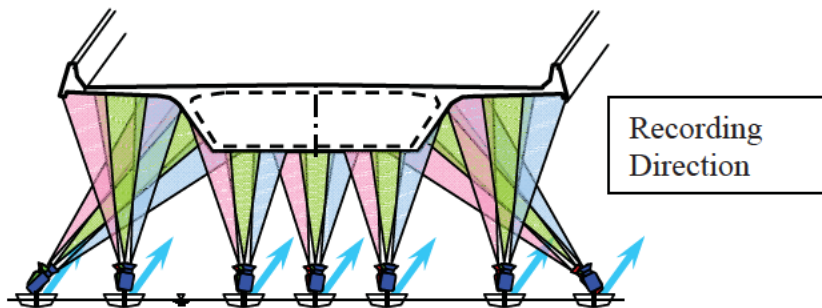


FIGURE 9 - RECORDING OF CONCRETE BRIDGE SUPERSTRUCTURE SURFACE BY THREE HDV CAMERAS

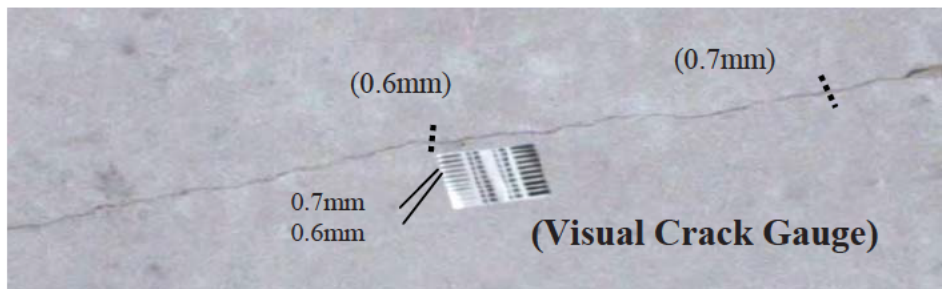


FIGURE 10 - ENLARGED IMAGE OF DETECTED CRACKS (EXAMPLE)

(3) Bridge Inspection Using Infrared Imagery Technology

The infrared images of the pilot project section were photographed by a boat-mounted camera from underneath the bridge. The time required to photograph the entire lower bridge superstructure surfaces (soffit, exterior stems and deck overhangs) of the seven spans was about 2 hours.

Since the accuracy of damage identification using infrared imagery is greatly affected by daily temperature variation, accurate monitoring of the infrared (IR) photographing environment is mandatory. FIGURE 11 shows the equipment used for monitoring the temperature condition on the concrete surface. Three concrete test pieces with artificial flaws were attached to the bridge's underside surface. Taking infrared images of the concrete 'set-up' test pieces enabled the field infrared imaging team to see if there was sufficient temperature difference between damaged and non-damaged areas at any given time to permit further diagnostic IR imaging of the test area. Based on analysis of a 24 hour time-temperature record, it was concluded that the best available time period to apply infrared technology was from 9pm to 2am. During the photographing process, the infrared images of set-up test pieces were periodically checked in order to make sure that the field infrared imaging team was always in proper IR imaging environment. Figure 12 (a)(b)(c) shows an example of test results using IR imagery technology. The result of damage rating in FIGURE 12(c) shows three clusters of red spots indicating "Critical" condition. However, by checking the digital

photo in FIGURE 12 (a), we can easily recognize that the spots at both sides are for drainage outlets. Using the output from the damage classification system, we can estimate the approximate spall area surrounded by red rectangle in Figure 12(c). Calculating the total spall area for each span or bridge provides engineers a quantified basis for prioritizing alternatives in a bridge structure rehabilitation plan.

Combining the results of HDV and IR imagery technology can produce synergetic effects that provide decision-makers with very useful structure condition information. By superimposing IR images, after specific location damage classifications have been made, onto the HDV image and resulting crack map of the same area, engineers can readily identify areas of likely structural damage, both on the surface and below the surface of the concrete.

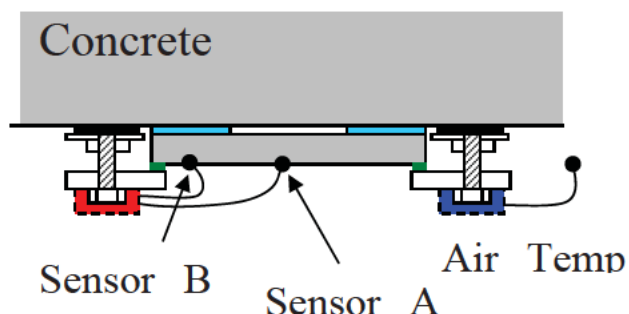


FIGURE 11 - THE “SET-UP TEST PIECE”

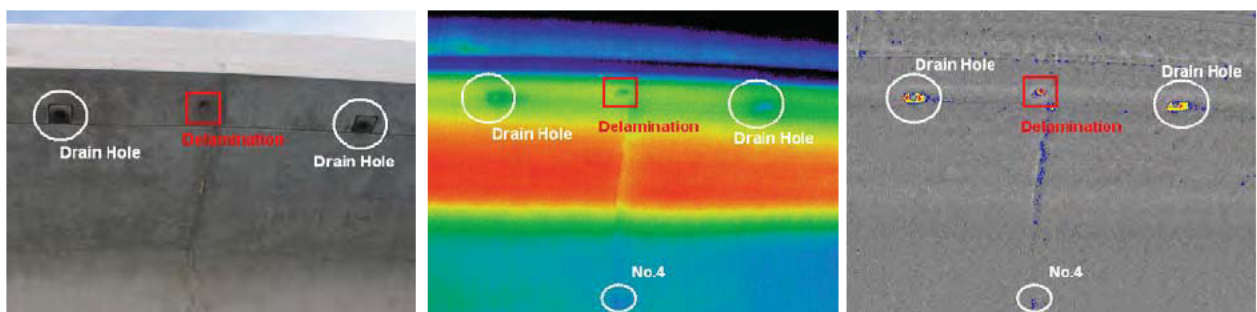


FIGURE 12 - RESULTS OF THE INSPECTION USING IR IMAGERY TECHNOLOGY - (A) PHOTOGRAPH (LEFT), (B) IR IMAGERY (CENTER), (C) DAMAGE RATING (RIGHT)

4. Potential Applications of HDV and IR Imagery Technologies

HDV and IR imagery technology can be applied for both in-service bridge inspection and checking new structures for specification compliance (in terms of crack area percentage) at the time of construction acceptance. HDV technology has also been used successfully for supporting night time striping reflectivity tests. IR imagery technology has many other uses as well. Among applications relevant to maintenance and rehabilitation is the ability to use IR imaging to monitor areas of structural distress

that have been covered with fiber reinforced polymer (FRP) materials (see FIGURE 13). Another application is to identify subsurface irregularities (grout covered rock pockets) in new construction structure immediately after the removal of form work.

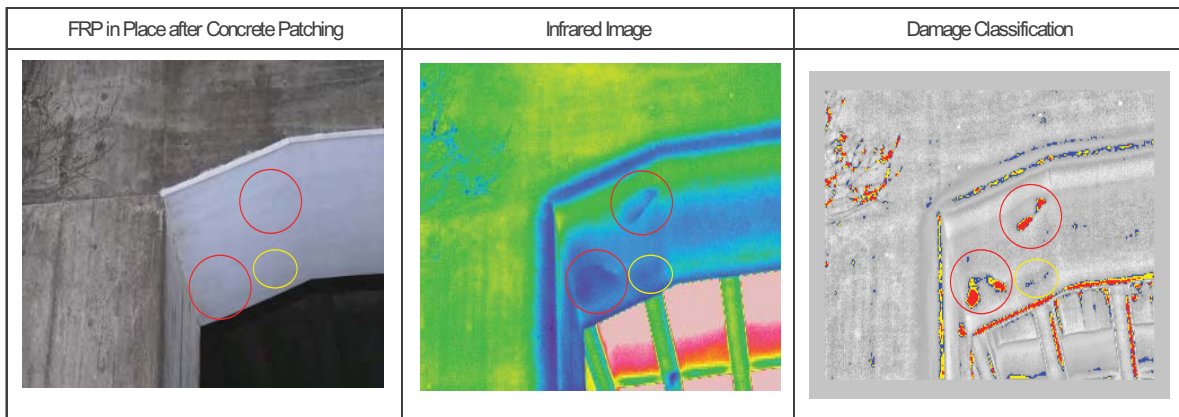


FIGURE 13 DETECTING POTENTIAL SPALL BENEATH THE FRP COVER

5. Summary and Conclusions

This paper described the mechanism of non-destructive bridge inspection methods using HDV and IR imagery technology and results of the on-site pilot project performed to evaluate the feasibility of applying these technologies for in service bridge inspection in the State of Florida, USA.

It was verified from the pilot project results that the accuracy of detection and measurement surface cracks and potential subsurface deterioration using these new technologies provided satisfactory and acceptable results for practical routine and special condition bridge inspections in compliance with recognized inspection practices. It was also demonstrated that new HDV and IR technologies could significantly reduce site inspection times and on-site inspection resource requirements.

With the quantity of roadway structure assets increasing annually, coupled with concurrent increasing rates of deterioration being experienced by many of the existing structures, bridge owners need to find new and creative ways to ensure the structural safety of their bridges while they all too often face problems of reduced budgets and dedicated bridge inspection resources. Using the proposed new HDV and IR technologies, bridge engineers can quickly and efficiently obtain objective current bridge condition information that has traditionally been obtained by more time consuming and, in some instances, more subjective close-up visual inspections and sounding tests. The digital output of these HDV and IR inspection techniques improves on-site inspection safety and objectivity and contributes to improved inspector efficiency by reducing significantly the amount of on-site inspection time in the field. However, it must be noted that while HDV and IR technologies do offer new efficiencies to the bridge inspection process, they are not a substitute for inspectors conducting on-site specific follow-up and detailed structure investigations. While

improved efficiencies in bridge inspection brought about by the application of HDV and IR technologies bring significant benefits to the overall bridge inspection process, they are not a substitute for the continued need for sound experienced engineering judgement.

Currently, costs of traditional and new inspection technologies are similar with new tech's lower field data collection costs being somewhat offset by additional costs for computer supported analysis. We expect with likely improvements in computer technology that these new inspection technologies will become increasingly cost effective. The authors believe that by offering experienced bridge engineers and inspectors new improved inspection technologies, bridge inspection programs will be strengthened through improved inspection data, increased safety and more economical operations...bringing tangible benefits to bridge owners and the motoring public alike.

Acknowledgments

The authors would like to express their sincere gratitude to Florida Department of Transportation, Transfield Services, Inc., The Monroe County Sheriff's Department, The Louis Berger Group Inc., Berger Avart Inc., Mr. Per Fostvedt of Infrared Services, Mr. Harry Stoltzfus of Harcon Bridge Access Services, Dr. Masanobu Sugimoto of Fuji Engineering Co. Ltd., Mr. Kazuaki Hashimoto of NEXCO-West Engineering Shikoku Co. Ltd., and Mr. Yuji Uchida of Ergo Vision Co. Ltd. for their cooperation and support during the pilot project.

References

1. Akashi K, Hashimoto K, Koide H, and Togawa M (2006.9): Development of Inspection Method using Infrared Thermography Technology and its Technical Consideration, Proceeding of JSCE 61st Annual Meeting, PP 1113-1114
2. Florida Department of Transportation (2008.2): Bridge Inspectors Field Guide Structural Elements,

CHARPY IMPACT TESTS WITH TEST SPECIMENS MADE WITH STOP-HOLE-SIZE CORES

Kiyoshi Ono¹, Kengo Anami² and Mitsuhiro Oikawa³

Abstract

In order to examine or repair fatigue damaged steel bridges, it is necessary to obtain information of mechanical and chemical properties of steel of damaged members or joints. However, for the old bridges, it is sometimes difficult to obtain such kinds of information from design articles. For such case, a sample material might be taken from the structures, but the sample should be as small as possible.

This study examines the use of small steel pieces regarded as cores, which are taken from stop-holes or bolt-holes. Test specimens for Charpy impact test are made with small steel pieces by Electron Beam Weld (EBW) and the effect of the steel piece size on Charpy absorbed energy are examined.

Introduction

Fatigue damage in steel bridges have been reported (Japan Road Association. 2007, 2009; Miki et al. 2007) and the number of reported fatigue damage has increased. Some of the fatigue damage are serious fatigue damage such as the fracture that extended halfway through the circumference of a steel pipe column of a pedestrian bridge and the crack on the web plate of a steel girder whose length is about 1.1m. In order to identify the cause of fatigue damage or examine the retrofitting methods of fatigue damage, it is necessary to gain the information on the mechanical, chemical and fracture properties of materials of steel bridges. Especially as for the old steel bridges, there are some cases that the information about the material does not remain or the standard of the material does not exist at all. In such cases, the test specimens or samples are picked from the base material of steel bridges. For example, test specimens of Charpy impact tests were made with the material removed from the base material and Charpy impact tests were carried out in order to examine the fracture toughness (Miki et al. 2009). However, it is desirable that the area picked from the sound base material is as small as possible.

By the way, there are cases that stop-holes are bored for preventing the crack propagation and the holes for high tension bolts are bored for retrofitting by the bolted splice steel plates. It is very effective and useful to use the stop-hole-cores or bolt-hole-cores as the test specimens or samples.

¹ Associate Professor, Dept. of Civil Engineering, Osaka University

² Associate Professor, Dept. of Civil Engineering, Shibaura Institute of Technology

³ Bachelor, Dept. of Civil Engineering, Shibaura Institute of Technology

In order to evaluate the fracture toughness by using stop-hole-size cores, this study examines to make the test specimens with the stop-hole-size cores and conduct Charpy impact tests by using the test specimens. To be concrete, a small steel piece including the V-notch area gained from the stop-holes or bolt-holes is connected to the other parts of the test specimen by electron beam weld (EBW) as shown in Figure1. The effect of the width of the small piece on the Charpy absorbed energy is investigated.

Mechanical and chemical properties of material

One of the major interest of this study is to investigate the material properties of the old steel. Therefore, the steel plates for the test specimens were picked from a web plate at a cross beam of a steel bridge constructed in the 1920's or 1930's and test specimens were made with the steel plates. The plate thickness of the targeted steel plate is 9mm. The information on the material properties does not remain at all. Therefore, the tensile tests and the chemical analysis were carried out in order to get the basic information on the material properties before Charpy impact tests.

Test specimens were removed in longitudinal direction of the cross beam and direction perpendicular to longitudinal direction. The number of test specimens in each direction is three and the total number is six. Table 1 indicates not only the average values of major mechanical properties about the strength and elongation in each direction but also the values specified in the 2008 JIS (Japanese Industrial Standards) as for SS400 that is rolled steel for general structures and SM400A that is rolled steel for welded structures. Figure 2 shows an example of stress-strain relationship gained from the tensile tests. As shown in Table 1, the mechanical properties of the steel satisfy the specifications of SS 400 and SM400A in the 2008 JIS.

Table 2 shows chemical analysis results and chemical components specified in the 2008 JIS in respect of SS400 and SM400A. As shown in Table 1, although the amount of "S" does not satisfy the specification as for SM400A in JIS, the other components in Table 2 satisfy the specifications as for SS400 and SM400A in JIS.

Assumed size of cores

The main purpose of this study to make the test specimens with the stop-hole-size cores for Charpy impact tests in order to evaluate the fracture toughness. Figure 1 shows an outline of test specimen examined in this study. As shown in Figure 1, a small steel piece including the V-notch area corresponding to a stop-hole core or a bolt-hole core is connected to the other parts of the test specimen by EBW. It is assumed that a diameter of the stop-hole or bolt-hole is 24.5mm or 26.5mm. It is thought that the stop-hole-size core whose diameter is 20mm can be obtained from the assumed stop-hole or bolt-hole. Figure 3 shows the relationship between an assumed stop-hole-size core gained from steel bridges and a small steel piece including the V-notch area of a test specimen. As shown in Figure 3, the square steel pieces whose size is 13mm can be gained from the stop-hole-size core whose diameter is 20mm. In

consideration of Figure 3, 13mm is decided as the maxim size "B" of square steel pieces gained from the stop-hole-size cores.

Procedure of making test specimens by EBW

The welding condition of EBW used in this study is as follows.

Voltage: 60(kV), Current: 65(mA), Welding speed: 650mm/min.

EBW was carried out from the one side of test specimens. The outline of the procedure of making test specimens is as follows.

- Small steel pieces corresponding the main part of test specimens including V-notch (① in Figure 4), steel spacers (② in Figure 4), edge parts of the test specimens (③ in Figure 4) and the bucking metal are set as shown in Figure 4. The steel grade of edge parts of the test specimens is SM490.
- EBW (Blue solid lines in Figure 4) is conducted.
- Cutting along the yellow dotted lines in Figure 4 is conducted.
- Making test specimens are completed by cutting and shaving off until the predetermined size and thickness of under-size Charpy V-notch impact test specimens specified in JIS.

Types of test specimens

It was impossible to make the standard-size Charpy V-notch impact test specimens whose thickness is 10mm because the thickness of targeted steel plates is 9mm. Therefore, under-sized Charpy impact V-notch test specimens whose thickness is 7.5mm were made in this study. In the case of making test specimens by welding, the influence of welding on the change in the material properties like the heat-affected zone should be considered. Moreover, some previous studies (Seo et al. 1982; Seo et al. 1983) pointed out that Charpy absorbed energy is effected by restriction by EBW and the adequate test results can not be gained if the distance between each EBW is small. Therefore, test specimens were set with focusing on the width of small steel pieces "B" in Figure 5. "B" corresponds to the distance of the center of each EBW as shown in Figure 5. Table 3 shows types of test specimens and the values of "B". In Table 3, the test specimen "B-0" indicates the test specimens without EBW. According to the experience of EBW until now, it is supposed that the width of the heat-affected zone by EBW whose welding condition is almost the same as that in this study may be 6mm. The width of the non heat-affected zone of each test specimens is supposed to be (B-6)mm as shown in Figure 5. Judging from this assumption about the width of the heat-affected zone by EBW, it is estimated that all over the V-notch area of test specimens "B-4" may become the heat-affected zone by EBW.

Macrostructure tests and Vickers hardness tests

Macrostructure tests and Vickers hardness tests were conducted in order to investigate the heat-affected zone by EBW. The weight of Vickers hardness test in this investigation was 9.8N. The location of the measuring points is the center of the height

of test specimens and the interval of the measuring points is 0.5mm. Pictures 1 and 2 show the results of the macrostructure tests of the test specimens "B-1" and "B-3". Figures 6 and 7 show the test results of Vickers hardness tests of those. In the pictures and the figures, "Front surface" indicates the surface in which electron beam was discharged and "Back surface" indicates the opposite side. In Figures 6 and 7, read dashed lines express the supposed center of EBW.

According to the results of the macrostructure tests and Vickers hardness tests, it is found that heat-effected zone by EBW on the front surface is wider than that on the back surface because the front surface is a surface in which electron beam was discharged. Judging from the hardness gained from Vickers hardness tests, it is thought that there is a correlation between " B " and the width of the non heat-affected zone " L ", in which the hardness is almost the same as that of the base material. The values of " L " are described in Table 3. As shown in Table 3, the values of " L " become smaller as those of " B " become smaller.

Results of Charpy V-notch impact tests

Charpy V-notch impact tests were conducted with under-sized test specimens whose thickness is 7.5mm. The temperature for the Charpy V-notch impact tests was 0°C, -30°C and -60°C. Figure 8 shows the results of the Charpy V-notch impact tests. The significant difference in the test results at -60°C and -30°C among all test specimens is not found and the values of the Charpy absorbed energy at -60°C and -30°C are very small as a whole. On the other hand, the difference in the Charpy absorbed energy at 0°C can be found depending on the type of the test specimens. The Charpy absorbed energy of the test specimens "B-13" whose " B " is 13mm is almost the same as that of the test specimens "B-0" that is test specimens without EBW although the variation in test results can be seen. The Charpy absorbed energy of the test specimens "B-4" in which all over the V-notch area is a heat-affected zone is the smallest of all types of test specimens. The Charpy absorbed energy of the test specimens "B-9" whose " B " is 9mm exist between that of "B-4" and that of "B-0" or "B-13". The test results show that the Charpy absorbed energy depends on the width " B " and the wider " B " leads the higher Charpy absorbed energy. Furthermore, the Charpy absorbed energy of the test specimens "B-13" whose " B " is 13mm is almost same as that of test specimens without EBW. Therefore, it is thought that the Charpy absorbed energy of test specimens made by EBW may converge to that of test specimens without EBW when " B " is almost 13mm. This fact indicates the possibility that the Charpy absorbed energy can be evaluated adequately with the test specimens made with stop-hole-size cores by EBW.

Concluding remarks

This study examines the use of small steel pieces regarded as cores, which are taken from stop-holes or bolt-holes. The targeted steel is the steel removed from a web plate at a cross beam of steel girder bridges constructed in the 1920's or 1930's. Test specimens for Charpy impact test are made with small steel pieces by Electron Beam Weld (EBW) and the effect of the steel piece size on Charpy absorbed energy are

examined.

As a result, it is found that the Charpy absorbed energy depends on the width of the steel pieces and the wider steel pieces leads the higher Charpy absorbed energy and it is thought that the Charpy absorbed energy of test specimens made by EBW may converge to that of test specimens without EBW when the width of the steel pieces is almost 13mm. This fact indicates the possibility that the Charpy absorbed energy can be evaluated adequately with the test specimens made with stop-hole-size cores by EBW.

Acknowledgments

This work was supported by the Grant-in-Aid for Scientific Research (S: No. 18106010) from the Japan Society for Promotion of Science (JSPS).

References

- Japan Road Association (2007): Collection of Example of Retrofitting of Highway Bridges. (in Japanese)
- Japan Road Association (2009): Collection of Example of Retrofitting of Highway Bridges. (in Japanese)
- Chitoshi Miki and Takuyo Konishi (2007): Retrofit Engineering for Steel Bridge Structures in Japan, A-0673, IABSE SYMPOSIUM, WEIMAR, 2007.
- C. Miki, K. Ono, K. Yokoyama and T. Harada (2009): Identification of the causes of fracture in the steel pipe column of a pedestrian bridge, Welding in the World, Vol.53(9/10), pp.229-237.
- Kenji Seo and Junichi Masaki (1982): Physical Interpretation for the Upper Shelf Energy of Weld Zone in Charpy Impact Test, Journal of the Japan Welding Society, Vol. 51, No.3, pp.39-45. (in Japanese)
- Kenji Seo, Junichi Masaki, Fumio Nogata and Kunihiko Sato (1983): Effect of Mechanical Heterogeneity on the Ductile-to-Brittle Transition Behavior of Weld Metal in Charpy Impact Test, quarterly journal of the Japan Welding Society, Vol.1, No.2, pp.123-129. (in Japanese)

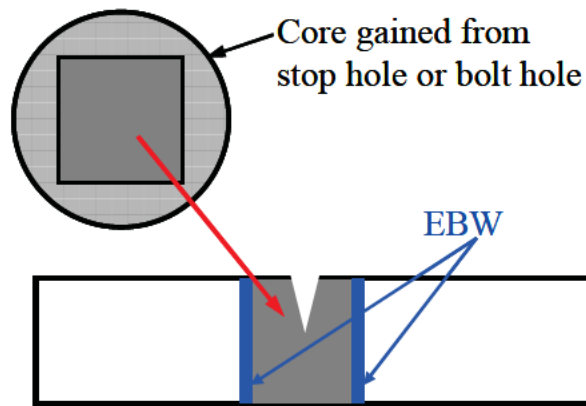


Figure 1 Image of test specimens made with stop-hole-size cores

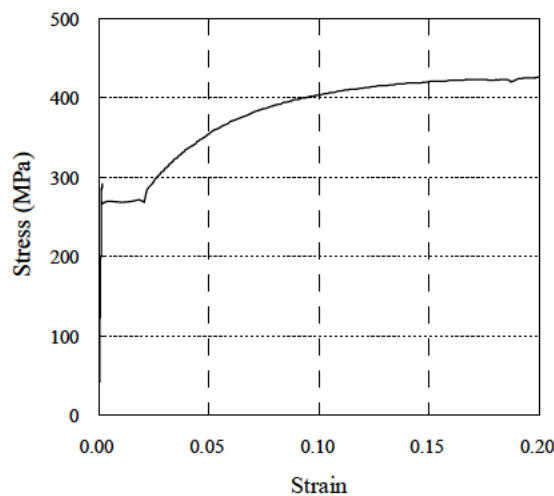


Figure 2 Stress-Strain relationship

Table 1 Mechanical properties

	Direction	Upper yield Stress σ_{yu} (MPa)	Lower yield Stress σ_{yl} (MPa)	Tensile Strength σ_b (MPa)	Elongation δ (%)
Targeted steel	Longitudinal	289	265	428	40.7
	Perpendicular	283	262	424	40.3
SS400(JIS-2008)		≥ 245	—	400~510	≥ 17
SM400A(JIS-2008)		≥ 245	—	400~510	≥ 18

Table 2 Results of chemical analysis

	C (%)	Si (%)	Mn (%)	P (%)	S (%)
Targeted Steel	0.18	0.01	0.46	0.031	0.038
SS400(JIS-2008)				≤ 0.050	≤ 0.050
SM400A(JIS-2008)	≤ 0.23		$\geq 2.5 \times C$	≤ 0.035	≤ 0.035

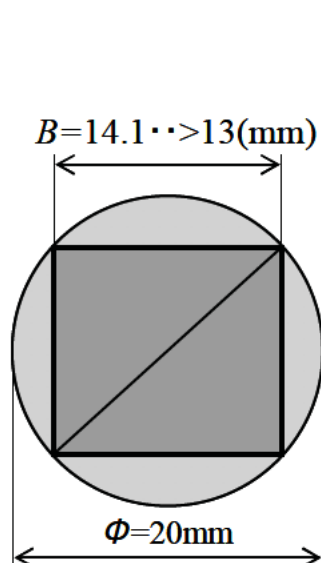


Figure 3 Relationship between assumed cores and gained steel pieces

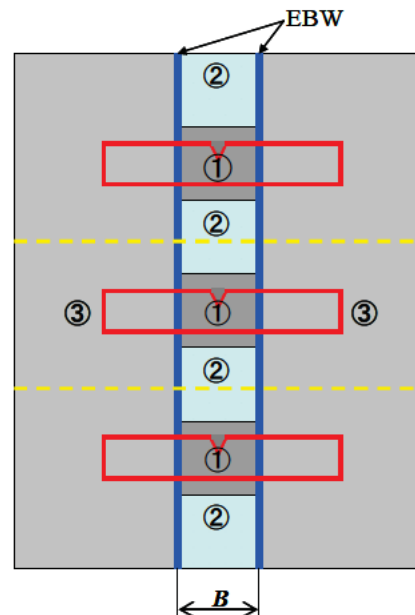


Figure 4 Procedure of making test specimens by EBW

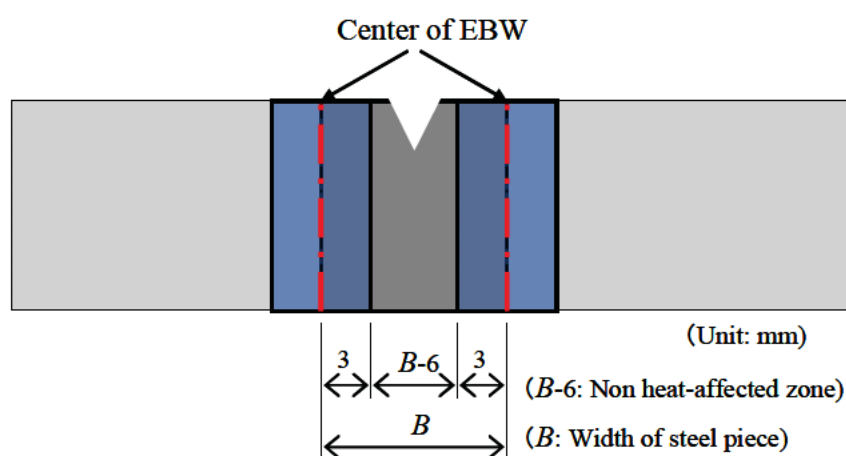
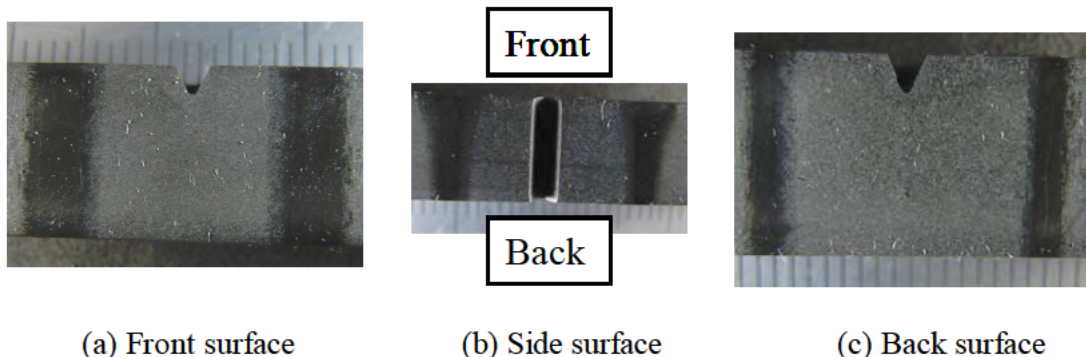


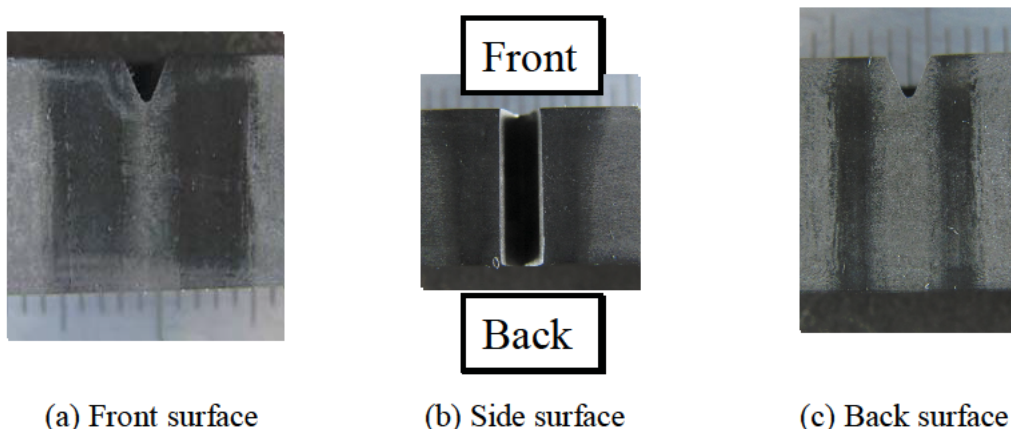
Figure 5 Test specimens made with stop-hole-size cores by EBW

Table 3 Types of test specimens and the values of "B", "B-6" and "L"

	Width of Steel Piece <i>B</i> (mm)	Width of Non Heat-affected Zone			
		Assumption <i>B</i> -6 (mm)	Based on Hardness: <i>L</i> (mm)		
			Front	Back	Average
B-13	13	7	8	10	9.0
B-9	9	3	3	4	3.5
B-4	4	- (0)	0	2	1.0
B-0		Non-EBW			



Picture 1 Results of macrostructure tests of test specimen "B-13"



Picture 2 Results of macrostructure tests of test specimen "B-4"

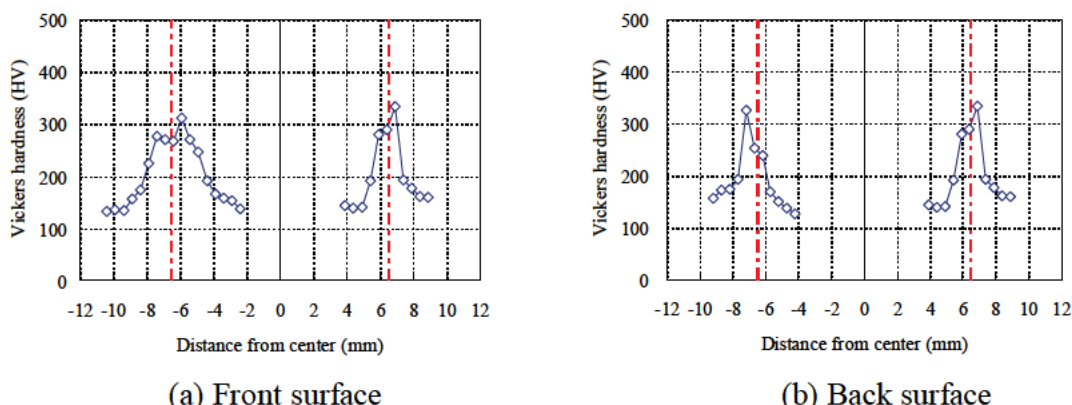


Figure 6 Results of Vickers hardness tests of test specimen "B-13"

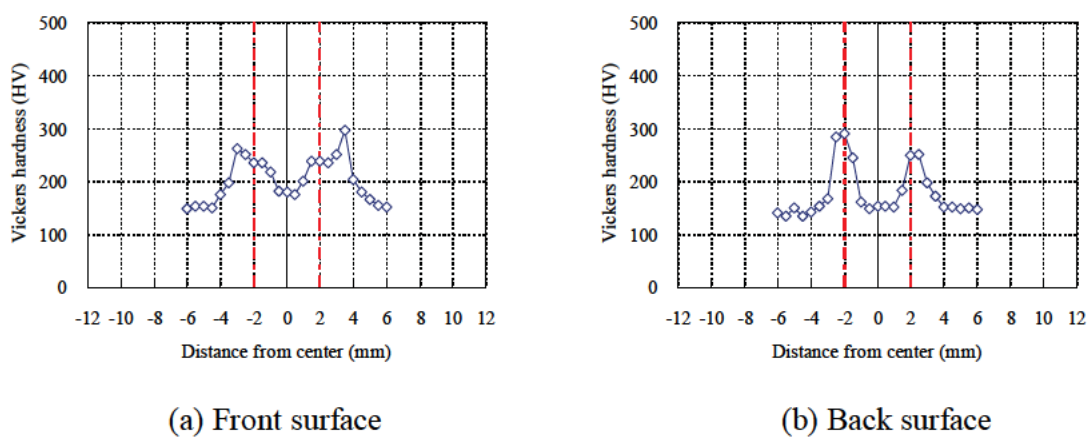


Figure 7 Results of Vickers hardness tests of test specimen "B-4"

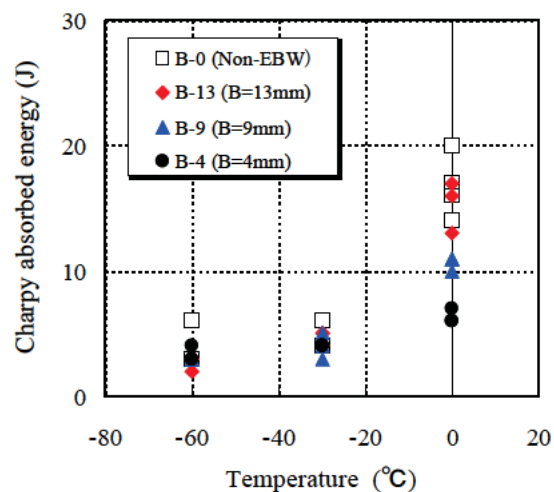


Figure 8 Results of Charpy V-notch impact tests

BRIDGES: THE NEXT GENERATION OF EXPERIMENTAL RESEARCH IN STRUCTURAL FIRES

John L. Gross¹ and Stephen A. Cauffman²

Abstract

Bridge fires, while not common, can have an enormous economic impact and can adversely affect the community served by the bridge, diminishing community resilience. Regulatory approaches that have been successful for buildings may not be applicable to bridges. And, while provisions addressing the protection of the structural elements of a bridge from high temperatures exist, little guidance is available to the bridge engineer to apply such provisions. This paper looks at these issues as well as a few examples of recent bridge fires, and attempts to make the case for the need to conduct large-scale experiments on bridges and bridge components under realistic fire conditions. Such tests can provide the technical basis for a performance-based approach to the design of bridges to resist fires. A new structural fire test facility, under construction at the National Institute of Standards and Technology, will enable the evaluation of the performance of large-scale bridge structures subjected to realistic fires. The capabilities of the National Fire Research Laboratory are presented along with its technical specifications.

Introduction

“Among the public safeguards that have been found necessary where buildings are built in proximity to each other are those pertaining to fire. Such regulations are founded on the long community experience that has been had with fires” [Ingberg, 1929]. Ingberg’s comment addresses, of course, the objectives of minimizing life and property loss due to building fires. If, however, one were to extend his tenet to include transportation systems, one would need to add the objectives of minimizing economic impact and increasing community resilience. Highways are critical lifeline systems enabling commerce and the transportation of people and goods within and among communities. Failure of a single bridge can have a significant economic impact in terms of direct costs and lost productivity due to traffic disruptions and detours.

Regulations intended to reduce the risk of damage or collapse and minimize economic impact by protecting bridge structures from high-temperature exposure do exist [NFPA, 2011], but guidance in their application is limited. A performance-based design

¹ Associate Director of Structures Research, National Fire Research Laboratory, NIST, Gaithersburg, MD, 20899 USA

² Deputy Division Chief, Materials and Structures Division, NIST, Gaithersburg, MD 20899 USA

approach for fire holds promise for bridge structures, but the technical basis for predicting analytically the performance of a bridge structure exposed to fire, including complex nonlinear behavior, is lacking. To date, there have been no fire tests on the performance of bridge structures to provide the required technical basis and analytical model validation.

Recent Bridge Fires

Garlock *et al.* [2011] have shown, through a literature review and case studies, that bridge fires can lead to significant structural damage, partial or complete collapse, as well as costly detours in traffic flow. Garlock *et al.* go on to report on the frequency of bridge fires and notes that a 2008 New York Department of Transportation national survey found that, of the 1746 bridge failures reported (the majority resulting from flooding or collision), 52 were due to fire and 19 due to earthquake; in other words, bridges were almost three times more likely to collapse due to fire than to earthquakes.

In this paper two recent examples which led to significant cost of repair and disruption are highlighted: the McArthur Maze fire which involved the collapse of a section of an overpass onto the roadway below, and the fire on the Mezcala (Mexico) cable-stayed bridge that involved the failure of one stay and damage to a second.

McArthur Maze Fire – Steel Plate Girder Failure

Early on the morning of April 29, 2007, a tanker truck carrying nearly 3400 L (9000 gallons) of gasoline overturned on the I-80/880 interchange in Oakland, California and burst into flames [Bulwa and Firmrite, 2007]. The accident occurred at 3:41 A.M. and just over 20 minutes later, at 4:02 A.M., the elevated roadway collapsed (see Figure 1). “As the fire progressed, the bolted connections in the collapsed girder began to weaken due to heat and were placed under increasing load from the weakening of the remainder of the bridge” [Kodur, *et al.*, 2010].



Figure 1 - Collapse of the McArthur Overpass
Photograph by Robert Campbell (used with permission)

Mezcala Bridge Fire – Stay Cable Failure

In March of 2007, a traffic accident involving two school buses and a truck transporting coconuts caused a fire on the Mezcala Bridge, a cable-stayed bridge in Mexico, that resulted in failure of one stay and damage to a second [Zoli and Steinhause, 2007]. It is reported that flammability of the exterior corrosion protection system on the bridge cables added to the thermal loading on the cables.

Structural Fire Resistance Regulations – A Historical Perspective

A historical look at the development of regulatory approaches to fire resistance of buildings provides the context for discussion regarding the challenges faced in determining the fire resistance of bridges.

Building Fires

In 1791, just four years after the U.S. Constitution was signed, President George Washington issued the first regulations limiting building heights in the nation's new capitol of Washington D.C., "concerned as much about structural and fire safety as about urban design" [Lewis, 1994]. Thus, regulations to limit the spread of fire dates back over 200 years.

The U.S. grew rapidly with population centers in Philadelphia, New York, Boston, Chicago and San Francisco. Along with this growth came devastating fires that

affected all of these burgeoning cities. The Great Chicago Fire of 1871, in which over 17,000 buildings were destroyed, marked a significant turning point in building practice whereby the fire resistance of a building began to be considered explicitly. “Although the early knowledge of the requirements for fire protection resulted from a study of the behavior of structures in fires and from examination of fire-damaged buildings, the development of skeleton-type construction made the necessity for fire endurance testing apparent” [Shoub, 1961]. New York City was the first American city to introduce a standard fire test method in the 1899 New York Building Code [Babrauskas and Williamson, 1978]. But it was the Great Baltimore Fire of 1904 that prompted the American Society for Testing and Materials (ASTM) to organize a national effort to standardize fire resistance testing; “A Standard Test for Fire-Proof Floor Construction” was issued just three years later in 1907. ASTM continued its work and in 1917 Committee C-5 issued a report that proposed a standard test method notable for two aspects, “the provision that structures be classified by their attained fire resistance” [Shoub, 1961], and the notion that “a furnace does not heat up instantaneously; for reproducible results, this initial heating should be quantified” [Babrauskas and Williamson, 1978]. The furnace time-temperature curve introduced by Committee C-5 remains unchanged to this day in the ASTM Standard E 119, *Standard Test Methods for Fire Tests of Building Construction and Materials* [ASTM, 2011], the standard commonly used in the United States for establishing fire resistance ratings.

It was Simon Ingberg of the National Bureau of Standards, now the National Institute of Standards and Technology(NIST), who introduced the fire “severity” concept suggesting that “all fires of the same severity have approximately the same effect on a structure” [Babrauskas and Williamson, 1978]. “Ingberg’s work on fire severity and fire resistance was adopted by national standards and model building codes...and his classification of building types [fireproof, incombustible, exterior-protected and wood] remains the basis for requirements for fire resistance of building components...” [Evans *et al.*, 2001]. Fire resistance ratings for buildings, as established by ASTM E 119, are intended to ensure the that a fire will not spread beyond the compartment of origin.

One significant addition to building codes in the United States has been the provision that “an approved automatic sprinkler system...shall be allowed to be substituted for 1-hour fire-resistance-rated construction” [ICC, 2006]. This provision, known as the “sprinkler tradeoff” provision, recognizes the effectiveness of automatic sprinklers in suppressing a fire in its early stages, thereby preventing the fire from becoming a threat to the building or its occupants.

Bridge Fires

Consideration for the need for fire protection for bridges is more recent. And, as noted in the introduction, the impact of a bridge fire extends beyond life safety and replacement cost to the broader impact on the community served by the bridge.

The National Fire Protection Association (NFPA) *Standard for Road Tunnels, Bridges, and other Limited Access Highways* [NFPA, 2011] contains provisions for the consideration of fire. Quoting directly from Chapter 6:

6.3.1 ...all primary structural elements shall be protected in accordance with this standard in order to:

- (1) Maintain life safety
- (2) Mitigate structural damage and prevent progressive structural collapse
- (3) Minimize economic impact

6.3.2 Critical structural members shall be protected from collision and high temperature exposure that can result in dangerous weakening or complete collapse of the bridge or elevated highway.

However, as pointed out by Garlock *et al.* [2011], "...current bridge design codes and standards offer limited information concerning the fire hazard."

A Case for Structural Fire Testing of Bridges

From the above discussion, one can identify three regulatory approaches to fire resistance for buildings: (1) construction restrictions (e.g., zoning and occupancy restrictions), (2) limiting the spread of fire beyond the compartment of origin (e.g., fire resistance rating requirements), and (3) active fire suppression (e.g., sprinklers). It is not at all clear, however, that any of these regulatory strategies would be effective in reducing the hazard from fire for bridges and elevated highway structures.

Additionally, results of tests on building components and assemblies are generally not applicable to bridge structures. For example, building fires are generally considered to be confined to a compartment, while bridges are likely to be exposed to plume fires. The combustible materials in a building (e.g., wood, paper, upholstery) are likely to have different burning characteristics than those affecting a bridge which may involve petroleum products (hydrocarbons). Finally, structural elements of a building are often different from elements found in bridges (e.g., steel plate girders or box sections, pre-stressed concrete beams, suspension cables, etc.). No systematic study has been

conducted to date to quantify the effects of damaging hydrocarbon pool fires on the wide variety of bridge forms in use today. Such a study is required to fully understand the behavior and modes of failure exhibited by the various structural forms when exposed to extreme temperatures.

By treating fire as a design condition in the design and analysis of bridges, one can implement a performance-based design approach. Performance-based design generally involves the calculation of the structural response of a bridge to the effects of a postulated fire, developed through consideration of possible fire scenarios. One of the main obstacles for moving towards performance-based fire safety design is the lack of knowledge about bridge fire response. Numerical models are needed as well as design tools, but these models and tools need to be validated with experiments since the bridge response under high thermal loads is complex and nonlinear.

To conduct such experiments requires a facility with the capability to:

- Conduct tests on real-scale structural systems and components
- Apply controlled loads to test structures to simulate true service conditions
- Create realistic fires that grow, spread and decay
- Characterize the fires in real time
- Measure the response of structural systems and components to the point of incipient collapse.

Until now, no laboratory in the world has possessed this combination of capabilities.

The National Fire Research Laboratory (NFRL)

The National Institute of Standards and Technology (NIST) is adding a new, unique facility that will serve as a center of excellence for fire performance of structures ranging in size from small components to large systems (see Figure 2). The laboratory, called the National Fire Research Laboratory (NFRL), will be led, managed and operated as a collaborative facility through a public-private partnership between NIST and industry, academia, and other government agencies.

The work of the laboratory will be focused on the NIST Engineering Laboratory mission: to promote US innovation and industrial competitiveness in areas of national priority by anticipating and meeting the measurement science and standards needs for technology-intensive manufacturing and construction in ways that enhance economic prosperity and improve the quality of life.



Figure 2 - Rendering of the new NIST facility for large-scale structural fire research

Scientists and engineers from industry, academia, and government agencies will work side-by-side with NIST researchers to address significant technical problems and fill critical knowledge gaps, and international scientists and engineers will be welcome to partner with NIST in areas of mutual interest. Projects may be funded by industry and government on a cost-shared basis.

The additional capabilities will allow NIST to:

- Test the performance of large-scale structures, including bridge components, subjected to realistic fires and structural loading under controlled laboratory conditions.
- Develop an experimental database on the performance of large-scale structural connections, components, subassemblies, and systems under realistic fire and loading.
- Validate physics-based models to predict fire resistance performance of structures.
- Enable performance-based standards for fire resistance design of structures and foster innovations in design and construction.

The NFRL is adding 1990 m² (21,400 sq ft) laboratory space to its existing Large Fire Laboratory (Building 205) (see Figure 3) and installing an environmental control system (ECS) to supplement the existing ECS to accommodate fires up to 20 MW heat release rate.

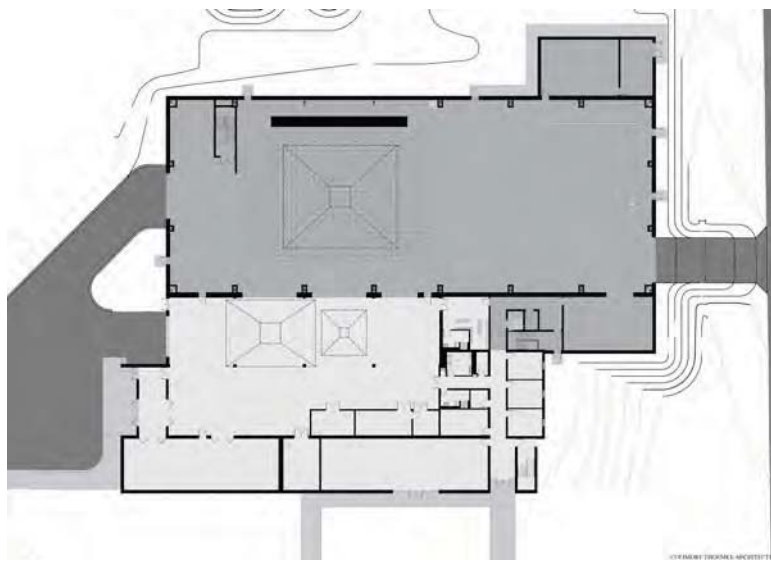


Figure 3 -Floor Plan of the National Fire Research Laboratory Expansion

The new laboratory space will accommodate structural systems or components 9 m (30 ft) high and roughly 12 m (40 ft) by 18 m (60 ft) in plan. Gravity loading will be applied using hydraulic actuators or fixed loads. Fully involved building fires, fueled by gas or liquid fuel, wood cribs, or actual building contents, will be employed to simulate building fire conditions. Characteristics of the fire (heat release rate) will be measured accurately using calorimetry.

The test area will consist of a 18.3 m × 27.4 m (60 ft × 90 ft) strong floor with anchor points on a 0.61 m × 0.61 m (2 ft × 2 ft) grid. The floor will be supported on a nine-cell reinforced concrete box girder providing a basement below the strong floor with a ceiling height of 2.7 m (9 ft). To one side of the strong floor will be a 9.1 m (30 ft) high × 18.3 m (60 ft) wide concrete strong wall with anchor points on the same grid as the strong floor. The strong wall will act to stabilize a test specimen to prevent uncontrolled failure, provide lateral restraint, or to laterally load a structure to simulate earthquake damage. A 13.7 m × 15.2 m (45 ft × 50 ft) hood, centered above the strong floor, will capture and remove smoke and hot gases.

The size of the test area was selected to enable the testing of large-scale structural systems or components; including bridge girders, cable systems, piers, etc.; under realistic hydrocarbon fires and controlled loading comprised of self-weight and vehicles. Technical specifications for the NFRL expansion are given in Appendix A.

Summary

In summary, the following points have been made:

- Fire represents a significant hazard in bridges
- Consequences of a bridge fire include:
 - structural damage, partial or complete collapse necessitating repair or replacement
 - disruption to traffic flow during repair or replacement
 - economic loss and adverse impact on community resilience
- The 100-plus year history of fire resistance regulations for building structures offers little guidance for bridge and transportation structures
- Current bridge design codes and standards offer limited information concerning the fire hazard
- Fire hazard can be overcome by addressing fire explicitly in the design and analysis of bridges
- Identification of failure modes and validation of advanced numerical models requires well controlled full-scale experiments
- The National Institute of Standards and Technology's new, unique fire/structure test facility, the National Fire Research Laboratory, will enable the evaluation of the performance of large-scale bridge components subjected to realistic fires.

References

- ASTM (2011). Standard Test Methods for Fire Tests of Building Construction and Materials, ASTM E 119 11 a, ASTM International, Conshohocken, Pa.
- Babrauskas, V. and Williamson, R. B. (1978). "The Historical Basis of Fire Resistance Testing – Part II," *Fire Technology*, Vol. 14, No. 4, Nov.
- Bulwa, D. and Firmrite, P. (2007). "Tanker Fire Destroys Part of McArthur Maze," *San Francisco Chronicle*, California.
- Evans, D., Gross, D. and Wright, R. (2001). "Test of the Severity of Building Fires," *A Century of Excellence in Measurements, Standards, and Technology*, Lide, D.R. (ed.), NIST Special Publication 958, National Institute of Standards and Technology, Gaithersburg, MD.
- Garlock, M., Payá-Zaforteza, I., Kodur, V., Gu, L. (2011). "Fire Hazard in Bridges: Review, Assessment and Repair Strategies" (submitted for publication in *Engineering Structures*, Elsevier).

ICC (2006). International Building Code, International Code Council, Falls Church, VA.

Ingberg, S.H. (1929). "Fire Resistance Requirements in Building Codes," Quarterly of the National Fire Protection Association, Vol. 23, No. 2, October 1929, NFPA, Boston, MA.

Kodur VR, Gu L, Garlock M.E. (2010). "Review and Assessment of Fire Hazard in Bridges" Journal of the Transportation Research Board No. 2172, Transportation Research Board of the National Academies, Washington D.C. (USA)

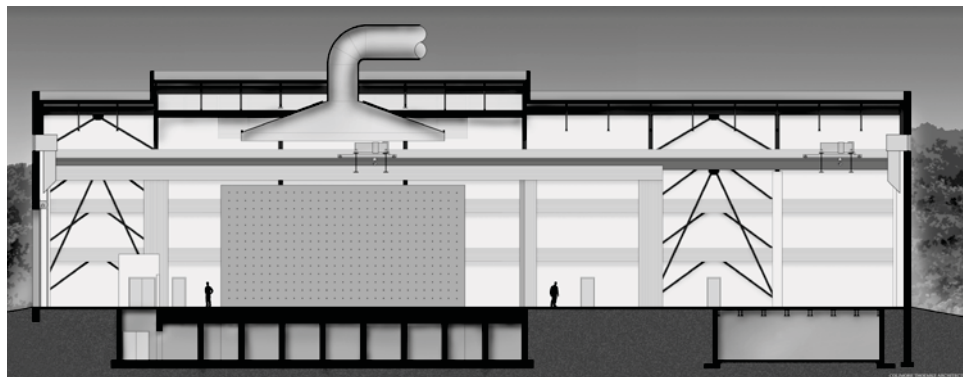
Lewis, R. (1994). "Testing the Upper Limits of D.C. Building Height Act," *The Washington Post*, Saturday, April 23, Washington, D.C.

NFPA (2011). *Standard for Road Tunnels, Bridges, and other Limited Access Highways*, AFPA 502, 2011 edition, National Fire Protection Association, Quincy, MA.

Shoub, H. (1961). "Early History of Fire Endurance Testing in the United States," Special Technical Publication No. 301, ASTM, Conshohocken, PA

Zoli, T. P., and Steinhouse, J. (2007). "Some Considerations in the Design of Long Span Bridges against Progressive Collapse," Proceedings of the 23rd U.S.-Japan Bridge Engineering Workshop, Tsukuba, Japan, Nov. 5-7

Appendix A - Technical Specifications



Strong Floor

- 18.3 m × 27.4 m (60 ft × 90 ft) post-tensioned floor with full basement
- 9 cell RC box girder with 406 mm (16 in) thick shear walls at 3.0 m (10 ft) o.c.
- Basement ceiling height: 2.7 m (9 ft)

- Floor thickness: 1.07 m (3 ft-6 in) with 152 mm (6 in) sacrificial top surface
- 1218 anchor points on 0.61 m × 0.61 m (2 ft × 2 ft) grid (sleeves or anchors)
- Load per anchor point: 445 kN (100 kip) up or down
- Shear capacity per anchor point: 222 kN (50 kip) (at top of slab)
- Moment capacity per anchor point: 136 kN·m (100 ft kip) (at c.g. of strong floor)

Strong Wall

- 9.1 m high × 18.3 m wide (30 ft high × 60 ft wide)
- 1.2 m (4 ft) deep post-tensioned concrete wall
- 420 anchor points on 0.61 × 0.61 m (2 ft × 2 ft) grid
- Horizontal load: 146 kN/m (10 kip/ft) at 9.14 m (30 ft)

ECS Hood and Pollution Control System

- 13.7 m × 15.2 m (45 ft × 50 ft) steel hood
- Height above floor: 12.5 m (41 ft) (excluding skirts)
- ECS maximum sustained capacity: 20 MW
- ECS maximum flow rate: 5100 m³/min (180,000 ft³/min)

Cranes

- Two 20-ton bridge cranes (sharing single set of rails)
- Height of rails above floor: 11.2 m (36 ft-8 in)
- Clearance, bottom of bridge-to-floor: 9.8 m (32 ft)

Configurable Hydraulic Loading System

- Hydraulic Power Unit 340 L/min (90 gal/min)
- Actuators (double acting) 762 mm (30 in) stroke w/ servo valve, load cell and swivels
 - Eight 240 kN (55 kip) Tension, 365 kN (80 kip) Compression
 - Two 445 kN (100 kip) Tension, 650 kN (145 kip) Compression
 - Two 956 kN (215 kip) Tension, 1470 kN (330 kip) Compression
- Four hydraulic service manifolds
- Controller

New Attempt to Maintenance of Steel Bridge Coating in Expressway

Shuhei Sakai¹, Dai Wakabayashi²

Abstract

In the steel bridge of the expressway in NEXCO, most of the rust prevention and protection method is painting. To reduce cost of the painting maintenance, the realization of an effective painting repair technique is necessary.

To solve this problem, we attempted a basic study on non destructive inspection technique with terahertz wave to grasp the corrosion degree under the coating, and confirmation about the effect of the simple coating removal technology using the special tool experimentally on the site. In this paper, summary and test result of these technique is described.

Introduction

Now, the expressway length that NEXCO manages is 8,732km¹⁾²⁾³⁾. As for the road structure ratio of the road structure, earthwork is about 75%, tunnel is about 10%, and bridge is about 15%. The bridge length is about 1,150km, and the number is 6700 bridges. As for the bridge type ratio, concrete bridge is about 70% and steel bridge is about 30%, the steel bridge length is about 2100km⁴⁾.

In the maintenance cost of the bridges, repair paint of the steel bridges accounts for most. Because it is predicted that these cost will be increased in future, a new effective paint repair technique is required.

From the background, we attempted two experimental study about a new paint repair technique. This report discuss the outline of these method.

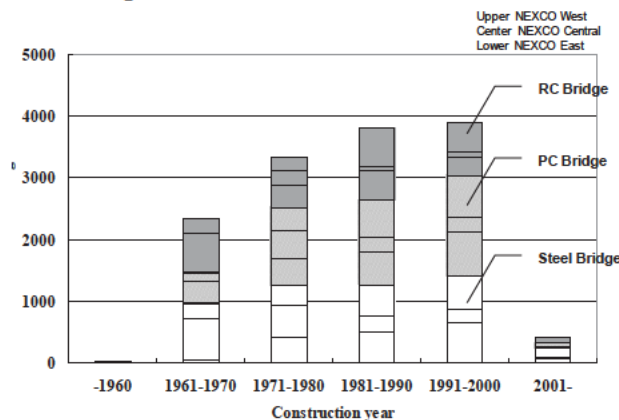


Fig.1 Bridge type ratio of expressway managed by NEXCO

¹ Nagoya B.O. Planning and Design Team Sub-leader, Central Nippon Expressway Co., Ltd. (NEXCO Central)

² Chief Researcher of Bridge Div., Nippon Expressway research institute Co., Ltd.

The maintenance Problem of the painting in the steel bridge

In the steel bridge of NEXCO more than 90%, the painting is used for rust prevention. The change of repainting coating specifications for general environment in NEXCO is shown in Fig.2.⁵⁾ As you can see, we changed its specification from general coating to heavy duty coating, considering life cycle cost and minimum maintenance.

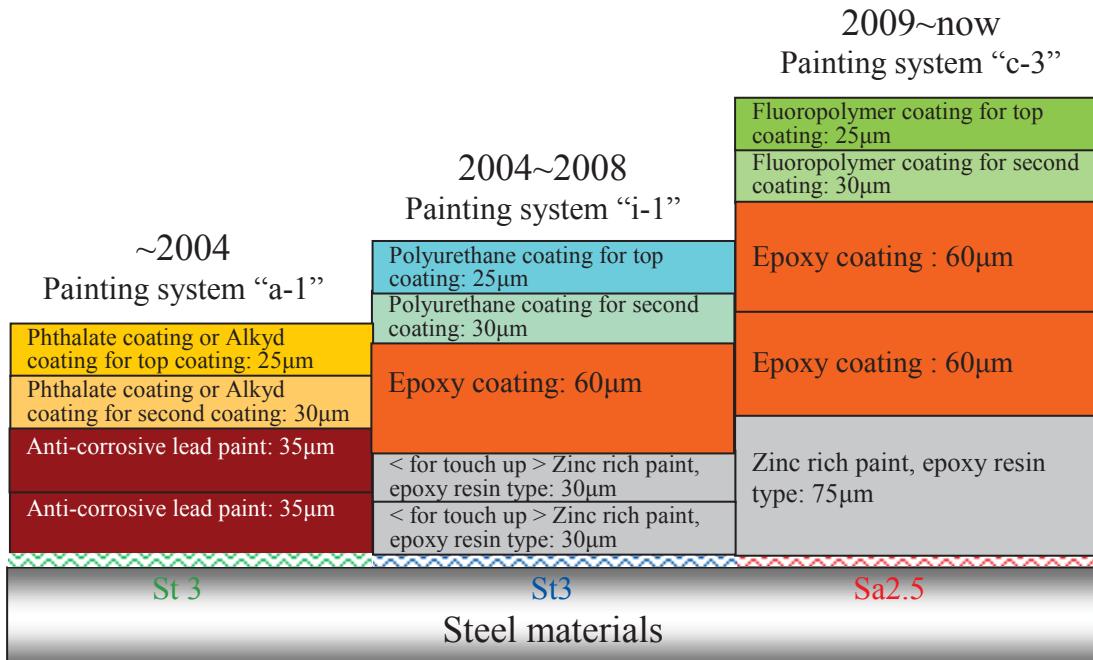


Fig.2 The change of painting specifications in NEXCO

For maintenance of the painting in NEXCO, Paint View System have been used. Paint View System detects the deteriorated coating with photograph, and it can judge necessity of painting repair from deterioration forms and the deterioration area ratio of the coating (Fig.3).

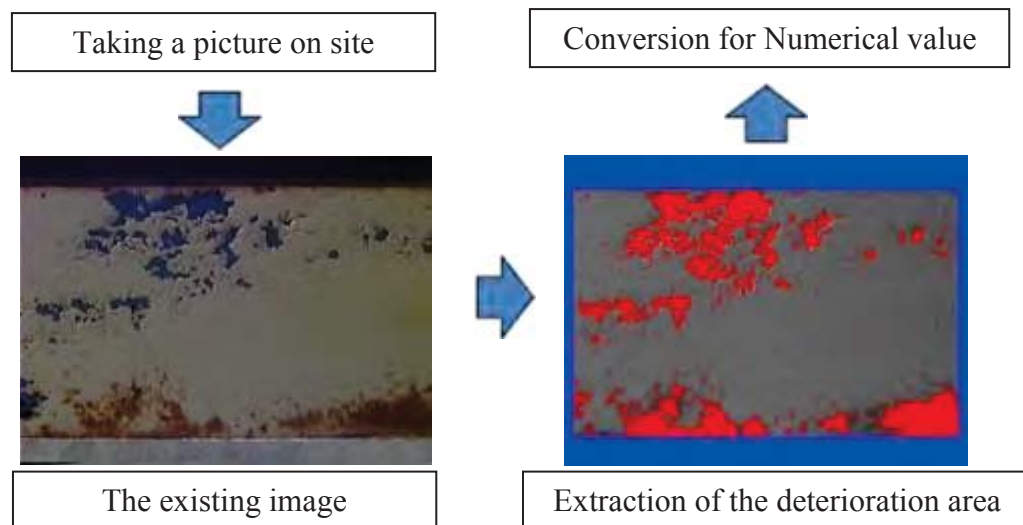


Fig.3 Detecting the deterioration area of painting using NEXCO Paint View System

Deterioration data of the coating are accumulated by the Paint View System. According to its data, deterioration of the general painting (painting system “A” or “a” painting system) progresses as shown in Fig.4. If painting life is when a deterioration area reached 5.0% , the average life of pro-general painting is about 17 years.

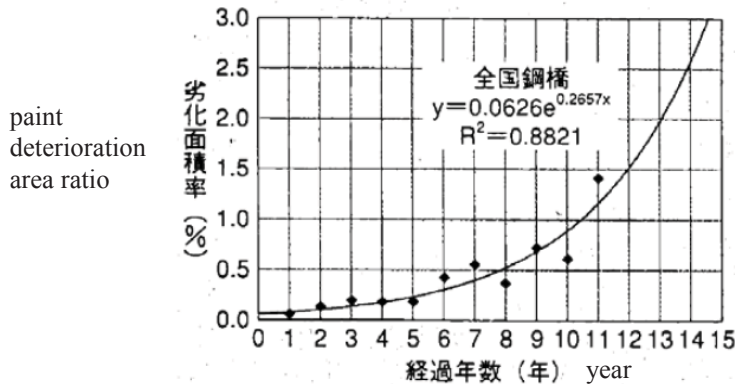


Fig.4 Deterioration curve of the painting (general painting system)⁶⁾

If dividing the number of bridges in NEXCO by life of the general painting by simple calculation, the repair painting is necessary higher than 120 bridges every year.

Therefore, high durable painting specifications have been adopted since 1997 in NEXCO. However, many old bridges using general painting system have repaired many times and gradually shorten for the repair cycle.

This reason is that deteriorated coating have been grinded by disk sander (According to ISO 8501-1 St 3) and general painting system have been painted repeatedly (Fig.5).

Some results of accelerate corrosion test to confirm painting durability in NEXCO Research Institute is shown in Fig.6. The method of remove rust by tool have been inferior in the durability. As for this reason, because the steel materials surface cannot be completely removed the rusts on irregularity surface made of the corrosion, such a point corrodes from the inside of the coating let accelerate the coating deterioration. Therefore, as for the deterioration after the repair painting, same parts often deteriorates early.



Fig.5 Grinding by power tool such as disk sander (According to ISO 8501-1 St 3)

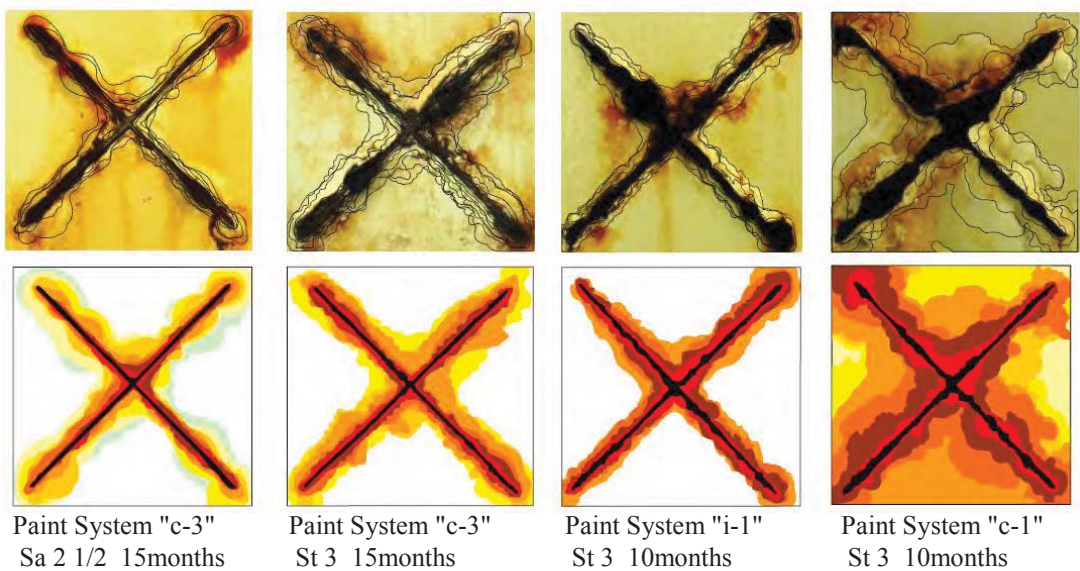


Fig.6 Accelerate corrosion test for painting

Because of its results, surface cleanliness method by blasting (According to ISO 8501-1 Sa2.5) has been focused recently. (Fig.7)

However, blasting on site is limited because of environmental problems such as scattering dust and loud noise from the construction site. In addition, the complicated structures such as gusset plate, stiffener often decrease the work space, so processing time of blasting becomes longer. Moreover, because the interval time from blasting to painting is limited, the construction efficiency is often very bad and its repair cost may be more expensive.⁷⁾



Fig.7 Cleanliness processing by blasting(According to ISO 8500-1 Sa2.5)

From these background, we attempted experimental study of two themes. One of these is a basic study on innovative non-destructive inspection to detect the corrosion area in coating. The other is a performance confirmation examination of the blasting method using the special tool on site. This method can remove the partial rust and corrosion economically and clear environmental problems.

Fundamental researches about the Non Destructive Inspection method of the coating deterioration using the Terahertz wave

1. Investigation contents and outline of Terahertz Imaging system

A steel material has no transmittance for electro-magnetic wave, however, it is reported in a past study that by using reflection imaging terahertz wave, the surface figure which is hidden under the coating is detectable.⁸⁾ Therefore we examined three following contents in this study.

- (1) Trial terahertz imaging using the deterioration coating specimen
- (2) Terahertz imaging using the specimen which made a rust shape to confirm detection performance intentionally
- (3) Examination to identify transmission properties of various paint using for a bridge

The examination was carried out in collaborative investigation with Iwate Prefectural College. The testing equipment used an apparatus as shown in Fig.8, and carried out the examination on a condition as shown in table 1.



Fig.8 Terahertz Imaging system
(Iwate Prefectural College owned)

Table 1 Terahertz Imaging measurement specifications

Item	Contents
Measuring system	Reflection imaging (probe scan)
Oscillation element	TUNNET 170GHz
Detector	0bias SBD at RT
Measurement area	Depends on each examination (about 60mm×60mm)
Scan size	0.5／1.0mmstep
Stabilization condition	8e-5, avg1 or 2

2. Investigation by the deterioration coating specimen

Prior to a detailed investigation, to grasp appropriate frequency condition of the terahertz wave and an image of the deterioration coating, we tested the examination measurement by the deterioration coating specimen.

The specimen exposed at Oyashirazu Coast exposure test area for about 13 years, and the back side was used. Painting specification of this specimen was the “I” painting system in the NEXCO painting standard. (first coating: Organic zinc Rich paint 75 μ m, middle coating: polyurethane resin paint for middle coating 30 μ m, final coating: Polyurethane resin paint for final coating 25 μ m)

Fig.9 is the result of a measurement. The back side of exposed specimen gets

rusty on the coating surface because of existing dew including the rust juice for a long time, and as for the rust spreads through the coating appearance and a real rust area becomes indistinct.

Terahertz imaging can be detected only a rust and corrosion point removing dirt with the rust juice in the coating surface.

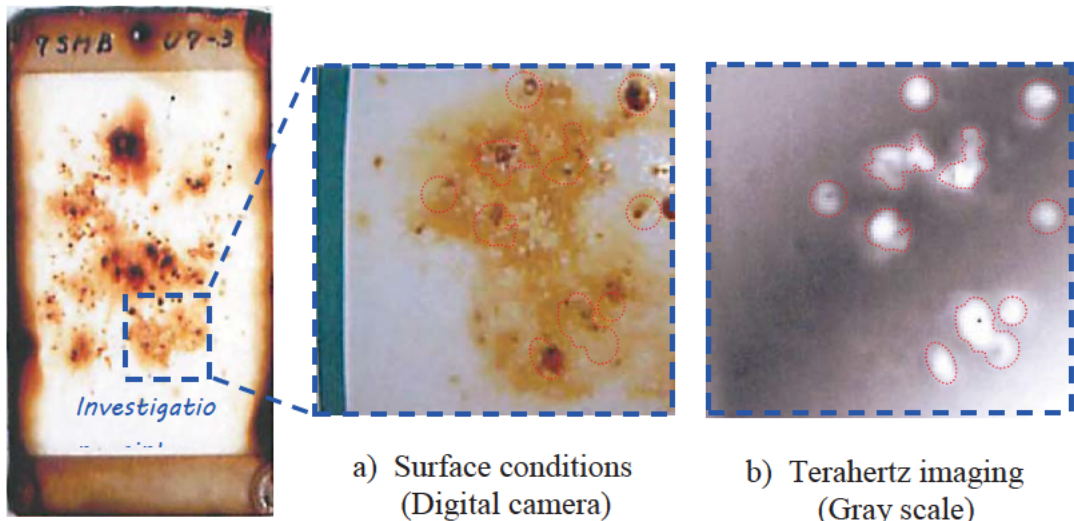


Fig.9 Investigation result by the deterioration coating specimen

3. Detection performance test of the corrosion in the coating

Painting specification of the specimen (Fig.10) were used two kinds of painting system. One is the “a-1” painting system (the phthalate series painting). The painting system was generally adopted in the past. The other is the “c-3” painting system. The coating is thickness and adopted for the repairing painting system at present.

The result of the terahertz imaging is shown in Fig.11. As a result, for both specimens of the “a-1” painting system and the “c-3” painting system, the rust area can be detected enough precisely.

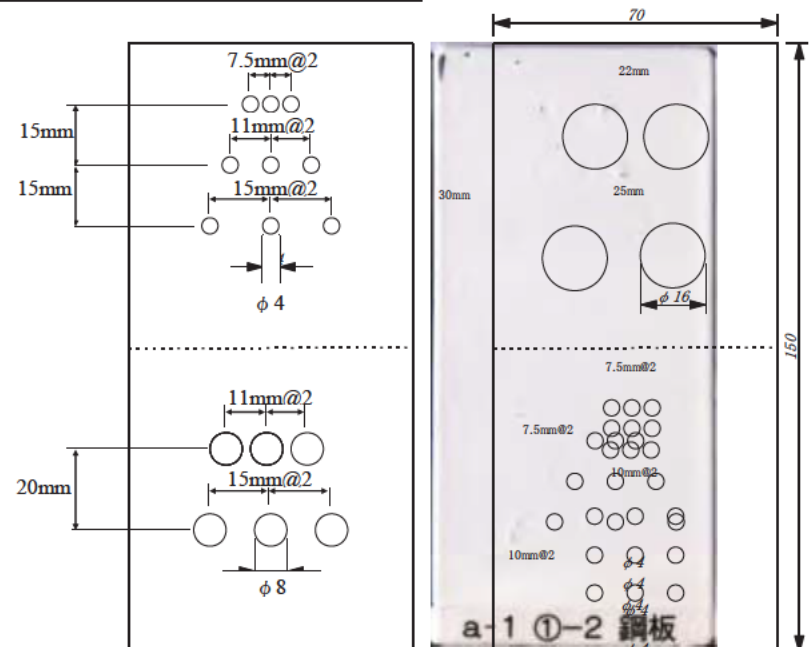


Fig.10 The position of the rust area and the painted specimen

Some absentminded point was seen partially. Because there is the place where strength of receiving wave is very week, so it seems the rotation of this area becomes hard to relatively distinguish it. However, the difference of the detection performance by the kind of painting specifications is small by this test result.

Seeing the results of other parts, an imaging of big rust area was clearer than the small rust area case. In addition, there was not combined every rust area. (The smallest distance between the rust is 5mm) Therefore, this method can be distinguished an individual rust area.

	Example of middle size diameter	
	Painting system "a-1"	Painting system "c-3"
Rust Type		
Imaging (Gray scale)		
Imaging (Color)		

Fig.11 Terahertz imaging of the specimen

4. Investigation into transmission properties by the difference in coating classification

We made single film test specimen of each painting classification and fixed it as shown in Fig.12. Then we measured incident power “P0” and transmission power “P1” of the terahertz wave and calculated the transmission ratio P1/P0.

The test result is shown in Fig.13, and Fig.14. As a result, it can be confirmed the following things.

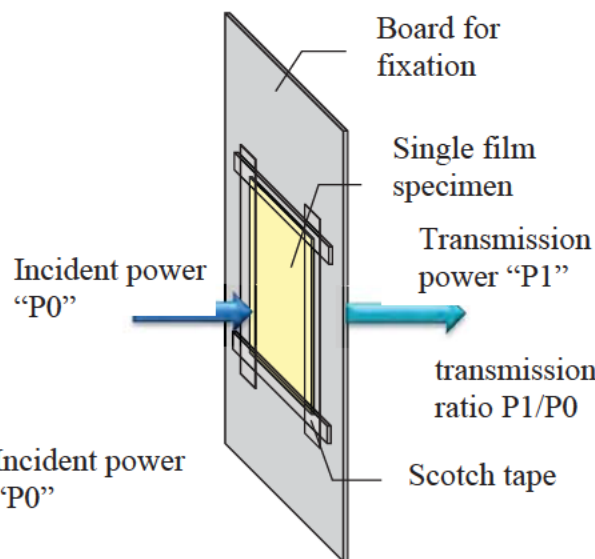


Fig.12 Investigation into transmission properties

As for Anti-corrosive lead paint ($40 \mu m$), Phthalate coating ($26 \mu m$), and Phthalate coating ($26 \mu m$), these transparency is very high. Therefore, the transparency of painting systems using those three (painting system “a-1”) is high.

As for Zinc Rich paint ($102 \mu m$), and Epoxy resin paint ($82 \mu m$), these transparency is comparatively low. As for Fluoropolymer coating (top coat is $49 \mu m$ and second coat $38 \mu m$), these transparency is very high. Therefore, the transparency of this painting system using those four (painting system “c-3”) is slightly lower, but its system has practical performance.

In addition, from a coating thickness of epoxy resin paint and relations of the absorbance, it was confirmed that if coating was thick, the transmission ratio is lower (absorbency is higher).

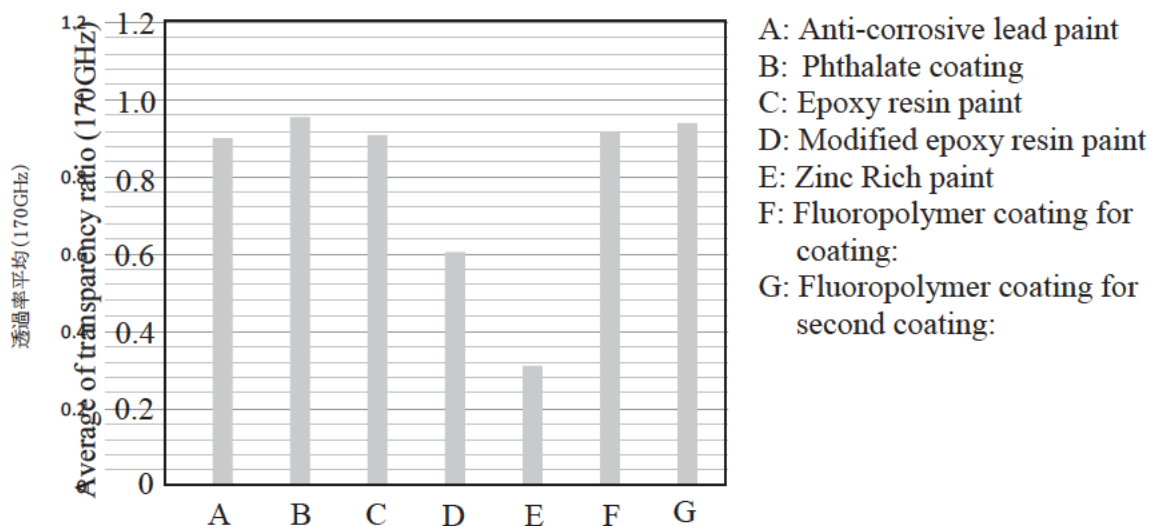


Fig.13 Average of transparency of each coating

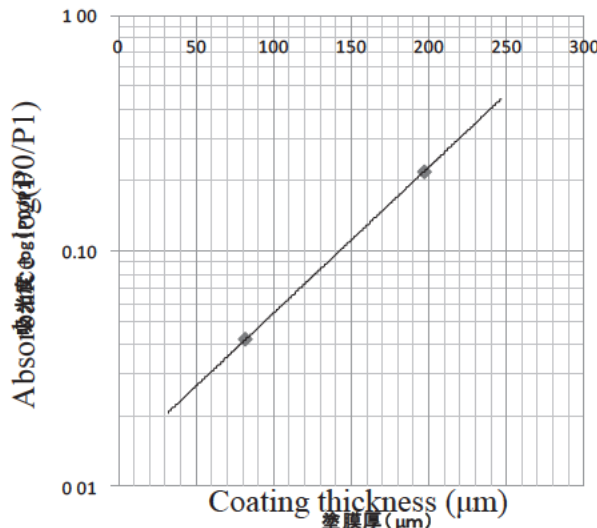


Fig.14 Relations of coating thickness and the absorbance of epoxy resin paint

5. Conclusion of Non Destructive Inspection using the terahertz

As a result of terahertz imaging investigation examination, the following matter can be confirmed.

- (1) The detection of rust and corrosion in the coating is possible using terahertz imaging.
- (2) Appropriate frequency of the electromagnetic wave to use in an investigation into rust and corrosion in the coating is around 170GHz.
- (3) Measurement time is about 20 minutes per one place (60*60mm) using the prototype.

This study is one fundamental research about the application to non destructive inspection of the terahertz technique. To be using on site, it is necessary to enable scanning a wide area at high speed. So the development of the apparatus is necessary.

Test construction for confirmation of application to the new blast method using the special tool on steel bridge coating repair construction site

1. New blasting method with the special tool

To remove the rust of deterioration coating, we generally use grinding method with a machine tool such as a disk sander, or blasting method with abrasives. Blasting method has environmental problems due to noise and dust, therefore did not hardly ever be used. On the other hand, blasting becomes necessary because of changing in the painting specifications. There are many methods improved the abrasives and blasting machine to solve these problems, but most of those method was too expensive. Therefore reasonable blasting method has been needed.

So we studied that the method which has been used in the field such as automotive, marine, plant recently, and can remove the rust as well as blasting method, can be applied to repair the steel bridge coating on site. The method need a special tool that named Bristle Blaster®(Fig.15), and developed in Germany. The principle of surface cleanliness is striking the subject with the many carbon spring steel or stainless steel spinning wires. The method with this tool can be the surface cleanliness as well as according to ISO 8501-1 Sa 2.5, as are also achieved for conventional blasting^{9~11)}.



Fig.15 The Special Tool of New Blasting Method

2. Test construction with the new surface cleanliness method

The test construction carried out at the steel bridge of Ise Expressway in Mie Pref. The bridge had the local deteriorated coating at the end of girders, because of the influence of leakage water in deicing salt from the expansion joint (Fig.16). In the test, we investigated the surface roughness, dust, noise, cleanliness performance at the web, corner, gusset plate and the corrosion surface, and processing time on the bridge repair construction site.



(1) Surface Roughness

Fig.17 shows the result of a 10-point average roughness of the surface by measure method of JIS. Compared to painted steel, rust steel, mill scale and

Fig.16 Horisaka Bridge (Ise Expressway in Mie Pref. conventional general paint 23years)

galvanized steel, all surface can be removed the rust and coating, and can be secured over the roughness of $50 \mu\text{m}$. Also, in comparison with grinding, this method is expected to improve adhesion of the coating than its method with disk sander.

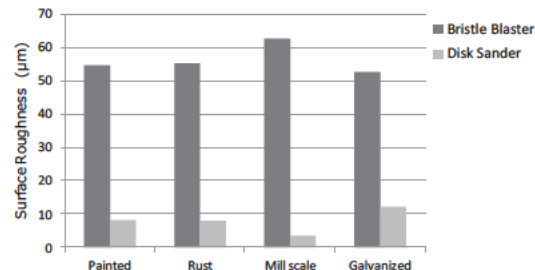


Fig.17 10-points ave. roughness of surface (by measure method JIS)

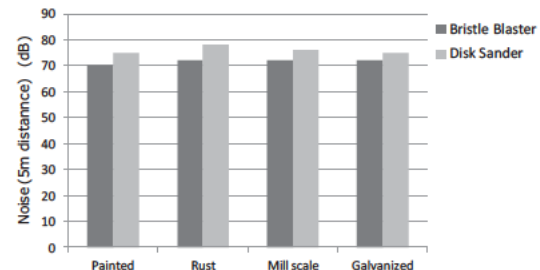


Fig.18 Noise Test

(2) Dust and Noise

Fig.18 shows the results of the noise measurement at 5m away from the work area. Regardless of the different surfaces, each sounds volume is same, and less than the sound volume of conventional grinding method with disk sander. Moreover, most of the dust did not occur.

(3) Surface Cleanliness

Fig.19(1) to (4) shows the treated surfaces after the work. This method is not worrying about cutting down the steel, the variations of surface cleanliness treatment is not much. Also, it can be good at the corner and around the bolts. Grinding with disk sander cannot be so. In addition, it can clean all the sever rusts (partial layered) on the corroded steel surfaces.

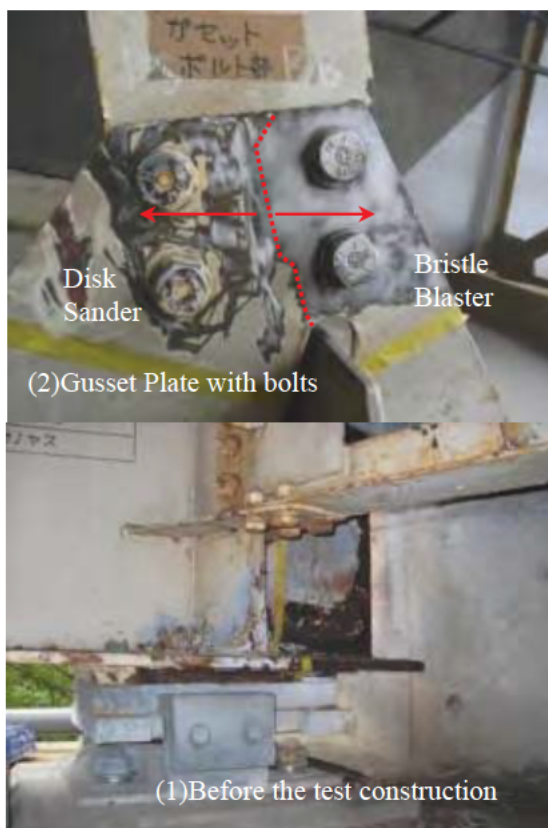


Fig.19 Treated Surfaces after the tests

(4) Workability and Processing time

We measured the processing time of cleaning at the web of the girder and around the bolts. Fig.20 shows the results. This result revealed that compared with the superior processing performance than grinding, in case of the conventional general painting.

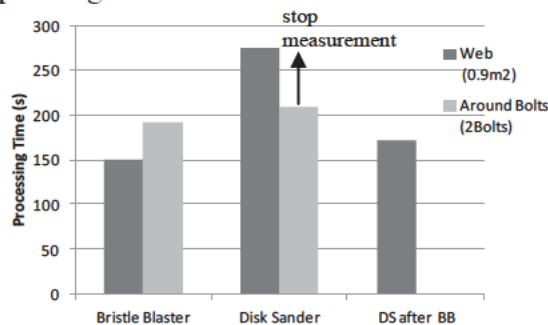


Fig.20 Processing time



Fig.21 Construction by new tool

As mention above, this method is reasonable, environmental and efficient than conventional grinding method with DS. And in case of repair at local deteriorated coating, the blasting with abrasives, this method is superior.

Conclusion

Durability of the coating to protect steel vary greatly on the condition of corrosive environment, coating specification, part of structure, construction and so on. If we can search the local weaknesses and remove and repair by proper method and specification, we can maintenance so good without significant cost increasing. Other than the above, we think that cleaning the girders is effective and has studying it.

We wish that this report is helpful to the maintenance of bridges in your future.

References

- 1) <http://www.e-nexco.co.jp/>, HP at East Nippon Expressway Co., Ltd , 2011.7
- 2) <http://www.c-nexco.co.jp/>, HP at Central Nippon Expressway Co., Ltd , 2011.7
- 3) <http://www.w-nexco.co.jp/>, HP at West Nippon Expressway Co., Ltd , 2011.7
- 4) Annual Report of Basic Data on Road Structures IN FY 2008, TECHNICAL NOTE of National Institute for Land and Infrastructure Management , No.545 / Oct.2009
- 5) The design standard for bridge management, East, Central, and west Nippon Expressway Co., Ltd , 2011.7
- 6) H. Yougai, W. Hatano, T. Okamoto : Study on the prediction of coating deterioration using the paint view , EXTEC No.64, 2003.3
- 7) S. Sakai, K. Fujino : Study on the coating removal method in the expressway, Structure Painting Vol.38 No.2, Japan Association of Structure Painting Constructors, 2010.9
- 8) T. Kurabayashi, P. Plotka, M. Watanabe, and others : Sub-terahertz imaging for Construction Materials, 33 rd International Conference on Infrared, Millimeter, and Terahertz Waves, 2008.9
- 9) KANSAI Paint Co., Ltd: <http://www.kansai.co.jp/new/press10/101101/index.html>
- 10) GOTO Electronic Works: <http://www.gotodenki.co.jp/>
- 11) MONTI-Werkzeuge GmbH: <http://www.monti.de/>

FHWA'S NEW INFRASTRUCTURE RESEARCH AND TECHNOLOGY STRATEGIC PLAN

Ian M. Friedland, P.E.¹

Abstract

In the fall of 2010, the Federal Highway Administration (FHWA) undertook an effort to develop a new, longer-term strategic plan and roadmap for infrastructure research and development, and technology deployment. This paper provides an overview of the new infrastructure R&D strategic plan, and deployment roadmap.

Background

Over the years, the Federal Highway Administration's (FHWA) bridge and structures research and development (R&D) efforts have addressed a range of topics and focal areas. Past efforts have included research as wide-ranging as that of assessing and reducing the seismic vulnerability of the U.S. national highway system, to curved steel I-girder bridge behavior, to understanding the forces associated with spill-through abutment scour, to the use of ground penetrating radar for concrete bridge deck inspection. R&D topics were typically developed based on the knowledge of technology gaps by FHWA engineers, input from a wide variety of stakeholders, and—occasionally—direction from the U.S. Congress. In addition, “failures” within the highway infrastructure also drove the decision-making regarding bridge and structures R&D.

Starting in the middle of 2006, the FHWA Office of Infrastructure R&D took a more strategic approach to its funded and planned research agenda. This approach looked at blending the two distinct infrastructure program areas – pavement R&D, and bridge and structures R&D – into a more comprehensive and integrated infrastructure R&D program. The overall focus of this effort was on long-term infrastructure performance. The result of this was a multi-tiered, multi-year strategic plan and research roadmap, as documented in the 2008 FHWA publication titled “Highways of the Future: A Strategic Plan for Highway Infrastructure Research and Development” (publication FHWA-HRT-08-068, July 2008).

The 2008 strategic plan addressed six primary R&D areas:

- Long Term Infrastructure Performance
- Durable Infrastructure Systems
- Accelerated Highway Construction

¹ Assistant Director for Bridge and Structures R&D, Federal Highway Administration, Washington, DC, USA

- Environmentally Sensitive Infrastructure
- Performance-Based Specifications
- Comprehensive & Integrated Asset Management

The basis for focusing on these six areas are the many critical challenges currently facing highway agencies, not only in the United States, but worldwide, including:

- The need to extend the service life of existing highway infrastructure.
- The need to build, rehabilitate, and rebuild infrastructure in ways that:
 - Minimizes the impact of construction activities on already congested highways.
 - Optimizes the overall cost/benefit for the improved infrastructure.
 - Facilitates future adaptation to accommodate changing demands.
- The need to effectively address the mobility challenges posed by natural or man-made extreme events and hazards – including earthquakes, hurricanes, floods, collisions, and acts of terrorism – by designing and constructing less vulnerable infrastructure to minimize loss, and employing rapid restoration techniques to restore functionality after a disaster occurs.

This FHWA infrastructure R&D strategic plan was the guiding document for all infrastructure R&D investments between 2007 and 2010.

The 2011 FHWA Infrastructure Research and Technology Strategic Plan

In the fall of 2010, FHWA initiated an effort to better integrate all elements of the agency's work related to highway infrastructure; i.e., not just R&D, but inclusive of all highway infrastructure technology and innovation development and deployment including design and construction, structures and pavement, asset management and long-term infrastructure performance. This required a more inclusive outreach within the agency which brought together all of FHWA's infrastructure offices and functions. The result was a new multi-year strategic plan and roadmap that describes the direction and outcomes to be pursued through FHWA's infrastructure Research and Technology (R&T) program for the next five to ten years. It is founded on and informed by input from a broad array of highway stakeholders gathered through both formal and informal mechanisms.

The United States highway system is entering an unprecedented era of change that brings with it significant challenges and opportunities for highway infrastructure. The country is experiencing unprecedented fiscal challenges to operate, maintain, and invest in infrastructure in order to maintain a state of good repair and provide the improvements needed to sustain and grow the economy. In these challenging times, there is no choice but to develop and apply innovative solutions to meet the needs of the travelling public.

Past infrastructure research and technology investments have produced and put into practice innovations that have resulted in longer-lived assets at lower costs, reduced environmental impacts, saved lives, and improved economic efficiency. Additional innovation will be needed to further improve safety, reduce congestion, address environmental and energy concerns, provide the quality highway system the nation's citizens expect and address the Department's Strategic Goals. Conducting research that addresses national highway infrastructure needs, developing new and updated policy, guidance and technologies to address these needs, and effectively deploying policy, guidance, and technologies are key programmatic activities that must be embraced to meet the challenges faced by the United States – and similarly worldwide. These efforts will be directed to ensure that highway infrastructure is delivered in ways that impact traveler mobility as infrequently as possible, for the shortest amount of time, providing the greatest mobility and safety. Transportation infrastructure must be managed in a way that addresses the new challenges and puts the needs of the American people and their communities first.

This overarching FHWA R&T infrastructure strategic plan and its supporting roadmap is now guiding FHWA's Infrastructure R&T efforts for the next 5 to 10 years. The plan provides a comprehensive focus and direction across organizational boundaries; assists in prioritizing program initiatives, allocating resources, and improves the processes relative to how FHWA achieves its mission well into the future; and recognizes the inter-relationships and interdependencies among the different infrastructure disciplines and provides a framework for collaboration across disciplines and with other FHWA programs.

The strategic direction articulated in this plan is founded in the **FHWA Strategic Plan**¹ and the **U.S. DOT Strategic Plan, FY 2010- FY 2015, Transportation for a New Generation**². The outcomes that will be achieved to support the goals identified in these plans are as follow:

1. Highway safety is improved;
2. Management of the infrastructure system is continuously improved;
3. Economic returns on transportation infrastructure investments are improved;
4. Delivery of high quality infrastructure projects is expedited;
5. Durability and longevity of highway infrastructure are improved;
6. The condition of the highway infrastructure is improved;
7. The sustainability of highway infrastructure design, construction, maintenance and operation is improved and adverse environmental impacts are reduced through environmental stewardship; and
8. Personal and commercial mobility is improved.

The specific objectives that will be pursued to achieve these outcomes and contribute to achievement of the FHWA and DOT strategic goals are as follows:

1. Reduce the number of fatalities attributable to infrastructure design characteristics and work zones.
2. Improve the safety and security of highway infrastructure.
3. Improve the management of infrastructure assets and advance the implementation of a performance-based program for the NHS.
4. Improve the ability of transportation agencies to deliver projects that meet expectations for timeliness, quality and cost.
5. Reduce user delay attributable to infrastructure system performance, maintenance, rehabilitation and construction.
6. Improve highway condition and performance through increased use of design, materials, construction and maintenance innovations.
7. Reduce the life-cycle environmental impacts of highway infrastructure (design, construction, operation, preservation, and maintenance).

The outcomes delivered through the objectives articulated in this strategic plan are aimed at delivering benefits to the American public by enabling improvements in safety, performance, and cost effectiveness of the U.S. highway infrastructure, while minimizing the environmental impacts of highway construction, maintenance, and rehabilitation. The results will make possible reductions in highway congestion, improved travel time reliability, improvements in highway safety, and enhancement of the overall driving experience for the American public.

FHWA Infrastructure R&T Program Roadmap – Objectives, Strategies, and Initiatives

Details on the FHWA Infrastructure R&T Strategic Plan are provided in the following program roadmap. As noted earlier, this plan and roadmap will drive FHWA's infrastructure R&D investments for the next 5 to 10 years.

Objective 1: Reduce the number of fatalities attributable to infrastructure design characteristics and work zones.

Strategy	Initiative
1.1 Develop and deploy best practices and opportunities to improve infrastructure safety performance.	1.1.1 Assessment of the adequacy of current policies and practices with regard to ensuring the safety of highway infrastructure and provide updated policy and best practice where warranted.
1.2 Develop and deploy technologies, standards, and test methods that optimize surface characteristics with regard to friction, texture and splash and spray.	1.2.1 Develop, standardize, and deploy test methods, technologies and specifications for enhancing friction/texture on new and existing surfaces.
	1.2.2 Identify and prioritize data needed to fully characterize the safety-related characteristics of highway infrastructure, including geometrics and surface

	<p>characteristics.</p> <p>1.2.3 Evaluate, refine, and standardize test methods for friction and texture for effectiveness, repeatability, and reproducibility.</p>
1.3 Develop and deploy technical guidance to support infrastructure safety management programs.	<p>1.3.1 Improve effectiveness of friction management programs.</p>
1.4. Develop and deploy construction administration practices that enhance safe operation of the highway system by reducing work zone exposure.	<p>1.4.1 Evaluate existing practices for accelerated construction practices related to contract administration for effectiveness to reduce crash risk in work zones.</p> <p>1.4.2 Update and enhance policy and technical guidance with regard to accelerated construction practices related to contract administration.</p> <p>1.4.3 Develop and deliver training and technical support for implementation of policy and technical guidance related to accelerated construction and contract administration.</p>

Objective 2. Improve the safety) and security of highway infrastructure.

Strategy	Initiative
2.1 Develop and deploy planning, analysis and design methodologies for highway infrastructure to reduce vulnerability to physical damage. (Design)	<p>2.1.1 Implement an integrated interagency Federal approach that consolidates capabilities in a unified effort for security to prevent human induced hazard events.</p> <p>2.1.2 Improve and optimize Infrastructure System design to improve safety and security.</p>
2.2 Develop and deploy hazard mitigation, adaptation and restoration strategies and techniques. (Rehab)	<p>2.2.1 Research, develop, and deploy strategies, technologies, and programs to mitigate specific known infrastructure hazards and adaptation needs.</p> <p>2.2.2 Development of hazard mitigation and adaptation countermeasures for existing and new structures that includes a national data archive resource that captures experimental data as well as field reconnaissance data.</p>
2.3 Develop and deploy improved decision support tools and sensing and monitoring technologies for hazard detection.	<p>2.3.1 Development of improved decision support tools and methodologies for assessing hazards to infrastructure.</p> <p>2.3.2 Research, develop, and deploy better detection and surveillance technologies for evaluation, prevention,</p>

(Monitoring and assessment)	and mitigation of extreme events.
2.4 Develop and deploy methodologies and guidance for assessing safety of infrastructure after a hazard event. (Repair and/or replace)	<p>2.4.1 Development of protocols/inspection techniques for rapid assessment of infra structures after a hazard event.</p> <p>2.4.2 Research and deployment of 'smart structure' designs that sense damage and provide active/semi-active control of structural response to hazard events.</p> <p>2.4.3 Research, develop, and deploy new infrastructure systems that can rapidly be repaired and reconstructed following a hazard event.</p>

Objective 3: Improve the management of infrastructure assets and advance the implementation of a performance-based program for the NHS.

3.1 Develop and deploy reliable performance prediction models and practices in the design, construction and management of the highway infrastructure.	3.1.1 Establish performance standards for infrastructure
	3.1.2 Identify and fill gaps in performance prediction models and practices across the asset life-cycle spectrum.
	3.1.3 Develop and deploy improved traffic prediction tools
	3.1.4 Develop and deploy improved prediction tools for environmental and climate change impacts on infrastructure performance.
	3.1.5 Conduct research to understand performance issues; and identify design, construction, preservation, and maintenance strategies to assure durability and longevity of infrastructure.
3.2 Develop and deploy sound measures and practices to assess infrastructure condition and to assure data quality in infrastructure management and performance predictions.	3.2.1 Develop improved methodologies & tools to more effectively collect and manage infrastructure condition data at the national, network and project levels to more effectively identify causes of deterioration and to make more informed decisions on system performance and health.
	3.2.2 Develop and deploy non-destructive evaluation (NDE) tools, software, and guidance for condition evaluation, construction quality assurance, and the prediction of key highway infrastructure performance at the network & project levels through the entire life

	<p>cycles of the infrastructure assets.</p> <p>3.2.3 Conduct research to develop and deploy new methods & technologies to monitor infrastructure conditions in real time.</p> <p>3.2.4 Develop tools and technologies for, and promote consideration of uncertainties and risks in, data quality.</p> <p>3.2.5 Develop and implement guidance, technical support, training, and technology transfer for data quality management and to control affects from data variability.</p>
<p>3.3 Develop and deploy decision support tools, systems, and processes to support rational, and comprehensive engineering and economic analysis methods for project, program, and national level investment decisions.</p>	<p>3.3.1 Identify, assemble, analyze the required data needs & develop analysis methodologies for an overall integrated asset management approach.</p> <p>3.3.2 Develop and deploy tools, technologies, and systems for project and program level management decisions</p> <p>3.3.3 Develop and deploy tools and technologies for cross-asset analysis involving existing assets and proposed future assets, and including the inherent uncertainties and risks.</p> <p>3.3.4 Develop tools and technologies for, and promote consideration of, uncertainties and risks inherent in longer term investment decision making process.</p>
<p>3.4 Develop and deploy guidance, management approaches, and policies for management of infrastructure assets and for implementation of a performance-based program for infrastructure on the NHS.</p>	<p>3.4.1 Define & deploy a consistent and reliable method to describe and project the health of the highway system in collaboration with stakeholders.</p> <p>3.4.2 Conduct research to determine the impact infrastructure condition has on users, and develop analysis tools to better assess those impacts.</p> <p>3.4.3 Develop and deploy management approaches and policies for corridors, tunnels, ancillary structures and other transportation assets.</p>

Objective 4: Improve the ability of transportation agencies to deliver projects that meet expectations for scope, timeliness, quality and cost.

Strategy	Initiative
<p>4.1 Develop and deploy expanded and consistent use of the elements of a quality assurance program to</p>	<p>4.1.1 Develop and deploy a composite index for project value that incorporates scope, costs, time, and quality.</p> <p>4.1.2 Develop guidance and tools, conduct program reviews, and deploy effective Quality Assurance plans</p>

improve infrastructure design, materials testing, construction, and inspection procedures.	and best practices.
4.2 Develop and deploy innovative processes and project management practices to enhance project delivery in highway design and construction.	<p>4.2.1 Identify, further develop, and deploy improved, streamlined and refined analysis, design, and construction procedures.</p> <p>4.2.2 Develop and deploy tools and guidance for innovative project delivery methods.</p> <p>4.2.3 Develop and deploy tools and technologies to assure and improve the quality & maintainability of accelerated construction projects.</p>
4.3 Develop and deploy contracting tools and practices to effectively manage risk in acceptance of and payment for construction and materials.	<p>4.3.1 Develop and deploy tools that project the long-term performance and value as a result of the as-built condition of the infrastructure asset.</p> <p>4.3.2 Develop and deploy approaches and specifications that link payment and acceptance to long-term performance and quantities to minimize agency risk.</p>

Objective 5. Reduce user delay attributable to infrastructure system performance, maintenance, rehabilitation and construction.

Strategy	Initiative
5.1 Develop and deploy tools and methodologies to assess the impact of decisions (design, construction, contracting, etc.) on user delay.	<p>5.1.1 Improve tools to more effectively assess user delay during design.</p> <p>5.1.2 Develop and deploy tools to evaluate the impacts of different construction delivery approaches on user delay (i.e. full closure vs. variable closures) at the project and corridor levels.</p> <p>5.1.3 Develop methods to evaluate the impacts of different contracting methods on user delay (i.e. design build, warranties).</p>
5.2 Develop and deploy construction, inspection, maintenance, preservation, and rehabilitation practices that minimize impact to users.	<p>5.2.1 Develop and deploy techniques for prefabricated construction of the infrastructure.</p> <p>5.2.2 Research, develop and deploy technologies and processes to accelerate construction and preservation.</p> <p>5.2.3 Develop and deploy approaches to automate the construction and preservation inspection, sampling and testing associated with the production and placement of highway related materials and systems (includes all related highway systems; pavement, bridge, culvert,</p>

	etc.). 5.2.4 Research, develop and deploy new approaches to conduct infrastructure condition inspections to minimize user delay.
--	--

Objective 6: Improve highway condition and performance through increased use of design, materials, construction and maintenance innovations.

Strategy	Initiative
6.1 Develop and deploy approaches to effectively and systematically preserve and improve the highway infrastructure condition and performance.	6.1.1 Develop methodologies to effectively apply treatments using asset management principles at the project and network levels. 6.1.2 Develop and deploy technologies and processes to enhance the effectiveness of preservation activities. 6.1.3 Develop and deploy technologies and techniques to enhance the effectiveness of rehabilitation and reconstruction activities.
6.2 Develop and deploy design and preconstruction technologies and innovations to improve infrastructure condition, durability and service life, and constructability.	6.2.1 Deploy existing and proven criteria, technologies and procedures to design infrastructure to more reliably achieve intended performance and service life. 6.2.2 Research and develop the next generation of analysis and design tools to improve design reliability to achieve intended performance and service life. 6.2.3 Develop and deploy contracting procedures to improve infrastructure condition and performance. (warranties, value engineering, etc. to allocate risk)
6.3 Develop and deploy alternative project delivery methods, construction approaches and specifications where the emphasis is on the long-term performance of the infrastructure system.	6.3.1 Develop and deploy tools to assist in the allocation of risk between agencies and industry. 6.3.2 Develop and deploy technologies to improve the efficiency of construction processes.
6.4 Develop and deploy methods that will improve the quality of materials and systems used for highway infrastructure.	6.4.1 Develop and deploy new tests and methods to more accurately and efficiently characterize materials. 6.4.2 Develop and deploy best practices for selection of materials and systems, tests and methods to assure and improve quality. 6.4.3 Develop and deploy innovative materials, and systems to improve the durability and longevity of

	highway infrastructure.
--	-------------------------

Objective 7: Reduce the life-cycle environmental impacts of highway infrastructure (design, construction, operations, preservation, and maintenance).

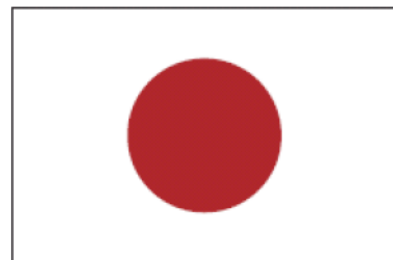
Strategy	Initiative
7.1 Advance the application of sustainable practices in project level infrastructure design.	7.1.1 Develop and deploy Life-Cycle Assessment (LCA) methodologies, tools, policy and guidance to implement and to quantify the environmental impacts of design. 7.1.2 Develop and deploy tools and practices for assessing sustainability in project-level decision-making. 7.1.3 Develop policy and guidance, and implement sustainable design approaches to adapt to the impacts of Climate Change. 7.1.4 Develop policy and guidance, and implement context sensitive design practices that improve sustainability. 7.1.5 Evaluate, develop policy and guidance, and implement sustainable aspects of existing and new materials, technologies and practices. 7.1.6 Develop policy and guidance, and evaluate practices that maximize the use of marginal and locally available materials.
7.2 Develop and deploy sustainable methods to reduce air pollutants and other emissions resulting from the construction and preservation practices.	7.2.1 Evaluate, develop policy and guidance, and implement aspects of infrastructure materials and technologies to reduce air pollutants and other emissions.
7.3 Develop and deploy sustainable methods to reduce water runoff and pollutants through improvements in design, construction, operations, maintenance, and preservation.	7.3.1 Evaluate, develop policy and guidance, and implement use of materials and technologies to reduce water runoff and pollutants. 7.3.2 Develop policy and guidance, and implement practices to improve storm water management. 7.3.3 Develop policy and guidance, and implement practices related to non-storm water runoff and pollutants.
7.4 Develop and advance sustainable practices that reduce noise during	7.4.1 Develop, standardize and deploy test methods for pavement noise to more effectively characterize noise performance of surfaces.

construction and throughout the service life.	7.4.2 Evaluate, develop policy and guidance, and implement use of materials and technologies that reduce noise such as optimizing pavement surface mix designs to reduce noise.
7.5 Identify, develop, and advance alternative energy sources for use during construction, operations, preservation and maintenance.	7.5.1 Evaluate, develop policy and guidance, and implement aspects of materials and technologies for the use of alternative energy sources.
	7.5.2 Develop policy and guidance, and implement infrastructure component technologies that generate energy.
7.6 Advance and increase the use of renewable, reusable, and recycled (3R) materials in highway-related infrastructure.	7.6.1 Evaluate the long-term performance of renewable, reusable, and recycled (3R) materials and implement the expanded use of 3R materials in highway-related infrastructure.
7.7 Minimize impacts of highway infrastructure on wildlife.	7.7.1 Develop, evaluate, improve, and deploy practices that minimize impacts on wildlife.
	7.7.2 Develop and deploy highway materials that are benign or less damaging to wildlife.

References

¹ FHWA Strategic Plan. Washington, DC : U.S. DOT, Federal Highway Administration, October 2008. Publication No. FHWA-PL-08-027.

² U.S. DOT Strategic Plan, FY 2010- FY 2015, Transportation for a New Generation, Washington, DC : U.S. Department of Transportation, April 15, 2010.



27th US-Japan Bridge Engineering Workshop

Session 7

Design and Analysis

Unbonded Prestressed Columns for Earthquake Resistance

By David H. Sanders, Alex S. Larkin, and M. Saiid Saiidi

Study on Corrosion Analysis with Fiber Model of Long-Span Truss Bridge

By Kunihiro Hayashi, Hideo Ohishi, Yukio Adachi, Misa Fujibayashi,
and Koichi Sugioka

Seismic Performance Assessment of Concrete Bridges Designed by
Displacement-Based Methods

By Kevin Mackie, Vinicio Suarez, and Oh-Sung Kwon

Local Buckling Analysis of Steel Truss Bridge under Seismic Loading

By Eiki Yamaguchi and Keita Yamada

Page Left Blank

UNBONDED PRESTRESSED COLUMNS FOR EARTHQUAKE RESISTANCE

Alex S. Larkin¹, David H. Sanders², M. Saiid Saiidi³

Abstract

The implementation of unbonded post-tensioning in bridge columns reduces damage and repair time by minimizing residual displacements. This research investigates the use of unbonded post-tensioned tendons in bridge columns. Two unbonded post-tensioned columns were tested that are identical except for the amount of longitudinal reinforcement crossing the joint between the footing and column base. The placement of post-tensioning in a full-scale column was taken into consideration which resulted in four tendons being placed around the center of the column cross section instead of one through the center of the column as has been done in previous experiments. The tendons are anchored in the side of the footing for ease of replacement following an earthquake.

Introduction

The number one concern for engineering seismic design is to maintain life safety. Once a structure can maintain life safety through an earthquake, the next step is to minimize the amount of damage to the affected structure. Minimizing the amount of damage will allow for rapid repairs and minimal closure time. For bridge columns, the use of unbonded post-tensioned tendons reduces the amount of residual displacement following an earthquake, allowing for minimal closure time of the bridge while repairs are made.

For full-scale columns, the amount of post-tensioning needed to promote re-centering effects would be between 8% and 10% $f_c A_g$. Typically, the initial stress in the tendons is between 20% to 30% f_{pu} . Therefore, if the column is 60 inches (1524 mm) in diameter, and 0.6 in (15.2 mm) strands are used, a total of between 62 and 86 strands would be needed. In addition to this being a large number for one tendon, multiple tendons allows for a tendon to be replaced while still maintaining post-tensioning and also increases redundancy. The columns being tested are 0.4-scale model, with a diameter of 24 in (610 mm). Therefore, to evenly distribute the force required for re-centering, four tendons, each with four 0.6 in (15.2 mm) Grade 270 ksi

¹Graduate Research Assistant, University of Nevada Reno

²Professor, University of Nevada Reno

³Professor, University of Nevada Reno

(1862 MPa) 7-wire strands were evenly spaced at 5.4 in. (137.2 mm) around the center of the column cross section (see Fig. 1).

Following a major earthquake, bridge columns are likely to have undergone large lateral displacements. Post-tensioned columns are typically designed to not have tendons yield or be damaged. It is critical for it to be possible to inspect and replace the tendons. Previous tests have utilized straight tendon or bar that exited through the bottom of the footing; this configuration makes it impossible to replace the tendon. By exiting out the side, or out the top of the footing for large footings (180 degree bend for the post-tensioning tendon), the tendons can be removed. For these specimens, the tendons exited out the side of the footing (see Fig. 2).

Literature Review

Excessive residual displacement is an issue with columns following an earthquake. Unbonded post-tensioned tendons have been used in columns that have shown reductions in residual displacements. Research performed by Ou showed the re-centering capabilities of unbonded post-tensioned columns. Ou's report also indicates that high lateral column displacements lead to high strain in the unbonded post-tensioned tendons (Ou et. al. 2009). Hewes has also indicated the importance in the selection of the initial post-tensioned force in the tendon. The higher tendon forces aid in reducing the residual displacements at low drift levels, but can lose their effectiveness at high drift ratios due to the yielding of the tendon. Hewes' report also indicates the benefit of using unbonded tendons as opposed to bonded tendons because the localized inelastic straining due to large drifts can be avoided, maintaining the re-centering force throughout testing or throughout an actual earthquake (Hewes and Priestley 2002). While the column may still show damage depending on the intensity of the earthquake, repairs can be made quicker when the column re-centers itself. Sakai concluded that adding a steel jacket to the column plastic hinge region as well as locally unbonding the mild reinforcing steel that cross the joint between the footing and column base prevented damage compared to a conventionally reinforced column and a partially prestressed column (Sakai et. al. 2006).

Justification

The amount of post-tensioning was selected by keeping the initial force (10% $f'_c A_g$) in the post-tensioning at or below a tendon stress of 20% f_{pu} . The amount of longitudinal reinforcement that crosses the joint between the footing and the base of the column was selected based on the literature review. Much of the previous post-tensioning experiments had very little to no longitudinal reinforcement crossing the

joint between the footing and column as past researchers were just interested in the re-centering effects of the tendon. Now that post-tensioning has shown excellent re-centering effects, the combination of post-tensioning with longitudinal reinforcement should be investigated. Sakai had a longitudinal reinforcement ratio of 0.65% with a single tendon in his report. This amount of reinforcement allows for some longitudinal column capacity in case of a tendon failure, and is small enough to allow for minimal residual displacement. While the research described in this paper utilized several tendons located around the center of the column cross section, it used a small longitudinal reinforcement ratio to capture the re-centering effects for one column. The second columns reinforcement ratio was doubled from the first to determine how the amount of longitudinal reinforcement affects re-centering.

Design of Specimens and Test Setup

The two columns selected for testing were initially targeted to have identical properties except for the amount of longitudinal reinforcement crossing the joint between the footing and the column base. Achieving identical forces in the tendons between the two columns was difficult and ended with slight variations in the initial post-tensioning ($\% f'_c A_g$) between the two specimens. The column parameters are shown in Table 1 and the cross section for each column is shown in Figure 1. The material properties for each column are shown in Tables 2 and 3.

The test setup for each column consisted of a reaction wall, strong floor, and a 220-kip actuator to produce the cyclic loading protocol in Figure 3. The reaction wall was created by stacking two columns of three 4x4x8 foot (1.22x1.22x2.44 m) concrete blocks, with one additional block added to the top of the front stack to achieve the proper height for the actuator to meet the column head. The reaction wall was secured to the strong floor using 1.25 in. (31.75 mm) DywidagTM post-tensioned bars. The footing of each column was secured to the 3 foot (0.91 m) deep strong floor with six 1.25 in. (31.75 mm) DywidagTM post-tensioned bars. Each DywidagTM bar for the reaction wall and footing had a 100 kip (444.84 kN) force applied.

A steel spreader beam was bolted to the top of the column to apply the axial dead load. Two hydraulic rams were attached to the top of the spreader beam on each side of the column and two high strength 1.25 in. (31.75 mm) threaded rods ran through the hydraulic ram, load cell, footing, and attached to the bottom of the strong floor to apply the axial dead load. The axial dead load was maintained through an accumulator which held constant and equal load in each of the hydraulic rams throughout testing. The test setup is shown in Figure 4.

Results

The cyclic loading for each column produced a lateral force and displacement hysteresis curve. The hysteresis curve was broken up into the positive backbone envelope, considered the push cycle, and the negative backbone envelope, considered the pull cycle. The absolute values from the negative backbone envelope were superimposed with the positive backbone envelope and an average curve was taken from the two envelopes. The average curve is considered the pushover curve for the column. The pushover curve for columns PT-LL and PT-HL are shown in Figures 5 and 6 respectively.

Column PT-LL had a first bar yield displacement of 0.63 in (16.0 mm). This was determined by finding the displacement when the first longitudinal bar yielded. This value was used to plot a straight line on the pushover curve, beginning at zero displacement and zero force. A straight line was then plotted across the top of the curve, where the area under the straight line bounded by the top of the pushover curve was equal to the area under the pushover curve bounded by the straight line. The point at which these two straight lines intersect is the effective yield displacement (0.95 in. (24.2 mm)). The ultimate displacement was defined as the displacement at 80% of the peak lateral force in the column. The ultimate displacement of column PT-LL was 8.64 in (219.5 mm) at a drift of 8.0%, and a displacement ductility of 9.1. Column PT-HL had a first yield displacement of 1.0 in (25.4 mm) that lead to an effective yield displacement of 1.36 in (34.5 mm). The ultimate displacement for column PT-HL was 9.17 in (232.9 mm) at a drift of 8.5% resulting in a displacement ductility of 6.7.

Each of the four tendons consisted of four 0.6" (15.24 mm) Grade 270 ksi (1862 MPa) 7-wire strands. Tendons 2 and 4 were located on the same axis that the column was rotated about. Tendons 1 and 3 were located on the extreme ends and felt the largest strains. The initial force in the tendons was carefully selected and kept within the lower elastic region so the tendons would not yield under large lateral displacements. Figures 7 and 8 show the microstrain in tendons 1 and 4 with respect to the drift ratio of the column. The outermost tendons (tendons 1 and 3) felt the largest strains as shown in Figure 7, compared with tendons located on the same axis the columns were rotated about (tendons 2 and 4) shown in Figure 8. The tendons do not begin to yield until a microstrain of at least 8000 is reached. It can be seen that even the most extreme tendons, such as tendon 1 did not reach their yield strains, even at very large drift ratios. Column PT-HL behaved very similarly to column PT-LL and did not reach a strain of more than 6500 microstrains, even at drift levels as high as 10%.

Figure 9 shows the full hysteresis curve for column PT-LL. During construction, the cover concrete was almost double the amount on one side of the column in relation to the other side. Uneven column cover lead to the core being shifted and not in the true center, causing residual displacements and peak loads to differ from a push and pull cycle. Figure 9 displays the enhanced re-centering effect provided by post-tensioning. At a drift level of 6% (6.48 in, 164.6 mm), column PT-LL had a residual displacement on the positive side of the hysteresis curve of 1.57 in (39.9 mm) and a residual displacement on the negative side of the hysteresis curve of 3.45 in (87.6 mm), resulting in an average residual displacement of 2.51 in (63.8 mm). The full hysteresis for column PT-HL is shown in Figure 10. The residual displacements are larger than PT-LL due to the increase in amount of longitudinal reinforcement. At a drift level of 6% (6.48 in, 164.6 mm), column PT-HL had a residual displacement on the positive side of the hysteresis curve of 3.12 in (79.2 mm) and a residual displacement on the negative side of the hysteresis curve of 3.31 in (84.1 mm), resulting in an average residual displacement of 3.22 in (81.7 mm).

Conclusions

Two unbonded post-tensioned columns have been tested for seismic design. The columns had identical properties except for the amount of longitudinal reinforcement crossing the joint between the footing and the base of the column. Each column had four tendons evenly spaced around the center of the column cross section to evenly distribute the force required for re-centering. While past research has anchored the tendons in the base of the footing, this research anchored the tendons in the side of the footing for the ease of inspection and replacement following an earthquake.

Tendon location and the initial tendon force selected (based on keeping the post-tensioning at or below an initial tendon stress of 20% f_{pu}) were satisfactory. The extreme tendons (tendons 1 and 3) did not begin to yield, even at large drift ratios of 10% (10.8 in, 274.3 mm). Tendons located at 22.5% of the column diameter from the center of the column cross section provide re-centering capabilities and do not yield at large drift ratios. Exiting the tendons out the side of the footing did not display any negative effects.

The amount of longitudinal reinforcement had a large impact on the re-centering capabilities of the column. PT-LL had a residual displacement of 1.5 in (38.1 mm) at 6% drift (6.48 in, 164.6 mm), while column PT-HL had a residual displacement of 3.1 in (78.7 mm) at 6% drift (6.48 in, 164.6 mm). The displacement ductility of column PT-LL was 8.1 as opposed to 6.7 for column PT-HL.

Acknowledgments

Support for this research was provided by the Nevada Department of Transportation. The findings herein are of the authors and do not necessarily represent those of the sponsoring organization

Conversions

US Customary Units	SI Equivalent
1 in	25.4 mm
1 ft	0.3048 m
1 kip	4.45 kN

References

Hewes, J. T., and Priestley, M. J. N. (2002). "Seismic Design and Performance of Precast Concrete Segmental Bridge Columns." Structural Systems Research Project, *Rep. No. SSRP-2001/25*, University of California, San Diego, La Jolla, California.

Ou, Y., Wang, P.-H., Tsai, M.-C., Chang, K.-C., and Lee, G. C. (2009). "Large-scale experimental study of precast segmental unbonded post-tensioned concrete bridge columns for seismic regions." *Journal of Structural Engineering, ASCE*

Sakai, J., H. Jeong and S. Mahin, "Reinforced Concrete Bridge Columns that Re-Center Following Earthquakes," *Proceeding, 8th national Conference on Earthquake Engineering, EERI*, San Francisco, CA, April 2006, Paper 1421.

TABLE 1: COLUMN PARAMETERS

Column	ρ_l	ρ_s	PT (initial)	Dead Load	Height, in (m)	Diameter, in (m)	Aspect Ratio
PT-LL	0.685% (10 #5's)	1.00%	8%fcAg, 157 kips (698 kN)	6%fcAg (122 kips)	108 (2.74)	24 (0.61)	4.5
PT-HL	1.33% (10 #7's)	1.00%	9%fcAg, 186 kips (827 kN)	6%fcAg (122 kips)	108 (2.74)	24 (0.61)	4.5

TABLE 2: CONCRETE PROPERTIES

Column	Segment	7-Day Strength, psi (MPa)	Test Day, psi (MPa)
PT-LL	Footing	4361 (30.1)	5384 (37.1)
	Column & Column Head	3380 (23.3)	4330 (29.9)
PT-HL	Footing	4361 (30.1)	5500 (37.9)
	Column & Column Head	3380 (23.3)	4570 (31.5)

TABLE 3: STEEL PROPERTIES FOR COLUMN PT-LL

Tested Bar	f_y , psi (MPa)	f_u , psi (MPa)
Transverse Bars: #3	71300 (492)	94500 (652)
Longitudinal Bars: #5	71800 (495)	96600 (666)
Longitudinal Bars: #7	69800 (481)	112200 (774)
Post-tensioned Strand: 0.6"	247000 (1703)	281000 (1937)

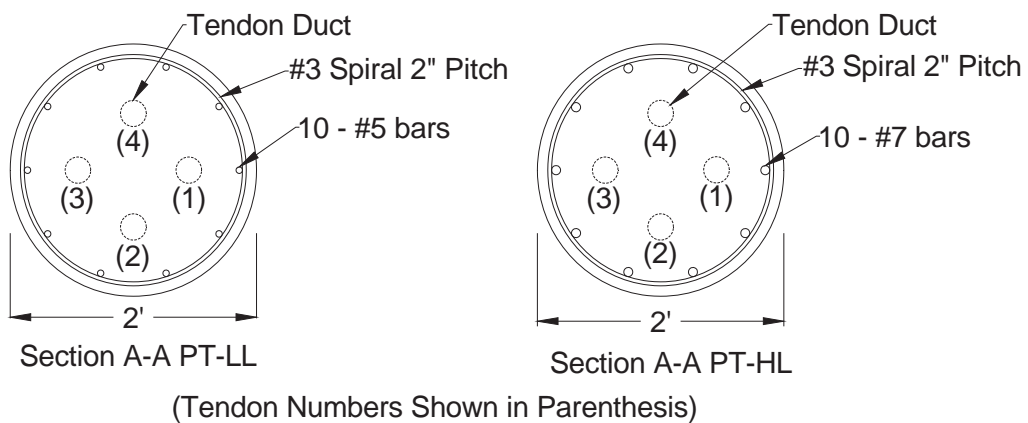


FIGURE 1: CROSS SECTION FOR PT-LL AND PT-HL

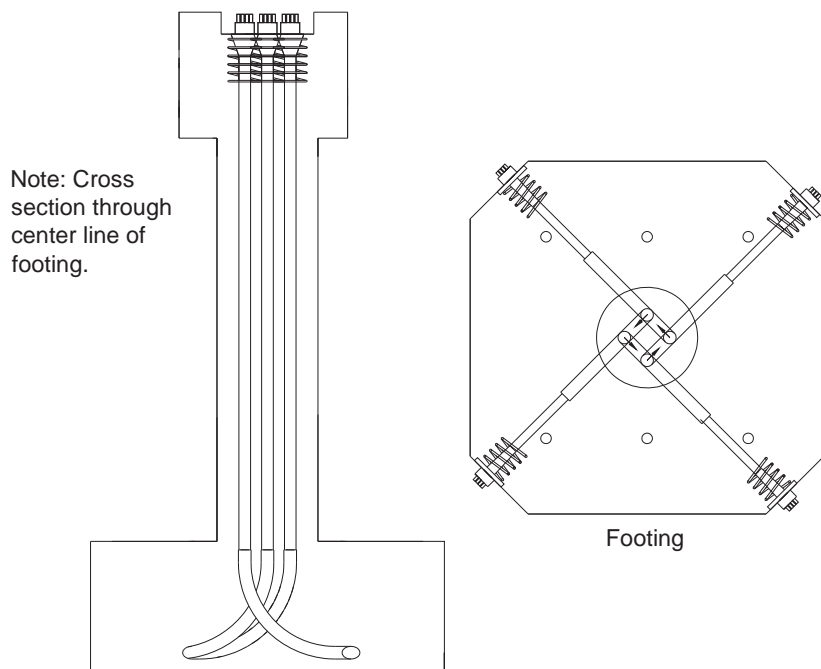


FIGURE 2: TENDONS EXITING OUT THE SIDE OF THE FOOTING

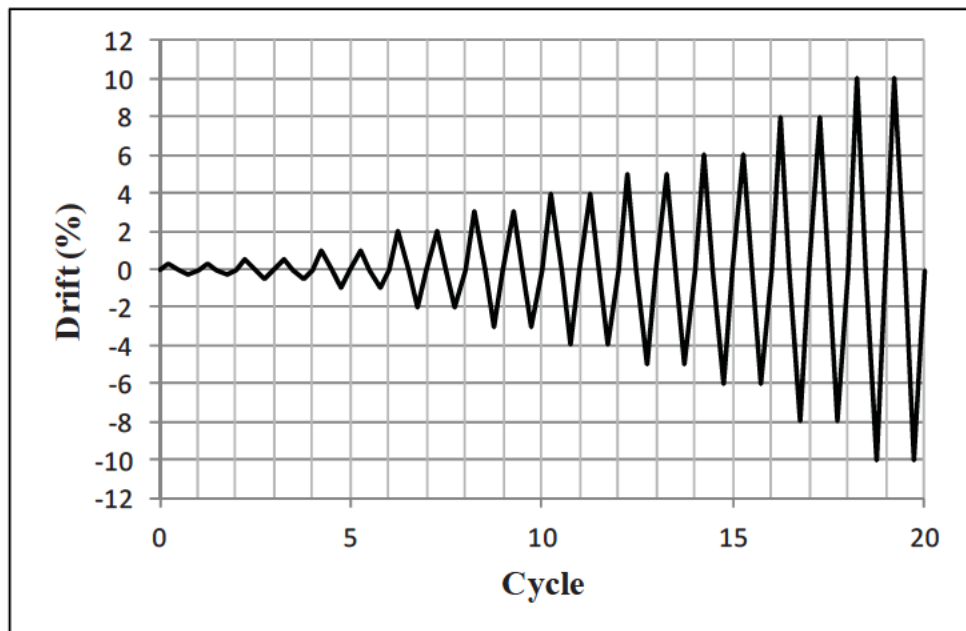


FIGURE 3: LOADING PROTOCOL



FIGURE 4: TEST SETUP

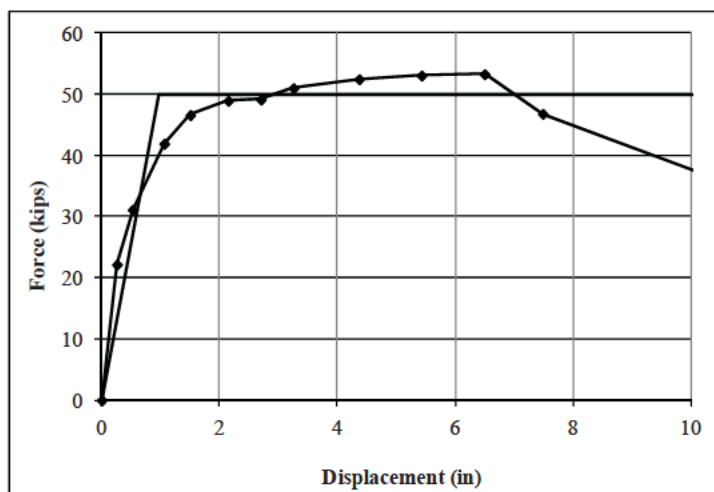


FIGURE 5: AVERAGE PUSHOVER PT-LL

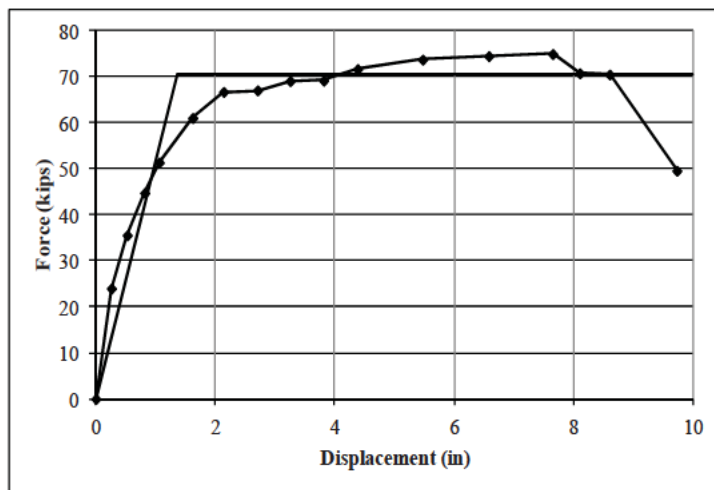


FIGURE 6: AVERAGE PUSHOVER PT-HL

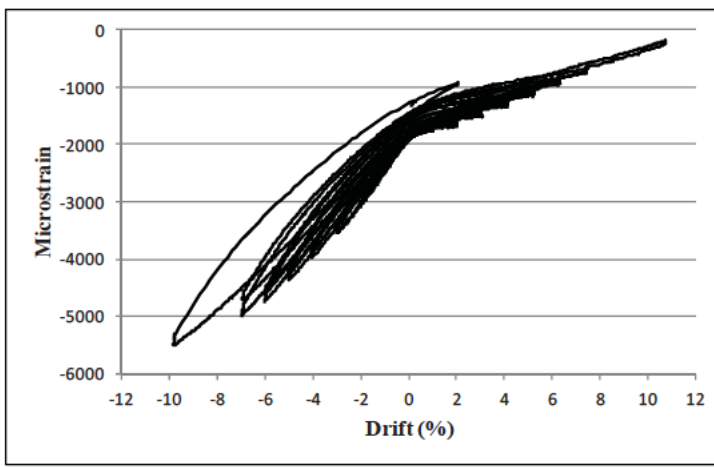


FIGURE 7: STRAIN IN TENDON 1 PT-LL

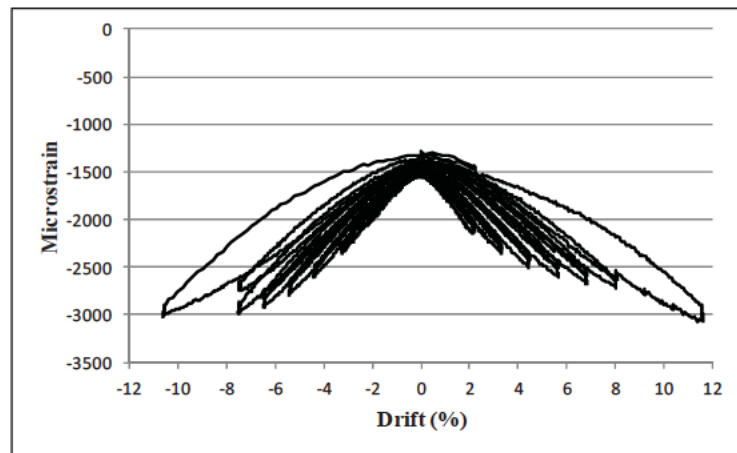


FIGURE 8: STRAIN IN TENDON 4 PT-LL

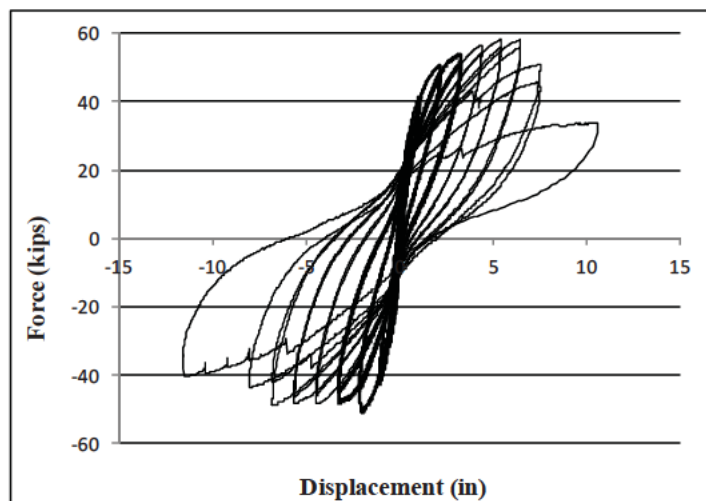


FIGURE 9: HYSTERESIS PT-LL

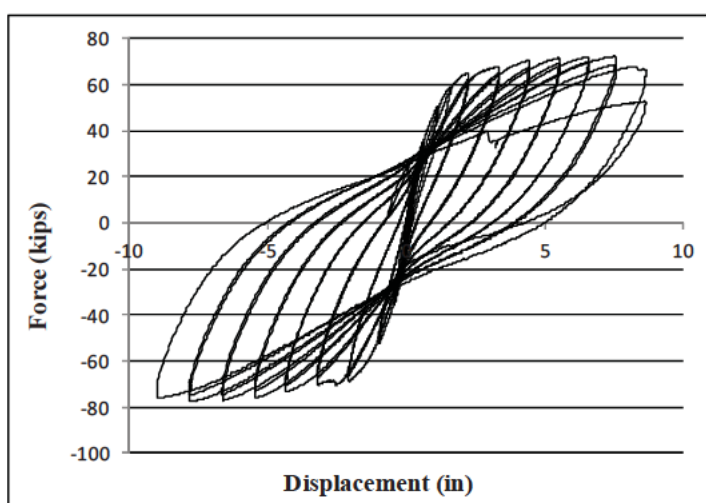


FIGURE 10: HYSTERESIS PT-HL

STUDY ON CORROSION ANALYSIS WITH FIBER MODEL OF LONG-SPAN TRUSS BRIDGE

Kunihiro Hayashi¹, Hideo Ohishi², Yukio Adachi³, Misa Fujibayashi⁴
and Koichi Sugioka⁵

Abstract

According to maintenance of long span bridges, especially inspection, it is required rational and feasible inspection programs, because these are large in scale and have numerous inspection points. To assist rationalization for long-span bridge inspection, the authors have considered features of structure and environment, and examined the maintenance plan in this study. We created the whole bridge system model of truss bridge and quantitatively identified the vulnerability to simulate in detail considered vertical load and horizontal load, those are earthquake and wind. Also we analyzed in case of member fracture. Furthermore, extracting significant inspection location considered engineering judgment was discussed.

Introduction

The Hanshin Expressway network, especially the Wangan Route located in the bay areas (FIGURE 1), has many long-span bridges. Inspection schedules for these long-span bridges are prepared individually, apart from the other bridges which are included in general inspections performed per route every 5 to 8 years (Hanshin Expressway Company Limited, 2005). Long-span bridges are extremely large in scale and composed of many members. Numerous locations need to be inspected, and inspection practices tend to be complicated. Many of them are also marine bridges with poor accessibility, which results in further increased costs of inspection and other maintenance activities. Because of these, it has been practically impossible to carry out inspections as initially intended.



FIGURE 1 HANSHIN EXPRESSWAY NETWORK

¹ Chief Engineer, Maintenance Engineering Group, Osaka Business and Maintenance Department, Hanshin Expressway Company Limited

² Assistant Manager, Planning and Research Division, Hanshin Expressway Management Technology Center

³ Manager, Maintenance Engineering Group, Osaka Business and Maintenance Department, Hanshin Expressway Company Limited

⁴ Engineer, Maintenance Engineering Group, Osaka Business and Maintenance Department, Hanshin Expressway Company Limited

⁵ Assistant Manager, Design Group, Engineering Department, Hanshin Expressway R&D Co., Ltd.

Recently more reducing the maintenance cost, it is required rational inspection with significant level of members. The authors simulated to determine limit states of the whole bridge system and to quantitatively identify impacts of corrosion-induced sectional loss on the safety performance of the whole bridge system, with a new modeling method considering effects of local buckling (Sugioka et al., 2011a, b). To pick up some weak members with quantitative evaluation, we think very useful means, in case of settling on optimum inspection plan of frequency or criteria. In this paper, assuming member corrosion of the Gerber truss bridge, we analyzed using the whole bridge system model with local buckling or initial imperfection, where was defined as corrosion analysis, and also examined maintenance rationalization for long-span bridges because of containing complicated structure and high redundancies.

Summary of Examination

The bridge under analysis is the long-span Gerber truss bridge of 980m length with the center span of 510m and the side spans of 235m each. The general view of bridge is shown in FIGURE 2. Analysis was conducted assuming corrosion by aged deteriorated member, so weak members were extracted as significant inspected one.

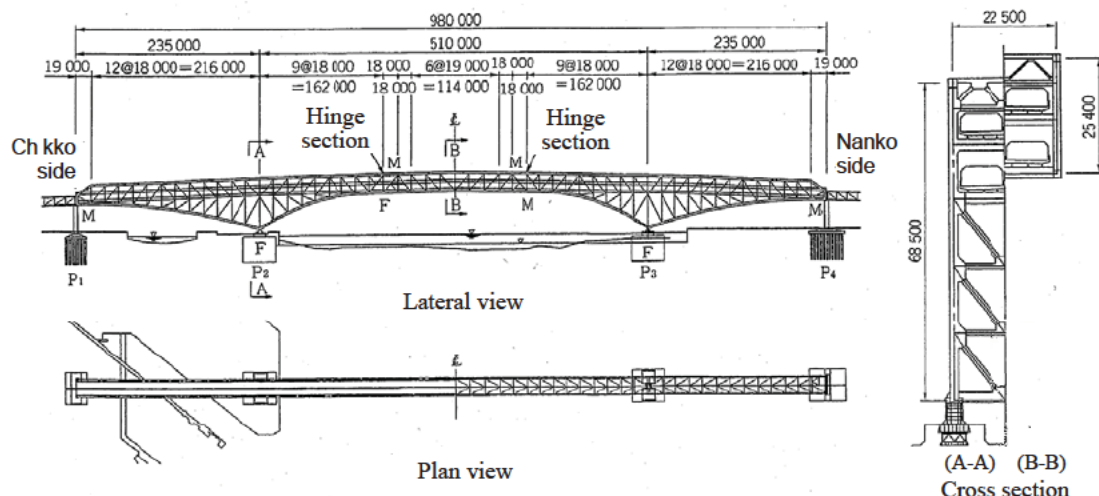


FIGURE 2 GENERAL VIEW OF LONG-SPAN GERBER TRUSS BRIDGE

The whole bridge system was modeled as shown in FIGURE 3, using the Fiber model for all members. The Fiber model that has Bernoulli-Euler theory cannot consider local buckling, so approximately evaluated axial compressive stress was equal to local buckling. The initial imperfection effecting global and local buckling stress

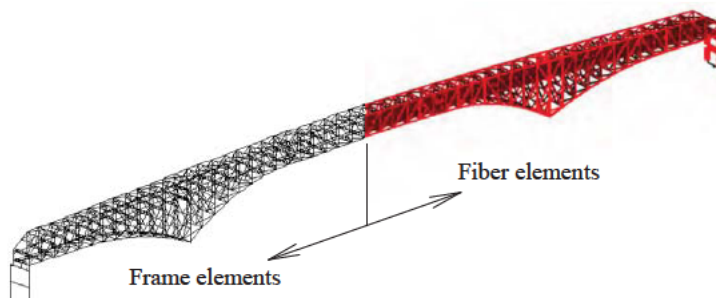


FIGURE 3 ANALYSIS MODEL OF WHOLE BRIDGE

was the initial deflection and residual stress. The initial deflection contained the deformation mode by loading D+L (for horizontal D+W, where D is dead load, L is live load and W is wind load) in advance and the deformation adjusted as L/1,000 where occurring the maximum displacement for each member. The residual stress, shown in FIGURE 4, was set up as initial stress at each integral point of fiber element. FIGURE 5 shows the contour figure of the initial imperfection. The created analysis model was proved the validation compared with the natural period, the cable tension and the support reaction of the original design.

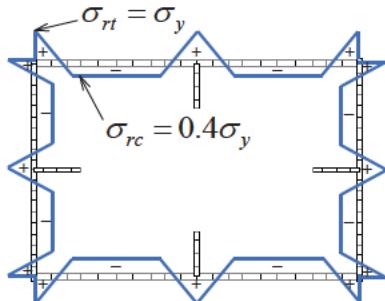


FIGURE 4 RESIDUAL STRESS

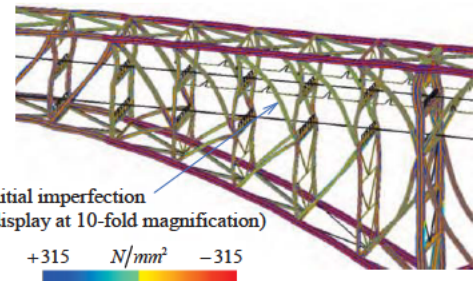


FIGURE 5 INITIAL IMPERFECTION

As corrosion was increased, the analysis stopping point emerged in structure instability. This is named the analytical limit. For steel members, the ultimate limit was judged automatically by the analytical limit through elastic-plastic finite displacement analysis. On the other hand, for the other members such as bearings did not judge the ultimate limit automatically, and adopted as the ultimate limit whether came first the analytical limit or the threshold to determine separately.

After loading dead load D, design load X was loading incrementally up to the ultimate limit of the whole bridge, which is D+βX. Design load X was applied dead load D and wind load W with loading fully, and seismic load set maximum acceleration distribution for dominant mode as load vector which simulated Level 1 earthquake response analysis in advance, as shown in FIGURE 6. In case of existing several dominant mode, seismic load was used for the central span. The bridge ultimate strength was reached at the ultimate limit on the minimum safety rate β , where magnification divided total load by design load. Also, for reference, we have calculated load ratio β' converted magnification of dead load D and design load X.

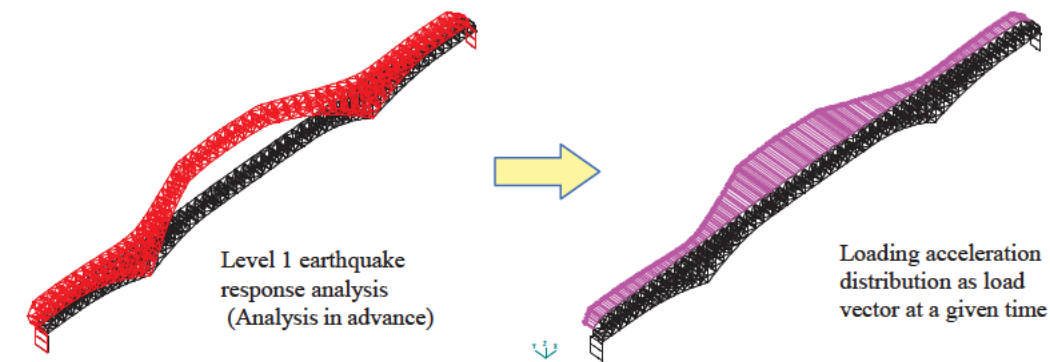


FIGURE 6 SETTING SEISMIC LOAD

Then, in the condition of loading design load that was live load, wind load and seismic load, section corrosion of the focused member increased, amount of displacement change for the focused position examined, and corrosion mass calculated when reached at the ultimate limit. The bridge under analysis is a symmetric structure, so 182 major members, quarter of whole bridge structure, were examination objects; where were 52 upper and lower chord members, 41 diagonal members, 27 vertical members, 57 cross beams, 1 eye bar support, 4 substructures. Analysis pattern was that the base was one member, without grouping corrosion members. and corroded at entire member for length and all around, as shown in through 90% of the base metal thickness in 10% increments (9 steps), it was organized the average thickness converted the base metal thickness of target members. Buckling strength was calculated for metal thickness of each corrosion step, the local buckling strength reduction was evaluated considering reduction of the yield stress. Design load was defined live load, wind load and seismic load (plane or out plane), and load vector was switched for each member of examine pattern if there were several dominant modes by dynamic response analysis of Level 1 earthquake.

By the way, some steel truss bridges in the country and overseas has been occurred damages, therefore, either to collapse whole bridge in a moment or avoid such a disaster. These are assumed to depend on differences of damage occurring position, structural redundancy and so on. To reveal the mechanism will be able to prevent an accident. In this study, live load ($D+L$) was applied to the whole bridge system model and elastic-plastic finite displacement analysis was performed in case of member fracture (buckling). Analysis case was based on one member without grouping corrosion members, and as shown in FIGURE 8 (URS Corporation, 2006.), some tension members were considered fracture impact force in $D+L$ loaded condition. Then, the member reached the analytical limit by this simulation was extracted as the significant member due to sudden fracture.

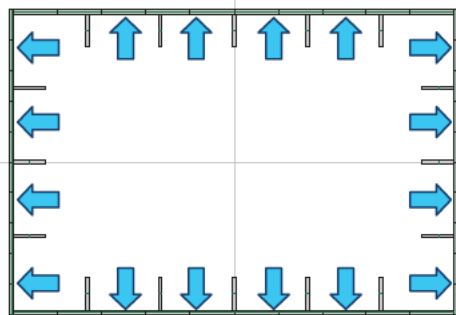


FIGURE 7 CORROSION DIRECTION

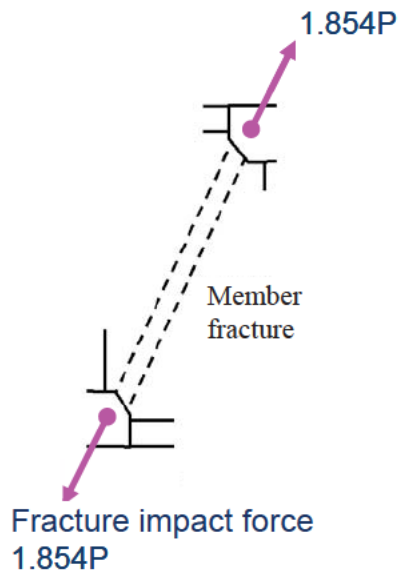


FIGURE 8 CONCEPT OF FRACTURE ANALYSIS

Analysis Results

Analysis results are shown in TABLE 1. The minimum ultimate strength is wind load ($D+\beta W$) and load ratio β is 1.57.

TABLE 1 ANALYSIS RESULTS OF ULTIMATE LIMIT

Judgment Value		Limit Value				Ultimate Limit
Examination Case	Monitoring Point	End Support	Intermediate Support	Pin of Eye Bar	Gerber Section	
D+L	$\beta' [\beta'(D+L)]$	-	-	-	-	$\beta'=1.54$ $\beta=5.46$
	$\beta [D+\beta L]$	-	-	-	-	
	Response/Allowable Value	0.14	0.59	0.90	0.00	
	Location	SH-P4L	SH-P2L	IB-P3L	SH-HP3U	
D+W	$\beta' [\beta'(D+W)]$	-	-	-	-	$\beta'=1.08$ $\beta=1.57$
	$\beta [D+\beta W]$	-	-	-	-	
	Response/Allowable Value	0.24	0.75	0.43	0.33	
	Location	SH-P4R	SH-P2R	IB-P3R	SH-HP2D	

FIGURE 9 shows one of analysis results in relationship between vertical displacement of the eye bar support bottom and corrosion mass of upper chord members in case of loading D+L. Here the vertical axis is the former and the horizontal axis is the latter that converted the average thickness of corrosion section. In this figure, the location named “01UB-17” was displaced drastically, the maximum vertical displacement 530mm at the eye bar support bottom, when average corrosion become 25mm. Analysis was stopped at the next step of 90% corrosion because of structural instability, so 80% corrosion was defined as the ultimate limit. FIGURE 10 shows corrosion mass of each upper chord member at the ultimate limit. Also the ultimate limits were organized for every analytical pattern of the lower chord members, the diagonal members and the vertical members; corrosion mass was made by different colors for each member as shown in FIGURE 11. Many diagonal members and vertical members were made the ultimate limit with corrosion mass of 20mm. Also the upper and lower chord

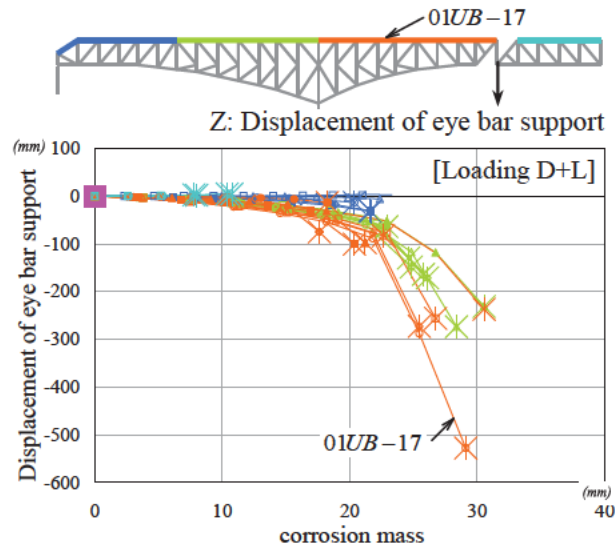


FIGURE 9 CORROSION AND DISPLACEMENT CURVE

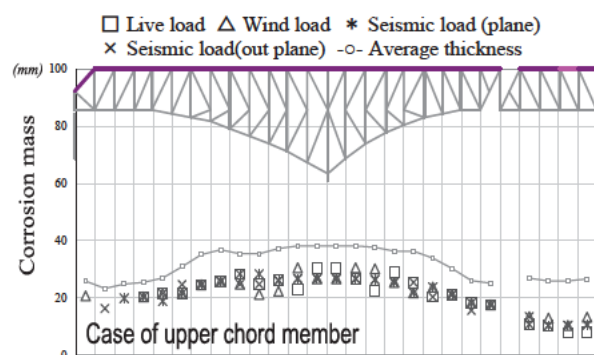


FIGURE 10 CORROSION AT ULTIMATE LIMIT

members that initial metal was thick were reached the ultimate limit with corrosion mass of 20 through 30mm. Otherwise, the eye bar support was very thick (average thickness was 75mm), so not to reach the ultimate limit but to displace much with progression of corrosion. If a less corrosion member, 0 through 10mm when its ultimate limit was reached, was regarded as weakness, some upper chord members of the suspended girder and diagonal members of the side span, displayed in red, were found weak points.

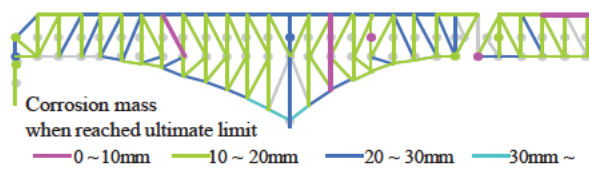


FIGURE 11 WEAK POINTS FROM ANALYSIS

Then, the results of local fracture analysis are mentioned. The fracture cases were 121 in total; where were 26 upper chord members, 26 lower chord members, 41 diagonal members, 27 vertical members and 1 eye bar support. In a condition of live load (D+L), compression members and tension members were classified, and the latters were considered fracture impact force 1.854P. FIGURE 12 shows fracture member at each axial force. From the results of fracture analysis, members that reached its ultimate limit were extracted as significant ones, shown in FIGURE 13. In each case, there were significant members at the same degree. The results were not reached to collapse in any case.

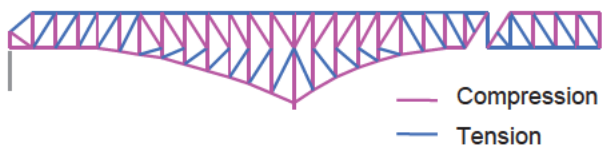


FIGURE 12 CLASSIFICATION OF MEMBERS

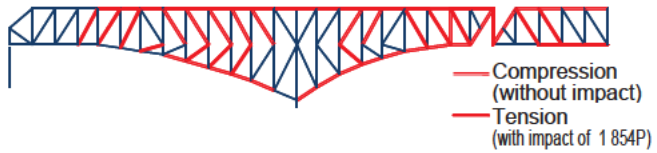


FIGURE 13 SIGNIFICANT MEMBERS

Here we examined the structure didn't make unstable even if the lower chord member near the intermediate bearing broken. The change of response axial force after fracture of the lower chord member was found that the force redistributed to the bottom laterals, the support members, the diagonal members, the main tower and the vertical members. TABLE 2 shows the increase-decrease rate of axial force share around the lower chord member before or after fracture. The lower chord member labeled No.(1) as shown in FIGURE 14 was broken, the bottom lateral No.(3) increased axial force

TABLE 2 INCREASE-DECREASE RATE OF AXIAL FORCE

		Before fracture: A	After fracture: B	Rate B/A
Lower chord member	L (1)	-95,000 kN (0.27 Ny)	0 kN (0.00 Ny)	0.0
	R (2)	-96,000 kN (0.27 Ny)	-161,000 kN (0.45 Ny)	1.7
Bottom lateral (side span)	L (3)	-4,000 kN (0.05 Ny)	-36,000 kN (0.48 Ny)	9.0
	R (4)	-4,000 kN (0.05 Ny)	-5,000 kN (0.06 Ny)	1.3
Bottom lateral (center span)	L (5)	-5,000 kN (0.06 Ny)	-13,000 kN (0.17 Ny)	2.6
	R (6)	-5,000 kN (0.06 Ny)	-14,000 kN (0.18 Ny)	2.8

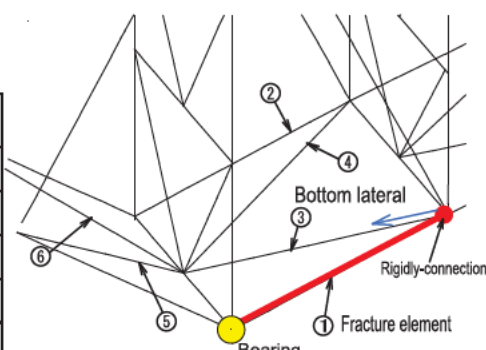


FIGURE 14 FRACTURE ELEMENT AROUND BEARING

mainly (9 times before fracture) had good margin: $0.48N_y$, where N_y was the yield axial force at full section. This was thought the force transmitted to (3) because every joint at panel point simulate as rigidly-connect. When (1) was actually broken, the gusset joint between (1) and (3) collapsed and the axial force was likely not to transmit to (3) normally. As mentioned above, this result of analysis had problem about the difference between analytical model and real structure. As it is now, however, significant part for each member was distributed by compositing structural significant member selection.

Optimum Inspection Policy

Since long-span bridges tend to have complicated structure with high redundancies, it is not necessarily reasonable to weigh all members equally in inspections. Therefore, in order to suggest priority of inspection frequency for each location, the flow diagram considered engineering judgment was made as shown in FIGURE 15 (Hanshin Expressway Company Limited, 2011). Inspection frequency was set 3 stages as “LOW”, “MIDDLE” or “HIGH”, and the location that cannot inspect with existing facilities was examined other inspection method. According to FIGURE 15, FIGURE 16 shows to suggest proper prioritization of structural members in inspection.

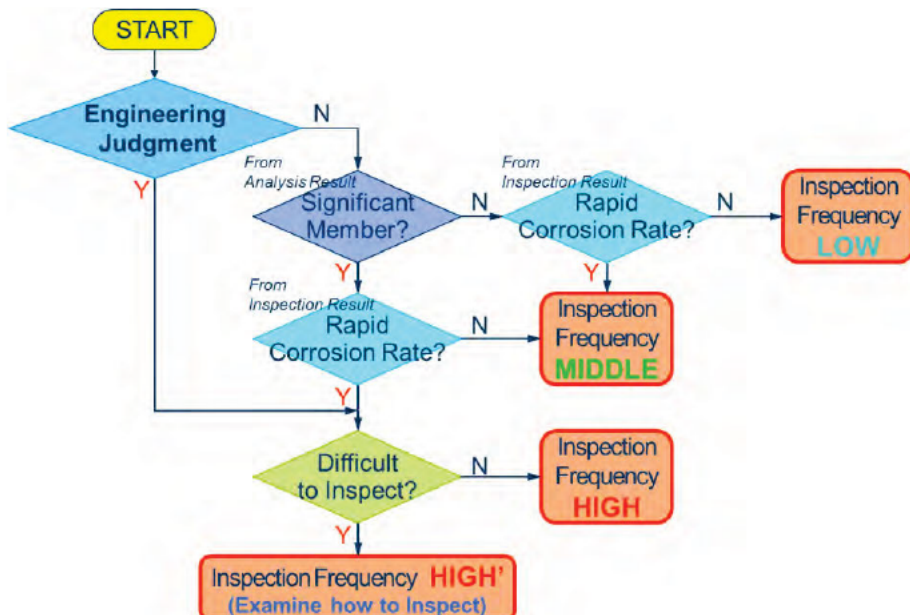


FIGURE 15 FLOW DIAGRAM OF INSPECTION FREQUENCY WEIGHT BY ENGINEERING JUDGMENT

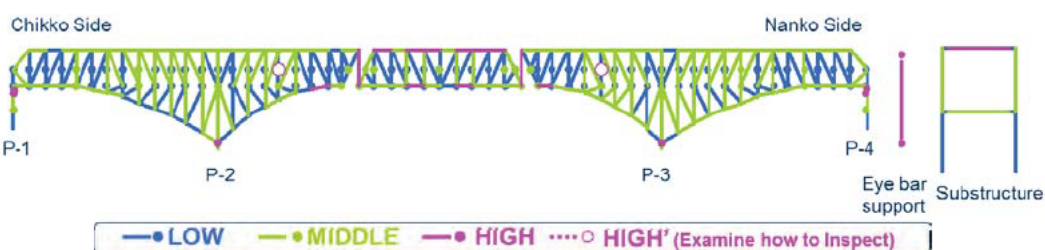


FIGURE 16 INSPECTION FREQUENCY OF LONG-SPAN TRUSS BRIDGE

The Hanshin Expressway manages, including the truss bridge under consideration, 15 long-span bridges such as the cable stayed bridge, the arch bridge and so in the Wangan Route. The inspection program for each long-span bridge was determined at the same time of initial design, so the contents of program have to be updated to reflect the condition of damages when the time comes to need a full-scale maintenance. In conjunction with the long-span bridge management techniques by Fault Tree Analysis have developed so far (Mashima et al., 2010), these techniques will be expended to rational and optimum inspection methods in the future.

Conclusion

This study was examined aging corrosion analysis with the sophisticated analytical fiber model of whole bridge system considered local buckling and initial imperfection, and presented a method to extract quantitatively weak members as significant inspection ones. Corrosion analysis was carried out for the long-span Gerber truss bridge using an whole bridge model and it was found that the some upper chord members of the suspended girder and diagonal members of the side span were the weak members. The selection of some significant inspection members from not only this analysis result but also engineering judgment enable to plan a rational inspection program of every long-span bridge.

Acknowledgments

This study has been reviewed at the Long-Span Bridge Inspection Rationalization Review Committee of the Hanshin Expressway. The authors would like to express their appreciation to Dr. Osamu Yoshikawa, a chairperson of the Committee and former professor at Osaka Institute of Technology, Dr. Masatsugu Nagai, a vice chairperson of the Committee and professor at Nagaoka University of Technology, and Dr. Kiyoyuki Kaito, a member of the Committee and associate professor at Osaka University. Appreciation of the authors is also extended to Mr. Kazuya Magoshi of Seismic Analysis Research Inc. who conducted the analysis.

References

- Hanshin Expressway Company Limited, 2005. Road Structure Inspection Procedures (in Japanese)
- Hanshin Expressway Company Limited, 2011. Summary of the Long-Span Bridge Inspection Rationalization Review Committee (in Japanese)
- Mashima, N., Sugioka, K., Kobayashi, H., Kanaji, H., Ohishi, H. and Kaito, K., 2010. Risk based inspection strategy considering structural redundancy of long span bridges, The 5th Int'l Conference on Bridge Maintenance, Safety and Management (full paper enclosed on CD-ROM), Philadelphia, USA.
- Sugioka, K., Matsumoto, S., Ohishi, H., Kanaji, H., Magoshi, K. and Nagai, M., 2011. Fundamental study on analysis of whole bridge system using fiber model considering local buckling, Journal of Structural Engineering, Vol.57A, pp.703-714 (in Japanese)

Sugioka, K., Matsumoto, S., Ohishi, H. and Magoshi, K., 2011. Redundancy analysis for rational maintenance of a long-span truss bridge considering corrosion effect, Proc. of Japan Society of Civil Engineering 2011 Annual Meeting, VI-243, pp.485-486 (in Japanese)

URS Corporation, 2006. Fatigue evaluation and redundancy analysis, Bridge No.9340, I-35W over Mississippi river, Draft report

SEISMIC PERFORMANCE ASSESSMENT OF CONCRETE BRIDGES DESIGNED BY DISPLACEMENT-BASED METHODS

Kevin Mackie¹, Vinicio Suarez², and Oh-Sung Kwon³

Abstract

With the advent of performance-based design, it is necessary to consider the performance of bridges as an intrinsic part of the design process. However, even when performance is measured in terms of deformations and displacement-based design is utilized, it is of interest to know whether designs actually result in the desired performance under ground shaking representative of the design hazard. Four case studies are designed in this paper, ranging from an elasto-plastic oscillator to a three-span continuous prestressed concrete bridge. The distribution of peak responses was assessed for each case study in reference to the original target displacement used for design.

Introduction

Performance-based design (PBD) aims to improve performance by defining performance criteria that must be satisfied at more than one earthquake level. Generally, better performance is expected for important structures and smaller earthquakes, while lower levels are required for ordinary structures and more rare events. Performance is no longer related to collapse prevention or life safety only; deformations, functionality, economic losses, and downtime are additional criteria (Mackie and Stojadinovic, 2007; Mackie et al., 2010). Yet, there is a question as to whether the PBD procedure actually results in a structure that meets the performance objectives.

PBD explicitly considers how a structure is likely to perform. The performance assessment requires detailed analysis because it becomes an intrinsic part of the design process. A good preliminary design will reduce or eliminate the need for iteration required to meet the performance objectives. Design procedures that are useful within this framework must: (i) Take any combination of earthquake level and performance criteria; (ii) Produce a design that meets the target performance; (iii) Be rational and easy to execute. Both force-based and displacement-based procedures are potential design methodologies for applicability as PBD tools; however, each with differing merits in terms of the three criteria listed above.

Regardless of the design methodology adopted; however, design should be carried out considering the following. First, seismic resistant bridges should have a

¹ Assistant Professor, Department of Civil, Environmental, and Construction Engineering, University of Central Florida, Orlando FL 32816-2450, USA.

² Director UCG, Universidad Tecnica Particular de Loja, Loja, Ecuador.

³ Assistant Professor, Department of Civil Engineering, University of Toronto, Toronto ON M5S 1A4, Canada.

simple configuration, such that their behavior can be easily modeled and analyzed. The chosen configuration should also aim to include energy dissipation in different components of the structure with ductile mechanisms. Second, in conventional bridges, pier columns provide the primary energy dissipation mechanism, while abutments can provide additional energy dissipation (Priestley et al., 1993). Recommended earthquake resisting systems for bridges are given in the Guide Specifications for LRFD Seismic Bridge Design (AASHTO, 2009). Finally, capacity design principles must be applied in all cases to protect the components outside the ductile mechanism and to prevent non-ductile modes such as shear.

Force-Based Design (FBD) and Displacement-Based Design (DBD)

Seismic design of bridges can be accomplished following different approaches. The traditional procedure is force based since damage in the structure is controlled by the assignment of a certain level of strength. The procedure uses strength reduction factors to reduce the elastic force demand while considering importance, assumed ductility capacity, over-strength and redundancy in the structure. FBD is found in the AASHTO LRFD Bridge Design Specification (AASHTO, 2004) and was first adopted by AASHTO in 1983 following recommendations of the Applied Technology Council (ATC, 1981).

There are several problems attributed to FBD. First, strength is used as a means to control damage, although these parameters do not correlate well. Second, it is assumed that strength and stiffness are independent. Third, force reduction factors (R) are used assuming that the ductility demand will be the same for each type of structure. Finally, the R factors are given generally for a single level “no-collapse” design. Multi-level design would require the specification of different R values.

After the Loma Prieta earthquake in 1989, extensive research has been conducted to develop improved seismic design criteria for bridges, emphasizing the use of displacements rather than forces as a measure of earthquake demand and damage in the structure. Research has also focused on the application of capacity design principles to assure ductile mechanisms and concentration of damage in specified regions. Several DBD methodologies have been developed including:

- Direct Displacement Based Design (DDBD) (Priestley, 1993)
- MCEER/ATC-49 Recommended LRFD guidelines for seismic design of bridges (ATC, 2003)
- Seismic Design Criteria (SDC) of Caltrans (Caltrans, 2004)
- Guide Specifications for LRFD Seismic Bridge Design (AASHTO, 2009)

DBD has gained popularity in the last fifteen years, as it addresses several shortcomings of the conventional FBD procedure, while serving as a useful tool for performance-based seismic design. The primary difference between DBD and FBD is that the former uses displacement as a measure of seismic demand and also as an indicator of damage in the structure. DBD takes advantage of the fact that displacement correlates better with damage than force. DBD also overcomes serious problems of FBD such as ignoring the proportionality between strength and stiffness

and the generalization of ductility capacity through the use of force reduction factors. DBD can be used with any combination of earthquake level and performance criteria.

Both conventional DBD and direct DBD are compared briefly below; however, DDBD is selected as the design procedure for the case studies presented in this paper. The primary differences in the AASHTO (2009) LRFD procedure and DDBD are linearization and the execution. The displacement demand assessment procedure in the AASHTO LRFD Seismic guide uses elastic analysis and the equal displacement approximation (Veletsos and Newmark, 1960) to obtain inelastic displacement demands (an amplification factor is used with short period structures). In the elastic analysis the structure is modeled with cracked section stiffness. DDBD uses the equivalent linearization to overcome the limitations of the equal displacement approximation (Suarez, 2008). In execution, the AASHTO LRFD uses a demand/capacity assessment procedure. In contrast to this, DDBD goes directly from target performance to required strength. The amount of reinforcement does not need to be assumed during design.

Conventional Displacement-Based Design approach

The Seismic Design Criteria by Caltrans (2004) shifted towards displacement-based design in 1999 by consolidating ATC-32 recommendations (ATC, 1996). Currently, Caltrans has an iterative design procedure in which the lateral strength of the system (size and reinforcement of the substructure sections) is assumed at the beginning of the process. Then, by means of displacement demand analysis and displacement capacity verification, it is confirmed that the bridge has an acceptable performance, otherwise, the strength is revised and the process repeated.

In the demand analysis, the peak inelastic displacement demands are estimated from a linear elastic response spectrum analysis of the bridge, with cracked (secant to yield point) component stiffness. Then, elastic peak displacements are converted to peak inelastic displacements using an equal displacement approximation (Veletsos and Newmark, 1960) with modification for short period structures. Once the displacement demands are estimated, the procedure requires the verification of the displacement capacity of each pier by means of a pushover analysis. Finally, the substructure sections and protected elements are designed and detailed according to capacity design principles.

The AASHTO Guide Specifications for LRFD Seismic Bridge Design (2009) recognizes the variability of seismic hazard over the US territory and it specifies different Seismic Design Categories (SDC). Each SDC links seismic hazard to expected performance. The design procedure in the AASHTO DBD approach is in concept similar to the Caltrans approach. Depending on the configuration of the bridge, the demand analysis is performed by the uniform load method for regular bridges, while spectral modal analysis can be used for all bridges. The capacity verification can be done using implicit equations for seismic design category B or by pushover analysis for categories C and D. As with the Caltrans approach, and with the exception of seismic category A, the proposed guide requires the use of capacity

design principles for the detailing of the substructure sections and protected elements.

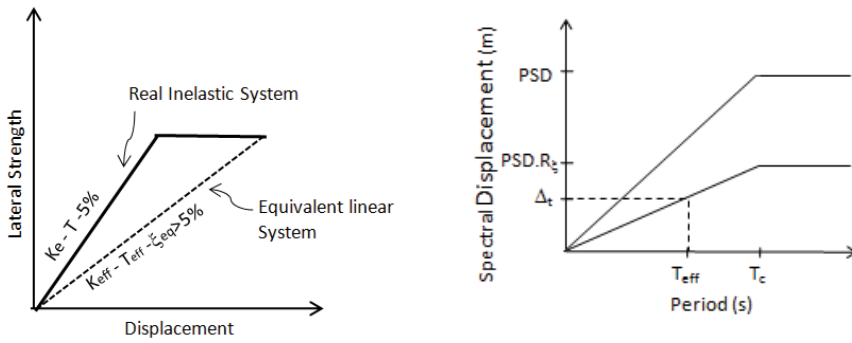
Current Caltrans and AASHTO approaches utilize acceleration spectrum curves to determine the displacement demand at the system level. The main limitations of this approach are:

- The use of the equal displacement approximation. Research conducted on displacement modification factors (FEMA 440, 2005) has shown that the ratio between inelastic and elastic displacement depends on period, hysteresis shape, and other factors. In addition to this, assuming that the elastic displacement demand equals the inelastic demand is not appropriate when additional damping exists in the structure as a result of soil-structure interaction or other sources.
- The use of acceleration response spectrum to compute displacement demand. The displacement spectrum seems a more rational source of seismic hazard for DBD.
- The procedure is iterative in nature since reinforcement in the pier sections must be guessed at the beginning of design. If the displacement capacity is ultimately less than the displacement demand, the process must be repeated increasing the amount of reinforcement. If the inverse occurs, no iteration is needed; however, the resulting design will be overly conservative.

Direct Displacement Based Design (DDBD)

DDBD has been conceived as a tool to achieve deterministic PBD, as a simple methodology that can be used to go from basic geometry to properly detailed sections and structural components. Research conducted in the last fifteen years have shown the method produces satisfactory bridge designs (Kowalsky et al., 1995, Calvi and Kingsley, 1995, Dwairi et al., 2006, Suarez and Kowalsky, 2007, Priestley et al., 2007), however a formal reliability study has not been yet conducted and the use of DDBD within the scope of probabilistic PBD requires further research. The DDBD method was initially proposed by Priestley (1993). In its current state, DDBD works with any combination of seismic hazard and performance criteria, and it is intended to produce structures that meet (theoretically in the mean), rather than be bounded by, the target performance. This makes DDBD a very attractive alternative for preliminary design since it reduces, and in some case might eliminate, the need for iteration in a general PBD procedure.

DDBD differs from the DBD procedure in the AASHTO Guide Specifications for LRF Seismic Bridge Design in the use of an equivalent linearization approach and in the execution of the procedure. DDBD starts with the definition of a performance-based target displacement for the structure and returns strength required to meet the target displacement under the specified earthquake. The method is referred to as “direct” since, in contrast to the traditional DBD procedure of AASHTO or Caltrans, the reinforcement and thus the strength of the structure does not need to be assumed at the beginning of the design and modified iteratively until a demand/capacity check is satisfied.



(a) Equivalent Linearization (b) Displacement Spectrum

FIGURE 1 - Fundamentals of DDBD

DDBD uses an equivalent linearization approach (Shibata and Sozen, 1976) where an inelastic system at maximum response is modeled by an equivalent elastic system with secant stiffness (K_{eff}) and equivalent viscous damping (ξ_{eq}) (FIGURE 1a). A design objective must be defined as a combination of a performance criterion and design earthquake. The performance can be specified in terms of material strains, curvature, drift, or ductility in the piers. In all cases, consideration of abutment displacements as a limit state, as well as P-Δ effects of bridge piers should also be addressed. The design objectives can also be those stated for each SDC in the AASHTO LRFD Seismic Guide Specification. The design earthquake is represented by a displacement spectrum that is reduced to the level of damping of the structure (FIGURE 1b).

In most cases DDBD can be applied with simple hand calculations. Modal spectral analysis or pushover analysis are not required. A major limitation of this approach is the target displacement can only be estimated for simple pier configurations (the most common at least). Since a pushover analysis is not carried out, the flexibility of cap beams and rotation of foundations (for example) cannot be incorporated without some iteration. In addition, the procedure is direct (no iteration) only when the shape of the displacement profile is known. This scenario occurs only in bridges with regular distributions of mass and stiffness. Curved bridges are design as straight.

Analysis Procedure

A DDBD procedure is carried out for four bridge case studies in this paper. A location is selected in the central United States to define an equal hazard spectrum for all four case studies, except for the final bridge structure that has a higher design spectrum. After a target displacement is selected for each structure based on appropriate limit state definitions (specific to reinforced concrete bridges), the performance of the case study structures was assessed using nonlinear time history analysis (THA) with recorded ground motions. The probabilistic assessment allows confirmation of whether the target displacement is achieved in the mean, reflecting an unbiased design procedure. Due to the assumptions surrounding the DDBD procedure, meeting the performance objective in the mean is unlikely; therefore, this

paper investigates whether the design procedure can be formulated to achieve a conservative design. Above and beyond this, it is demonstrated that under a given performance objective and probabilistic acceptance criterion, a modifier on the initial design displacement can be specified so that the procedure retains the advantages of being non-iterative (see FIGURE 2).

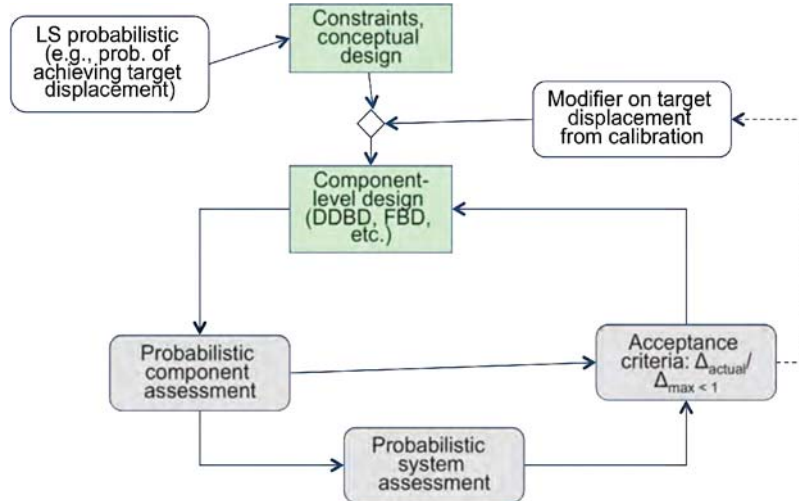


FIGURE 2 - Probabilistic considerations in DDBD and assessment

A complicating factor for nonlinear assessment of structures designed according to DDBD is that bridges are inherently three-dimensional (3D) systems. Two important phenomena are illustrated in the case studies presented in this paper: 1.) 3D excitation and response impact performance in ways that are difficult to account for in only longitudinal or transverse simplifications (or combination rules), and 2.) the bridge responds as a system, with contributions from several load-resisting components such as shear keys, abutments, foundations, and the superstructure itself. Therefore, assessment often yields different response quantities than the initial design. The choice of assessment procedure and degree of model complexity also influence agreement between design and assessment. Allowance for different assessment techniques (linear dynamic, nonlinear static, nonlinear dynamic, etc.) should be considered when proposing any modification factors on the initial target displacement; however, only nonlinear THA is considered in this paper.

Hazard, DDBD, and Case Study Details

A site near the New Madrid seismic zone was selected (-90.196, 35.212). Multi-level hazards are defined based on USGS seismic hazard maps. Spectral acceleration curves were generated for three hazard levels: 10%--, 5%--, and 2%-probability of exceedance in 50 years and 5% equivalent viscous damping. The acceleration spectra were converted to displacement spectra and then linearized (relationship between T and Sd). The peak spectral displacement was assumed to occur at the corner period of 3 sec. Based on extrapolation of the Sd curve, the Sd at corner period are 5.76, 16.1, 33.4 (cm) for each of the three hazard levels. The spectral displacement hazard at the 2% probability of exceedance in 50 year level was

raised to 72 cm for the bridge in case study as it was originally designed for a site in California with substantially higher hazard.

Once the design objective has been selected, the main steps of the DDBD procedure are: (i) Select the dimensions of the components of the earthquake resisting system on the basis of past experience. (ii) Compute a target displacement based on the performance level for the structure. Depending on whether this is specified as a strain, ductility, etc., it may be necessary to use a plastic hinge model to relate these to peak displacements. (iii) Evaluate the effective mass and equivalent viscous damping for the system. Priestley et al. (2007) defined a ductility vs equivalent damping relationship. (iv) Compute the spectral reduction factor that corresponds to the equivalent damping level in the structure and find a reduced design spectrum. The spectral reduction factor for inelastic structures is based on Eurocode (1998). (v) Determine the required effective period, secant stiffness and required strength. (vi) Distribute the required strength, design plastic hinges and protected elements using capacity design principles.

The four case studies considered in this paper are: 1.) a single-degree-of-freedom elasto-plastic oscillator, 2.) a two-dimensional reinforced concrete bridge bent with a single column subject to transverse excitation, 3.) the same two-dimensional bridge bent subject to both lateral and vertical excitation, and 4.) a 3D reinforced concrete bridge with 3 continuous spans and explicit foundation and abutment representations.

Case Study 1: Single-degree-of-freedom (SDOF) system

The SDOF system was selected as the simplest case of design where the period of the structure (both loading and unloading) is constant and the yield point defines the perfectly plastic plateau. Therefore, the only unknowns are the period and the yield strength. A factor of 55 was used in the expression for equivalent damping of the elasto-plastic system. The benefit of using a SDOF oscillator is that it is not necessary to use nonlinear THA to assess the performance of the system, other approximate techniques can be readily used (such as R- μ -T relationships). The oscillator was assumed to have a yield displacement of 0.05 m (typically the yield displacement is obtainable from the structure's geometry) and a target ductility of 4. For the 2%-in-50-year hazard defined previously, the effective period becomes 3.28 sec and the target strength is 0.73 kN.

The properties of the oscillator were then used in two separate analyses. The first was to use a common relationship between R- μ -T to obtain the achieved ductility at the target spectral displacement. The second was to perform inelastic THA with the specified oscillator properties. A total of 160 ground motions were scaled to the target spectral displacement before performing the analysis and the distribution of achieved maximum displacements is shown in FIGURE 3 below. The individual ground motion realizations are shown in the top pane of the figure while the cumulative distribution function (CDF) is shown in the bottom pane. The actual time history CDF is shown with lower (LCB) and upper (UCB) bound indicators. Finally, the data is

assumed to follow a lognormal distribution and two parameters are estimated using maximum likelihood.

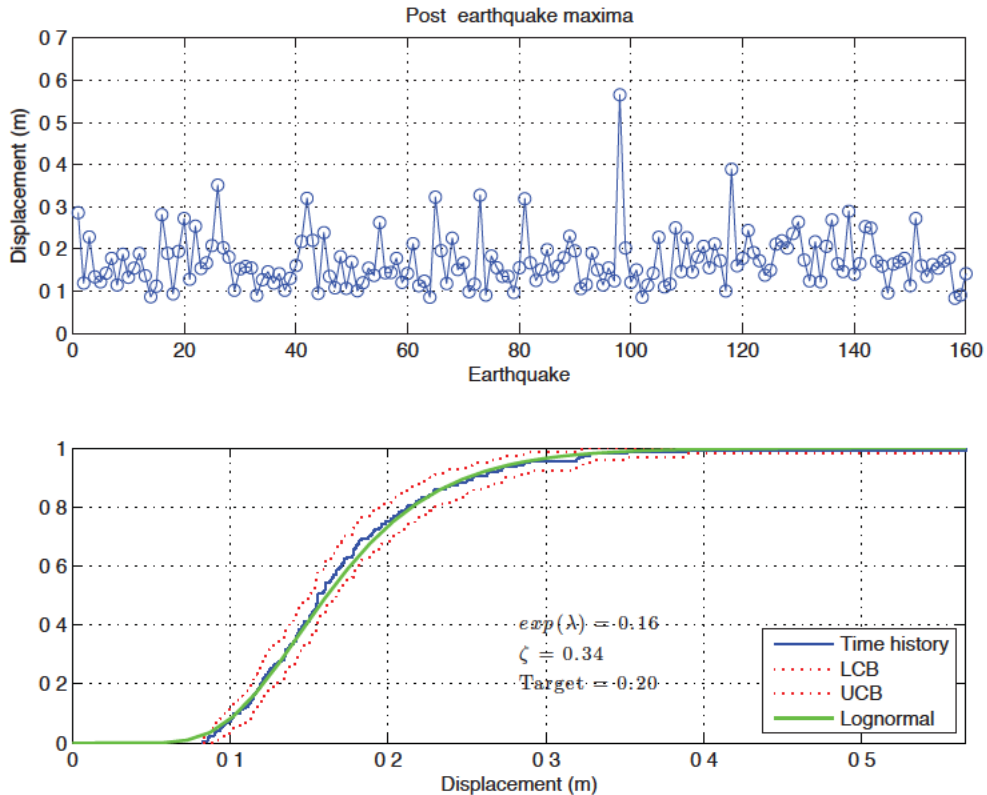


FIGURE 3 - Response statistics for SDOF oscillator in Case study 1

The mean displacement from the R- μ -T and THA analysis methods were 0.17 and 0.17 m, respectively (the THA mean was obtained from the method of moments considering the fitted lognormal parameters). An equivalent statement is that a system with 15% less strength (than that required by DDBD) would be required to exactly produce the target displacement. The R- μ -T relations provide only mean or central value information, but the THA provides the actual distribution of responses. It can be observed that the probability of exceeding the target design displacement is 0.26.

Case Study 2: Single bent with transverse excitation

A regular two-lane RC box girder bridge with single column piers that are integral with the superstructure is selected for a more realistic case study (FIGURE 4). The piers are supported on a rigid pile group. The spans are 50 m long and the weight of the superstructure is 180 kN/m. The bridge is assumed to behave like a SDOF system, but exhibits material and geometric nonlinearity typical of a reinforced concrete structure rather than an idealized bilinear elasto-plastic material. The height is 6 m (pier) + 0.8 m (rigid within superstructure to center of mass), and the column diameter is 1.3 m. Other values that were assumed for the analysis and design are: expected concrete compression strength (f_{ce}) 45000 kPa, expected yield strength of

main reinforcement (f_y) 462000 kPa, expected yield strength of transverse reinforcement (f_{ys}) 462000 kPa, diameter of longitudinal bars (d_b) 32 mm, diameter of spiral (d_{bs}) 22 mm, pitch of spiral (s) 100 mm, and 50 mm cover to main reinforcement. The design assumptions result in a volumetric spiral ratio (ρ_s) of 0.013 and an axial load ratio (ALR) of 0.154.

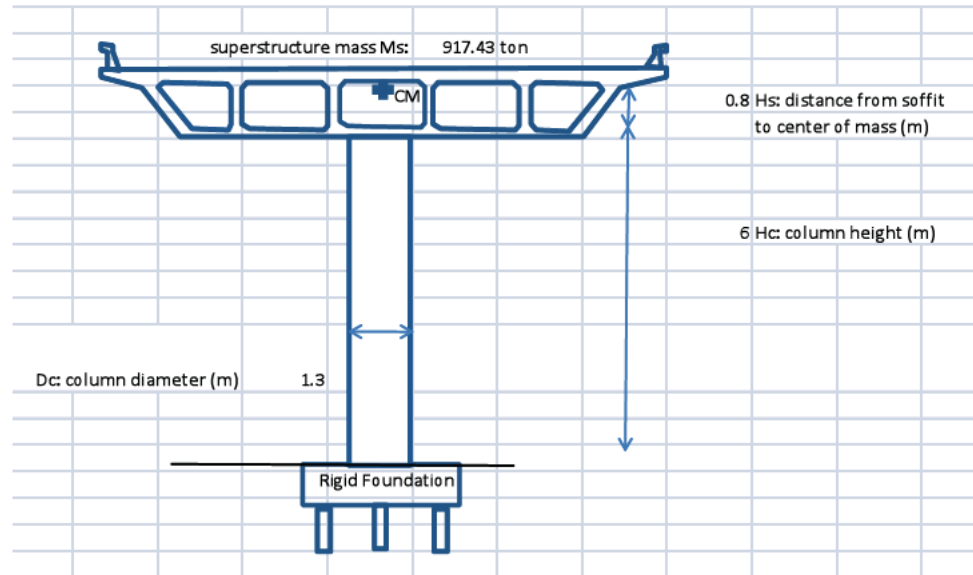


FIGURE 4 - Design schematic for single-column bent transverse analysis case study

The target displacement was defined by the drift ratio required for initiation of spalling, as defined by Berry and Eberhard (2003), or 0.13 m. Nonlinear THA was performed on the bent using 160 ground motions scaled to the spectral displacement demand at the initial elastic period. The initial elastic period was calculated after gravity load analysis but without any equivalent linearization or secant approximations. As with the SDOF oscillator, the distribution of maximum displacements were obtained and plotted in FIGURE 5. The mean achieved displacement is 0.11 m and the probability of exceeding the target displacement is 0.27.

Case Study 3: Single bent with transverse and vertical excitation

The same reinforced concrete bent from the previous case study is reused, but an additional two components of excitation were added. The case study demonstrates the effects of varying axial loads and potential P- Δ effects without the need for combination rules; however, is only a simple extension as it does not consider rotational inertia or boundary conditions at the top of the column. For ground motion amplitude, the design spectrum was treated as the geometric mean of the two lateral components. The response metric was taken as the maximum of the instantaneous vector combination of the two orthogonal lateral components (known as the square-root-sum-of-squares). While (as expected for circular columns) the response is very similar to the previous case study, the mean achieved displacement increased slightly to 0.14 m (FIGURE 6). This increase brings to the probability of exceeding the target

displacement to 0.50, but is more representative of the difference in the lognormal fit to the data than the actual change in the mean. The change in shape in the distribution is indicative of several larger displacement realizations obtained from bidirectional displacement orbits.

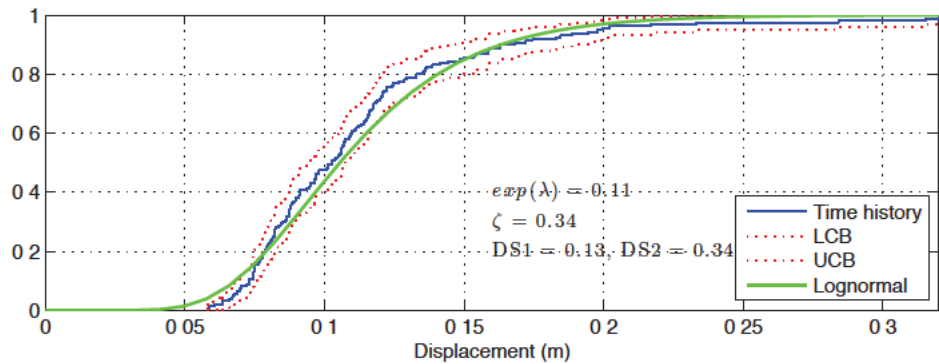


FIGURE 5 - Distribution of maximum transverse displacements for Case study 2

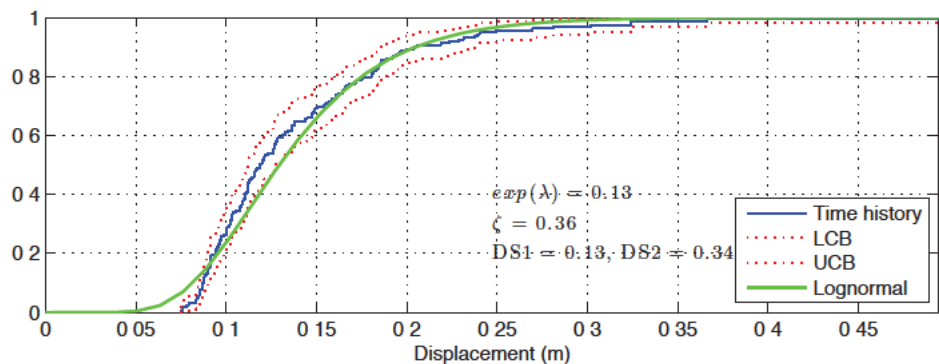


FIGURE 6 - Distribution of maximum SRSS displacements for Case study 3

Case Study 4: Typical three-span California bridge

The problem is generalized to a 3D case (both structure and excitation) to assess the effect of multiple components (lateral) of excitation and response, as well as the impact of system performance on components design according to the DDBD procedure. Explicit representations of the stiffness and strength of the abutments and superstructure are included in the assessment model. The case study is taken directly from the LRFD design example (AASHTO, 2006) for a bridge typical to California that falls into SDC D. Conventional DBD was performed for this bridge in the example and subsequently DDBD was also performed on the same structure (Suarez and Kowalsky, 2010). The DDBD detailing to achieve a target displacement of 0.64 m is used for assessment in this case study.

The bridge has three spans of 38.41, 51.21, and 35.98 m with a continuous prestressed reinforced concrete box girder superstructure, as shown in FIGURE 7.

The two bents are skewed 20 degrees and have two 1.83 m diameter columns supported on piles (FIGURE 8). Column height varies from 13.4 m at bent two to 14.3 m at bent three. The columns are pinned at the bottom and fixed to an integral bent in the superstructure. The bridge is founded on seat type abutments with elastomeric bearings and a break-off wall once the gap closes in the longitudinal direction. Exterior shear keys prevent transverse motion under lower intensity motions and service loads. The superstructure is capacity designed to remain elastic at the target displacement and is therefore modeled using an elastic section with cracked properties. No explicit representation of the tendons or mild steel was created in the analytical model.

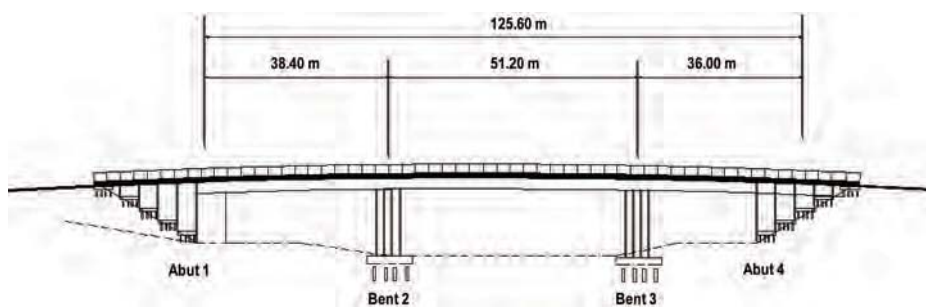


FIGURE 7 - Elevation of 3-span continuous case study bridge (Suarez and Kowalsky, 2010)

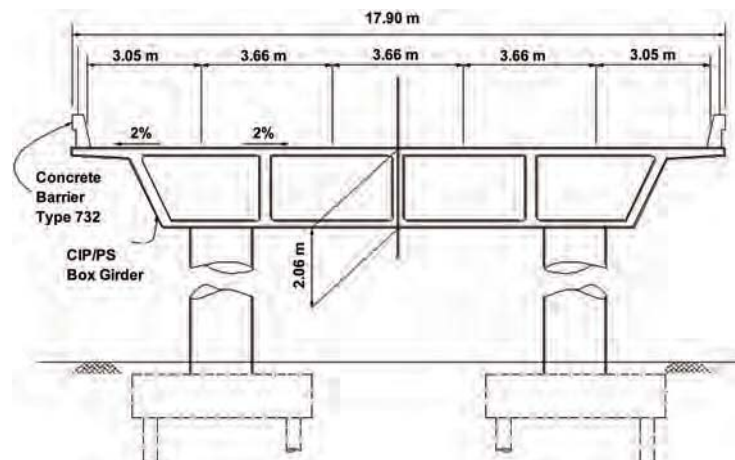


FIGURE 8 - Bent configuration and superstructure cross section for 3-span continuous case study bridge (Suarez and Kowalsky, 2010)

The expected concrete compression strength was 36000 kPa, expected yield strength of main reinforcement 455000 kPa, diameter of spiral 25 mm, pitch of spiral 125 mm, and 50 mm cover to main reinforcement were consistent with the DDBD design. The superstructure elastic properties were obtained from the LRFD design example appendix and were factored by 0.5 for cracked moment of inertia and 0.25 for cracked torsional constant. The bent cap is modeled explicitly and also contains cracked elastic properties based on initial gross dimensions. The two columns per

bent are modeled with a rigid extension into the bent cap where the elements for the superstructure are placed at the center of gravity. An integral diaphragm at the abutments allows for the placement of abutment spring elements at the transverse extremes of the superstructure cross section. To be consistent with the design assumptions, both the longitudinal and transverse abutment responses were assumed elasto-plastic. The longitudinal response is mobilized only in compression (movement of the deck into the backwall). Due to the skew of the bridge, the abutment springs were aligned parallel and perpendicular to the abutment diaphragm (not in the global bridge longitudinal direction).

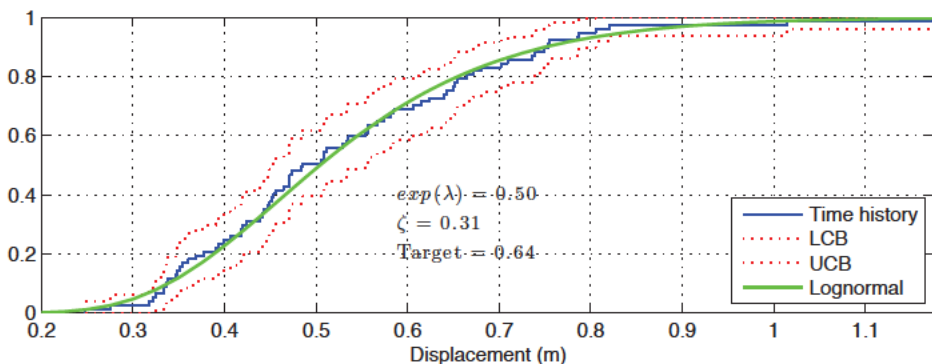


FIGURE 9 - Three-span bridge maximum SRSS displacements for Case study 4

A total of 80 ground motions were used for nonlinear THA. The CDF of maximum response is shown in FIGURE 9. The mean response was 0.53 m and the probability of exceeding the target displacement was 0.22. Similar to the previous case studies, the DDBD target displacement is conservative to the maximum response achieved using nonlinear THA. However, in the previous case studies it was possible to control for many variables that potentially differ between DDBD and analysis. This more realistic case study contains complete 3D nonlinear element interaction, 3D excitation, nonlinear geometry, and 3D response. In addition, the bents are skewed, causing interaction between the longitudinal and transverse bridge directions. Assumptions were also made on the analytical side, such as not explicitly representing the foundations or the fill above the pile caps, the tendons and axial forces in the superstructure, the mild steel and concrete nonlinearity in the box girder and bent cap, selection of equivalent viscous damping and damping model, period selected to decide scale factor for each ground motion, and shear deformations and any other non axial-flexural modes.

Design for Target Performance Objective

While this paper has yet to fully characterize the reliability of the DDBD procedure, it does provide some insight into the target vs achieved displacements for a variety of bridge structures. Based on the consistency of the results, it was postulated that the probability of exceeding the target displacement could be specified apriori as part of the performance objective for design. For example, for Case study 1, if the target displacement is 0.2 m and the maximum permissible probability of exceedance

is 50% (most likely too high from a risk perspective), then the inverse problem can be solved. A modifier on the target displacement (0.28 m) will result in a new period and required strength (0.523 kN). Assessment of this modified system yields a mean displacement of 0.2 m. For the SDOF system, this phenomenon is easily explored analytically using the expression for spectral factor based on the equivalent damping. Continuing work will demonstrate the relationship between the distribution of this parameter and the resulting responses. The numerical level of conservatism (and therefore the ability to achieve target risk levels for each displacement) will be demonstrated and related to the brief inverse problem described in this section. It is also worth noting that as the target displacement (with modifier) is increased, the selection of recorded ground motions that meet the target spectral displacement for design diminish. Therefore, scale factors on ground motion amplitude are used that would likely cause a bias in the observed response distribution.

Conclusions

This paper investigates performance-based assessment of the direct displacement-based design (DDBD) procedure. Four case studies were selected ranging from an elasto-plastic oscillator to a three-span continuous prestressed concrete box girder bridge. Each case study was designed using DDBD for a specified hazard level. Subsequently, a nonlinear time history analysis was conducted to assess the performance of each, or more specifically, the probabilistic distribution of peak displacement responses in reference to the original target displacement used for design. It is demonstrated that, consistent with earlier findings, the DDBD leads to a slightly conservative design whereby the target displacement is exceeded less than 50% of the time. In all the case studies (except Case 3), the probability of exceeding the target displacement is approximately 25%. It was demonstrated that this information enables a modifier to the original target displacement to achieve a specified risk level (acceptable probability of exceeding target displacement) without iteration. Further work is necessary to determine the nature of the response distribution for different structure types and modeling assumptions before such a technique can be used more broadly to achieve performance-based design objectives.

References

- AASHTO, 2006, LRFD Design Example B November 3, 2006 – Version 1.1, <http://cms.transportation.org/?siteid=34&pageid=1800>, (accessed April 18, 2008).
- Berry, M.P., and Eberhard, M.O., 2003, Performance models for flexural damage in reinforced concrete columns, Report No. 2003/18, Pacific Earthquake Engineering Research Center, University of California Berkeley.
- Calvi G.M. and Kingsley G.R., 1995, Displacement based seismic design of multi-degree-of-freedom bridge structures, *Earthquake Engineering and Structural Dynamics*, 24, 1247-1266.
- Dwairi, H. and Kowalsky, M.J., 2006, Implementation of inelastic displacement patterns in direct displacement-based design of continuous bridge structures, *Earthquake Spectra*, 22(3), 631-662.
- EuroCode 8, 1998, Structures in seismic regions – Design. Part 1, General and

Building”, Commission of European Communities, Report EUR 8849 EN

Kowalsky M.J., Priestley M.J.N. and MacRae G.A. 1995. Displacement-based design of RC bridge columns in seismic regions, *Earthquake Engineering and Structural Dynamics*, 24, 1623-1643.

Mackie, K.R., and Stojadinovic, B. 2007. Performance-based seismic bridge design for damage and loss limit states. *Earthquake Engineering and Structural Dynamics*, 36(13), 1953-1971.

Mackie, K.R., Wong, J-M., and Stojadinovic, B. 2010. Post-earthquake bridge repair cost and repair time estimation methodology. *Earthquake Engineering and Structural Dynamics*, 39(3), 281-301.

Priestley, M. J. N., 1993, Myths and fallacies in earthquake engineering-conflicts between design and reality, *Bulletin of the New Zealand Society of Earthquake Engineering*, 26 (3), 329–341.

Priestley, M. J. N., Calvi, G. M. and Kowalsky, M. J., 2007, Direct Displacement-Based Seismic Design of Structures, Pavia, IUSS Press.

Shibata A. and Sozen M. Substitute structure method for seismic design in R/C. *Journal of the Structural Division, ASCE* 1976; 102(ST1): 1-18.

Suarez, V.A. and Kowalsky, M.J., 2007, Displacement-based seismic design of drilled shaft bents with soil-structure interaction, *Journal of Earthquake Engineering*, 11(6): 1010 – 1030.

Suarez, V.A., 2008, Implementation of direct displacement-based design for highway bridges, PhD Dissertation, North Carolina State University.

Suarez, V.A. and Kowalsky, M.J., 2010, Direct Displacement-Based Design as an Alternative Method for Seismic Design of Bridges, ACI Special Publication, SP-271(4): 63 - 78.

Veletsos, A. and Newmark, N. M., 1960, Effect of inelastic behavior on the response of simple systems to earthquake motions”, *Proceedings of 2nd World Conference on Earthquake Engineering*, pp. 895 – 912.

LOCAL BUCKLING ANALYSIS OF STEEL TRUSS BRIDGE UNDER SEISMIC LOADING

Eiki Yamaguchi¹, Keita Yamada²

Abstract

In the 2004 Mid Niigata Prefecture Earthquake, a steel truss bridge was damaged: the lower chord member underwent local buckling. The axial force in that member is not necessarily compression-dominant: tensile axial force is also expected. Since many steel bridge piers were subjected to local buckling in the 1995 Kobe Earthquake, the criterion for local buckling in the member under axial compression has been studied rather extensively. However, the local buckling in the member under the other states of axial force has not. In the present study, the local buckling in the lower chord member of a truss bridge is to be looked into. To that end, the existing criterion for local buckling in terms of average strain is tested for the case when tensile yielding precedes compression, failing to confirm its applicability. Then the criterion is modified by introducing the updated average strain. The seismic response analysis is then conducted to show the significance of the proposed criterion.

Introduction

One of the largest earthquakes in the recorded history, the Tohoku Earthquake, just hit Japan in March, 2011, causing very serious damage in the eastern part of Japan. Yet the memory of the damage to structures in the 1995 Kobe Earthquake is still fresh and vivid for many structural engineers. Between the two large earthquakes, numerous earthquakes occurred as well, some of which were quite large and comparable to the 1995 Kobe Earthquake. The damage in each big earthquake has posed a new challenge for engineers; some of them are yet to be solved.

In the 2004 Mid Niigata Prefecture Earthquake, a steel truss bridge was damaged: the lower chord member underwent local buckling at its fixed end. The axial force in that member is not necessarily compression-dominant: tensile force can be expected. Since many steel bridge piers experienced local buckling in the 1995 Kobe Earthquake, the criterion for local buckling in the member under axial compression has been studied rather extensively (Ono et al. 2007, Committee 2008). However, the local buckling of the member under the other states of axial force has not. In the present study, the local buckling in the lower chord member of a truss bridge is to be looked into.

Existing Criterion for Local Buckling

Local buckling can be simulated in the finite element analysis (FEA) with shell

¹ Professor, Dept. of Civil Engineering, Kyushu Institute of Technology, Kitakyushu

² Graduate Student, Dept. of Civil Engineering, Kyushu Institute of Technology, Kitakyushu

elements. Even though it is not impossible to model the whole bridge by shell elements and conduct nonlinear dynamic FEA, that is not a practical approach to structural design; beam elements are employed exclusively for the analysis of seismic design. However, since the cross section of a beam element does not deform, the direct simulation of the local buckling by beam elements is not possible. To overcome the difficulty, various efforts have been made, which includes the detection of the local buckling by the magnitude of strain (Ono et al. 2007, Committee 2008) and the implementation of strength reduction due to local buckling in the constitutive relationship (Yamaguchi 2009).

The criterion of the local buckling due to Committee (2008) is based on the average strain ε in a compressive flange over the characteristic length L_C . For a box-section member, the characteristic length L_C is given by

$$L_C = \text{Min}(0.7b, a) \quad (1)$$

where a is the distance between two adjacent diaphragms and b the width of a flange. Min indicates that the smaller of the two values in the parenthesis shall be taken. On the other hand, the limit strain ε_u for an unstiffened box-section member is computed by

$$\left| \frac{\varepsilon_u}{\varepsilon_y} \right| = \frac{0.24}{(R_f - 0.2)^{2.8} (1 + N_c/N_y)^{2.4}} + \frac{2.8}{(1 + N_c/N_y)^{0.6}} \leq 20.0 \quad (2)$$

where ε_y is the yield strain, R_f the width-to-thickness ratio parameter, N_c the compressive axial load and N_y the squash load. The validity of the equation has been verified for $0.2 \leq R_f \leq 0.7$, $0.0 \leq N/N_y \leq 1.0$.

The criterion for the local buckling is then that the member is judged to undergo local buckling at the instance when the average strain ε reaches the limit strain ε_u . It is noted that N_c changes during earthquake so that the limit strain ε_u varies with time as well.

Equation 2 has been obtained under compressive loading applied monotonically. Therefore, the validity of Equation 2 is not clear if tensile yielding precedes compression. The investigation is needed herein since the lower chord member in a truss bridge may yield in tension.

To this end, a short box-section member shown in Figure 1 is constructed. It is pulled first and then compressed until local buckling occurs. This nonlinear problem is analyzed by ABAQUS (Dassault 2008) using 1280 shell elements: the local buckling can be simulated directly. The material is steel with Young's modulus E equal to $2.0 \times 10^5 \text{ N/mm}^2$ and the yield stress σ_y equal to 235 N/mm^2 . The stress-strain relationship is of a bilinear type with the slope after yielding being $E/100$ (Figure 2).

Six cases are considered, between which the difference lies in the initial

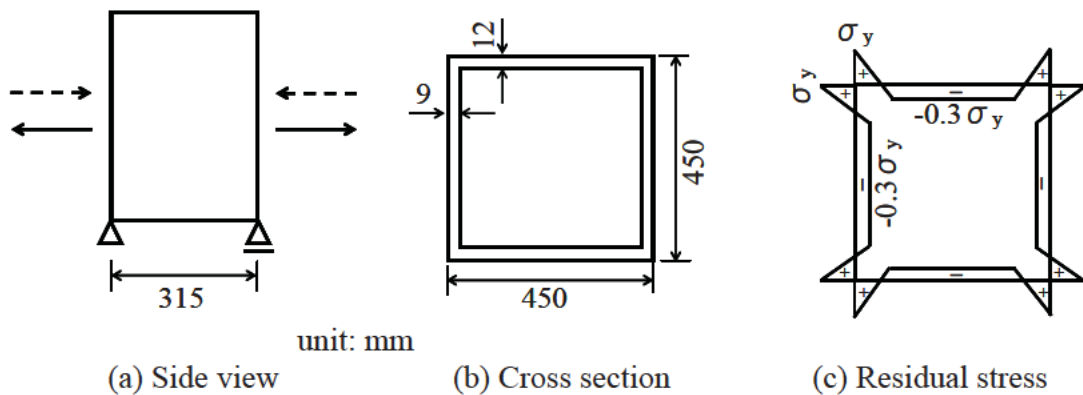


Figure 1 Short box-section member

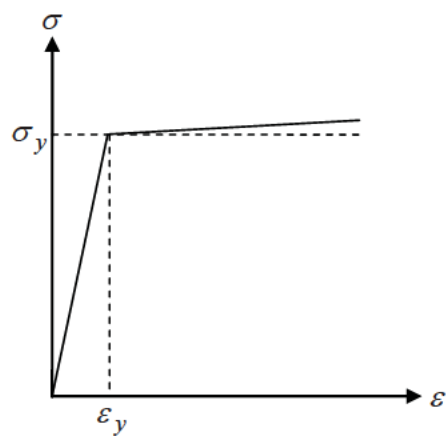


Figure 2 Stress-strain relationship of steel

elongation: the maximum initial tensile strain ε_t in the six cases are $\varepsilon_t = 2\varepsilon_y$, $3\varepsilon_y$, $4\varepsilon_y$, $5\varepsilon_y$, $7\varepsilon_y$, and $10\varepsilon_y$, respectively.

The average strain ε at the initiation of the local buckling in each case is presented in Figure 3. The limit strain ε_u is also given in the same figure. Note that the limit strain ε_u is common to all the cases since Equation 2 has nothing to do with the maximum initial tensile strain ε_t .

Significant difference between ε and ε_u is observed. When the initial elongation is large, the local buckling occurs, even when the average strain ε is still tensile. This result shows that the criterion with the average strain ε and the limit strain ε_u given by Equation 2 is not valid if tensile yielding precedes compression.

Proposed Criterion for Local Buckling

Once an elastic-plastic material yields, strain does not vanish even when all the loads are removed completely. However, upon reloading, the material behavior would be similar to that of the original material except that the subsequent yield point may be

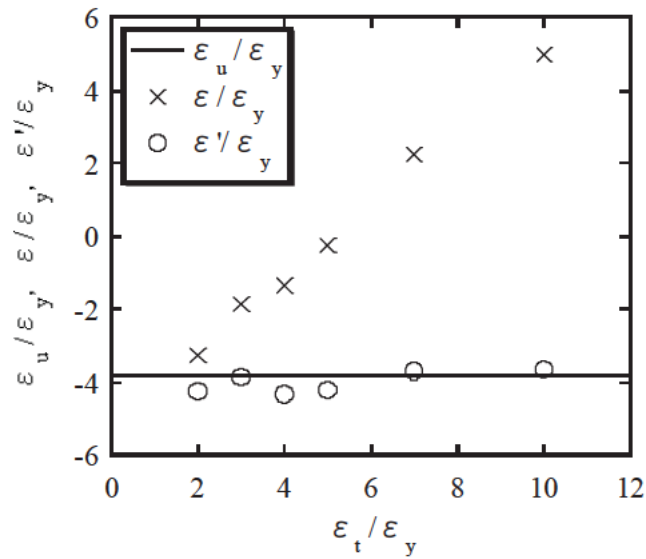


Figure 3 Average strain ε and updated average strain ε' at instance of local buckling after pre-yielding ε_t

different from the initial value according to the plasticity theory (Chen 1994).

Likewise, once a steel member elongates beyond the yield point, deformation remains even when all the loads are removed completely. Yet, the member behavior would be similar to that of the original member except that the subsequent yielding occurs at different loading level.

This observation suggests that instead of the average strain ε , the updated average strain ε' should be used for the comparison with the limit strain ε_u to see if local buckling occurs. The definition of the updated average strain ε' is given schematically in Figure 4: the origin of the updated average strain ε' is located at the state of the complete removal of stress.

To verify the validity, the updated average strain ε' at the instance of the local buckling is obtained in the analysis of the short box-section member for the six cases mentioned above. The results are presented in Figure 3. The updated average strains ε' at the local bucklings are in good agreement with the limit strain ε_u given by Equation 2.

It is then proposed that the updated average strain ε' instead of the average strain ε is to be compared with the limit strain ε_u in Equation 2 for the judgment on the initiation of local buckling. Needless to say, the proposed criterion is also good for monotonic loading, since the updated average strains ε' is nothing but the average strain ε under monotonic loading.

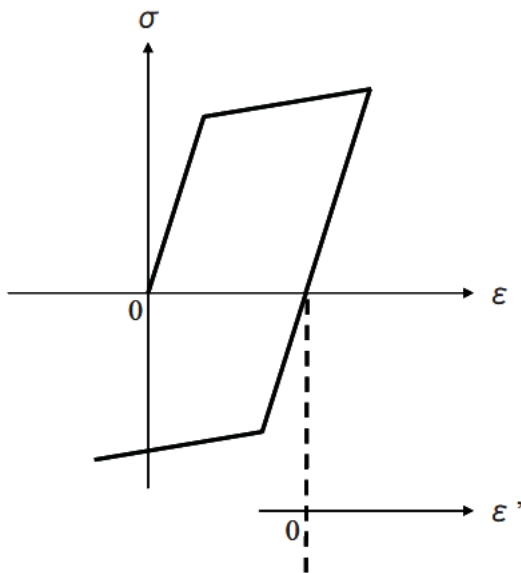


Figure 4 Schematic definition of updated average strain ε'

Seismic Response of Truss Bridge Model

Figures 5 and 6 show a truss bridge model to be analyzed in the present study. It is a simply-supported bridge with the length of 74.4 m. The bridge end denoted by A in Figure 5 is fixed longitudinally. The truss members are made of steel that has the same material properties as those of the short box-section member including the stress-strain relationship (Figure 2). The floor slab is concrete and 220 mm thick. Young's modulus of concrete is 1/7 of that of steel, and the stress-strain relationship is shown in Figure 7 where ε_0 is 0.002, ε_{cu} 0.0035, σ_{ck} 30 N/mm².

The time history of seismic acceleration in Figure 8 is applied. This is an actual seismic data recorded in the 2004 Mid Niigata Prefecture Earthquake. Dead load is also considered simultaneously.

Using the model mentioned above, nonlinear dynamic analysis is conducted by the finite element software Y-FIBER3D (Yamato 2000) to obtain the seismic response of the truss bridge.

Figure 9 (a) shows the numerical result where the average strain ε in the lower chord member near the bridge end A together with the limit strain ε_u is presented. Note that the cross section of the bridge end A is the same as that given in Figure 1 (b). The average strain ε fluctuates and is compressive from time to time at the initial stage, but tensile strain dominates at the later stage. The average strain ε and the limit strain ε_u do not cross, indicating that the local buckling does not occur if the average strain ε is used for the judgment.

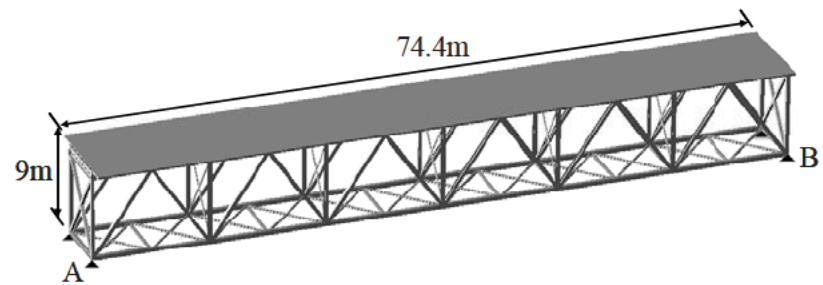
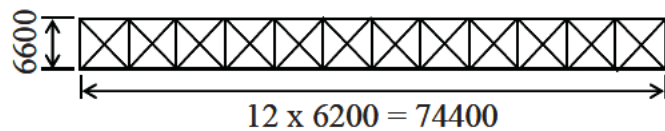
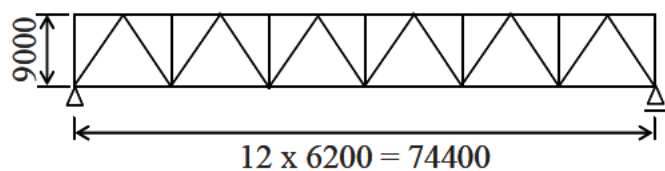


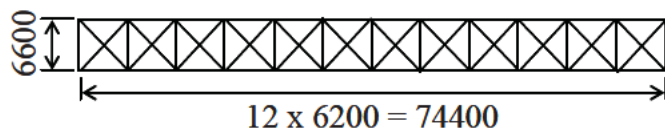
Figure 5 Schematic of truss bridge model



(a) Top view



(b) Side view



(c) Bottom view

Figure 6 Main truss (Unit: mm)

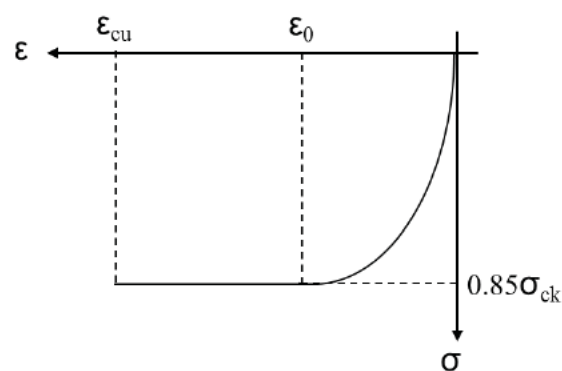


Figure 7 Stress-strain relationship of concrete

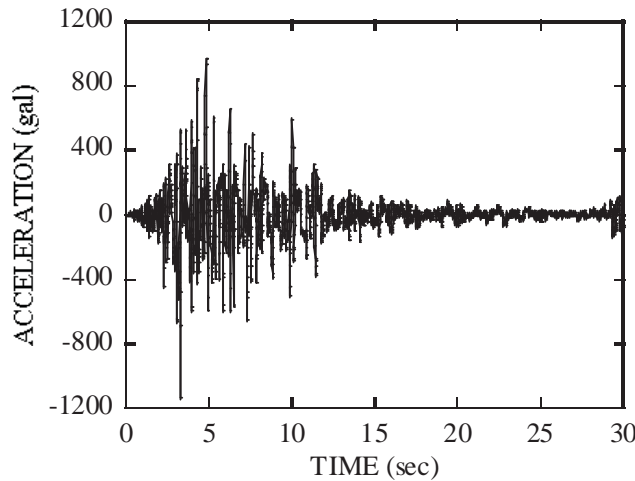


Figure 8 Acceleration recorded in 2004 Mid Niigata Prefecture Earthquake

The updated average strain ε' is plotted in Figure 9 (b). It is very different from the average strain ε in Figure 9 (a): the updated average strain ε' does meet the limit strain ε_u so that the local buckling is judged to take place. The significance of the proposed criterion is thus obvious.

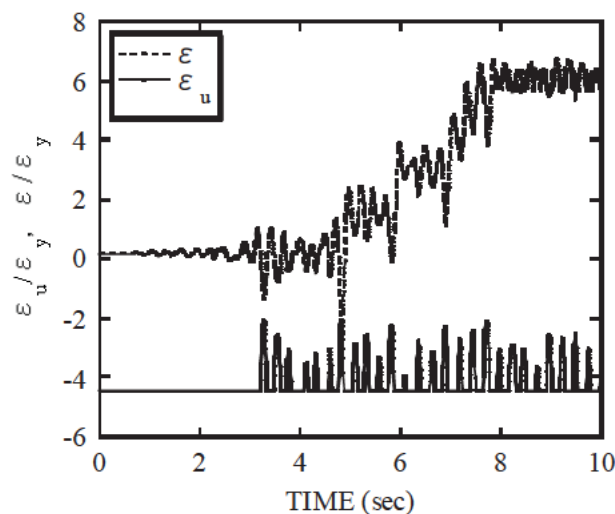
Concluding Remarks

When beam elements are employed for the seismic response analysis of a bridge, the criterion for local buckling is necessary. However, it has been concluded in the present study that when tensile yielding preceded, the existing criterion could not give the correct judgment.

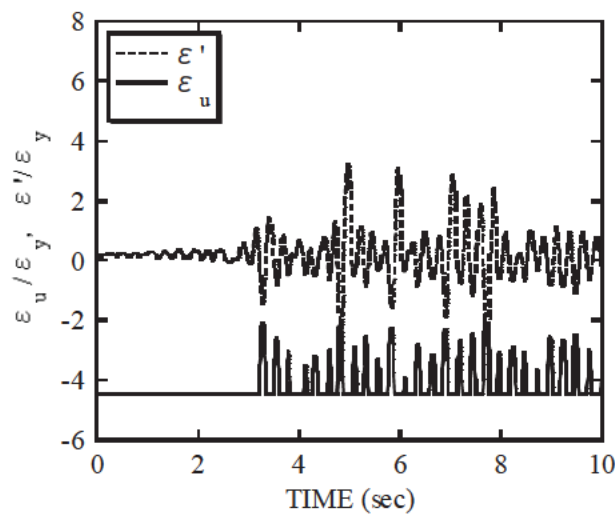
The modification of the criterion in which the average strain was replaced by the updated average strain has been proposed. The seismic response analysis of a steel truss bridge then demonstrated the significance of the proposed criterion.

References

- Chen, W.F.: Constitutive Equations for Engineering Materials, Vol.2. Amsterdam, Elsevier, 1994.
- Committee on Steel Structures: Standard Specifications for Steel and Composite Structures - 2008 IV Seismic Design, Tokyo, Japan Society of Civil Engineers (JSCE), 2008.
- Dassault Systemes Simulia Corp.: ABAQUS: User's Manual, ABAQUS Ver. 6.8, 2008.
- Ono, K., Hashimoto, A., Nishimura, N., Yamaguchi, E.: Seismic evaluation method of stiffened box members with fiber model, Bridge and Foundation Engineering, Vol. 41, No. 6, pp. 26-33, 2007.
- Yamato Design Co., Ltd.: User's Manual for Y-FIBER3D, 2000.



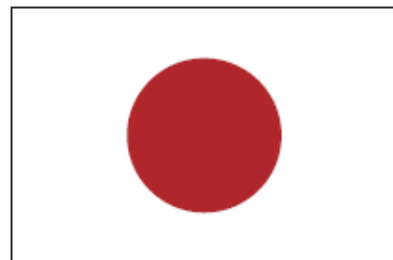
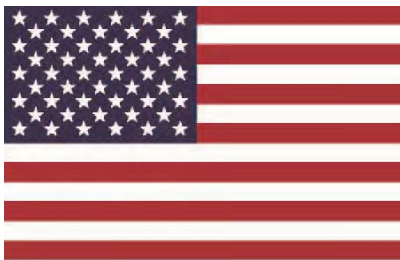
(a) Average strain ε and limit strain ε_u



(b) Updated average strain ε' and limit strain ε_u

Figure 9 Variation of strain with time

Yamaguchi, E.: Practical finite element procedure for achieving mesh objectivity in local buckling analysis of steel structures by beam elements, International Journal of Advanced Steel Construction Vol. 5, No. 3, pp. 224-236, 2009.



27th US-Japan Bridge Engineering Workshop

Session 8

Construction and Maintenance3

Use of Precast I-Girders for Accelerated Bridge Construction in High Seismic Regions

By Sri Sritharan, Justin Vander Werff, and Rick Snyder

How to Build a Bridge - Fast

By John Stanton

Research and Repair of Reinforcement by Overlaying Floor Slab Method in Expressway

By Hidekazu Hayashi

Repairing Fatigue Cracks in a Steel Deck Plate Girder Bridge of Unusual Structure

By Haruhiko Nakata, Yoshiyuki Takamura, and Ken Tokumasu

Development of Eddy Current Test to Detect Fatigue Damages on Orthotropic Steel Deck

By Hiroki Sugiyama, Akiko Tabata, Hiroyuki Nakajima, Tetsuji Yamagami,

Sigeaki Tsukamoto, Akira Shiraishi, and Takaaki Yamada

Page Left Blank

USE OF PRECAST I-GIRDERS FOR ACCELERATED BRIDGE CONSTRUCTION IN HIGH SEISMIC REGIONS

Sri Sritharan¹
Justin Vander Werff²
Rick Snyder³

Abstract

This paper summarizes the experimental investigation of an integral bridge pier system consisting of a concrete column, I-shaped precast concrete girders, and an inverted-tee concrete cap beam that facilitates accelerated bridge construction methods in seismic regions. The research focus included the behavior of the girder-to-cap connections and the overall system behavior. Two girder-to-cap connections—one that has already been implemented in practice and another that is proposed for future use—were studied in one large-scale test unit, which exhibited good seismic response with successful formation of plastic hinges in the column as intended. Both the as-built and the improved girder-to-cap connections performed well, with the improved connection showing more dependable response than the as-built connection.

-
1. Wilson Engineering Professor, Department of Civil, Construction and Environmental Engineering, Iowa State University, Ames, Iowa
 2. Assistant Professor of Engineering, Dordt College, Sioux Center, Iowa; and Researcher, Iowa State University, Ames, Iowa
 3. Laboratory Engineer, University of Minnesota, Minneapolis, Minnesota

Introduction

Precast concrete members in bridge systems are appealing because they lend themselves well to incorporating accelerated bridge construction (ABC) methods. In addition, integral column and cap beam systems for bridges utilizing precast concrete girders have several advantages over structures consisting of steel girders or cast-in-place concrete alternatives. However, the use of precast concrete girders for the design of earthquake-resistant bridges is limited, primarily because of the lack of research and design information regarding the connection between critical bridge components (Theimann 2009, Snyder 2010). The research detailed herein was conducted to investigate the seismic design of a bridge system utilizing a cast-in-place reinforced concrete column integrally connected to a cast-in-place concrete inverted-tee cap beam supporting I-shaped precast concrete girders. Of specific interest were (a) ensuring the girder-to-cap connection would have sufficient shear as well as positive and negative moment capacity to enable successful formation of a plastic hinge at the column top, thus exhibiting good overall system behavior; (b) experimental validation and documentation of the girder-to-cap connections; and (c) developing suitable design recommendations and specifications to promote and advance the use of such designs for ABC techniques. This paper focuses on the large-scale experimental validation tests conducted for the connection regions.

New bridge designs and bridge retrofits developed using the capacity design philosophy have proven to perform well compared to structures designed and built prior to advances made as a result of the Loma Prieta Earthquake in 1989 and the Northridge Earthquake in 1994 (Snyder 2010; Priestly, Seible, Uang 1994). Although a significant amount of research has been aggressively carried out, some structural details have yet to be investigated. One such area is the connection between the substructure and the superstructure when precast girders are implemented in the superstructure. Successful completion of analytical and experimental investigations of such connections will enhance the ability to build quality bridges at an accelerated and efficient pace in seismic regions. The improvements associated with using precast components are resulting in these methods becoming the preferred choice over traditional cast-in-place construction techniques (FHA 2009).

Inverted-tee Bent Cap

A particular connection detail that requires further investigation is the inverted-tee bent cap-to-girder connection. The inverted-tee bent cap system can be used for single or multi-column bent configurations and consists of a cap beam in the shape of an upside-down letter "T" that is placed on top of the columns. Precast girders, typically with dapped ends, are then placed with ease in the field on the ledge of the inverted-tee without requiring any falsework. Thus, this connection is well-suited for implementation in ABC methods. The bridge is made continuous for live load by casting a concrete

diaphragm around the girders and cap followed by construction of the concrete deck over the length and width of the structure.

The inverted-tee connection detail has been used in a number of bridges throughout the state of California. When this detail had been implemented, the column was designed assuming a fixed connection at the base and a pin support at the column top adjacent to the cap (SDC 2006). Having a pin support at the column-to-cap connection is not efficient for seismic design, because it prevents the possibility of forming a plastic hinge at the top of the column, thereby increasing the foundation costs and making the precast option cost prohibitive. Although assumed as a pin connection in previous designs, analysis completed as a part of the project presented herein illustrated that inverted-tee connections, when properly designed, can be expected to behave more like fixed connections, with adequate resistance to both positive and negative moment at the girder-to-cap beam connection regions (Theimann 2009, Snyder 2010). The moment resistance of the previously assumed pin connection, along with its effect on the behavior of the remainder of the bridge, had not previously been investigated. Thus, the experimental investigation was conducted to quantify its behavior and possibly lead to design methods that can utilize the moment resistance of an inverted-tee connection for seismic design. Also of interest regarding the inverted-tee connection was the shear force transfer from the girder-to-cap beam, since such a transfer through the inverted-tee connection would be compromised if the girder-to-cap connection experienced deterioration. A further objective of this research was to develop and investigate means by which to improve this type of connection.

The inverted-tee bent cap system has a number of significant advantages over traditional cast-in-place systems. First, the inverted-tee bent caps allow for the use of precast girders. Shop construction results in higher-quality girders than would be produced in the field and allows for economic savings, being well-suited for ABC practices. The benefits of ABC methods have been well documented in recent years and include reduced field construction time and labor, reduced traffic control or divergence and hence reduced congestion, and reduced noise and air pollution (Billington, Barnes, Breen 1999; Caltrans 2008). In addition to ABC benefits, the inverted-tee system decreases the required depth of the superstructure compared to more traditional bent caps. This benefit is especially apparent when girders with dapped ends are utilized. Also, the inverted-tee system requires less supporting falsework than a method that utilizes splicing of the precast girders in the field, because falsework is only required for casting the inverted-tee bent cap itself. Hence, the girders can be placed directly on the bent cap without any direct support from falsework, which results in economic, time, and environmental savings.

Despite the aforementioned benefits, precast components are still not implemented frequently for bridges in areas of seismic activity. It is highly likely that the use of precast construction would become widely accepted in seismic areas if a design methodology were developed and proven to be reliable. The advantages of doing so

would be numerable, as already discussed above. Successful improvement and testing of the specific connection between commonly used precast I-girders and an inverted-tee bent cap would likely to increase ABC of bridges in high seismic regions.

Prototype Bridge

The prototype bridge, shown in Figure 1, was selected for the experimental study. This bridge was designed in accordance to the AASHTO LRFD Bridge Design Specifications 3rd Edition with 2006 Interims and California Amendments (AASHTO 2003) as well as the Caltrans Bridge Design Aid (BDA 1995). In addition, Caltrans Bridge Design Specifications (BDS 2003) and Seismic Design Criteria v. 1.4 (SDC 2006) were also used in the design. Computer software packages WinRECOL (TRC/ Imbsen), Xtract (TRC/Imbsent), and Conspan (Bentley 2008) were used to aid in the design. The majority of the prototype design was completed by the structural design firm PBS&J with consideration to finite element work conducted as a part of this project. The outcomes of the finite element analysis as well as discussion and calculations for the design of the column, cap beam, girder dapped end and slab for the prototype have been documented in Thiemann (2009).

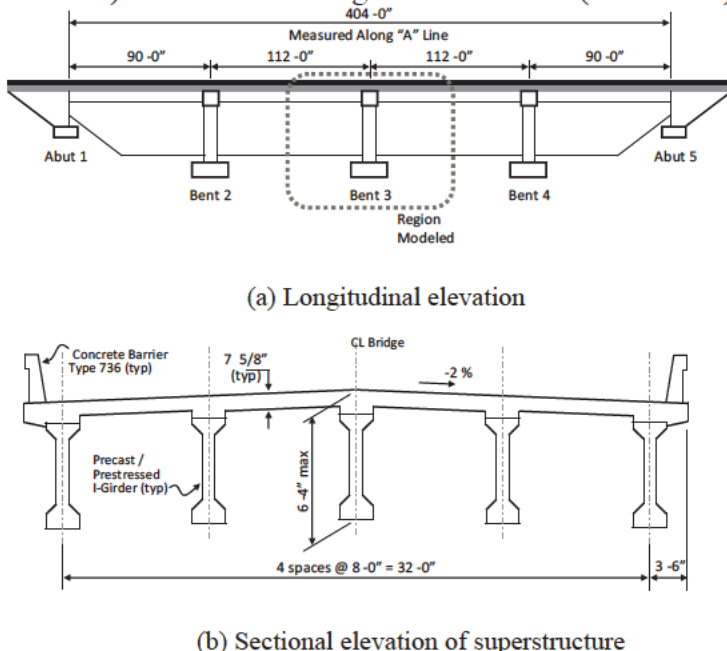


Fig. 1 Prototype Bridge (1 ft = 0.3048 m; 1 in. = 25.4 mm)

Experimental Unit and Test Plan

The test unit was developed based on a 50% dimensional scale of the center portion prototype structure, which represented a typical inverted-tee bridge. The specifics regarding the design of the test unit are outlined in Snyder et al. (2011). Since the behavior of the connection between the girders and the inverted-tee cap beam was the main focus of this study, only one column, with half of a span on each side, was constructed. Therefore, the test unit consisted of a single column with an inverted-tee cap beam and a superstructure of five I-girders overlaid with a deck on each side. In order to test both the “as-built connection” as well as an “improved connection” without building two test units, one side of the inverted-tee cap beam was constructed using the as-built details while the other was constructed using the improved connection details for the

girder-to-cap region. The column was expected to develop a plastic hinge at the top, and thus this region was designed with adequate confinement. Since a majority of the negative moment contribution would be provided by the longitudinal reinforcement in the deck (Hastak, Mirmiran, Miller, Shah, Castrodale 2003), both connections were expected to provide comparable negative moment resistance. As a result, based on whether the superstructure of the test unit was subjected to a horizontal push or pull direction of loading, damage to either of the positive moment connection was expected to be adequately reflected in the overall response of the test unit. Test unit plan details are provided in Figure 2, and further information on the test unit has been documented in Snyder et al. (2011).

Figure 3 provides the details of the test unit's girder-to-cap connection, which was the primary focus of the experimental study. The connection shown in Figure 3 utilized the "as-built" details on the right side, replicating a connection detail that has already been used in practice, while the left side of the connection incorporated an "improved" detail. The enhancement of the improved detail was accomplished using a grouted, unstressed post-tensioning strand connecting each of the girders to the pier cap. In a new bridge design, this unstressed strand would run continuously through both girders on either side of the pier cap. However, since the right side of the pier cap, as shown, was intended to be the as-built condition, the unstressed strand was terminated at the right face of the pier cap.

As is typical for such details, hooked reinforcement was placed between the cap and diaphragm to establish a connection between the diaphragm and inverted-tee bent

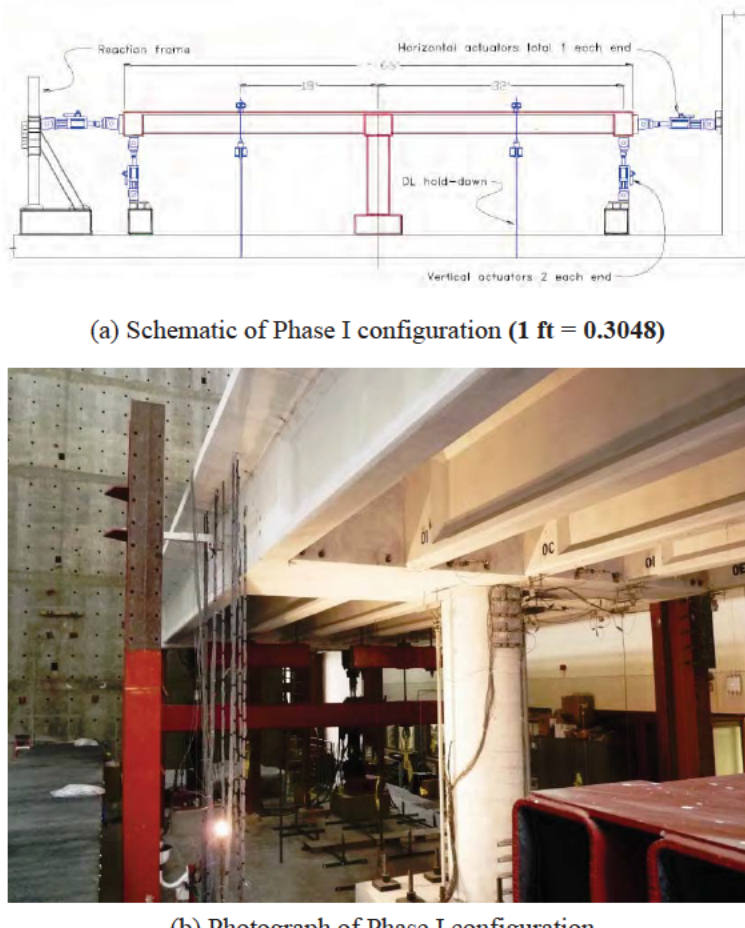


Fig. 2 Inverted-tee Test Unit at 50% scale

cap. Additionally, following another common technique, dowel bars were placed within the girders which extended into the diaphragm in order to further establish a connection between the embedded ends of the girders and the diaphragm.

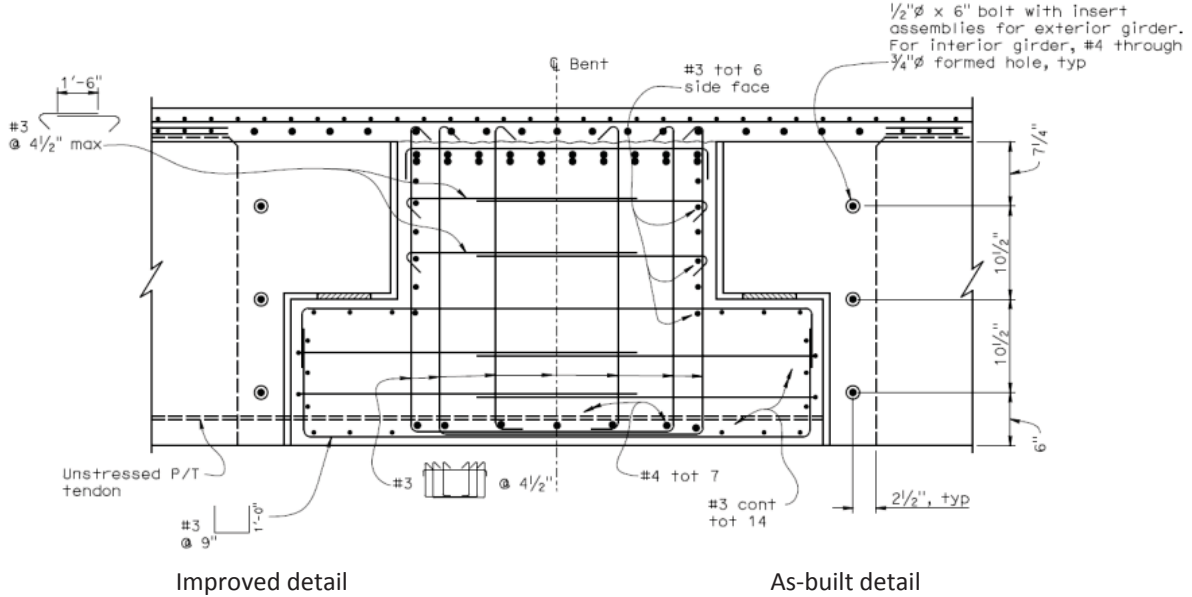


Fig. 3 Girder-to-cap Connection Detail for the Test Unit (1 ft = 0.3048 m; 1 in. = 25.4 mm)

The experimental investigation for this project was divided into two main phases. The first phase, referred to as Phase I, was primarily geared towards investigating the sufficiency of the cap-to-girder connection in having adequate capacity to develop the plastic hinge in the column under simulated gravity and horizontal seismic load. This phase of experimental work is the main focus of this paper. The second phase, designated Phase II, subjected the precast girders to cyclic vertical loads to fully exercise the cap-to-girder connections and to establish the ultimate capacity of the connections.

Phase I testing consisted of horizontal cyclic quasi-static loading of the superstructure. Using two horizontally mounted actuators on each end of the abutment, the superstructure was cyclically pushed and pulled through a series of increasing system displacement ductility levels, μ_d , until the specimen reached a maximum displacement ductility of 10. Phase I was intended to investigate the connection's ability to provide good system performance, including successful development of a plastic hinge at the column top just below the cap beam, a key component of such a bridge designed according to the capacity design philosophy for seismic loading.

Throughout Phase I testing, the gravity load effects on the test unit were simulated using two sets of vertical tie-downs and four actuators positioned in the vertical direction. The tie-downs were positioned appropriately to closely model the scaled shear and

moment values at the girder-to-cap connection that would be experienced by the prototype structure.

Phase I Test Results

When subjected to a combined gravity and horizontal seismic load in a cyclic manner, Phase I loading of the test unit revealed excellent performance for both the as-built and improved connections as well as for the overall system. Plastic hinges were successfully developed at the top and bottom column ends. The test structure achieved a displacement ductility of 10, corresponding to 7 in. (178 mm) of total horizontal displacement, at which point the buckling of column longitudinal reinforcement and confinement failure in the plastic hinge regions were observed. Both the improved and as-built connections between the precast I-girders and the inverted-tee cap beam behaved as fixed connections and did not show significant signs of degradation. Visual observations revealed less-than-expected degradation of the positive as-built connection and almost no damage to the improved connection. Data analysis following the test confirmed a slight difference in the behavior of the as-built connection compared to the improved connection. Deck cracking that resulted from the Phase I test consisted almost exclusively of transverse cracks that extended across the entire width of the deck. The cracks were more tightly spaced near the cap beam, with spacing increasing further away. This extent of flexural cracking indicated that all of the girders were engaged in resisting the horizontal seismic load.

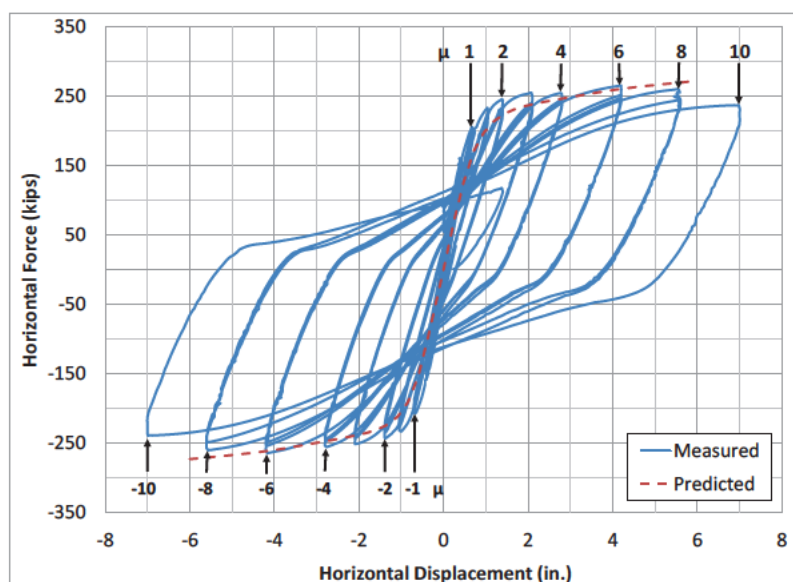


Fig. 4 Comparison of Measured vs. Predicted Force-displacement Response (1 in = 25.4 mm; 1 kips = 4.448 kN)

A comparison of critical data collected during the test to the predictions made prior to the test based on a SAP2000 grillage model analysis (Snyder 2010) showed generally good results. The horizontal force vs. lateral displacement of the superstructure is shown in Figure 4, which shows slight disagreement at small displacements as the grillage model used an effective cracked stiffness for both the column and superstructure sections, rather than the actual gross values for the crack-free stage of the test. However,

the analytical and experimental results began to converge progressively with increasing lateral displacement as more of the structure began to soften due to the development of cracks and yielding of longitudinal reinforcement.

Furthermore, the force-displacement behavior in Figure 4 is seen to be quite similar in the two displacement directions, indicating that both the as-built and improved connections behaved similarly, in terms of their contribution to overall system behavior, when exposed to the horizontal seismic load testing in Phase I.

The test unit as a system behaved well, as the connections exhibited excellent seismic performance. The as-built girder-to-cap connections behaved as a fixed connection instead of a pinned connection, contrary to current assumptions (SDC 2006) regarding precast girder connections to an inverted-tee bent cap. This observation suggests that minimal measures would be required to the as-built bridges in order to ensure a satisfactory performance of the inverted-tee/I-girder bridges in the field. It was also established that a satisfactory agreement was achieved between the predicted response of the grillage model and the measured response of the test unit.

Phase II Test Results

Following the Phase I test, the loading setup for the test unit was reconfigured by removing the vertical tie-downs and horizontal actuators and reinstalling actuators in a vertical configuration closer to the mid-span of the girders on either side of the column, as shown in Figure 5. This configuration offered the opportunity to displace the girder ends vertically while retaining the fixed configuration of the column. Initial loading for Phase II consisted of using the vertical actuators to apply a hold-down force to the test unit simulating the moment at the girder-to-cap interface at the end of construction. Primary testing for Phase II followed, where the girder ends on both sides of the cap were simultaneously subjected to cyclic positive and negative displacements at gradually increasing magnitudes.

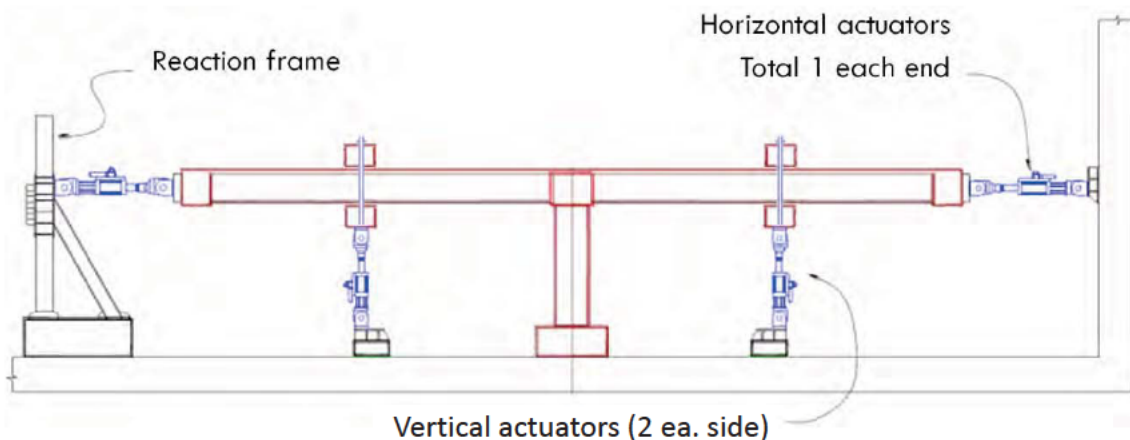


Fig. 5 Phase II Test Configuration

The goal of the Phase II test was to fully exercise the as-built and improved girder-to-cap connections in order to fully investigate their performance. The focus was placed on examining the ultimate moment capacity of each connection type as much as possible in order to determine the validity of the current design approach (SDC 2006), which assumes the as-built connection will eventually degrade to a pin condition under positive moments.

The test structure was subjected to a maximum positive (i.e., upward) displacement of 3 in. (76 mm) and a maximum negative (i.e., downward) displacement of 6 in. (152 mm). Both the positive and negative responses matched or exceeded expectations. In fact, the force vs. displacement plot indicated the structure still had additional negative moment capacity when the test was terminated, as a significant drop in strength was not recorded. Therefore, it is likely that a displacement greater than negative 6 in. (152 mm) could have been achieved. However, extensive and significant cracking was noticed in the deck at the end of the test, with the largest cracks corresponding to the stem of the inverted-T and the outer edge of the diaphragm. Since the cracks spanned the entire width of the structure, it was demonstrated that all of the girders were still actively engaged in resisting the applied moment.

Phase II was successful in exercising the as-built connections to their full capacity under positive moments, establishing the moment capacities, and ensuring a satisfactory shear transfer through the as-built girder-to-cap connection. The as-built connection was clearly observed to have a significant reserve capacity for both positive and negative moments, contrary to current design assumptions for this connection. Phase II subjected the connection to maximum negative and positive moment magnitudes that were approximately 4.9 and 1.4 times greater, respectively, than the demands imposed during Phase I.

The Phase II test did not, however, allow complete quantification of the improved connection performance. This limitation occurred progressively as the as-built connection began to fail and due to the damage to the column ends that was sustained during the Phase I test. The combination of the as-built connection degradation, and the column hinges that developed during Phase I testing produced a pinned-like mechanism, so larger vertical actuator displacements tended to only produce larger rotations in damaged regions, failing to significantly increase the moment demand in the improved connections. Although the pin-like behavior due to the as-built connection deterioration dominated the load-displacement response on both sides of the pier cap, careful reduction of the data revealed that the positive moment demand on the as-built side began decreasing while improved connections responding elastically throughout Phase II testing, providing clear indication that the improved connection exhibited better performance.

Conclusions

This experimental investigation was conducted to examine the performance of both an as-built and an improved girder-to-cap connection for precast concrete I-girders and an inverted-tee pier cap. The following conclusions have been as a result of this study:

- Contrary to current design assumptions, the as-built connection of the inverted-tee pier cap to the precast I-shaped girder behaved as a fully continuous connection instead of a pinned connection.
- The improved cap-to-girder connection performed as expected, ensuring fully continuous behavior under both positive and negative moments.
- Both the as-built and improved connections successfully transferred shear forces from the superstructure into the cap beam during both phases of testing.
- The inverted-tee pier cap detail can be used in an integral connection design to develop a plastic hinge in the top of the column. Thus, the inverted-tee pier cap is an excellent way to implement precast concrete girders in seismic regions and promote accelerated bridge construction in these regions.
- The improved cap-to-girder connection is sufficient to achieve the design goals intended in an integral connection. However, full quantification of the improved cap-to-girder connection was not achieved due to the degradation of the as-built connection. Further work is planned to complete this portion of the investigation.
- Since the as-built bridges are expected to have sufficient moment connections to act as fixed connections based on the details adopted, the columns are expected to develop plastic hinges at the top adjacent to the cap beam. In consideration of minimizing cost, only the column tops in these bridges are suggested for retrofitting with adequate confinement reinforcement so that this region can successfully develop a plastic hinge. It should be noted, however, that doing so will increase the column shear demand as well as other demands within the system, so these effects should be investigated prior to retrofitting to ensure satisfactory seismic performance of bridges in future earthquakes.
- The force vs. displacement predictions from a grillage model were observed to correlate well with the measured response of the test unit for both phases of testing. Thus, the grillage model is an adequate means of predicting the behavior of current and future inverted-tee bridge structures.

Acknowledgements

The research team thanks the following individuals for their support and assistance in the completion of the experimental study presented in this paper. Without their help and kindness, much of this research would not have been possible:

- Caltrans for sponsoring this research project and Mike Keever and Charly Sikorsky for their input, advice, and assistance with project management;
- Sami Megally of PBS&J for his expertise and guidance in the design and construction of the test unit; and
- Professor Jose Restrepo and the staff at UCSD and the Charles Lee Powell Laboratories for their assistance in the construction and testing of the test unit.

References

- AASHTO LRFD Bridge Design Specifications, 3rd Edition*, AASHTO, 2003.
- Accelerated Bridge Construction Applications in California, A Lessons Learned Report, Version 1.1*, Caltrans, 2008.
- Billington, S.L., Barnes, R.W., Breen, J.E., “A Precast Segmental Substructure System for Standard Bridges,” *PCI Journal*, V. 44, No. 4, July/August 1999, pp. 56-72.
- Bridge Design Aids*, Caltrans, 1995.
- Bridge Design Specifications*, Caltrans, 2003.
- “Connection Details for Prefabricated Bridge Elements and Systems.” Publication No. FHWA-IF-09-010., FHA, 2009.
- Conspan*, Bentley Systems, Inc., 2008.
- Hastak, M., Mirmiran, Al, Miller, R., Shah, R., and Castrodale, R. “State of Practice for Positive Moment Connections in Prestressed Concrete Girders Made Continuous,” *Journal of Bridge Engineering*, 2003, pp. 267-272.
- Priestley, M.-N., Seible, F., and Uang, C., *The Northridge Earthquake of January 17, 1994*, The University of California, 1994.
- Seismic Design Criteria, Version 1.4*, Caltrans, 2006.
- Snyder, Richard M., *Seismic Performance of an I-girder to Inverted-T Bent Cap Bridge Connection*, 2010.
- Snyder Richard M., Vander Werff, J., Theimann, Zachary J., Sritharan, Sri, and Holombo, Jay *Seismic Performance of an I-Girder to Inverted-T Bent Cap Connection*, Final California Department of Transportation, Iowa State University, 2011.
- Theimann, Zachary J., *3-D Finite Element Analysis of the Girder-to-Cap Beam Connection of an Inverted-tee Cap Beam Designed for Seismic Loadings*, Iowa State University, 2009.
- WinRECOL*, TRC/Imbsen Software Systems.
- Xtract*, TRC/Imbsen Software Systems.

HOW TO BUILD A BRIDGE - FAST

John Stanton¹

Abstract

A new connection has been developed for connecting precast bridge columns to cast-in-place spread footings. It is quick and simple to construct, and has excellent seismic resistance as well. It is made by precasting the column; setting, plumbing and leveling it on site; fixing the footing steel; and casting the concrete for the footing. No steel crosses the interface between the precast column and the spread footing; the column bars are all straight and are terminated with heads for anchorage. The column has a roughened surface that transfers the shear stresses (due to column axial load and bending) across the column-footing interface. Tests were carried out on the system. The paper describes the design criteria and methodology, the results of the tests, and recommendations for use of the system in practice.

Introduction

Bridge construction frequently leads to traffic delays, which result in wasted time and fuel. Bridge owners are therefore seeking methods to accelerate bridge construction, referred to as ABC. Such methods also offer reduced environmental impacts, better worker safety, higher quality construction and lower lifecycle costs (Wacker et al. 2005). Use of precast concrete represents a promising technology for ABC, and has been successfully used for bridge substructures in non-seismic regions (Matsumoto et al. 2001). Connections are typically made at the beam-column and column-foundation interfaces to facilitate fabrication and transportation. However, for structures in seismic regions, those interfaces represent the locations of high moments and large inelastic cyclic strain reversals. Devising connections that are not only sufficiently robust to accommodate those inelastic cyclic loads, but are also readily constructible, is challenging.

A bridge bent system has been developed at the University of Washington, in collaboration with WSDOT and Berger/ABAM Engineers, that is intended to satisfy the combined needs of seismic performance and rapid construction. Different connection systems are used at the column-to-foundation and the cap beam-to-column interfaces, because of the different conditions that exist at each location. The cap-beam connection is described in Pang et al. (2010) and is shown in Figure 1. It consists of bars that project from a precast column and are grouted into ducts in the precast cap beam. The distinction between it and other grouted bar systems is that large bars (up to #18 US, or D57) are used in large ducts. That approach allows the use of a small number of bars, which minimizes the number of bar fit-ups needed on site and maximizes the size of the ducts, both of which improve constructability.

¹ Professor, University of Washington, Seattle, WA 98195, USA.

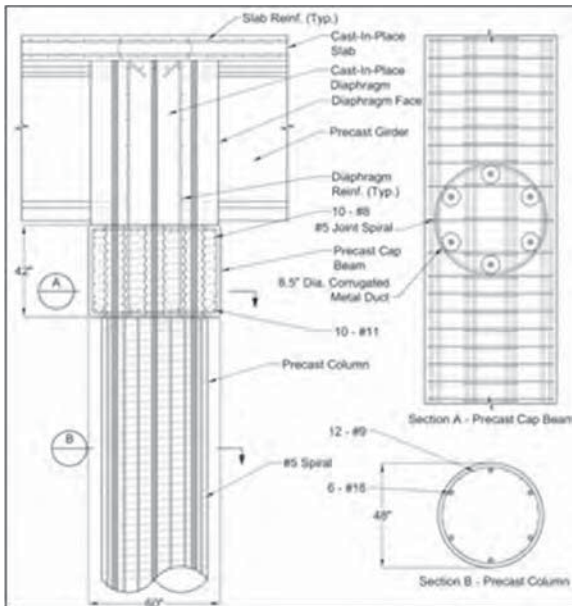


FIGURE 1. COLUMN TO CAP BEAM CONNECTION CONCEPT. (1 inch = 25 mm)

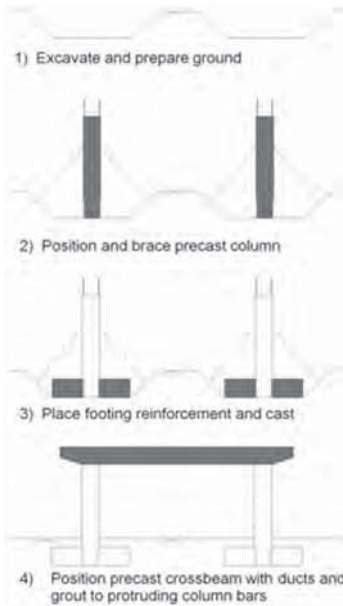


FIGURE 2. CONSTRUCTION SEQUENCE

The potential drawback of the use of large bars is their anchorage within the depth of the cap beam. However, extensive testing (Steuck et al. 2009) showed that even #18 (D57) bars could easily be anchored within the depth of a typical cap beam and that, under cyclic lateral load, the connection behaved like a cast-in-place system with conventional detailing and bar sizes (Pang et al. 2010).

This paper describes the socket connection between the column and spread footing, for which the same requirements, namely simplicity of construction and good seismic performance, exist. Research to extend the concept to the use of drilled shafts is ongoing.

The construction sequence for the new socket connection is shown in Figure 2. The column is precast with a roughened outer surface at the bottom. Once the footing has been excavated (Step 1 in Figure 2), the precast column is brought to site, plumbed, leveled, and braced (Step 2). Footing reinforcement is then placed, and the footing is cast (Step 3) around the column.

The final step is to connect the column to the precast cap-beam (Step 4) by grouting the large bars in the large ducts. In comparison with conventional cast-in-place construction, the primary advantage of this system is construction speed; a footing and column can be built in little more time than is needed to cast the footing alone. Further, the use of a precast cap beam is estimated to save several weeks.

The structural details differ from those of a conventional, cast-in-place system in two ways. First, no bars pass from the footing into the column, so the only

resistance to vertical load comes from shear friction across the precast to cast-in-place interface. That interface is intentionally roughened to facilitate this load transfer.

Second, the longitudinal column bars are not bent out at the bottom, but instead, they are developed by headed anchors. This choice simplifies transportation and handling of the columns, because no steel projects from the sides, and it eliminates the hazard that would otherwise be posed by protruding bars. The configuration also provides a much simpler and more direct flow of internal forces than is possible with bent-out bars. The distribution of internal forces is illustrated by the strut-and-tie model shown in Figure 3 for both a bent-out bar system and an anchored bar system. In the headed bar system, the node that connects the vertical column bar to the diagonal strut is a CCC node, which is extremely efficient, robust and reliable, because the concrete is in triaxial compression. In the conventional bent-out bar system, the load must be transferred from the diagonal strut to the bar by bond around the bend of the bar. This is a poor transfer mechanism and leads to diagonal cracks in the footing at relatively low stresses. These cracks are often referred to as "joint shear" cracks. The Caltrans Criteria (2006) require significant amounts of tie steel in the footing to overcome the poor transfer mechanism. That tie steel is not needed when headed bars are used.

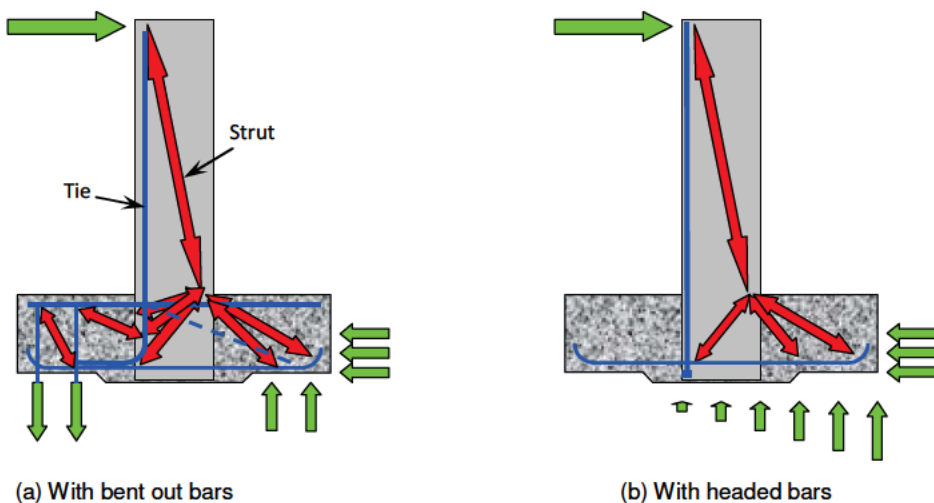


FIGURE 3. STRUT AND TIE MODELS OF CONNECTION.

This socket connection was used in a bridge over I-5 in Washington State that was constructed during the summer of 2011.

Design Requirements

The footing must satisfy several design requirements imposed by the AASHTO LRFD Design Specifications and the AASHTO Guide Specifications for LRFD Seismic design. The latter are largely based on the Caltrans Seismic Design Criteria (2006), but the Caltrans Criteria contain some requirements beyond the AASHTO ones, and they are expected to be incorporated into the next edition of the AASHTO

Guide Specifications. Therefore they were included too. The primary requirements are:

- The soil pressure under the footing, under vertical load plus overturning, must remain below the allowable bearing pressure.
- The resultant vertical reaction, under vertical load plus overturning, must remain within the middle two-thirds of the footing.
- The connection between the footing and column must provide sufficient strength to force the failure to occur in the column. The goal is to avoid footing failure, which can be expensive to inspect and repair.

The first two requirements, based on soil properties, essentially define the plan dimensions of the footing and are not discussed further here. The structural requirements for the connection can be identified from the potential modes of failure. The primary ones are:

- Bending strength of the footing.
- One-way shear strength of the footing.
- Anchorage failure of the bars.
- Punching shear failure under vertical load (assumed to occur on a conical surface).
- Transfer of combined vertical load and moment between the column and footing.
- Shear friction failure across the precast to cast-in-place interface.
- Joint-shear failure within the connection.

The longitudinal column bars are equipped with headed anchors, which should be selected from commercially available products and may thus be assumed to provide adequate anchorage. The other structural requirements depend on the flow of forces in a system that is highly statically indeterminate. While the distribution of internal forces is expected to follow the general pattern shown in Figure 3, the resistance in each potential failure mode is not well defined and so needs to be determined by testing. The characteristics that were expected to influence the resistance were:

- The ratio of footing depth to column diameter.
- The quantity of column longitudinal reinforcement.
- The quantity of shear reinforcement in the column within the joint region.
- The quantity of transverse reinforcement in the footing.

Test Program

The number of characteristics exceeded the number of tests (three) that could be conducted within the program resources, so choices had to be made. All the test specimens consisted of cantilever columns projecting from spread footings, in which the columns were subjected to constant vertical load and cyclic lateral load. The test specimens consisted of 20-in. (500 mm) diameter columns and represented at 5/12

scale a notional prototype with a 4-ft (1200 mm) diameter column. Specimens SF-1 and SF-2 each contained a column splice above the plastic hinge region. However, the splice is not an essential part of the system, and is not discussed further here.

In many columns in the field, the longitudinal column reinforcement ratio is close to the AASHTO minimum of 1%. Therefore this ratio was used for all three tests. The spiral steel in the column is also typically carried down into the footing at the same pitch as in the body of the column, so that was also done in all of these test specimens. It provided joint shear some resistance.

The primary test variables were the ratio of footing thickness to column diameter and the quantity of transverse steel used in the footings. In addition several other details of the footing steel were varied between specimens. The specimen details are summarized in Table 1. The test program was carried out while the Washington State Department of Transportation, WSDOT, was designing a bridge that uses the system. The bridge construction started only eight months after that laboratory testing was complete, and is now finished. The geometry of the test specimens represented, at 1: 2.4 scale, the geometry of the prototype bridge components.

TABLE 1. TEST SPECIMEN DETAILS

Spec. No.	Column dia. (-) (in)	Vertical rft ratio (%)	Spiral rft ratio (%)	Footing depth (in)	Footing Ties (-)	Diagonal steel sets (-)
SF-1	20	1.12	0.88	22	full	3
SF-2	20	1.12	0.88	22	half	1
SF-3	20	1.12	0.88	10	none	0

(Note: 1 inch = 25 mm).

Specimen SF-1 was regarded as the most conservative detailing, intended to represent as closely as possible a direct conversion from cast-in-place to precast construction. Thus some of the flexural steel in the bottom of the footing passed directly under the column, and this required casting a slot into the bottom of the column, as shown in Figure 4. The goal was to ensure the best possible engagement of the footing steel with the column steel. A plan view of the test specimen is also shown in Figure 5.

In all three specimens, the column projected slightly below the structural part of the footing in order to locate the anchor head on the column bar just below the bottom node in the strut and tie model shown in Figure 3. This choice would cause the node to behave as a CCC node, with the attendant stable load transfer properties and absence of anchorage problems. A void was also left between the underside of the column and the top of the test floor to ensure that all of the applied vertical load was resisted by the connection between the column and footing, because none could pass in bearing to the platen of the test machine under the footing.

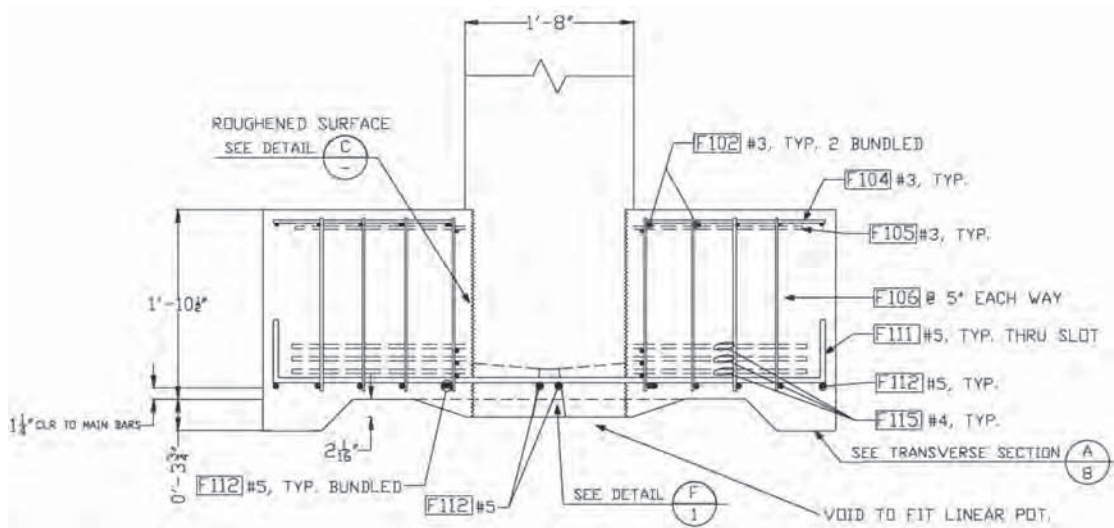


FIGURE 4. SPECMEN SF-1: SECTION. (1 inch = 25 mm)

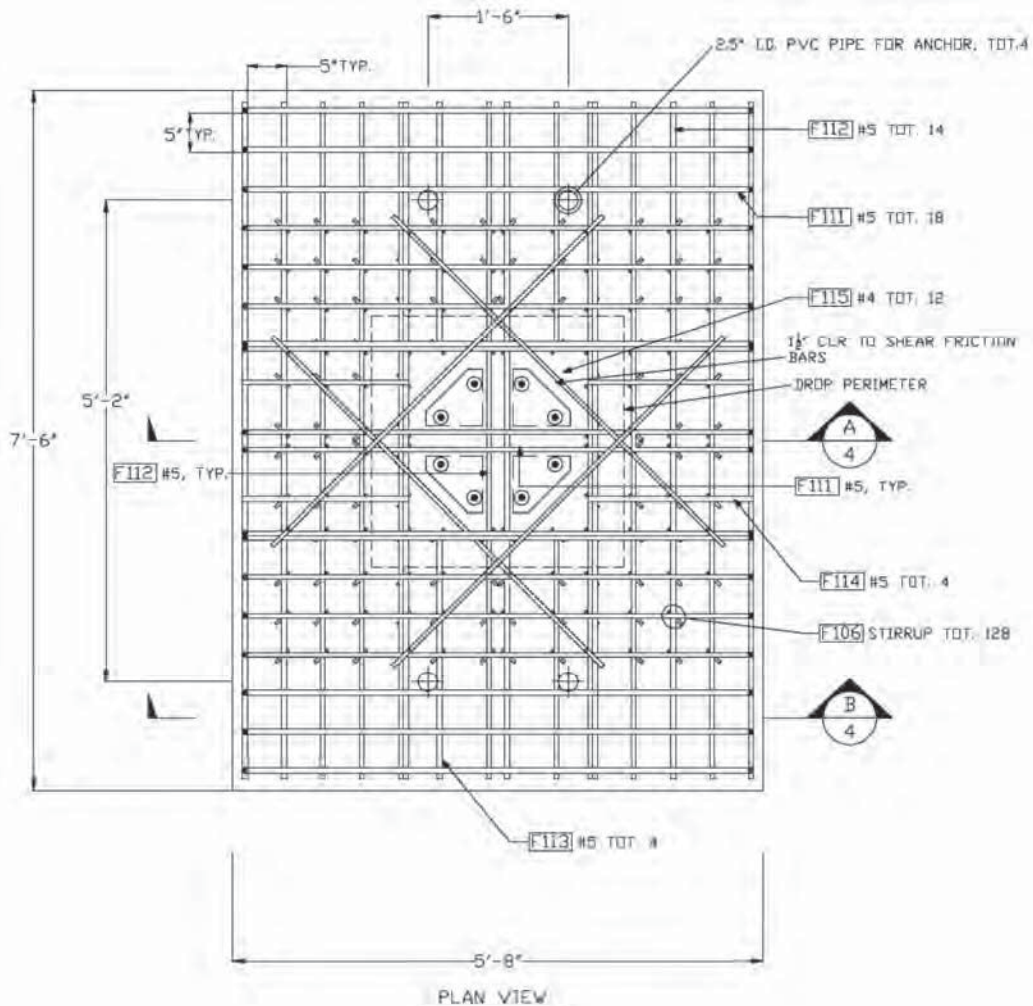


FIGURE 5. SPECMEN SF-1: PLAN VIEW. (1 inch = 25 mm).

Figure 5 also shows sets of diagonal bars in the footing. These were placed both to provide some reinforcement in the otherwise unreinforced corners of the square region of cast-in-place concrete surrounding the octagonal column, and to provide a tension capacity across the pc-cip interface for the purpose of generating shear friction resistance there. Last, the footing of Specimen SF-1 contained the full complement of transverse reinforcement required by the Caltrans Criteria (2006). That reinforcement is intended to resist joint shear forces. It should be noted that, unlike a beam-column joint in a building frame, the region that constitutes the joint, and in which the reinforcement can be placed, includes a region of the footing outside the column itself.

Specimen SF-2 was similar to SF-1 except that no footing steel was placed under the column, thereby eliminating the slots in the bottom of the column. The same total amount of footing steel was used, but some bars were moved to just outside the column where they were bundled with other bars already in that location. The diagonal shear friction steel was also reduced to a single set of bars, rather than three sets, and the amount of transverse steel in the footing was halved. The basis for reducing the diagonal steel was that, in both specimens, the normal force due to the flexural steel was ignored in evaluating the shear friction resistance, even though it appears logical to count it. (This is evident from the strut and tie model in Figure 3b). The transverse steel was reduced because the tests underlying the Caltrans Requirements were all conducted on cast-in-place systems in which the column bars were bent out. That arrangement prevents formation of the strut and tie model of Figure 3b, in which case the forces must follow a more complex path, such as that in Figure 3a (from Xiao et al. 1996). It was hypothesized that replacement of the bent-out bars by anchor heads in the present study would reduce or eliminate the need for additional transverse reinforcement.

Specimen SF-3 was designed and constructed after testing SF-1 and SF-2. Because those two suffered essentially no damage in the connection region, they provided only lower bounds on the connection strength. To obtain an upper bound as well (and therefore to bracket the true value), failure in Specimen SF-3 had to be forced into the connection region. To do that, it was designed with a 20-in. (500 mm) diameter column, as in Specimens SF-1 and SF-2, but a footing that was only 10 in. (250 mm) thick. The column steel remained the same, but the flexural steel in the footing had to be much heavier to provide the same flexural strength with a smaller lever arm.

To avoid a spurious one-way (“beam”) shear failure, a small number of footing ties were needed for one-way shear strength. They were placed so that they contributed to one-way shear resistance but not to punching shear resistance. A single set of diagonal “shear friction” steel bars was used, as was done in Specimen SF-2, to provide a minimum of reinforcement in the otherwise reinforced corners of the region around the column. The results of tests on Specimens SF-1 and SF-2 had shown that the stress in the diagonal bars never exceeded about 5% of yield, so they were not expected to contribute significantly to shear friction resistance in Specimen SF-3.

Test Results

Each test specimen was first subjected to a pure axial load test to investigate the possibility of shear failure at the precast-cast-in-place interface. The axial load for Specimens SF-1 and SF-2 was 240 kips (1077 kN), which was the factored DL + LL on the prototype bridge to be built over I-5, scaled to specimen size. Specimen SF-3 was subjected to 1.4 times this load. No signs of cracking or damage were seen in any of the three specimens under this loading.

Each test specimen was then subjected to the lateral displacement history shown in Figure 6. Displacements were applied under stroke control.

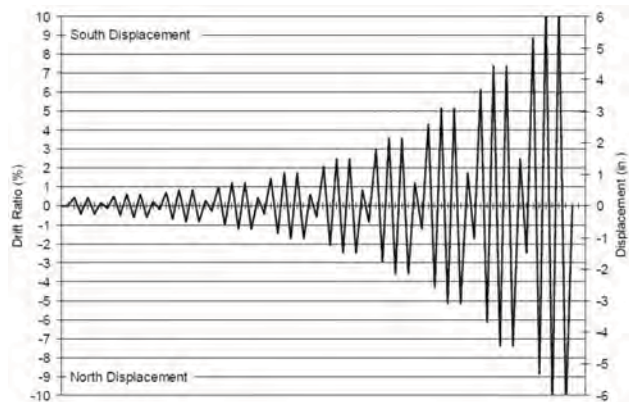


FIGURE 6. LATERAL DISPLACEMENT HISTORY.

The load-displacement plots for all three specimens are shown in Figure 7.

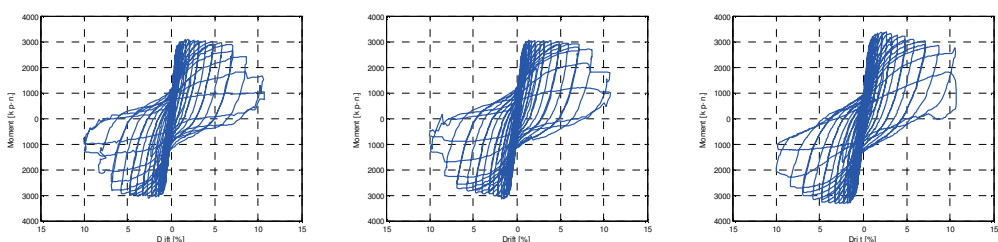


FIGURE 7. LOAD-DISPLACEMENT RESPONSE FOR SPECIMENS SF-1, SF-2 AND SF-3. (1 inch-kip = 113 N-m).

The responses of Specimens SF-1 and SF-2 were nearly identical, and furthermore they were essentially the same as that of a cip reference specimen tested earlier (Pang et al. 2010). All the damage occurred in the column, which failed by combined axial load and flexure in a conventional plastic hinge. The proximate cause of failure was fracture of some of the bars, which was in turn caused by buckling and re-straightening of those bars under cyclic loading. Bar buckling was first observed at approximately 6% drift ratio in both cases, after which the lateral strength started to drop. The only cracks in the footing were hairline, and all the footing steel displayed stresses well below yield. The footing was thus behaving as if it were made from mass concrete with no reinforcement.

Specimen SF-3, with the thinner footing, behaved differently. In the early stages of loading it appeared to be behaving in the same way as the other two, with

some spalling of the column concrete and yielding of the longitudinal column steel. However, at about 6% drift, some spalling of the footing concrete became visible around the column. The column bars did not buckle or fracture, but the footing started to sustain more damage. Eventually, at 10% drift, the specimen failed by combined vertical force and moment transfer in the connection region. Because a void had been deliberately left under the column to prevent vertical support from the test floor, the column sank approximately 3 in. (75 mm) through the footing when failure occurred. Thus the objective of forcing failure to occur in the footing was achieved. However, the extensive yielding of the column bars and the fact that no footing damage was visible until quite late in the loading history suggest that the specimen was only just connection-critical, in which case the ratio of column diameter to footing thickness used in the specimen represents a fairly tight upper bound on the value needed to avoid footing failure.

Figure 8 shows Specimen SF-3, seen from below, after failure. The column can be seen to be relatively intact, with all the damage concentrated in the surrounding footing concrete. The failure surface suggests a punching shear failure under combined vertical load and bending.



FIGURE 8. SPECCEIMEN SF-3 AFTER FAILURE (FROM BELOW).

After the lateral-load testing, Specimens SF-1 and SF-2 were subjected to a vertical load test to failure, in order to evaluate the remaining strength of the connection under vertical load alone. The test could not be applied to Specimen SF-3 because the connection region in it had already failed. In both cases, the column was able to carry approximately 840 kips (3740 kN) before crushing in the plastic hinge region of the column. It should be noted that the spiral and several longitudinal bars had already fractured in the lateral load testing, before this vertical load was applied. No damage occurred in the footings during this loading. The peak load of 840 kips (3740 kN) was limited by the axial strength of the previously-damaged column, so the footing capacity may have been much higher. The load represents 3.5 times the factored dead plus live load in the prototype bridge, adjusted to laboratory scale. It is thus clear that for footings of these proportions, the shear friction capacity across the pc-cip interface is easily sufficient to resist the vertical load.

Conclusions

The following conclusions were drawn from the study:

- **Connection concept.** The column-to-footing socket connection can be designed so that the system behaves like a comparable cast-in-place column-to-footing connection. The precast columns can be designed following the same specifications as are used to design conventional cast-in-place columns.
- **Need for mechanical anchors.** The use in the column of headed straight bars, instead of bent out bars, simplifies construction and improves the force flow in the footing, but necessitates the use of headed anchors on the bars.
- **Design against footing failure.** The procedures outlined in the AASHTO Guide Specifications for LRFD Seismic Design for determining the required flexural strength of the footing were effective in preventing footing failure in all three column tests.
- **Vertical ties in the footing.** When the column steel consists of straight bars equipped with headed anchors, rather than the conventional bent-out bars, the prescriptive vertical footing ties specified by the AASHTO Guide Specification perform no useful function and can be omitted. This conclusion applies only to the prescriptive ties, and not to ties that are needed to supply shear resistance required to resist computed shear demands.
- **Shear-friction push-through resistance of connection.** The strength of the connection in shear friction was sufficient to prevent any sign of slip, much less sliding failure, across the pc-cip interface, in any of the three test specimens. The flexural reinforcement provides normal forces across the potential sliding interface, which induce sufficient friction to resist the demands. Thus additional reinforcement (here placed diagonally) is not necessary for that purpose. However, a small amount of diagonal “trimming” reinforcement is still desirable to avoid the existence of a large region of unreinforced concrete at the corners of the embedded column.

Acknowledgements

Support for this work was provided by the Federal Highway Administration, through their Highways for Life program, by the Washington State Department of Transportation, and by the Valle Foundation at the University of Washington. The findings and conclusions contained herein are those of the authors alone. Thanks are extended to former graduate students Kyle Steuck and Laila Cohagen, Laboratory Manager Vince Chaijaroen, Mr. Greg Ritke and the staff of Tri-state Construction, Mr. Steve Seguirant of Concrete Technology Corporation, Dr. Bijan Khaleghi and Mr. Jugesh Kapur of the WSDOT, and Dr. Lee Marsh of Berger/ABAM Engineers for their valuable assistance, without which the project would not have been possible.

References

- “AASHTO (2009). “*LRFD Bridge Design Specifications*” 4th ed., American Association of State Highway and Transportation Officials, Washington, DC.
- “AASHTO *Guide Specification for LRFD Seismic Bridge Design*” (2009). AASHTO, Washington DC.
- Building Seismic Safety Council for the FEMA. (2004) “*NEHRP Recommended Provisions for Seismic Regulations and for New Buildings and Other Structures (FEMA 450) 2003 Ed.*,” Washington D.C.
- Caltrans (2006). “*Seismic Design Criteria Version 1.4*”. Caltrans, Sacramento, CA.
- Matsumoto, E., Waggoner, M., Sumen, G., Kreger, M., Wood, S., and Breen, J. (2001). “*Development of a Precast Bent Cap System*,” Center for Transportation Research, Research Project 0-1748, University of Texas at Austin.
- Pang, J. B.K., Eberhard, M.O. and Stanton J.F. (2010). “Large-Bar Connection for Precast Bridge Bents in Seismic Regions”. *ASCE, Jo Bridge Eng.* 15 (3) May-Jun: 231-239.
- Steuck, K., Stanton, J.F. and Eberhard, M.O. (2009) "Anchorage of Large-Diameter Reinforcing Bars in Ducts," *ACI Structural Journal*, July-August, pp 506-513.
- Wacker, J., Hieber, D., Stanton, J.F., and Eberhard, M.O. (2005). “*Design of Precast Concrete Piers for Rapid Bridge Construction in Seismic Regions*,” Washington State Transportation Center Report, Seattle, WA.
- Xiao, Y., Priestley, M.J.N., and Seible, F. (1996). “*Seismic Assessment and Retrofit of Bridge Column Footings*”. *ACI Structural Journal*, ACI, Farmington Hills, MI. Jan-Feb., pp. 79-94.

RESEARCH AND REPAIR OF REINFORCEMENT BY OVERLAYING FLOOR SLAB METHOD IN EXPRESSWAY

Hidekazu Hayashi¹

Abstract

NEXCO has been reinforcing floor slabs by overlaying for about 15 years as a measure against deterioration and increasing live load on steel bridges. However, re-deterioration has become noticeable on repaired bridges. This document is a summary of the measures taken to cope with the issue.

Introduction

In Japan, live load has raised, and the damage of floor slab has increased. The "Design and Construction Manual for Overlaying"¹⁾ was compiled as a guideline for reinforcing floor slabs and has been applied from 1995 on more than 400 bridges. But, recently, damages have been found in short periods after reinforcement and the number has been escalating as well. The following gives an outline of the overlay method, description of the deterioration factors, study results on improving the durability of the method and the resin injection method used to repair re-deteriorated floor slabs.

Outline about the reinforcement of overlaying¹⁾⁽²⁾

A repair method is decided by the location and the degree of deterioration which are determined by examining the floor slab. The repair method is selected from the followings: slab waterproofing, partial slab exchange, overlaying floor slab from bottom face, overlaying floor slab and full slab exchange.

In the overlaying method, load bearing capacity is recovered or improved by casting steel fiber reinforcement concrete on the existing floor slab. (Fig.1).

Steel fiber reinforcement concrete is cast thinly after polishing and sweeping the milling face. Rapid hardening cement is often used to shorten the construction and accompanying traffic control period. Steel fiber reinforcing concrete is generally produced exclusively at a large-sized plant and is laid and tamped by a concrete finisher dedicated for that purpose. It is used to prevent cracks and control the size of cracks if cracks develop. The design strength is the same as the existing concrete. The slump is to be around 5cm to reduce dry shrinkage and correspond to longitudinal and cross slopes. Most steel fiber is 30mm in length and has an aspect ratio of 50-60, and a mixture rate of 1.27vol.% as standard.

At present, more than 400 bridges adopt this method as a repair method of deteriorated floor slab in expressway.

¹ Researcher, Road Research Department Bridge Division, Nippon Expressway Research Institute Co Ltd., Tokyo

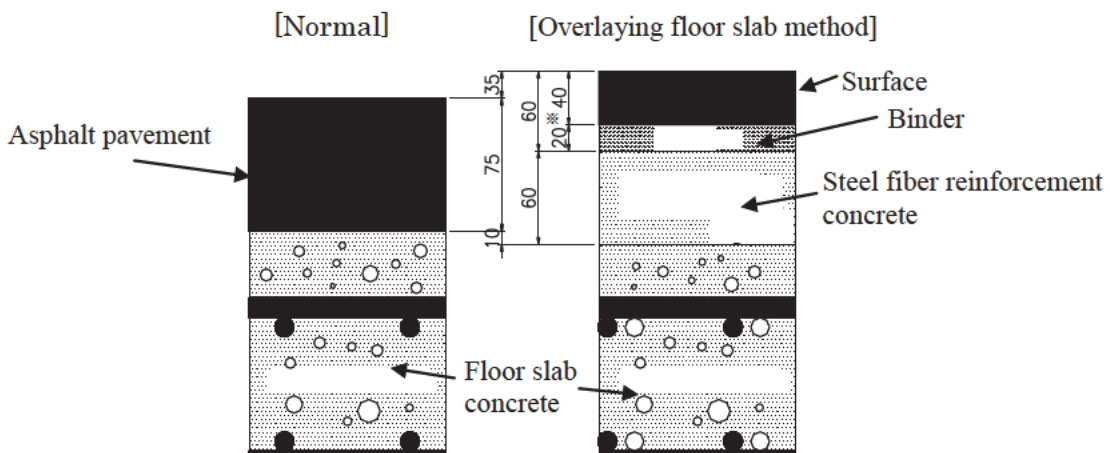


Fig.1 Cross section of overlaying floor slab method

Re-deterioration factor³⁾

Re-deterioration of floor slab has been reported from about 1998. The problem has become noticeable as potholes and cracks in the pavement.

We did a questionnaire survey, in 2006, for about 400 bridges repaired by overlaying. The survey showed that re-deterioration occurred in 12% of bridges. When we studied the record of damage and analyzed damage positions, we found that potholes occurred most at the construction joint between lanes (Fig.2) and tended to be near the shoulder next to running position of large-sized vehicles. Fig.3 shows the cross section of floor slab where many potholes were found. The damage state indicates infiltration of water from the construction joint and staying of slag at the boundary between existing floor slab and overlaying.

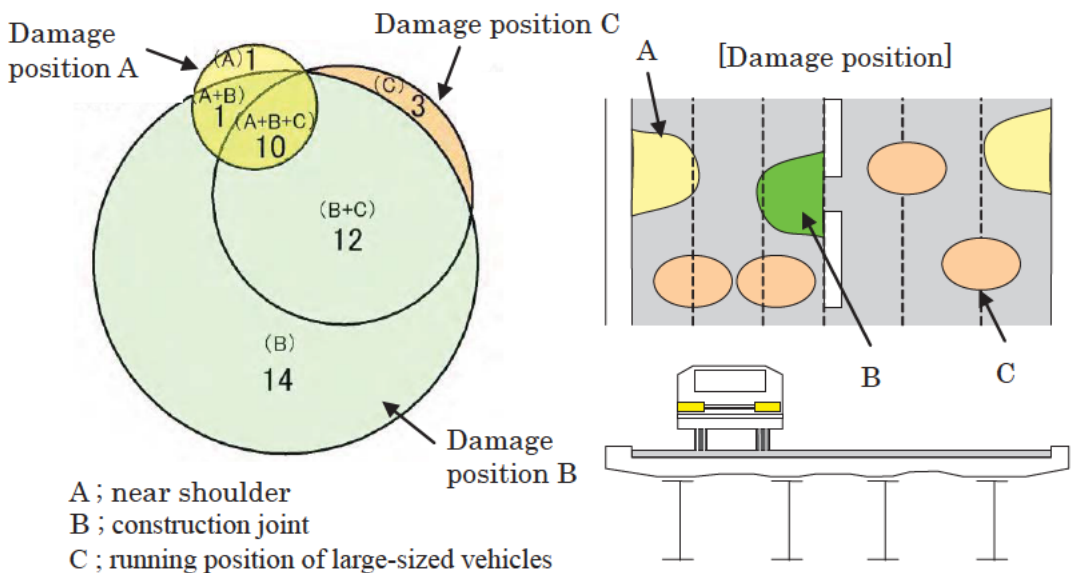


Fig.2 Damage position of overlaying floor slab

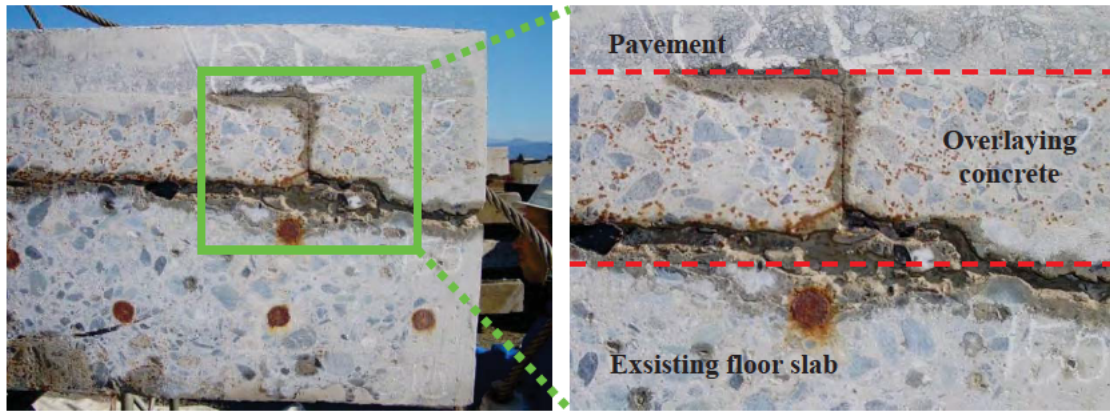


Fig.3 Section of floor slab with many potholes at construction joint

We analyzed the questionnaire survey statistically to find the causes for the re-deterioration. We roughly classified the re-deterioration factors as follows: structure factors, environmental factors, material factors, level of health and construction factors. Of the factors, those which we were able to find a tendency for occurrence are described below.

Structural factors: Steel bridges accounted for 70% of the bridges reinforced with the overlay method and re-deterioration was noticeable in plate girder bridges (Fig.4). In addition, much of the deterioration was found in bridges designed between 1971 and 1979 — design standards used for these bridges are not much different from the current standards.

Environmental factors: Re-deterioration tended to become noticeable when the cumulative quantity of anti-freezing agents used and the cumulative days of when minimum temperature is lower than zero degrees exceed a certain quantity (Fig.5, 6).

Construction factors: Milling machines and surface preparation may cause cracks in floor slabs. It was tested and confirmed on a test piece that minute cracks developed in existing floor slabs when floor slabs were cut or chipped with a milling machine or breaker.

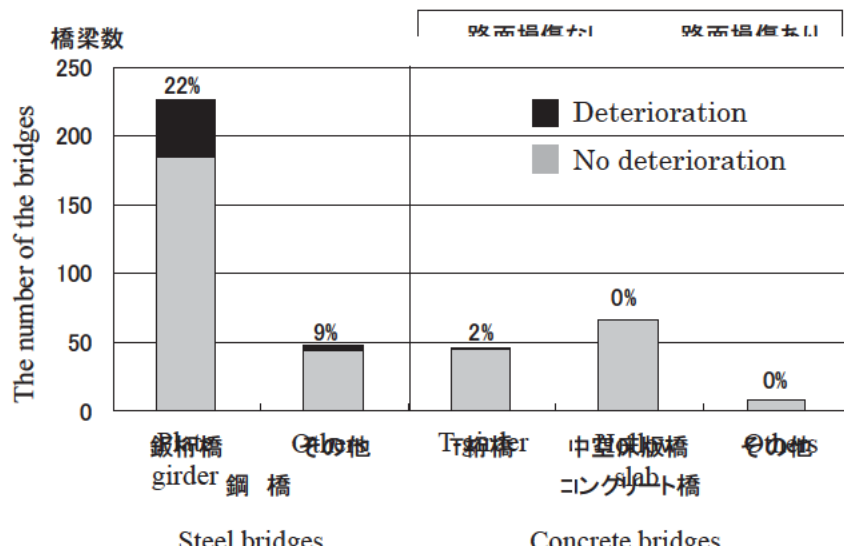


Fig.4 Relations of structure and deterioration

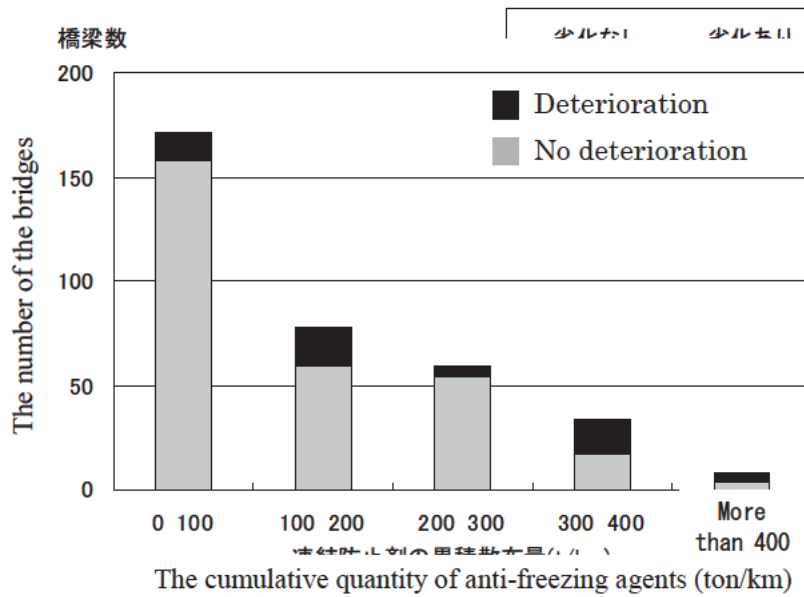


Fig.5 Number of deterioration caused by anti-freezing agents

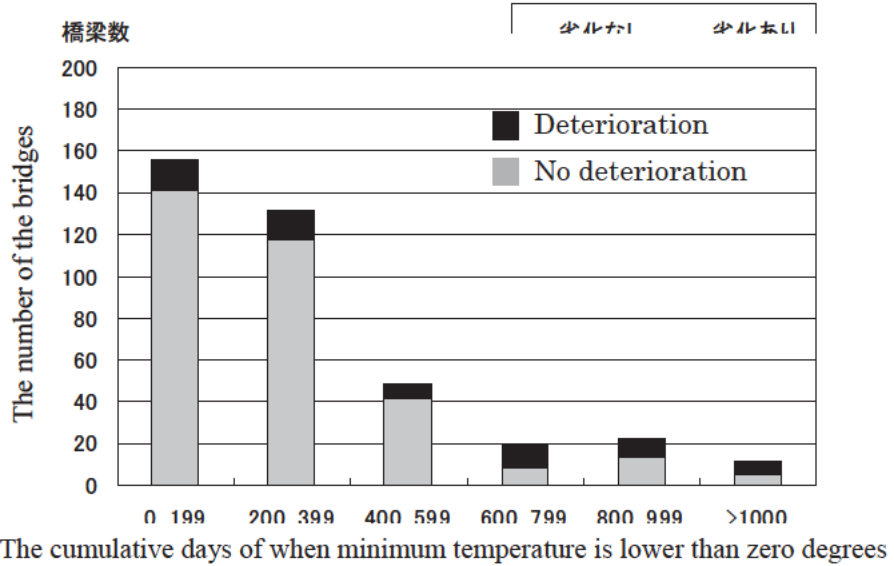


Fig.6 Number of deterioration caused by daily temperatures lower than zero degrees

We found that in many cases re-deterioration begins from the construction joint. A standard procedure in the overlay method is to polish and sweep the existing floor slab with a shot-blast machine after milling. Although the shot-blast machine is placed along the construction joint, the area which is 150mm from the construction joint cannot be sufficiently polished and swept. We also found that although a sweeper cleans after milling, chips were not fully removed and tended to remain at the edge (Fig.7). Poor adhesion may occur when concrete is casted in this state. Therefore, vibrators are used for tamping by hand.

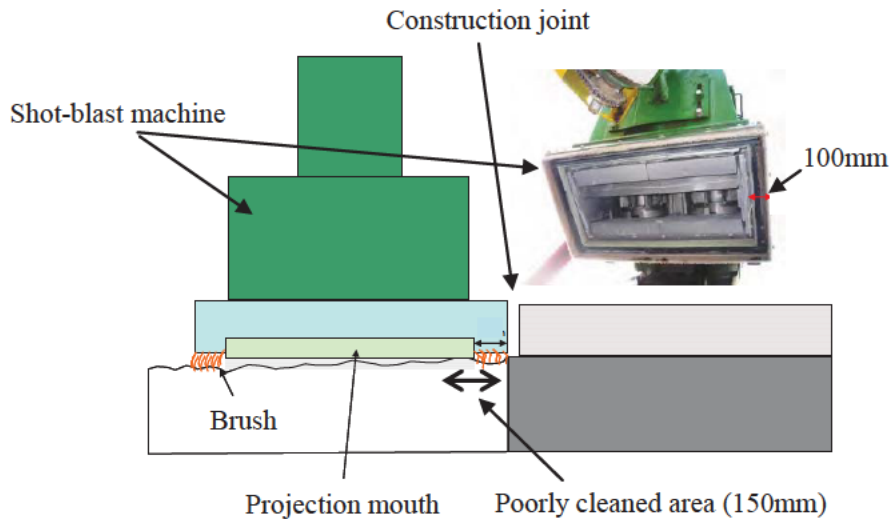


Fig.7 Position of a shot-blast machine at edge

Repair of re-deteriorated floor slab⁴⁾

In 2002, we repaired a re-deteriorated floor slab of a steel truss bridge which was reinforced by overlaying in 1990 (Fig.8). As some ten years had passed since the repair, potholes were often found in the pavement. Inspections showed that there was separation between the existing floor slab and overlaying concrete. It was assumed that this separation caused the damage to the pavement. Thereupon, we tried injecting resin in the interface of the re-deteriorated floor slab. This method was selected considering safety of road users and so that roadwork restrictions to control traffic are held down as much as possible as traffic on the bridge was more than 80,000 vehicles per day.



Fig.8 The bridge repaired by overlaying floor slab

Before the actual repair was carried out, a section of the re-deteriorated floor slab was cut out and resin was injected in the interface. Then a fatigue test using the accelerated load tester was conducted to confirm the effectiveness of the repair method. The result was compared with the fatigue test result of the section before injecting resin. Recovery of stiffness, improvement of durability and degree of separation were confirmed. The size of the section taken from floor slab of the actual steel truss bridge was 2.5m*5.0m.

Before injecting resin in the interface, approximately 2.5 liters of water was poured in from the injection holes at the center of the specimen. This was to wet the interface for the injection. Injection holes are placed at about 0.5m - 1.0m intervals. The qualities considered when selecting the resin for filling are filling characteristics, impregnation characteristics, the influence the mud on the boundary surface has on the resin, adhesiveness of the concrete and adhesiveness when surface is wet. Several hydrophilic materials were tested and an epoxy resin-based material with high filling performance was chosen.

The fatigue test showed that the number of loading (counting back and forth as one trip) before breakdown was 23,000 times for the test piece without resin injected. On the other hand, it was 139,000 times for the test piece with resin. This shows that durability is approximately 6 times more when resin is injected.

Fig.9 shows a section of the bridge actually repaired by injecting resin. After cutting the pavement, injection holes 100mm deep and with a diameter of 10mm were drilled, and the resin was injected. The resin was partly injected from the pavement surface as traffic control requirements restricted the work that can be carried out (Fig.10). In either case, the holes were cleaned by air (compressed air infusion) after drilling. But places where the concrete have turned to gravel were washed with water. Resin was injected every 1m in both longitudinal and perpendicular directions. Core sampling was performed after injection, and it was confirmed that filling was satisfactory in most of the repaired locations.

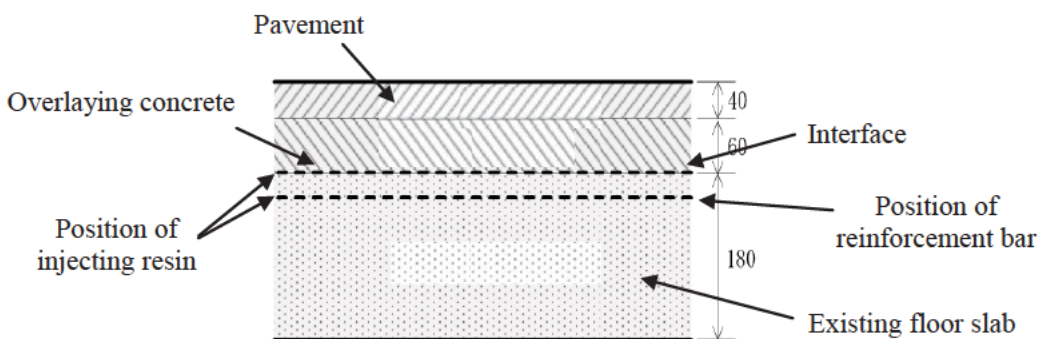


Fig.9 Section where resin was injected



Fig.10 Shows resin being injected

Examination results of reinforcement effect after repair⁵⁾

Repairs by injecting resin were carried out on a trial bases, and not many locations where the method was applied exist. Therefore, its effectiveness and the durability obtained were not verified. So to find out, we examined a re-deteriorated floor slab which had been repaired seven years ago.

Static loading test using load vehicle and frequency measurement using load of vehicles actually travelling on the bridge were conducted. In addition, separation of floor slab were tested by hammering for the upper part and visually from below for the bottom part of the floor slab.

To verify the effectiveness, the test results were compared with the results of the tests conducted in 2002 when the bridge was repaired by injecting resin. The tests were conducted under the same condition. Fig.11 shows the measurement position of the static loading test. Fig.12 shows the measurement position of deflection.

The results are as follows.

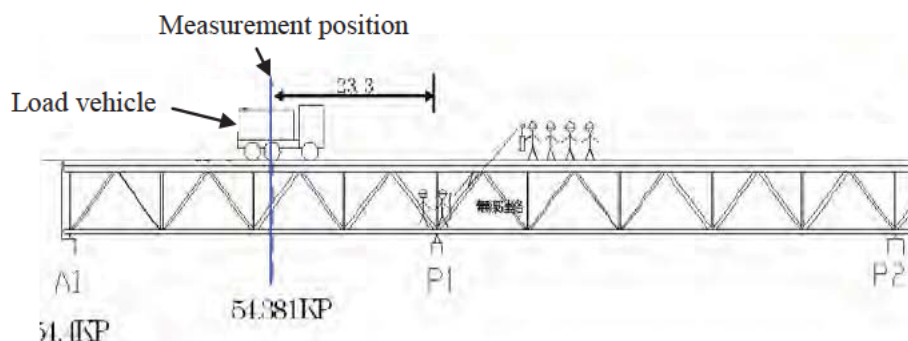


Fig.11 Measurement position of static load test

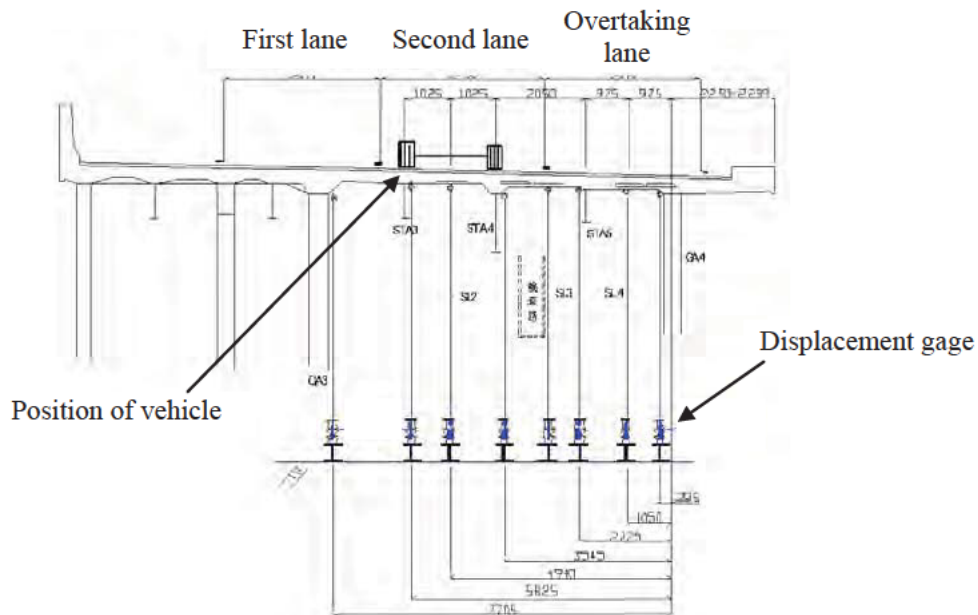


Fig.12 Measurement position of deflection

1. Static loading test

The results of the measurements of floor slab deflection, distortion of reinforcement bar and crack displacement are as follows.

The initial value was set on the assumption that there is no vehicle on the bridge and deflection was measured using a load vehicle. The "relative deflection" was compared. The value was relatively calculated, supposing that the position of an upper chord material of the main truss and the stringer were steady points.

Fig.13 shows the maximum measured deflection. The deflection decreased after repair. We found that the deflection measured “seven years after” repair is equal to the value measured immediately “after repair” and assumed that the load bearing capacity increased by the repair lasts.

The distortion of reinforcement bar was checked by measuring main reinforcement bar and distributing bar of floor slab. The measurements were compared in terms of stress, with the initial value set assuming that no vehicle is on the bridge. Though in some parts it seemed that the value for "seven years after" repair is larger than that for "before repair," when the values for immediately "after repair" and "seven years after" repair are compared, they are about equal. Therefore we assume that increased load bearing capacity continues.

Crack displacement was also measured in the same way. The results of measurements are similar to the distortion. We concluded that the possibility of cracks progressing rapidly is low.

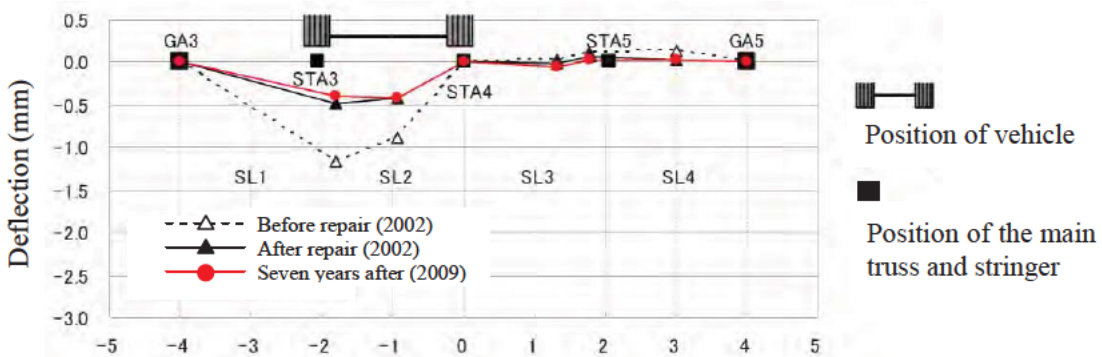


Fig.13 Distribution of relative deflection of floor slab

2. Frequency measurement using load of vehicles

Reinforcement bar distortion and crack displacement taken in the frequency measurement are as follows. The traffic density for 24 hours, the number of vehicles and the mix rate of large-size vehicles in the traffic on the day of measurement were the same as in 2002, when “after repair” confirmation tests were carried out.

Distortion was measured at main reinforcement bar and distributing bar at the bottom of floor slab. The distortion of main reinforcement bar of “seven years after” repair was the same value as immediately “after repair”. It was confirmed that the tendency was the same as the static loading test result. The distributing bar also had a similar tendency.

Crack displacement was measured for cracks in the longitudinal and perpendicular direction of the bridge axis. Fig.14 shows the measurement of a crack in the perpendicular direction. The crack displacement shows the range of crack displacement caused by vehicles travelling on the bridge. Though the displacement of “seven years after” repair is approximately 2 times that of immediately “after repair”, the displacement is low and is half that of “before repair”. Because the remaining crack width was between 0.10-0.20mm, we assumed that the crack did not tend to noticeably progress.

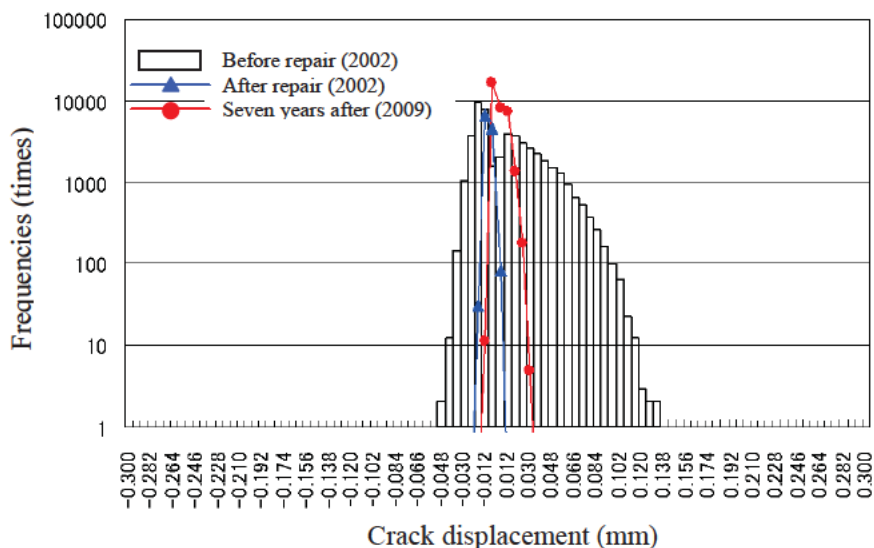


Fig.14 Frequency distribution of crack displacement

3. Examination of separation on the pavement

The area of separation was approximately 2% of the area inspected using a test hammer. (area : 6*6m). Little separation has developed after repair, and we can assume that the effectiveness of the repair is maintained.

4. Visual inspection of the floor slab bottom

A visual inspection of the floor slab bottom between A1 – P1 was performed. Though crack density progressed slightly after repair, deterioration of free lime and leakage water didn't occur. Therefore, we assume that the pace of deterioration is slow.

Conclusion

Most re-deterioration of floor slabs occurred at the construction joint between the lanes. Deterioration tended to be remarkable when large amounts of anti-freezing agents are used and when there are many days when the daily minimum temperature is below zero degrees. I would like to add that currently we apply an adhesive agent at the construction joint to improve adhesion.

Injecting resin has helped maintain floor slab condition for seven years after repair. Therefore, we can say that this method is effective as a repair method to prolong the life of the re-deterioration floor slab.

Reference

- 1) Express Highway Research Foundation of Japan: Design construction manual of overlaying floor slab method, 1995.7
- 2) NEXCO: Expressway Standard Specification by NEXCO for Bridge Maintenance Design, 2011.7
- 3) T.Nagatani, K.Wada, T.Ogata: Deterioration reproduction experiment of a part of construction joint on overlaying floor slab, Proceedings of the Japan Concrete Institute Vo1.32, No.2, 2010
- 4) S.Kubo, M.Fujii, Y.Miyasaka, M.Matsumoto, T.Itabashi: Consideration on repair method of deteriorated floor slab, Japan Society of Civil Engineers 2010 Annual Meeting, 2003.9
- 5) A.Goto, T.Nagatani, T.Ogata, M.Matsumoto: Examination of overlaying floor slab repaired by injecting resin, Proceedings of the Japan Concrete Institute Vo1.33, No.2, 2011

REPAIRING FATIGUE CRACKS IN A STEEL DECK PLATE GIRDER BRIDGE OF UNUSUAL STRUCTURE

Haruhiko Nakata¹, Yoshiyuki Takamura¹, Ken Tokumasu²

Abstract

Morinomiya section of the Hanshin Expressway Higashi Osaka Route (#13) was opened to traffic in 1978. In October 2010 significant fatigue cracks were found in some main girder support areas of a three-span continuous steel deck plate girder bridge in this section. These cracks were found to have initiated in weld beads on the sole plate or around the bearing set bolts and propagated partly into the webs in only four years. This paper identifies damage cause through structural analysis and field measurement and presents an emergency repair measure which takes into account ease of operation and fatigue durability.

Introduction

A three-span continuous plate girder bridge with steel decks (spans: 9.8 m + 10.0 m + 9.8 m; total width: 16.0 m) on the Hanshin Expressway Higashi Osaka Route (#13) was found to have fatigue cracks in some main girder support areas in 1993 after 15 years of service. They were repaired by patching, and old steel bearings were replaced with rubber ones. However, fatigue cracks were again found in the main girder support areas in October 2010. Cracks originating at weld beads on the sole plate or around the bearing set bolts were found penetrating through the bottom flange of the main girder or end cross beam and propagating partly further into the webs. Since no cracks were found during the latest inspection in 2006, these fatigue cracks were thought to have initiated and propagated in about four years. It was decided to take immediate measures to prevent possible rapid growth of these cracks.

Structural overview

The bridge with the fatigue cracks is a part of a bridge system consisting of simple or continuous plate girder steel deck bridges. The steel deck plate girder type was selected for its light weight because this section passing over the ruins of the ancient NANIWA PALACE SITE needed to be designed to protect architectural remains of the palace.

The Higashi Osaka Route is a heavy traffic road connecting Osaka City area and its eastern suburb of Higashi Osaka, travelled by about 85,000 vehicles per day on average, including 17,800 heavy vehicles which account for about 20%.

The superstructure of this bridge is larger in width (16 m) than in span length (10 m) and, therefore, has a very limited girder height of 700 mm. The bottom flanges of main girders and those of end cross beams are on the same plane and connected to

¹ Hanshin Expressway Engineering Company Limited, Osaka, Japan

² Hanshin Expressway Company Limited, Osaka, Japan

each other by welding, which inevitably results in a low fatigue strength.

This bridge has an unusual structure in which only three of seven main girders are supported by bearings.

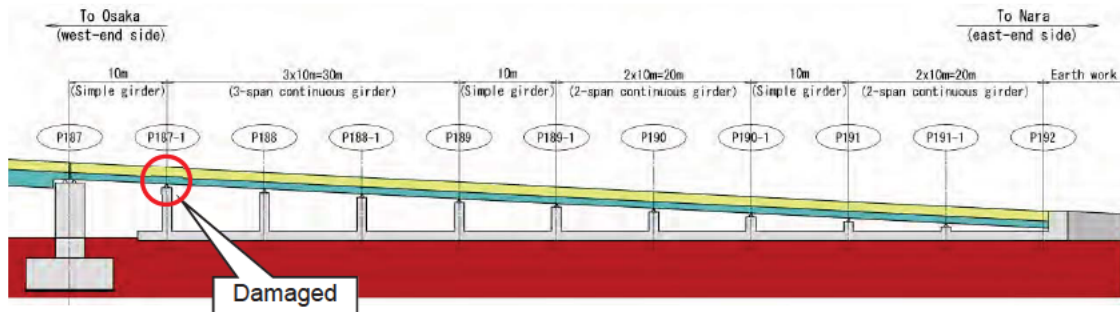


FIGURE 1 SIDE VIEW OF THE WHOLE BRIDGE SYSTEM

The fatigue cracks were found in girders G1 and G7 at the end support (P187-1) of the three-span continuous steel deck plate girder bridge which was located on the west-end side of this section.

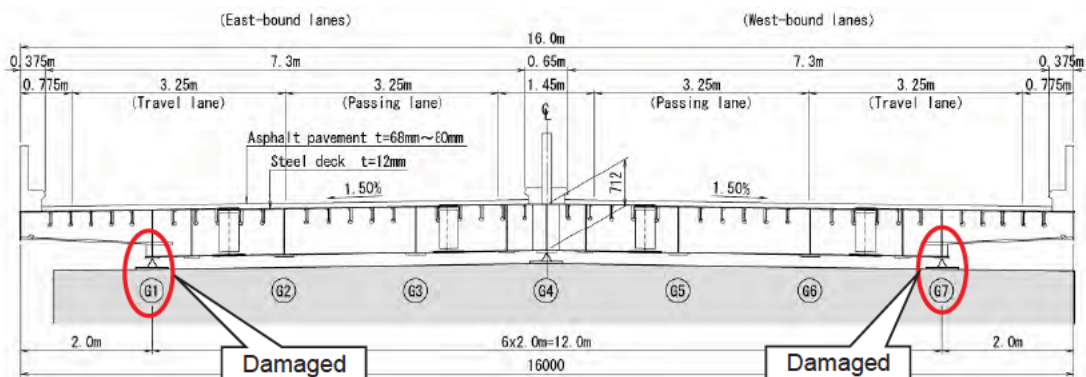


FIGURE 2 SECTIONAL VIEW OF THE SUPERSTRUCTURE

Inspection and repair histories

Every route of the Hanshin Expressway is inspected routinely and periodically for proper maintenance. Periodic inspection is primarily a visual examination from a close distance and is conducted every five to eight years. Routine inspection is conducted six times a year by primarily observing the structure at a distance from the ground using a binocular.

The first periodic inspection on the bridge in this report was performed in 1987 after nine years of service. The bridge then underwent five more periodic inspections by the end of 2006 and was found to have some damage at every close-up examination.

Table 1 shows a list of years of periodic inspections and damage found during each inspection.

TABLE 1 PERIODIC INSPECTION AND DAMAGE HISTORIES

Year of periodic inspection	Years in service	Damage in girder G1 and repairs	Damage in girder G7
1978	--	Opened to traffic.	
1987	9 years	No damage was found.	
1991	13 years	Cracks in welds between the sole plate and the main girder bottom flange Cracks in the main girder and end cross beam bottom flanges These cracks were repaired and bearing replacement was implemented in 1993.	No damage was found.
1996	18 years	Movements of the bearings Gap between the top shoe and the rubber	
2004	26 years	Same as above.	
2006	28 years	Movements of the bearings Gap between the top shoe and the sole plate	

Damage was first found in 1991 after 13 years of service when fatigue cracks were detected in girder G1 in a support area. Cracks originating at weld beads between the sole plate and main girder bottom flange or around the bearing set bolts were found propagating toward the edge of the main girder bottom flange. These fatigue cracks were welded and patched for repair, and the existing bearings were replaced with new ones.

Main girder damage was found only in 1991, and other defects detected during periodic inspections included movements of the bearings.

No damage has been detected in Girder G7 which was found in healthy state during periodic inspection in 2006.

Field investigation

Damage in girders G1 and G7 at the supports

Field investigation was carried out by close-up visual examination. Magnetic particle testing was also performed to obtain accurate locations of the cracks.

Cracks in girder G1 initiated in weld beads between the sole plate and the end cross beam bottom flange and grew penetrating through the flange and partly propagating further into the weld between the flange and the web of the end cross beam. Cracks were also found in the main girder bottom flange, originating at around the bearing set bolt. None of them was propagating into the main girder web which had a patch plate on it.

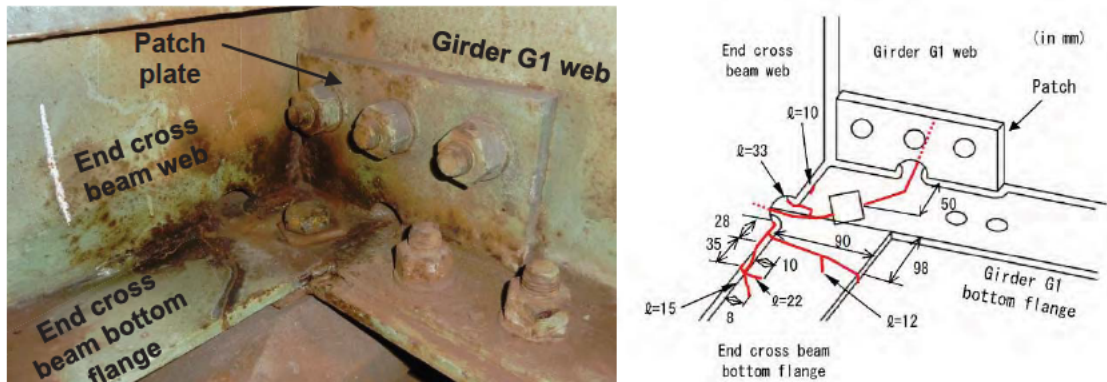


PHOTO 1 CRACKS IN GIRDER G1

Cracks in girder G7 initiated in weld beads between the sole plate and the main girder bottom flange and penetrated through the flange. They propagated into the weld between the flange and the web of the main girder, and partly further into the web.

Gap was found between the sole plate and the top shoe in both girders G1 and G7. The girders were found to move in the vertical direction with every passage of vehicle, generating metal sound.

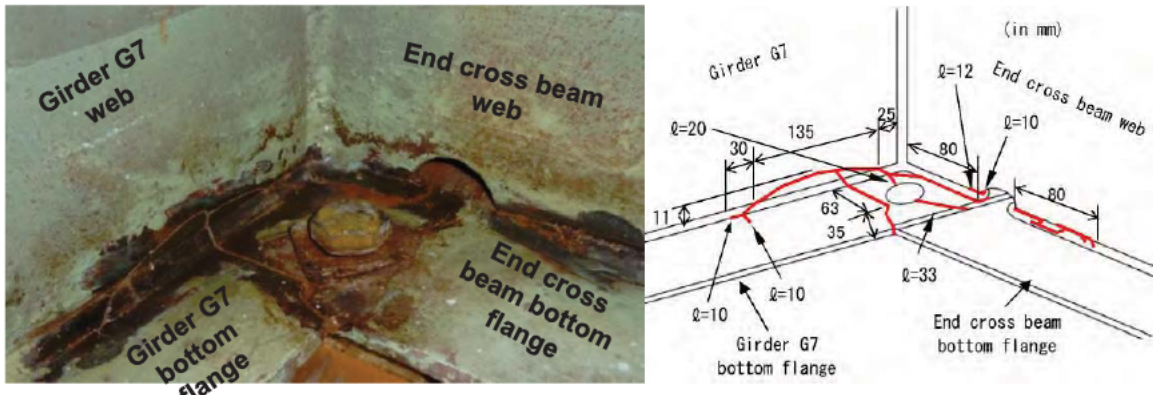


PHOTO 2 CRACKS IN GIRDER G7

Other damage

Beside fatigue cracks, shoe base mortar was found damaged on girders G1 and G4. There was corrosion in the main girders due to leakage of water from the expansion joints, but without any reduction in cross-section. No cracks were found in the longitudinal ribs or deck plates of the steel decks.

Checking surface height differences at expansion joints

The vertical movements of girders G1 and G7 with the passage of vehicles suggested the presence of surface height differences at the expansion joints between the longitudinally adjacent girders. Road surface was investigated at the expansion joints, and it was found that there were surface differences of 12 mm and 8 mm,

respectively, in the west-bound lanes (in the side of girder G7) and in the east-bound lanes (in the side of girder G1).

Heights of girders G1 and G7 were adjusted in an attempt to eliminate surface height differences. However, jacking up girder G1 made girder G7 lower, and jacking up girder G7 made girder G1 lower. Such behavior like a balancing toy suggested that the superstructure was in an unstable state balancing on a fulcrum at girder G4.

Damage cause estimation

Process from damage cause estimation to emergency repair decision

Figure 3 shows the process how emergency repair was decided based on the inspection and repair histories and field investigation results.

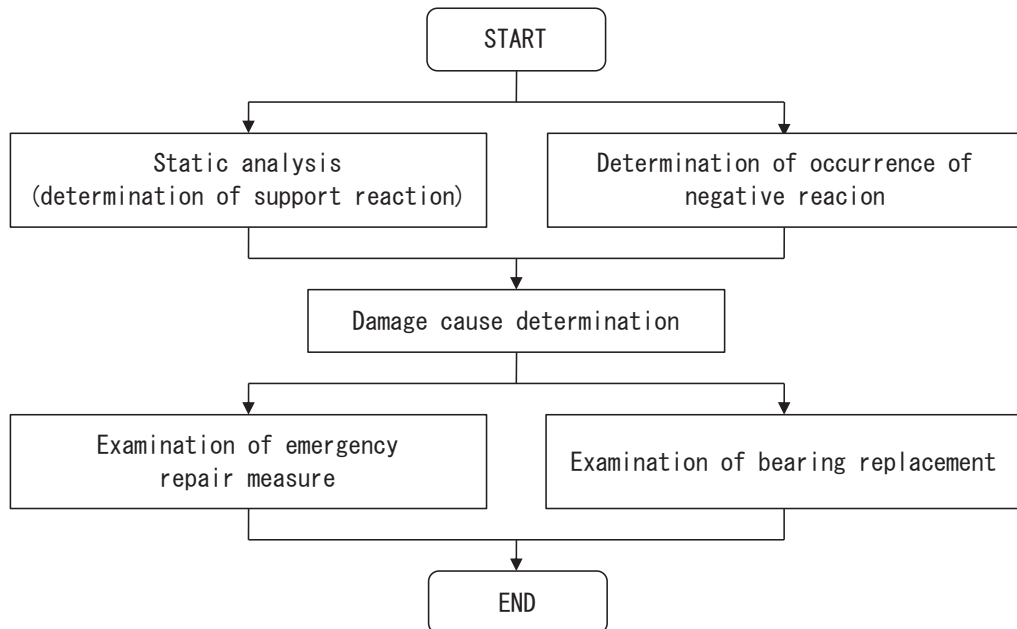


FIGURE 3 PROCESS TO EMERGENCY REPAIR DECISION

Static analysis

Static analysis was carried out first in order to understand support reactions. Using a plane frame model of the superstructure, lattice analysis was made to obtain support reaction values. Design live load of this bridge at construction was TL-20. In order to evaluate reactions under current standards, the analysis was also made for L and T loads of B live load. T load was included in addition to L load because the effects of T load were considered to be significant in this superstructure where the width, 16 m, was larger than the span length, 10 m (JRA, 2002).

Table 2 shows a list of reaction values obtained by the lattice analysis.

TABLE 2 REACTION VALUES

(in kN)

		End supports (P187-1, P189)				
		Dead load (D)	Maximum live load (L_{max})	Minimum live load (L_{min})	$D + L_{max}$	$D + L_{min}$
TL-20	Girder G1	101.9	389.1	-40.5	491.0	61.4
	Girder G4	128.7	526.0	-63.3	654.8	65.5
	Girder G7	101.9	389.1	-40.5	491.0	61.4
	Total	332.5	--	--	--	--
B live load (T load)	Girder G1	101.9	541.8	-43.3	643.7	58.6
	Girder G4	128.7	683.0	-50.0	811.8	78.8
	Girder G7	101.9	541.8	-43.3	643.7	58.6
	Total	332.5	--	--	--	--

The static analysis results showed no negative reactions at either support under normal conditions (dead load reaction + live load reaction). However, dead load reaction was found to be about 100 kN and live load reaction was about 540 kN, which made a ratio of 1:5. This large ratio of live load reaction suggested that stress from live load fluctuations was significant in this superstructure.

Determination of occurrence of negative reaction

Although no occurrence of negative reaction was indicated by the static analysis, the analysis values were based on the assumption that the superstructure was correctly manufactured and erected as designed. The vertical movements of the damaged main girders observed with every passage of vehicle during the field investigation suggested occurrence of negative reaction. In order to determine whether negative reaction actually occurred at supports or not, vertical strain under vehicle traffic was measured, using strain gauges attached to some members in a support area. It was expected that fluctuations in support reaction might be estimated from dynamic measurement of strain response to vehicle traffic in the main girder web, end cross beam web and support stiffener in the support area. Any strain occurring in the tensile direction should indicate occurrence of negative reaction overwhelming dead load reaction.

Members and points for vertical strain measurement in the support area

Because accurate stress measurement was impossible with the damaged members, the authors selected girder G7 on P189 which had the same detail but no damage for the vertical strain measurement. Figure 4 shows the measurement points: three on the main girder web, one on the support stiffener and three on the end cross beam web in the support area. Continuous measurement was carried out for 72 consecutive hours on weekdays to represent typical vehicle traffic conditions.

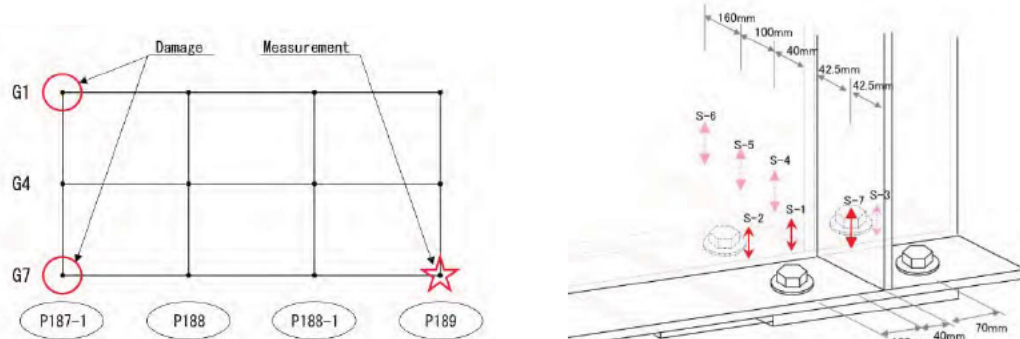


FIGURE 4: STRAIN MEASUREMENT LOCATIONS AND POINTS

Results on occurrence of reaction

Figure 5 shows stress waveforms under vehicle traffic obtained from the vertical strain measurements in the support area. As shown here, no negative reaction occurred with the passage of vehicle. There was a slight stress in the tensile direction at point S-6 on the end cross beam, which was attributed to the wheel load on the overhang causing the backup plate of bracket to uplift.

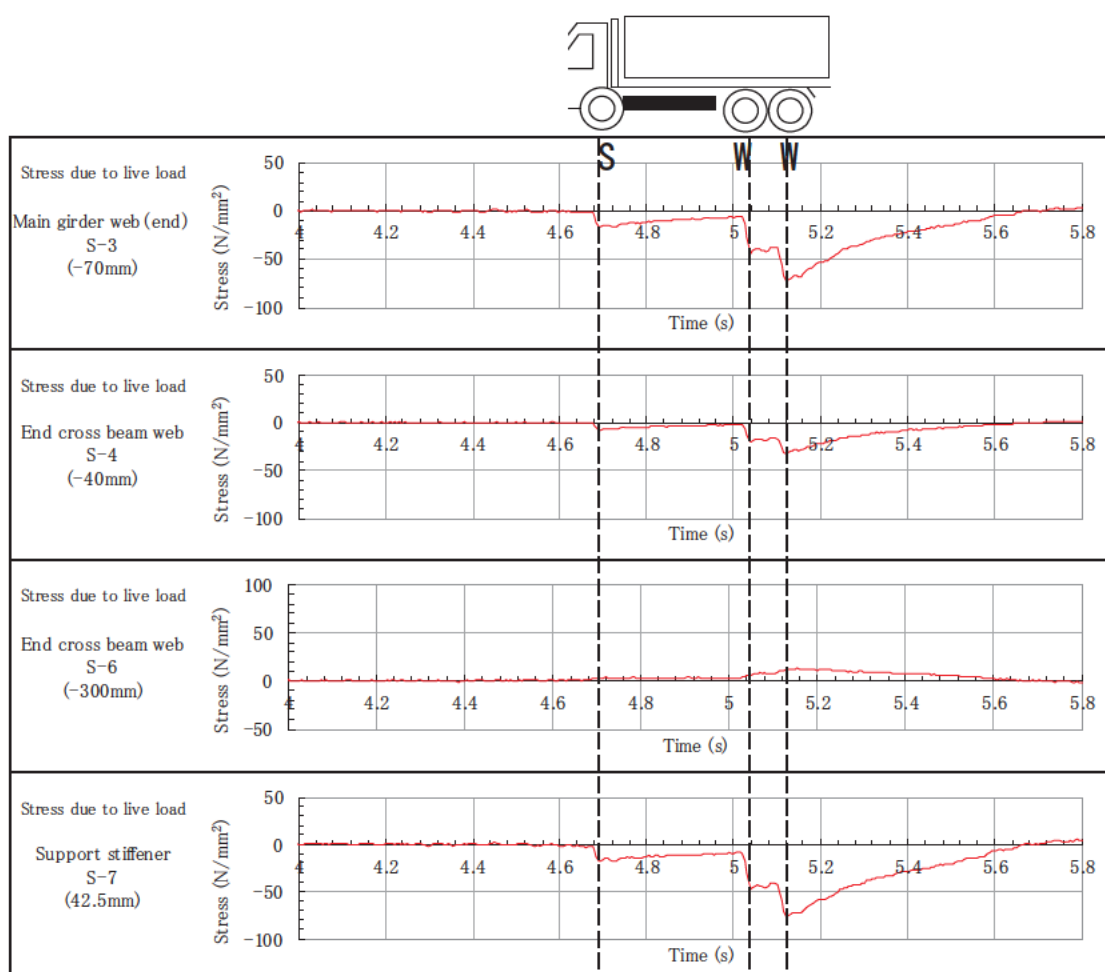


FIGURE 5 STRESS WAVEFORMS UNDER VEHICLE TRAFFIC

Damage cause estimation

The static analysis and stress measurement revealed no occurrence of negative reaction in the support areas. Therefore, it was concluded that what caused the damage was not an uplift of the girders due to negative reaction.

The focus was then moved to the damage to the shoe base mortar on girders G1 and G4. The assumption was that deterioration of the shoe base mortar with time caused settlement of the bearings, which resulted in vertical movements of the main girders, giving impacts to the damaged parts (Figure 6).

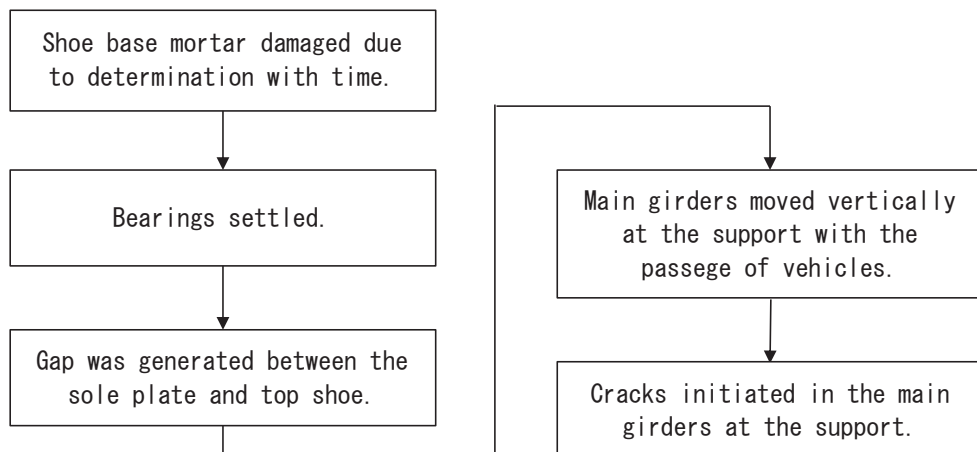


FIGURE 6: COURSE OF DAMAGE EVOLUTION

Emergency repair measure

Examination of emergency repair measure

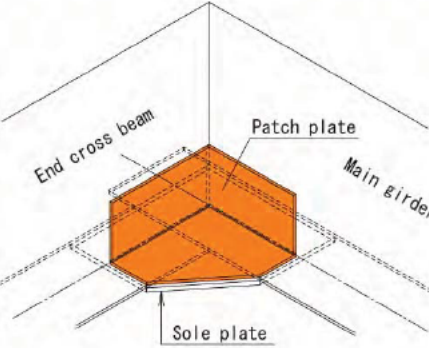
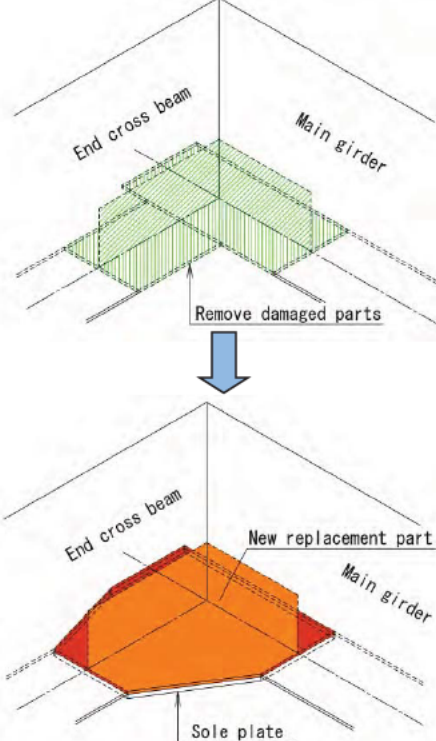
The fact that the cracks found in the main girders in the support areas grew in a very short period indicated an urgent need for some action. It was decided to carry out emergency repair as an immediate measure. There were two plans for emergency repair: (1) patching; and (2) partial replacement. Replacement of bearings was also taken into account because of the damage to the shoe base mortar of girders G1 and G4. Through a comparative examination, the partial replacement plan was selected to take advantage of complete removal of cracks which could eliminate possible future concerns and provide improved fatigue durability to the structure.

Table 3 shows a comparative table of the two plans.

High tension bolts were selected for the connection of parts, while field welding was also possible. The repair work needed to be carried out while the expressway was open to traffic, and the headway available for work space was very limited. Field welding under such conditions was considered to be difficult, especially in terms of quality control. In addition, the large stress amplitude due to live load might cause

damage to the new weld in future. In contrast, high tension bolts were considered to be easy to install even under normal traffic and capable of providing more secure connection than field welding.

TABLE 3 EMERGENCY REPAIR MEASURE COMPARATIVE TABLE

	PLAN 1: PATCHING	PLAN 2: PARTIAL REPLACEMENT
Schematics		
Description	<ul style="list-style-type: none"> Patch plates are fitted to the main girder web, end cross beam web and their bottom flanges to cover the cracks. Cracks remain as they are. 	<ul style="list-style-type: none"> Parts with cracks are removed, and new shop-manufactured parts are installed. Cracks are removed completely.
Structure	<ul style="list-style-type: none"> Fatigue durability does not change. 	<input type="triangle"/> <ul style="list-style-type: none"> Cracks are removed, leaving no concerns about their growth. Fatigue durability increases as the main girder and end cross beam bottom flanges are unified in the new part.
Ease of operation	<ul style="list-style-type: none"> Work under normal traffic is possible. Work period is shorter than Plan 2. Limited headway makes the work difficult. 	<input type="circle"/> <ul style="list-style-type: none"> Work under normal traffic is possible. Removal of the parts with cracks requires a longer work period. Limited headway makes the work difficult.
Economics	<ul style="list-style-type: none"> Economic efficiency is high. 	<input type="circle"/> <ul style="list-style-type: none"> Economic efficiency is low.
Maintenance	<ul style="list-style-type: none"> Existing cracks may grow in future. Existing cracks cannot be monitored because a check hole cannot be made in the patch plate. 	<input checked="" type="cross"/> <ul style="list-style-type: none"> Increased fatigue durability due to the replacement provides excellent maintenance properties.
Overall evaluation	<input type="triangle"/>	<input type="circle"/>

Features of the partial replacement plan are described below.

- (1) To improve fatigue durability, the main girder and end cross beam bottom flanges were unified in the new replacement part.
- (2) The planar dimensions of the sole plate were made larger to reduce stress concentration in the support area.
- (3) The ends of the sole plate were tapered to alleviate stress concentration due to drastic change in cross-section around the sole plate.
- (4) High tension bolts were used for the connection with the sole plate, main girder bottom flange and end cross beam bottom flange, to improve fatigue durability.
- (5) In order to assure stiffness in the main girders in the support areas, splice plates were installed on the main girder web to a height one half the girder height which was the effective buckling length above the support point.
- (6) Angle steels were installed where the main girder web met the end cross beam web, to ensure transmission of vertical force between the new and existing parts above the support point.
- (7) As a fatigue countermeasure for the support stiffener, stiffness of the overhang bracket was enhanced to control deflection.

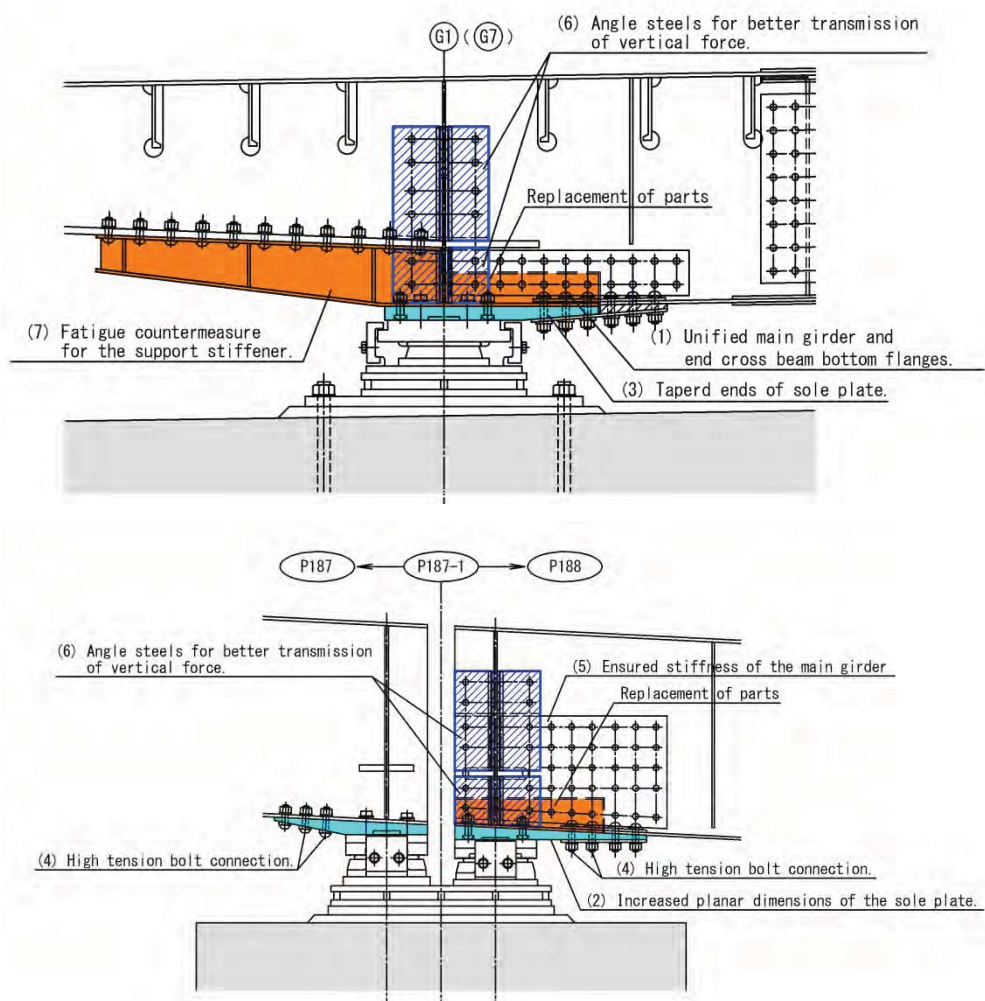


FIGURE 7 SCHEMATIC DIAGRAMS OF THE REPAIR

Figure 7 shows the schematic diagrams of the partial replacement plan. The numbers in the diagrams correspond to the numbers in the above list. The parts marked with red color are those to be replaced, and the blue-colored part is the new sole plate to be installed.

Study on bearing replacement

The damage found in the existing shoe base mortar on girders G1 and G4 suggested influences on the capacity to carry reaction force. On the other hand, the limited headway required the existing bearings to be temporarily removed for the emergency repair work to create a sufficient work space. However, fine height adjustment was difficult with the existing bearing system in which the higher bearing on the west-end side and the lower bearing on the east-end side were mounted on the same block, sharing one base plate, one height adjustment plate and one bottom shoe (Figure 8).

Consequently, it was decided to replace the bearings at the same time with the emergency repair work. Steel bearings were employed to replace the existing rubber ones so that reaction force would be carried more properly. In order to make height adjustment in the field easy, the height adjustment plate was divided into two parts for the two bearings.

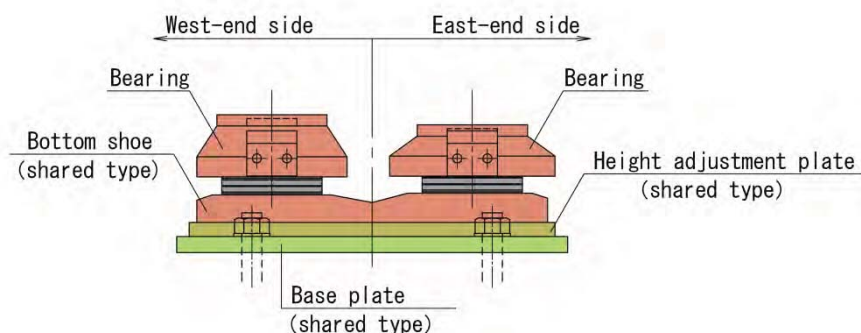


FIGURE 8 SIDE VIEW OF THE EXISTING BEARINGS

There was significant leakage of water from the expansion joints. Rainwater could have penetrated through the damage in the shoe base mortar, causing corrosion of the bearing anchor bolts. Ultrasonic measurement was carried out on the existing bearing anchor bolts, and it was found that their embedment length was about 400 mm at minimum against 610 mm in as-built drawings.

Since corrosion and possible reduction in cross-section of the existing bearing anchor bolts were suggested by the measurement results, the existing anchor bolts were discarded and replaced with new ones for the new bearings.

Conclusions

In this paper damage cause was estimated from structural analysis and field measurement results, and emergency repair measure was discussed, with fatigue durability emphasized for the prevention of possible similar problems in future. Key findings are summarized below.

- 1) Static analysis revealed that the superstructure was subject to live load effects, with a ratio of dead load reaction to live load reaction being 1:5.
- 2) The static analysis and stress measurement revealed no occurrence of negative reaction. Therefore, it was concluded that what caused the damage was not an uplift of the girders due to negative reaction.
- 3) The damage cause was assumed to be impact from vertical movements of the main girders due to settlement of the bearings caused by deterioration of shoe base mortar with time.
- 4) Partial replacement was selected for the emergency repair to take advantage of complete removal of cracks which could eliminate future concerns about growing cracks and provide improved fatigue durability to the structure.
- 5) High tension bolts were used for the connection with the sole plate, main girder bottom flange and end cross beam bottom flange to improve fatigue durability.
- 6) The bottom flange of the main girder and that of the end cross beam were unified in the new replacement part for improved fatigue durability.
- 7) Although no damage was found in the support stiffener in this study, damage was detected in other locations with the same detail in other spans. Therefore, fatigue countermeasure was taken as a preventive maintenance by improving stiffness of the overhang bracket to control deflection.
- 8) Bearings were replaced at the same time with the emergency repair work. This allowed to obtain a sufficient work space in the limited headway, improving ease of operation.
- 9) In the new bearing system the height adjustment plate was divided into two parts for the two bearings on the west- and east-end sides to make height adjustment in the field easy.

Closing remarks

The emergency repair project described in this paper has just been completed. Photo 3 shows girder G7 after removal of the damaged parts. Photo 4 shows the same girder after the partial replacement, with the bearings also replaced.

Stress measurement is planned in the vicinity of the emergency repair site to evaluate the repair effect by comparing the measurement results with those for other locations with the same detail but no damage.

This section of the expressway consists of similar structures to this bridge which is subject to live load effects. Permanent repair including in-depth modification will be conducted on this section next year.



PHOTO 3 GIRDER G7 IMMEDIATELY AFTER REMOVAL OF THE PARTS WITH CRACKS



PHOTO 4 GIRDER G7 AT THE COMPLETION OF EMERGENCY REPAIR

References

- [1] Japan Road Association (JRA): Specifications for Highway Bridges and Commentary, Part II Steel Bridges, March 2002.

DEVELOPMENT OF EDDY CURRENT TEST TO DETECT FATIGUE DAMAGES ON ORTHOTROPIC STEEL DECK

Hiroki Sugiyama & Akiko Tabata¹

Hiroyuki Nakajima, Tetsuji Yamagami & Sigeaki Tsukamoto²

Akira Shiraishi & Takaaki Yamada³

Abstract

In recent years, a number of fatigue damages in steel orthotropic deck bridges have been reported. Among them, those occurring in the welded connections between orthotropic deck and U-shaped ribs, in which cracks starting at the weld roots develop in the direction of the deck thickness, penetrating into the deck plate, raise a serious problem. In case these cracks develop along a long extension, they may cause the road to sink and harm to third parties, requiring early detection and measures from the road administrators. As these cracks cannot be seen without the removal of the asphalt, various types of non-destructive testing methods, including ultra-sonic inspection methods, were carried out, without effective results. Thus, the Hanshin Expressway group has developed a sophisticated method to detect these cracks, by integrating infrared, eddy current and phased array ultrasonic inspections. Among these methods, efforts were made in the development of the eddy current method as an effective inspection method.

Introduction

Steel road bridges having orthotropic decks, due to its lightness and short construction time, have been widely applied in the costal area of urban highways. In recent years, with the increase in the traffic amount and the constant occurrence of overloaded vehicles, fatigue damages on orthotropic decks have been reported.

As it is shown in Figure 1, fatigue damages on orthotropic decks can be classified into 4 groups.

- ① Cracks occurring in along the weld between the deck and U-shaped rib
- ② Cracks occurring in the weld between the U-shaped rib and transverse beams.
- ③ Cracks occurring in the butt weld between U-shaped rib and transverse beams
- ④ Cracks occurring in the weld between the deck plate and the vertical stiffeners

In particular, type① cracks originated in the root of the weld between the U-shaped rib and the deck can be classified into 3 types.

- ①-1 Weld bead crack
- ①-2 Cracks originated in the weld bead and developing into the U-shaped rib base material
- ①-3 Cracks developed into the deck surface.

¹ Hanshin Expressway Company Limited, Osaka, Japan

² Hanshin Expressway Engineering Company Limited, Osaka, Japan

³ Nihon Densokuki Co. Ltd., Fukuoka, Japan

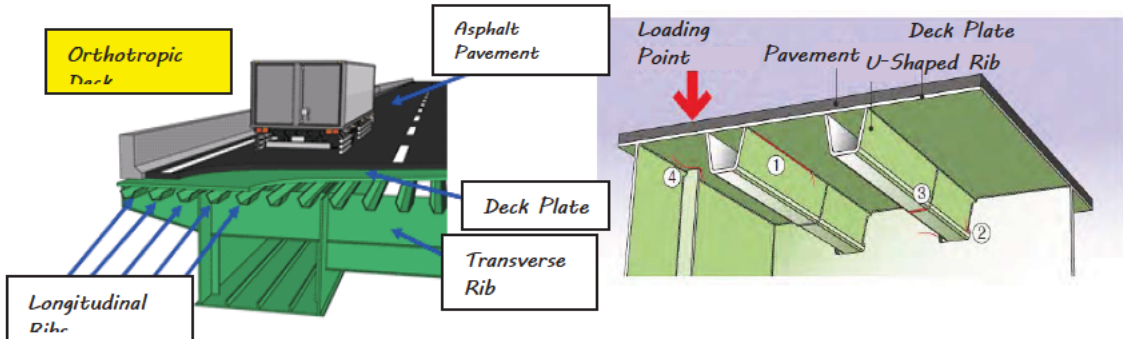


Figure 1. Types of fatigue damages

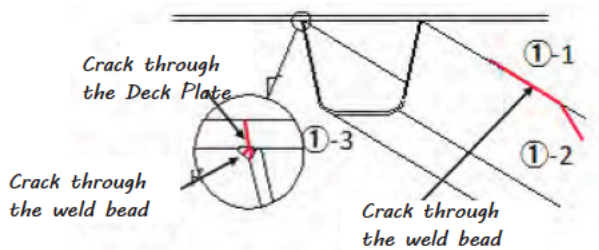


Figure 2. Fatigue cracks between deck plate and U-shaped ribs

In type ①-3 in case the crack penetrates through the deck plate into the surface of the deck and extends along a long length, not only it affects the asphalt but also, causes the local reduction of the deck strength, what may cause local collapse of the road and consequent risk of harm to third parties.

Therefore, early detection and reinforcement of fatigue cracks in orthotropic decks, specially of type ①-3, are required from the road administrators.

Thus, the Hanshin Expressway is performing inspections focusing in fatigue cracks in orthotropic decks. These inspections are carried out mainly by experienced inspectors and are based on visual inspection of the orthotropic deck from its lower surface. In case abnormality is found in the visual inspection, detailed inspections are carried out through non-destructive testing such as, eddy current test, penetrant test and ultrasonic test.

However, among crack types ① to ④, cracks of type ①-3 develop from the weld root in the direction of the deck upper surface. These cracks not only cannot be visually detected from the lower surface of the deck, as it shown in Figure 3, but they cannot also be found by visual inspection of the upper surface of the deck without removing the pavement, as it is shown in Figure 4.

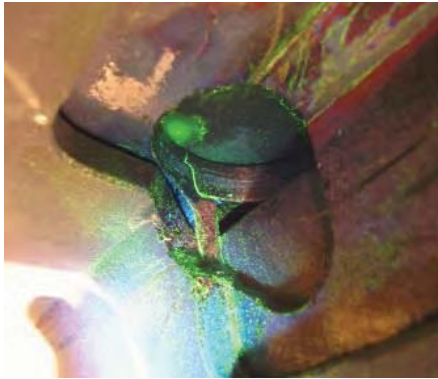


Figure3. Lower surface of the deck plate Figure 4. Upper surface of the deck plate
(without pavement)



Therefore the only inspection method available was the ultrasonic inspection carried out from the bottom surface of the deck plate.

However, ultrasonic inspections have the following disadvantages.

- Because they require contact with the steel orthotropic deck, proper equipment and scaffolding works are necessary.
- In high viaducts or water crossing, they require large-scale overall scaffolding works.
- Because of the above mentioned requirements, the efficiency or the whole inspection is not good.
- Comparing the inspection costs, the costs of the facilities are high, having budget restraints.
- Although the cycle of the inspections are not yet defined, periodic inspections are necessary.

Thus, a rational and economic inspection method with high performance to detect cracks penetrating the deck plate is required.

As rational and economic methods, ①infrared inspection, ②eddy-current inspection and ③phased array ultrasonic inspection can be mentioned. Among these methods focus was made on the eddy-current method as an effective method and an inspection of orthotropic decks was developed.

Eddy current inspection

When detecting cracks that perforate the deck plate and cannot be visualized through non-destructive tests, inspections can be carried out either from the upper, or from the bottom surface of the steel orthotropic deck.

As it was mentioned in the above lines, inspections from the bottom surface of the orthotropic deck are not effective due to the necessary scaffolding works. Thus, an inspection method that can be carried out from the pavement surface, without any physical contact with the deck surface, would provide a better performance.

The characteristics of the non-destructive methods considered in the present

study are presented in Figure 5.

		[Non destructive test equipment]		
Type		upper surface crack	lower surface crack	perforating crack
Eddy Current	non contact max. lift off			
Phased Array	contact image processing			
Continuous Magnetic Saturation	non contact min lift off			

Figure 5. Testing methods

Considering that inspection through the pavement will have to be carried out without physical contact with the deck surface, the present investigation focused on the eddy current method, which can be carried out even with relatively high lift-offs. The eddy current test, being a test which can be carried out without contacting the surface of the members, has been applied to slender pipes in thermal transformers of electrical plants. As shown in Figure 6, inspections were carried out inside slender pipes in a speed of over 2 m/s to detect cracks and corrosion without touching the pipes surface.

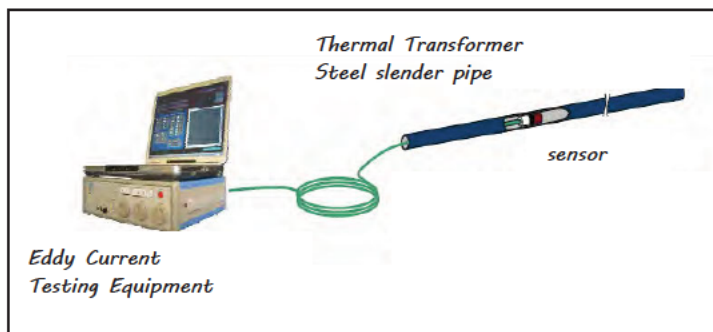


Figure 6. Eddy current test for slender pipes of thermal transformers

The development was carried out on a method applying the techniques of the eddy current inspection. The following problems were found in developing the present method.

- ① The traditional eddy current method is one-dimensional, whereas the steel deck is a two-dimensional structure
- ② The maximum pavement thickness being about 80 mm, is extremely big compared to the ordinary lift-offs found in eddy current tests.
- ③ The effects of the pavement on the magnetic field generated in the eddy current test are still not clear.

To solve these problems, the following steps were carried out in the development of a new method

- ① Laboratory Tests (vacant lift-off tests)
- ② Laboratory Tests (pavement lift-off tests)
- ③ Test in situ (vacant lift-off tests)
- ④ Test in situ (actual pavement tests)

Laboratory tests (vacant lift-off test)

Crack detection tests were carried out in specimens having the same thickness of that of the actual orthotropic deck plate, $t=12$ mm. The specimens also contained artificial cracks having a width of 0.5 mm and a length of 10 cm. As shown in Figure 7, eddy current detectors having horizontally distributed coils (DIF type) and vertically distributed coils (ABS type) were fabricated and comparisons were made.

Crack detection tests were carried out with lift-offs of 5 mm to 70 mm. To avoid the effects of surface roughness, an acrylic plate of 5mm was placed on the contact surface. (Figure 8)

The signal of the detection test is shown in Figure 9. With the increase in the lift-off, the ABS type was able to detect the crack through a lift-off of 70mm. However, for the DIF type, there was an inclination to decrease the detection rate and cracks could not be detected for a 70 mm lift-off. Therefore, the ABS type was selected for the sensor.

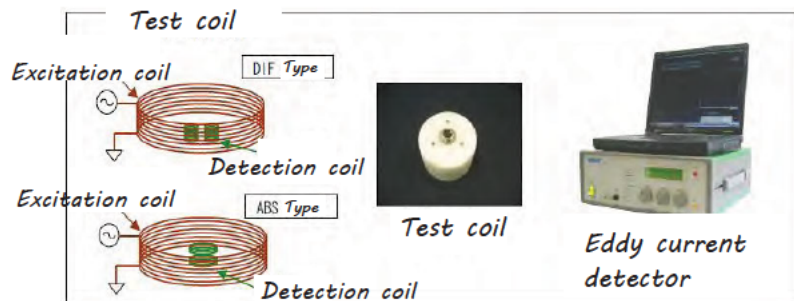


Figure 7. Eddy current test equipment



Figure 8. Laboratory tests

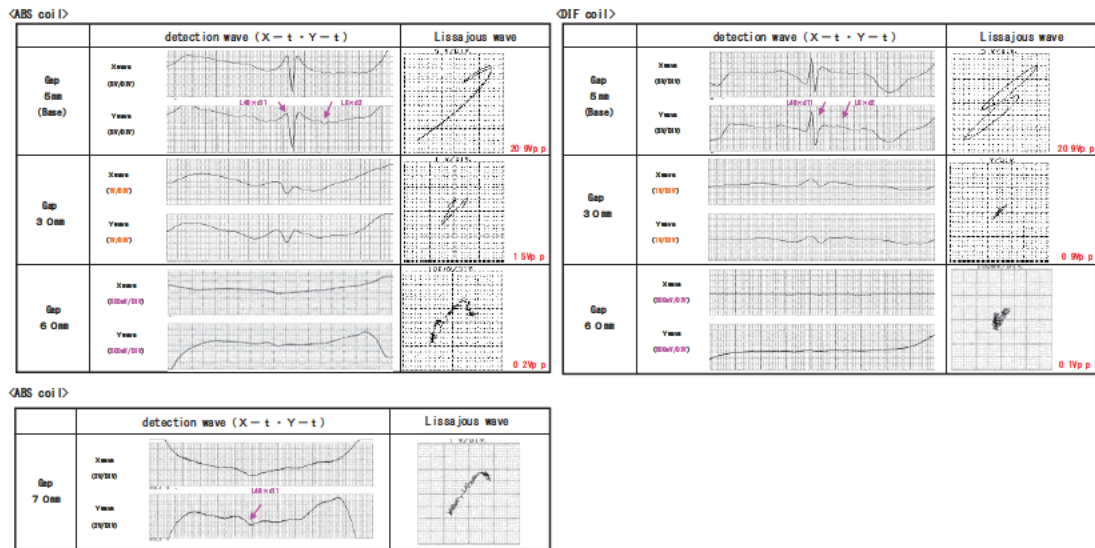


Figure 9. Laboratory tests (comparison of coils)

Laboratory tests (pavement lift-off test)

To investigate on the effects of the pavement during detection inspections performed in actual bridges, pavement blocks having thicknesses of 20 mm and 40 mm were placed on the specimens mentioned in the former section. Detection tests for lift-off of 25 mm and 45 mm were carried out, and the results were compared.

Detection signal data are shown in Figure 10. Comparison between the specimens with and without pavement, it was concluded that there is no influence of pavement on the detection test results.

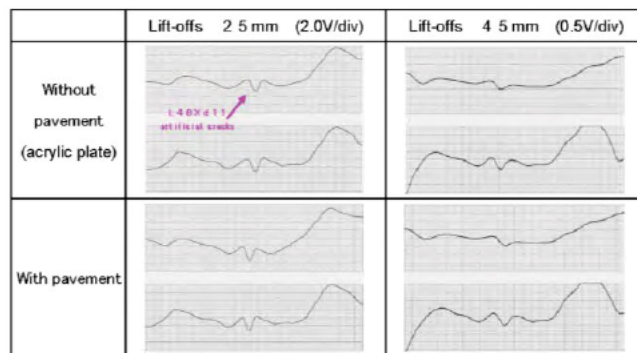


Figure 10. Laboratory tests for pavement lift-offs

Tests in situ (vacant lift-off test)

As shown in Figure 11, detection tests were carried out on cracks perforating the deck, found during pavement replacement works in the Hanshin Expressway. The detected crack was 245mm long.



Figure 11. Eddy current test (without pavement)

調査箇所：欠陥部
Detection tests were carried out for lift-offs of 5 mm, 30 mm, 55 mm and 85 mm. The results are shown in Figure 12.

It was confirmed that the cracks can be detected even for a lift-off equivalent to the pavement thickness.

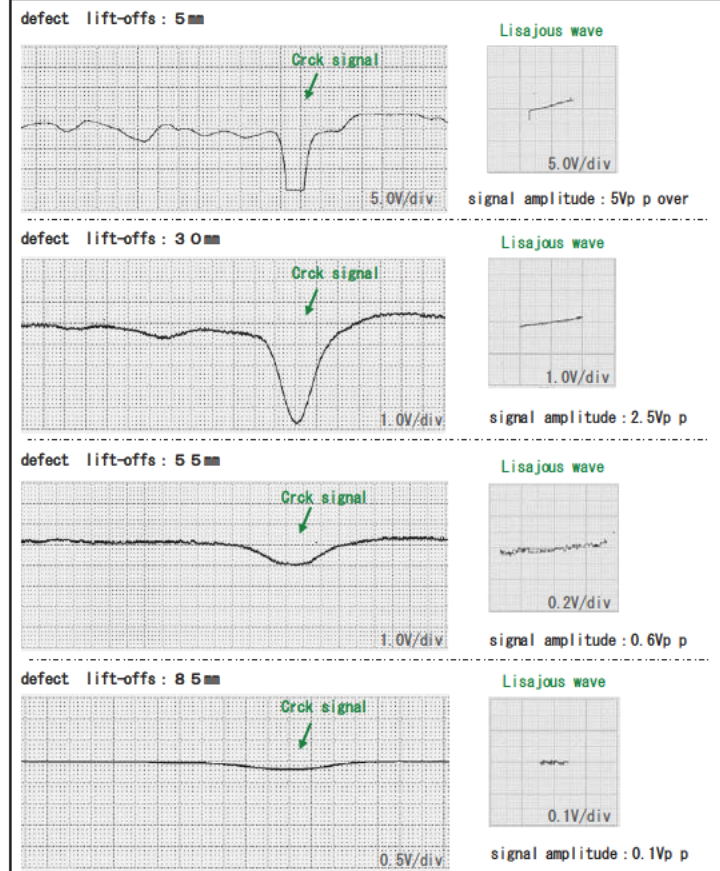


Figure 12. Detection tests in situ

Tests in situ (actual pavement test)

(1) Test 1

On the day after the executing pavement works after the completion of the detection tests, the sensor was improved and detection tests on the actual pavement surface were carried out (Figure 13). Because the pavement of this bridge has a thickness of 65 mm, detection tests for a lift-off of 70 mm, including the acrylic plate, were carried out. As shown in Figure 14, it was possible to obtain the crack signal.



Figure 13. Eddy current test
(with pavement)
(2) Test2

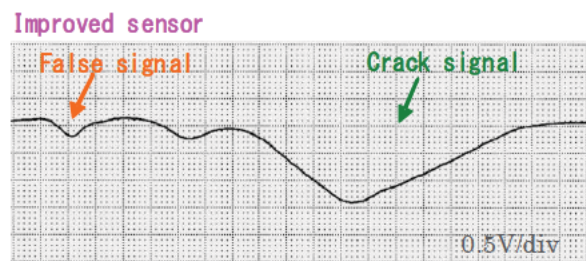


Figure 14. Improved sensor wave
(85 mm lift-offs)

Verification tests were carried out at locations where damages in the pavement had been repaired. Eddy current inspections were carried out over the pavement layer to verify whether the crack perforating the deck plate can be detected. Precision of the eddy current method was also verified by calibrating the results obtained by the eddy current test and the crack perforating the deck, after the removal of the asphalt layer.

As a result, the signal due to crack perforating the deck was detected. Comparing the results with the crack perforating the deck after the removal of the asphalt, it was confirmed that the results obtained by the eddy current test executed over the asphalt detected with good precision the crack perforating the deck along a length of about 500mm.



Figure 15. Field inspection on
actual pavement

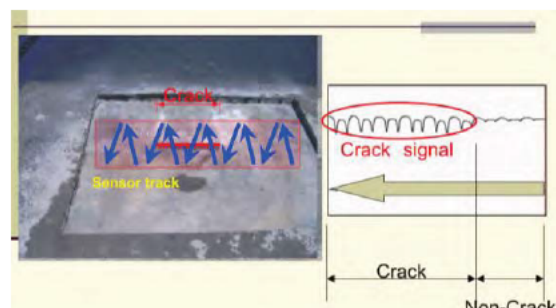


Figure 16. Output of eddy current test

Development of an automotive eddy current inspection device

Under the present conditions, the eddy current test method has to be executed manually, what is a limitation for the improvement of the test efficiency. Thus, to rationalize the inspections and tests works, with the objective of detecting early cracks in orthotropic decks, an automated eddy current device that can replace the manual works was developed.

The testing device system is composed by a multi-channel eddy current testing system, a detector with a scanning system, a power generator and a tractor to tow the whole system.

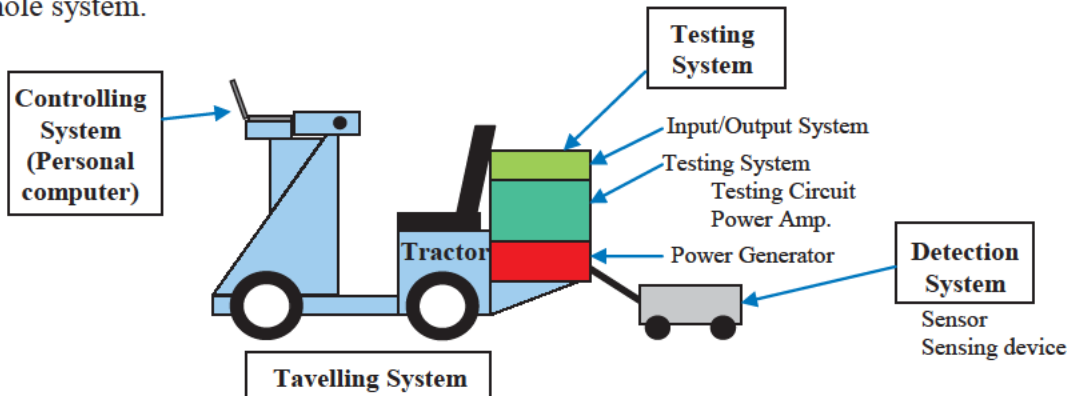


Figure 17. Scheme of the automated detection system

The detection device is pulled by the driving vehicle, and 4 coils mounted on it as sensors, with 1 coil measuring 1 U-rib weld line. The sensor is capable of moving in zigzag over the movement direction (transverse to the weld line) in a determined speed.

Required specifications

- One round trip per traffic control period (about 4 working hours), 1 span (about 80m), 1 lane (about 3.5m, 8 weld lines)
- Able to detect 100mm cracks perforating decks over an asphalt thickness of 100mm,
- Running speed: during measurement 1-10 cm/sec; while moving, 50 cm/sec.
- Load: 80kg (1 person riding)

Measurement device: about 140kg

Driving device: about 130kg (including detection device and control PC)

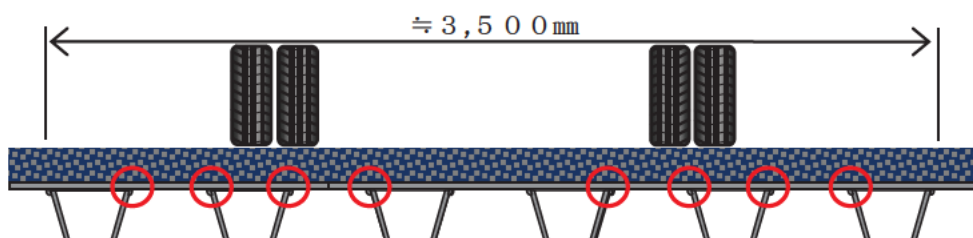


Figure 18. Sweep per lane (3.5m, 8 welding lines)



Figure 19. Automated detection system

Conclusions

It was confirmed that cracks perforating the deck can be detected through eddy current test carried out on the pavement surface, with good efficiency.

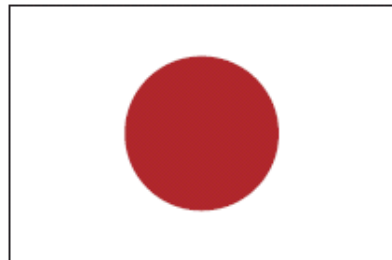
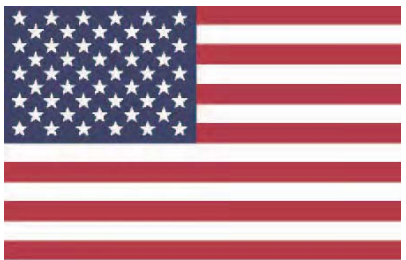
The detection limit for the improved sensor is 100 mm for length and a maximum of 85 mm for lift-offs.

The eddy current inspection can be applied as a simplified method of health diagnostic in the areas where cracks perforating the decks were found by screening through the infrared inspection mentioned in article 1.

With the increase in the heavy traffic volume and the consequent increase of the accumulated traffic volume, the number of occurrence of fatigue cracks is expected to increase. The authors shall continue to collect inspection data and make efforts to improve the detection limits and precision.

References

- Tukamoto, S., Hayashida, M. & Tabata, A. 2009. Development of a compound test method with the objective of detecting cracks perforating steel orthotropic deck. *Proceeding of the 64th Annual Meeting of Japan Society of Civil Engineers*: 6-346, 691-692.
- Sugiyama, H., Sakiya, K., Kobayashi, H., Tabata, A., Yamagami, T., Tukamoto, S. & Takamura, Y. 2009. Detection of cracks perforating steel orthotropic deck using phased-array ultrasonic detection. *28th Japan Road Congress, Japan Road Association*.
- Sugiyama, H., Sakiya, K., Kobayashi, H., Takamura, Y. & Tukamoto, S. 2009 Detailed inspection and reinforcement design of cracks perforating steel orthotropic decks. *Journal of Constructional Steel, Japanese Society of Steel Construction*: vol. 17, 345-350.



**27th US-Japan
Bridge Engineering Workshop**

Appendix 1:

Japan Participants

Page Left Blank

Taku Hanai

Senior Researcher

Bridge and Structural Technology Research Group

Center for Advanced Engineering Structural Assessment and Research

Public Works Research Institute (PWRI)

1-6, Minamihara, Tsukuba, Ibaraki, 305-8516, Japan

Phone: +81-29-879-6773

Fax: +81-29-879-6739

E-mail: hanai@pwri.go.jp

Hidekazu Hayashi

Researcher

Road Research Department Bridge Division

Nippon Expressway Research Institute Company Limited

1-4-1, Tadao, Machida-shi, Tokyo, 194-8508, Japan

Phone: +81-42-791-1625

Fax: +81-42-791-2380

E-mail: h.hayashi.ac@ri-nexco.co.jp

Kunihiro Hayashi

Chief Engineer of Osaka Business and Maintenance Department,

Hanshin Expressway Company Limited, Osaka

3-1-25 Ishida, Minato-ku, Osaka, 552-0006 JAPAN

Phone: +81-6-6576-3881

Fax: +81-6-6576-1907

Email: kunihiro-hayashi@hanshin-exp.co.jp

Jun-ichi Hoshikuma

Chief Researcher

Bridge and Structural Technology Research Group

Center for Advanced Engineering Structural Assessment and Research

Public Works Research Institute (PWRI)

1-6, Minamihara, Tsukuba, Ibaraki, 305-8516, Japan

Phone: +81-29-879-6793

Fax: +81-29-879-6739

E-mail: hosikuma@pwri.go.jp

Masahiro Ishida

Chief Researcher

Bridge and Structural Technology Research Group

Center for Advanced Engineering Structural Assessment and Research

Public Works Research Institute (PWRI)

1-6, Minamihara, Tsukuba, Ibaraki, 305-8516, Japan

Phone: +81-29-879-6793

Fax: +81-29-879-6739

E-mail: ishida@pwri.go.jp

Shojo Kataoka

Senior Researcher

Earthquake Disaster Prevention Division

National Institute for Land and Infrastructure Management (NILIM)

Ministry of Land, Infrastructure, Transport and Tourism (MLIT)

1 Asahi, Tsukuba 305-0804, Japan

Phone: +81-29-864-7682

Fax: +81-29-864-0598

Email: kataoka-s92rc@nilim.go.jp

Kazuhiko Kawashima.

Professor

Department of Civil Engineering

Tokyo Institute of Technology

M1-10, O-Okayama,Meguro, Tokyo, 152-8552, Japan

Phone: +81-3-5734-2922

Fax: +81-3-5734-3810

E-mail: kawashima.k.ae@m.titech.ac.jp

Yoshitomi Kimura

Chief Researcher

Bridge and Structural Technology Research Group

Center for Advanced Engineering Structural Assessment and Research

Public Works Research Institute (PWRI)

1-6, Minamihara, Tsukuba, Ibaraki, 305-8516, Japan

Phone: +81-29-879-6793

Fax: +81-29-879-6739

E-mail: y-kimura@pwri.go.jp

Kenji Kosa

Professor of Civil Engineering
Kyushu Institute of Technology
Department of Civil Engineering
Kyushu Institute of Technology
Sensui 1-1, Tobata, Kitakyushu, 804-8550 JAPAN
Phone & Fax: +81-93-884-3123
E-mail: kosa@civil.kyutech.ac.jp

Tetsurou Kuwabara

Director of Bridge and Structural Engineering Research Group,
Center for Advanced Engineering Structural Assessment and Research
Public Works Research Institute (PWRI)
1-6 Minamihara, Tsukuba-shi, Ibaraki-ken 305-8516 Japan
Phone: +81-29-879-6793
Fax: +81-29-879-6739
E-mail t-kuwa@pwri.go.jp

Koji Mitani

President and CEO, NEXCO-West USA, Inc.
1015, 18th Street, N.W., Suite 504
Washington, D.C., 20036
Phone: 202- 223-7040
Fax: : 202- 296-5373
Email: k.mitani@w-nexco-usa.com

Jun Murakoshi

Chief Researcher,
Bridge and Structural Technology Research Group
Center for Advanced Engineering Structural Assessment and Research
Public Works Research Institute (PWRI)
1-6, Minamihara, Tsukuba, Ibaraki, 305-8516, Japan
Phone: +81-29-879-6773
Fax: +81-29-879-6739
E-mail:murakosi@pwri.go.jp

Shunji Nagahashi

Staff of Bridges Department, Public Works Division,
Public Works Bureau of Osaka City Government
ATC-building ITM 6F, 2-1-10 Nankokita Suminoe-Ku Osaka City 559-0034, Japan
Phone: +81-6- 6615-6824
Fax: +81-6- 6615-6582
E-mail: s-nagahashi@city.osaka.lg.jp

Keita Nakasu

Senior Researcher,
Bridge and Structures Division, Road Department,
National Institute for Land and Infrastructure Management (NILIM)
Ministry of Land, Infrastructure and Transport (MLIT)
1 Asahi, Tsukuba, Ibaraki, 305-0804 JAPAN
Phone: +81-29-864-4919
Fax: +81-29-864-0178
Email: nakasu-k92gy@nilim.go.jp

Haruhiko Nakata

Inspection and Survey Division, Engineering Department,
Hanshin Expressway Engineering Company Limited
ORIX building 12F, 1-4-1, Nishi-hommachi, Nishi-ku, Osaka City
Phone: +81-6- 6110-7200
Fax: +81-6- 6110-7300
Email: haruhiko-nakata@hex-eng.co.jp

Shoichi Nakatani

Chief Researcher
Bridge and Structural Technology Research Group
Center for Advanced Engineering Structural Assessment and Research
Public Works Research Institute (PWRI)
1-6, Minamihara, Tsukuba, Ibaraki, 305-8516, Japan
Phone: +81-29-879-6773
Fax: +81-29-879-6739
E-mail: nakatani@pwri.go.jp

Toshiaki Nanazawa

Principal Senior Researcher

Bridge and Structural Technology Research Group

Center for Advanced Engineering Structural Assessment and Research

Public Works Research Institute (PWRI)

1-6, Minamihara, Tsukuba, Ibaraki, 305-8516, Japan

Phone: +81-29-879-6773

Fax: +81-29-879-6739

Email: nanazawa@pwri.go.jp

Hideaki Nishida

Senior Researcher

Bridge and Structural Technology Research Group

Center for Advanced Engineering Structural Assessment and Research

Public Works Research Institute (PWRI)

1-6, Minamihara, Tsukuba, Ibaraki, 305-8516, Japan

Phone: +81-29-879-6773

Fax: +81-29-879-6739

Email: nisida@pwri.go.jp

Fumihiko Nomura

Researcher,

Bridge and Structures Division, Road Department,

National Institute for Land and Infrastructure Management,

Ministry of Land, Infrastructure and Transport (MLIT)

1 Asahi, Tsukuba, Ibaraki, 305-0804 JAPAN

Phone: +81-29-864-4919

Fax: +81-29-864-0178

Email: nomura-f92td@nilim.go.jp

Kiyoshi Ono

Associate Professor of Civil Engineering

Osaka University, Department of Civil Engineering

Graduate school of Engineering

Osaka University

2-1 Yamadaoka, Suita City, Osaka 565-0871, Japan

Phone: +81-6-6879-7598

Fax: +81-6-6871-7601

E-mail: k-ono@civil.eng.osaka-u.ac.jp

Junichi Sakai

Senior Researcher

Bridge and Structural Technology Research Group

Center for Advanced Engineering Structural Assessment and Research

Public Works Research Institute (PWRI)

1-6, Minamihara, Tsukuba, Ibaraki, 305-8516, Japan

Phone: +81-29-879-6773

Fax: +81-29-879-6739

E-mail: sakai55@pwri.go.jp

Shuhei Sakai

Central Nippon Expressway Co., Ltd.

Dept. of Planning and Design Team Nagoya B.O. NEXCO Central

Mitsui-Sumitomo Bank Nagoya Building

2-18-19 Nishiki Naka-ku Nagoyashi Aichi Prefecture 460-0003, JAPAN

Phone: +81- 52-222-1594

Fax: +81- 52-232-3718

Email: s.sakai.ac@c-nexco.co.jp

Hiroshi Sato

Advisor

IHI Infrastructure Systems Co., Ltd.

Ohama-Nishimachi 3, Sakai-ku, Sakai-shi, Osaka, 590-0977, Japan

Phone: +81-72-223-0980

Fax: +81-72-223-0854

Email: hiroshi_sato@iis.ihi.co.jp

Hiroki Sugiyama

Chief

Design Management and Engineering Research Group,

Engineering Department

Hanshin Expressway Company Limited, Osaka, Japan

4-1-3, Kyutaro-machi, Chuo-Ku, Osaka, 541-0056, Japan

Phone: +81-6-4963-5790

Fax: +81-6-6252-4583

Email: hiroki-sugiyama@hanshin-exp.co.jp

Takashi Tamakoshi

Head,

Bridge and Structures Division, Road Department

National Institute for Land and Infrastructure Management

Ministry of Land, Infrastructure, Transport and Tourism (MLIT)

1 Asahi, Tsukuba, Ibaraki, 305-0804 JAPAN

Phone: +81-29-864-4919

Fax: +81-29-864-0178

Email: tamakoshi-t92gd@nilim.go.jp

Keiichi Tamura

Research Coordinator for Earthquake Engineering

Center for Advanced Engineering Structural Assessment and Research

Public Works Research Institute (PWRI)

1-6 Minamihara, Tsukuba-shi, Ibaraki-ken 305-8516 Japan

Phone: +81-29-879-6721,

Fax: +81-29-879-6739

E-mail: ke-tamura@pwri.go.jp

Yoshiki Tanaka

Senior Research Engineer

Bridge and Structural Technology Research Group

Center for Advanced Engineering Structural Assessment and Research

Public Works Research Institute (PWRI)

1-6, Minamihara, Tsukuba, Ibaraki, 305-8516, Japan

Phone: +81-29-879-6773

Fax: +81-29-879-6739

E-mail: tanakay@pwri.go.jp

Yukihiro Tsukada

Director of Road Department,

National Institute for Land and Infrastructure Management,

Ministry of Land, Infrastructure, Transport and Tourism (MLIT)

1 Asahi, Tsukuba, Ibaraki, 305-0804 JAPAN

Phone: +81-29-864-4919

Fax: +81-29-864-0178

Email: tsukada-y27x@nilim.go.jp

Shigeki Unjoh

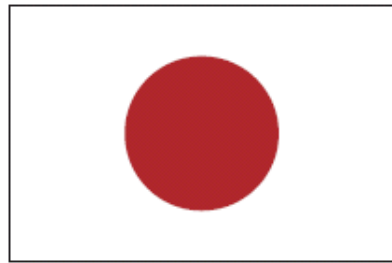
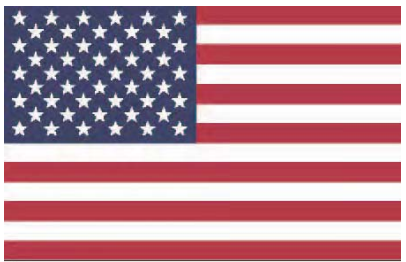
Research Coordinator for Earthquake Disaster Prevention
National Institute for Land and Infrastructure Management (NILIM)
Asahi 1, Tsukuba-shi, Ibaraki-ken 305-0804 Japan
Phone: +81-29-864-4963
E-mail unjoh@pwri.go.jp

Eiki Yamaguchi

Professor of Civil Engineering
Dept. of Civil Engineering
Kyushu Institute of Technology
Kitakyushu, 804-8550, Japan
Phone: +81-93-884-3110
Fax: +81-93-884-3100
E-mail: yamaguch@civil.kyutech.ac.jp

Guangfeng Zhang

Researcher
Bridge and Structural Technology Research Group
Center for Advanced Engineering Structural Assessment and Research
Public Works Research Institute (PWRI)
1-6, Minami-hara, Tsukuba, Ibaraki, 305-8516, Japan
Phone: +81-29-879-6773
Fax: +81-29-879-6739
E-mail: tyou44@pwri.go.jp



**27th US-Japan
Bridge Engineering Workshop**

Appendix 2:

US Participants

Page Left Blank

Ian Buckle

Professor

Department of Civil and Environmental Engineering

University of Nevada, Reno

1664 N. Virginia St/MS 258

Reno, NV 89557-0258

Phone: 775-784-4213,

Fax: 775-784-1390

E-mail: igbuckle@unr.edu

Genda Chen

Professor of Civil Engineering and Associate Director

Mid-America Transportation Center

Department of Civil, Architectural, and Environmental Engineering

Missouri University of Science and Technology

328 Butler-Carlton Hall 1401 N. Pine Street

Rolla, MO 65409-0030

Phone: 573-341-4462

Fax: 573-341-6215

Email: gchen@mst.edu

Waseem Dekelbab

Senior Program Officer

National Cooperative Highway Research Program

500 Fifth Street, NW

Washington, DC 20001

Phone: 202-334-1409

Fax: 202-334-2006

Email: WDekebab@nas.edu

Ian M. Friedland

Acting Director, Office of Freight Operations and Management

Federal Highway Administration

Phone: 202-366-9615

Email: ian.friedland@dot.gov

John L. Gross

Director of Structures Research, NFRL

National Institute of Standards and Technology

100 Bureau Drive, Stop 8611

Gaithersburg, MD 20899-8611

Phone: 301-975-6068

Email: john.gross@nist.gov

Bruce Johnson

State Bridge Engineer
Oregon DOT Bridge Section
4040 Fairview Industrial Dr SE, MS#
Salem, OR 97302
Phone: 503-986-3344
Email: Bruce.V.Johnson@odot.state.or.us

Kevin R. Mackie

Assistant Professor
Civil, Environmental, and Construction Engineering
University of Central Florida
Orlando, FL 32816-2450
Phone: 407-823-2857
Fax: 407 823-3315
Email: Kevin.Mackie@ucf.edu

Lee Marsh

Senior Project Manager
BergerABAM
33301 Ninth Avenue South, Suite 300
Federal Way, Washington 98003-2600
Phone: 206-431-2340
Email: lee.marsh@abam.com

David Sanders

Professor
Department of Civil and Environmental Engineering
University of Nevada, Reno
1664 N. Virginia St/MS 258
Reno, NV 89557-0258
Phone: 775-784-4288
Fax: 775-784-1390
Email: sanders@unr.edu

Sri Sritharan

Wilson Engineering Professor
376 Town Engineering Bldg.
Civil, Construction & Environmental Engineering
Iowa State University
Ames, IA 50011-3232
Phone: 515-294-523
Fax: 515-294-8216
Email: sri@iastate.edu

John Stanton

Professor of Civil Engineering
214 More Hall, Box 352700
University of Washington,
Seattle, WA 98195.
Phone: 206-543-6057
Email: stanton@u.washington.edu

Peter Weykamp

Bridge Maintenance Program Engineer
New York State Department of Transportation
50 Wolf Road, Pod 5-1
Albany, NY 12232
Phone: 518-457-8485
Fax: 518-457-4203,
Email:pweykamp@dot.state.ny.us

W. Phillip Yen

Principal Bridge Engineer - Structural Dynamics
Office of Bridge Technology, FHWA
1200 New Jersey Avenue, S.E., Room 73-421
Washington, DC 20590
Phone: 202-366-5604
Email: Wen-huei.yen@dot.gov